Coalbed methane in the Upper Cretaceous Fruitland Formation, San Juan Basin, New Mexico and Colorado

Edited by W. B. Ayers, Jr., and W. R. Kaiser

Published in cooperation with

Bureau of Economic Geology, The University of Texas at Austin, Report of Investigations No. 218

Colorado Geological Survey, Division of Minerals and Geology, Department of Natural Resources, Resource Series 31

BULLETIN 146 New Mexico Bureau of Mines & Mineral Resources 1994

A DIVISION OF
NEW MEXICO INSTITUTE OF MINING AND TECHNOLOGY

COVER—Westward view of the Hogback monocline between Carbon Junction and Florida River, northern San Juan Basin. The Pictured Cliffs Sandstone forms the Hogback monocline. Above the Pictured Cliffs Sandstone (left of the Hogback) is the Fruitland Formation. Fruitland coal beds occur in the strike-parallel valleys, whereas thin Fruitland sandstones form the minor ridges. The Farmington Sandstone forms a prominent ridge at the south (left). Meteoric recharge along the Hogback accounts for artesian overpressure in coal beds and high water production rates in coalbed methane wells in the northern part of the San Juan Basin. Photograph by W. B. Ayers, Jr.

Bulletin 146

New Mexico Bureau of Mines and Mineral Resources

A DIVISION OF
NEW MEXICO INSTITUTE OF MINING AND TECHNOLOGY

Coalbed methane in the Upper Cretaceous Fruitland Formation, San Juan Basin, New Mexico and Colorado

Edited by W. B. Ayers, Jr., and W. R. Kaiser

Bureau of Economic Geology, The University of Texas at Austin, Austin, Texas 78713-7508

DOI: https://doi.org/10.58783/cgs.rs31.jxgu1990

Research funded by the Gas Research Institute
under contract no. 5087-214-1544

Published in cooperation with

Bureau of Economic Geology
The University of Texas at Austin
Austin, Texas 78713-7508
(Report of Investigations No. 218)

Colorado Geological Survey
Division of Minerals and Geology
Department of Natural Resources
1313 Sherman St., Room 715
Denver, Colorado 80203
(Resource Series 31)

SOCORRO 1994

Original Printing

Published by Authority of State of New Mexico, NMSA 1953 Sec. 63-1-4 Printed by University of New Mexico Printing Services, July 1994

Available from New Mexico Bureau of Mines & Mineral Resources, Socorro, NM 87801 Published as public domain, therefore reproducible without permission. Source credit requested.

Contents

Preface

Coalbed methane is playing an increasingly important role in meeting the energy needs of the United States. According to one estimate, this unconventional gas may supply 4-5% of the domestic natural gas in 1994. In the San Juan Basin, Fruitland Formation coal beds contain an estimated 43 to 49 trillion cubic feet (Tcf) of methane. This basin is the most active area of coalbed methane development and production in the United States. The San Juan Basin led the nation in coalbed methane production in 1992, when nearly 2,100 Fruitland coalbed wells produced approximately 447 billion cubic feet (Bcf) of coalbed methane-81% of the total U.S. coalbed methane production of approximately 553 Bcf.

From August 1987 through July 1990, the Bureau of Economic Geology (BEG) at The University of Texas at Austin evaluated geologic and hydrologic controls on the occurrence and producibility of coalbed methane in the Fruitland Formation for the Gas Research Institute (GRI). The Colorado Geological Survey and the New Mexico Bureau of Mines and Mineral Resources participated in the research through subcontracts with BEG. Results from the first two years of research were summarized in annual reports to GRI (GRI88/0322.1 and GRI-90/0014.1, respectively). A topical report submitted to GRI in 1991 (GRI-91/0072) superseded those annual reports, integrating their contents with research results from the final year of the study. This publication includes all except two papers from that topical report. Themes of the omitted papers were generic; therefore, those papers were omitted to focus this publication on the San Juan Basin.

The unpublished GRI contract reports had limited distribution. Their goal was the timely transfer of technology to industry. Because requests for the topical report exceeded the number of copies printed and because many of the topics covered in this research appeal to a broad audience of geoscientists and engineers, this publication was issued to increase the availability of the research results. This report discusses five areas that relate to controls on the occurrence or producibility of coalbed methane.

The first topic, the *tectonic setting* of the San Juan Basin, reviews regional tectonic controls on depositional systems and coalbed attitude. Among the most important geologic factors affecting the occurrence and producibility of coalbed methane is the *depositional setting,* which is covered in the second part of this report; a chapter on the regional depositional setting of Fruitland coalbed methane is followed by two chapters describing local studies. *Fracture patterns* in Fruitland coal beds and adjacent strata are addressed in three chapters that discuss regional cleat trends and lineament analysis. Studies of *hydrology, thermal maturity, and gas composition* are essential to understanding and predicting regional hydrodynamics and coalbed gas content and composition; these considerations are the subject of two chapters. Finally, the last topic is the *integration of geologic and hydrologic studies.* In this section we summarize gas and water production from Fruitland coal beds, and on the basis of the relations between production, geologic setting, and hydrodynamics, we divide the San Juan Basin into regions in which Fruitland coal beds have similar reservoir characteristics.

Acknowledgments

This research was funded by the Gas Research Institute (GRI) under contract no. 5087-214-1544. To our benefit, we discussed various aspects of the research with personnel of GRI contractors and with the GRI coalbed methane project managers, R. A. McBane and R. C. Klem. We also benefited from discussions with Brad Boyce, Terry Britt, Ernie Busch, Jay Close, Brent Hale, W. B. Hanson, Tom Hemler, W. F. Hoppe, A. C. Huffman, Jr., P. D. Jenden, Robert Kemp, Jack McAnear, Paul Oldaker, and Jeff Peace. The contributions of others are acknowledged in the appropriate chapters. The report was reviewed internally at BEG, and each paper was read by one or more outside reviewers, who are acknowledged in the respective chapters.

Several companies supplied data that advanced the study's objectives, strengthening its results and conclusions; among these were Amoco Production, R. L. Bayless, Blackwood & Nichols, Chevron Oil Field Research, Dugan Production, El Paso Natural Gas, Holditch & Associates, McKenzie Methane, Mesa Petroleum, Mobil Oil, Northwest Pipeline, Phillips Petroleum, and Resource Enterprises. We thank the Southern Ute Indian tribe and other landowners for access to their properties and BHP-Utah International, Pueblo Coal, and Kaiser Steel Resources, Inc., for mine access.

We thank C. F. Brandenburg, GRI Director for Natural Gas Supply, for recognizing the need for an integrated study of geologic controls on the occurrence and producibility of coalbed methane. R. J. Finley, BEG Associate Director for Gas Resources, played a critical role in the initiation of this project.

During this study, capable assistance was provided by J. D. Bechman, W. J. Garey, D. R. Grote, G. J. Hawkins, S. A. Jones, R. G. McMurry, Wahiduzzaman Mirza, M. M. Newton, P. S. Reiss, Ting-Ya Hsieh, T. E. Swartz, G. A. Warren, J. S. Yeh, and S. D. Zellers, all Research Assistants at The University of Texas at Austin. The cartographic, editorial, and publication staffs of the BEG and the publication staff of the New Mexico Bureau of Mines and Mineral Resources contributed greatly to the completion of this report. The computing staff at BEG, managed by Ken Duncan, provided guidance in data processing and computer-assisted mapping. Drafting was by the cartographic staff of the BEG under the direction of R. L. Dillon, chief cartographer. Other BEG staff members contributing to the publication of this report were Susan Lloyd and Diane Ruetz, word processing, and Bobby Duncan, editing, under the direction of Susann Doenges, editor-in-chief.

We also wish to thank Carol Hjellming of the New Mexico Bureau of Mines and Mineral Resources for her editorial assistance and publication production.

W. B. Ayers, Jr.
W. R. Kaiser

1. Tectonic setting of the San Juan Basin

S. E. Laubach[1] and C. M. Tremain[2]

[1]*Bureau of Economic Geology and 'Colorado Geological Survey*

Abstract—Tectonic history influenced Mesozoic and Cenozoic depositional patterns, coal occurrence, and gas generation in the San Juan Basin of New Mexico and Colorado. Tectonic events also affected or controlled the distribution and orientation of folds and fractures in coals and adjacent rocks. This chapter summarizes basin origin and evolution in order to provide a framework for studies of depositional patterns and fracture occurrence in Cretaceous and Tertiary rocks. An understanding of the tectonic setting, combined with the studies in the following chapters, provides a basis for predicting coalbed methane occurrence and producibility in this and other western coal basins.

Location and structure of the basin

The San Juan Basin occupies the east-central part of the Colorado Plateau in northwestern New Mexico and southwestern Colorado. It is a roughly circular, asymmetrical, structural basin of Late Cretaceous to early Tertiary age (Fig. 1.1). The structures that bound the basin include the Hogback monocline on the west and northwest, the San Juan uplift on the north, the Nacimiento uplift to the southeast, and the Chaco slope and Zuni uplift to the south and southwest. The depocenter and the synclinal axis of the basin on Upper Cretaceous strata occur near, and parallel, the northern and the northeastern margins of the basin.

Rocks in the basin range in age from Precambrian through Cenozoic. In the deepest part of the basin, Precambrian crystalline basement rocks are more than 14,000 ft (>4,270 m) beneath the surface. Coal is present throughout the Cretaceous System, but the largest coal and coalbed methane resources are in the Fruitland Formation, which is the focus of this study. The area of Fruitland Formation outcrop occurrence encompasses approximately 6,700 mi^2 (~17,350 km^2). Fruitland coal seams occur from outcrop to depths as great as 4,200 ft (1,280 m).

Evolution of the basin

During the Cretaceous, the area of the present San Juan Basin was on the western margin of the Western Interior seaway, a rapidly subsiding, elongate, asymmetric trough. At that time, the basin was occupied by a shallow sea (Fig. 1.2) that extended from north to south across much of the Midcontinent (Kauffman, 1977; Merewether and Cobban, 1986; Weimer, 1986). The Western Interior Basin was bounded on the west by the Cordilleran orogenic belt, a fold and thrust belt that is exposed west of the San Juan Basin in Utah and Nevada (Armstrong, 1968; Burchfiel and Davis, 1975; Royse and others, 1975) and southwest of the Colorado Plateau in southeastern California, western and southern Arizona, New Mexico, and west Texas (Burchfiel and Davis, 1975). The western margin of the Western Interior Basin was the site of the greatest subsidence, which was controlled by tectonism in the orogenic belt. The eastern part of the basin was shallow and adjacent to a broad, stable platform (Hattin, 1965; Kauffman, 1977).

A major time of subsidence in the Western Interior Basin during mid-Cretaceous (Aptian Cenomanian) time is interpreted as recording the initiation of thrusting in the adjacent overthrust belt (Heller and others, 1986). The correlation of transgressions and regressions of the Upper Cretaceous shoreline with episodic thrust-fault movement and uplift shows that basin subsidence was accelerated by thrust-loading deformation (Jordan, 1981). The structure and stratigraphy of the Western Interior Basin is complicated by spatial and temporal variability of thrusting and subsidence, by intermittent uplift of broad, gentle flexure-related arches in the foreland, and by eustasy.

Rocky Mountain intermontane basins and uplifts formed in this tectonic regime (Chapin and Cather, 1981; Dickinson and others, 1988). During the Laramide orogeny, which began in the Late Cretaceous, peaked in the Paleocene, and waned in the Eocene (approximately 80 to 40 m.y. ago), the San Juan structural basin formed in the east-central Colorado Plateau. The Eocene San Jose Formation is the oldest rock unit for which isopachs clearly indicate a separate depocenter in the San Juan Basin (Stone and others, 1983, figs. 18, 21, and 27; Fassett, 1985).

A protracted extension event followed Late Cretaceous to early Tertiary thrusting in the western United States, creating the Basin and Range province. The Colorado Plateau is a coherent, uplifted crustal block surrounded by the extended terrain of the Basin and Range and Rio Grande Rift provinces (Thompson and Zoback, 1979). It began to decouple from the Basin and Range province and the Rio Grande rift about 32 m.y. ago (Aldrich and others, 1986, fig. 3). The plateau was affected by mild Cenozoic extension and volcanism, but major post-Laramide faults and folds are rare on the Colorado Plateau, deformation being limited to minor structures and episodes of uplift or subsidence.

Reactivation of basement metamorphic fabrics or faults (Cordell and Grauch, 1985; Huffman and Taylor, 1991) and Paleozoic faults (Kluth and Coney, 1981; Ross and Ross, 1986) may have localized Mesozoic and Cenozoic deformation or controlled structural trends. Interpretation of seismic lines throughout the San Juan Basin by the U.S. Geological Survey (Taylor and Huffman, 1988; Huffman and Taylor, 1991) indicates a rectilinear pattern of high-angle faults in the basement with dominant northwest and northeast strikes. Predominantly dip-slip separation is inferred for most of these faults, although map patterns of some of the faults resemble patterns associated with strike-slip movement. Fault movement occurred intermittently during the Pennsylvanian to Permian, Jurassic to Early Cretaceous, and Late Cretaceous to early Tertiary. Locally, Mesozoic rocks either drape over buried basement faults or are cut by them. Locally, faults juxtapose permeable coal beds and less permeable shale and sandstone.

Regional extension was accompanied by the eruption of voluminous Oligocene volcanic rocks to form the San Juan volcanic field and by the emplacement of igneous intrusives beneath the volcanic pile along the northern side of the San Juan Basin (Steven, 1975; Lipman and others, 1978). In the northeastern San Juan Basin, the north-trending Dulce dike swarm yields radiometric ages of 28 to 22 Ma, indicating east-west least principal horizontal stress when the Rio Grande rift was forming on the east side of the Colorado Plateau (Aldrich and others, 1986). The Dulce dikes had only a local heating effect on the basin, as indicated by the lack of deflection of coal rank contours across the dike swarm (Meissner, 1984, fig. 18; Kelso and others, 1988, fig. 19; Scott and others, this volume, Fig. 9.3). However, the late Oligocene thermal event is a probable regional heat source for

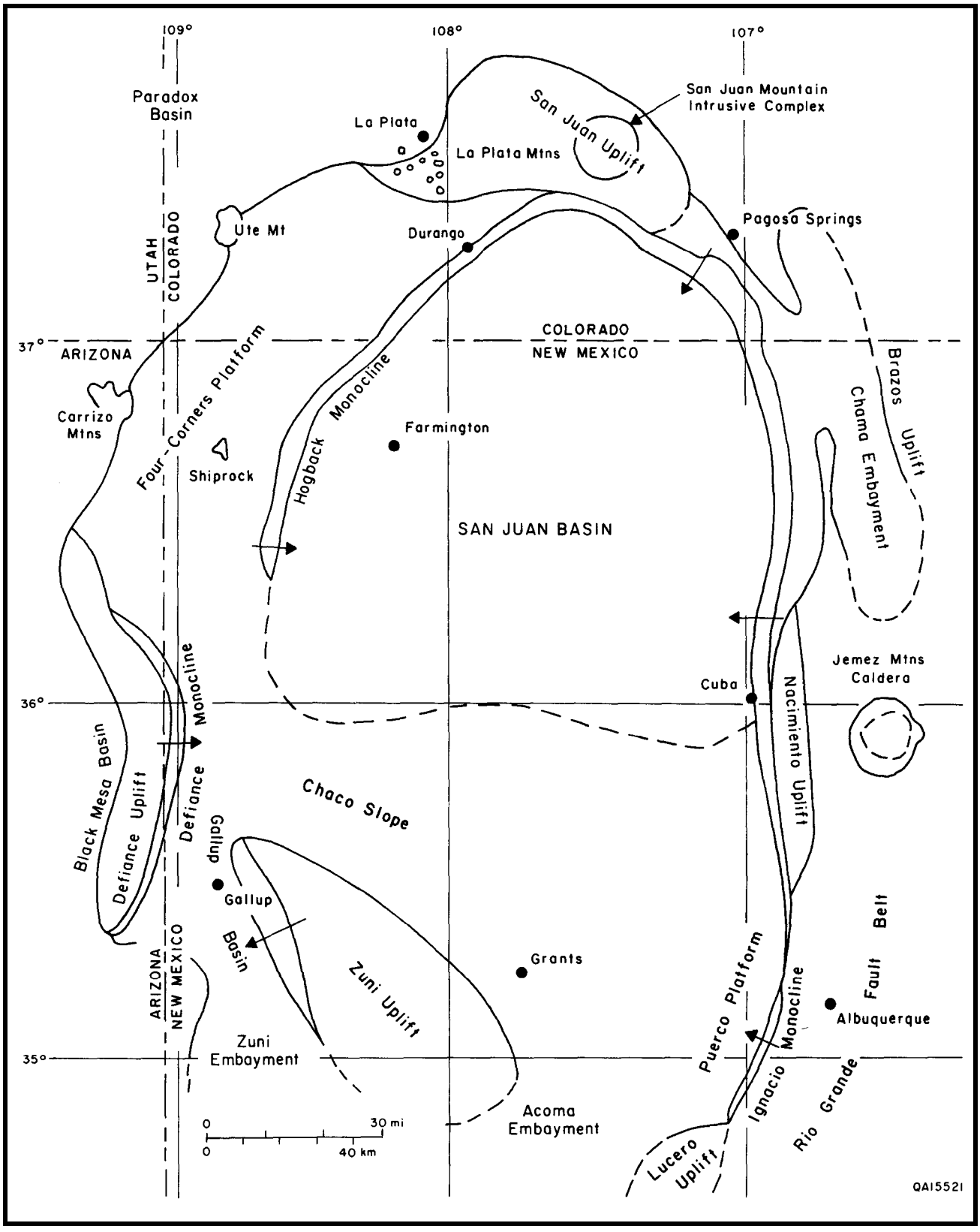

FIGURE 1.1—Regional tectonic setting of the San Juan Basin. Steeply dipping strata form the Hogback monocline that rims the northwestern part of the basin. Modified from Fassett and Hinds (1971) after Kelley (1951, p. 125).

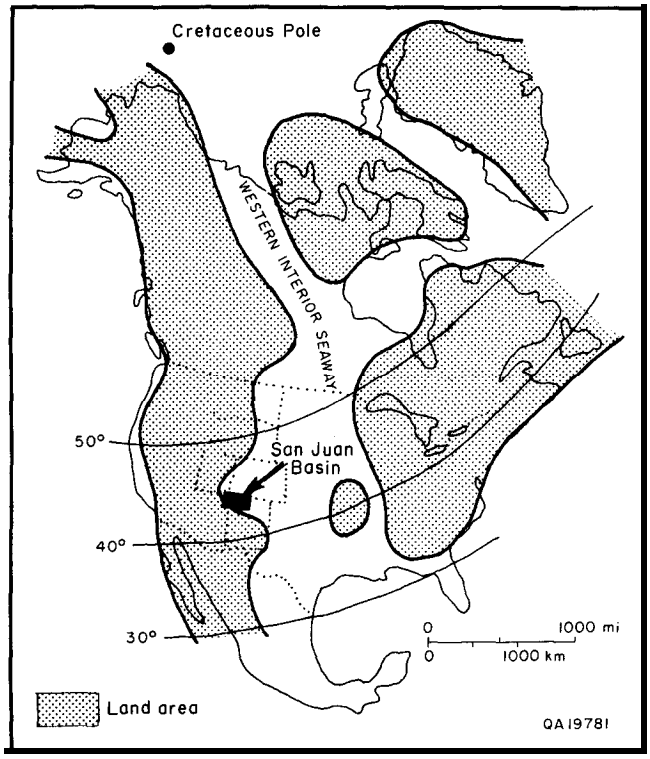

FIGURE 1.2—Location of the San Juan Basin relative to the Western Interior seaway. Modified from Palmer and Scott (1984) after Williams and Stelck (1975) and Irving (1979).

hydrocarbon generation in the San Juan Basin (Choate and Rightmire, 1982; Bond, 1984; Meissner, 1984; Clarkson and Reiter, 1988).

Regional uplift of the Colorado Plateau began in the Miocene and has continued to the present (Epis and Chapin, 1975). Erosion of basin fill from the San Juan Basin has contributed to the post-Oligocene cooling of the basin (Meissner, 1984). Especially important from the standpoint of this report is the erosion of Oligocene volcanic and volcaniclastic rocks over the upturned outcrop of the Fruitland Formation along the northern flank of the basin, which allowed meteoric recharge of elevated sandstones and coal seams to cause artesian conditions and overpressuring in the Fruitland Formation in the northwestern part of the basin (Kaiser and Swartz, 1988, 1989; Kaiser and others, this volume, Chapter 8).

Minor structures and stress regime

Natural fractures (joints and cleats) are widespread in Cretaceous and Tertiary rocks in the San Juan Basin. Within the Fruitland Formation and adjacent rocks, opening mode (extensional) fractures are prevalent (Laubach and Tremain, this volume, Chapter 6; Tremain and others, this volume, Chapter 5). Systematic, closely spaced fractures (cleats) that intersect at approximately 90° are well developed within the Fruitland coal seams. A structural map of the San Juan Basin shows only minor anticlinal and synclinal noses and small normal faults superimposed on large areas of homoclinal dip (Ayers and others, this volume, Chapter 2). These minor folds and faults, which may cause fracture-enhanced permeability in coal seams (Yeh and others, 1991), have structural relief of less than 200 ft (<61 m).

Studies of seismicity, young faults, and in situ stress indicators suggest that the present stress regime of the Colorado Plateau is extensional, the minimum horizontal stress being oriented east-northeast. This stress direction is rotated approximately 70° counterclockwise from the west-northwest direction of the surrounding Rio Grande rift—Basin and Range extensional province (Zoback and Zoback, 1980, 1989; Wong and Humphrey, 1989).

Acknowledgments

We thank N. H. Whitehead, III for his contributions to this summary.

2. Coalbed methane in the Fruitland Formation, San Juan Basin: depositional and structural controls on occurrence and resources

W. B. Ayers, Jr., W. A. Ambrose, and J. S. Yeh

Bureau of Economic Geology

Abstract—The San Juan Basin is the leading producer of coalbed methane in the United States; production from the Upper Cretaceous Fruitland Formation was more than 65 Bcf in 1989 and was approximately 447 Bcf in 1992, when it accounted for 2.5% of the United States' natural gas production. To evaluate geologic controls on the occurrence and producibility of Fruitland coalbed methane, we used data from 2,500 geophysical well logs to make structure, lithofacies, isopach, and coal-occurrence maps and to calculate coal and coalbed methane resources. Fruitland coal accumulated southwest of the Pictured Cliffs wave-dominated shoreline, which prograded northeastward. The shoreline crossed an inferred northwest-striking structural hingeline; sporadic faulting downdropped the basin floor north of the hingeline, which created accommodation space and caused shoreline stillstands and transgressions, recorded in upper Pictured Cliffs tongues. These stillstands allowed extensive peat deposits to form and to spread over abandoned shoreline- and fluvial-sandstone complexes. The thickest Fruitland coal occurs in northwest-trending belts parallel to and landward of associated Pictured Cliffs tongues. Net coal thickness in these belts locally exceeds 100 ft (>30 m), and individual coal seams can be more than 30 ft (>9 m) thick. Northeast-trending coal deposits are common in the southwestern part of the basin, where they occur between dip-elongate fluvial-sandstone complexes. Coal resources of the Fruitland Formation are calculated to be 245 billion short tons; this coal contains an estimated 43 to 49 Tcf of coalbed methane in place.

Introduction

Depositional systems and structural features (fractures and faults in coal beds) are the primary geologic controls on coalbed methane resources and recoverability. The depositional system controls the occurrence, geometry, and thickness of coal seams by building platforms for peat (coal) accumulation and by bounding the seams. Additionally, the framework sandstones of the depositional system commonly are conduits for fluid flow. Although coal seams are the primary aquifers in the Fruitland Formation, these coal beds and associated sandstones perform as a single regional aquifer in the San Juan Basin (Kaiser and others, this volume, Chapter 8). However, fluid migration in coal seams, and hence producibility of coalbed methane, is locally enhanced or impeded by faults and fractures. Therefore, this section integrates sedimentology, coal occurrence, and structure of the Fruitland Formation and the Pictured Cliffs Sandstone to clarify geologic controls on coalbed methane occurrence and producibility.

Regional geologic setting and stratigraphy

During the Late Cretaceous (Campanian), the region of the present San Juan Basin was on the west margin of the Western Interior seaway (Laubach and Tremain, this volume, Fig. 1.2). The coastline migrated to the northeast, depositing a vertical succession of shelf through coal-bearing continental sediments. The Pictured Cliffs Sandstone is a coastal facies that was deposited as the Late Cretaceous shoreline prograded northeastward into the Western Interior seaway. In geophysical well logs (Fig. 2.1) and at outcrop, the Pictured Cliffs Sandstone is divisible into genetically related upper and lower units. The lower unit is composed of a series of upward-coarsening subunits and is interpreted as shelf and shoreface mudstone and sandstone interbeds (Fig. 2.1). The upper unit has a blocky well-log response and is composed of amalgamated sandstone bodies having a composite thickness of 40 to 120 ft (12 to 36 m); it is inferred to be the framework facies of prograding barrier-strandplain or wave-dominated delta depositional systems (Fig. 2.1).

Conventionally, the base of the Pictured Cliffs Sandstone is placed at the base of the upward-coarsening units (Fig. 2.1). However, that boundary is time-transgressive because the Pictured Cliffs Sandstone intertongues with the Lewis Shale (Figs. 2.2 and 2.3). The marine Lewis Shale (Figs. 2.12.3) contains several bentonite beds that are excellent marker beds for correlation. However, only the Huerfanito Bentonite Bed has been correlated throughout the San Juan Basin (Fassett and Hinds, 1971). Contemporaneity of the coastal (blocky) and shoreface and shelf (upward-coarsening) units is documented by marker beds, representing time lines, that cross the proximal shelf and shoreface to intersect and terminate in the Pictured Cliffs coastal sandstones (Fig. 2.2). The Pictured Cliffs Sandstone and equivalent marine units thicken basinward above the Huerfanito Bentonite Bed partly because of differential subsidence in the northern part of the basin. Progradation of the Pictured Cliffs shoreline resulted in basinward offset of the landward pinch-outs of these marker beds.

In subsurface studies, the contact between the Pictured Cliffs Sandstone and the Fruitland Formation (Fig. 2.1) is "placed at the top of the massive sandstone below the lowermost coal of the Fruitland except in those areas where the Fruitland and Pictured Cliffs intertongue" (Fassett and Hinds, 1971, p. 8). Pictured Cliffs sandstones are the depositional platforms on which Fruitland peat (coal) accumulated, and ultimately Pictured Cliffs shoreline sandstones bound coal seams in the basinward direction. Progradation of the Pictured Cliffs shoreline, dependent on complex interactions of sediment supply, basin subsidence, and eustasy, was intermittent, resulting in shoreline stillstands. Intertonguing of the Pictured Cliffs and the Fruitland Formation resulted from temporary landward shifts of the shoreline during overall regression of the Late Cretaceous shoreline. In this study, the Pictured Cliffs sandstones that intertongue with the Fruitland Formation are called upper Pictured Cliffs sandstones, or upper Pictured Cliffs tongues. There are three upper Pictured Cliffs tongues in the basin; individually, they are called UP1, UP2, or UP3 in this volume (Fig. 2.2). Together, they account for approximately 270 ft (82 m) of stratigraphic rise of the Pictured Cliffs over a 25-mi (40-km) distance in the northern third of the San Juan Basin (Fig. 2.2). The upper Pictured Cliffs tongues are upward-coarsening sequences on geophysical logs (Fig. 2.1), and each is

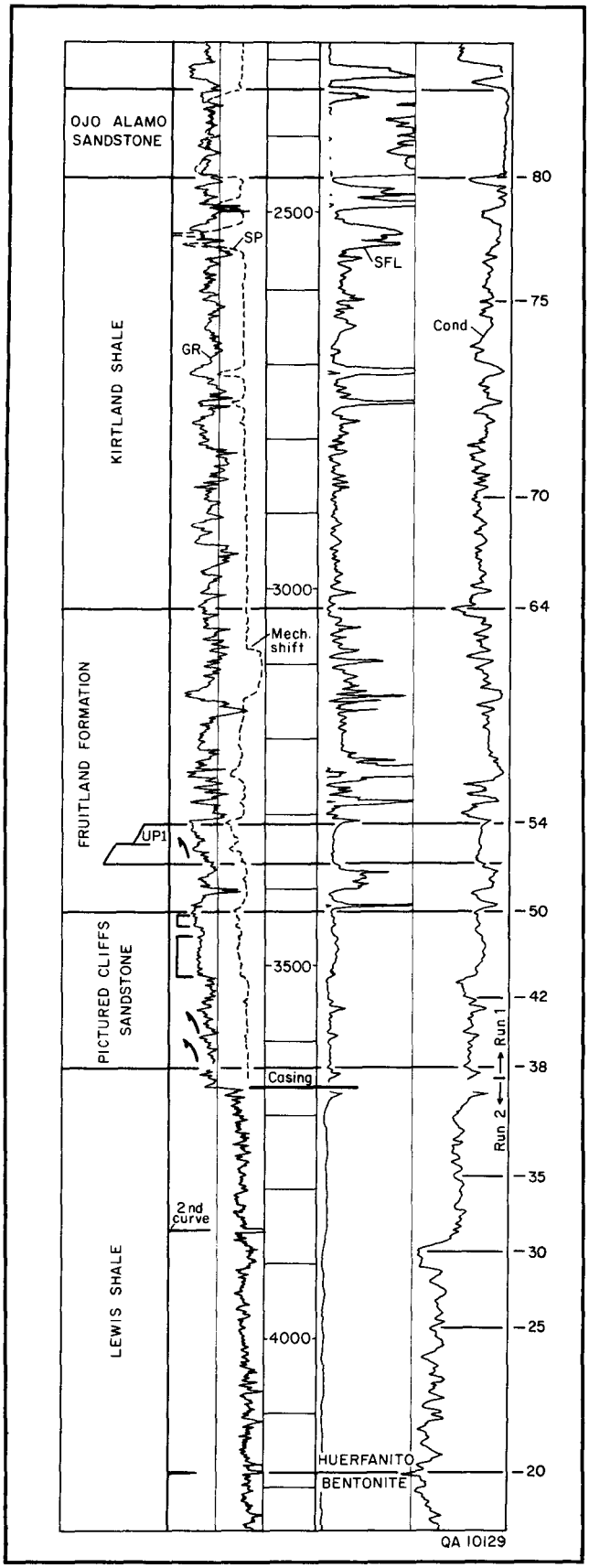

FIGURE 2.1—Type log showing Upper Cretaceous stratigraphy in the San Juan Basin. See Fig. 2.5 for well location and Fig. 2.13 for identification of Fruitland coal seams. Two-digit numbers on the right margin of the conductivity curve refer to marker beds used in this study. From Ayers and Ambrose, 1990.

composed of wave-dominated deltaic or northwest-trending, amalgamated barrier-strandplain sandstones up to 100 ft (30 m) thick.

The Fruitland Formation (Fig. 2.1), the primary coal-bearing formation in the San Juan Basin and the focus of this study, is the continental facies deposited landward of the Pictured Cliffs Sandstone shoreline. It is composed of sandstone, mudstone, and coal interbeds. In past regional subsurface studies, the contact between the Fruitland Formation (Campanian) and the overlying Kirtland Shale (Campanian and Maastrichtian) was placed at the top of the highest coal bed or carbonaceous shale bed; for the most part, the Kirtland lacks coal and carbonaceous shale (Fassett and Hinds, 1971). However, because coal and carbonaceous shale occur locally in the Kirtland, that boundary is erratic. Therefore, in this study the Fruitland—Kirtland contact was placed at a high-conductivity peak that occurs at the top of an upward-fining sequence (Figs. 2.1-2.3). This high-conductivity peak corresponds to the base of a regionally extensive shale (lower Kirtland Shale) that may have formed as a consequence of a short-lived marine transgression over the Fruitland coastal plain. Foraminifera have been reported in this interval (Dilworth, 1960). This marker is at approximately the same stratigraphic position as the boundary chosen by earlier workers (Fassett and Hinds, 1971; Molenaar and Baird, 1989), and it has more genetic significance and less variability than the previously selected boundary.

The Kirtland Shale, which overlies the Fruitland Formation, is composed of the lower shale member, the Farmington sandstone, and the upper shale member (Fig. 2.1). The basal contact of the Paleocene Ojo Alamo Sandstone (Fig. 2.1) is unconformable with the Kirtland Shale and Fruitland Formation (Figs. 2.2 and 2.3); a hiatus of approximately 11 million years (m.y.) is reported at the southern margin of the basin (Fassett, 1985), but this hiatus diminishes in magnitude northwestward. Near the eastern margin of the basin, the fluvial Ojo Alamo Sandstone truncates the Kirtland Shale and Fruitland Formation, and in the southeastern part of the basin, the Kirtland Shale and Fruitland Formation are truncated by a pre-Ojo Alamo unconformity that merges westward with the Ojo Alamo unconformity (Fig. 2.4). This pre-Ojo Alamo unconformity is at the base of an upward-fining unit inferred to be a fluvial sandstone, and the boundary between the fluvial sandstone and underlying strata is an angular unconformity (Fig. 2.4). Although some earlier workers recognized that this sandstone differed in character from adjacent sandstones, they generally assumed that it was a facies variation of either the Fruitland Formation (Fassett and Hinds, 1971, p. 17) or the Ojo Alamo Sandstone (Sikkink, 1987, pp. 89-90). However, a pre-Ojo Alamo unconformity at the southeastern margin of the basin was suggested from an earlier outcrop study on the basis of thickness variations in the Fruitland Formation and Kirtland Shale and lithologic differences in pre-Ojo Alamo and Ojo Alamo sandstones (Baltz, 1967, p. 34).

Previous studies

Fassett and Hinds (1971) described the regional geology and energy resources of the Fruitland Formation in the San Juan Basin. They used measured sections and data from approximately 325 well logs to calculate 200 billion short tons of Fruitland coal in the basin, but they did not report coalbed methane resources. Choate and others (1984) summarized previous studies in which TRW, Inc., working under contracts with the U.S. Department of Energy, estimated 31 Tcf of methane in Fruitland coal seams. This estimate was made by multiplying the coal-tonnage estimate of Fassett and Hinds (1971) by gas-content values for Fruitland

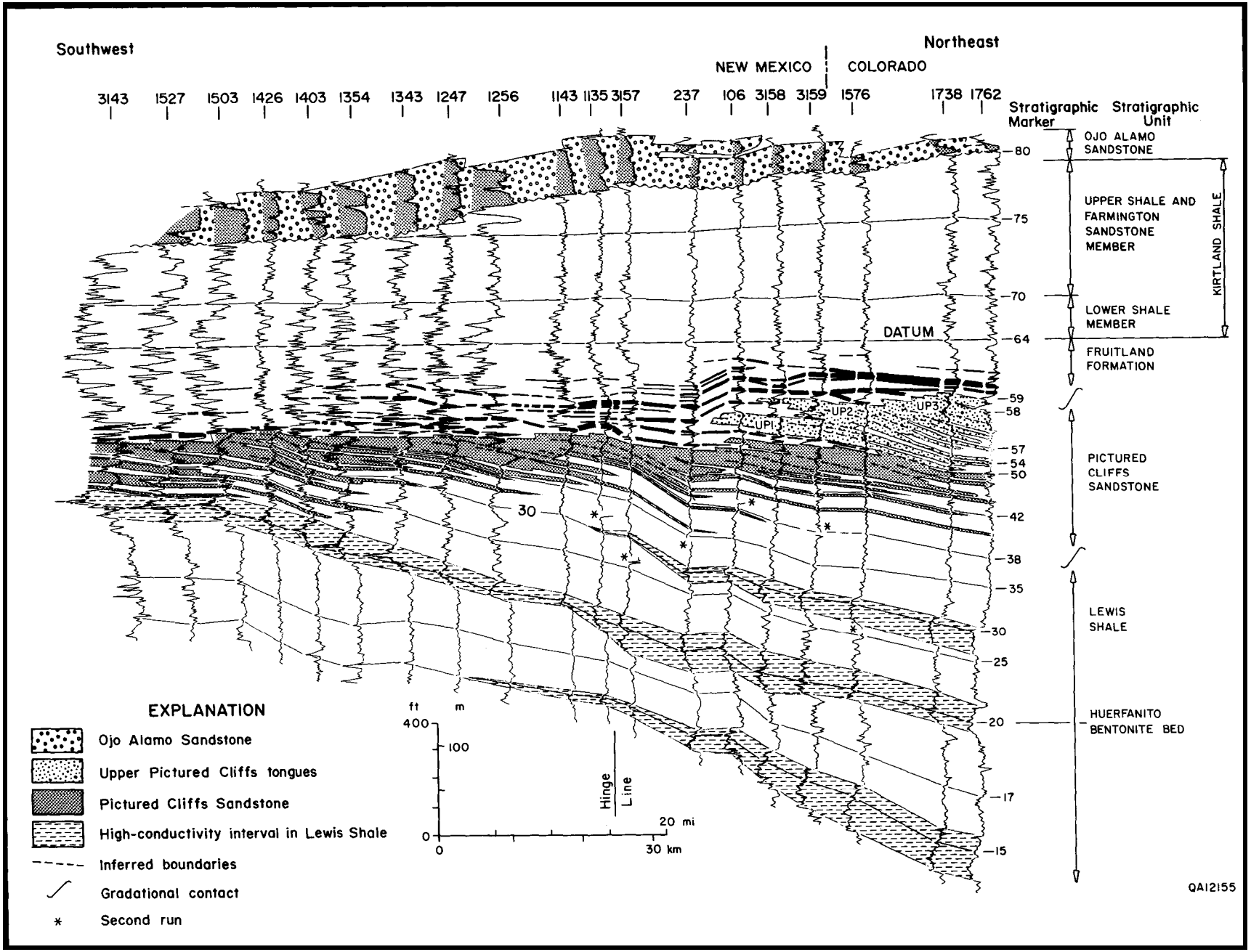

FIGURE 2.2—Stratigraphic dip section D20, located in Fig. 2.8. Traces of conductivity curves are shown for wells in this section; datum is the base of the Kirtland Shale, defined as a high-conductivity zone at the top of an upward-fining sequence in the upper Fruitland Formation. Log 106 ties with strike section S10 (Fig. 2.3). From Ayers and Ambrose, 1990.

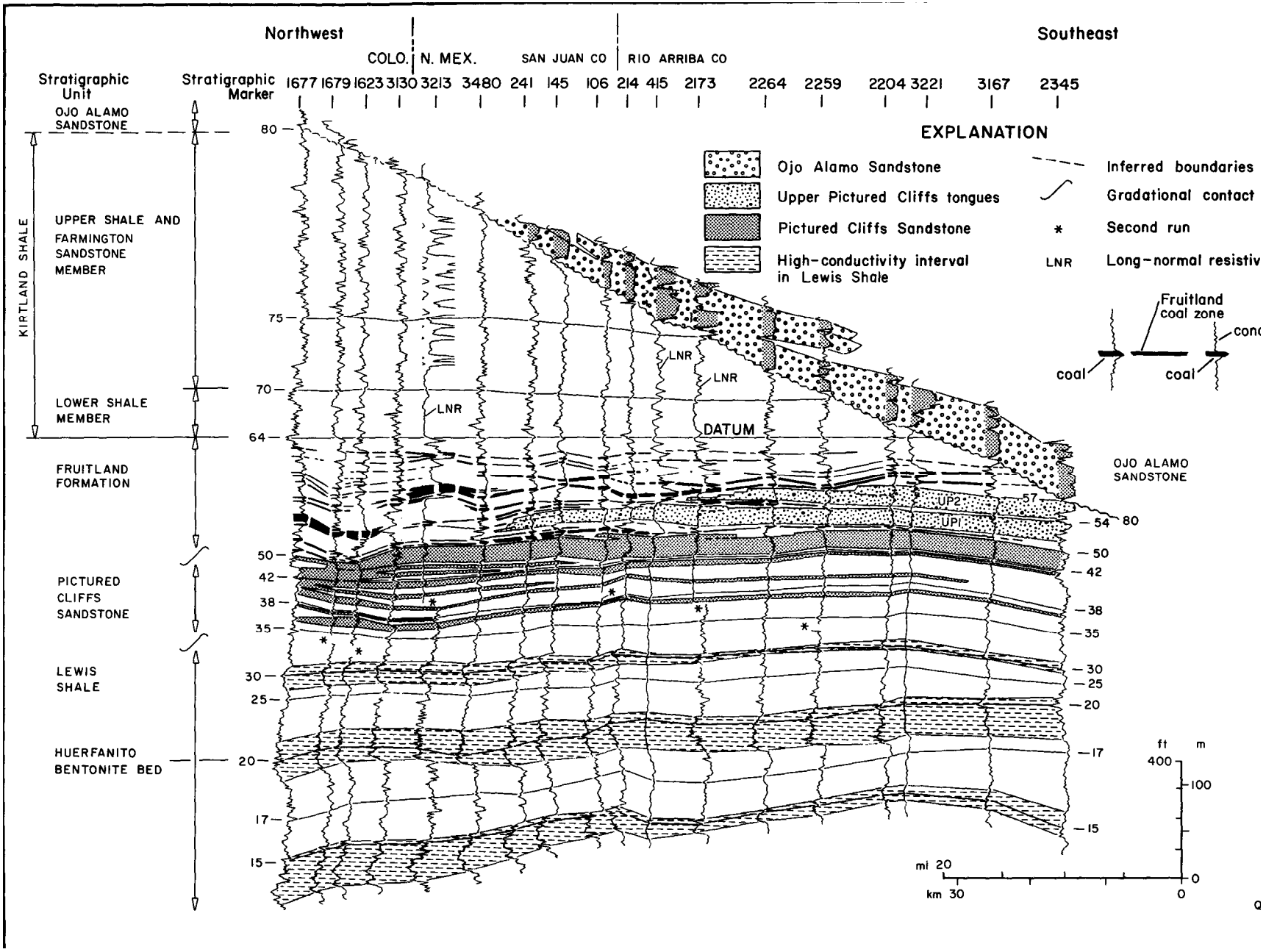

FIGURE 2.3—Stratigraphic strike section S10, located in Fig. 2.8. Log traces not labeled as long-normal resistivity are traces of conductivity logs. Datum is the high-conductivity, low-resistivity marker also used in dip section D20 (Fig. 2.2). Log 106 ties with dip section D20 (Fig. 2.2). From Ayers and Ambrose, 1990.

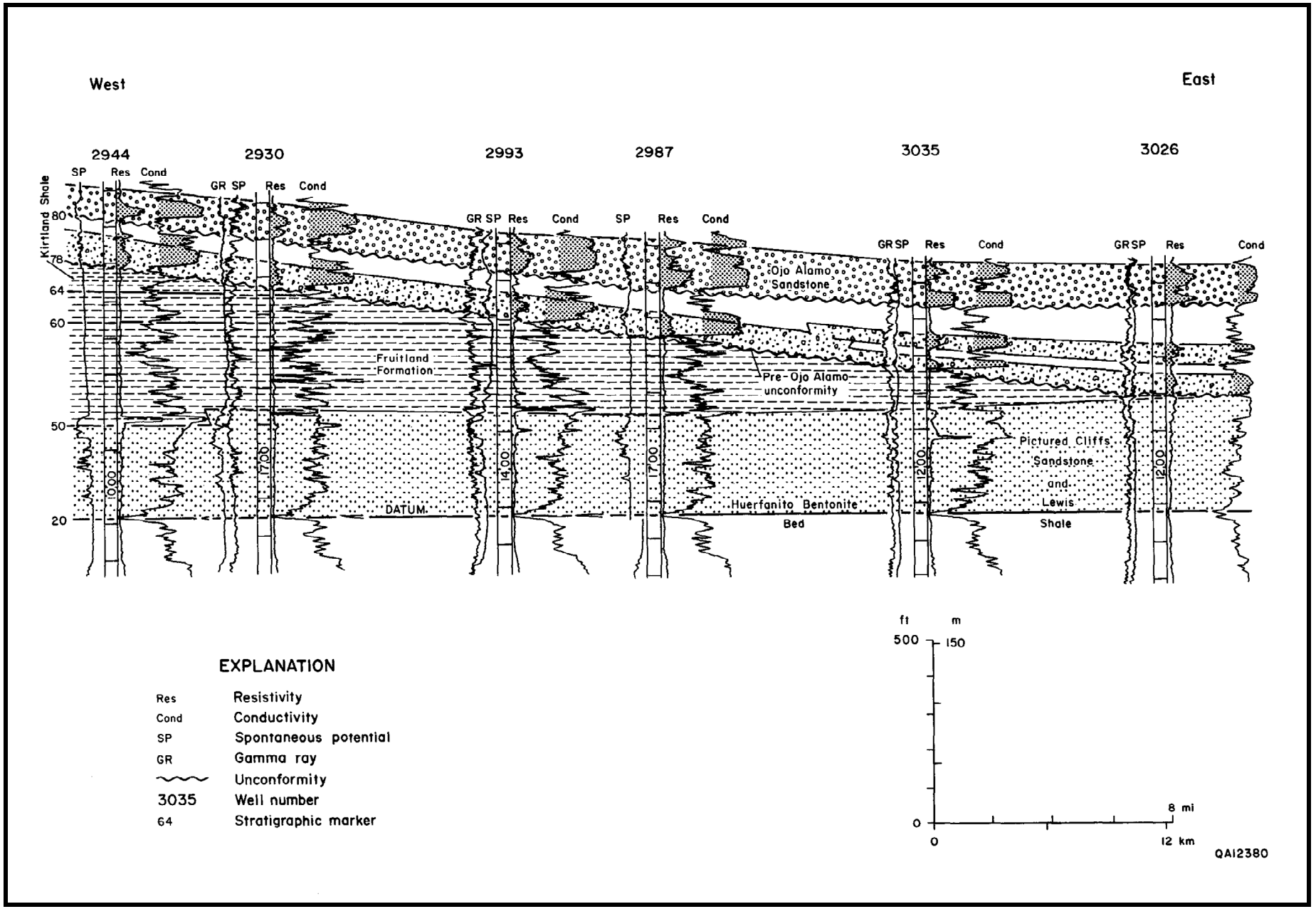

FIGURE 2.4—Stratigraphic strike section in the southeast part of the San Juan Basin, illustrating truncation of the Kirtland Shale, Fruitland Formation, and Pictured Cliffs Sandstone by a pre-Ojo Alamo unconformity. Cross section is located in Fig. 2.11. From Ayers and Ambrose, 1990.

coal seams. The gas-content estimates were based on limited data. Kelso and others (1988) reevaluated coal and coalbed methane resources in the Fruitland Formation. For their estimate, they used coal-thickness data from 549 geophysical well logs to calculate coal volume and desorbed-gas values from 28 coal samples to calculate gas content; Kelso and others (1988) estimated 219 billion short tons of coal and 50 Tcf of coalbed methane in Fruitland coal seams thicker than 2 ft (>0.6 m). Although the previous regional studies defined regional coalbed methane resources of the Fruitland Formation, they did not address geologic and hydrologic controls on the occurrence and producibility of the methane.

In a study of the Navajo Lake area, Ayers and Zellers (1988; this volume, Chapter 4) used closely spaced well control (approximately 400 well logs in a 215-m^2 [557-km^2] area) to show that geologic conditions that affect the occurrence and producibility of coalbed methane are more complex than inferred from regional studies conducted with sparse data. Using a datum above rather than below the coal-bearing Fruitland Formation, as had been done by previous researchers, they showed that basin subsidence indirectly controlled the occurrence of thick coal seams by causing reversals in the direction of shoreline migration and deposition of interfingering upper Pictured Cliffs sandstones. They also concluded that, although lower Fruitland coal seams pinch out behind Pictured Cliffs shoreline sandstones, upper Fruitland seams may override abandoned-shoreline sandstones, thereby forming extensive coalbed methane reservoirs.

Objectives

Goals of this study were to (1) evaluate the structural evolution of the San Juan Basin as it applies to the distribution and maturation of Fruitland coal, (2) define depositional systems, (3) delineate the regional occurrence and continuity of coal seams and evaluate geologic controls on coal occurrence, geometry, and trends, and (4) identify structural features that may enhance coal permeability or affect coalbed continuity. Results from this study of the geologic framework will be integrated with other results from studies of structure, gas composition, and hydrology to interpret controls on coalbed methane occurrence and producibility (Kaiser and Ayers, this volume, Chapter 10).

Methods

In the San Juan Basin, which covers approximately 6,700 m^2 (~17,350 km^2) encompassed by the Fruitland Formation outcrop, more than 17,000 oil and gas wells have been drilled and logged, providing an excellent data base for a subsurface study of Fruitland coalbed methane. In this study we used approximately 2,500 geophysical logs from these wells. Well logs were used to make interlocking cross sections, and stratigraphic units, defined by 18 marker beds in the Upper Cretaceous and lower Tertiary section, were correlated in these cross sections. All remaining logs were correlated to these sections. Structure, isopach, lithofacies, and coal data from the logs were tabulated in computer files; these data were used to make computer-contoured maps, or they were posted by the computer for hand contouring. The cross sections and maps were then evaluated to interpret evolution of the San Juan Basin and geologic controls on the occurrence and producibility of coalbed methane. Geologic interpretation from subsurface data was verified in studies of outcrops and cores.

Structural evolution of the San Juan Basin

Structure affected the availability and producibility of Fruitland coalbed methane in four ways. First, increased subsidence north of an inferred hingeline affected a shoreline stillstand and allowed thick peat to accumulate. Second, the timing of structural development of the San Juan Basin affected the burial depth and, hence, thermal maturity of Fruitland coal seams. Third, structural deformation caused fractures that may enhance coalbed permeability or offset the coal beds and impede flow. Finally, structural folding uplifted and exposed Fruitland strata at the basin margin, thereby greatly affecting the water movement by exposing truncated beds (especially coal beds) for recharge or expulsion of fluids and by providing potential energy for fluid movement.

Structure of Huerfanito Bentonite Bed

The structure map of the Huerfanito Bentonite Bed (Fig. 2.5) was made using data from approximately 2,500 well logs (Fig. 2.6). Structural relief on the Huerfanito Bentonite Bed in the basin exceeds 4,500 ft (>1,370 m). The steeply dipping Hogback monocline is apparent around the northern, northwestern, and eastern margins of the basin. In the southern half of the basin, dip is 1° (92 ft/mi [17m/km]) to the northeast. The structural axis of the basin is complex and is strongly displaced to the northeastern side. The basin floor is the conspicuously flat area below 2,600 ft (790 m) (Fig. 2.5) that trends northwestward and measures about 20 x 30 m^2 (50 x 75 km^2). Dip on the floor is approximately 0.1° (10 ft/mi [2 m/km]). An inferred structural hingeline coincides with the 2,600-ft (790-m) contour at the southwestern margin of the basin floor and projects to crop out at the La Plata mine (Fig. 2.5).

This structural hingeline is interpreted to be a zone of complex, northwest-trending, en echelon normal faults, with net downdrop to the north; width of the zone is 6 to 10 mi (10 to 16 km). Its presence is inferred from the coincidence of geologic anomalies that are apparent in regional maps and cross sections. Among these are (1) change in structural attitude from northeast-dipping beds on the southwest to flat-lying but folded and faulted beds on the northeast (Fig. 2.5); (2) faults identified in well logs in this area (Ambrose and Ayers, this volume, Fig. 3.3); (3) marked thickening of the interval from the Huerfanito Bentonite to the top of the uppermost Pictured Cliffs sandstone (Fig. 2.2); (4) southwestward thinning or pinch-out of high-conductivity units in the Lewis Shale (Fig. 2.2, marker beds 15, 20, and 30); (5) highly organized gravity values that trend northwestward, parallel to the hingeline, and are closely spaced (Scott and others, this volume, Fig. 9.4); (6) closely spaced contours in maps of vitrinite reflectance (Scott and others, this volume, Fig. 9.3), potentiometric surface, and pressure gradient (Kaiser and others, this volume, Figs. 8.1 and 8.8); (7) marked changes in coalbed-gas composition (Scott and others, this volume, Figs. 9.9 and 9.10); (8) increased net coal thickness on the northeast; and (9) permeability contrasts in the Fruitland Formation (Kaiser and others, this volume, Chapter 8) and the Pictured Cliffs Sandstone. Additionally, northwest-trending normal faults, having as much as 70 ft (21 m) of displacement (Roberts and Uptegrove, 1991), are present where the hingeline projects to outcrop along the western margin of the basin, and from studies of reflection seismic data, the U.S. Geological Survey reports northwest-trending faults affecting basement rock in this area (Huffman and Taylor, 1991). The significance of this hingeline to Pictured Cliffs shoreline trends and Fruitland coal and coalbed methane occurrences will be developed further in subsequent discussions.

Coal seams may have fracture-enhanced permeability in major folds like the Hogback monocline and Ignacio anticline (Fig. 2.5). From the northern margin of the basin, a complex structural promontory consisting of several folds extends southward approximately 25 mi (~40 km). The most prominent of these folds is the Ignacio anticline in Colorado

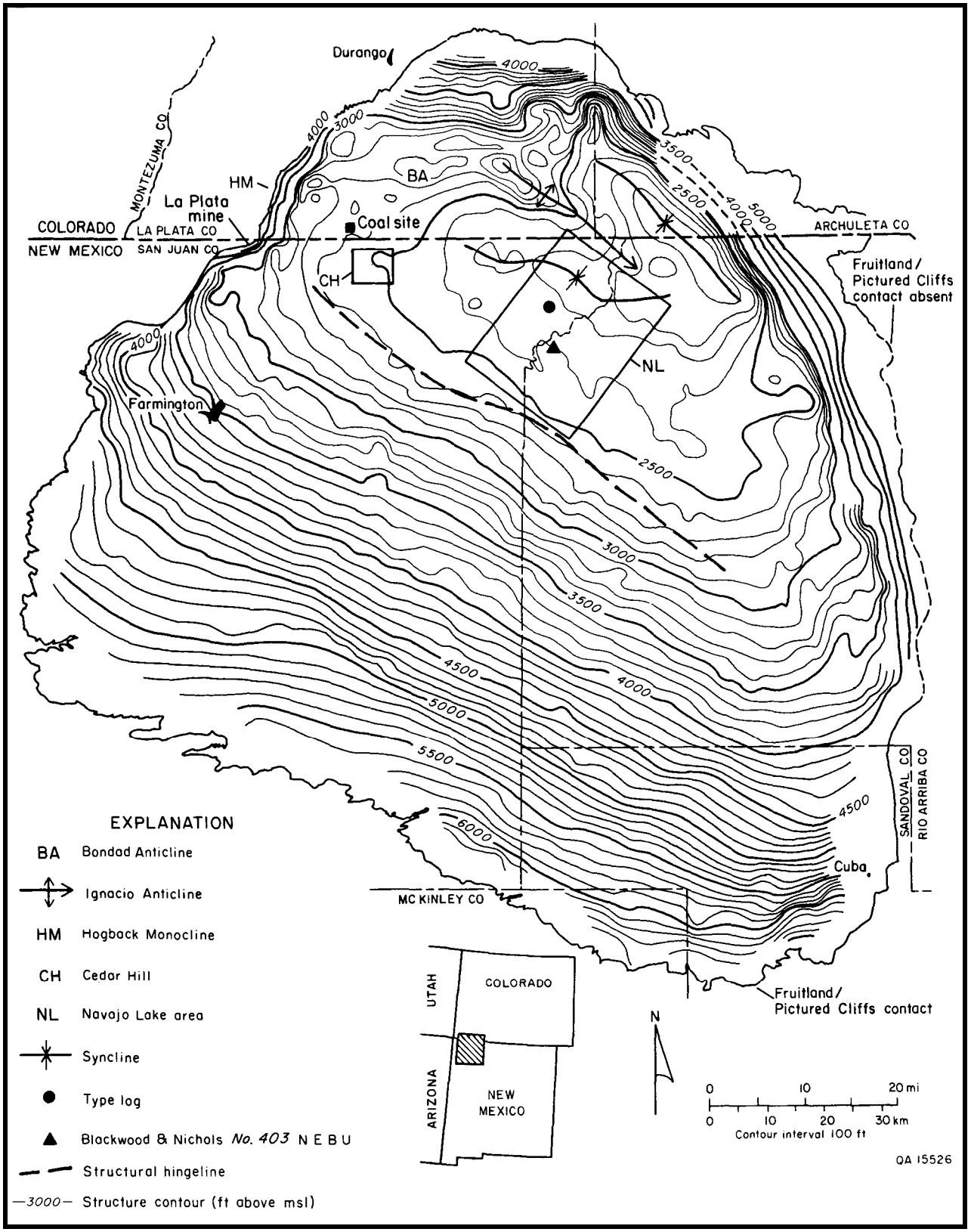

FIGURE 2.5—Structure map of the San Juan Basin, contoured on the Huerfanito Bentonite Bed, and location of type log (Fig. 2.1) and Blackwood and Nichols NEBU No. 403 (Ayers and Zellers, this volume, Fig. 4.5). The basin displays gentle dips on the southern margin and steep dips on the north margin along the Hogback monocline. Modified from Ayers and Ambrose, 1990.

that plunges southeastward. Maximum structural relief on the anticline is approximately 250 ft (~75 km).

Minor folds with structural relief less than 100 ft (<30 m) may also form structural traps and contribute fracture-enhanced permeability to coal seams. These minor folds occur throughout the basin and are especially apparent where the regional dip changes, such as near the Hogback monocline and at the periphery of the basin floor. Northwest-plunging folds occur in the Navajo Lake area (Ayers and Zellers, this volume, Chapter 4), and a tightly folded, east-plunging syncline bisects Cedar Hill field (Fig. 2.5; Ambrose and Ayers, this volume, Fig. 3.4). These minor folds were not apparent in an earlier regional structural map of the Huerfanito Bentonite Bed that was made using a data density of one to two well logs per township and a contour interval of 400 ft (122 m) (Fassett and Hinds, 1971, fig. 15).

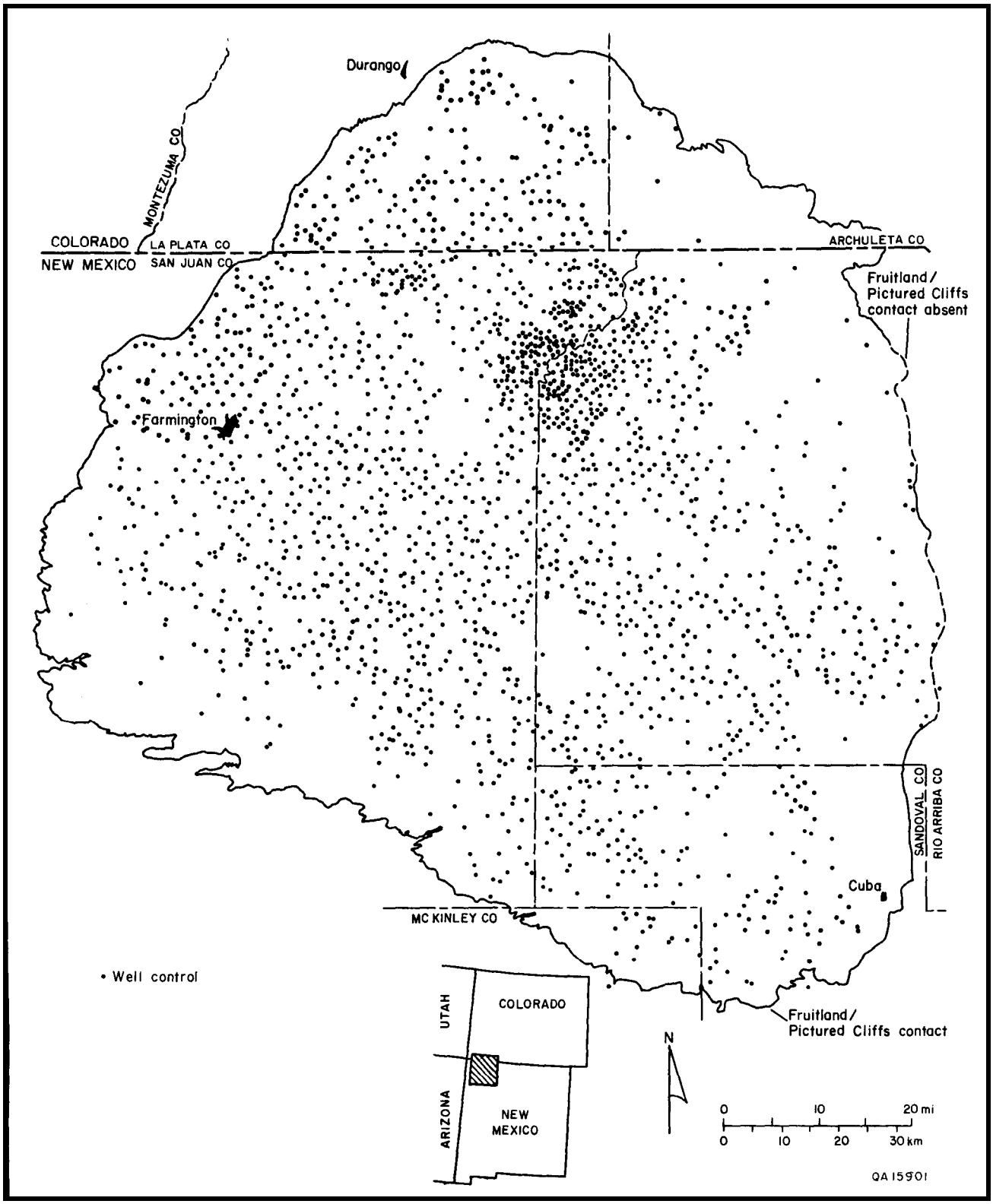

FIGURE 2.6—Locations of wells used in this study.

Elevation of Pictured Cliffs Sandstone

The elevation of the top of the Pictured Cliffs Sandstone (Fig. 2.7) was mapped because it is subjacent to the thick lower Fruitland coal beds in the southern two-thirds of the basin, whereas the Huerfanito Bentonite Bed is as much as 700 ft (215 m) below the Fruitland Formation in that area. This is not a true structure map because the Pictured Cliffs Sandstone is time-transgressive (Fig. 2.2). Relief on top of the Pictured Cliff Sandstone is approximately 3,500 ft (1,065 m), which is considerably less than structural relief on the Huerfanito Bentonite Bed (>4,500 ft [>1,370 m]); this difference is due to northward thickening of the Huerfanito to Pictured Cliffs interval (see "Huerfanito to top of Pictured Cliffs Sandstone"). The map shows, with minor differences, the structural features delineated on the Huerfanito Bentonite man (Fig. 2.51. confirming that formation of the struc-

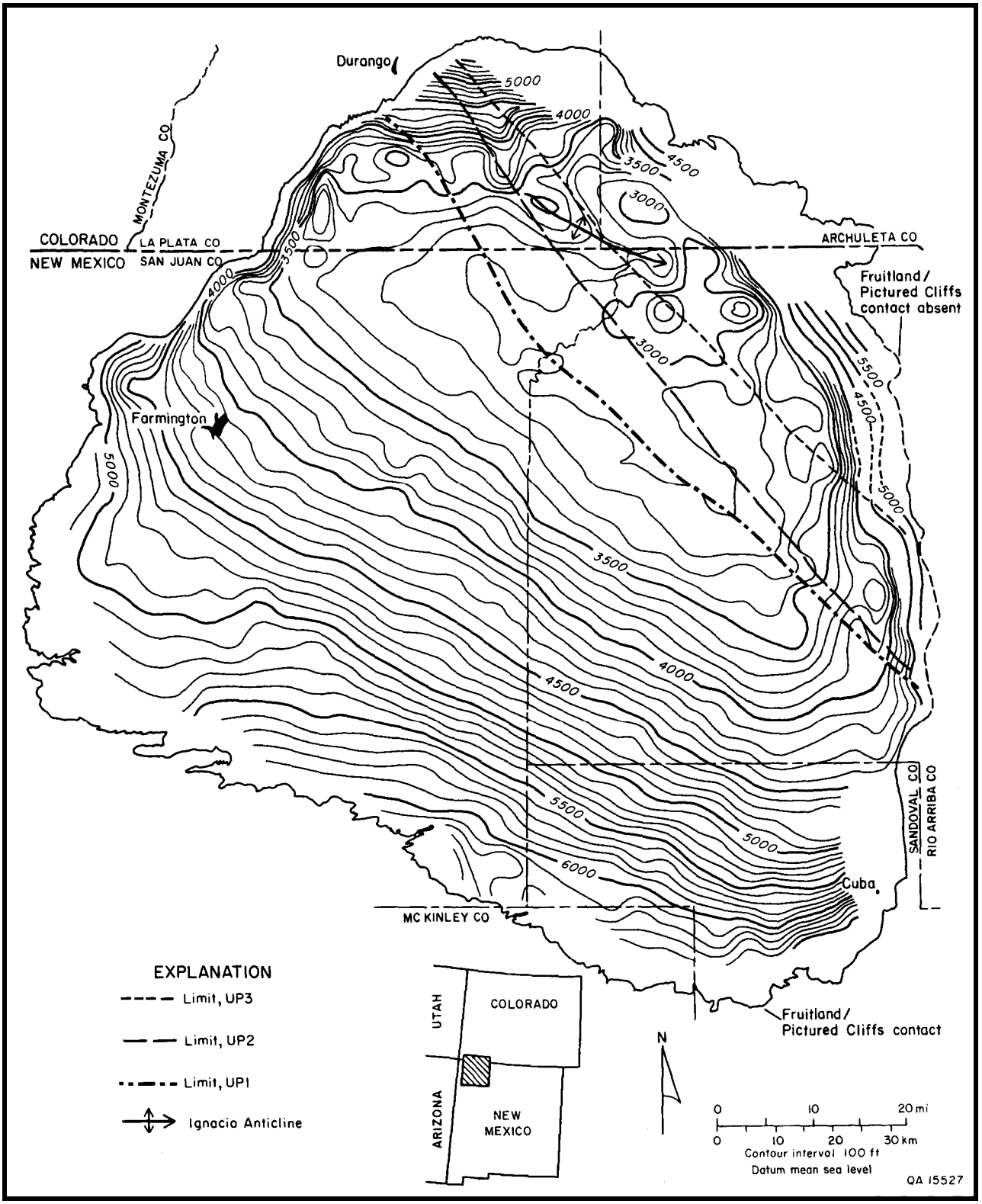

FIGURE 2.7—Elevation of the top of the Pictured Cliffs Sandstone, showing structural features similar to those in the structure map of the Huerfanito Bentonite Bed (Fig. 2.5). Modified from Ayers and Ambrose, 1990.

tural basin mostly postdates deposition of the Pictured Cliffs Sandstone.

Depositional framework of the Pictured Cliffs Sandstone and the Fruitland Formation

The thickness, continuity, and extent of Fruitland coal seams were controlled by their depositional setting, which in turn was controlled by syndepositional tectonic activity. To interpret the tectonic and depositional controls on coal seam occurrence, we made cross sections and isopach and lithofacies maps. Formation-thickness, or isopach, maps are useful in defining the regional paleoslope, basin evolution, and local syndepositional structural features. The intervals mapped in this study are shown in Figs. 2.2 and 2.3. They are identified either by stratigraphic name or by bounding marker beds that were numbered consecutively, beginning with the lowest (oldest) marker bed. These two-digit numbers were used to facilitate computer manipulation of data in this study and are not suggested as official names or as replacements for existing stratigraphic nomenclature. In this study, isopach maps were made of the (1) top of the Huerfanito Bentonite Bed (marker 20) to the top of the Pictured Cliffs Sandstone (marker 50) or to the top of the uppermost Pictured Cliffs tongue (marker 58), where present; (2) Pictured Cliffs Sandstone to the top of the Fruitland Formation (markers 50 to 64); and (3) Huerfanito Bentonite Bed to the base of the Ojo Alamo Sandstone (markers 20 to 80). Other maps in this report are isopach, isopleth, and isolith maps of the upper Pictured Cliffs tongues (markers 50 to 58).

Huerfanito Bentonite Bed to top of upper Pictured Cliffs tongues (markers 20 to 58)

This map (Fig. 2.8) is equivalent to the Huerfanito to Pictured Cliffs Sandstone isopach of Fassett and Hinds (1971, fig. 7); the interval includes lower Fruitland tongues and is bounded by the top of the uppermost Pictured Cliffs tongue. This interval thickens from less than 100 ft (<30 m) on the southwest to more than 1,200 ft (>365 m) on the northeast, consistent with a paleoslope to the north or northeast; bas-inward thickening of the interval (900 ft over 90 mi [275 m over 145 km]) averages 10 ft/mi (2 m/km) in the southern two-thirds of the basin, south of the 750-ft isopach. Throughout the southern part of the basin, isopach trends are oblique to updip (southwest) pinch-out lines of marker beds in Lewis Shale, demonstrating that isopach trends, although useful in evaluating paleoslopes, do not necessarily parallel depositional strike (Ayers and others, 1990). The rate of thickening northeast of the 800-ft isopach is approximately 15 ft/mi (~3 m/km). The 800-ft contour nearly coincides with the UP1 pinch-out line (Fig. 2.8). In the northern part of the basin, isopach trends are discordant (rotated about 30° clockwise) with the Huerfanito-Pictured Cliffs Sandstone isopach trends in the southern part of the basin, suggesting initiation of differential subsidence across the hingeline at the southwest floor of the basin and realignment of the upper Pictured Cliffs shoreline parallel to that hinge. Contours are closely spaced north of the 800-ft contour (for example, the 900- to 1,000-ft contour) where UP2 and UP3 pinch out, particularly in the northwestern part of the basin. The interval thins at minor anticlines in northwestern Rio Arriba County and at Bondad anticline (Fig. 2.5), suggesting that these structures were active during deposition of upper Pictured Cliffs tongues.

Upper Pictured Cliffs tongues (markers 50 to 58)

In the northeastern half of the San Juan Basin, thick lower Fruitland coal seams occur landward (southwestward) of shoreline deposits of the upper Pictured Cliffs tongues. To evaluate controls on Fruitland coal occurrence, we mapped the net thickness of the undivided upper Pictured Cliffs tongues (Fig. 2.9; see Fig. 2.2, markers 50 to 58), the number and net thickness of major sandstones (Figs. 2.10a and 2.10b, respectively), and the maximum sandstone thickness (Fig. 2.10c). Maps of the major sandstones (here defined as those >20 ft [>6 m] thick) and maximum sandstone (thickest individual sandstone) delineate the depositional framework facies that bound thick Fruitland coal beds in the northeastern part of the basin.

Isopach—The isopach map (Fig. 2.9) of the combined upper Pictured Cliffs tongues (markers 50 to 58) and the interbedded Fruitland tongues shows strike-elongate (northwest-trending) contours that parallel the structural grain of the basin. The northwest-trending pinch-out line of UP1 parallels the southern margin of the structural floor (hingeline) and nearly coincides with structural axes of the basin as mapped on the Pictured Cliffs Sandstone (Fig. 2.7), suggesting that transgression was initiated by subsidence of the basin floor and that landward pinch-out of UP1 was against this hingeline. The depocenter is near the northern margin of the basin, where interval thickness locally exceeds 350 ft (>105 m) (Fig. 2.9). Thickness of the composite interval (60 to 350 ft [18 to 105 m]) is less than the sum of the maximum thicknesses of component sandstones (UP1 through UP3) because of a basinward offset (Fig. 2.2, shingled or imbricated relation) of successive depocenters. Rates of thickening are greatest north of the pinch-out lines of individual Pictured Cliffs tongues. For example, the greatest rate of thickening (30 to 60 ft/mi [6 to 12 m/km]) is north of the UP3 pinch-out line.

Lithofacies—The upper Pictured Cliffs sandstone interval is composed of 1 to 3 tongues (UP1, UP2, and UP3) (Figs. 2.2 and 2.10a). The updip (southwestern) limits of these tongues are defined by contours in the major-sandstone isopleth map (Fig. 2.10a, contours 1, 2, and 3), and they coincide with the 20-ft, 60-ft, and 140-ft contours, respectively, on the net-major-sandstone map (Fig. 2.10b). Sand-body geometries of upper Pictured Cliffs tongues (Figs. 2.10b and 2.10c) are consistent with deposition in a wave-dominated shoreline setting. Both dip-elongate and strike-elongate (northeast- and northwest-trending, respectively) sandstone bodies occur northwest of the Rio Arriba County Line, where a wave-dominated delta system (Cedar Hill delta system) is inferred to have caused the Pictured Cliffs shoreline to prograde to the northeast (Figs. 2.10b and 2.10c). Dip-elongate sandstone bodies (distributaries) in the upper Pictured Cliffs tongues northwest of Rio Arriba County project landward (southwestward) to tie with fluvial/distributary channel-fill sandstones in the Fruitland Formation in the Cedar Hill area (Ambrose and Ayers, this volume, Chapter 3). In Rio Arriba County, dominance of strike-elongate sand-body trends in the upper Pictured Cliffs tongues suggests a strandplain-barrier system (Fig. 2.10c, Navajo strandplain-barrier complex) whose sediments were derived primarily from the Cedar Hill deltaic complex by long-shore drift. Southeastward convergence of the UP2 and UP1 pinch-out lines (Fig. 2.10a) and lower values of net major sandstone thickness (Fig. 2.10b) near the eastern margin of the basin suggest lower rates of sediment input in this area. Subordinate dip-elongate sand-body trends in Rio Arriba County suggest sediment input from minor Fruitland fluvial systems.

Fruitland Formation isopach (markers 50 to 64)

The interval from the top of the Pictured Cliffs Sandstone to the top of the Fruitland Formation (markers 50 to 64) includes the coal-bearing Fruitland Formation and, in the northeastern part of the basin, the upper Pictured Cliffs tongues (Fig. 2.2). From a rather uniform thickness of 300

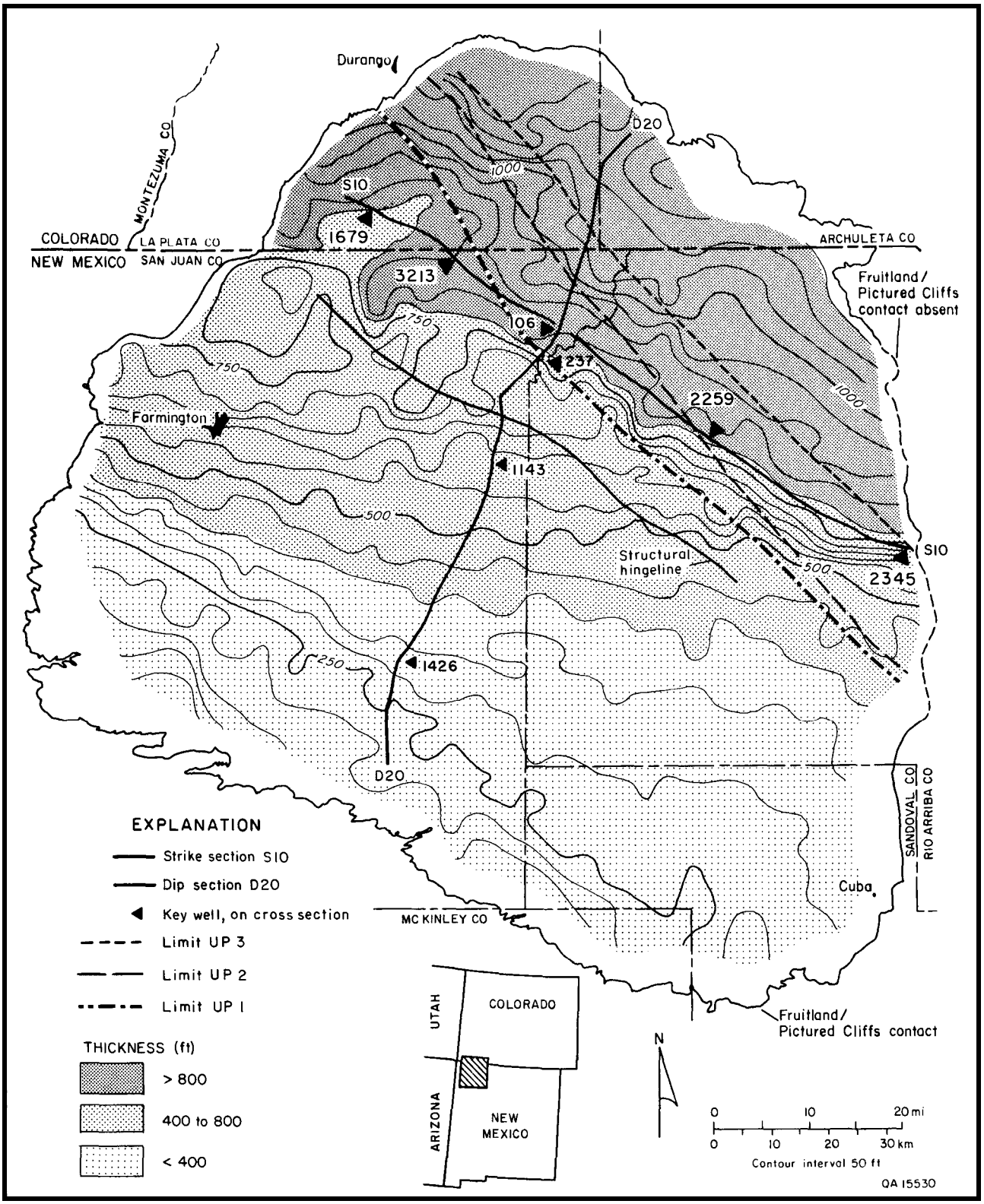

FIGURE 2.8—Isopach map of the Huerfanito Bentonite Bed (marker 20) to the uppermost upper Pictured Cliffs Sandstone (markers 50 to 58). Closely spaced contours show abrupt thinning across the updip (southwest) limit of UP1, UP2, and UP3. Cross sections D20 and S10 are shown in Figs. 2.2 and 2.3, respectively. From Ayers and Ambrose, 1990.

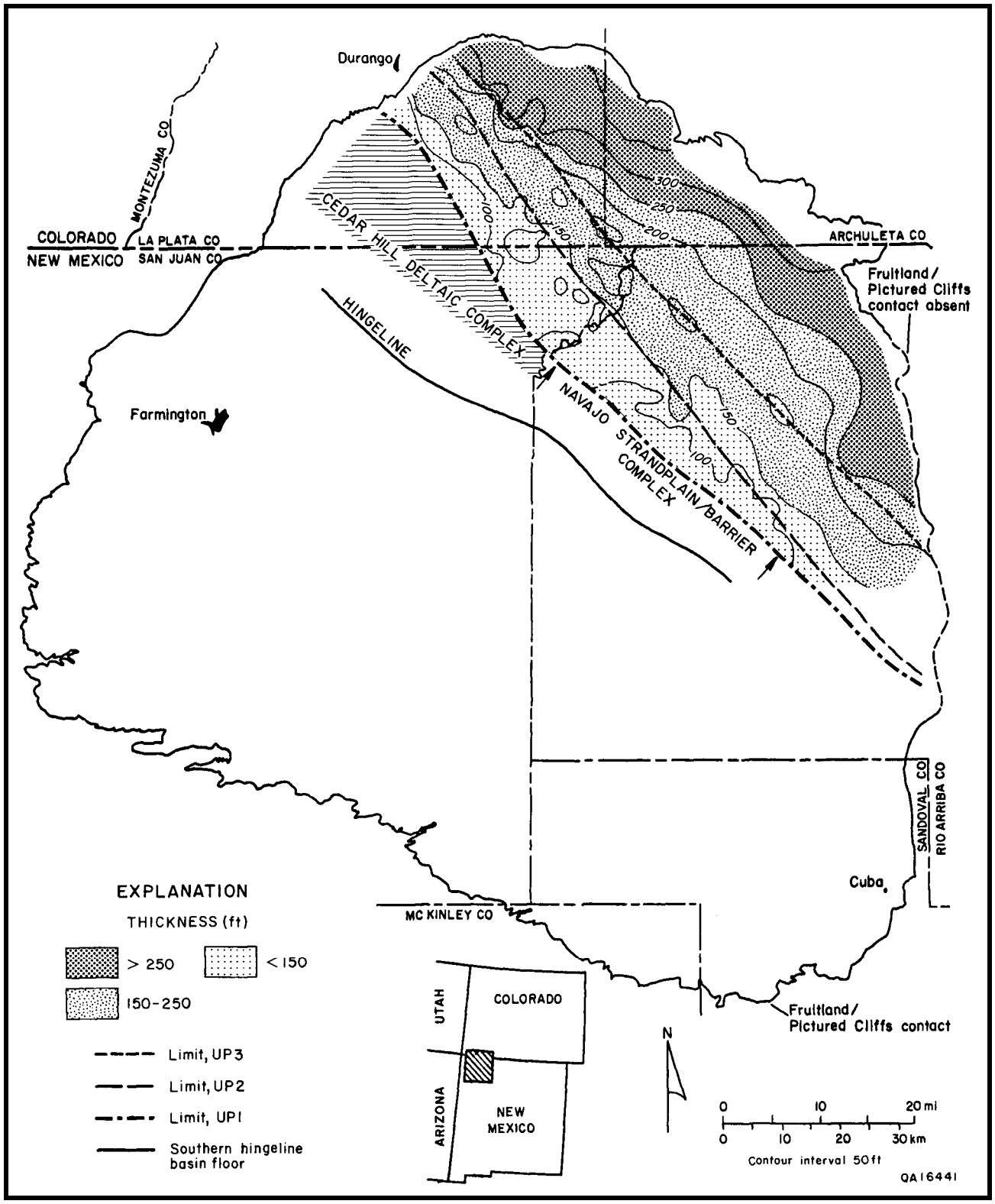

FIGURE 2.9—Isopach map of the top of the Pictured Cliffs Sandstone to the top of UP3 illustrating combined thickness of UPI, UP2, and UP3. From Ayers and Ambrose, 1990.

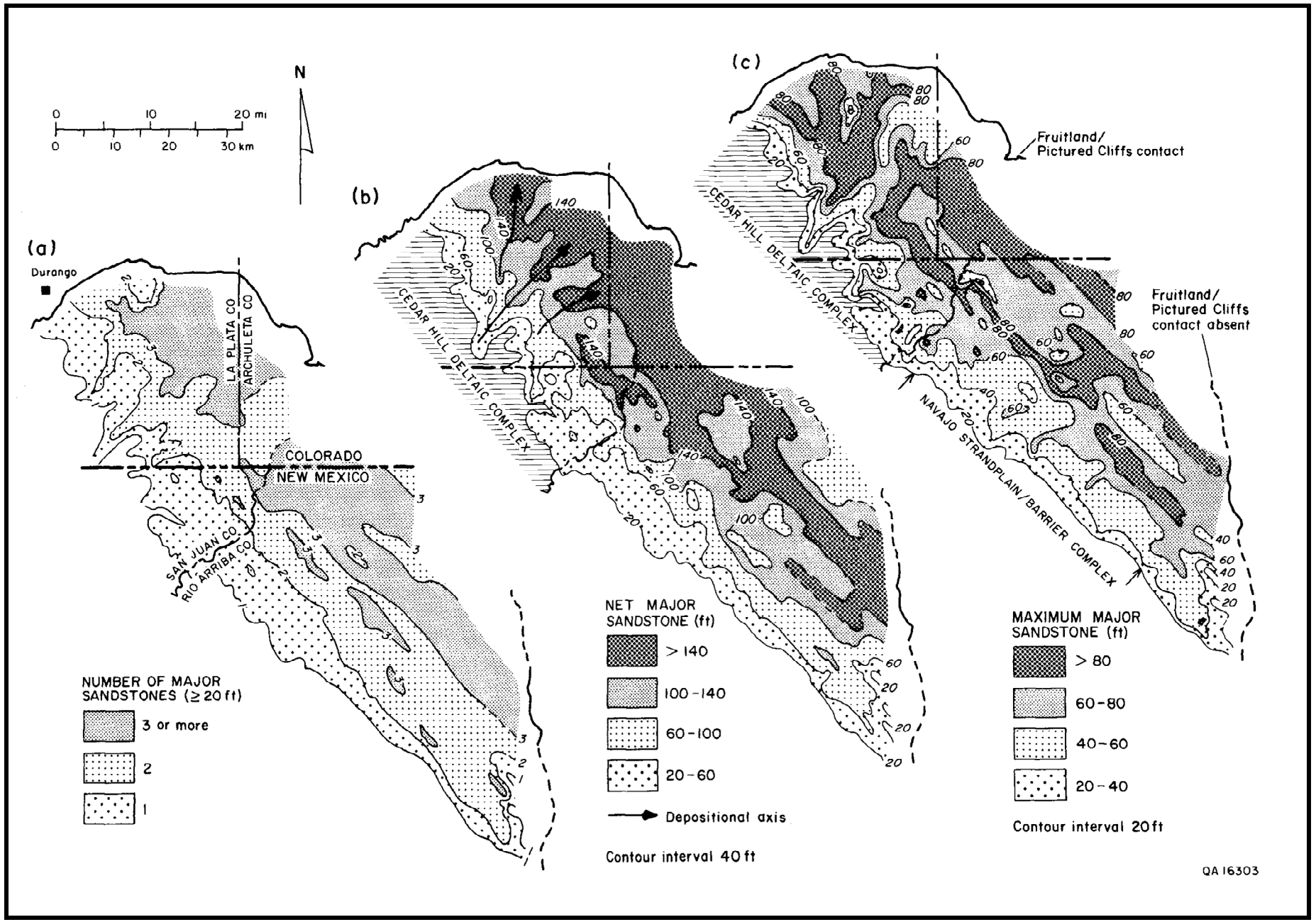

FIGURE 2.10—Maps of upper Pictured Cliffs Sandstone showing (a) the number of major (<40 ft [<12]m thick) sandstones in the upper Pictured Cliff tongues (markers 50 to 58), (b) the net thickness of major sandstones in the upper Pictured Cliffs tongues (markers 50 to 58), and (c) the thickest upper Pictured Cliff sandstone in each borehole.

to 350 ft (90 to 110 m) in the southern half of the basin, this interval thickens to more than 650 ft (200 m) in the northern half of the basin (Fig. 2.11). Marked eastward thinning and truncation of the Fruitland Formation near the eastern margin of the basin resulted from erosional beveling (Figs. 2.3 and 2.4). Local thickening in the northwestern San Juan Basin near the Colorado—New Mexico State Line may reflect the Fruitland depocenter that was described by earlier workers (Silver, 1951; 1957). If so, then southeastward thinning of the Huerfanito—Ojo Alamo interval may not be due entirely to postdepositional erosion of the Kirtland Shale, as concluded by Fassett and Hinds (1971), and uplift of the southeast rim of the basin may have started during Pictured Cliffs—Fruitland deposition.

Eastward and southeastward thinning of the Kirtland Shale in the southern and southeastern parts of the basin was also partly attributed to deposition rather than exclusively to the effects of erosion (Dane, 1936, pp. 120-121). During deposition of the Fruitland Formation and Kirtland Shale, local uplift occurred at the southeastern margin of the basin (Baltz, 1967, p. 34). Therefore, lower subsidence rates and reduced basin accommodation (thus, more oxidizing conditions) may have existed along the eastern margin even before Kirtland time and may partly explain the absence of thick coal seams in the eastern part of the basin.

Huerfanito Bentonite Bed to base of Ojo Alamo Sandstone (markers 20 to 80)

Northeast-trending contours on the isopach map of this interval (Fig. 2.12) are the result of truncation of Upper Cretaceous strata by the southeastward-dipping unconformity at the base of the Ojo Alamo Sandstone. This interval is not mapped in the northwestern part of the basin where the Ojo Alamo Sandstone is unrecognized, because of either facies change or erosional truncation of the Ojo Alamo. Fassett (1985) suggested that the pre-Ojo Alamo strata were eroded by a northwestward-flowing fluvial system that pre-dated the southward-flowing Ojo Alamo fluvial system that was deposited above the unconformity. The second-order, northwest-trending bands of isopach thinning were present in an earlier map and were inferred to be paleovalleys (Fassett and Hinds, 1971; Fassett, 1985). However, we have identified and mapped an unconformable surface 50 to 200 ft (15 to 61 m) below and discordant with the Ojo Alamo unconformity in the southeastern part of the basin (Fig. 2.4).

Because of erosional truncation, Upper Cretaceous strata thin southeastward from more than 2,200 ft (>670 m) thick in the northwest to less than 500 ft (<150 m) thick in the southeastern part of the basin (Figs. 2.3 and 2.12). Closer spacing of contours in the northwestern part of the basin indicates that the surface of the unconformity is steeper there, suggesting that there was relatively little tilting in the southeastern part, which was uplifted as a platform and was bounded to the northwest by a poorly defined, northeast-trending hingeline. Rate of thinning in the platform area is 35 ft/mi (6.6 m/km) northwest and 15 ft/mi (3 m/km) southeast of the 1,000-ft contour.

Fruitland coal

Fruitland coal rank is subbituminous B to high volatile A bituminous around much of the southern and western margins of the San Juan Basin; rank increases into the basin to low volatile bituminous in T34N R8W (Scott and others, this volume, Fig. 9.3). However, the area of highest coal rank does not coincide with present depth of burial or basin structure (Kaiser and Swartz, 1988). Ash content ranges from 10 to 30% and commonly is greater than 20%; sulfur averages less than 1%, and moisture averages 10% in New Mexico and approximately 2% in Colorado (Keystone, 1986; Fassett, 1987).

Coal identification

On geophysical well logs, coal is identified by low density, high neutron and density porosities, low sonic velocity, and/or low neutron count (Fig. 2.13). Low natural gamma response can be used to reliably identify coal seams in some basins. However, gamma response in Fruitland coal seams is variable, probably because of high and variable ash content of the coal. In Fig. 2.13, the thick coal at 3,225 to 3,255 ft is split by a parting at 3,240 ft. Coal above the parting is more radioactive (higher gamma count) than coal below the parting; response in the upper coal is similar to that in the overlying sandstone (3,180 to 3,215 ft). The upper coal has a higher bulk density than coal below the parting, implying greater ash content in the upper coal. The gamma-ray curve is useful for correlation locally; high gamma counts (peaks) in coal seams and associated Fruitland deposits (Fig. 2.13) can be correlated for several miles. These natural gamma peaks are attributed to thin clastic beds that are interpreted as volcanic ash layers (tonsteins) in the coal or attributed to organically bound radioactive elements in adjacent sediments. Volcanic ash beds are described in Fruitland coal seams from the southern margin of the basin (Fassett and Hinds, 1971), and bentonite beds are common in the Lewis Shale. The abundant tonstein layers most likely contribute to the high-ash content of Fruitland coal seams. Formation resistivity is of limited use for coal identification in the northern San Juan Basin. However, it can be used to reliably identify coal in the southern part because there are no other highly resistive beds in the Fruitland Formation in this area (Fassett and Hinds, 1971).

On geophysical logs, the thickness of a bed is commonly measured halfway between the shale baseline and the peak corresponding to that bed. On the bulk density log (Fig. 2.13), coal-seam thickness was measured at a density of approximately 1.80 g/cm^3, which is a slightly conservative measurement. We recorded the thickness of coal seams thicker than 2 ft (>0.6 m); partings thinner than 2 ft (<0.6 m) in thick coal seams were included as coal because of the limits of resolution of the geophysical logs. High-ash coal is also a source and reservoir rock for coalbed methane, and inclusion of minor thicknesses of high-ash coal does not conflict with our goals of delineating the distribution and depositional setting of the coal seams. A 3-ft (0.9-m) parting cutoff in thick coal seams was used by Fassett and Hinds (1971) in mapping the thickest individual (maximum) coal in the Fruitland Formation. However, Fassett and Hinds (1971) excluded partings thicker than 1 ft (0.3 m) when mapping total coal thickness. Kelso and others (1987, 1988) did not state the maximum thickness of partings included in coal-seam measurements for their resource calculations.

Coal stratigraphy

In the southern San Juan Basin, thick coal seams occur in the lower half (150 to 200 ft [45 to 60 m]) of the Fruitland Formation (Fig. 2.2). In the central part of the basin, some of these thick lower Fruitland coal beds pinch out against the Pictured Cliffs Sandstone, and the thickest coal seams in the northern part of the basin are stratigraphically equivalent to the thin upper Fruitland coal seams in the south. The lower Fruitland Formation and coal seams of the southern part of the basin are absent in the north because of pinching out between Pictured Cliffs tongues UP1, UP2, and UP3 (Fig. 2.2). Thick coal seams in the north either pinch out against or override upper Pictured Cliffs tongues. However, because they are immediately above UP1, UP2, or UP3, these coal seams are commonly referred to as lower

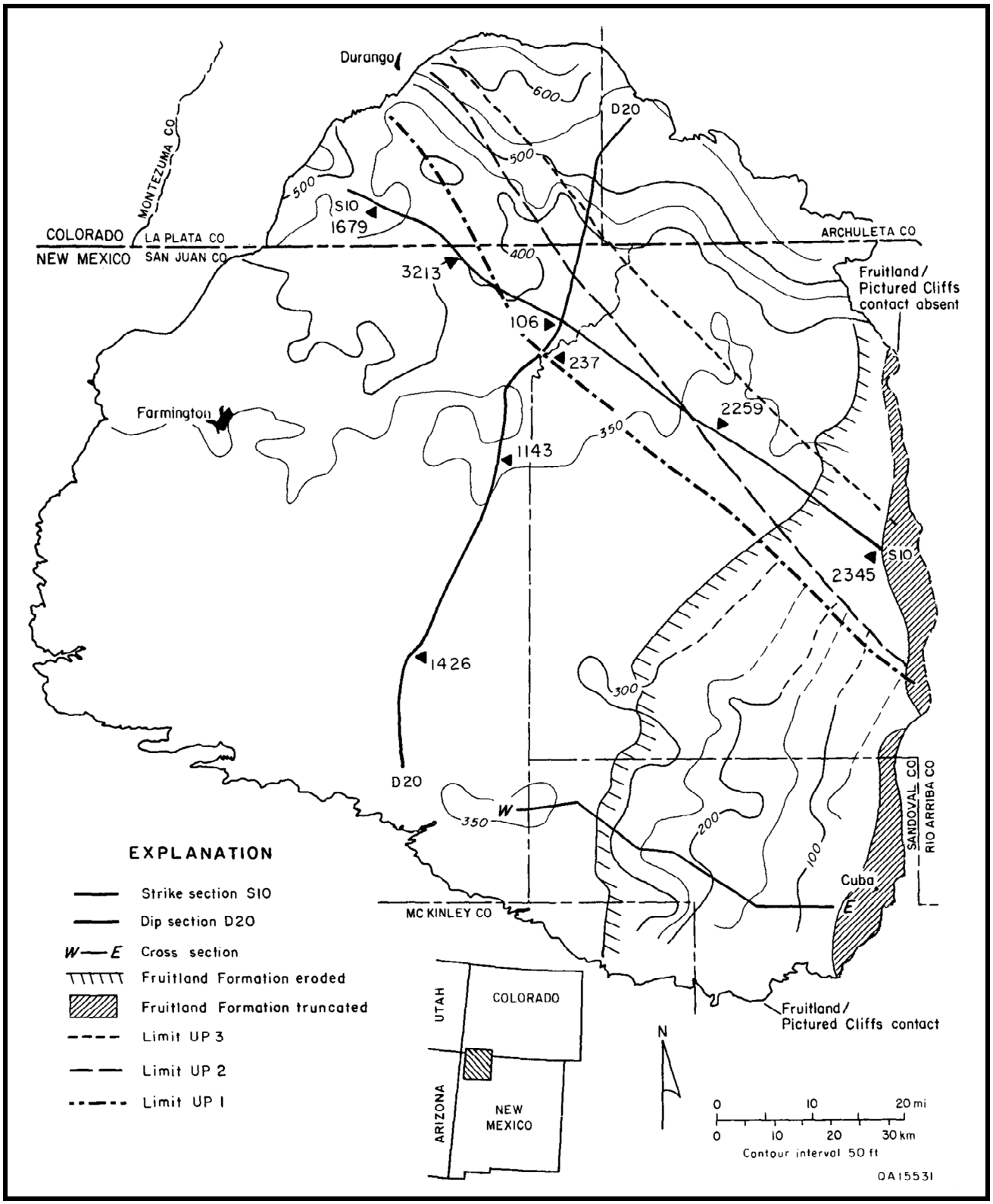

FIGURE 2.11—Isopach map of the Fruitland Formation including upper Pictured Cliffs tongues UP1, UP2, and UP3. Cross sections D20, S10, and E-W are shown in Figs. 2.2, 2.3, and 2.4, respectively. From Ayers and Ambrose, 1990.

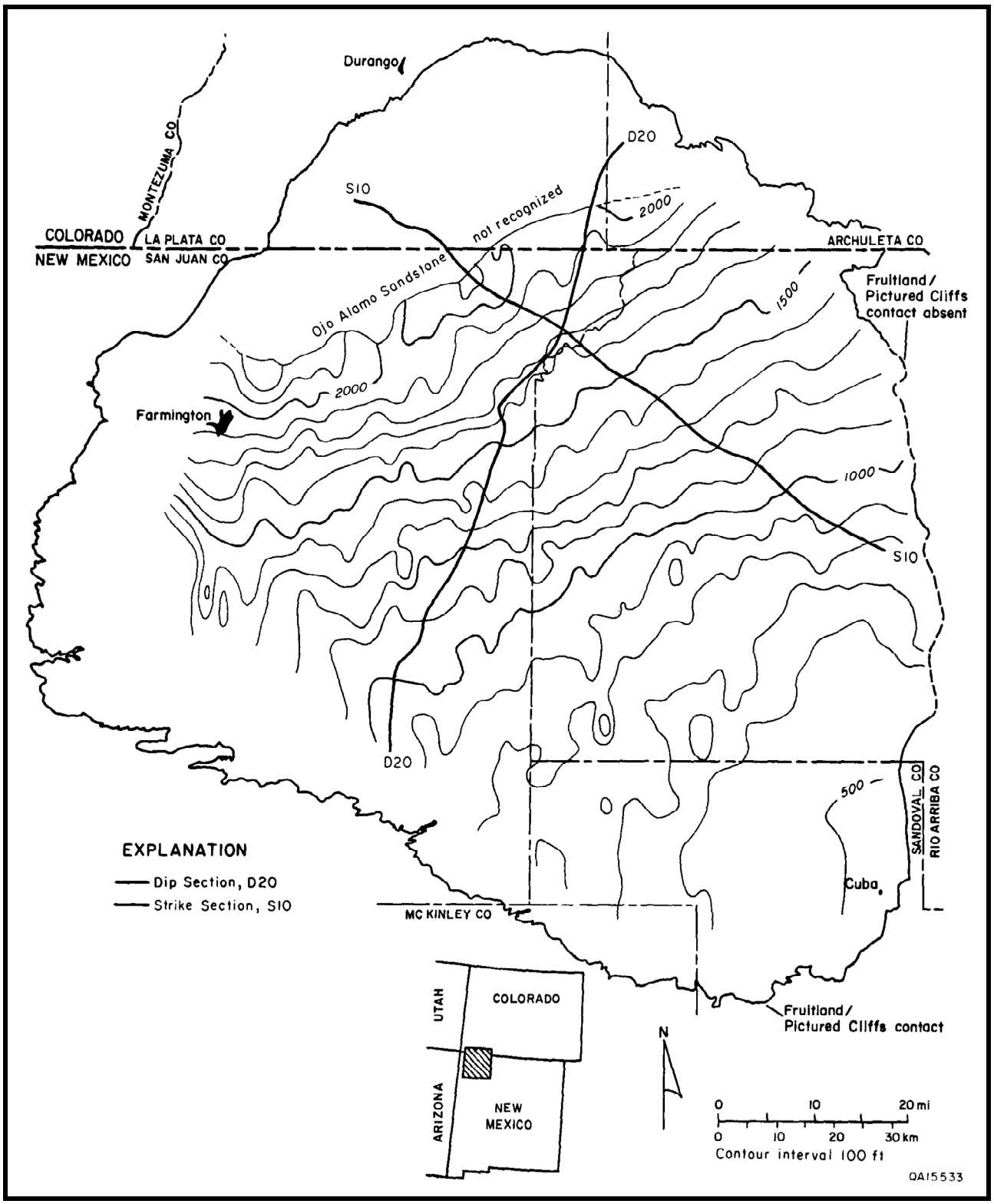

FIGURE 2.12—Isopach map of the Huerfanito Bentonite Bed to base of the Ojo Alamo Sandstone. East–northeast orientation of contours results from combination of eastward-dipping erosional surface of the Ojo Alamo unconformity and basinward thickening of the Pictured Cliffs Sandstone. Cross sections D20 and S10 are shown in Figs. 2.2 and 2.3, respectively. From Ayers and Ambrose, 1990.

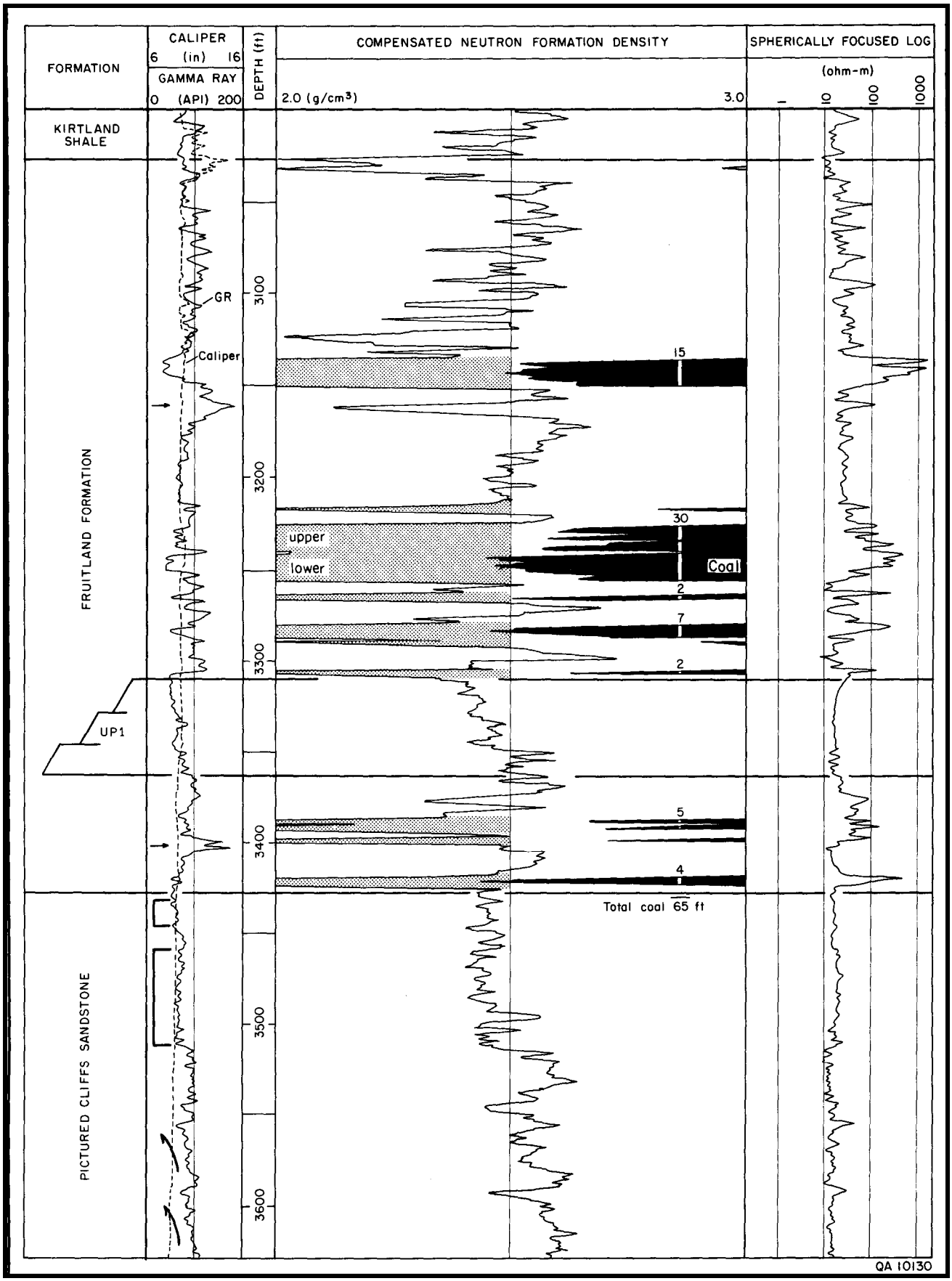

FIGURE 2.13—Identification and measurement of Fruitland coal in type log in Fig. 2.1. High natural gamma-ray responses, indicated by arrows, are attributed to volcanic ash beds and to organically bound radioactive elements in coal seams. From Ayers and Ambrose, 1990.

Fruitland seams, even though they are stratigraphically higher than thick coal seams in the south. As pointed out by Fassett (1987), the terms "upper and lower" Fruitland have little validity in regional discussions because the Pictured Cliffs-Fruitland boundary is time-transgressive.

Coal overburden

The depth to Pictured Cliffs Sandstone or the uppermost Pictured Cliffs tongue, where present (Fig. 2.14, overburden map), indicates approximate thickness of the overburden for sealing Fruitland coal seams and the drilling depth required to evaluate all Fruitland coal seams. Depth to the top of the Pictured Cliffs reflects present topographic relief, basin structure, and stratigraphic rise of Pictured Cliffs tongues. Overburden is thickest in the eastern part of the basin, in a north-northwest-trending area, where Fruitland coal seams are as deep as 4,200 ft (1,280 m). However, overburden thickness (present burial depth) does not relate to greatest coal rank (Kelso and others, 1988; Scott and others, this volume, Fig. 9.3). Southeastward thinning of the Huerfanito Bentonite Bed-Ojo Alamo Sandstone interval (Fig. 2.12) suggests lesser burial depths in the eastern part of the basin. Thus, Fruitland coal seams there are inferred to be lower rank. Coal seams are absent near the eastern margin of the basin because the Fruitland Formation is truncated (Fig. 2.3).

Coal distribution

To evaluate the occurrence of coal and coalbed methane, we mapped net, maximum, and average coal thickness as well as the number of coal seams in the Fruitland Formation. These maps were compared to identify trends of persistent coal occurrence. These trends are summarized in Fig. 2.15. Thick Fruitland coal seams occur in several major northwest-trending, strike-parallel belts (belts A-G) and in minor northeast-trending, dip-elongate belts (belts 1-3). Fruitland coal and coalbed methane are concentrated northeast of the hingeline (see "Geologic controls on coal occurrence").

Net coal thickness—The greatest Fruitland net coal thickness occurs in a northwest-trending belt in the northeastern half of the basin where net coal thickness exceeds 50 ft (>15 m) and is locally as much as 110 ft (33 m) (Fig. 2.16); this complex belt, which encompasses belts E and F in Fig. 2.15, is about 50 mi (80 km) wide in the northwest and narrows southeastward, terminating about 12 mi (19 km) from the eastern margin of the basin. Narrowing of this belt is due to erosional beveling of the Fruitland Formation and truncation of coal seams by the post-Cretaceous unconformity (Figs. 2.3 and 2.16).

The major northwest-trending region of thick coal was described in earlier regional maps (Fassett and Hinds, 1971; Kelso and others, 1987). However, these earlier studies used less data and showed fewer secondary coal trends. For example, these studies did not show the presence of numerous dip-elongate belts of coal, 1 to 8 mi (1.6 to 13 km) wide and 30 to 70 ft thick (9 to 21 m), that extend southwestward from the main northwest-trending belt of 50 to 100 ft (15 to 30 m) of net coal to the Fruitland outcrop at the southwestern margin of the basin (Fig. 2.16).

Maximum coal thickness—The maximum coal map (Fig. 2.17) was made by contouring the thickest Fruitland coal seam recorded in each well, regardless of its stratigraphic position. Therefore, it does not record an individual seam across the basin. However, individual thick seams are mapped locally, where a persistent thick seam occurs.

Maximum Fruitland coal-seam thickness is as much as 40 ft (12 m). Coal seams thicker than 20 ft (>6 m) occur primarily in northwest-trending belts (Fig. 2.17) that coincide with trends of greatest net coal thickness (Fig. 2.16). In these strike-elongate belts, the thickest individual coal seams are more than 30 ft (>9 m) thick, have podlike geometries, and are 2 to 8 mi (3.2 to 13 km) across. Northwest-trending belts of coal containing individual seams more than 30 ft (>9 m) thick (Fig. 2.15, belts E and F) occur in the northern third of the basin (Fig. 2.17). A second northwest-trending belt of thick coal (Fig. 2.15, belt G) occurs near the northeastern margin of the basin (Fig. 2.17). Less prominent, northwest-trending belts of thick coal (Fig. 2.15, belts A and B) occur at the southwestern margin of the basin (Fig. 2.17). Northeast-trending, dip-elongate belts, in which the maximum coal thickness is greater than 10 ft (>3 m) (Fig. 2.15, belts 1, 2, and 3), intersect the northwest-trending coal belts (Fig. 2.17). An earlier regional maximum coal map (Fassett and Hinds, 1971, fig. 22), which was made with fewer data, shows the major northwest-trending belts of maximum coal but little evidence of the secondary northeast-trending coal deposits.

Number of coal seams—Fruitland coal occurs in as many as 16 seams in the San Juan Basin (Fig. 2.18); these coal seams are most abundant in a 40-mi-wide (64-km), northwest-trending belt of six or more coal seams that bisects the basin; seams are most numerous in the northwestern half of this trend. Areas with the greatest numbers of coal seams (more than nine) coincide with areas of greatest net coal thickness (>70 ft [>21 m], Fig. 2.16) and with the thickest individual seams (>30 ft [>9 m] thick, Fig. 2.17).

Average coal thickness—The map of average coal thickness (Fig. 2.19) clearly delineates coal occurrences and geometries. In the northern half of the San Juan Basin, three distinct belts of northwest-trending, thick coal (Fig. 2.15, belts E, F, and G) are defined by areas where average coal thickness exceeds 9 ft (>2.7 m) (Fig. 2.19). The northernmost belt (Fig. 2.15, belt G) of thick coal is better defined in this map than in other coal maps; although there are few coal seams in this area (Fig. 2.19), individual seams are commonly greater than 30 ft (>9 m) thick (Fig. 2.17). Belts A and B coincide with the northeast-trending belts of high values of net coal thickness (Fig. 2.16). In the southwestern part of the basin, there are three strike-elongate belts (Fig. 2.15, belts A, B, and C) in which the average coal seam is more than 6 ft (>1.8 m) thick (Fig. 2.19). Several dip-oriented belts (Fig. 2.15, belts 1, 2, and 3) occur in which the coal seam thickness is greater than 6 ft (>1.8 m) (Fig. 2.19). These northeast-trending belts are common in the southwestern part of the basin.

Geologic controls on occurrence of coal seams

Previous studies

Coal seams are facies or subsets of genetically related sedimentary units called depositional systems (Fisher and others, 1969). The depositional system controls the occurrence, trend, and thickness and greatly influences the quality of coal (McGowen, 1968; Home and others, 1978; Kaiser and others, 1978; Donaldson and others, 1979; Houseknecht and Iannacchione, 1982). Therefore, the relations between depositional systems and coal occurrence, determined from maps and cross sections, are predictive and are useful tools in coalbed methane exploration.

Pictured Cliffs and Fruitland sandstones are the depositional framework facies that control the occurrence, trend, and thickness of Fruitland coal seams. Previous studies of the depositional setting of the Pictured Cliffs Sandstone and of the Fruitland Formation and other coal-bearing and coal-bounding strata in the San Juan Basin (Sears and others, 1941; Scruton, 1961; Fassett and Hinds, 1971; Erpenbeck, 1979; Devine, 1980; Kelso and others, 1980; Cumella, 1981; Flores and Erpenbeck, 1981; Palmer and Scott, 1984; Wright,

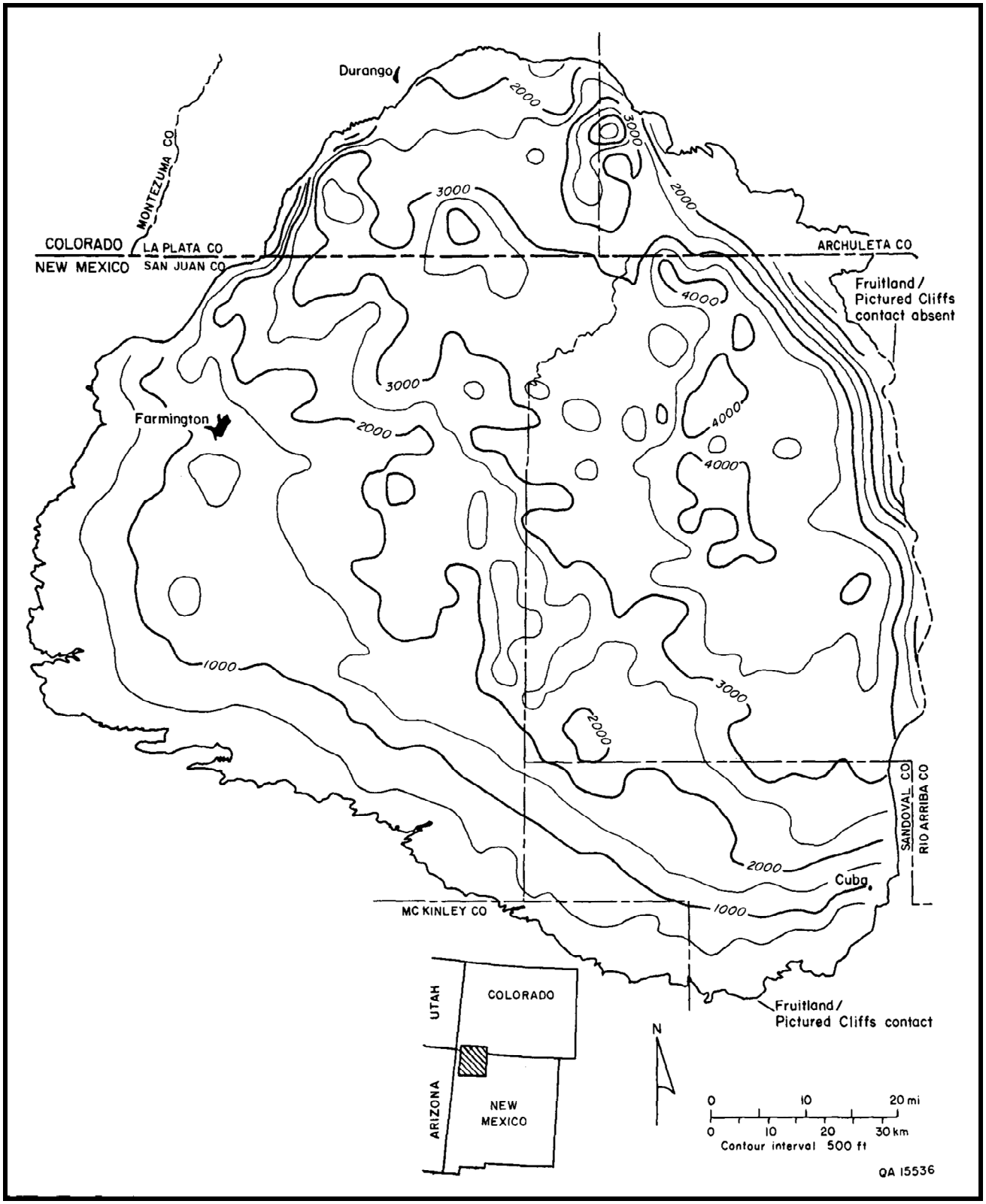

FIGURE 2.14—Coal-overburden map, defined as the depth to the top of the Pictured Cliffs Sandstone or to the top of the uppermost Pictured Cliffs tongue. From Ayers and Ambrose, 1990.

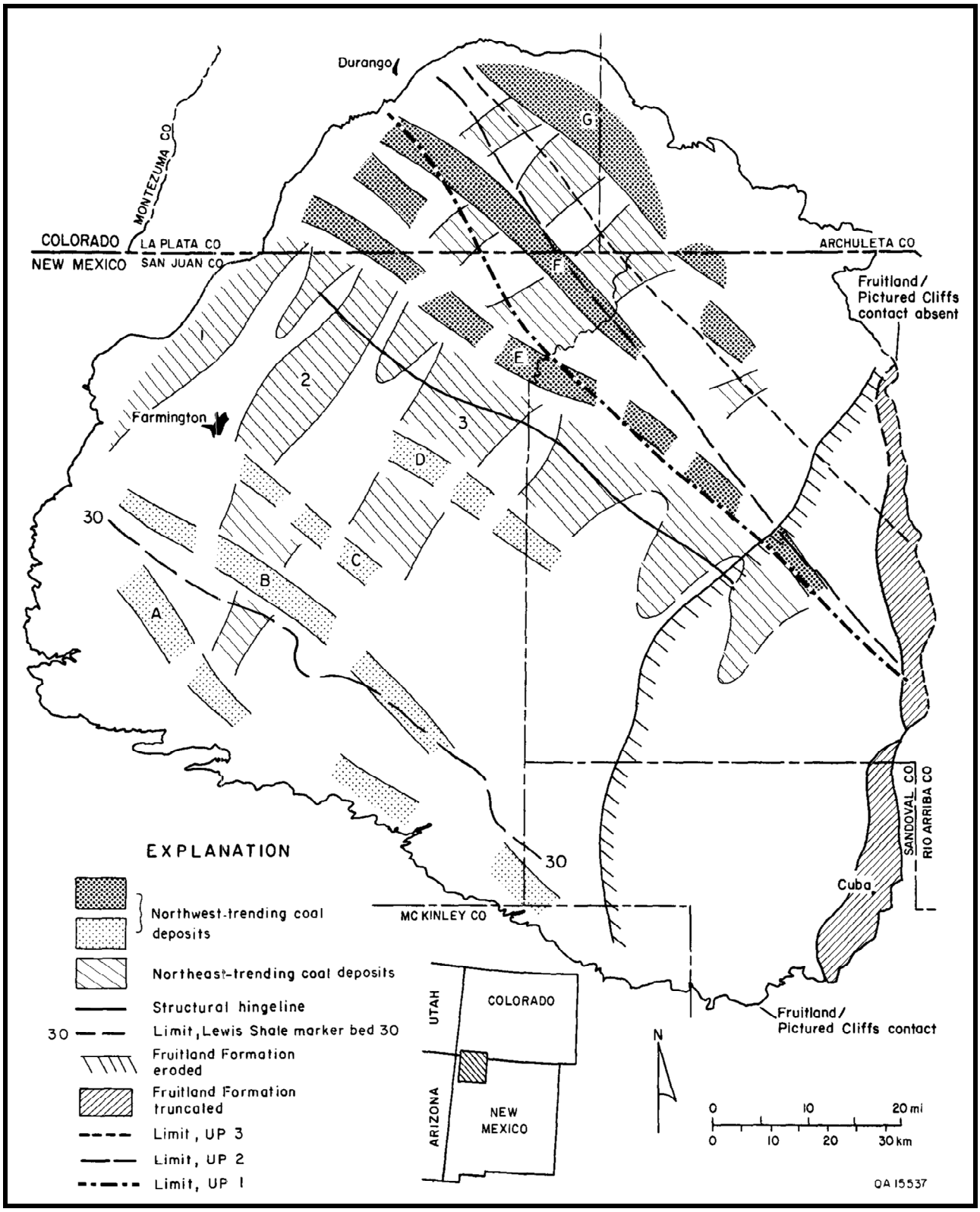

FIGURE 2.15—Major coal-occurrence trends in the Fruitland Formation, summarizing Figs. 2.16-2.19. Thickest coal seams occur northeast of the structural hingeline and parallel the northwest-trending upper Pictured Cliffs tongues, UP1, UP2, and UP3. Southwest of the hingeline, anomalously thick coal either strikes northwest and parallels minor Pictured Cliffs shoreline buildups or trends northeast and lies between Fruitland fluvial systems. From Ayers and Ambrose, 1990.

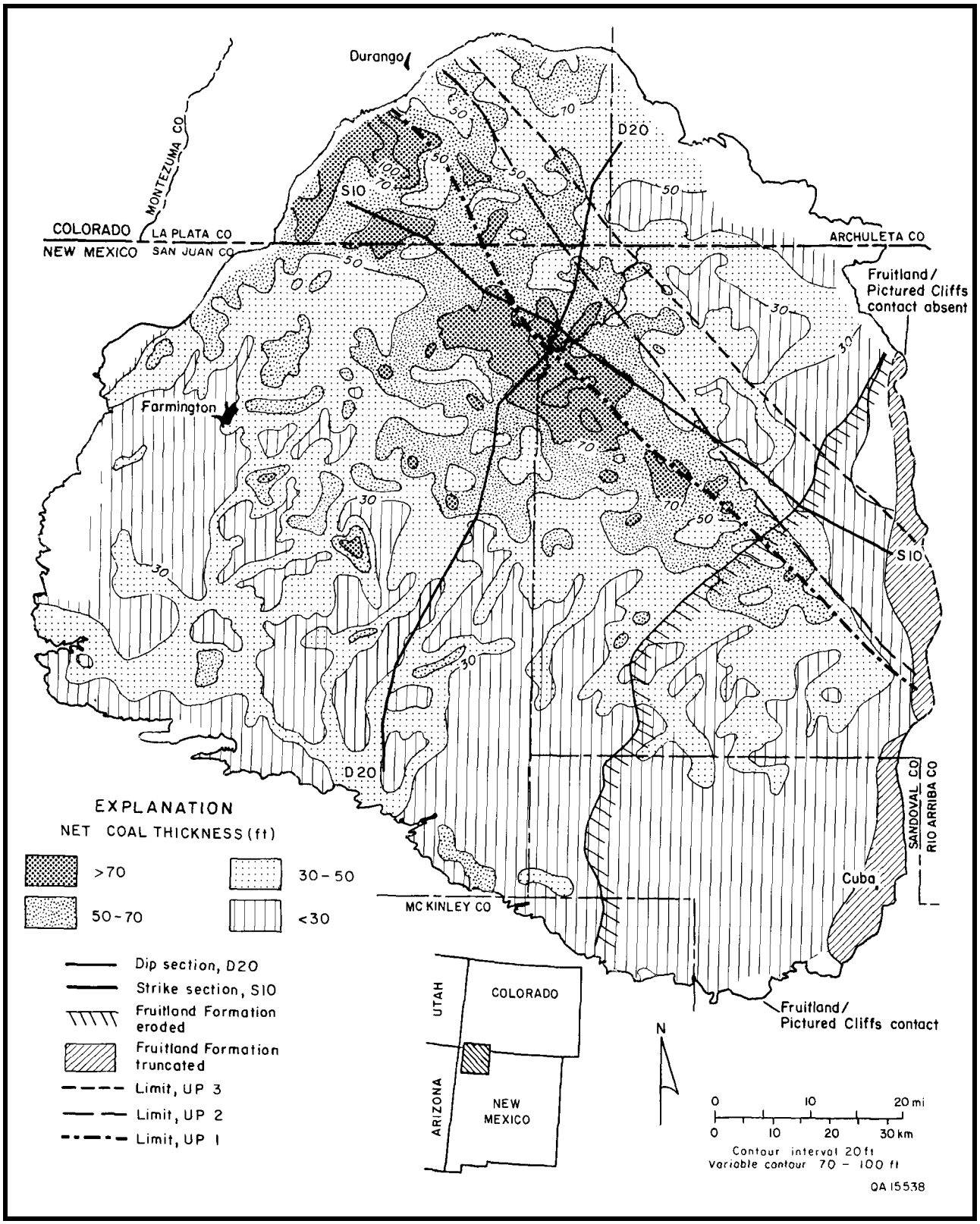

FIGURE 2.16—Fruitland net coal map. Greatest net coal thickness occurs in a northwest-trending belt in the north-central part of the basin. Narrow, dip-oriented net coal deposits trend southwestward from this belt and are inferred to have formed in a floodplain setting. Cross sections D20 and S10 are shown in Figs. 2.2 and 2.3, respectively. From Ayers and Ambrose, 1990.

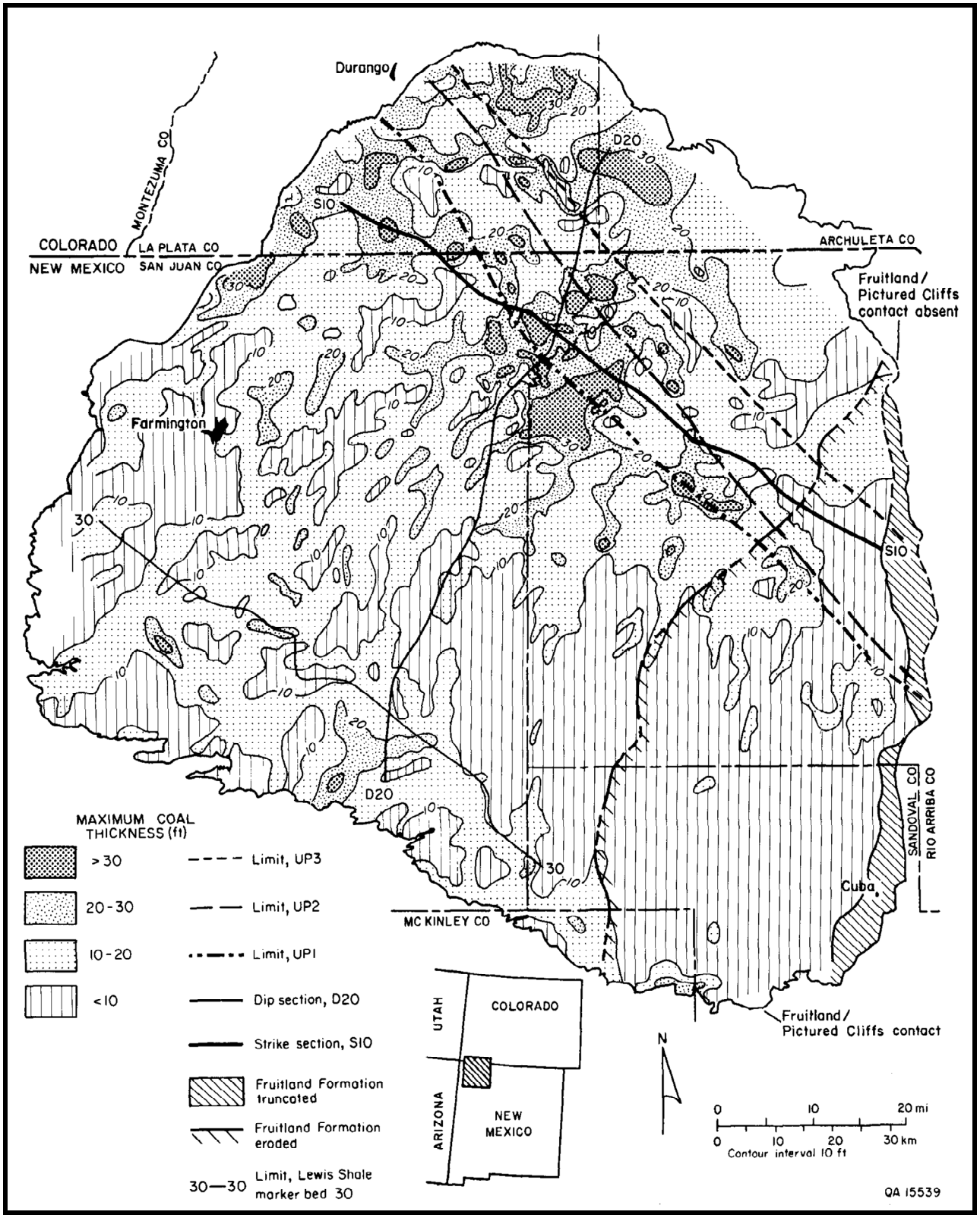

FIGURE 2.17—Fruitland maximum coal map. The thickest coal beds occur in the northern part of the basin. Strike-elongate coal deposits in the southwestern part of the basin are genetically related to the 30–marker bed (see Figs. 2.1-2.3). Cross sections D20 and S10 are shown in Figs. 2.2 and 2.3, respectively. From Ayers and Ambrose, 1990.

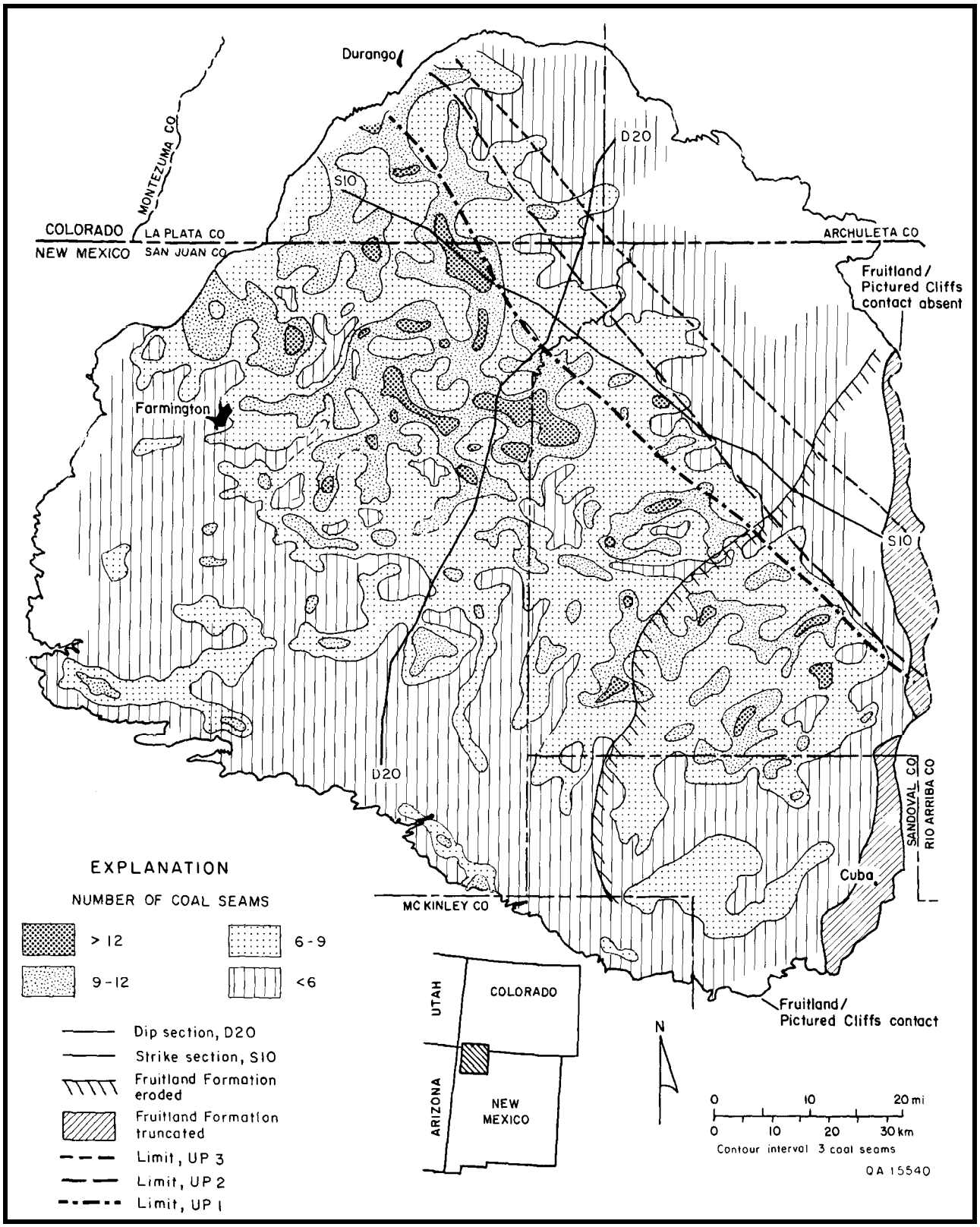

FIGURE 2.18—Fruitland coal isopleth map. Coal seams are most numerous in a broad, strike-elongate belt in the central basin; this belt is landward (southwest) of UP1, UP2, and UP3 shorelines. Cross sections D20 and 510 are shown in Figs. 2.2 and 2.3, respectively. From Ayers and Ambrose, 1990.

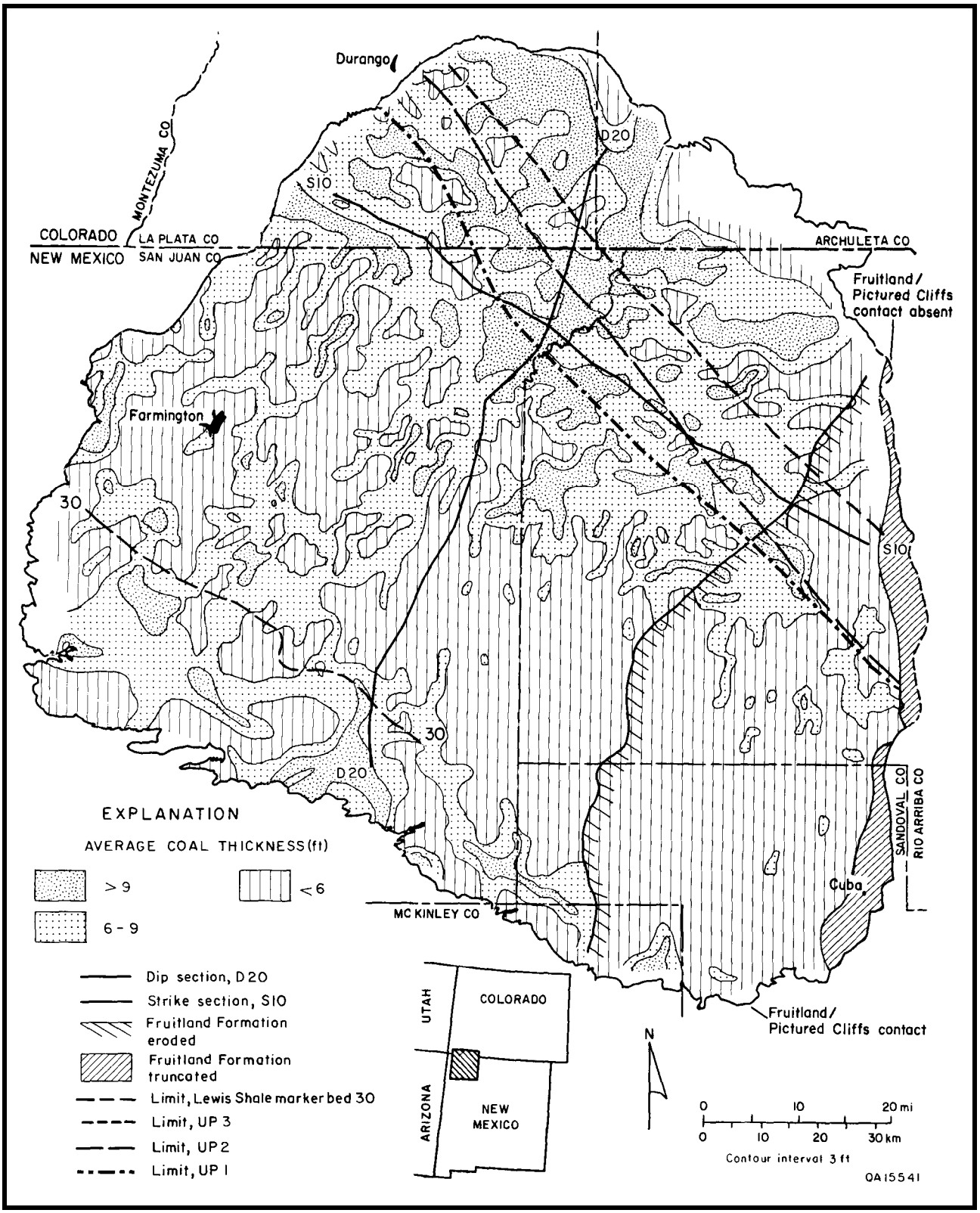

FIGURE 2.19—Fruitland average-coal-thickness map. Trends of coal occurrence are similar to those in other Fruitland coal maps. Strike-elongate trends are well developed landward (southwest) of UP1, UP2, and UP3. Cross sections D20 and S10 are shown in Figs. 2.2 and 2.3, respectively. From Ayers and Ambrose, 1990.

1986) were reviewed in Ayers and Zellers (1988). Wave-dominated coastal processes and resulting wave-dominated deltas and barrier-strandplain systems have long been suggested for the Pictured Cliffs and earlier coastal units in the basin. However, "fluvial-influenced" deltas flanked by barrier strandplains were described for the Pictured Cliffs in the southwestern quarter of the basin by Flores and Erpenbeck (1981, p. 33) and Erpenbeck (1979, p. 67), who suggested that Fruitland coal seams occur in two depositional settings. The thickest coal seams are in the lower Fruitland and are dip-elongate seams flanked by distributary channel-fill sandstones. These workers concluded that Fruitland back-barrier coal seams are thinner and contain abundant carbonaceous shale.

The depositional setting of Fruitland coal seams (Fig. 2.20) was established from coal-seam geometry and distribution and from the relations between the coal seams and the Pictured Cliffs and Fruitland depositional framework facies. At Cedar Hill field, coal beds are dip elongate and formed in upper delta-plain to lower alluvial-plain settings (Cedar Hill deltaic complex, Figs. 2.10b and 2.10c; Ambrose and Ayers, this volume, Chapter 3). Palynologic studies (Manfrino, 1984) and the low sulfur content of Fruitland coal seams indicate peat accumulation in a fresh-water setting that was isolated from marine influence, suggesting that peat accumulation occurred inland behind abandoned and foundering shoreline deposits. In the Navajo Lake area, the thinness of Fruitland fluvial sandstone complexes and their poor definition on lithofacies maps (Ayers and Zellers, this volume, Chapter 4) suggest that fluvial systems in the north-central part of the basin (Navajo Lake area) were minor and too small to form fluvially dominated deltas where they debouched into the Western Interior seaway. This conclusion is supported by linear geometry of the Pictured Cliffs shoreline sandstone tongues (Figs. 2.10b and 2.10c), which suggests a wave-dominated coastline. Additionally, coal seams are thickest and most numerous landward of upper Pictured Cliffs tongues (Fig. 2.20). These relationships suggest that thick coal formed in persistent and recurring swamp environments landward of the upper Pictured Cliffs strandplain-barrier shorelines.

From cross sections and maps made in this regional study and in previous studies, we conclude that syndepositional tectonic activity controlled the depositional system and, indirectly, the occurrence of thick Fruitland coal (Fig. 2.20). Pulsatory differential subsidence across the hingeline at the

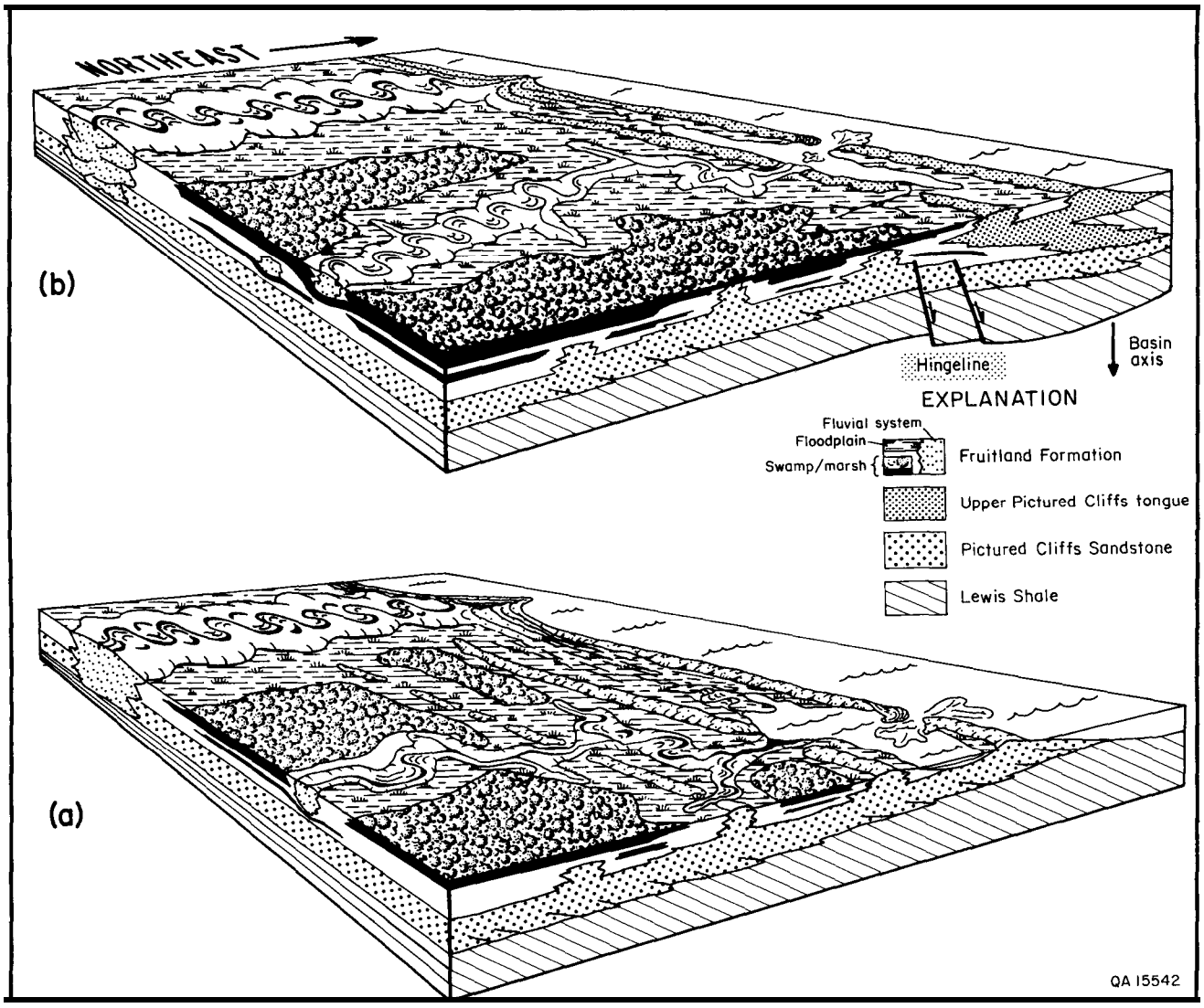

FIGURE 2.20—Depositional model of Fruitland coal seams in the Navajo Lake area. (a) Peat is deposited behind, and overrides, abandoned and foundered Pictured Cliffs shoreline sandstones that occur inland and downdrift of a postulated wave-dominated delta. Area is crossed only by minor fluvial feeders that shift periodically. (b) Intermittent subsidence along basin axis temporarily halts regression, causing a shoreline stillstand and allowing accumulation of thick, extensive peat deposits. Not to scale. From Ayers and Zellers, 1988.

southwestern margin of the basin floor (Figs. 2.2 and 2.8) caused a relative sea-level rise, which resulted in stillstands of the Pictured Cliffs shoreline (UP1, UP2, and UP3). These stillstands allowed ample time for peat (coal) to aggrade and to overspread abandoned shoreline- and fluvial-sandstone complexes. Hence, the greatest concentrations of coal resources occur in northwest-trending belts, north of the hingeline.

Relations between depositional systems and coal occurrence

Northwest-trending belts of thick Fruitland coal (Figs. 2.15-2.19) are related to Pictured Cliffs shoreline positions. The oldest Fruitland coal in the basin is in belts A and B (Fig. 2.15) and formed behind a shoreline associated with initial Pictured Cliffs shoreline progradation. In contrast, belt G contains the youngest Fruitland coal, formed as the Pictured Cliffs shoreline prograded beyond the northern margin of the present San Juan Basin. The initial Pictured Cliffs shoreline progradation temporarily reached a limit in the southern part of the basin, marked by the updip pinch-out of the 30—marker bed (Figs. 2.2 and 2.15). The 30 marker occurs in a high-conductivity shale that was deposited during a minor transgression over an early Pictured Cliffs pro-gradational wedge. Individual coal seams as much as 30 ft (9 m) thick and net coal as much as 50 ft (15 m) thick locally occur at the updip limit of this 30—marker bed (Figs. 2.16 and 2.17). Following the transgression associated with the 30 marker, the Pictured Cliffs shoreline prograded rapidly to the north-central third of the San Juan Basin. As the Pictured Cliffs shoreline advanced basinward, relatively thin peats (coal seams <20 ft [<6 m] thick; Fig. 2.17) formed in floodplains between northeast-flowing Fruitland rivers that supplied sediment to the prograding Pictured Cliffs shoreline. This northeast-trending system of interfluvial coal seams was superimposed over older, northwest-trending belts of shoreline-related coal seams as the Pictured Cliffs shoreline prograded toward the northeast. Areas that were occupied by inferred Fruitland rivers correspond to areas of low values of net, maximum, and average coalbed thickness (Figs. 2.16, 2.17, and 2.19); in contrast, interfluvial areas correspond to narrow (1-8-mi-wide [1.6-13-km]), dip-elongate pods of relatively thick coal. In the southwestern part of the basin, a wide band of thick coal (Fig. 2.15, belts 1, 2, and 3; Figs. 2.16, 2.17, and 2.19) formed in a relatively stable part of the coastal plain that was not occupied by major Fruitland fluvial systems.

The thickest and most laterally continuous Fruitland coal seams were deposited in back-barrier settings that correspond to the northwest-trending belts, E, F, and G (Fig. 2.15). These belts of thick coal are landward (southwest) of pinch-out lines of upper Pictured Cliffs tongues that were deposited during periods of shoreline stillstand and/or marine transgression (retrogradation). Two minor, discontinuous belts of northwest-trending coal (Fig. 2.15, belts C and D) were also deposited during short-lived Pictured Cliffs shoreline stillstands associated with deposition of transgressive shales represented by the 35- and 38-marker beds (Figs. 2.2 and 2.3).

As much as 100 ft (30 m) of coal locally occurs landward of UP1, the oldest upper Pictured Cliffs tongue (Fig. 2.16). This is the thickest belt (Fig. 2.15, belt E) of Fruitland coal in the basin, which suggests a long period of stability of the Pictured Cliffs shoreline. This belt of thick coal encompasses Cedar Hill field and the Navajo Lake area (Fig. 2.5), two of the most productive Fruitland coalbed methane areas in the basin (Kaiser and Ayers, this volume, Chapter 10). Downdip (northeast) of coal belt E in the north-central part of the basin, the number of coal seams (Fig. 2.18) and the net coal thickness (Fig. 2.16) decrease as the Fruitland Formation thins at the expense of Pictured Cliffs tongues UP1 and UP2 (Fig. 2.2); commonly, net coal thickness is less than 70 ft (<21 m) landward of UP2 and 50 ft (15 m) landward of UP3.

Geologic controls on producibility of coalbed methane

Locally in the San Juan Basin, Fruitland coal seams are folded because of tectonic activity, and structure maps can indicate areas of fracture-enhanced permeability. In other areas, coal seams may be folded over or under Fruitland channel-fill sandstones or Pictured Cliffs shoreline sandstones because of differential compaction. Such compactional folding of brittle coal beds may cause fractures that enhance coalbed permeability. If fracture systems of differential-compaction origin are sufficiently developed, areas of interbedded sandstones and coal seams would be good targets for coalbed methane exploration.

Earlier workers concluded that Fruitland coal seams have limited extent and that they are bounded on their basinward (northeast) margins by Pictured Cliffs shoreline sandstone and along paleostrike (northwest—southeast) by Fruitland fluvial sandstones (Fassett and Hinds, 1971; Fassett, 1986). However, some Fruitland coal seams may be regionally continuous, overriding the Pictured Cliffs Sandstone and Pictured Cliffs tongues with continued progradation. This implies that many Fruitland coal seams are time-transgressive, and it conflicts with the previous interpretation that Fruitland coal beds are "essentially time-equivalent throughout their extent" (Fassett, 1988, p. 35). In at least one area of the San Juan Basin, thick Fruitland coal seams override an upper Pictured Cliffs tongue in the paleodip direction (Ayers and Zellers, this volume, Fig. 4.16). Along paleostrike, coal seams split and interfinger with fluvial channel-fill sandstone complexes (Ayers and Zellers, this volume, Fig. 4.17). Areas where Fruitland coal seams drape over upper Pictured Cliffs tongues may be sites of compaction-induced fractures.

The significance of this complex coal-seam geometry is threefold: (1) coal seams, and hence coalbed methane reservoirs, are more extensive than previous workers suggested; (2) compaction-induced fractures, and therefore enhanced coalbed permeability, may occur in areas where coal seams drape over shoreline sandstones or form zigzag splits with channel-fill sandstone complexes; and (3) the greater lateral extent of coal seams, inferred from this research, is critical to the interpretation of ground-water flow and abnormal pressure in the Fruitland Formation (Kaiser and Swartz, 1988, 1989). The abundance of folds and their potential contribution to enhanced production justify further study. Evaluations of compaction and tectonic folds, in both subsurface and outcrop studies, will be required for clarification of the relations between folding and fracturing.

Coal and coalbed methane resources

In this study, we calculated coal and coalbed methane resources only in Fruitland coal seams deeper than 400 ft (>122 m). Coal resources in the Fruitland Formation were calculated to be 245 billion short tons. This estimate is 11% greater than that of Kelso and others (1988 [219 billion short tons]), and it is 23% greater than that of Fassett and Hinds (1971 [200 billion short tons]). Coalbed methane in place was calculated to be 43-49 Tcf, which is 2-14% less than the 50 Tcf estimate reported by Kelso and others (1988) but is 39-58% greater than the estimate by Choate and others (1984). Approximately 2,500 geophysical well logs were used to make most maps in this study. Of these logs, 1,731 were of sufficiently good quality to be used to evaluate and map

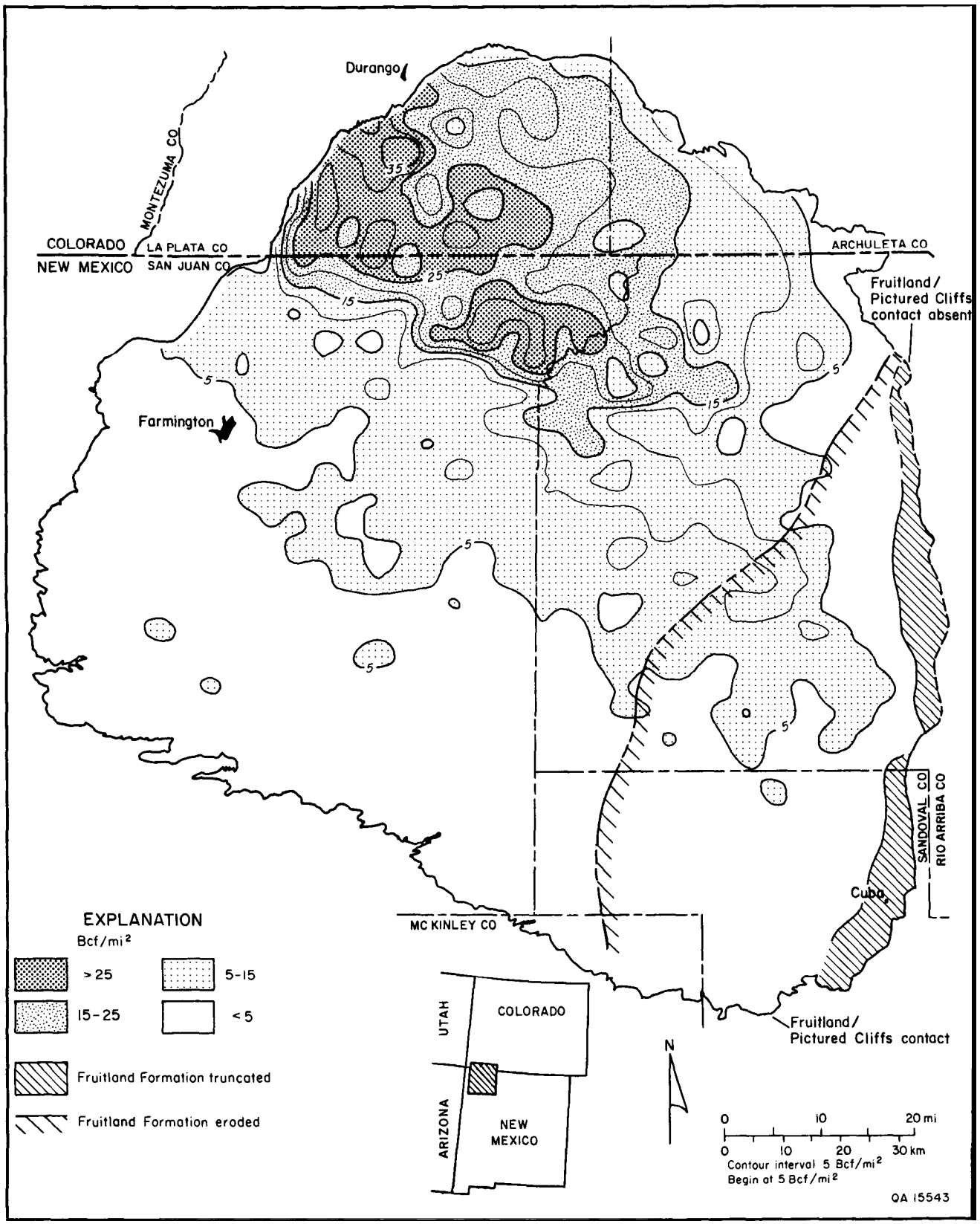

FIGURE 2.21—Gas-in-place map for Fruitland Formation coal seams, calculated on the basis of 20% average ash content in coal. High values of gas in place occur in the west-central part of the San Juan Basin and reflect the presence of thick coal seams, high coal rank, and high formation pressure. From Ayers and Ambrose, 1990.

Fruitland coal beds. This data base was much larger than that used in previous studies, and it resulted in better definition of coal occurrences and trends and in a larger coal resource estimate than in previous studies. Fassett and Hinds (1971) used data from approximately 325 well logs to calculate Fruitland coal resources; the coalbed-methane-resource estimate of Choate and others (1984) was based on Fassett and Hinds' (1971) coal-resource estimate. Kelso and others (1988) used 549 well logs to calculate coal and coalbed methane resources.

Although coal resources estimated in this study are 11% greater than those estimated by Kelso and others (1988), the gas in place in Fruitland coal seams estimated in this study is 2 to 14% less than that of Kelso and others (1988). Differences between the coalbed methane estimates stem from differences in the methods of calculation and from assumed ash content of coal seams. Kelso and others (1988) calculated coalbed methane resources on the basis of average coalbed thickness, rank, depth, and gas content in each township; the total resource is the sum of the resources in individual townships. To account for the reduced gas content of the coal because of the presence of inorganic material (commonly referred to as ash) in coal seams, Kelso and others (1988) assumed that the ash values (10-36%) mapped by Fassett and Hinds (1971, fig. 24) reflected regional trends common in all Fruitland coal seams (B. S. Kelso, pers. comm. 1989). In the present study, resources were calculated by computer on a well-by-well basis using coal thickness and depth data recorded from well logs. Values for gas content and coal density were those used by Kelso and others (1988). Rather than assuming that the ash content of one coal sample was representative of all Fruitland coal seams at that locality, we used average ash contents of 20% and 30% to calculate 49 Tcf and 43 Tcf, respectively, of methane in Fruitland coal seams.

Gas in place in Fruitland coal seams locally exceeds 35 Bcf/mi^2 in the north-central part of the basin (Fig. 2.21). Gas in place, although influenced by coal rank and present depth, is predominantly controlled by coal thickness. Gas contents greater than 35 Bcf/mi^2 (Fig. 2.21) generally coincide with northwest-trending areas where net coal thickness exceeds 70 ft (>21 m) (Fig. 2.16) and maximum coal thickness exceeds 20 ft (>6 m) (Fig. 17); the 10-Bcf/mi^2 contour (Fig. 2.21) generally coincides with the 50-ft net coal thickness contour (Fig. 2.16).

Conclusions

1. Geologic factors that affected the occurrence and producibility of coalbed methane in the San Juan Basin were tectonic controls on sedimentation, depositional controls on coal occurrence and geometry, and structural controls on the permeability of coal seams.

2. Pictured Cliffs shoreline sandstones accumulated in northwest-trending barrier strandplains. Retrogradational deposits, upper Pictured Cliffs tongues UP1, UP2, and UP3, were caused partly by differential basin subsidence; UP1 pinches out northeast of and parallel to a structural hinge-line that separates the northeast-dipping monocline of the southern half of the basin from the low-relief basin floor.

3. The thickest and most continuous coal seams in the Fruitland Formation occur in the northwestern part of the basin and are associated with upper Pictured Cliffs tongues. These coal deposits occur in three northwest-trending belts that are updip (southwest) of and parallel to these upper Pictured Cliffs shoreline sandstones. Other northwest-trending belts of thick Fruitland coal seams in the southern part of the basin are genetically related to older, minor Pictured Cliffs transgressions.

4. Dip-elongate belts of thick Fruitland coal seams project landward (southwestward) from the northwest-trending belts of thick coal and are inferred to have formed in a floodplain setting. These belts of Fruitland coal were identified and the geometry of the northwest-trending belts of thick coal were better defined in this study than in previous studies because regional maps were made using more data (12 to 15 well logs per township versus 2 to 5 wells per township).

5. The Fruitland Formation thins eastward in the southeastern part of the San Juan Basin because of syndepositional uplift. Coal seams are thinner and fewer in that area. Postdepositional uplift of the southeast part of the basin caused pre-Ojo Alamo erosion that beveled the Fruitland Formation, truncating coal seams near the eastern margin of the basin.

6. The northwest-trending belts of thick coal crop out along the northern and northwestern margins of the basin where they may receive or discharge fluids; hydrologic maps suggest that these Fruitland coal seams are major aquifers that are regionally overpressured because of the elevated recharge area and coal-seam pinch-out (Kaiser and Swartz, 1988, 1989). These northwest-trending seams are poorly connected to dip-elongate coal seams in the southwestern part of the basin because coal seams pinch out to the southwest and, possibly, because coal seams are offset by faults along the structural hingeline.

7. Coal and coalbed methane resources in the Fruitland Formation are 245 billion short tons and 43 to 49 Tcf, respectively, at depths of 400 ft (122 m) or more. These resources are most abundant in the northwestern part of the basin where Fruitland gas in place may exceed 35 Bcf/mi2.

8. Targets for increased coalbed methane production because of fracture-enhanced permeability may exist along minor tectonic folds such as those developed along the Hogback monocline or at the margin of the basin floor. Coal seams commonly override sandstones to extend tens of miles in either the paleodip or the paleostrike direction. Potential targets for enhanced permeability caused by compaction-induced fractures occur where Fruitland coal seams drape Pictured Cliffs and Fruitland sandstones.

Acknowledgments

This study benefited from discussions with W. B. Hanson, W. F. Hoppe, A. C. Huffman, Jr., W. R. Kaiser, B. S. Kelso, and Robert Kemp. C. M. Tremain and N. H. Whitehead, III, contributed data and geologic insights and assisted with field work. Data from Roybal and others (1985) were used to map coal in the shallow subsurface near the southern margin of the basin. D. R. Grote, Areef Ahamad, J. D. Beckman, P. S. Reiss, G. A. Warren, W. J. Garey, M. M. Newton, R. G. McMurry, and J. N. Ashton assisted with data collection and processing. We gratefully acknowledge review comments by J. C. Close, D. K. Murray, and W. R. Kaiser.

3. Geologic controls on coalbed methane occurrence and production in the Fruitland Formation, Cedar Hill field and the COAL site

W. A. Ambrose and W. B. Ayers, Jr.

Bureau of Economic Geology

Abstract—The Cedar Hill field area contains some of the most productive coalbed methane wells in the San Juan Basin. To determine geologic controls on occurrence and producibility of coalbed methane at Cedar Hill field and the Completion Optimization and Assessment Laboratory (COAL) site, structure, coal occurrence, net sandstone thickness, and production were mapped.

The primary targets for coalbed methane production in Cedar Hill field are the thick lower Fruitland Formation coals (coal group A), which formed in a lower coastal-plain setting. Group A coal beds are the thickest, up to 35 ft (11 m), and most continuous coal beds at Cedar Hill field. In contrast, at the COAL site the thickest coal beds are more than 30 ft (>9 m) thick and occur in the middle Fruitland Formation (coal group C).

Fruitland coal seams form complex reservoirs at Cedar Hill field and the COAL site because of coalbed-sandstone relations and minor structural deformation. Compactional folding in coal beds is present where they underlie or override Fruitland channel-fill sandstones. Coal beds may be more intensely fractured, and thus more permeable, where folded. Northwest-trending (?) faults along the basin hingeline and a syncline that bisects Cedar Hill field also contribute to coal seam complexity. Faults at the hingeline offset coal beds and may hinder fluid flow, thus causing the boundary between overpressured and underpressured strata.

Introduction

Cedar Hill field, in the north-central San Juan Basin (Fig. 3.1), has the longest history of coalbed methane production in the basin. Developed by Amoco Production Company in 1977, Cedar Hill field produces from basal Fruitland Formation coal seams at a depth of approximately 2,800 ft (854 m). Coal seams there contain an estimated 313 million tons of coal and 89 billion cubic feet (Bcf) of gas in place (Decker and others, 1988). Approximately 17.2 Bcf of coalbed methane and 737,000 bbls of water were produced in Cedar Hill field from 1977 through 1989 (Petzet, 1990).

The COAL site, located approximately 2.5 mi (~4 km) northwest of Cedar Hill field (Fig. 3.1) in Colorado, has a coalbed methane field research laboratory operated jointly by Amoco Production Company and the Gas Research Institute (GRI). Research at the COAL site is designed to compare the effectiveness of open-hole cavity completions with cased-hole, hydraulically fractured completions, and to determine the parameters that favor open-hole cavity completions. At both Cedar Hill field and the COAL site, the Fruitland Formation is overpressured. Because overpressuring is due to artesian conditions, most coalbed methane wells in the area produce water.

Objectives

The objectives of this study were to (1) identify Fruitland coal groups and depositional subunits, (2) define geologic control on the thickness, continuity, and structural attitude of major coal seams (reservoirs) that occur in each coal group, and (3) characterize the boundary between overpressured and underpressured Fruitland strata. The geologic characteristics defined in this study will be compared with coalbed methane production trends to determine geologic and hydrologic controls on coalbed methane producibility (Kaiser and Ayers, this volume, Chapter 10). This area was selected because (1) Cedar Hill field has the longest history of coalbed methane production in the basin, and (2) geologic characterization of the COAL site provides an interpretation of coalbed methane research results by describing controls on coalbed reservoir complexity and productivity.

Methods

Data from 260 geophysical logs, including 22 from shallow (<600 ft [<183 m] deep) boreholes near the Fruitland outcrop, were used in this study. Outcrops were described to document relationships between Fruitland and Pictured Cliffs stratigraphic units, to evaluate coalbed continuity, and to support interpretations of depositional systems.

Stratigraphic units below, above, and in the Fruitland Formation were correlated on eight structural and strati-graphic cross sections to provide a framework for determining the lateral extent of Fruitland coal seams and sandstones. Marker beds that were correlated included the Huerfanito

Bentonite Bed, five shale marker beds in the Lewis Shale and Pictured Cliffs Sandstone, tonsteins (ash layers) in Fruitland coal seams, carbonaceous shales in the Fruitland Formation, and a high-conductivity shale at the Fruitland–Kirtland contact (Ayers and others, this volume, Chapter 2).

The Fruitland Formation was divided into three depositional subunits, each bounded by continuous coal beds or locally by shale and sandstone beds. Depositional models of subunits were based on a comparative analysis of net coal thickness, net sandstone thickness, isopach, and structure maps. Sandstone thickness was determined from resistivity and natural-gamma curves; coal identification was confirmed with bulk-density logs. We recorded coal seams thicker than 2 ft (>0.6 m); partings thinner than 2 ft (<0.6 m) were included as coal because of the limits of resolution of the geophysical logs. For logs without a density curve, natural-gamma, neutron, and resistivity curves were used; coal seams in these logs were identified by correlation with coal seams in nearby logs having bulk-density curves.

Stratigraphic and structural setting

At Cedar Hill field and the COAL site, the Fruitland Formation is 430 to 470 ft (131 to 143 m) thick; it thickens northwest toward the Fruitland outcrop, where it is more than 570 ft (>174 m) thick (Fig. 3.1). The Fruitland Formation was divided into three depositional subunits (lower, middle, and upper) that contain four coal groups in as-

cending stratigraphic order (A, B, C, and D) (Figs. 3.2 and 3.3). In areas where the bounding coal groups pinch out, subunit boundaries are replaced by locally occurring shale or sandstone beds. Although coal seams that bound Fruitland subunits pinch out locally in the area of Cedar Hill field and the COAL site, they are present over most of the study area.

The lower Fruitland subunit, which directly overlies the Pictured Cliffs Sandstone (Figs. 3.2 and 3.3), consists of sandstone, mudstone, and two coal groups (A and B). Coal beds in group A occur at the base of the Fruitland Formation, and those in group B are bounded by two sandstones, LF1 and LF2 (Fig. 3.3). LF1 was mapped separately, whereas thinner, underlying sandstones in the interval that includes coal group A were mapped collectively.

The middle and upper subunits compose most of the Fruitland Formation and contain coal groups C and D, respectively. Group C coal seams overlie LF1 sandstones in

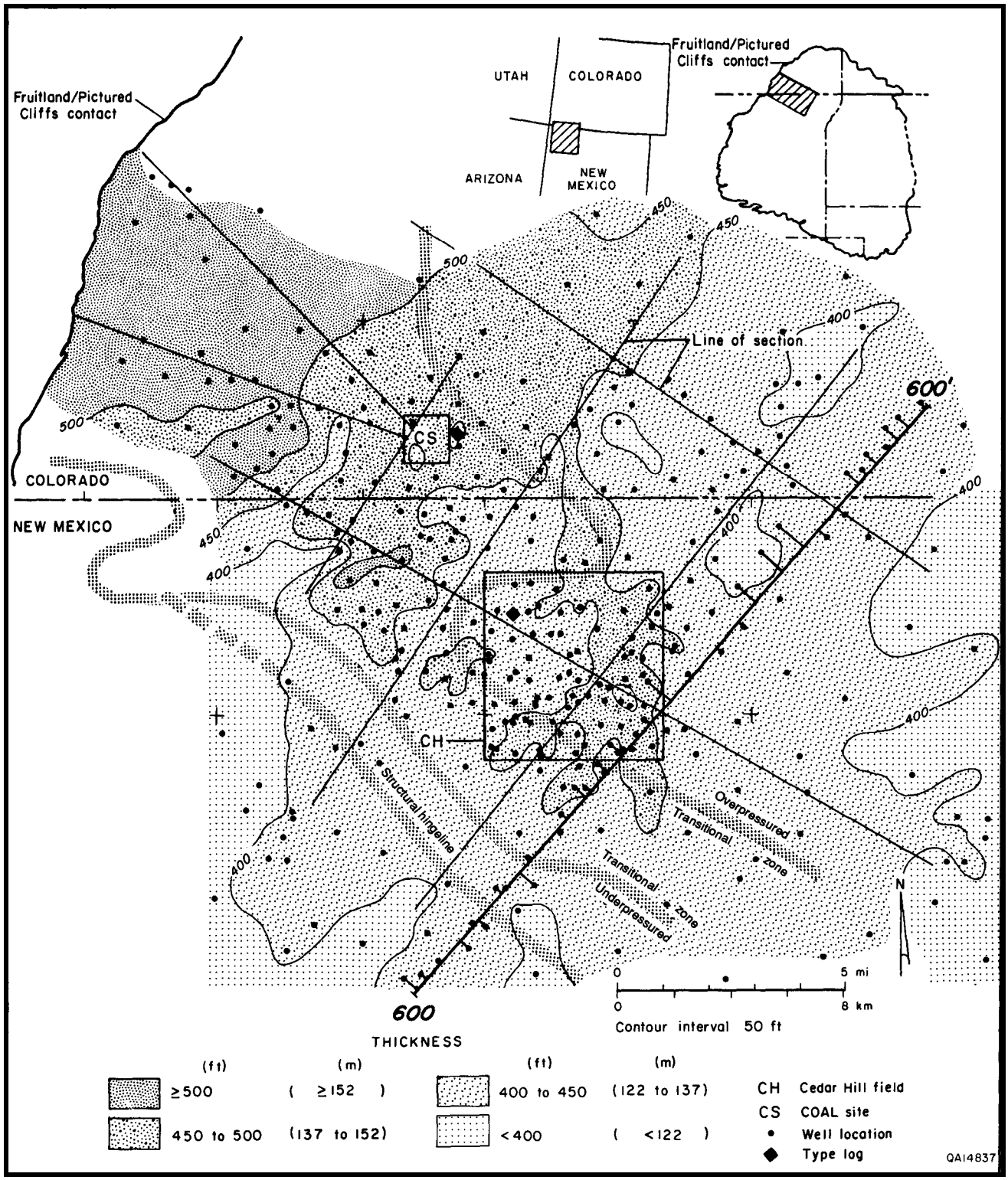

FIGURE 3.1—Isopach map of the Fruitland Formation at Cedar Hill field and the COAL site. The Fruitland Formation thickens northwestward toward the outcrop belt.

Cedar Hill field but override LF2 sandstones northeast of the field (Fig. 3.3). Group C coal seams are thicker and more continuous than group D seams, which occur between thick channel-fill sandstones in the upper Fruitland subunit.

The Fruitland—Kirtland contact is a regionally extensive, high-conductivity shale (Fig. 3.2). This shale interval is inferred to be a marine condensed section deposited over older Fruitland coastal-plain deposits (Ayers and others, this volume, Chapter 2). Foraminifera have been reported in this shale (Dilworth, 1960), which has a geophysical-log response (high natural-gamma, high conductivity) and regional continuity similar to that described for other marine condensed sections in the Western Interior seaway (Leckie and others, 1990).

Cedar Hill field is bisected by an east-plunging syncline (Fig. 3.4). In the syncline, Fruitland strata are more tightly folded (Fig. 3.4a) than the underlying Huerfanito Bentonite Bed (Fig. 3.4b). Structural relief on the base of Fruitland coal group A across Cedar Hill field is 70 ft (21 m) (Fig. 3.4a). Up to 40 ft (12 m) of structural relief occurs across faults and where coal seams override sandstones (Fig. 3.3).

Depositional systems

Pictured Cliffs Sandstone

The Pictured Cliffs Sandstone, which forms a sandstone platform at the base of the Fruitland Formation, consists of northwest-trending, strike-elongate shoreline deposits of barrier-island and wave-dominated delta systems that pro-graded northeastward (Ayers and others, this volume, Chapter 2). North of the study area, the upper Pictured Cliffs Sandstone intertongues with the Fruitland Formation. The lower Pictured Cliffs Sandstone intertongues with the Lewis Shale and is 175 ft (53 m) thick, 2 mi (3.2 km) updip (southwest) of the basin hingeline (Fig. 3.3). However, it is 250 ft (76 m) thick in Cedar Hill field, and 4 mi (6.4 km)

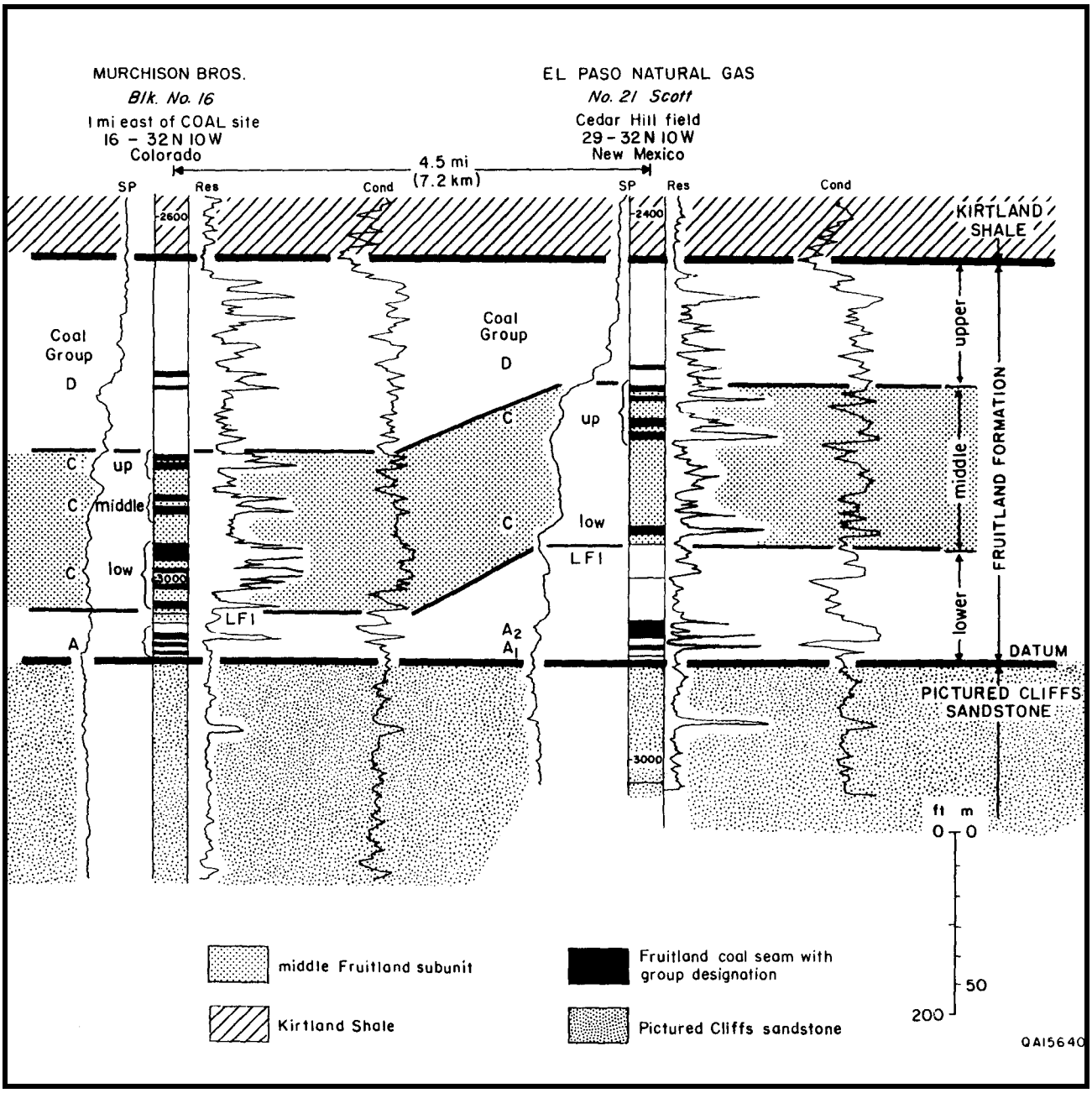

FIGURE 3.2—Type logs (located in Fig. 3.1) showing Fruitland stratigraphic units in Cedar Hill field and in the area of the COAL site. Group B coal seams and the overlying LF2 sandstone (shown in Fig. 3.3) are absent in Cedar Hill field and the COAL site.

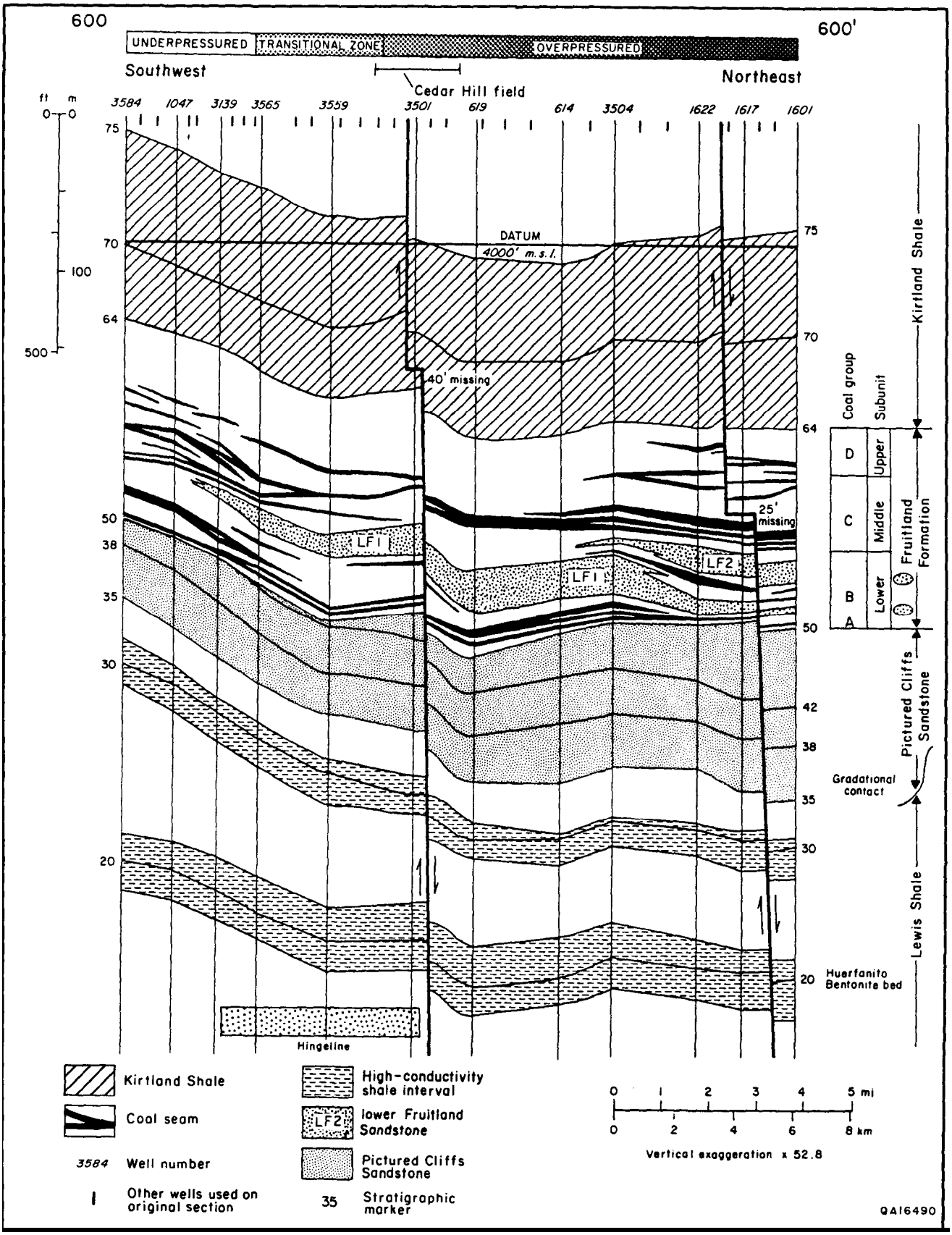

FIGURE 3.3—Structural dip section in northwestern San Juan Basin (see Fig. 3.1 for location). A transition from gently northeast-dipping to nearly flat-lying but folded and faulted strata occurs at the hingeline and the southwest margin of regional overpressuring.

northeast of the field it thickens basinward to more than 350 ft (>107 m). Marker beds in the Lewis Shale, used to correlate well logs in this study, represent isochronous surfaces across proximal-shelf and shoreface facies. These marker beds intersect and are unresolvable in Pictured Cliffs coastal sandstones (Ayers and others, this volume, Chapter 2). Similar stratigraphic marker beds have been described in pro-gradational coastline deposits in the Upper Cretaceous Point Lookout Sandstone in the southern part of the San Juan Basin (Wright, 1986).

Fruitland Formation

The Fruitland Formation, the primary coal-bearing formation in the San Juan Basin, is the nonmarine facies tract consisting of interbedded sandstone, mudstone, and coal beds (Fig. 3.3) deposited landward of the marine (barrier-island and delta-front) facies tract of the Pictured Cliffs Sandstone. In the Fruitland Formation, dip-elongate (northeast-trending), fluvial and lower coastal-plain sandstone bodies form the depositional framework. Net sandstone thickness in the Fruitland Formation ranges from 110 to 230 ft (34 to 70 m) (Fig. 3.5).

Lower Fruitland subunit—Thin, northeast-trending sandstones associated with coal group A, below LF1 (Figs. 3.2 and 3.3), were mapped to determine depositional controls on occurrence of lower Fruitland coal beds. Sandstones in the lower Fruitland subunit are locally more than 40 ft (>12 m) thick at Cedar Hill field, but thin to only 10 ft (3 m) northeastward (Fig. 3.6a). They are interpreted to be distributary-channel and crevasse-splay complexes deposited in a lower delta-plain setting, on the basis of their stratigraphic position (directly overlying the Pictured Cliffs Sandstone) in the offlapping Fruitland-Pictured Cliffs facies tract. The Pictured Cliffs delta front, inferred from pinch-outs of associated distributary-channel sandstones, was 3 to 6 mi (4.8 to 9.6 km) northeast of Cedar Hill field and the COAL site.

Northeast-trending LF1 sandstones, locally more than 40 ft (>12 m) thick (Fig. 3.6b), are interpreted to have been deposited in upper delta-plain fluvial systems that were deposited over older, lower delta-plain deposits associated with coal group A. A major LF1 channel-belt system in the eastern half of Cedar Hill field is defined by sandstones more than 40 ft (>12 m) thick. In contrast, the COAL site is located between LF1 depositional axes, where net sandstone thickness is less than 10 ft (<3 m). LF2, a lenticular sandstone less than 20 ft (<6 m) thick, occurs above coal group B, but was not mapped because it is present only locally at the margin of the study area (Fig. 3.3).

Middle Fruitland subunit—The middle Fruitland subunit consists of strata from the base to the top of coal group C (Figs. 3.2 and 3.3). Sandstone bodies display a strongly dip-elongate geometry in the middle Fruitland subunit. Net sandstone thickness is 40 to 60 ft (12 to 18 m) in Cedar Hill field and more than 80 ft (24 m) near the northwestern margin of the basin (Fig. 3.7a). The inferred depositional setting of the middle Fruitland subunit is a transition between upper coastal plain and lower alluvial plain; as the Pictured Cliffs shoreline prograded northeastward, there was a corresponding seaward shift in depositional environments of overlying, younger Fruitland strata. During deposition of the middle Fruitland subunit, the Pictured Cliffs shoreline was located farther basinward than it was during deposition of the lower Fruitland subunit because of the seaward-stepping geometry caused by net shoreline pro-gradation.

Upper Fruitland subunit—The upper Fruitland subunit consists of all Fruitland strata above coal group C (Fig. 3.2). Sandstones occur in dip-elongate (northeast-trending) belts; these belts are less than 2,000 ft (<610 m) wide at Cedar Hill field (Fig. 3.7b). The upper Fruitland subunit contains the thickest Fruitland sandstones, with thickness of individual sandstone bodies up to 50 ft (15 m) and net sandstone thickness up to 130 ft (40 m). The upper Fruitland subunit is interpreted to be the most landward part of the Fruitland fluvial facies tract. At Cedar Hill field and the COAL site, sandstone belts are interpreted to be tributary-stream deposits that merge down the paleoslope (northeastward) to form alluvial trunk-stream deposits.

Fruitland coal groups

The four Fruitland coal groups (A, B, C, and D) consist of one or more individual coal seams (Figs. 3.2 and 3.3). Coal seams in these groups vary in thickness and continuity because of deposition of peat in different settings and presence of lenticular sandstones that locally replace coal seams. Coal group B occurs only locally and pinches out approximately 1 mi (~1.6 km) northeast of Cedar Hill field (Fig. 3.3); therefore, it was not evaluated in this study. In this section we describe coal groups A, C, and D, and relate coal characteristics to depositional setting.

Fruitland net coal thickness at Cedar Hill field and the COAL site ranges from less than 40 ft (<12 m) to as much as 100 ft (30 m) (Fig. 3.8a). Coal deposits commonly are parallel to depositional dip (northeast-trending) at Cedar Hill field and south of the COAL site. Dip-elongate bands of 60 to 80 ft (18 to 24 m) of coal merge toward depositional dip (northeastward) to form a strike-elongate (northwest-trending) sheet of more than 80 ft (>24 m) of net coal, approximately 3 mi (~4.8 km) northeast of Cedar Hill field. The dip-elongate coal deposits in the Fruitland Formation formed in floodplain and interdistributary environments, whereas the strike-elongate coal deposits accumulated in swamps landward (southwest) of Pictured Cliffs shoreline sandstones. Similar depositional controls on coalbed geometry have also been described in the Upper Cretaceous Ferron Sandstone in central Utah (Ryer, 1981).

Coal group A

Coal group A consists of as many as three coal seams. In the northwestern San Juan Basin, the greatest net coal thickness in group A (35 ft [11 m]) occurs in northeast-trending bands in Cedar Hill field (Fig. 3.8b), where this group is the main target for coalbed methane production. Coal seams in group A pinch out 1 to 3 mi (1.6 to 4.8 km) from the northwestern margin of the basin.

The thickest coal in group A in the study area coincides with a 3-mi-wide (4.8-km-wide) area centered on Cedar Hill field, where thickness of underlying and interbedded sandstones exceeds 20 ft (>6 m). This relation suggests that peat in coal group A accumulated on a sand-rich platform in a deltaic depocenter at Cedar Hill field (Fig. 3.6a). However, net coal thickness of group A in the Cedar Hill deltaic depocenter is locally greatest (>30 ft [>9 m] thick) in sand-poor, narrow (<1 mi [<1.6 km] wide) interdistributary deposits, where net sandstone thickness is less than 20 ft (<6 m) (Fig. 3.6a). The depositional setting of coal group A is similar to that described by Levey (1985) for lower delta-plain coal seams in the Upper Cretaceous Rock Springs Formation in southwestern Wyoming. Thick Rock Springs coal seams formed from peats that had overspread abandoned-delta lobes, and the greatest accumulation occurred between distributaries.

Coal group C

Coal group C occurs in the middle Fruitland subunit (Figs. 3.2 and 3.3). Net coal thickness in group C is greatest northwest of Cedar Hill field, where thickness exceeds 60 ft (>18 m) (Fig. 3.9). Coal occurs in dip-elongate deposits that merge

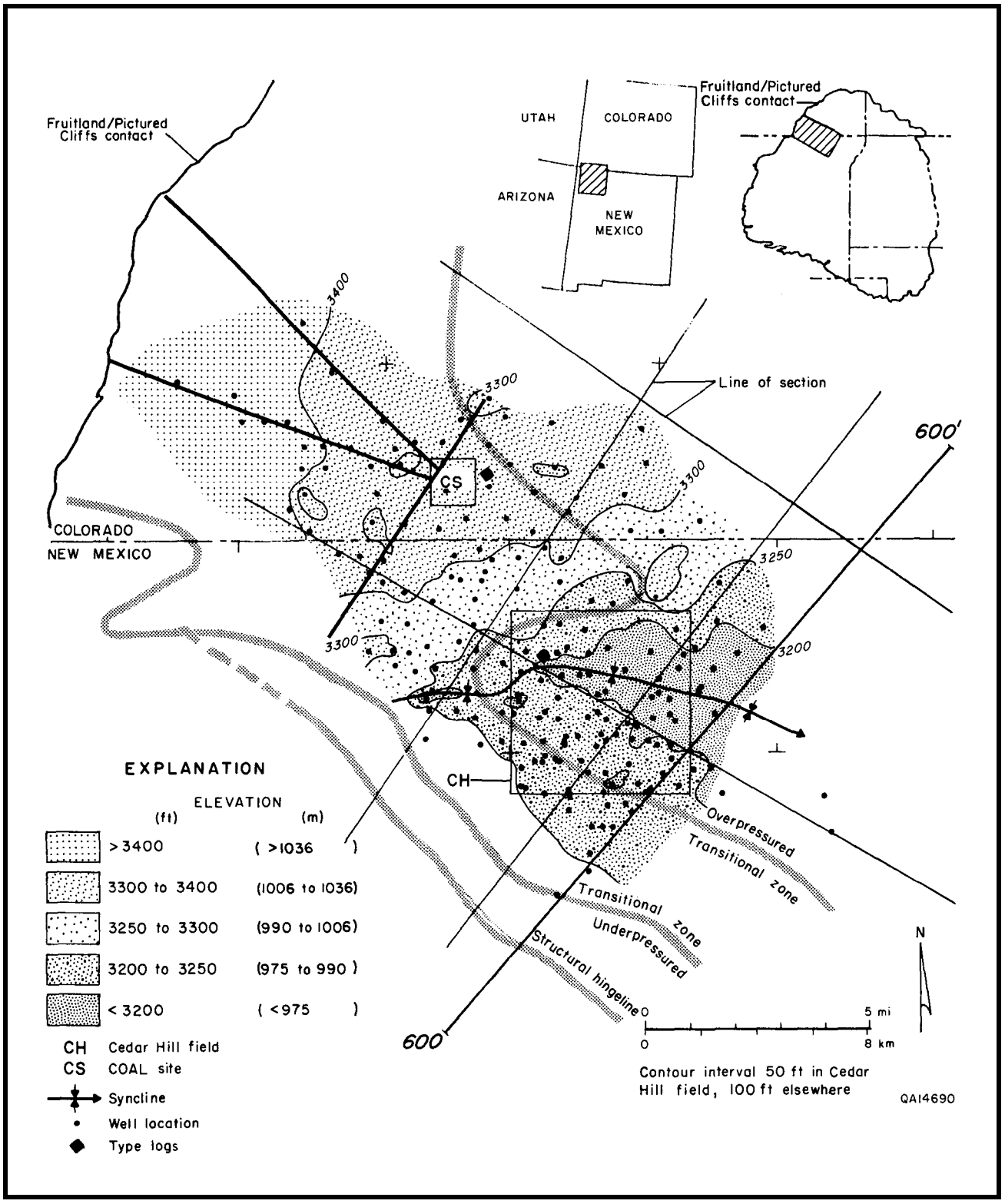

FIGURE 3.4—(a) Structure map of the base of Fruitland coal group A at Cedar Hill field and the COAL site. An east-plunging syncline bisects Cedar Hill field.

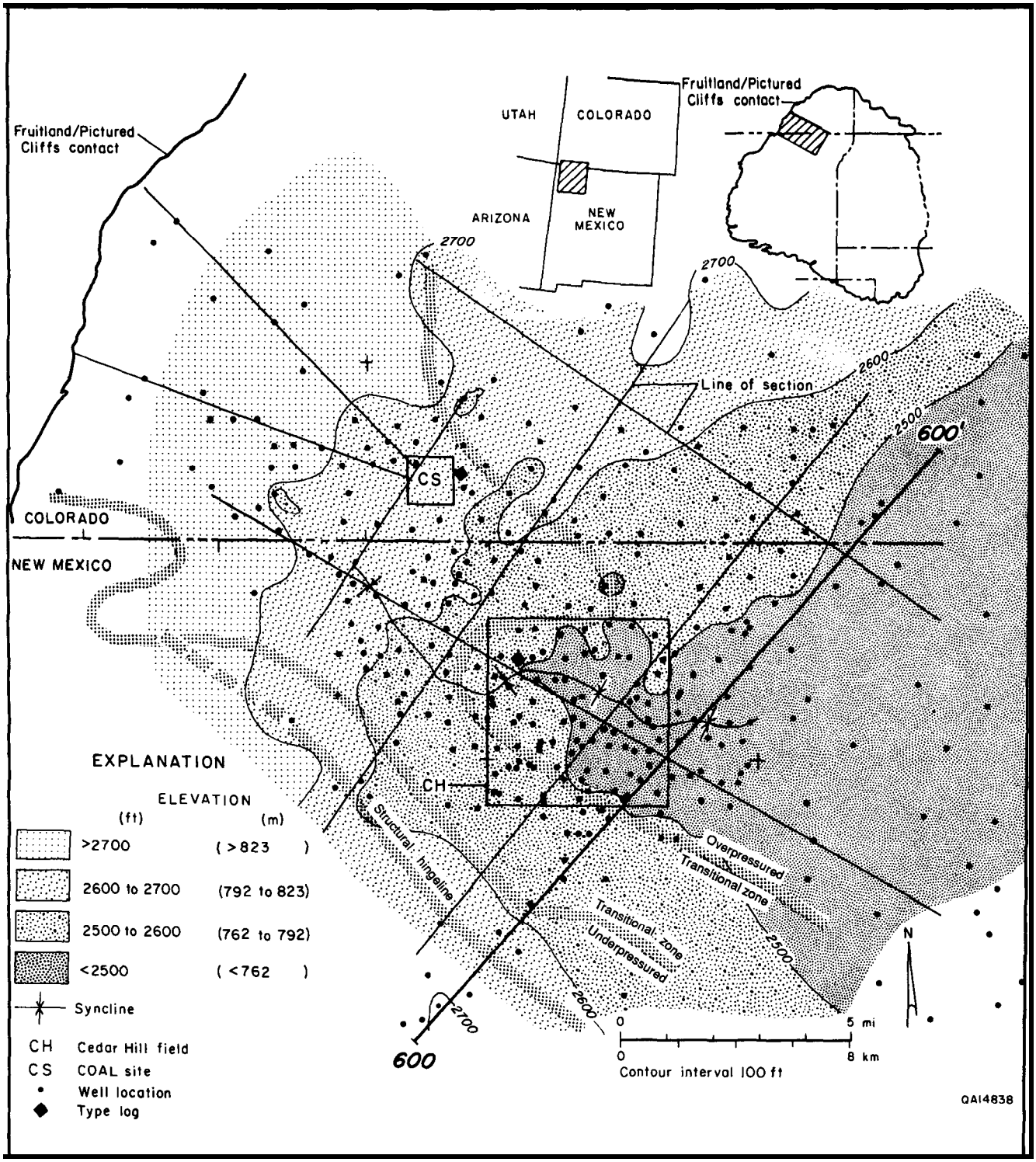

FIGURE 3.4—(b) Structure map of the Huerfanito Bentonite Bed in the Lewis Shale. The synclinal axis at Cedar Hill field is more open in this map than in the structure map of Fruitland coal group A.

downdip (northeastward) to form a strike-elongate sheet north of Cedar Hill field. Net coal thickness is generally less than 40 ft (<12 m) in Cedar Hill field, where coal group C overlies thick LF1 sandstones (Fig. 3.6b). Coal group C is divided into lower, middle, and upper seams that will be described separately.

Lower C coal seams—Lower C coal seams are the thickest seams in group C. They overlie LF1 sandstones at Cedar Hill field and at the COAL site (Fig. 3.2). Two net coalthickness trends (>30 ft [>9 m] of net coal) are present in lower C coal seams (Fig. 3.10a). Dip-elongate (northeast-trending) belts occur south of the COAL site. These belts merge downdip (northeastward) into a strike-elongate sheet. Lower C coal seams overlie thick LF1 channel sandstones over much of the area, but at Cedar Hill field they pinch out against them. These sandstones vary from 20 to 100 ft (6 to 30 m) thick in Cedar Hill field (Fig. 3.6b), producing considerable structural relief on lower C coal seams.

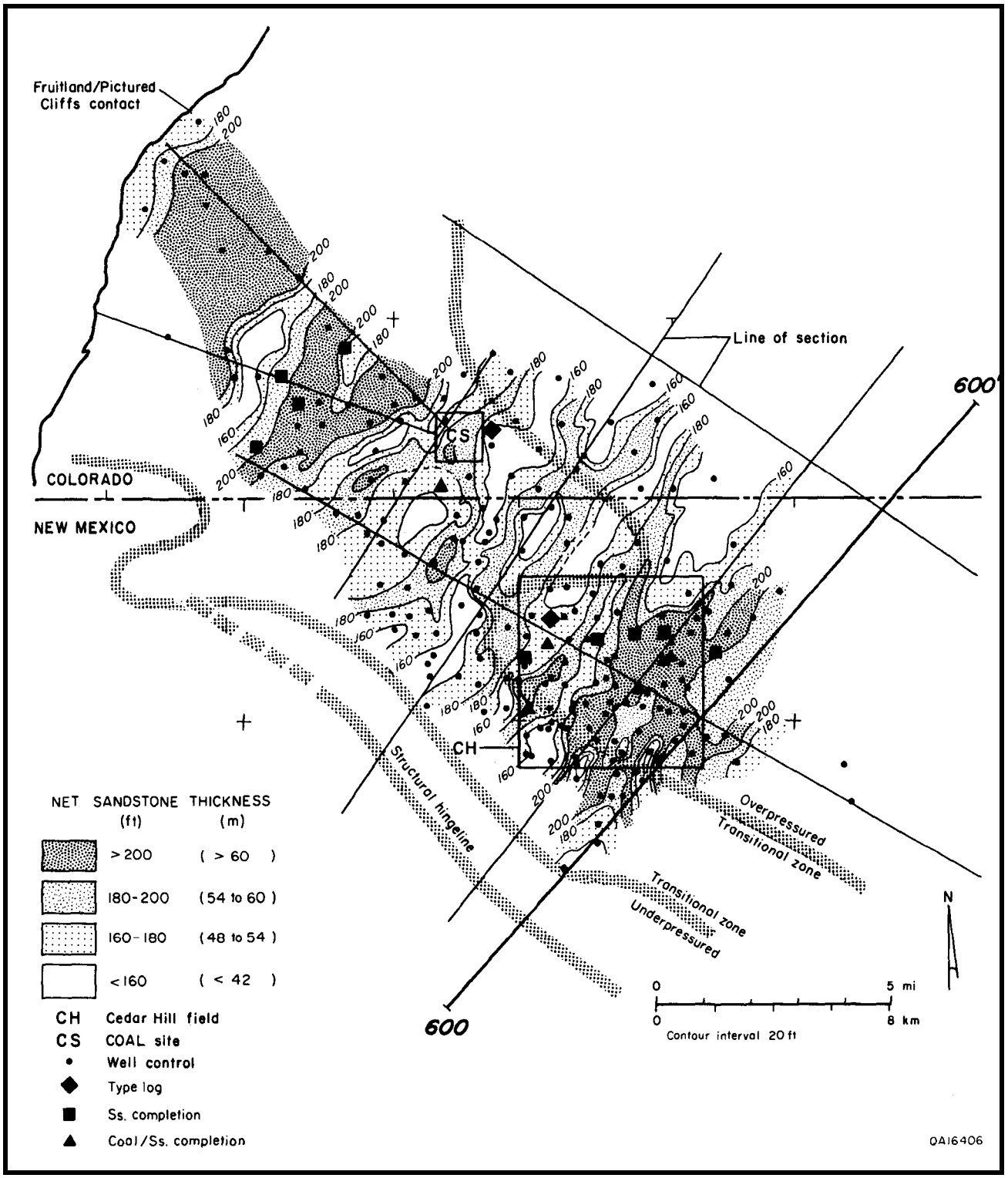

FIGURE 3.5—Sandstone isolith map of the Fruitland Formation. Net thickness of dip-elongate, northeast-trending sandstone bodies exceeds 200 ft (>61 m) near the Fruitland outcrop.

Middle and upper C coal seams—Middle and upper C coal seams (Fig. 3.2) are thin and discontinuous; because of similarities in these two subgroups, only middle C coal seams will be described. Like the lower C seams, middle C seams are absent in the eastern part of Cedar Hill field (Fig. 3.10b). However, there are notable differences in net coal thickness (hence, reservoir continuity) of middle and lower C coal seams at the COAL site. Middle C coal seams are thinner (<10 ft [<3 m] thick) than lower C coal seams that are locally more than 30 ft (>9 m) thick. However, middle C coal seams are more than 40 ft (>12 m) thick near the Fruitland outcrop at the northwestern margin of the basin.

Coal group D

Coal seams in group D are associated with the upper Fruitland subunit (Figs. 3.2 and 3.3). These seams are the thinnest and least continuous coal seams in the Fruitland Formation. They occur in discontinuous, dip-elongate pods with net coal thickness of less than 10 ft (<3 m) at Cedar Hill field and the COAL site (Fig. 3.11a). The net coal thickness of group D coal seams is greatest (>15 ft [>4.6 ml thick) near the Fruitland outcrop.

Group D coal seams are thin, discontinuous, and northeast trending because they formed in an unstable floodplain setting between northeast-trending, upper Fruitland fluvial channels (Fig. 3.7b). Aggradation of the coastal plain resulted in stacked channel-fill sandstones that are locally thicker than 130 ft (>40 m). Channel avulsion and lateral migration resulted in destruction of short-lived peat swamps on unstable floodplains.

Depositional controls on coalbed continuity and structural attitude

The thickness and original continuity of Fruitland coal seams were controlled by depositional environment. In the southwestern part of the study area, thick Fruitland coal seams occur in northeast-trending belts between fluvial channel-fill sandstone complexes, whereas in the northeastern part, they occur in northwest-trending sheet deposits that formed landward of Pictured Cliffs coastal deposits.

Depocenters for Fruitland coal beds (reservoirs) shifted northwestward with time (Fig. 3.11b). Thick coal beds in group A are the main coalbed reservoirs in Cedar Hill field, but these coal beds are thin at the COAL site (Fig. 3.8b), where thick lower C coal beds are the primary coalbed methane target (Fig. 3.10a). Fruitland coal beds vary considerably in thickness across the basin, and although they collectively are an integrated, regional reservoir, individual beds may be in poor hydraulic communication locally. Stratigraphic studies of these coal beds are required to (1) delineate limits of individual reservoirs and (2) evaluate locations and spacing of coalbed methane wells.

The relationship between sandstone LF1 and lower C coal seams is an example of sandstone-body control on the extent and thickness of coal seams. Lower C coal seams have an inverse thickness relation to underlying LF1 sandstones. At Cedar Hill field, these seams thin and pinch out over thick (>40 ft [>12 m]) LF1 sandstones. Conversely, at the COAL site, where lower C coal seams are thick (locally >30 ft [>9 m]), LF1 sandstones are thin (<5 ft (<1.5 m]).

Coal seams overlying channel-fill sandstones are the result of peat having accumulated over antecedent, abandoned-channel complexes, whereas coal seams that underlie channel-fill sandstones represent subsequent channel avulsion that redirected streams into swamps. Where they override and underlie lenticular sandstone bodies, coal seams commonly are folded because of differential compaction of sandstones and adjacent mudstones and coal beds. Such compactional folding of coal beds may cause fractures (Donaldson, 1979; Houseknecht and Iannacchione, 1982) that enhance coalbed permeability.

At Cedar Hill field and the COAL site, coal seams occur above or below channel-fill sandstone complexes that are less than 2,000 ft (<610 m) wide. Changes in structural attitude of overriding coal seams can be abrupt. In a cross section located near the northwestern margin of the basin, stratigraphic relief on Fruitland coal seams is as great as 60 ft (18 m) where coal seams underlie or override thick (up to 80 ft [24 m]) channel sandstones (Fig. 3.12). The significance of continuous coal seams that override and underlie sandstones but are sharply folded at facies boundaries is twofold: (1) coal seams (methane reservoirs) are more laterally extensive than inferred by previous workers, and (2) folding-induced fractures, and therefore enhanced coalbed permeability, may occur where coal seams are associated with sandstone complexes.

Controls on coalbed permeability

Permeability in coal beds is controlled by the intensity and interconnectedness of fractures. The orientation of coalbed cleats (fractures) is determined by regional stresses present during coalification. At Cedar Hill field, face cleats (dominant fracture) trend northeastward (Tremain and others, this volume, Chapter 5). Also, Cedar Hill field is bisected by a synclinal axis (Ayers and others, this volume, Chapter 2). Coal beds in this east-plunging syncline (Fig. 3.4) are folded, and therefore may have high fracture intensity and enhanced permeability. Coalbed continuity in the Cedar Hill field area is partly controlled by the structural hingeline of the basin, which is inferred to consist of a complex of northwest-trending normal faults. Individual faults in this complex offset coal beds by as much as 40 ft (12 m).

Formation pressure

In the San Juan Basin, the Fruitland Formation is abnormally pressured relative to the fresh-water hydrostatic gradient (0.433 psi/ft). The north-central part of the basin is overpressured, whereas much of the rest of the basin is underpressured (Kaiser and others, this volume, Chapter 8). Because Fruitland overpressuring is due to artesian conditions, most overpressured coalbed methane wells are water productive. The pressure gradient at Cedar Hill field, which is located near the southwestern margin of regional Fruitland overpressuring, is approximately 0.50 psi/ft. At Cedar Hill field, the southwest boundary of overpressured Fruitland strata conforms to a synclinal fold (Fig. 3.4). The transition between overpressured and underpressured Fruitland strata is marked by pronounced steepening of the potentiometric surface and potential for upward flow (Kaiser and others, this volume, Chapter 8). High productivity from overpressured Fruitland coal beds near the transition zone may reflect potential for upward flow and free gas in conventional stratigraphic traps along the southwestward pinch-out of aquifer coal beds.

Coalbed methane resources

The Cedar Hill field area contains some of the highest gas-in-place values of the Fruitland Formation (>25 Bcf/mi^2) in the San Juan Basin. This high gas resource reflects the presence of thick coal beds, high coal rank, and high formation pressure (Ayers and others, this volume, Chapter 2). Cedar Hill field is in a transitional area where gas-inplace values range from 15 to 25 Bcf/mi^2. This range reflects the change from the locally thick, northeast-trending fluvial floodplain coal deposits in the southern part of the basin to the extensive, thick, northwest-trending delta-plain and back-barrier coal deposits in the northern part of the basin.

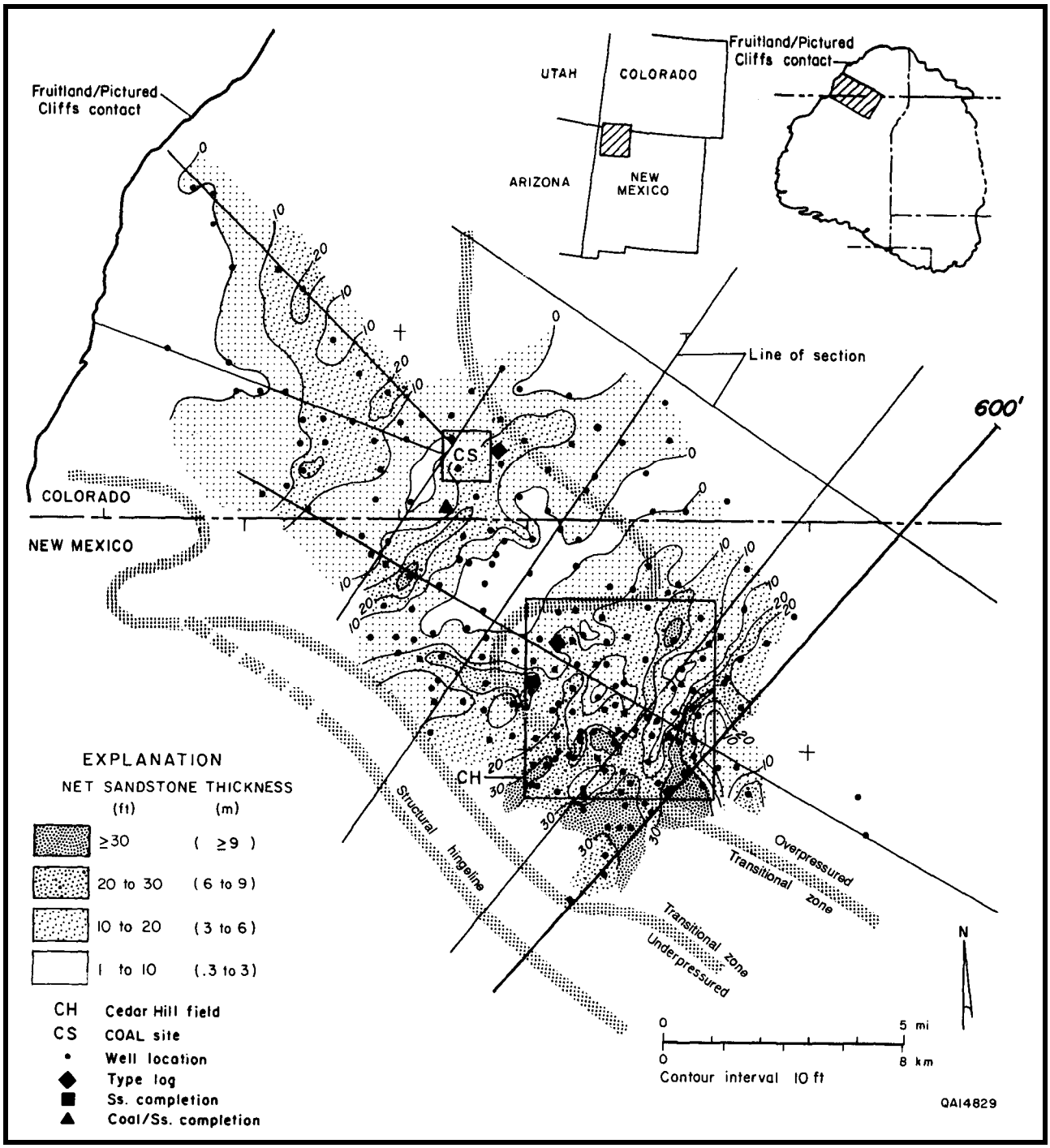

FIGURE 3.6—(a) Sandstone isolith map of the part of lower Fruitland subunit associated with coal group A. Multiple, dip-elongate sandstone bodies are more than 30 ft (>9 m) thick.

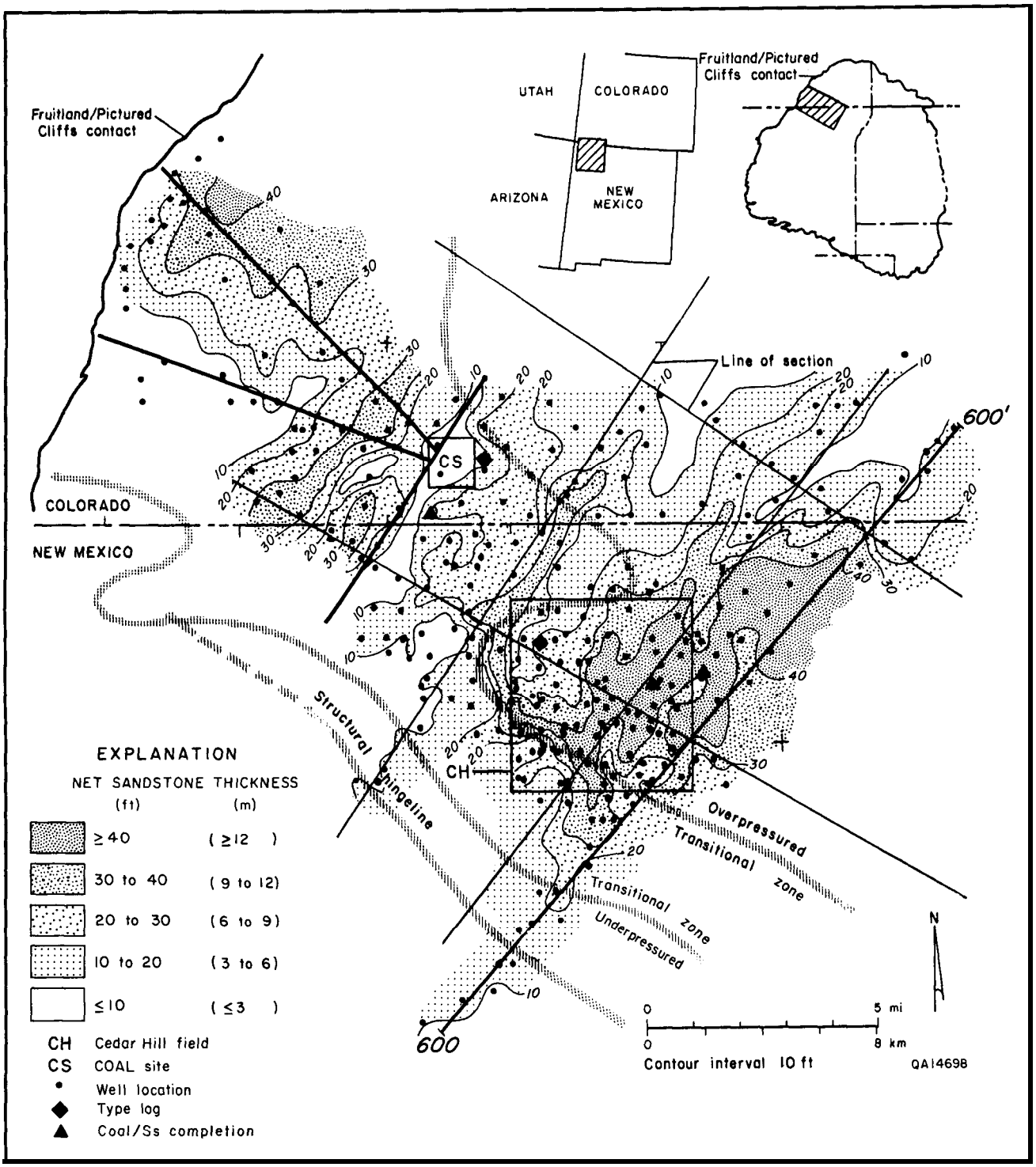

FIGURE 3.6—(b) Sandstone isolith map of lower Fruitland sandstone LF1. Deltaic depocenter at Cedar Hill field is defined by dip-elongate sandstone bodies that are locally more than 40 ft (>12 m) thick.

Gas production trends

The most productive coalbed methane wells in the San Juan Basin are completed in overpressured Fruitland coal beds along the southwestern margin of the overpressured region (Kaiser and others, this volume, Chapter 8). This highly productive trend occurs in thick, northwest-trending Fruitland coal beds of delta-plain and back-barrier origin and includes Cedar Hill field. In this northwest-trending belt, highest production (>1,000 Mcf/d) is in locally occurring, northeast-trending pods that reflect the presence of thick, interchannel coal beds.

Production at Cedar Hill field reflects the northeastward trend of coal beds and channel-fill sandstones (Fig. 3.13). Individual coalbed methane wells in the field typically produce 300 to more than 1,000 Mcf/d. In 1980, the average coalbed gas production per well at Cedar Hill field was approximately 600 Mcf/d; by 1990, average well production had increased to 1,000 Mcf/d. Northeast-trending belts of high production (maximum production more than 1,500 Mcf/d) in the southwestern part of the field coincide with thick (locally >30 ft [>9 m]) lower Fruitland coal beds (coal group A; Fig. 3.8b). In contrast, low production (maximum

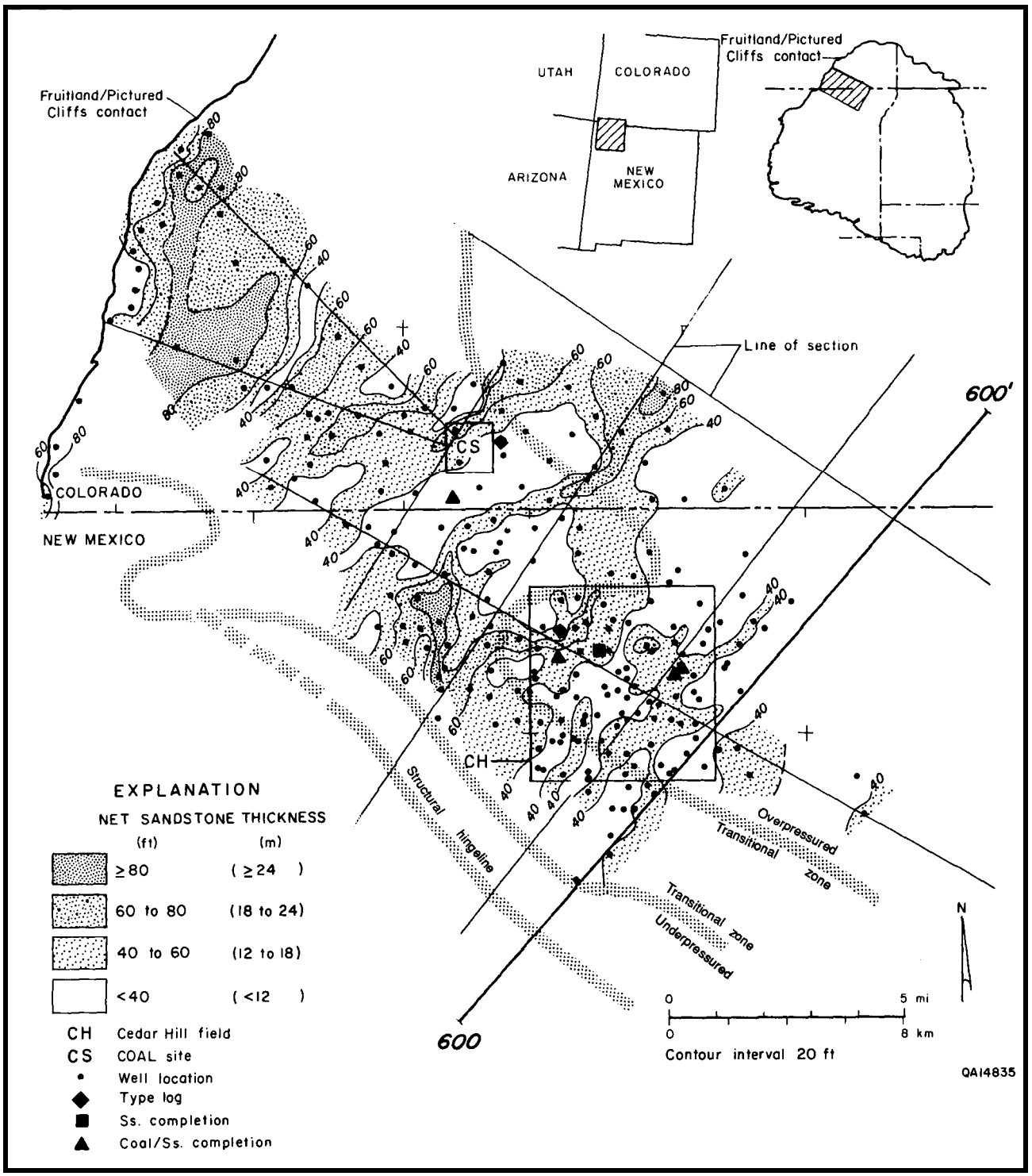

FIGURE 3.7—(a) Sandstone isolith map of the middle Fruitland subunit.

production <500 Mcf/d) in the southeastern part of Cedar Hill field coincides with thin coal beds in coal groups A and C (Figs. 3.8b and 3.9). The most productive wells (maximum production >1,800 Mcf/d) are on the southern flank of the synclinal axis in the eastern part of Cedar Hill field (Fig. 3.13), where folding may have caused fracture-enhanced permeability.

Water production

Overpressured wells in Cedar Hill field commonly produce water, requiring disposal of brines and adding to operation costs. Areas of greatest water production (20 to 152 bbls/d) in Cedar Hill field occur in central and eastern areas along the syncline that bisects the field. Wells in Cedar Hill field are still dewatering; in 1980 the average water production per well was approximately 200 bbls/d. By 1990, average water production had declined to 20 bbls/d per well.

Conclusions

1. At Cedar Hill field and the COAL site, four Fruitland coal groups occur in three Fruitland depositional subunits. The characteristics of coal seams in these groups reflect their depositional setting and associated clastic facies geometry and continuity. The thickest, most continuous coal seams occur in the lower and middle Fruitland subunits; these seams (coal groups A and C) formed in delta-plain and

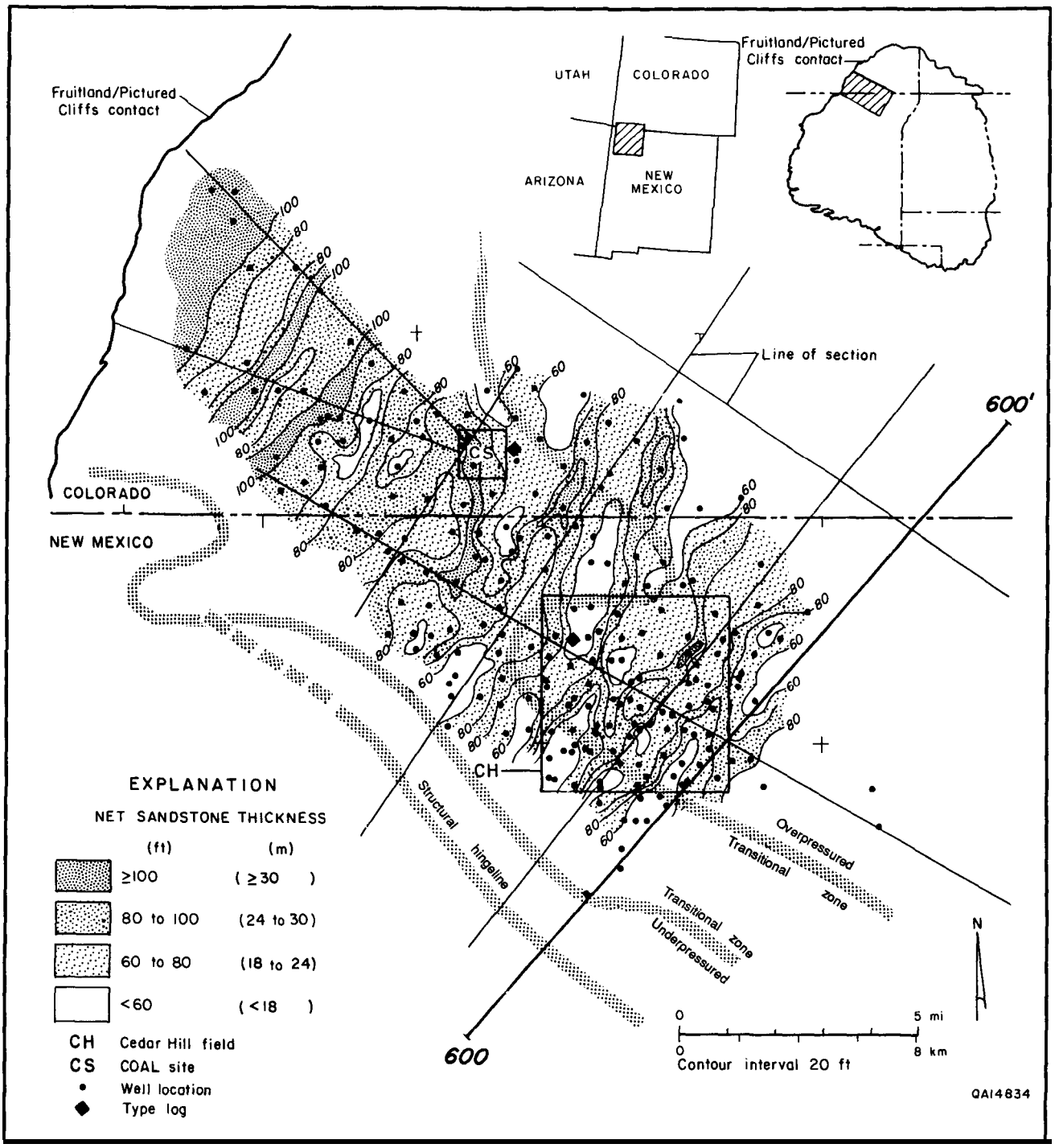

FIGURE 3.7—(b) Sandstone isolith map of the upper Fruitland subunit.

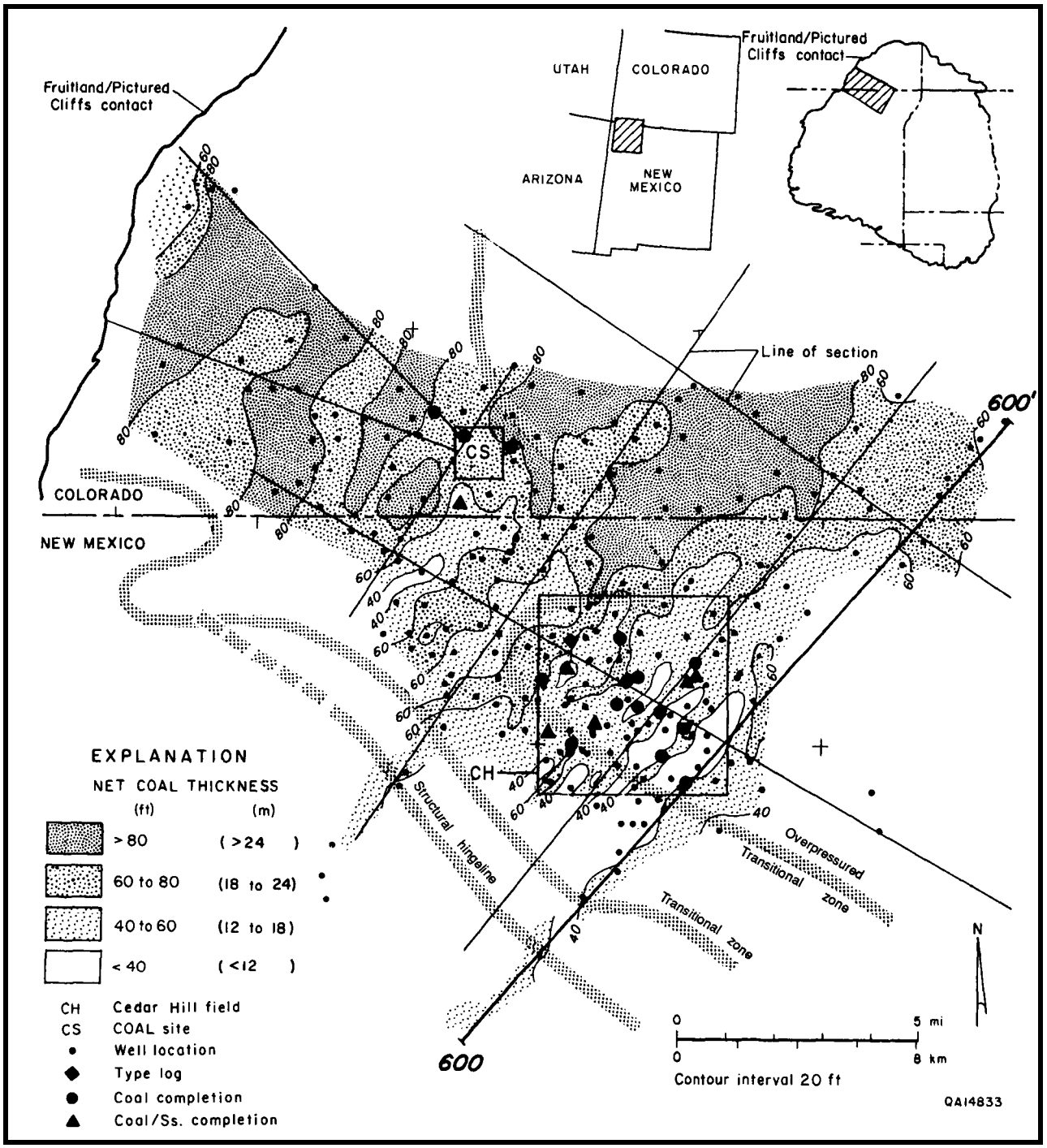

FIGURE 3.8—(a) Coal isolith map of the undivided Fruitland Formation. Dip-parallel deposits of more than 80 ft (>24 m) of coal broaden and merge downdip of Cedar Hill field and the COAL site.

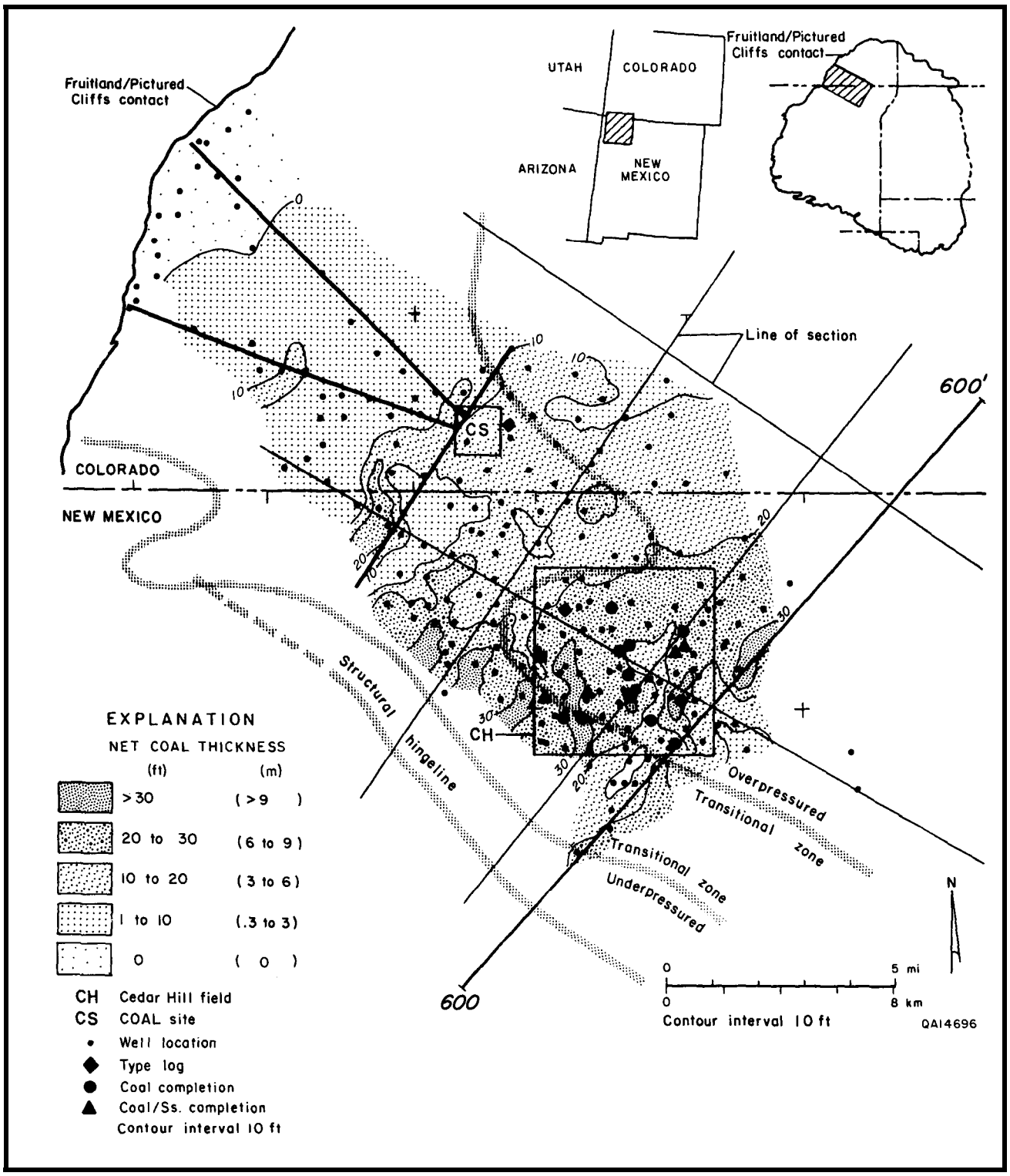

FIGURE 3.8—(b) Coal isolith map of Fruitland coal group A, the thickest coal group at Cedar Hill field.

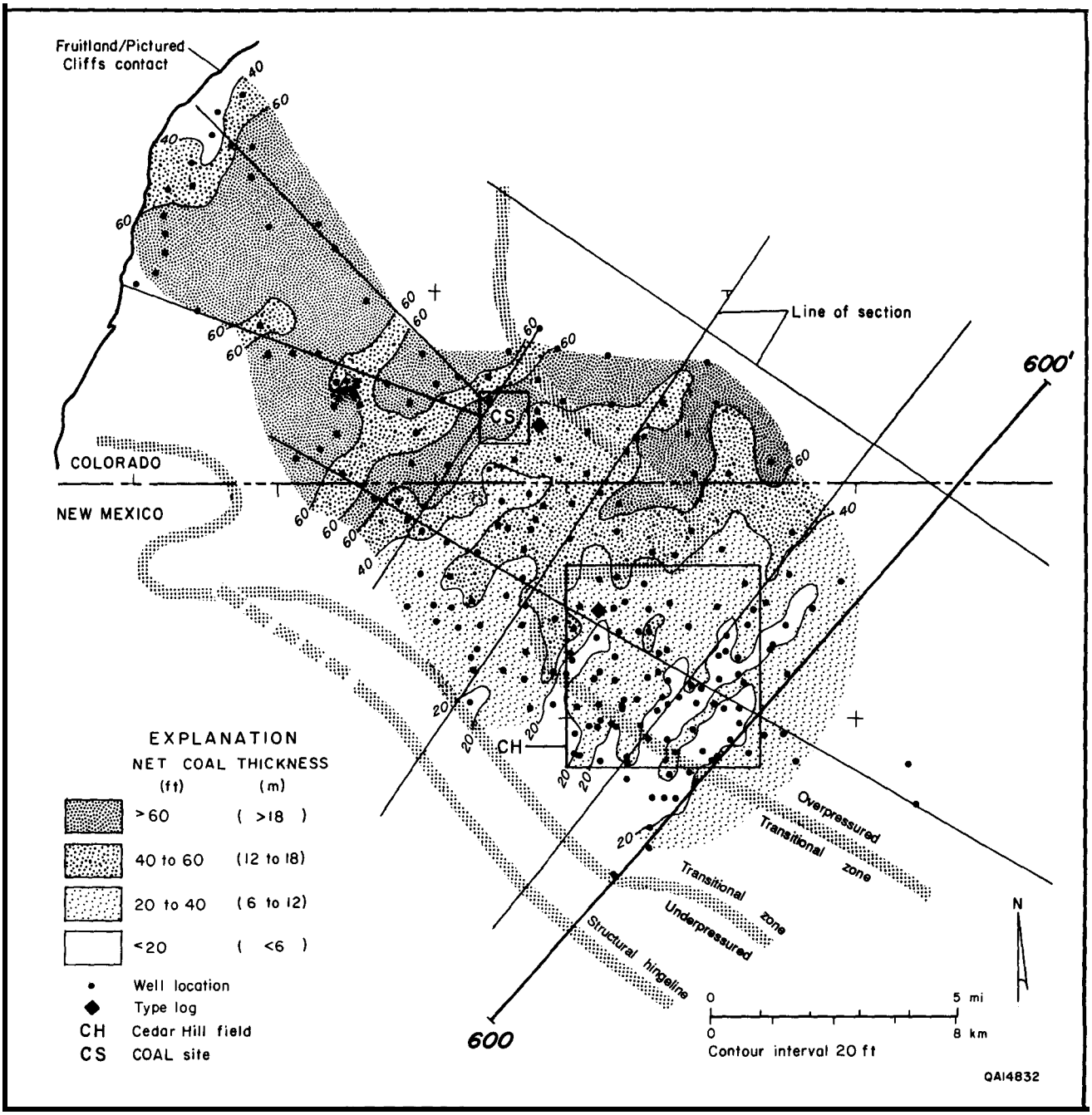

FIGURE 3.9—Coal isolith map of the undivided coal group C at Cedar Hill field and the COAL site.

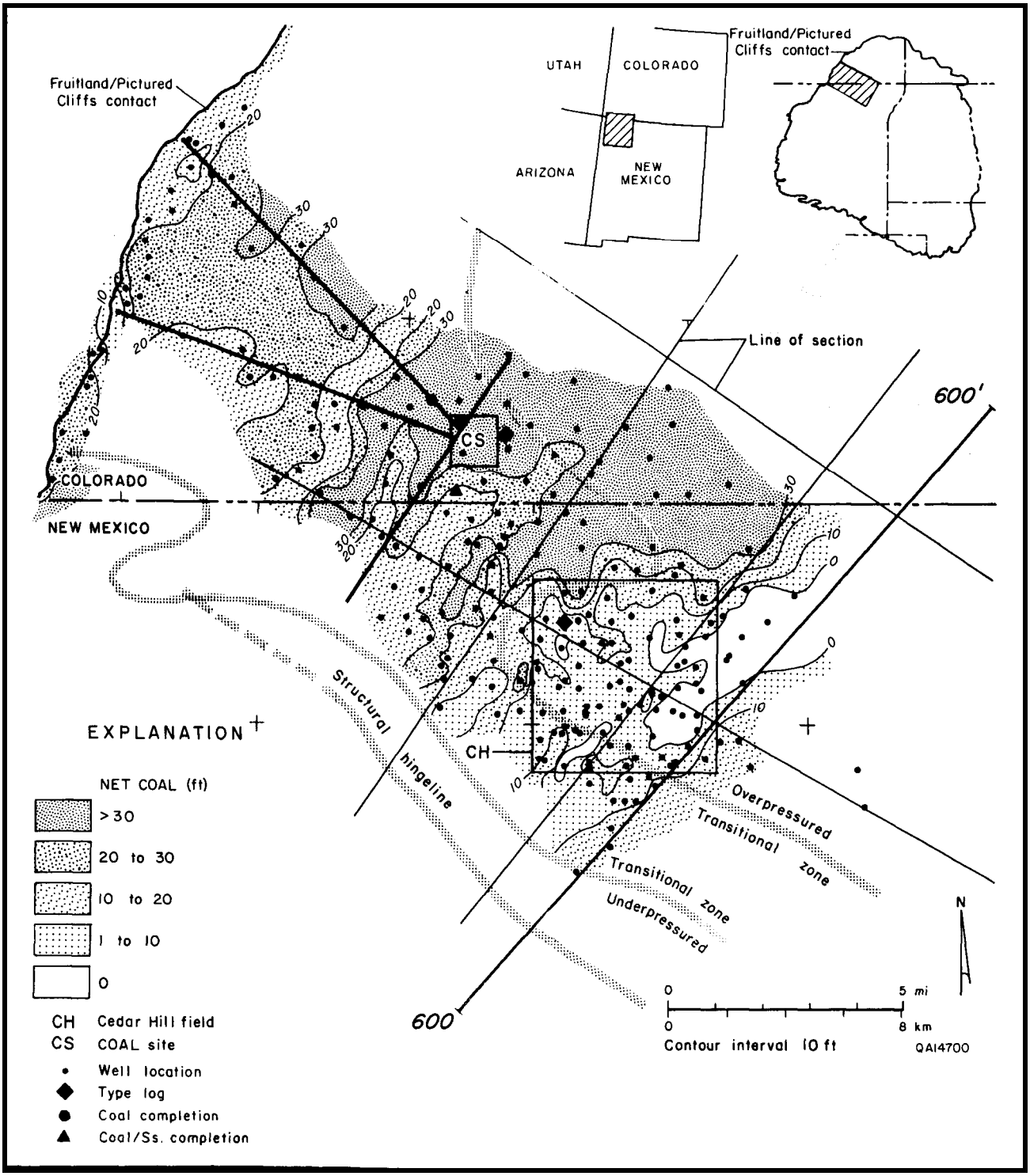

FIGURE 3.10—(a) Coal isolith map of lower C coal seams in Cedar Hill field and the COAL site. Lower C coal seams are absent over thick LF1 sandstones (Fig. 3.6a) in the eastern part of Cedar Hill field.

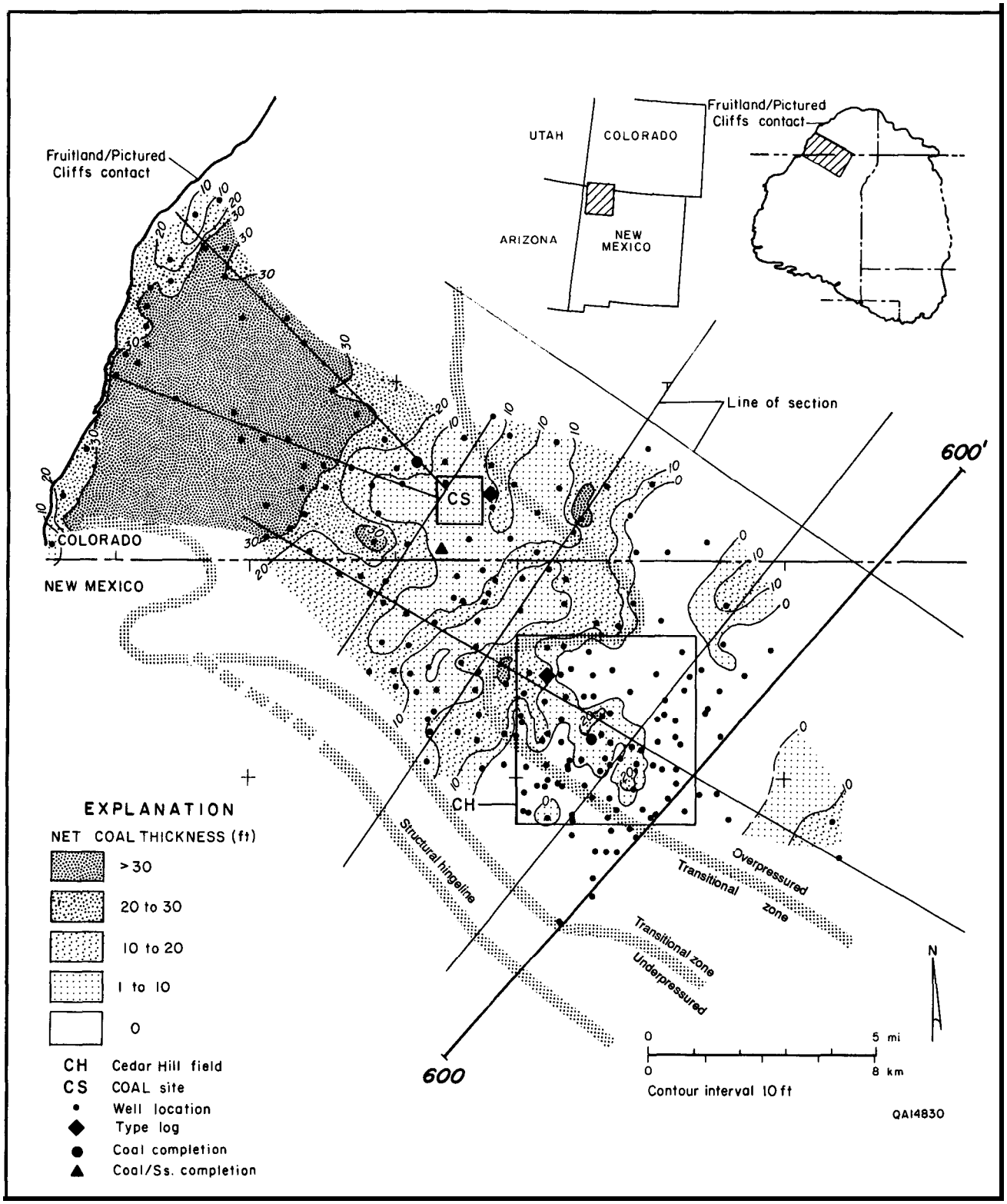

FIGURE 3.10—(b) Coal isolith map of middle C coal seams. Net coal thickness of middle C coal seams is less than that of lower C coal seams at the COAL site. However, middle C coal seams thicken northwestward toward the Fruitland outcrop.

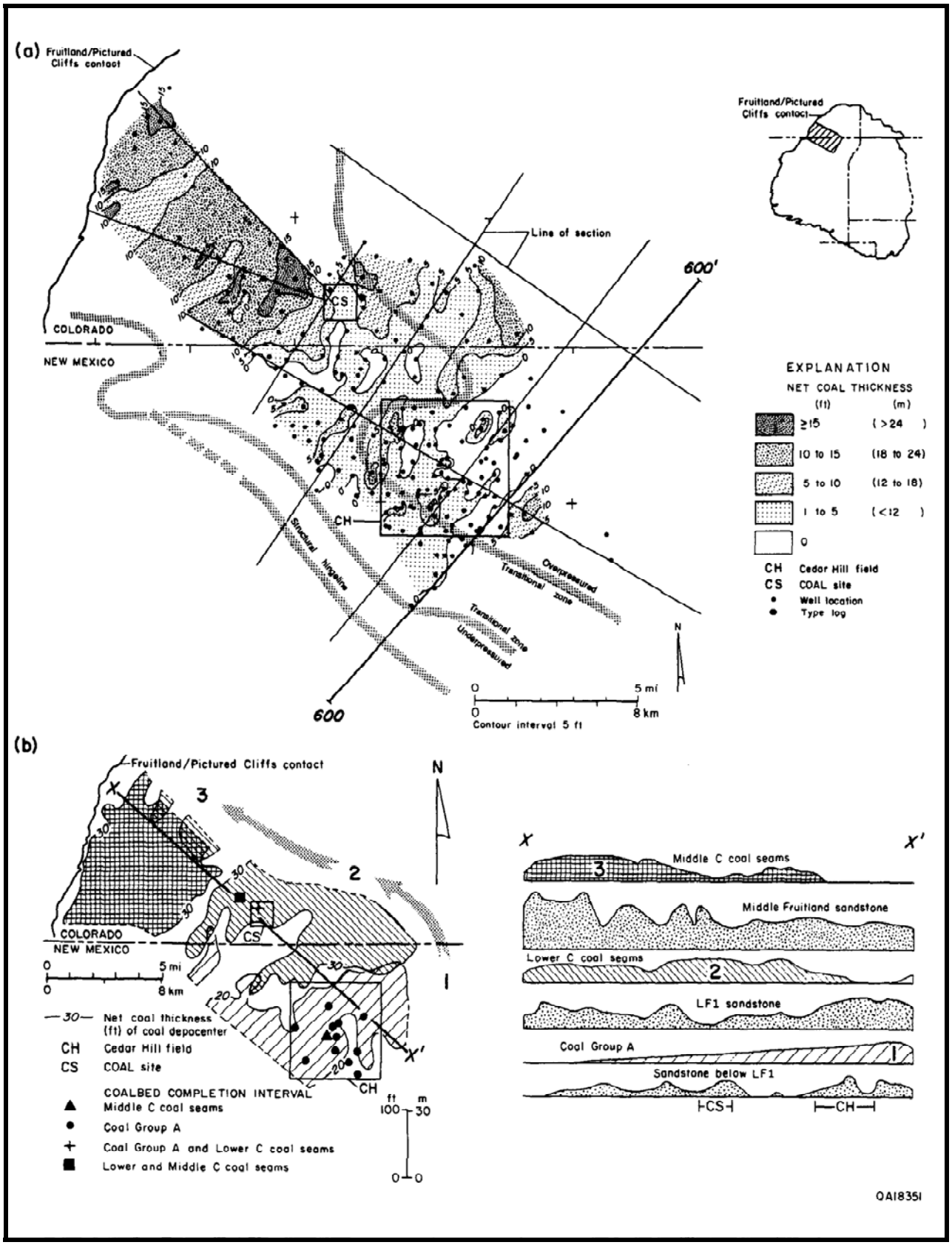

FIGURE 3.11—(a) Coal isolith map of coal group D in the upper Fruitland subunit. (b) Fruitland coal depocenters (coal groups A, lower C, and middle C) and well distribution by coalbed completion interval at Cedar Hill field and the COAL site. Coal depocenters, defined by area of greatest net coal thickness, shifted northwestward with time. Net thickness of lower C coal beds is inversely related to thickness of underlying Fruitland sandstone, LF1.

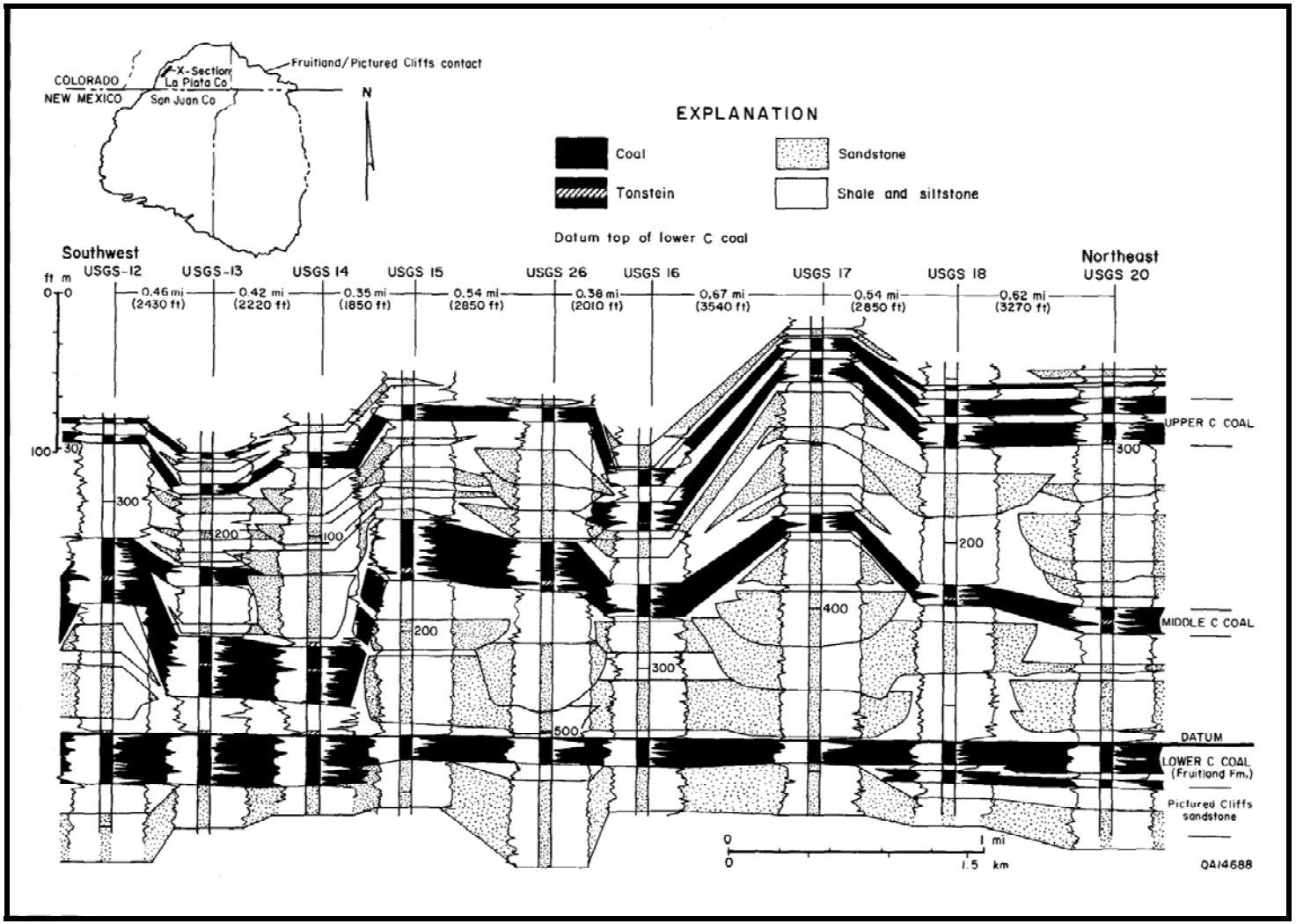

FIGURE 3.12—Stratigraphic dip section in the shallow subsurface near the Fruitland outcrop belt in the northwestern part of the San Juan Basin, illustrating complex Fruitland coalbed and sandstone architecture. Coal seams are complex reservoirs where they overlie, underlie, or pinch out between channel-fill sandstones. Data from Roberts (1989).

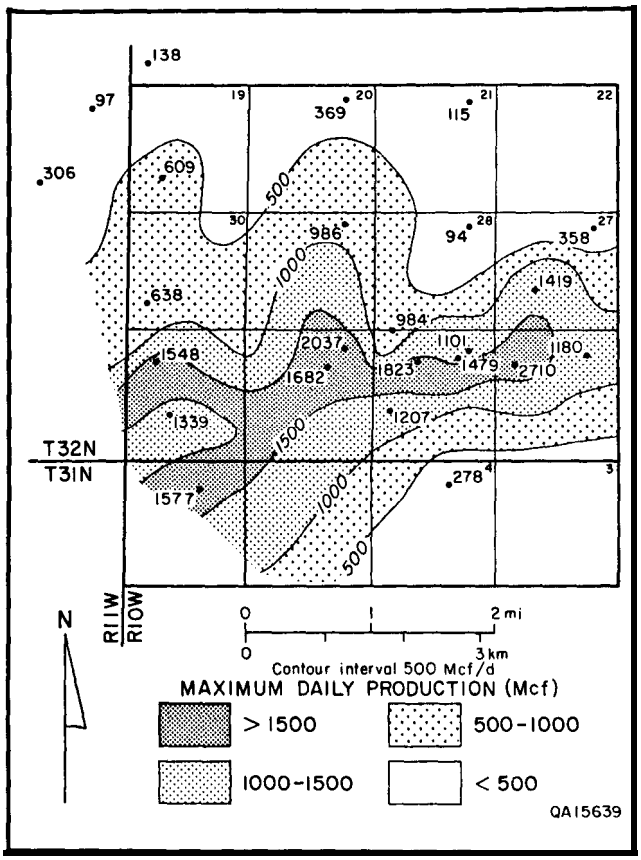

FIGURE 3.13—Fruitland coalbed methane production at Cedar Hill field. Values are average daily production (Mcf/d) in the well's most productive year.

lower alluvial-plain settings associated with seaward-stepping, shallow-marine facies tracts. Seams in coal groups A and C are continuous and commonly override and underlie channel-fill sandstone bodies. In contrast, upper Fruitland coal beds (coal group D), as a result of having formed in an unstable floodplain setting far landward of the Pictured Cliffs coastline, are thin and discontinuous and commonly pinch out against channel-fill sandstone bodies.

2. Lower and middle Fruitland coal groups (groups A and C) are not equally well developed in the northwestern part of the San Juan Basin because they formed in local depocenters on the Fruitland coastal plain. At Cedar Hill field, the thickest and most extensive coal seams occur in group A, but these seams pinch out near the northwestern margin of the basin. At the COAL site, seams are best developed in coal group C, which is thin or absent to the southeast, at Cedar Hill field.

3. Increased fracture intensity, and therefore enhanced coalbed permeability, may occur where coal seams are folded. Tectonic folding has formed synclines at Cedar Hill field and the COAL site. Also, many lower and middle Fruitland coal seams are folded where they underlie and overlie northeast-trending channel-fill sandstone complexes. Locally, structural relief on Fruitland coal seams at Cedar Hill field and the COAL site is more than 40 ft (>12 m) because of offset by faults and differential compaction adjacent to less compactible sandstones.

4. Cedar Hill field is located at the southwestern margin of regionally overpressured Fruitland strata. The northwest-trending structural hingeline south of Cedar Hill field nearly coincides with the overpressure/underpressure boundary. The hingeline may result from a northwest-trending fault complex that offsets overpressured, water-saturated coal beds in the northern part of the basin from underpressured, predominantly gas-saturated coal beds in the southern part of the basin.

5. Coalbed gas occurrence and producibility in Cedar Hill field are primarily controlled by the coupled relationship between sandstone and coal facies in a coastal-plain setting; productivity trends are dominantly northeast-trending in the field and coincide with thick, northeast-trending coal beds that formed in interchannel areas. Other coalbed methane production trends in the area are controlled by structure; a high-productivity trend occurs along a syncline that bisects Cedar Hill field. Coalbed permeability may also be enhanced where coal beds are locally fractured because of differential compaction.

Acknowledgments

This manuscript benefited from reviews by Mike Gardner, Jay C. Close, Richard C. Klem, Tucker F. Hentz, and Andrew Scott. Dwight's Energydata, Inc., provided gas and water production data.

4. Coalbed methane in the Fruitland Formation, Navajo Lake area: geologic controls on occurrence and producibility

W. B. Ayers, Jr., and S. D. Zellers

Bureau of Economic Geology

Abstract—The most productive coalbed methane wells in the United States, with production commonly greater than 250 Mcf/d per well, occur in the Navajo Lake area. Coal-occurrence, lithofacies, structure, and isopach maps were made to clarify geologic controls on coalbed methane resources and producibility in this area. Structural activity and depositional systems controlled coal occurrence. The thickest coal deposits trend northwestward and occur in a back-barrier setting; increased subsidence north of a structural hingeline created accommodation space and initiated a shoreline stillstand, allowing thick, strike-elongate peat deposits to form. Individual coal beds are dip elongate but laterally continuous, pinching and swelling in the paleostrike direction. Coal beds are the major aquifers in the Fruitland; they are more permeable than adjacent Fruitland and Pictured Cliffs sandstones. Therefore, coalbed geometry and extent control hydrologic and reservoir conditions in the Fruitland Formation. Structural features in Fruitland coal beds are both tectonic and compactional in origin; minor folds are common. Structural attitude of coal beds is unique to each coal bed. High productivity from coalbed methane wells in the Navajo Lake area is attributed to presence of thick coal beds (reservoir rock), Fruitland hydrodynamics, and enhanced coalbed permeability, possibly because of folding-induced fractures.

Introduction

Geologic controls on coalbed methane occurrence and producibility commonly are more complex than is apparent from regional studies. Therefore, we used closely spaced data to study these controls in the Fruitland Formation at Navajo Lake in northern San Juan and Rio Arriba Counties, New Mexico (Ayers and others, this volume, Fig. 2.5). This area, encompassing 215 mi^2 (557 km^2) and including the Northeast Blanco Unit and the Meridian 400 coalbed methane wells, was selected because it (1) contains some of the thickest Fruitland coal beds in the San Juan Basin, (2) contains two upper Pictured Cliffs sandstone tongues that bound the thick coal, causing a major stratigraphic rise of the Pictured Cliffs, (3) has the most productive coalbed methane wells in the basin and a history of coalbed methane production extending from the early 1950s, and (4) has no major structural features in the area that might contribute to the high productivity.

Objectives

The objectives of this study were to (1) evaluate the structural evolution of the San Juan Basin as it applies to the distribution and maturation of Fruitland coal, (2) define depositional systems and evaluate the interconnectedness of depositional framework (sandstone) facies, (3) define the occurrence and continuity of coal seams and evaluate framework facies control on coal occurrence, geometry, and trends, (4) identify structural features that may enhance coal permeability or affect coalbed continuity, and (5) relate coalbed methane reservoir conditions to the geologic and hydrologic settings.

Methods

The primary data used for this study were approximately 400 geophysical well logs from oil and gas tests. Geophysical logs were used to make 10 interlocking cross sections, and all remaining logs were correlated to those sections. Structure, isopach, lithofacies, and coal data from the logs were tabulated in computer files and were used to make computer-contoured maps and to post data for hand contouring. The cross sections and maps were then evaluated to interpret geologic controls on the occurrence and producibility of coalbed methane.

Regional geologic setting and stratigraphy

During the Late Cretaceous, the region of the present San Juan Basin was on the western margin of the Western Interior seaway (Tremain and others, this volume, Fig. 5.2). In the Late Cretaceous (Campanian), the coastline migrated northeastward, resulting in deposition of a vertical succession of shelf (Lewis Shale) through coastal (Pictured Cliffs Sandstone) to coal-bearing continental sediments (Fruitland Formation) (Fig. 4.1).

The contact between the Pictured Cliffs Sandstone and the Fruitland Formation (Fig. 4.1) was placed at the top of the massive coastal sandstone complex below the lowermost Fruitland coal; because the shoreline migrated basin-ward, this boundary is time-transgressive. The Fruitland–Kirtland contact was placed at a high-conductivity peak that occurs in a shale at the top of an upward-fining Fruitland sequence (Fig. 4.1). This shale is inferred to be the base of the regionally extensive lower Kirtland shale, which may have formed as a consequence of a short-lived marine transgression over the Fruitland coastal plain. The Kirtland Shale (Campanian/Maastrichtian) conformably overlies the Fruitland Formation and is unconformably overlain by the fluvial Ojo Alamo Sandstone (Paleocene). For a more detailed stratigraphic review, see Ayers and others (this volume, Chapter 2).

Structural evaluation

Structural activity has impacted the availability and producibility of coalbed methane in four ways: (1) syndepositional structural activity influenced depositional systems and, hence, coal occurrence, (2) the structural development of the San Juan Basin affected the burial depth and thermal maturity of Fruitland coal seams, (3) structural deformation caused fractures that may offset the coal beds (reservoirs), and (4) minor folds formed structural traps, and fractures that formed during folding may enhance coalbed permeability.

Structure of Huerfanito Bentonite Bed

The Huerfanito Bentonite Bed, present in the Lewis Shale throughout much of the basin (Fassett and Hinds, 1971), was used as a structural horizon and as a boundary for isopach maps. To delineate the presence of structural fea-

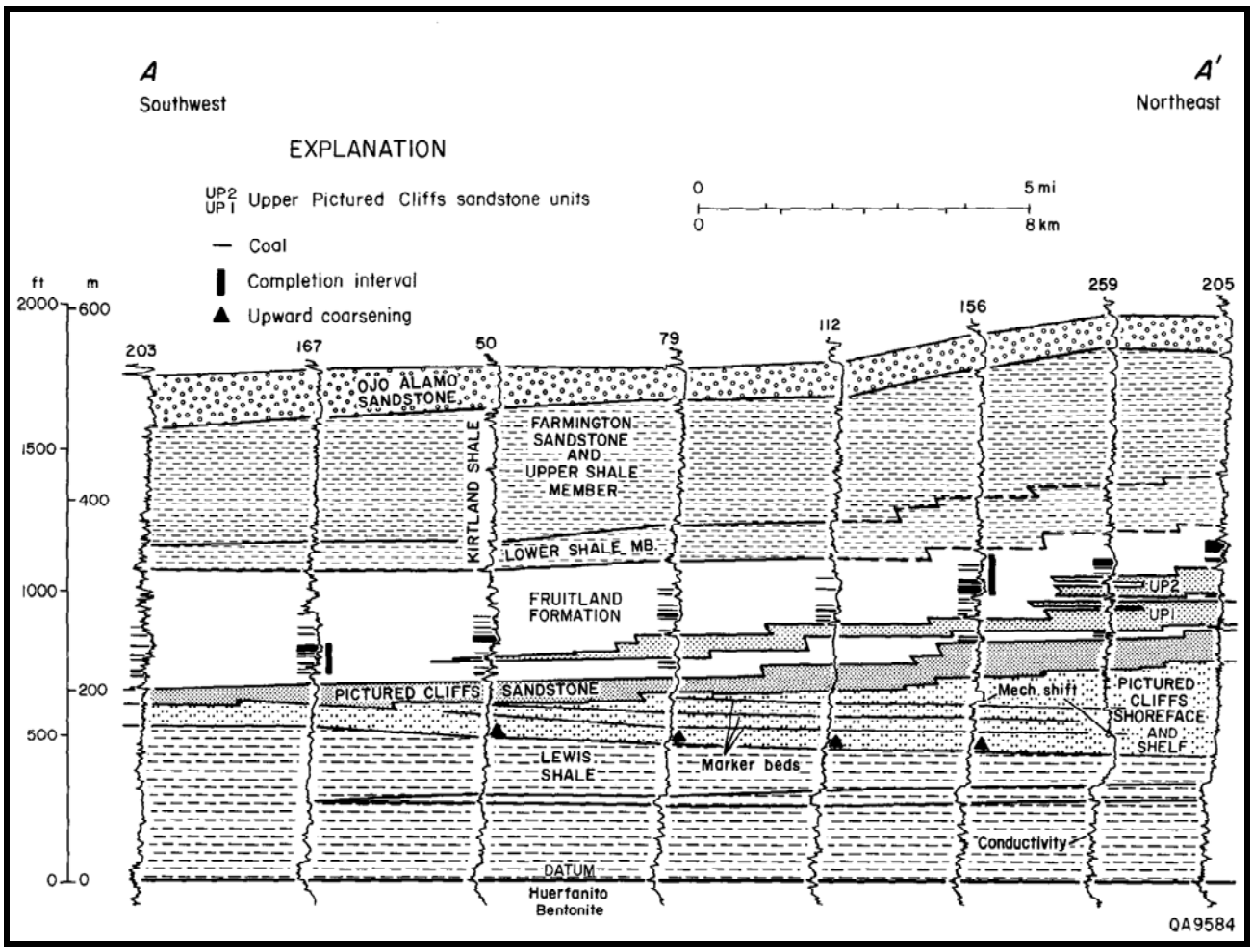

FIGURE 4.1—Stratigraphic cross section A–A'. The coal-bearing Fruitland Formation is a coastal plain unit deposited landward (southwest) of the regressive Pictured Cliffs Sandstone that prograded into the Western Interior seaway. Thick coal seams in the northeast that overlie upper Pictured Cliffs sandstones (UP1 and UP2) are stratigraphically higher than thick seams in the southwest. See Fig. 4.2 for location.

tures that may affect the continuity of Fruitland coal seams, we made a computer-contoured structure map of the Huerfanito Bentonite. In the Navajo Lake area, structural relief on the Huerfanito Bentonite is 450 ft (135 m) (Fig. 4.2). A major synclinal axis in the San Juan Basin crosses the northeast quarter of the area, approximately 7 mi (11 km) north of the Meridian wells. South of the synclinal axis, an anticline, centered in T30N and T31N, R7W, has 75 to 100 ft (22 to 30 m) of structural relief and plunges northward toward the syncline. It is flanked on the west by a northward-plunging syncline with similar amplitude, and on the east by a series of lower amplitude, northeast-plunging folds. Minor faults (displacements less than 50 ft [<15 m]) are inferred in some areas where structural relief changes abruptly, and faults are documented in some well logs. The northwest-trending structural hingeline of the basin (Ayers and others, this volume, Chapter 2) crosses the southern part of the area, 1 to 5 mi (1.6 to 8 km) south of the Meridian wells (Fig. 4.2). This hingeline is inferred to be a diffuse, complex zone of northwest-trending faults.

Elevation of Pictured Cliffs Sandstone and top of the Fruitland Formation

Throughout the San Juan Basin, the most prospective coalbed methane reservoirs are thick lower Fruitland coal seams. The elevation of the top of the Pictured Cliffs Sandstone (Fig. 4.3) was mapped because it immediately underlies these thick coal beds, whereas the Huerfanito Bentonite Bed is 675 to 850 ft (205 to 260 m) below the Fruitland in the study area. Although this is not a true structure map because the Pictured Cliffs Sandstone is time-transgressive, the map shows, with minor differences, the structural features delineated in the Huerfanito Bentonite map (Fig. 4.2), confirming that most structural features in the Navajo Lake area postdate deposition of the Pictured Cliffs Sandstone. A structure map of the top of the Fruitland Formation also has several major features in common with the Huerfanito structure map (Fig. 4.2). A minor northeast-plunging anticline with less than 50 ft (<15 m) of relief is located just south of the Phillips No. 6-17 well (Fig. 4.2). There is further evidence from structure maps of coal seams that pre-Fruitland structural features may not reflect present structural attitude of Fruitland coal seams (see "Structural controls on producibility of coalbed methane").

Isopachous trends

Huerfanito Bentonite—Pictured Cliffs Sandstone isopach

Thickness variations are useful indicators of paleoslope and syndepositional structural activity. Sedimentary units

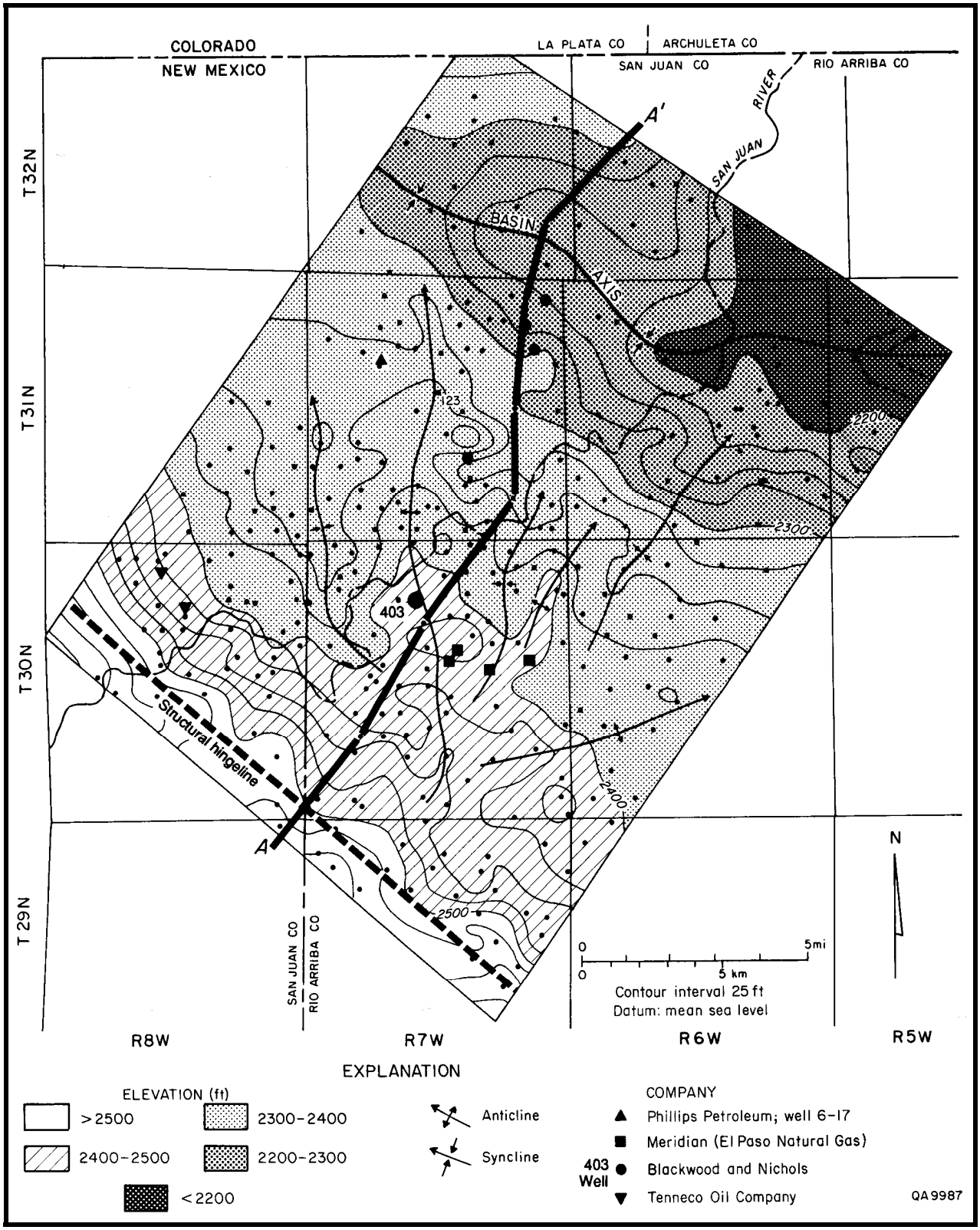

FIGURE 4.2—Structure map of the Huerfanito Bentonite Bed showing location of cross section A-A' (Fig. 4.1). A major synclinal axis crosses the northern quarter of the area, and the structural hingeline crosses the southwest part of the map. Minor folds may form conventional traps and contribute fracture permeability to Fruitland coal seams. See Ayers and others (this volume, Fig. 2.5) for location of Navajo Lake area.

commonly (but not always) thicken in the paleoslope direction and pinch and swell over uplifted and down-dropped areas, respectively. The Huerfanito BentonitePictured Cliffs Sandstone interval thickens from 675 ft (205 m) at the south to 850 ft (260 m) at the north end of the Navajo Lake area (Fig. 4.4), consistent with a paleoslope to the north or northeast; basinward thickening of the interval, 175 ft over 17 mi (52 m over 27 km), averages 10 ft/mi (1.9 m/km). Slight thinning and thickening at the axes of the minor anticlines and synclines, respectively, and greater increases of thickness coincident with structural steepening on the south side of the basin axis suggest syndepositional

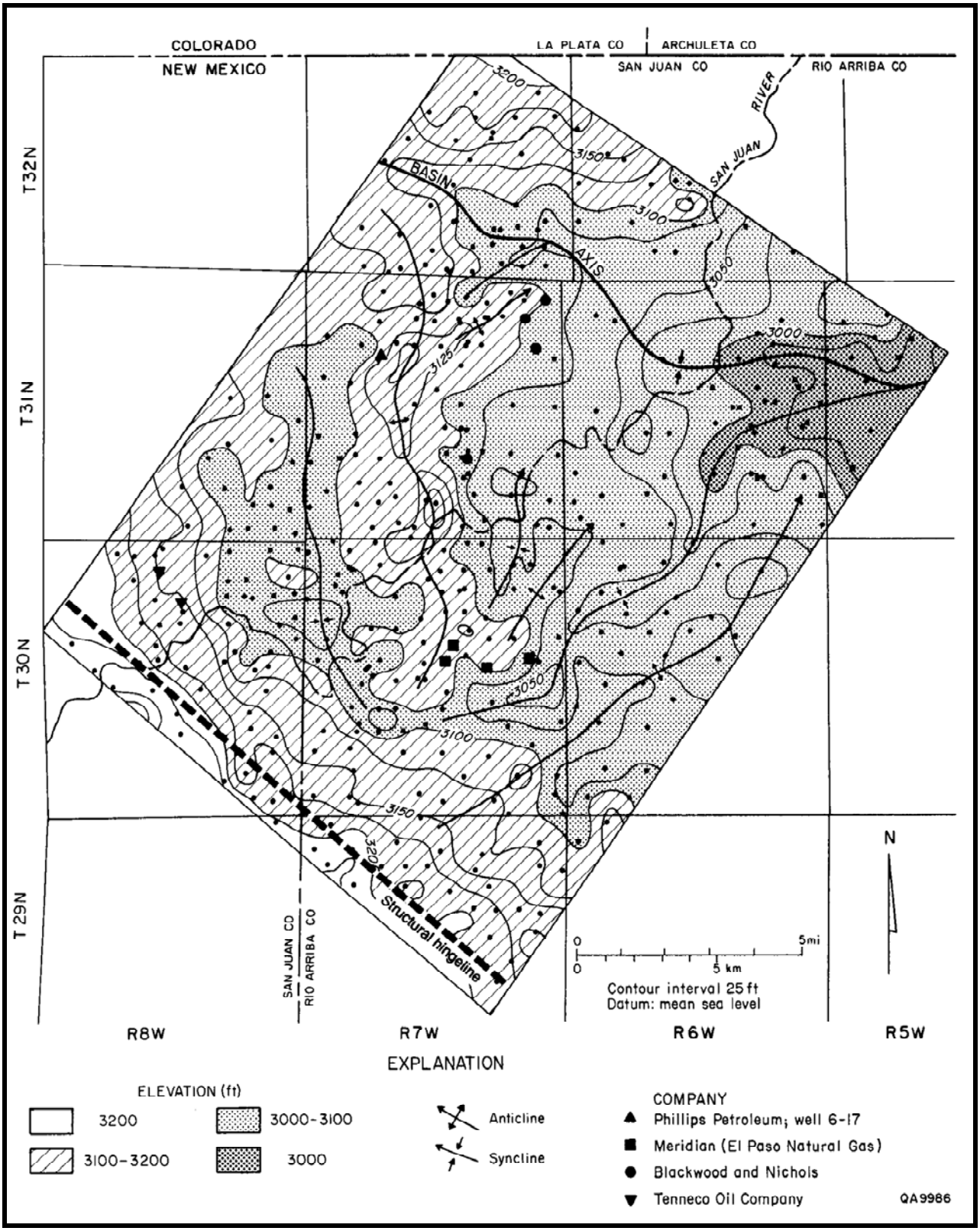

FIGURE 4.3—Elevation of the top of the Pictured Cliffs Sandstone results primarily from structural features (compare with Fig. 4.2) and secondarily from sedimentary fades changes.

folding (compare Fig. 4.2 with Fig. 4.4). A minor increase in thickness (25 ft [7.5 m]) along the structural hingeline indicates possible syndepositional faulting.

Fruitland Formation isopach

The Fruitland Formation thickens from 350 ft (105 m) on the east side of the area to 450 ft (135 m) on the west side of the Navajo Lake area, which may indicate a depocenter in the northwestern San Juan Basin (Silver, 1951, 1957). If so, then southeastward thinning of the Huerfanito Bentonite—Ojo Alamo interval (Ayers and Zellers, 1988, fig. 13) may not be due entirely to postdepositional erosion of the Kirtland Shale, as concluded by Fassett and Hinds (1971); uplift of the southeastern rim of the basin may have started during Pictured Cliffs—Fruitland deposition.

Sedimentary facies

Depositional framework facies are composed of the coarsest sediments and are deposited by the highest energy pro-

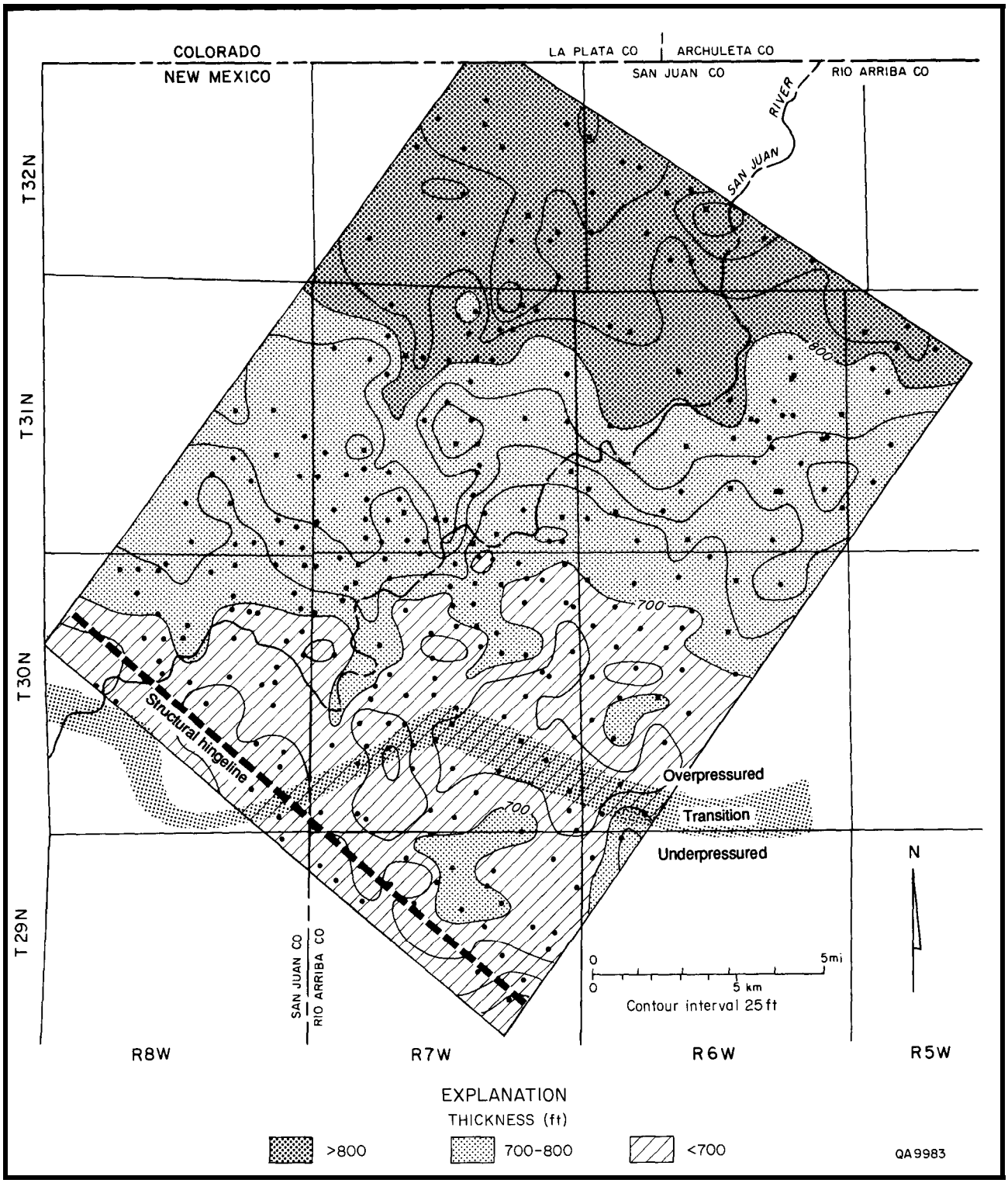

FIGURE 4.4—Isopach map from Huerfanito Bentonite Bed to top of Pictured Cliffs Sandstone. The interval thickens northward. Boundary between overpressured and underpressured Fruitland strata is from Kaiser and others (this volume, Fig. 8.7).

cesses operating within a depositional system; they are the skeletons of the depositional systems. In the Pictured Cliffs Sandstone, framework facies are barrier-strandplain, delta-front, and distributary/tidal channel-fill sandstones, and in the Fruitland Formation, framework facies are fluvial channel-fill sandstones deposited by rivers that carried sediments to the Pictured Cliffs shoreline.

Sediments marginal to the framework facies, representing deposition by lower energy processes acting in many environments, collectively are called nonframework facies. Nonframework facies of Pictured Cliffs barrier-strandplain and deltaic systems are washover fan, tidal flat, lagoon, back-barrier marsh, and delta plain; common nonframework facies in Fruitland Formation are natural levee, flood-plain, lacustrine, and swamp (coal) facies. To determine controls on coal occurrence, thickness, and trends, we mapped depositional framework facies in the coal-bearing Fruitland Formation and in the Pictured Cliffs Sandstone, which bounds Fruitland coal beds on their basinward side.

Pictured Cliffs lithofacies

Pictured Cliffs Sandstone—Pictured Cliffs shoreline sandstones are the depositional platforms upon which Fruitland peats (coals) accumulated; ultimately these sandstones bound coal seams in the basinward (northeast) direction. In geophysical logs, the Pictured Cliffs is divisible into upper and lower units. The lower unit is composed of a series of upward-coarsening sequences that are interpreted as upward-shoaling, shelf and shoreface mudstone and sandstone interbeds (Fig. 4.1; Ayers and others, this volume, Fig. 2.1). The upper unit of the Pictured Cliffs Sandstone has a blocky log signature and is interpreted to be amalgamated barrier-strandplain and/or wave-dominated deltaic sandstones. In a core from the Blackwood and Nichols NEBU No. 403, the upper unit of the Pictured Cliffs contains well-sorted and crossbedded sandstone (Figs. 4.5 and 4.6). Grain size increases slightly upward to medium sand near the top of the unit, but the upper 2 to 4 ft (0.5 to 1.2 m) of the Pictured Cliffs consists of fine sand. This upper part of the unit contains planar and contorted laminae; plant fragments are common, and the interval is organically stained. In the Navajo Lake area, two successive Pictured Cliffs amalgamated sandstone units range from 40 to 120 ft (12 to 36 m) in thickness and strike northwest (Fig. 4.7, shorelines 1 and 2), oblique to thickness trends defined in the Huerfanito Bentonite-Pictured Cliffs isopach map (Fig. 4.4).

Upper Pictured Cliffs sandstones (UP1 and UP2)—The Pictured Cliffs Sandstone and equivalent marine units thicken basinward above the Huerfanito Bentonite Bed of the Lewis Shale because of progradation into a subsiding basin. Note the basinward shift of the updip limits of marker beds (time lines), which originate in the shelf facies and terminate in the shoreline facies (Fig. 4.1). Progradation of the Pictured Cliffs shoreline, dependent on complex interactions of sediment supply, basin subsidence, and eustasy, was intermittent, resulting in shoreline stillstands. Periodically, shoreline movement reversed direction, and the Pictured Cliffs shoreline migrated (transgressed) southwestward over the Fruitland Formation, resulting in intertonguing of upper Pictured Cliffs transgressive-regressive sandstone beds with the Fruitland Formation. Two upper Pictured Cliffs tongues (UP1 and UP2) are present in the Navajo Lake area (Fig. 4.1).

Upper Pictured Cliffs tongues typically consist of crossbedded, burrowed, fine sandstone that overlies a coal-bearing lower Fruitland tongue (Figs. 4.5 and 4.6). These sandstones grade upward into planar-bedded, medium sandstones that make up the upper two-thirds of the Pictured Cliffs tongue (Fig. 4.6). UP1 and UP2 sandstones trend

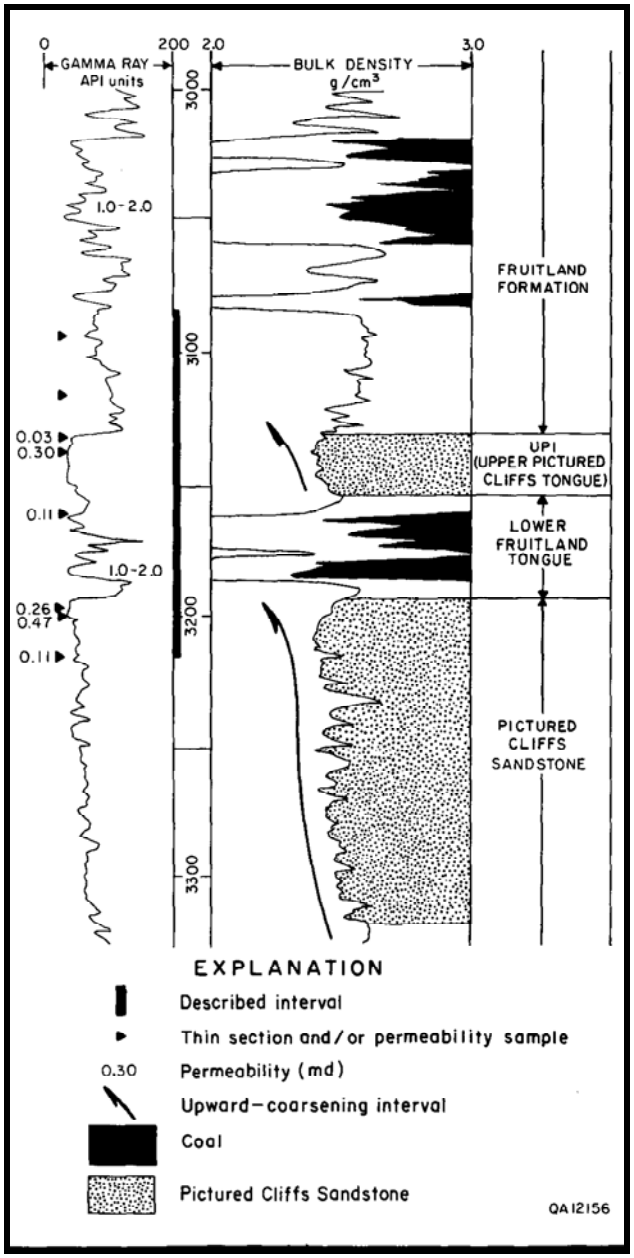

FIGURE 4.5—Gamma-density log of Blackwood and Nichols NEBU No. 403, shown in Fig. 4.2. Cored interval is described in Fig. 4.6. Permeabilities are from core plugs in sandstones and well tests in coal beds.

northwestward and are as much as 100 ft (30 m) thick (Figs. 4.8 and 4.9). The Pictured Cliffs tongues thin updip (southwestward), and their boundaries were placed where net sandstone thickness is 20 ft (6 m). Together, UP1 and UP2 account for approximately 150 ft (~45 m) of stratigraphic rise of the Pictured Cliffs over a 10-mi (16-km) distance from the southern third to the northern border of the study area (Fig. 4.1).

The depocenter of UP1, defined by the 70-ft (21-m) contour in Fig. 4.8, coincides with a depocenter of the underlying Pictured Cliffs Sandstone (Fig. 4.7), suggesting structural or subsidence control of shoreline position. Northeast-oriented fluvial or tidal channel-fill sandstones are inferred where the 60-ft contour projects landward (southwest) from areas of more than 90 ft (>27 m) of UP1 sandstone (Fig. 4.8). UP1 pinches out basinward, northeast of the study

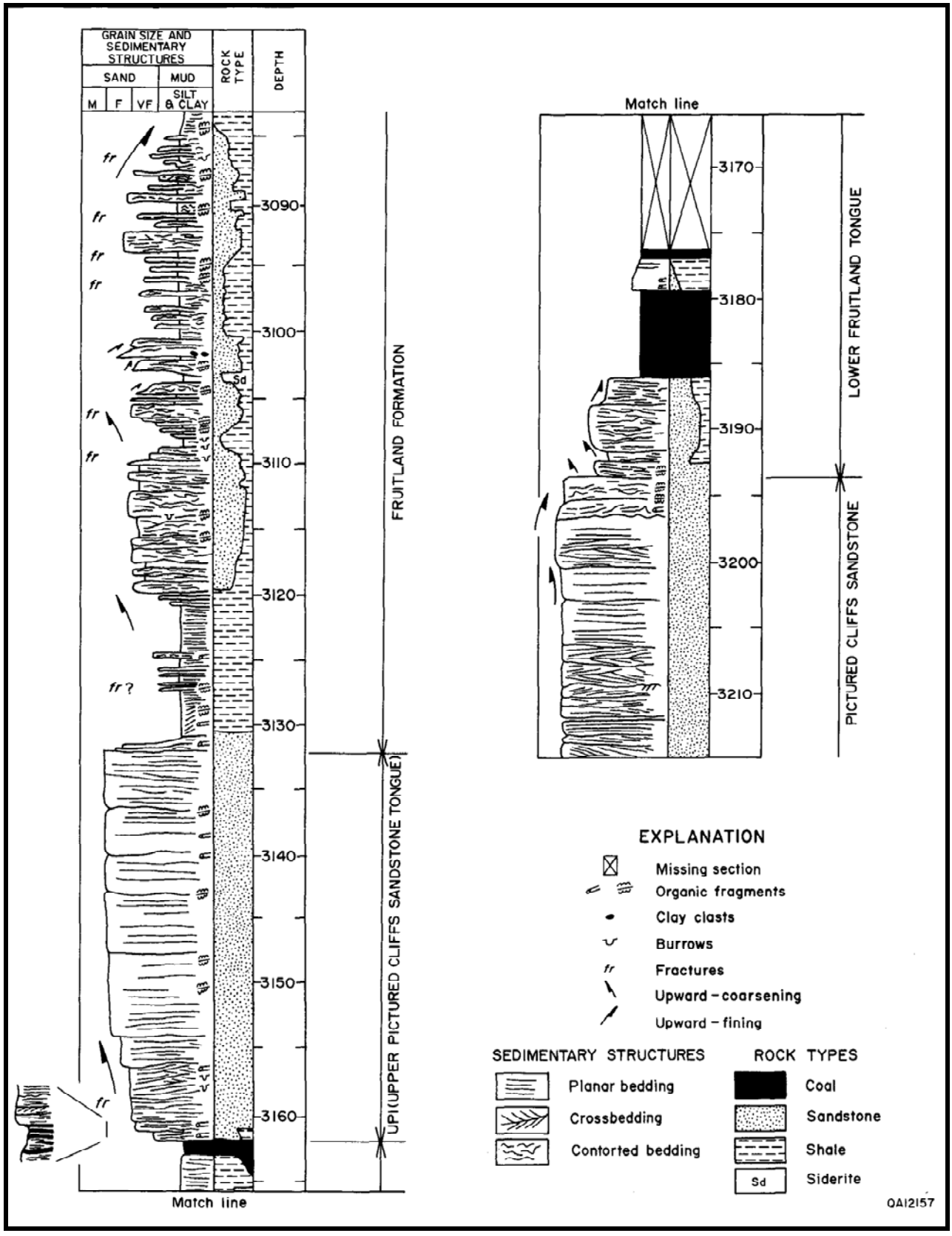

FIGURE 4.6—Core description of Pictured Cliffs Sandstone, lower Fruitland tongue, upper Pictured Cliffs tongue (UP1), and Fruitland Formation in Blackwood and Nichols NEBU No. 403 (see Fig. 4.5).

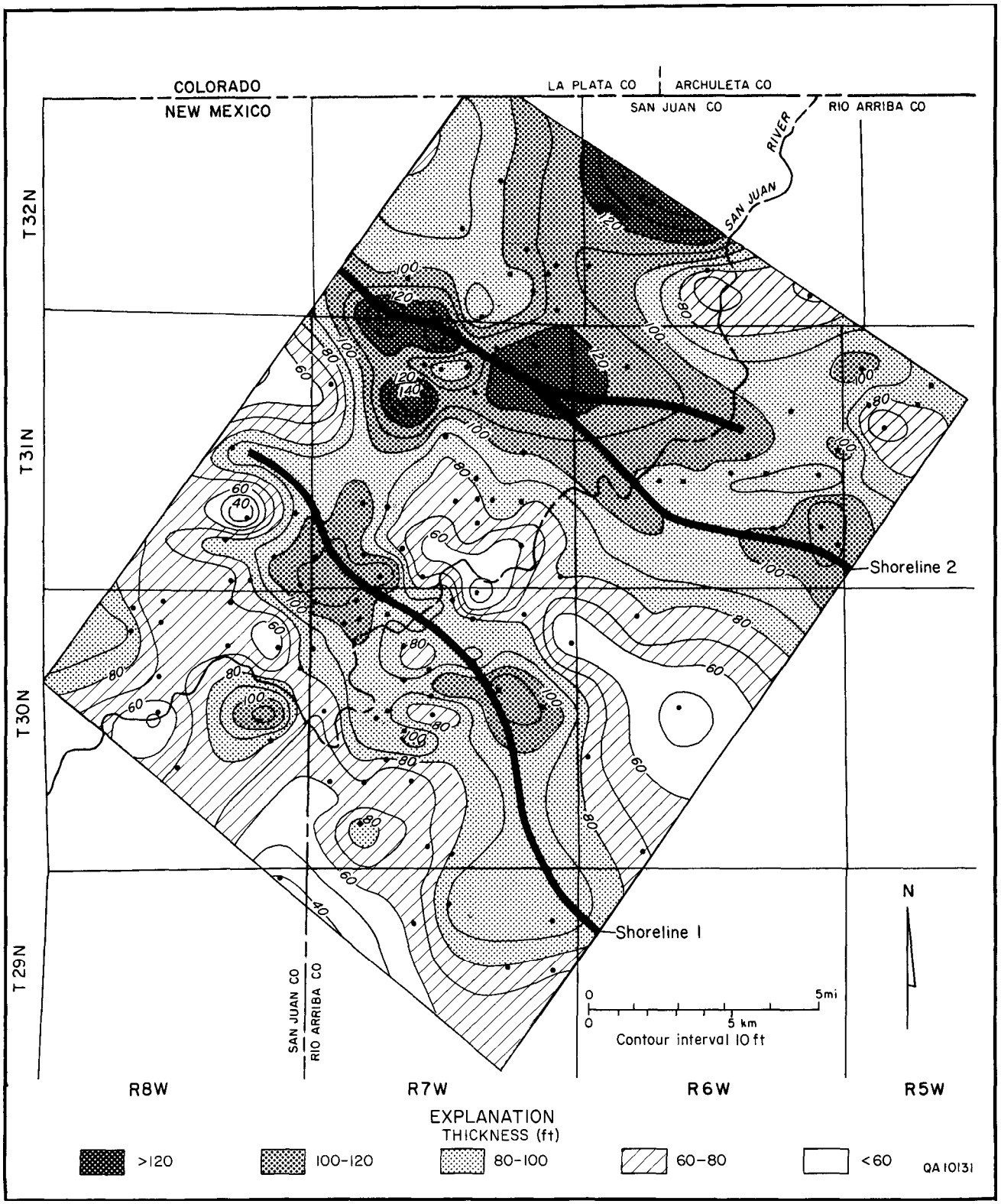

FIGURE 4.7—Sandstone isolith map of the Pictured Cliffs Sandstone. Net sandstone thickness trends of the Pictured Cliffs Sandstone suggest two successive, subparallel, northwest-trending shoreline sand bodies.

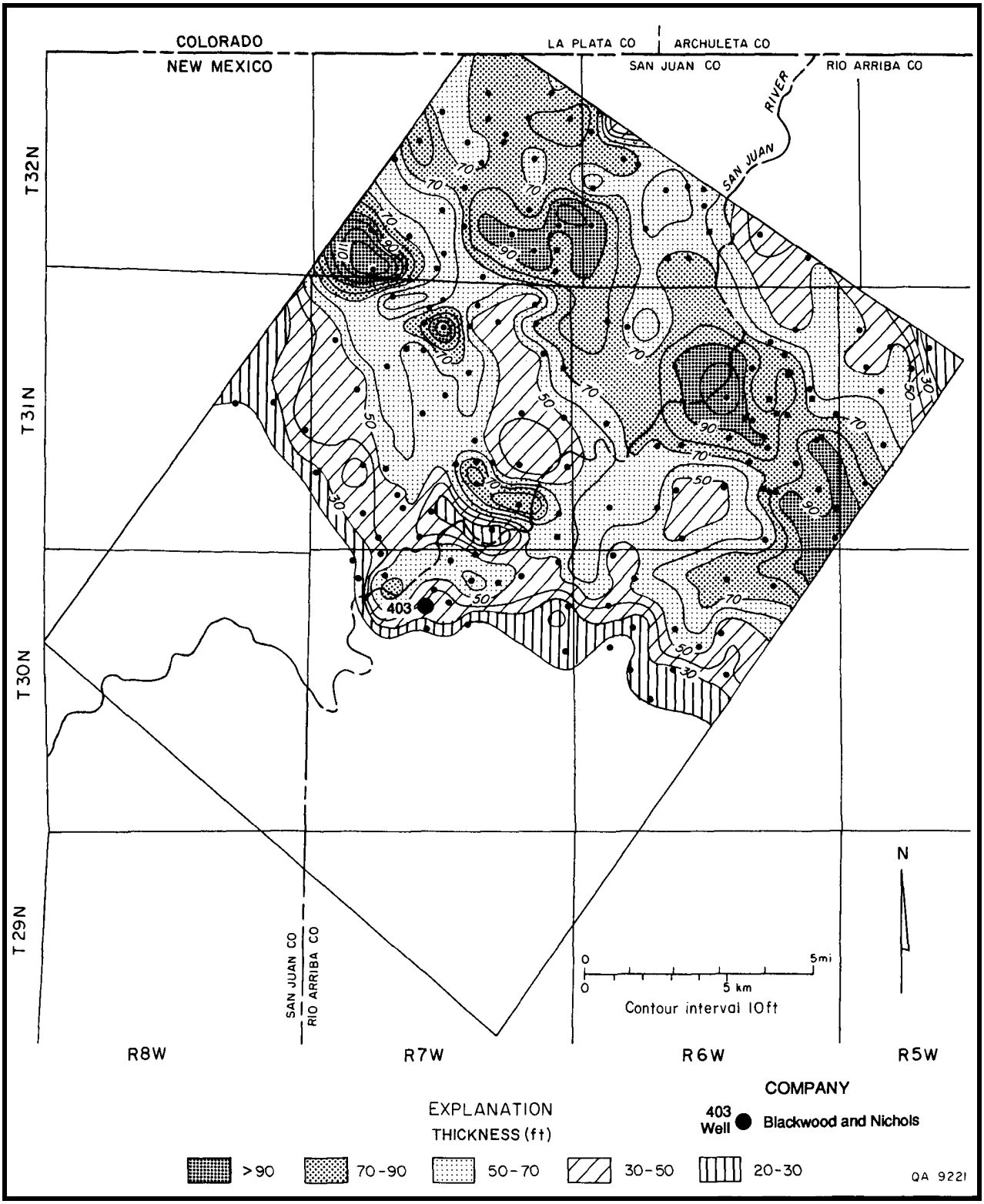

FIGURE 4.8—Sandstone isolith map of UP1 (Figs. 4.1, 4.5, and 4.6), showing strike-elongate geometry of the barrier-strandplain shoreline. Landward deflections of the 60-ft contour may represent dip-elongate fluvial or tidal channel-fill sandstones. Area mapped is where net sandstone thickness exceeds 20 ft (6 m).

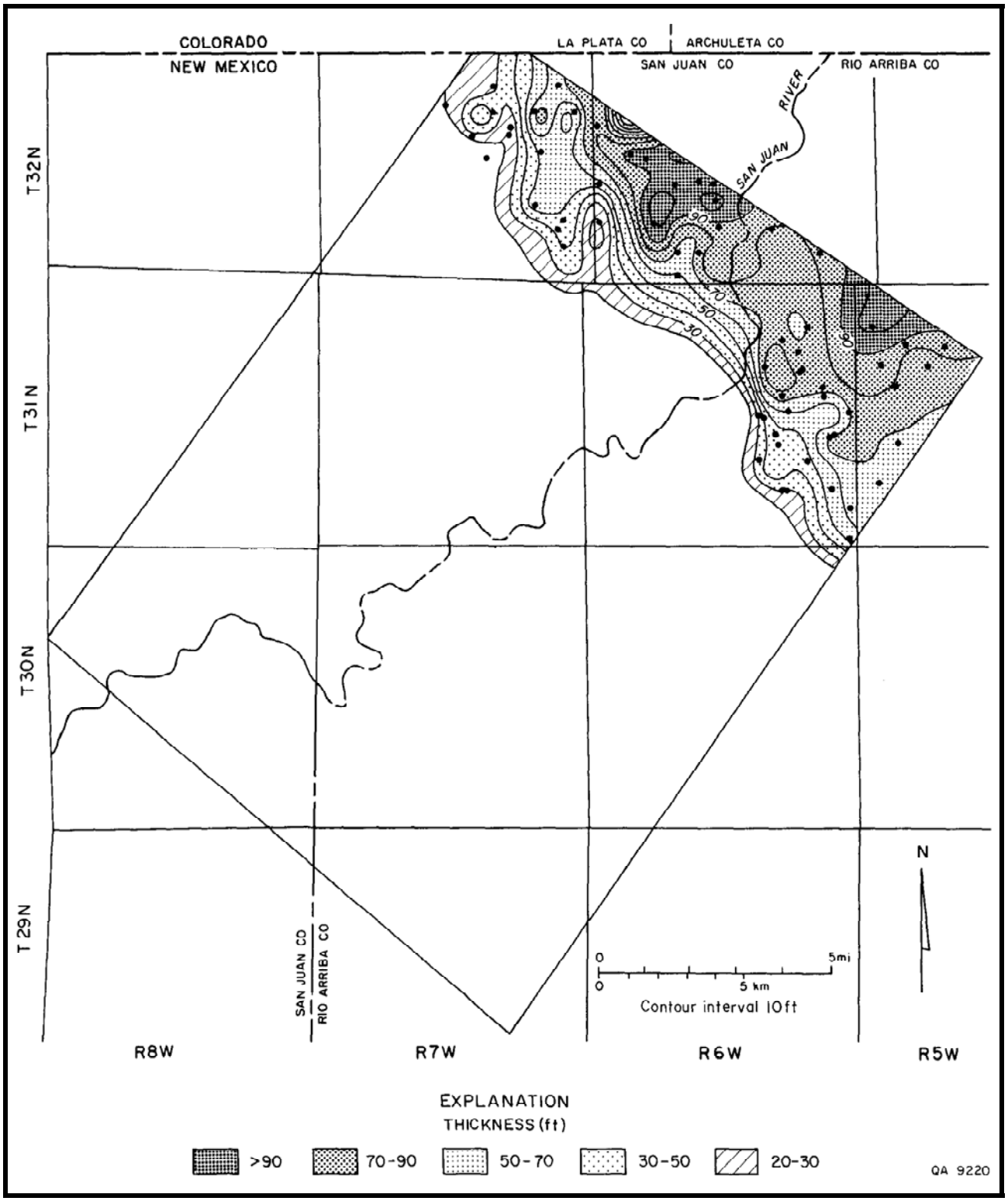

FIGURE 4.9—Sandstone isolith map of UP2 (Fig. 4.1). Depocenter of strike-elongate coastal sandstone is offset basinward of UP1 (Fig. 4.8). Area mapped is where net sandstone thickness exceeds 20 ft (6 m).

area. UP2 overlaps UP1, but its depocenter is offset bas-inward (northeast) of UP1, reflecting net Pictured Cliffs regression (Figs. 4.8 and 4.9). Lower Fruitland mudstone and coal that separate UP1 and UP2 in the southwest pinch out in the northeast area, where UP2 rests on UP1 (Fig. 4.1).

Fruitland Formation lithofacies

The coal-bearing Fruitland Formation is a coastal plain unit deposited landward of the Pictured Cliffs shoreline (Fig. 4.1). It is composed of sandstone, mudstone, and coal interbeds. Framework fades of the Fruitland Formation were delineated in the net and percent sandstone maps (Figs. 4.10 and 4.11). The net thickness of Fruitland sandstone ranges from 30 to 100 ft (9 to 30 m) (Fig. 4.10). Net sandstone thickness is lowest in the northern third of the area where the Fruitland Formation intertongues with the upper Pictured Cliffs sandstones. Sandstone commonly composes 15 to 30 percent of the Fruitland Formation (Fig. 4.11). In the Navajo Lake area, individual Fruitland framework sandstones are less than 40 ft (<12 m) thick and, most commonly, are 20 to 30 ft (6 to 9 m) thick. These sandstone bodies are elongate and trend northeastward (Fig. 4.11), parallel to the inferred paleoslope, and log signatures of Fruitland sandstones are upward fining, spiky, and serrate, consistent with the fluvial interpretation.

Fruitland rivers flowed northeastward but bypassed Fruitland swamps and supplied sediment to the Pictured Cliffs shoreline. The thinness of Fruitland sandstones suggests that fluvial systems in the Navajo Lake area were minor and too small to form fluvially dominated deltas. This conclusion is supported by linear geometry of the Pictured Cliffs shoreline sandstone (for example, UP1 [Fig. 4.8]), which suggests a wave-dominated coastline. The dip-elongate sandstone-body trends described in UP1 (Fig. 4.8) coincide with Fruitland sand-body trends, reinforcing the interpretation of Fruitland sandstones as minor fluvial feeders to the Pictured Cliffs shoreline.

Fruitland nonframework sandstones typically are thin, ranging from a few inches to less than 15 ft (<4 m) thick (Fig. 4.6). These sandstones are fine grained, rich in plant fragments, and commonly interbedded with silty mud-stone. They contain poorly defined sedimentary structures that have been distorted by soft-sediment deformation, microfaults, and burrowing. Fruitland nonframework sandstone beds occur in upward-coarsening sequences 3 to 6 ft (1 to 2 m) thick and amalgamated or upward-fining sequences as much as 15 ft (4 m) thick; these nonframework sandstones are interpreted to be crevasse-splay and natural levee deposits.

Coal occurrence

Net coal thickness

The criteria for identifying coal beds and for determining coal thickness on geophysical logs are summarized by Ayers and others (this volume, Chapter 2). The net thickness of Fruitland coal seams in the Navajo Lake area ranges from 40 to 110 ft (12 to 33 m) (Fig. 4.12). The greatest net coal thickness, more than 70 ft (>21 m), occurs in the south, and the least net coal thickness is in the northeastern quarter of the area, which has 30 to 50 ft (9 to 15 m) of coal. The local northwest trend in the Navajo Lake area (Fig. 4.12) is also present in regional maps (Fassett and Hinds, 1971; Kelso and others, 1987; Ayers and others, this volume, Fig. 2.16).

Maximum coal thickness

The maximum coal map (Fig. 4.13) was made by contouring the thickest individual Fruitland coal seam recorded in each well, regardless of its stratigraphic position. Therefore, it does not record seams that extend throughout the area. However, locally, as in the southeast corner of the map, individual thick seams are mapped. Maximum coal thickness ranges from 15 to 50 ft (4 to 15 m) (Fig. 4.13). Depocenters for thick coal, where individual coal seams are thicker than 30 ft (>9 m), occur in pods 2 to 6 mi (3 to 10 km) in diameter. Coal seams thin radially from those depocenters, but they extend throughout most of the Navajo Lake area. A thick coal seam (>30 ft [>9 m]; T29 and 30N, R7W) in the south coincides with an area of great net coal thickness (Fig. 4.12) and indicates an area of persistent peat-forming conditions. Although a regional maximum coal map shows little internal complexity in northwest-trending belts of thick maximum coal (Ayers and others, this volume, Fig. 2.17), the maximum coal map of the Navajo Lake area, which was made with closely spaced well control, suggests that geometry of individual coal seams in the northwest-trending belts is podlike or dip elongate.

Number of Fruitland coal seams

In the Navajo Lake area, Fruitland coal occurs in 2 to 14 seams, which are most numerous in the southwest and least numerous in the northeast (Fig. 4.14). A northwest strike is also apparent in this coal isopleth map. The greatest number of coal seams (14 seams) coincides with the location of greatest total coal thickness (>90 ft [>27 m]; Fig. 4.12) and the thickest individual seam in the south (>30 ft [>9 m]; Fig. 4.13).

Depositional controls on coal occurrence, trends, and thickness

The depositional setting of Fruitland coal seams in the Navajo Lake area was determined from coalbed trends and from relations between coal beds and Pictured Cliffs and Fruitland framework sandstones. Principal aspects of these relations are summarized in Fig. 4.15, a map of depositional elements, and in the depositional model (Ayers and others, this volume, Fig. 2.20).

In coal isolith and isopleth maps (Figs. 4.12 and 4.14), strike-elongate trends are apparent, and coal seams are thickest and most abundant landward of upper Pictured Cliffs tongues. These relations suggest that thick coal formed in persistent, recurring swamps located landward of upper Pictured Cliffs linear shorelines. Although some coal beds terminate behind shoreline sandstones (Figs. 4.15 and 4.16), other coal beds override them (Fig. 4.16, upper two seams) to form laterally extensive coal beds. In the maximum coal map (Fig. 4.13), coalbed geometry is podlike and dip elongate rather than strike elongate because thick coal seams formed in peat depocenters between dip-elongate, Fruitland channel-fill sandstone complexes (Figs. 4.15 and 4.17). Palynologic studies (Manfrino, 1984) and the low sulfur content of Fruitland coal seams indicate that peat accumulated in a fresh-water setting. Therefore, we conclude that the thickest peats formed inland, behind abandoned and foundering shoreline deposits of the Pictured Cliffs Sandstone (Ayers and others, this volume, Fig. 2.20).

Structural controls on depositional systems

Fruitland net coal thickness is greatest landward of the greatest Pictured Cliffs stratigraphic rise, and yet, as pointed out by Fassett (1986), analogous thick coals are not associated with stratigraphic rises in subjacent coal-bearing formations. This implies that a process (or processes), absent when previous San Juan Basin coal beds were deposited, operated during Fruitland deposition. We suggest that structural activity caused a higher rate of subsidence in the

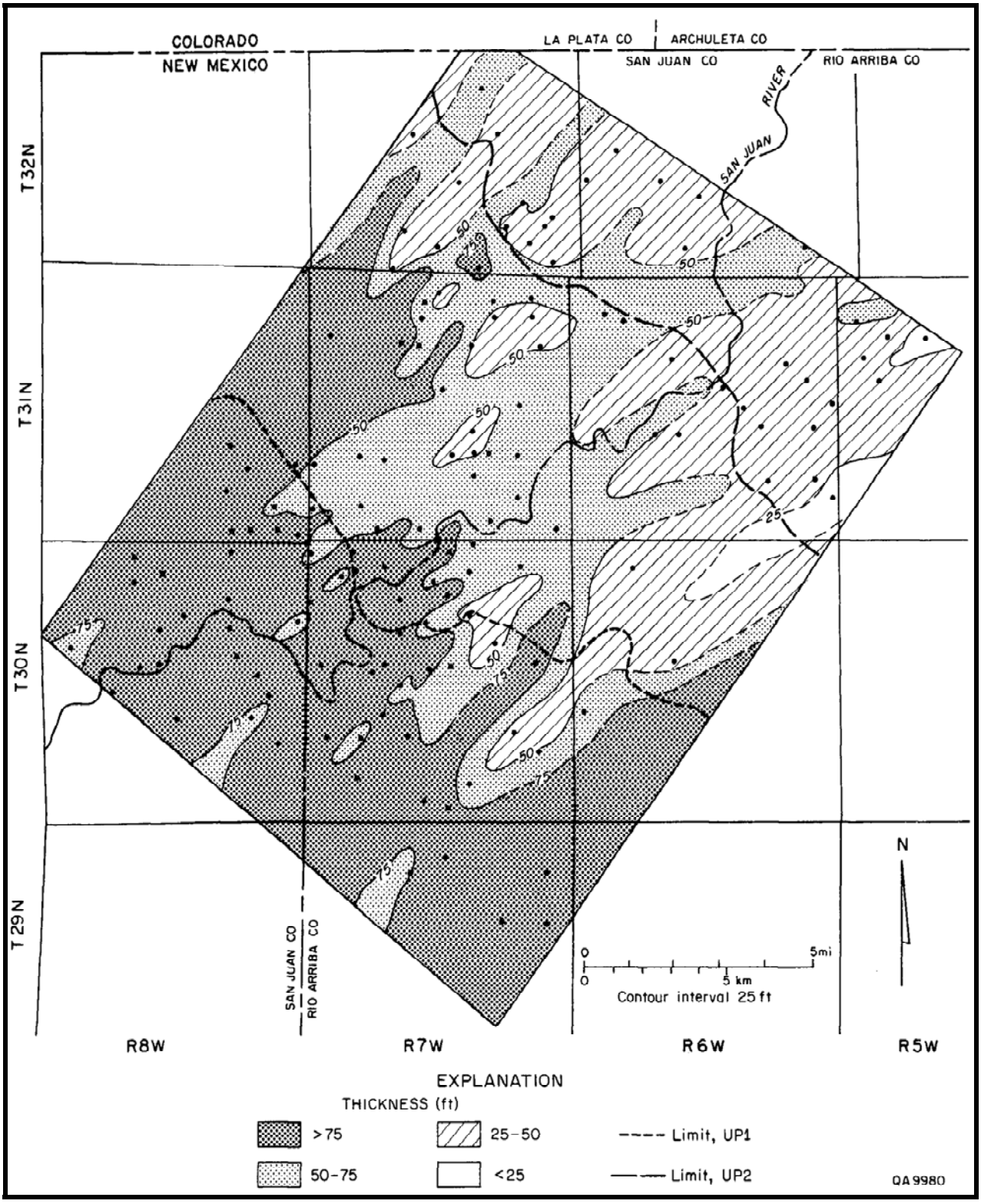

FIGURE 4.10—Sandstone isolith map of the Fruitland Formation. Net thickness of Fruitland sandstones is greatest in the southwest part of the area. Dip-elongate sandstone bodies were deposited by minor Fruitland fluvial systems that supplied sediment to Pictured Cliffs shoreline.

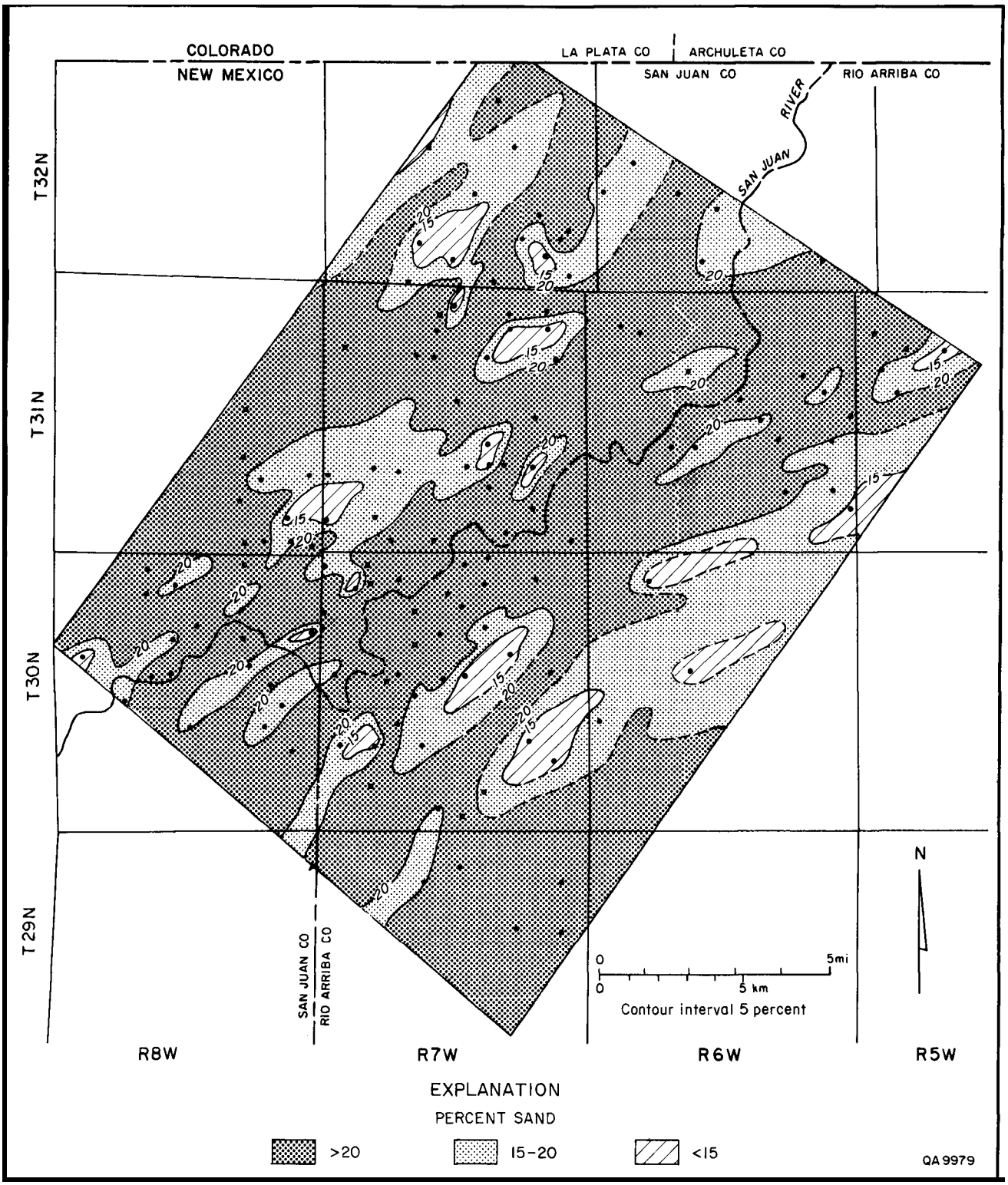

FIGURE 4.11—Sandstone percent map of the Fruitland Formation. Dip-elongate sandstone bodies make up 15 to 30% of the formation.

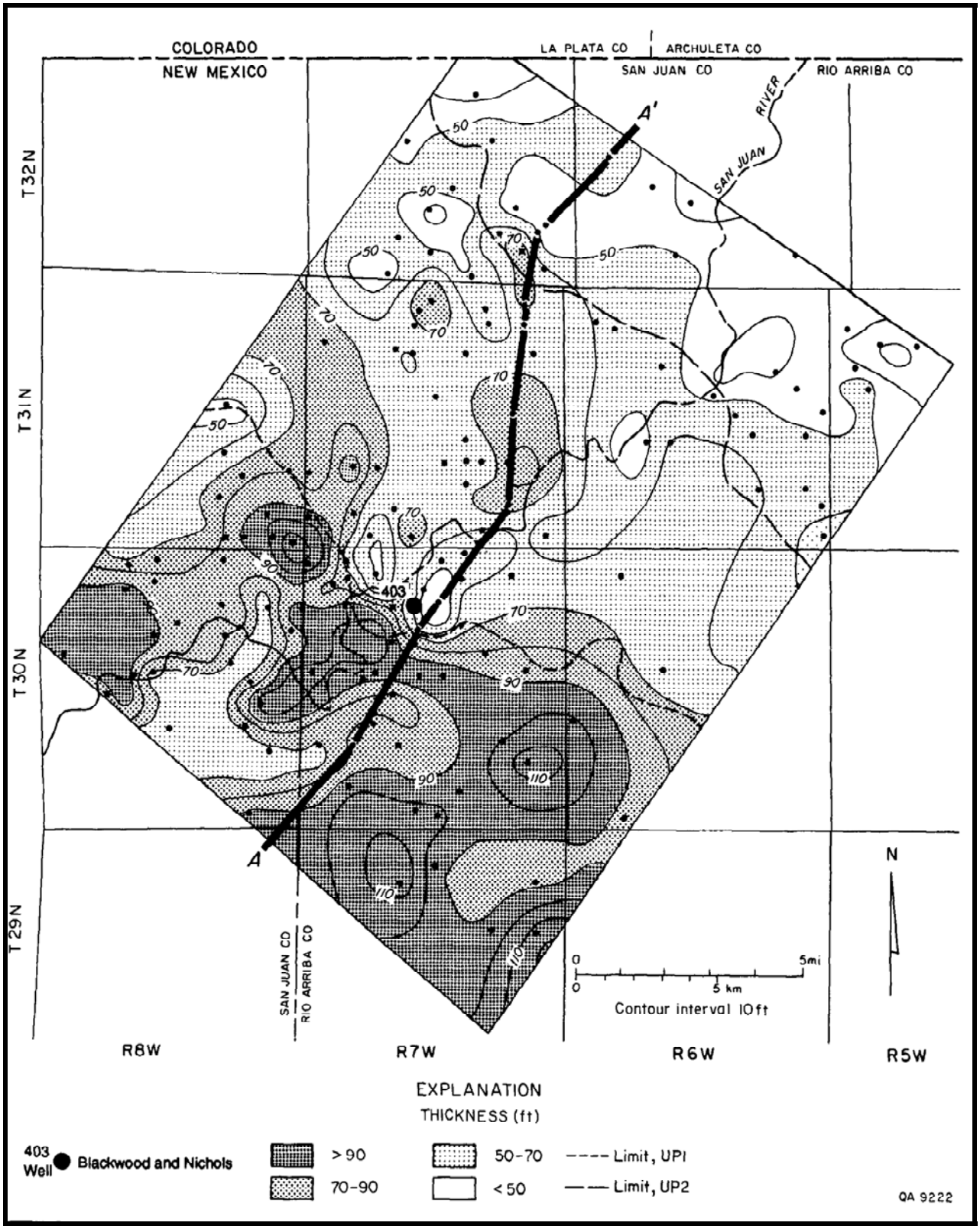

FIGURE 4.12—Fruitland coal isolith map. Net coal thickness ranges from 40 to 110 ft (12 to 33 m). Greatest net coal thickness is in the southern third of the area, and thickness trends strike northwestward, parallel to, and landward of the trends of upper Pictured Cliffs shoreline sandstones UP1 and UP2 (Figs. 4.8 and 4.9).

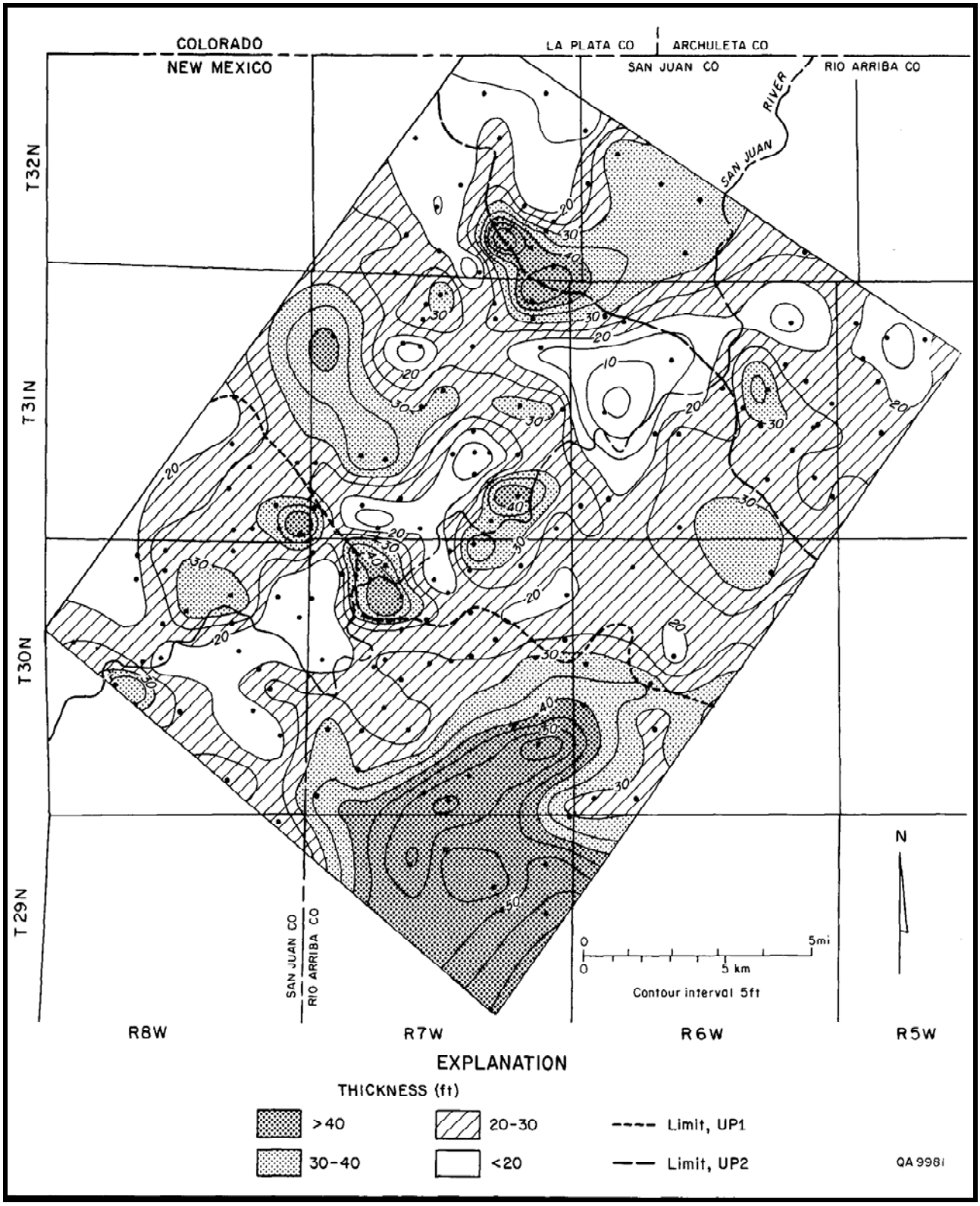

FIGURE 4.13—Fruitland maximum coal map. Map of the thickest individual coal seam at each location shows a thickness range from 15 to 50 ft (4 to 15 m). Thickest coal is in the south, and no preferred orientation is apparent.

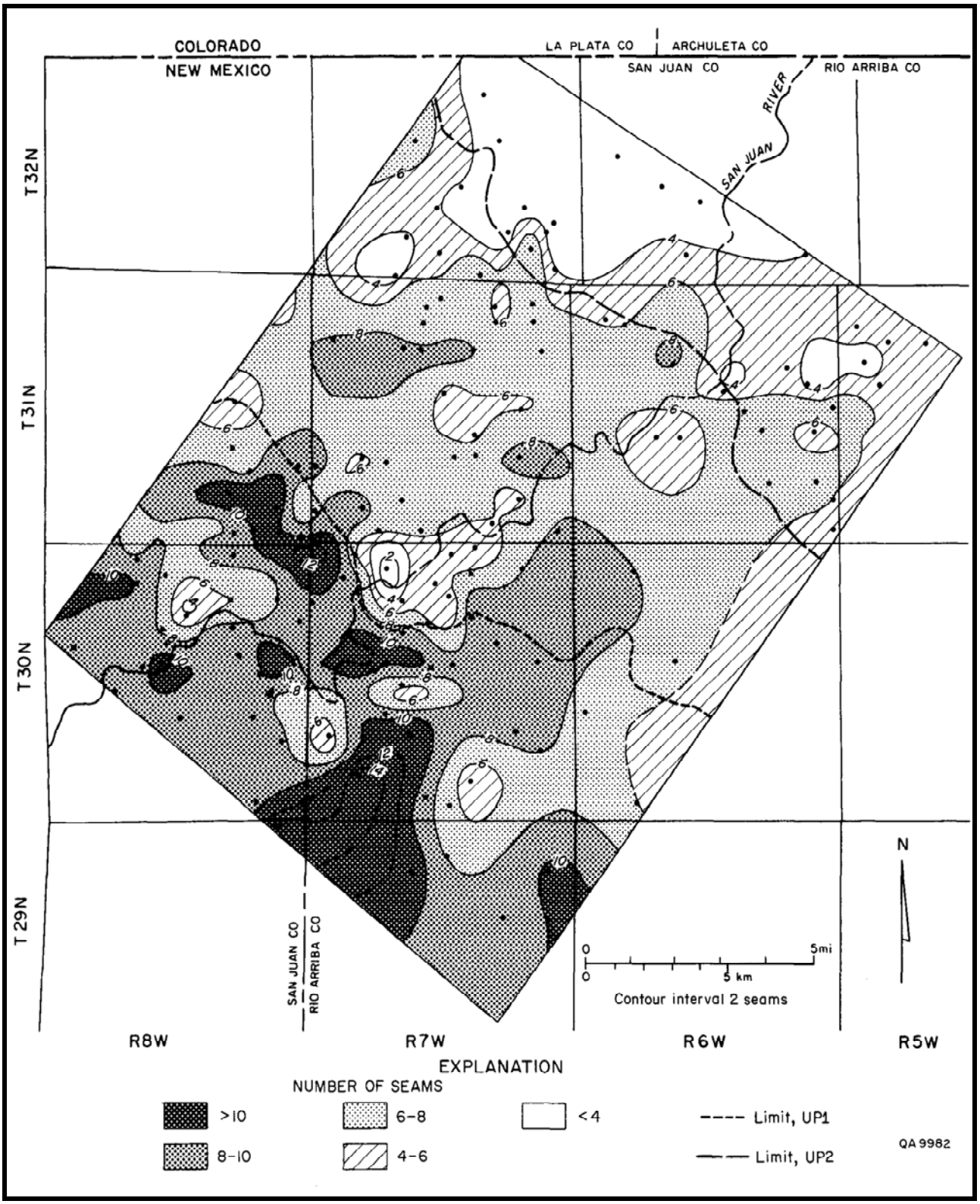

FIGURE 4.14—Fruitland coal isopleth map. Fruitland Formation coal occurs in 2 to 14 seams that trend northwestward, parallel to upper Pictured Cliffs sandstones UP1 and UP2 (Figs. 4.8 and 4.9).

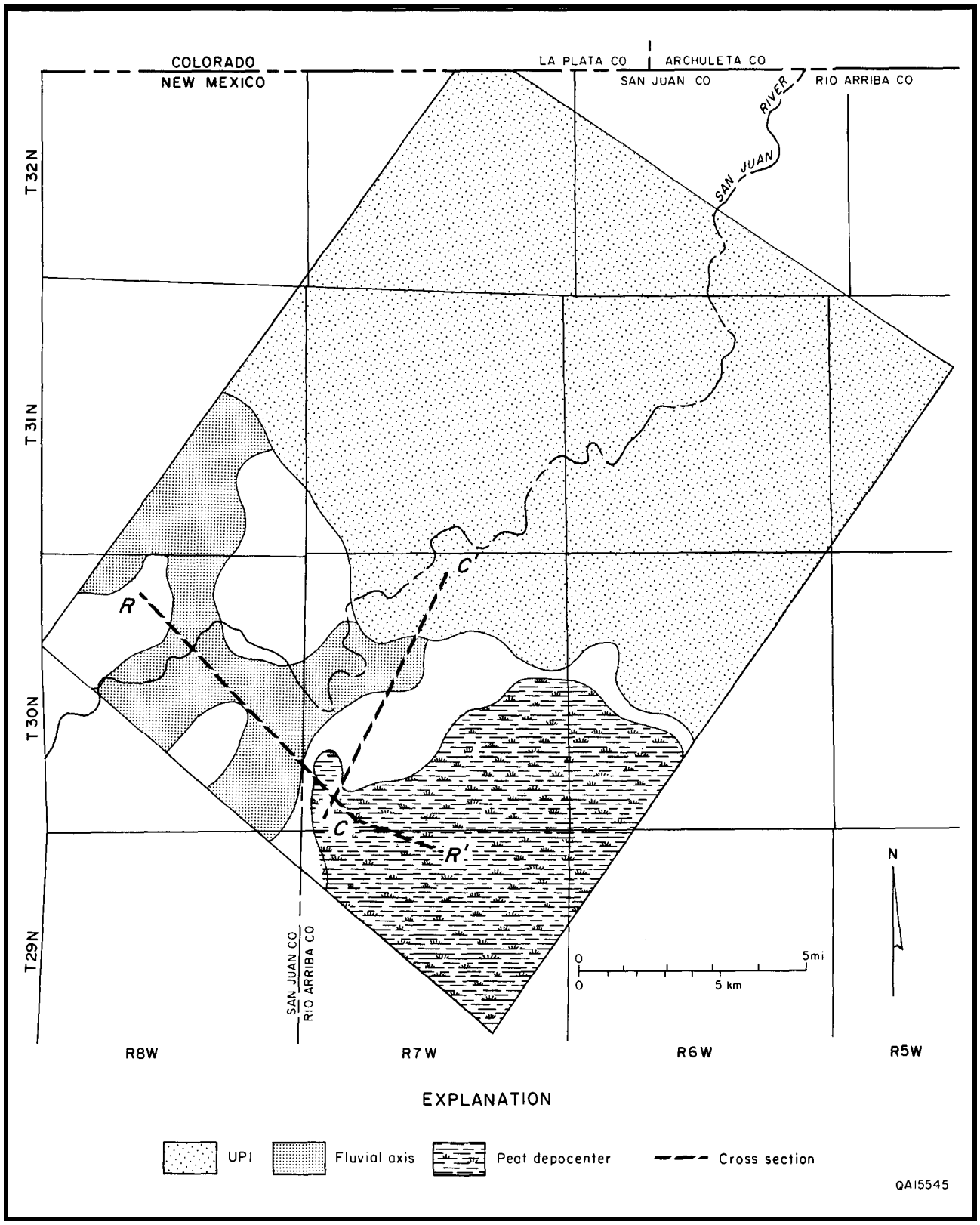

FIGURE 4.15—Depositional elements of Fruitland Formation and upper Pictured Cliffs tongue (UP1) in the Navajo Lake area. Peat depocenter persisted southwest of the Pictured Cliffs shoreline and lateral to Fruitland fluvial depositional axes. Cross sections C—C' and R—R' are shown in Figs. 4.16 and 4.17.

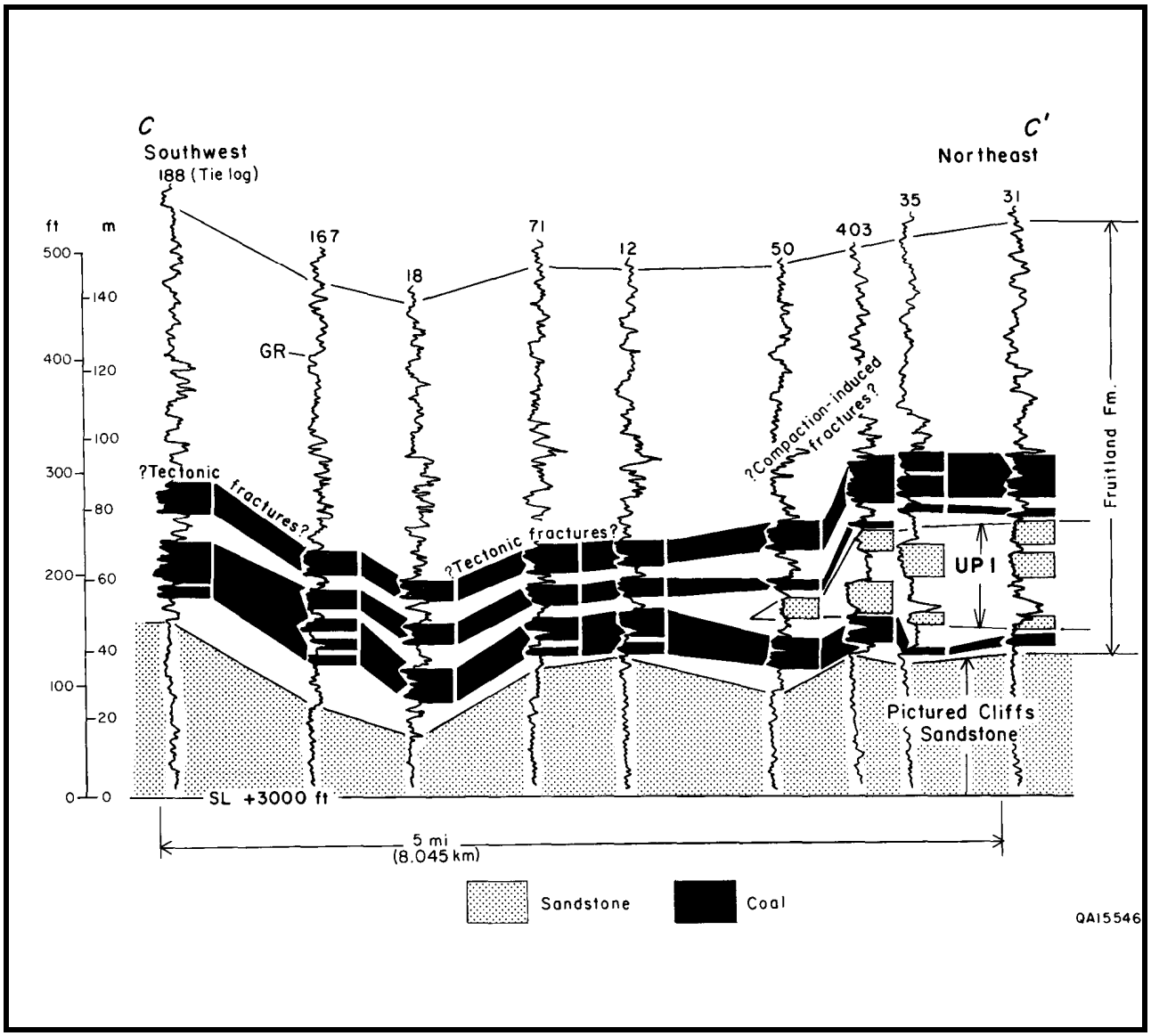

FIGURE 4.16—Structural cross section C–C'. Although lower Fruitland coal seams pinch out landward of Pictured Cliffs shoreline sandstones, a thick upper Fruitland coal seam overrides UP1. Fractures may occur in areas of tectonic folding, such as between wells 188 and 71 in all seams, and in areas of compaction-induced folding where coal seams override shoreline sandstones, such as between wells 50 and 403 in the upper two thick seams. Well 188 ties with Fig. 4.17. See Fig. 4.15 for location.

northern part of the basin, northeast of the structural hinge-line (Ayers and others, this volume, Chapter 2). This greater subsidence created more accommodation space, causing a stillstand of the Pictured Cliffs shoreline and allowing the accumulation of thick Fruitland peats.

Fassett and Hinds (1971) used the Huerfanito Bentonite of the Lewis Shale as a datum for correlating Fruitland coal seams because it is stratigraphically the closest regional marker to the Fruitland Formation. However, the Huerfanito Bentonite is 675 to 850 ft (205 to 260 m) below the Fruitland in the Navajo Lake area (Fig. 4.4). Although it is an excellent regional marker, the Huerfanito Bentonite has limitations in Fruitland coal evaluations. Fassett (1987) reported that Fruitland coal seams parallel the Huerfanito Bentonite, but Fruitland coal seams can parallel the Huerfanito only if (1) stratigraphic rise of the Pictured Cliffs is due to eustasy (impossible, considering the magnitude of thickening-1,200 ft [365 m] across the basin) or a uniform subsidence rate across the entire basin, which is inconsistent with isopach maps and other findings expanded on below, and (2) there has been no differential compaction of the underlying Pictured Cliffs Sandstone and Lewis Shale. Use of the Huerfanito Bentonite as a datum suggests that all coal seams terminate abruptly against Pictured Cliffs sandstones (Fig. 4.18a). It also requires rapid aggradation of the continental Fruitland facies to keep pace with rapid rise of relative sea level (Fig. 4.18a); however, rapid aggradation of coastal plain sediment is incompatible with persistent peat accumulation.

Use of a datum above the Fruitland Formation (Fig. 4.18b) gives a different perspective of basin-filling processes and suggests structural control of the Pictured Cliffs shoreline and, indirectly, the distribution of thick Fruitland coal seams. Fassett and Hinds (1971, p. 38) stated that "the pre-Ojo Alamo surface was probably a relatively flat peneplain." Cross section B–B' is aligned with the present-day strike of that surface (Ayers and Zellers, 1988, fig. 10c), which, in turn, nearly parallels the Pictured Cliffs–Ojo Alamo isopach strike. Therefore, the base of the Ojo Alamo Sandstone was used as a local datum. From Fig. 4.18b we surmise that

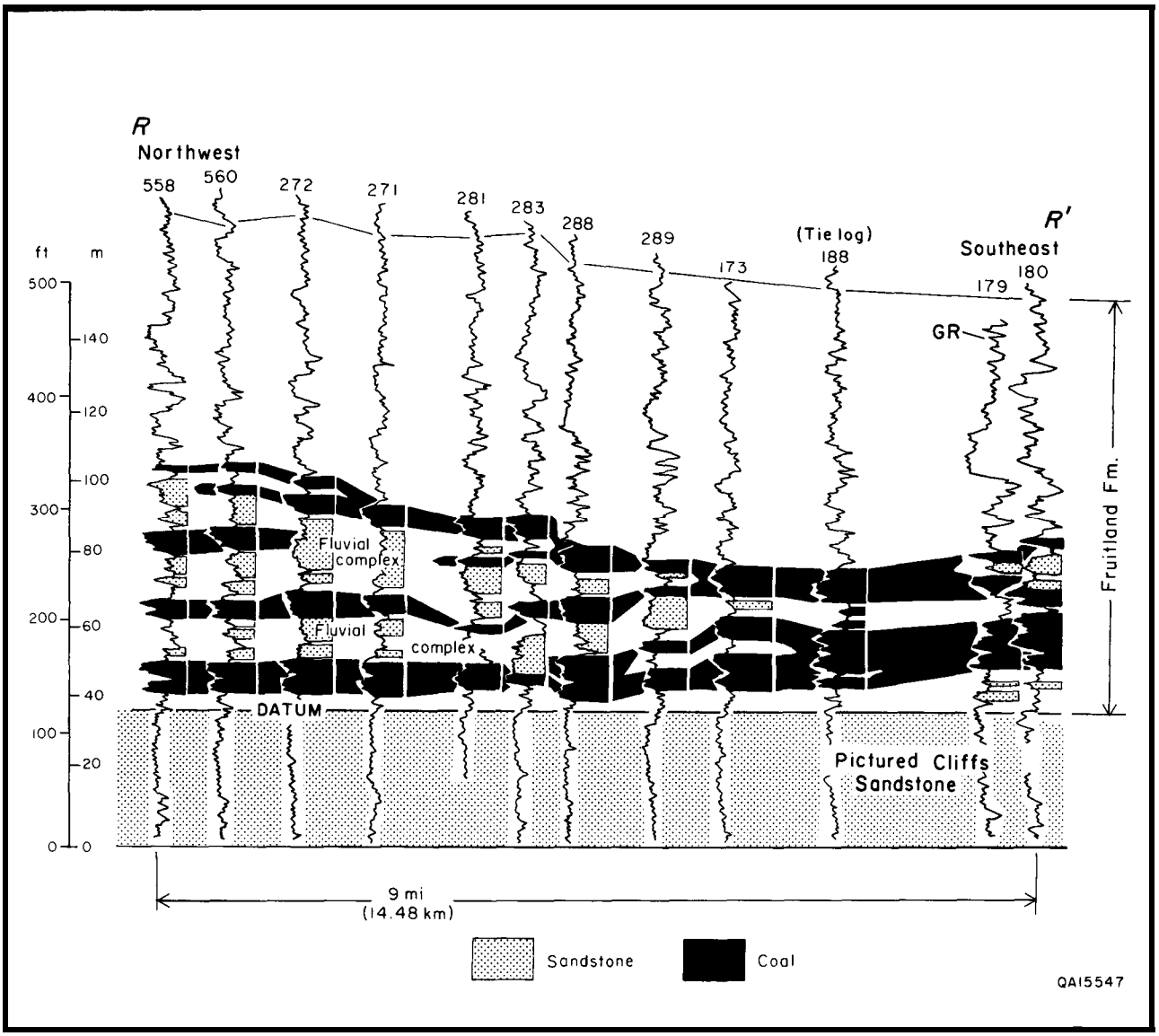

FIGURE 4.17—Stratigraphic cross section R–R'. Thick Fruitland coal in well 188 forms zigzag splits to the northwest where more compactible peat (coal) interfingers with fluvial complexes (sandstones) along paleostrike. These folds may cause fracture-enhanced permeability. Because the datum is the top of the Pictured Cliffs Sandstone, true structural attitude of the coal beds is not shown. Well 188 ties with Fig. 4.16. See Fig. 4.15 for location.

differential subsidence north of a structural hingeline (Fig. 4.2; Ayers and others, this volume, Fig. 2.20) controlled movement of the Pictured Cliffs shoreline by creating more accommodation space in the northern part of the basin.

In Fig. 4.18b, it is apparent that (1) if the increased thickness of Lewis Shale between wells 70 and 213 is due to differential subsidence, then thick coals in well 70 may override UP1 and UP2 in well 213 rather than terminate against them as suggested in Fig. 4.18a, and (2) if less rapid aggradation is required at well 70 to keep pace with aggradation in well 213, then more time is available for uninterrupted peat accumulation at well 70, and hence the greater thickness of peat southwest of UP1. Because Upper Cretaceous strata thicken basinward, in part because of increased basin subsidence, coal seams are not parallel to the Huerfanito Bentonite.

Evidence in support of a higher rate of subsidence in the northern part of the basin includes the following observations: (1) if basinward thickening of the Huerfanito Bentonite—Pictured Cliffs Sandstone interval is due to eustasy or uniform platform subsidence, the unconformable base of the Ojo Alamo Sandstone should not parallel the stratigraphic rise of the Pictured Cliffs (Fig. 4.18a); (2) UP1 is stacked on an underlying Pictured Cliffs Sandstone shoreline (Figs. 4.7 and 4.8), and it pinches out at approximately the same area as a marine marker zone above the Huerfanito (Fig. 4.1) and a similar marker zone (not shown) below the Huerfanito; (3) the inclined marker beds in Pictured Cliffs shelf and shoreface deposits (Fig. 4.1) show notable thickening of these deposits basinward, northeast of well 50, whereas to the southwest of well 50, shelf and shoreface markers are horizontal and the deposits are thin; and (4) although stratigraphic rise of the Pictured Cliffs occurs in the southern part of the basin, the greatest stratigraphic rise is northeast of the structural hingeline. The regional Huerfanito Bentonite—upper Pictured Cliffs Sandstone isopach shows a realignment of contours from an east trend in the central part of the basin to a northwest trend in the area of greatest stratigraphic rise (Ayers and others, this volume, Fig. 2.8).

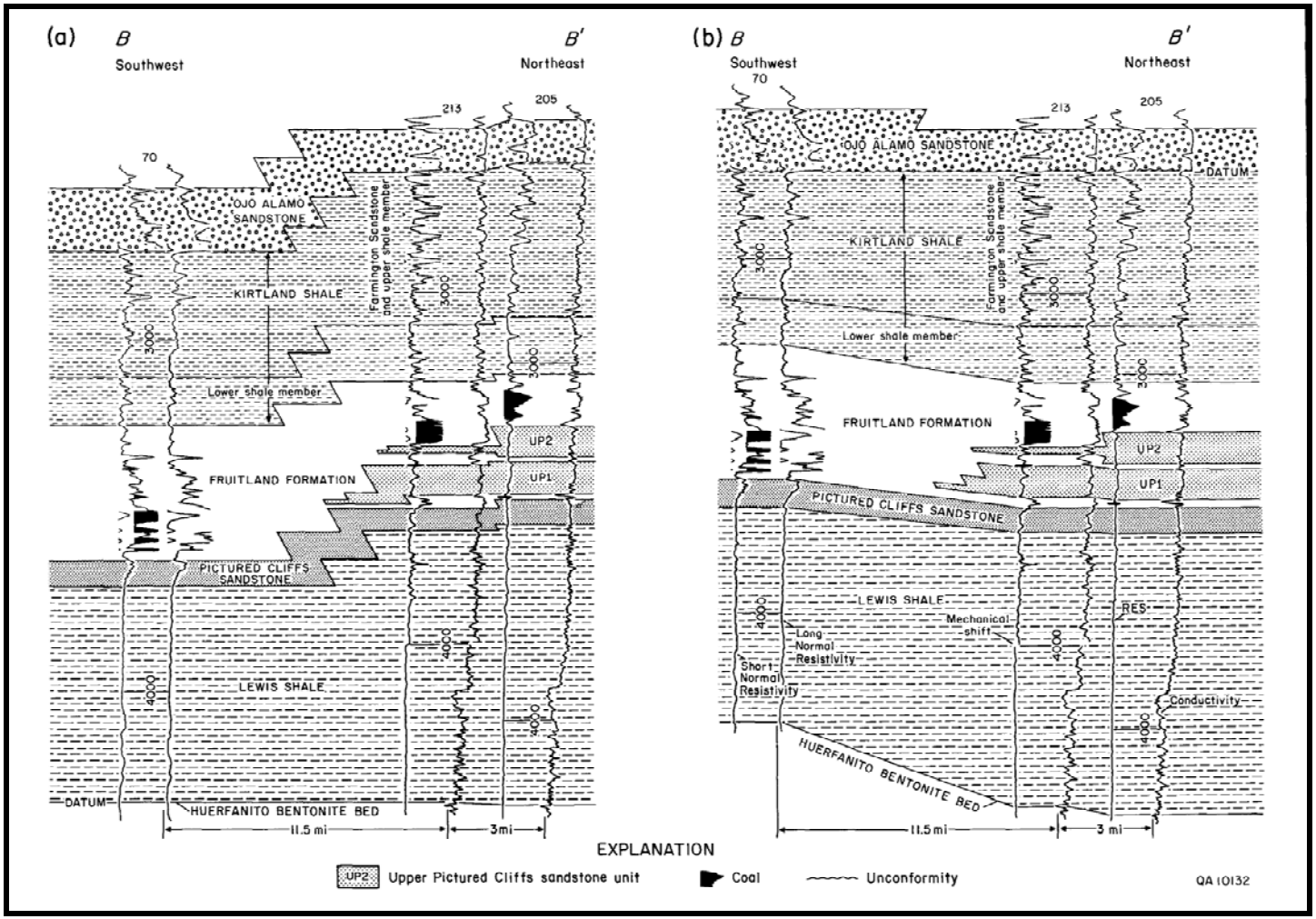

FIGURE 4.18—Cross section B—B'. (a) Datum is the Huerfanito Bentonite. Use of this datum suggests that coal seams terminate abruptly against Pictured Cliffs shoreline sandstones. (b) Datum is base of the Ojo Alamo Sandstone. Use of a datum above the Fruitland Formation suggests that swamp fades (coal seams) migrated over abandoned, foundered Pictured Cliffs shoreline sandstones. See Fig. 4.19 for location.

We suggest that structural activity contributed to relatively greater stratigraphic rise in this area and, indirectly, to the distribution of thick Fruitland coal seams (Ayers and others, this volume, Fig. 2.20). The Pictured Cliffs shoreline prograded rapidly basinward across the southern half of the basin. After the shoreline crossed the structural hinge-line, sporadic structural activity began and the northern part of the basin subsided more rapidly to accommodate a greater thickness of sediment. The changing balance between sediment input and pulsatory subsidence north of the hingeline resulted in oscillation and aggradation of the shoreline, accounting for the most significant stratigraphic rise of the Pictured Cliffs in the basin and allowing time for thick peat accumulation landward of the oscillating shoreline. This model explains why the greatest net thickness of Fruitland coal is in the northern part of the basin, and why coal seams in the Fruitland Formation are thicker than those in subjacent continental strata. Further testing is needed to verify the existence of the structural hingeline; seismic studies would be especially useful. A regional map of structural elements that were identified in regional reflection seismic lines shows northwest-trending faults in the area of this hingeline (Huffman and Taylor, 1991).

Structural controls on producibility of coalbed methane

Earlier studies suggested that Fruitland coal seams have limited extent and that they are bounded on their basinward (northeast) margins by Pictured Cliffs shoreline sandstone and along paleostrike (northwest—southeast) by Fruitland fluvial sandstones (Fassett and Hinds, 1971; Fassett, 1986). However, as we have demonstrated, some Fruitland coal seams may be regionally continuous, overriding and thinning over upper Pictured Cliffs tongues (Figs. 4.16 and 4.18) in the paleodip direction. Updip pinch-out lines of upper Pictured Cliffs tongues may be areas where Fruitland coal seams drape over shoreline sandstones and have a higher fracture density because of compaction-induced fractures. The structural attitude of an upper Fruitland coal bed (Fig. 4.19) differs markedly from the structural attitude of other strata, such as the Huerfanito Bentonite (Fig. 4.2). Along paleostrike, coal seams split and interfinger with fluvial channel-fill sandstone complexes (Fig. 4.17), and many of these coal benches, rather than terminating against the channel sandstones, override or underlie them, forming zigzag splits similar to those described in coal-bearing strata in other basins (Britten and others, 1975; Ayers and Kaiser, 1984). Although these coal seams pinch and swell, they are laterally continuous, which contributes to their effectiveness as aquifers. Fractures related to compactional folding of coal beds are well documented (Donaldson, 1979; Houseknecht and Iannacchione, 1982; Tyler and others, 1991). If such fracture systems are sufficiently developed, areas of interbedded sandstones and coal seams would be good targets for coalbed methane exploration (Fig. 4.20).

This study has shown that Fruitland coal beds are more extensive and complex than previously inferred (Figs. 4.164.18). The significance of these findings is threefold. First, coalbed methane reservoirs are larger (more extensive) than previously thought. Second, compaction-induced fractures, and therefore enhanced coalbed permeability, may occur in areas where extensive coal seams drape over shoreline sandstones or form zigzag splits with channel-fill sandstone complexes. Finally, the greater lateral extent of coal seams, inferred from this research, is critical to the interpretation of ground-water flow and abnormal pressure in the Fruitland Formation (Kaiser and others, this volume, Chapter 8).

The viability of the hypothesis of increased fracture density where coal beds are folded is uncertain; additional subsurface and outcrop studies are required. However, given the abundance of folds and the potential for folding-induced fractures to contribute to enhanced coalbed methane production, such studies are warranted.

Coalbed methane activity and reservoir conditions

The Navajo Lake area has a long and noteworthy history of coalbed methane production. The Phillips No. 6-17 well (Figs. 4.2 and 4.3) is often referred to as the discovery well for coalbed methane in the San Juan Basin. This well, which is an open-hole completion in upper Fruitland coal beds and sandstones, is located on the northwest flank of a minor, north-plunging anticline. It has operated for more than 25 yrs with little decline in gas production (averaging 160 to 180 Mcf/d) or pressure (Hale and Firth, 1988). The well produces little or no water, indicating some element of structural and/or stratigraphic trapping. Although Hale and Firth (1988) discount structural trapping, their interpretation was based on a structure map of the Huerfanito Bentonite, which does not accurately reflect the structural attitude of Fruitland coal beds. Since 1985, Meridian Oil and Blackwood and Nichols have completed several coalbed methane wells in the Navajo Lake area, including the most productive coalbed methane wells in the United States. Some Meridian wells in this area (Figs. 4.2, 4.3, and 4.19) have produced at a rate of 300 to 15,000 Mcf/d (see Kaiser and Ayers, this volume, Chapter 10, for discussion of production). Meridian 400 wells are completed in lower Fruitland coal beds on the margin of a syncline and near the updip pinch-out of UP1 (Fig. 4.19).

In the Navajo Lake area, Fruitland coal beds are mostly in the area of regional overpressuring and highest Fruitland bottom-hole pressures; overpressuring is attributed to artesian conditions (Kaiser and others, this volume, Chapter 8). The boundary between overpressured and underpressured strata crosses the southern part of the area (Fig. 4.4); this boundary may be caused by southwestward pinch-out and/or offset of aquifer coal beds across faults that are inferred to make up the structural hingeline (Fig. 4.2). Both gas- and water-saturated coal seams are present in the Navajo Lake area. In this area, Fruitland coal rank increases from high volatile B bituminous at the south to medium volatile bituminous at the north (Scott and others, this volume, Fig. 9.3), and it contains more than 10 Bcf of methane/mi^2 (Ayers and others, this volume, Fig. 2.21). Fruitland coalbed gas is dry (C_1/C_{1-5} >95%), and it contains a high percentage of carbon dioxide (commonly 3-10%) (Scott and others, this volume, Fig. 9.10). Primary fractures (face cleats) in oriented cores from Blackwood and Nichols NEBU No. 403 trend northeastward, consistent with regional cleat trends in the southern part of the basin (Tremain and others, this volume, Fig. 5.1). Highly productive wells in the Navajo Lake area are reported to have fracture-enhanced permeability that may be predicted from lineament analysis. However, a recent study showed no significant relations between methane production and lineament attributes in the northern San Juan Basin (Baumgardner, this volume, Chapter 7). Geologic and hydrologic controls on producibility of coalbed methane in the Navajo Lake area are further discussed by Kaiser and Ayers (this volume, Chapter 10).

Summary and conclusions

In summary, we suggest both depositional and structural controls affect the occurrence and producibility of Fruitland coalbed methane in the Navajo Lake area. The distribution of thick coal seams was controlled by depositional setting, which in turn was structurally controlled; tectonically induced subsidence north of the hingeline temporarily confined the Pictured Cliffs shoreline to a narrow belt, and this

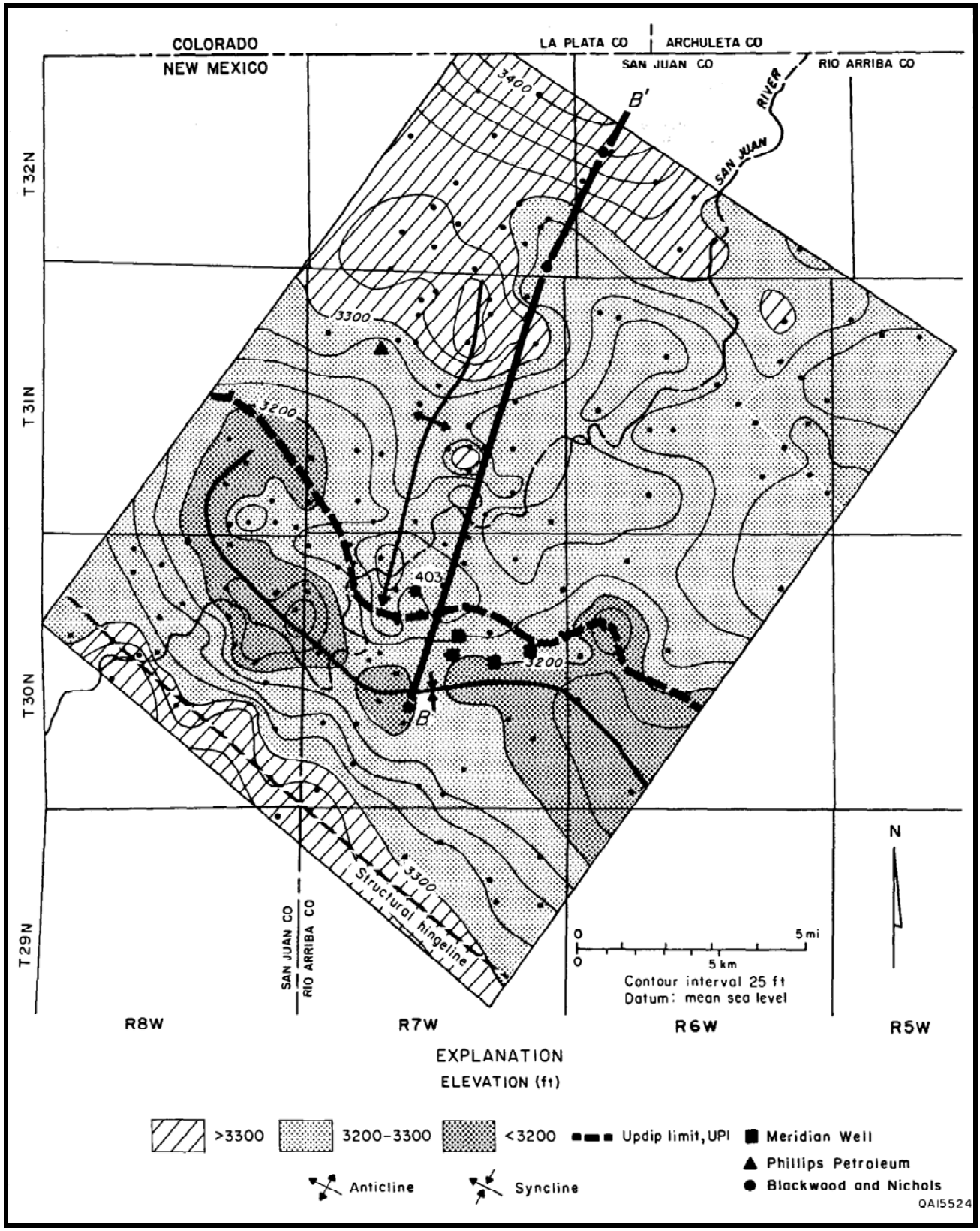

FIGURE 4.19—Structure map of upper Fruitland coal seam in Fig. 4.16. Attitude of the coal bed differs markedly from that of the Huerfanito Bentonite and the Pictured Cliffs Sandstone (Figs. 4.2 and 4.4, respectively). Structural trough occurs southwest of the pinch-out of UP1. Cross section B–B' is in Fig. 4.18.

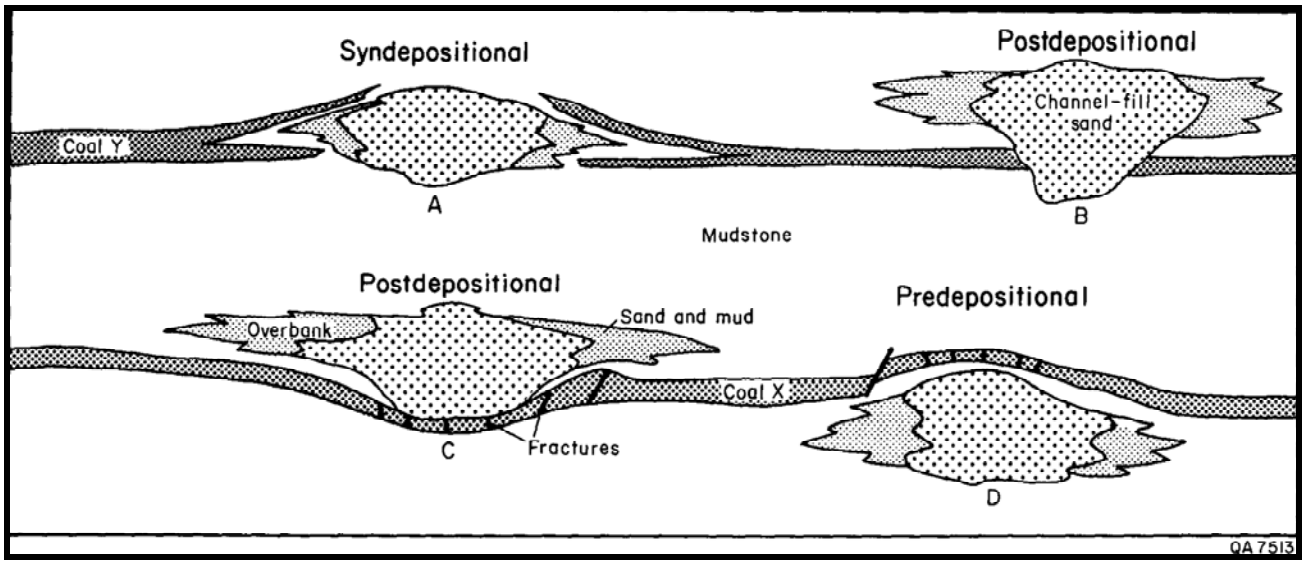

FIGURE 4.20—Relationship between depositional framework facies and coal seams. Coal seam Y splits and pinches out at interface with channel-fill sandstone A; seam Y was removed postdepositionally by channel B. Coal seam X is folded and fractured under postdepositional channel-fill sandstone C, and over channel-fill sandstone D (from Ayers and Zellers, 1988; concepts from Donaldson, 1979).

stillstand resulted in thick Fruitland coal seams by allowing thick peat to accumulate. Locally, low-amplitude folds of tectonic or differential-compaction origin may form conventional structural traps. Fractures associated with the folds may enhance permeability of Fruitland coal seams locally, thus improving the producibility of coalbed methane. We conclude the following.

1. In the Navajo Lake area, thick Fruitland coal formed in a back-barrier setting. During the Late Cretaceous, the Pictured Cliffs barrier-strandplain system prograded rapidly northward across the area of the present San Juan Basin. Sporadic subsidence north of a northwest-trending structural hingeline is inferred to have caused two major shoreline reversals and deposition of upper Pictured Cliffs transgressive-regressive sandstones, UP1 and UP2, that interfinger with the continental Fruitland Formation to the southeast.

2. Increased accommodation space north of the hingeline caused the Pictured Cliffs shoreline to aggrade within a narrow belt, favoring the accumulation of thick Fruitland peat; as much as 110 ft (33 m) of coal occurs in as many as 14 seams. Regionally, coal seams show strike-elongate geometry, with both the greatest net coal thickness and greatest number of coal seams occurring landward of the northwest-trending upper Pictured Cliffs shoreline sandstones. Although thin coal seams pinch out behind Pictured Cliffs shoreline sandstones, thick seams appear to override abandoned shoreline sandstones, commonly thinning basinward. Individual coal seams are podlike or dip elongate rather than strike elongate because along paleostrike they interfinger with, or thin and override dip-elongate Fruitland channel-fill sandstones.

3. In the Navajo Lake area, coal seams may be isolated from, or in contact with, Fruitland and Pictured Cliffs sandstones. Also, upper Pictured Cliffs sandstone tongues and the Pictured Cliffs Sandstone commonly are isolated from each other but are locally in contact. Permeabilities of Fruitland coal beds exceed those of Fruitland and Pictured Cliffs sandstones, but all of these units produce some gas. Because the dominant trend of the most extensive permeable units (Fruitland coal seams and Pictured Cliffs sandstones) is northwest, all other factors being equal, regional fluid movement parallel to that trend is favored.

4. From isopach maps, we conclude that during Fruitland and Kirtland deposition, a depocenter existed in the northwestern San Juan Basin and the Nacimiento uplift was active. The regional distribution of coal supports this conclusion; both the maximum and the net coal thicknesses decrease eastward in the basin, which may reflect deposition under less reducing conditions because of slower rates of subsidence. These conditions suggest lesser burial depths and thermal maturity for coal seams in the southeastern part of the basin.

5. Most structures in the Navajo Lake area formed after deposition of the Pictured Cliffs Sandstone. Minor structures that may cause conventional trapping and fracture-enhanced permeability are common in the San Juan Basin. However, minor structures mapped on the top of the Fruitland Formation may not parallel structures mapped on Fruitland coal seams because of differential compaction of Fruitland sand, mud, and peat.

6. Coalbed methane may be hydrodynamically trapped where thick coal seams pinch out to the southwest and where they are offset at the structural hingeline; the most productive wells in the basin are less than 5 mi (8 km) northeast of the structural hingeline.

Acknowledgments

We thank W. A. Ambrose, T. F. Hentz, W. R. Kaiser, and R. L. Hawks for their review comments. W. A. Ambrose described the Blackwood and Nichols NEBU No. 403 core.

5. Fracture (cleat) patterns in Upper Cretaceous Fruitland Formation coal seams, San Juan Basin

C. M. Tremain[1], S. E. Laubach[2], and N. H. Whitehead, III[3]

[1]*Colorado Geological Survey,* [2]*Bureau of Economic Geology,* [3]*New Mexico Bureau of Mines and Mineral Resources*

Abstract—Matrix permeabilities in Upper Cretaceous Fruitland Formation coals are low. Outcrop observations and production data indicate gas and water flow is through partially open, interconnected systems of short, discontinuous opening-mode fractures (cleats) and localized zones of more intense fracture development associated with faults and fracture swarms. Fracture pattern attributes relevant to gas-well development and completion design include spacing variation related to changes in coal rank, composition, and bed thickness, regional shifts in strike of systematic fractures resulting in two directions of strongly developed cleat trends in different parts of the basin, and fracturing and offset associated with faults. To evaluate controls on fracture (cleat) patterns in coal seams in the Fruitland Formation, we studied fractures in coal and adjacent sandstones in 11 cores and at 90 outcrop stations along the basin margin and mapped fractures in selected areas.

Introduction

Coal fractures (cleats) enhance gas and water flow in coal beds. With the increasing importance of coalbed methane as a natural gas source, information on cleat patterns is becoming critical for planning coalbed methane well placement and spacing. Moreover, fracture patterns in coal and adjacent rocks can affect the success of completion and stimulation techniques such as horizontal drilling, open-hole cavitation, and hydraulic fracture treatment. More than 1,000 methane wells have been drilled in the Fruitland Formation of the San Juan Basin of Colorado and New Mexico in the past decade, making it one of the most important coalbed-methane-producing areas in the country. The aim of our study is to document cleat characteristics and patterns in the Fruitland Formation in this basin. Results can help guide coalbed methane development in the San Juan Basin and provide a standard of comparison for cleat patterns in other coalbed-methane-producing basins in western North America.

Previous studies of cleat on the northwestern margin of the San Juan Basin documented northwest, north, and northeast fracture strikes (Newman and McCord, 1980; Condon, 1988), and northwest and northeast fault strikes (Fig. 5.1). Newman and McCord reported joint strikes in sandstones at 70 locations in the Colorado part of the San Juan Basin and cleat strikes at approximately a dozen stations. Condon measured cleat and/or joint strikes at 37 locations on the northwest side of the Colorado part of the basin. Our study builds on this previous work with observations of fracture orientations and intensity made from 90 outcrop stations and 7 oriented and 5 unoriented cores from wells in Colorado and New Mexico. We mapped fracture patterns in coal and adjacent sandstone bedding plane (pavement) outcrops and documented cleat orientation, length, spacing, and mineral fill.

Characteristics of Fruitland Formation cleat

Cleats are systematic fractures in coal that are equivalent to joints in other sedimentary rocks. Cleats in Fruitland Formation coal beds are opening-mode fractures that are perpendicular to bedding, generally planar, commonly uniform in strike within an outcrop or core, and arranged in subparallel sets (Table 5.1). Crossing or mutually abutting fracture patterns are present locally, but relative ages of cleats can be generally determined on the basis of abutting relations, where a younger fracture terminates against a preexisting fracture. The earliest formed fractures, against which other fractures terminate, are called face cleats (Fig. 5.2). Face cleats are planar, smooth-sided fractures that *usually* make up the most prominent fracture set. They may be as much as several meters long in plan view. Butt cleats formed later and in most cases strike perpendicular to face cleat, with average angles of intersection typically between 80° and 90°. A single face-cleat set and an associated, nearly orthogonal butt-cleat set are present in most exposures. However, butt cleats are locally absent in core and in some outcrops. Butt cleats are much shorter than face cleats, having lengths commonly less than 4 inches (<10 cm). Their surfaces are predominantly irregular and hackly, and they are typically less continuous and less well developed than associated face cleats, although in some areas or in particular coal beds both cleat sets are equally developed (Table 5.1, locations 18 and 19).

Fractures in regional cleat sets in the San Juan Basin coal seams cut across subhorizontal compaction fabrics defined by flattened objects such as coalified wood. Locally, fractures in cleat sets cross rigid concretions. Cleats are perpendicular to bedding planes regardless of bedding plane dip. Consequently, face- and butt-cleat inclinations are locally as low as approximately 30° to 40° in the northern San Juan Basin, where coalbed dips of up to 50° occur on the Hogback monocline.

Cleat strikes are generally uniform over wide areas of the basin (Fig. 5.1), but curved cleats are evident in some large exposures and in several mine floors (Figs. 5.3a and 5.3b). In addition to face and butt cleats, other systematic, generally less closely spaced fracture sets occur in some coal outcrops (Table 5.1). Among these are fractures that are indistinguishable from cleats except for their divergent strike. These fractures occur in association with typical face and butt cleats; abutting relations suggest that some of these fractures predate the main face-cleat set whereas others are younger. Fractures with polygonal patterns occur in some dull (bone) coals where other cleat sets are absent. Faults and associated fractures crosscut cleat in some areas; elsewhere, cleats curve as they approach faults.

Cleat types and cleat spacing

Cleat spacing in Fruitland Formation coal ranges from less than 0.04 inch (<0.1 cm) to more than 1 ft (>30 cm). To obtain cleat spacing measurements that can be compared from one station to another, we define a hierarchy of cleat (fracture) sizes that can exist within a given bed. These range from primary cleats that extend across one or several coal-type (lithotype) layers, to secondary and tertiary cleats that are vertically discontinuous within coal-type layers (Fig. 5.4). These fractures and associated butt cleat (which also shows a hierarchy of sizes) give coal its blocky appearance.

We distinguish three measures of fracture intensity in Fruitland coal: primary-face-cleat spacing; total fracture in-

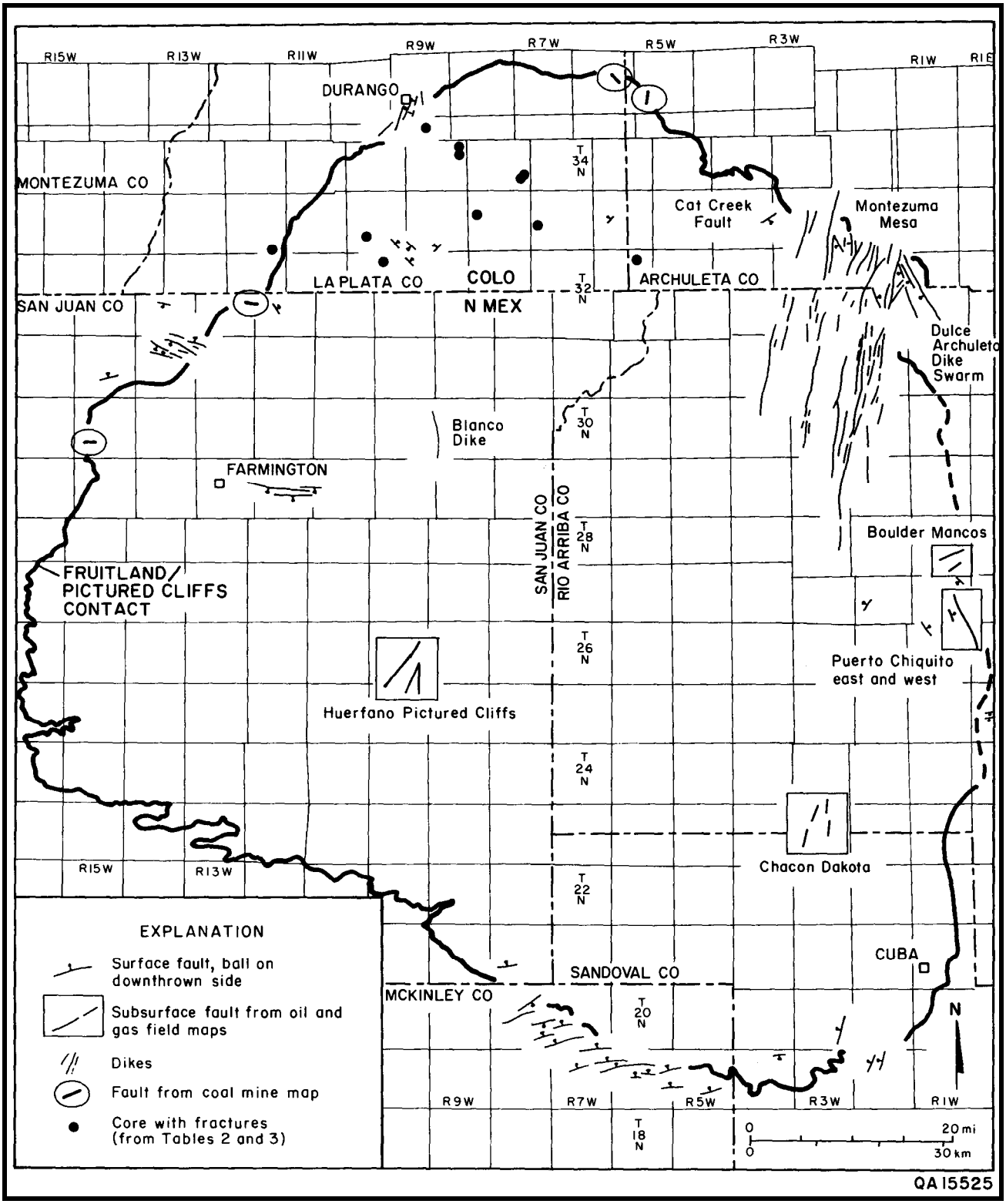

FIGURE 5.1—Faults and dikes in the San Juan Basin

tensity, defined as total number of fractures (primary, secondary, and tertiary) along a given distance in a coal seam; and fracture density, defined as total length of all fractures in a given area. Such measurements and fracture connectivity indices (Laubach and Tremain, this volume, Chapter 6) may provide a better indication of fluid flow in coal. In this report we use primary-face-cleat spacing as our standard measure of cleat intensity in outcrop because many of the exposures we studied are too small for fracture density measurements. Total fracture intensity was used in core measurements.

Primary cleats are the prominent cleat set in most Fruitland exposures. Two scales of primary cleat are evident locally. The most common primary cleats in Fruitland coals have average spacing of 1 to 3 inches (2 to 8 cm), are 1 inch to over 3 ft (several centimeters to over a meter) long, and

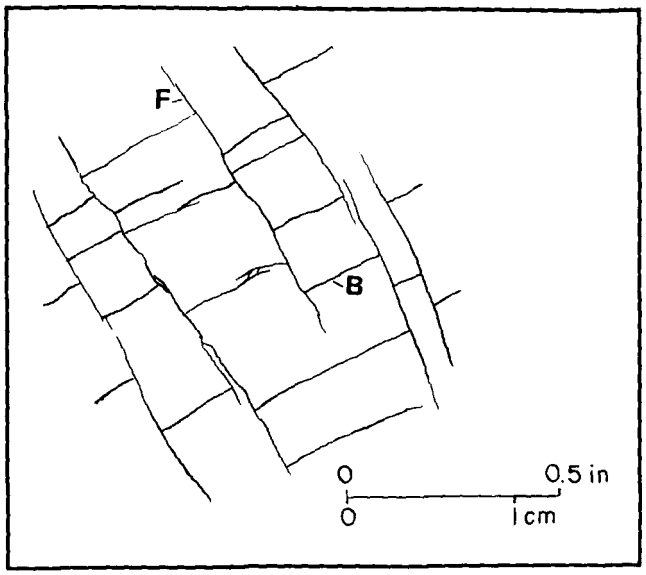

FIGURE 5.2—Diagram illustrating abutting relations between face (F) and butt (B) cleats.

commonly have oxidized surfaces indicating fluid flow. Their height is equal to the thickness of the coal lithotype layer in which they occur, from a foot or more (several tens of centimeters) tall in thick layers to less than half an inch in thin vitrain layers. They rarely cross interbedded tonsteins or thin shale partings, even where interbeds are less than half an inch thick. For example, in one lower Fruitland coal bed in the Pinto pit (Navajo mine), fewer than 20% of cleats penetrate or cross interbeds 0.2 inch (0.5 cm) thick or less. Master cleats (Henkle and others, 1977) are primary cleats that cross several coal-type layers. Master cleats are visible in some large Fruitland outcrops and coal pits, where spacing ranges from 1 to 3 ft (30 cm to 1 m). Where coal seams are less than 6.5 ft (<2 m) thick, master cleats may cross the entire seam.

Secondary cleats are fractures parallel to primary cleats that are *vertically discontinuous* within a lithotype. Secondary cleat spacing is commonly 1 to 2.5 inches (2.5 to 6.3 cm) in subbituminous to high volatile C bituminous coals in the southern part of the basin and 0.25 to 0.5 inch (0.6 to 1.2 cm) in high volatile B bituminous coals in the west. Spacing ranges from 0.12 to 0.25 inch (0.3 to 0.6 cm) in high volatile A bituminous coals in the northern part of the basin. Length and height of secondary cleats are generally less than 1 inch (<2 cm). The distinction between primary and secondary cleats is obvious in outcrop but less so in core.

The hierarchy of fracture sizes applies to butt cleat as well as face cleat. Most butt cleats could be classified as secondary cleats in that they rarely extend completely across coal lithotype layers; they are vertically and laterally less persistent than associated face cleats. Butt-cleat spacing is generally greater than face-cleat spacing in the southern San Juan Basin, but it is commonly similar to or closer than face-cleat spacing in the central and northern San Juan Basin.

Tertiary cleats *are* closely spaced fractures and micro-fractures with spacing and height on the order of 0.04 to 0.12 inch (0.1 to 0.3 cm) or less that occur between primary or secondary cleats. Intensity of tertiary cleats is commonly greater in weathered outcrops, and locally, where fresh coal can be traced into weathered exposures, tertiary cleats become more prevalent. Lack of mineral infill or staining, greater intensity in weathered outcrops, and terminations at open horizontal unloading fractures suggest that tertiary

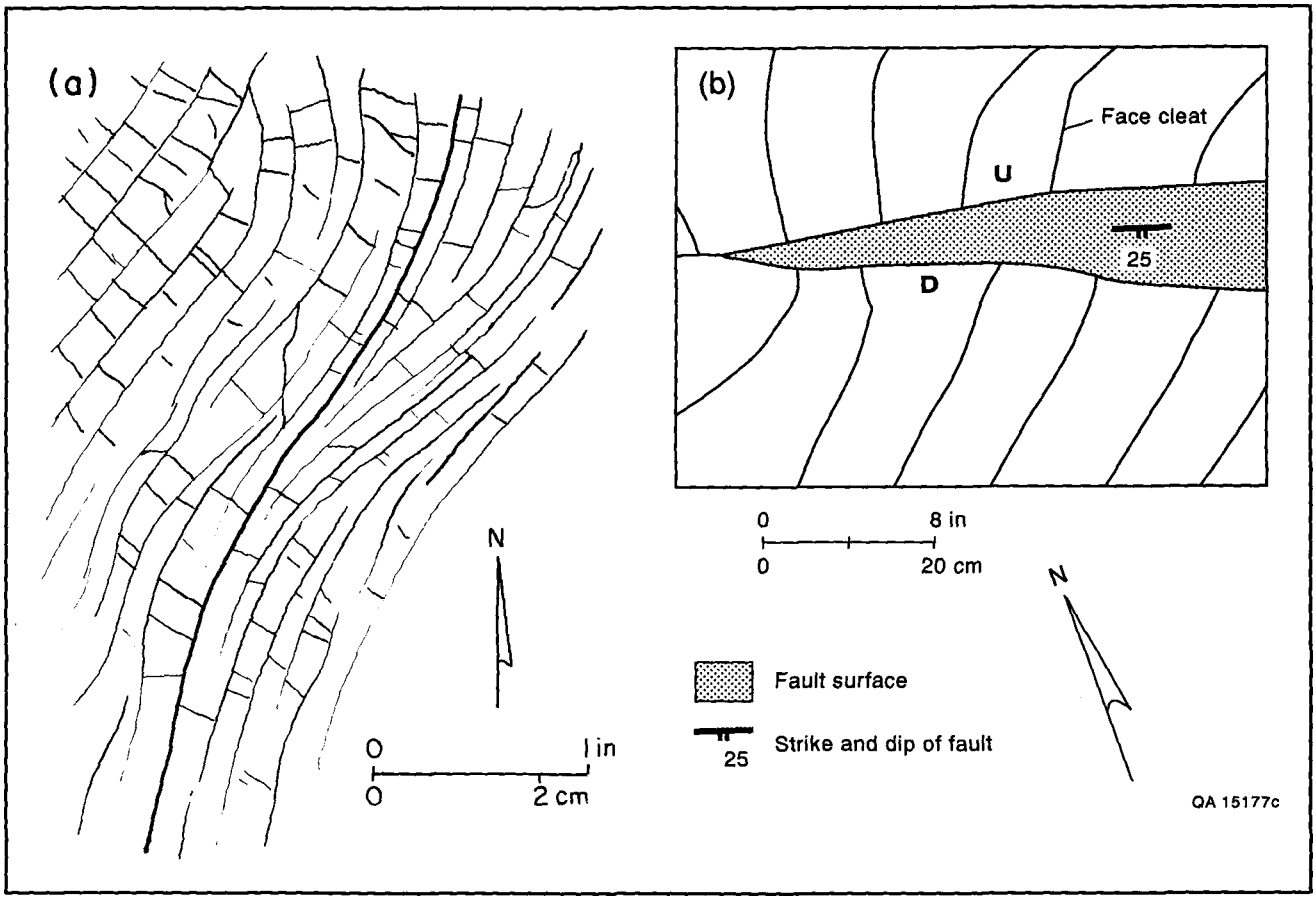

FIGURE 5.3—(a) Bundle of curved cleat traces in flat-lying coal, Fossett Gulch. (b) Curved cleats near small normal fault, Navajo mine.

TABLE 5.1-Fruitland coal cleat stations.

Loc. no.	Location	Mean face strike	Primary spacing (inches)	Secondary/ tertiary spacing (inches)	Coal/seam attitude (strike/dip)	Position	Luster and rank	Comments (see below)
1	A+B mine NWNE 32, 33N, 2W	334	1½	-	356/2	3.3 ft above PC	HVA	2
2	Old Talian mine SENESW 16, 33N, 3W	336	¼ 1¾	1/16	288/33	lower Kf	Bright	1, 6
3	Chimney Rock strip NE 30, 34N, 4W	329	-	-	310/7	mid Kf	A-HVB B-HVA C-HVA	4
4	East Fosset Gulch Road NWNE 24, 34N, 5W	42	2¾	1/32-3/8	318/7	lower Kf	Dull	2, 6, 5, 10
5	West Fosset Gulch Road NENE 15, 34N, 5W	324	¼	1/32	328/31 290/35	24-ft seam near PC	HVA	3, 5, 11
6	Squaw Creek CNE 9, 34.5N, 5W	326	-	1/16	325/26	lower Kf	HVA	2, 4, 9, 19, 21
7	Beaver Creek Road SESE 13, 35N, 6W (2 seams)	2 314	- 1½	- 1/16 ¼	- 294/30	lower Kf	- Dull HVA	11, 20
8	Los Piños mine SWNW 14, 35N, 7W	16	¾ 1½	1/8	295/40	lower Kf	Moderate bright HVA	5
9	South Fork Texas Creek NWSE 7, 35N, 7W, CW½ 8, 35N, 7W	345 356	½ 2¼	1/8 ¼	76/21 95/29	lower Kf	Weathered Dull	1, 5, 8, 19
10	Florida River 24, 35N, 9W	325	¼ 2	1/32 1/8	42/40 67/62	lower Kf+ Kf tongue	Moderate dull	5, 12, 15
11	La Plata mine SE 27, 35N, 9W (4 seams)	344	-	-	-	mid Kf	-	1, 6
		338	1 10	1/32	59/41	mid Kf	-	
		330	¾ 2½	1/16 -	40/40	lower Kf	HVA	
		337	-	-	50/35	Kf tongue	-	
12	Carbon Junction strip SESE 33, 35N, 9W NWNE 53, 34, 5N, 9W	340	½ 6	1/32 ¼	48/26 -	Kf tongue	HVA	13, 20
13	Carbon Junction road cut SWNW 4, 34N, 9W	340	-	1/16	27/24	lower Kf	-	1, 8, 20
14	East Gap NWSW 17, 34N, 10W NE 18, 34N, 10W (2 seams)	356	¾ 1½	¼ 1/8	355/23 330/9	mid-lower Kf	Weathered ?	3, 5, 12
15	West Gap SENE 13, 34N, 11W	353	¾-1½	¼-1/8	40/11	lower Kf	Weathered	3, 5, 7
16	Houston well SWSE 9, 33N, 11W	286	-	¼	38/31	lower Kf	-	6
17	Fort Lewis mine NENE 1, 32N, 12W NESE 36, 33N, 12W	NW	¼-12	1/32-¼	25	lower Kf	HVA	2, 3, 6, 14
18	Old Soda Springs mine CSE 1, 32N, 12W	314	-	¼-½	25/9	lower Kf	HVA-HVB	5, 7, 22
19	Cinder Buttes NENE 14, 32N, 12W	317	1 12	-	17/11 32/12	lower Kf	HVB	1, 5, 7

1 = planar cleat
2 = curved cleat
3 = local curved cleat
4 = variable strike
5 = "third cleat" present
6 = friable
7 = blocky
8 = poor butt-cleat development
9 = striations (slickensides)
10 = "third cleat" abuts face cleat
11 = 2 stations combined
12 = 3 stations combined
13 = 5 stations combined
14 = 27 stations combined
15 = Fruitland SS jnts strike 330-350
16 = Fruitland SS jnts strike 330
17 = Fruitland SS jnts strike 345-350
18 = Fruitland SS jnts strike 347, 285
19 = Fruitland SS jnts strike 016, 355
20 = Fruitland SS jnts strike NW
21 = calcite-filled veins in PC strike 330
22 = gas bleeding from coal

HVA = high volatile A bituminous
HVB = high volatile B bituminous
Dash indicates attribute not determined.

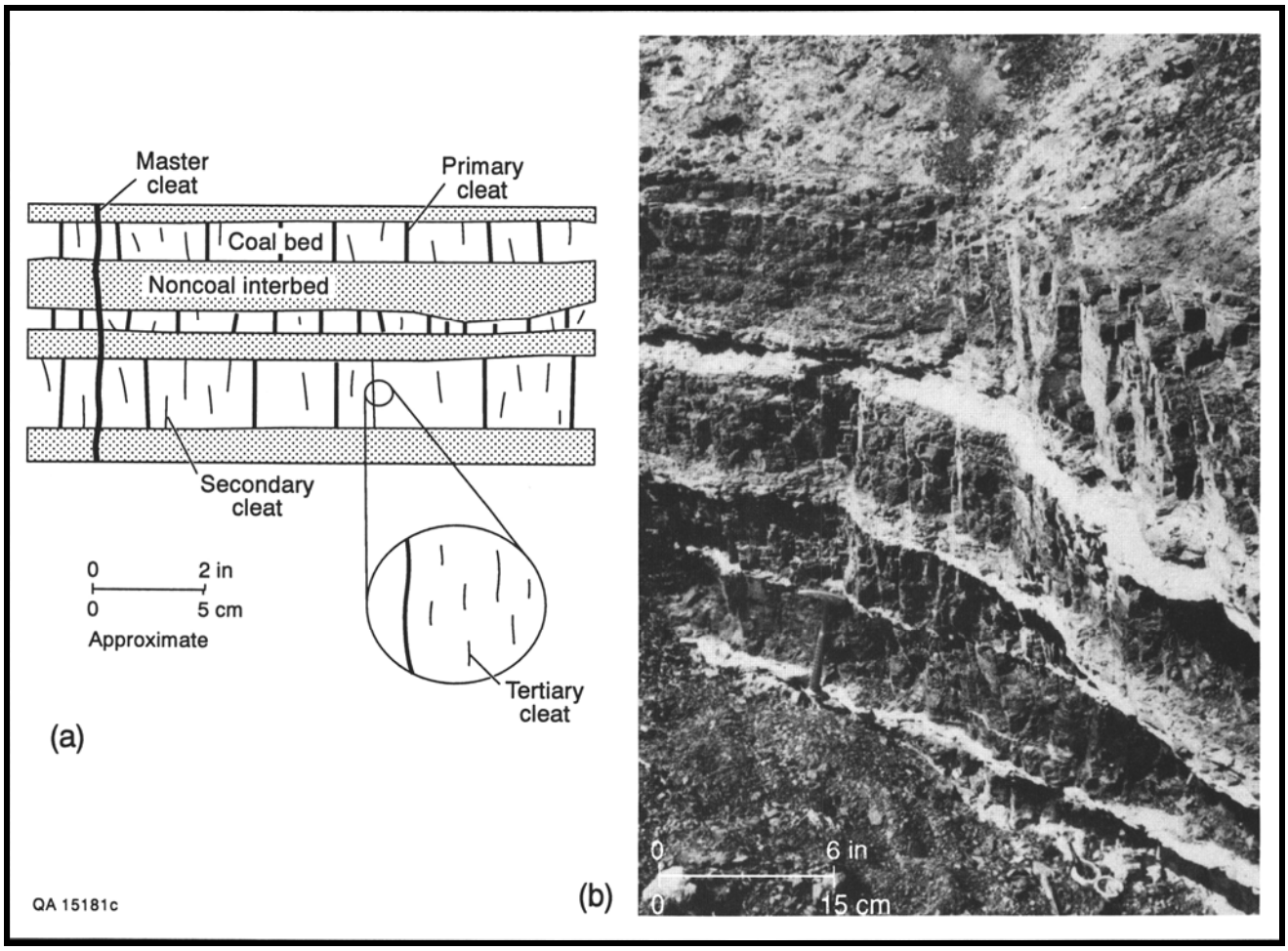

FIGURE 5.4—Hierarchy of cleat sizes. (a) Diagram illustrating primary, secondary, and tertiary cleats. (b) Photograph showing primary cleats terminating at interbedded tonsteins and secondary cleats terminating within coal-type layers. This hierarchy of fracture sizes suggests that approaches that account for scaling properties of fracture patterns (fractal geometry) should be applied to coal fractures (see Laubach and Tremain, this volume, Chapter 6).

cleats formed near the Earth's surface and may not have been present at depth.

Cleat spacings in coal cores are similar to those in coal beds at outcrop (Tables 5.1, 5.2, and 5.3). In core, cleat spacing ranges from less than 0.04 inch to an inch or more (0.1 to several cm). Core observations do not indicate significant variation in cleat spacing with depth, but cleat intensity appears to be greater in bright coals and thinner coal beds, as is the case in outcrop. In core and in fresh mine exposures, secondary and tertiary cleats are less prevalent and less closely spaced than in natural outcrops.

Spacing of coal fractures in regional cleat sets (total fracture intensity) is uniform over distances of as much as a mile where coal occurs above sandstones with planar upper surfaces. For example, in a single 4-inch-thick (10-cm) layer of uniform-composition coal approximately 15 ft (~4.6 m) above the Pictured Cliffs Sandstone that is exposed in a highwall over a distance of 2,300 ft (700 m) in the Navajo mine, most cleat spacing values fall within one standard deviation of the mean of the entire data set (Fig. 5.5). Where sandstones have irregular contacts, and locally near lateral terminations or beneath thick parts of lenticular fluvial sandstones, cleat intensity increases by as much as 25%. Such an increase in fracture intensity could arise from several processes, including fracturing caused by stress concentrations at irregularly shaped lithologic boundaries. Variation in primary regional cleat spacing and localization of other fracture types such as small faults at or near irregular rock-type boundaries occur in some Cretaceous coals in the western United States (Tyler and others, 1991).

Causes of variation in cleat spacing

Previous studies suggest that cleat spacing is controlled by coal rank and lithotype as well as bed thickness (Ammosov and Eremin, 1960). Primary cleat spacing in the San Juan Basin depends on coal rank and type, and to a lesser extent, within areas of equal rank, on stratigraphic and structural position and on the thickness of individual coal beds within a seam. In Fruitland coal beds, average primary face cleat is closer in the higher rank coals in the northern third of the basin than in the lower rank coals to the south. Mean primary-face-cleat spacing is 1.5 inches (4 cm) in outcrops along the northern and western margins of the basin. In the southern San Juan Basin, where coal rank is lower, spacing ranges from 0.75 to 6 inches (2 to 15 cm), but typically is between 2.5 and 3.5 inches (6.5 and 9 cm) for medium-brightness coal. Decreased cleat spacing with increased bituminous coal rank has been reported in other basins (Ammosov and Eremin, 1960; Ting, 1977).

Primary cleat spacing depends in part on coal type (Ammosov and Eremin, 1960; Ting, 1977). In Fruitland coals, spacing is closest in bright vitrain-rich layers and widest in dull durain-rich layers. Some primary cleats in 0.1-inch-

TABLE 5.2—Mineralization in fractures in coal core.

Well name	Location	Core depth (ft)	Mineralization	References
USGS Core Hole A-15	Sec. 1 T23N R13W	262-295	Gypsum	Wilson and Jentgen, 1980
USGS Core Hole A-4	Sec. 30 T24N R13W	276-296	Pyrite, gypsum	Wilson and Jentgen, 1980
El Paso Natural Gas Gasbuggy No. 1	Sec. 36 T29N R4W	3803-3819, 3880-3910	Calcite, pyrite	Fassett, 1967
Blackwood & Nichols NEBU No. 403	Sec. 9 T30N R7W	3025-3059	Calcite	Mayor and Close, 1989a
Tenneco Pritchard No. 9	Sec. 1 T30N R9W	2467-2491, 2621-2651	Calcite, gypsum	CGS files
Western Coal P-70	Sec. 22 T30N R15W	384-414	Calcite, pyrite	TRW Preliminary Well Test Report, 1978
USGS Core Hole SJ 23-4	Sec. 23 T30N R15W	461-471, 583-608	Pyrite, gypsum	Beach and Jentgen, 1978
Tiffany Glover No. 1	Sec. 2 T32N R6W	3062-3111	Calcite	Jones, 1985
Mobil Colorado 32-7, No. 9	Sec. 4 T32N R7W	2783-2804	Pyrite	COGCC files
USGS No. 2	Sec. 23 T32N R12W	61-119	Pyrite	Roberts, 1989
USGS No. 10	Sec. 31 T33N R11W	337-397, 416-460	Pyrite	Roberts, 1989
Amoco Hott 29-1, No. 2	Sec. 29 T33N R6W	3021-3031	Calcite	COGCC files
USGS No. 8	Sec. 36 T33N R12W	75-129	Pyrite	Roberts, 1989
SUTEC Oxford No. 1	Sec. 25 T34N R8W	2769-2787	Calcite	CGS files
SUTEC Oxford No. 2	Sec. 25 T34N R8W	2832-2850	Calcite, gypsum, pyrite	CGS files
Tenneco Fassett 2-13	Sec. 13 T34N R9W	2468-2482	Calcite	CGS files

CGS = Colorado Geological Survey

COGCC = Colorado Oil and Gas Conservation Commission

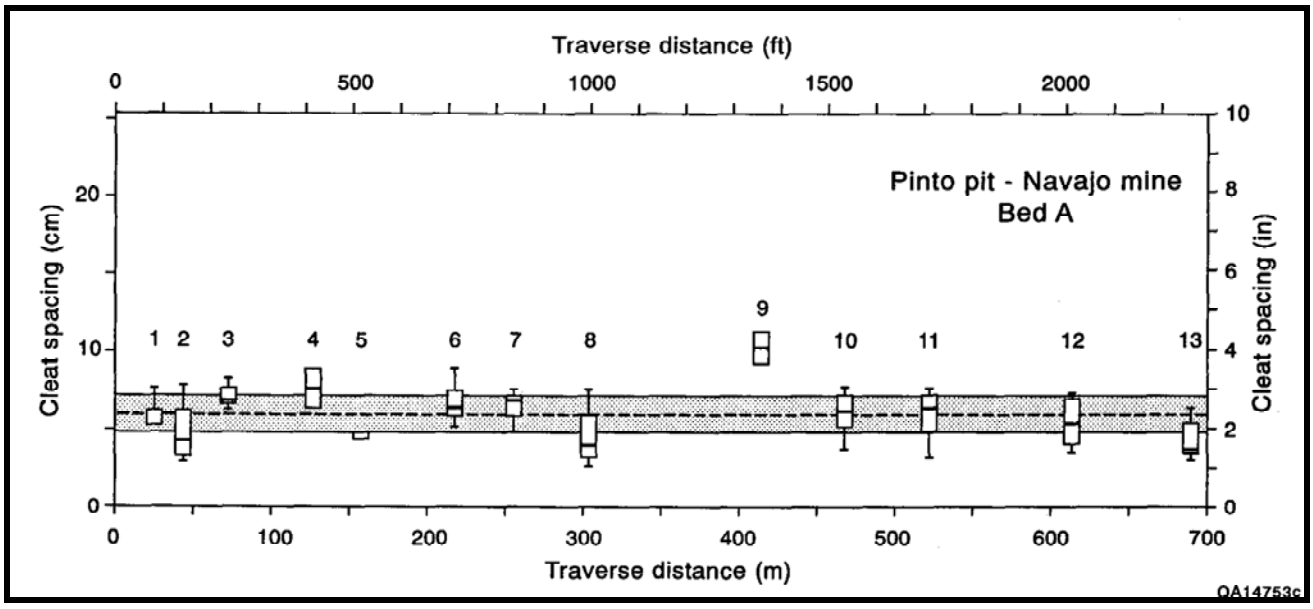

FIGURE 5.5—Cleat spacing versus traverse distance in a bed of uniform dip, thickness, and composition, Navajo mine. Center half of the data at each station is represented by a rectangle (box) and median is indicated by a bar. Dashed line and shaded area represent mean and one standard deviation of measurements from all stations.

TABLE 5.3-Oriented cores.

Well name and location	Cleat orientation	Cleat frequency (number/cm)	Cleat length	Fruitland coal stratigraphic position	Coal sample depth (ft)	Coal rank	Comments and references
Bowen-Edwards McCulloch 28-1 SWSE sec. 28 T34N R10W[1]	Face: 320-340° Butt: 40-70°	-	0.4 mm-13.4 cm 75% avg. 1.11 cm 25% > 2.54 cm	Lower	3140.5-3143	?	COGCC[2]
Amoco Southern Ute Tribal H No. 1 NWNW sec. 18 T32N R10W	Face: 20-40° Butt: 280-320°	Face: 4.3-17/cm avg. 7.1/cm Butt: 3.3-15/cm avg. 6.1/cm	Face: <0.1-4.5 cm avg. 2.3 cm Butt: <0.1-3.7 cm avg. 1.8 cm	Lower	3110-3131		(TerraTek, 1990)
Mesa Hamilton No. 3 SWSW sec. 30 T32N R10W1	Face: 30-50° Butt: 300-320° Third: 0-10°	All beds: 1-16/cm Core 2: 1-8/cm	All beds: avg. 4 cm Core 2: max. 9 cm	Upper	(1) 2652-2670.6 (2) 2673.8-2680.9	HVA	"Cleat frequency, length .. . inversely proportional to ash content" (Decker and others, 1989)
		Core 3: max. 12/cm	Core 3: 0.1 mm-18 cm	Lower	(3) 2872-2886.8		
Mobil Colorado 32-7 No. 9 SWSW sec. 4 T32N R7W	Face: 0-20° Butt: 80-110°	Face: 2-22/cm Butt: 3-18/cm Thin vitrain: Face: 28/cm Butt: 20/cm	Face: 1-3 mm	Lower	2906.6-2911.7	MV	"Some gouge and calcite filled fractures in sandstone below coals, strike same as cleats" (GRI-90/0043 Mayor and Close, 1989c)
Tiffany Glover No. 1 NESE sec. 2 T32N R6W	Face: 294°	Face: 2/cm Butt: 1/cm	-	Lower	3074-3089	MV	"Some calcite on cleats" (Jones, 1985)
Blackwood & Nichols NEBU No. 403 SENE sec. 9 T30N R7W	Face: 20-40° Butt: 300-320°			Upper	3025.5-3058.5	HVA	"Calcite in joints and cleats, late-stage joints in face cleat direction"; "cleat . . . varies inversely with lithotype thickness"; "cleats terminate at partings" (GRI-90/0041 Mayor and Close, 1989a)
				Lower	3160.6-3186		
McKenzie Methane So. Ute Mobil 36-1 SENE sec. 36 T34N R10W	Face: North	avg. 6/cm in thin vitrain: avg. 15/cm max. 40/cm	avg. 6 mm max. 3 cm 0.5-5 mm (layer thickness1	Mid	2415.2-2453.9	MV	(GRI-90/0042 Mayor and Close, 1989b)

MV = medium volatile bituminous
HVA = high volatile A bituminous
[1]Well number on Fig. 1
[2]Geological well report, Colorado Oil and Gas Conservation Commission
Dash indicates attribute not determined

thick (0.25-cm) vitrain-rich layers or lenses have spacing of less than 0.04 inch (<0.1 cm), whereas some thin dull (or bone) coal layers are virtually uncleated. However, these thin lenses of very bright or dull coal are volumetrically insignificant (<10%); most Fruitland coals that we examined are of intermediate composition, ranging from medium bright to medium dull. We used a qualitative visual field assessment of coal brightness to distinguish three categories of medium-brightness coal. Within this range of coal composition, no significant trend of cleat spacing with coal type is evident (Fig. 5.6).

Fracture spacing in coal and in many other stratified rocks is commonly inversely proportional to bed thickness, with more closely spaced fractures in thinner beds and spacing somewhat less than bed thickness (Ladeira and Price, 1981; Spears and Caswell, 1986). Thickness of coal beds (those divisions of a coal seam separated by noncoal layers such as shale partings or tonsteins) within medium-brightness coal seams in the northern and western San Juan Basin ranges from less than 0.4 inch (<1 cm) to more than 20 inches (>50 cm), with a mean thickness of 4 inches (10 cm). Primary-face-cleat spacing in these beds ranges from 0.04 to 12 inches (0.1 to 30 cm), with a mean spacing of 1.6 inches (4 cm). Although primary cleat spacing can be as much as 4 inches (10 cm) for a bed 2 inches (5 cm) thick, most beds less than 8 inches (<20 cm) thick have cleat spacing of less than 2 inches (<5 cm), and several beds that are between 10 and 12 inches (25 and 30 cm) thick have spacing of less than 4 inches (<10 cm). No systematic increase in cleat spacing is evident for beds thicker than 4 inches (>10 cm).

Some variation in cleat spacing for a given bed thickness may be due to compositional effects, because a range of coal compositions has been included in the medium-brightness coal data set. In some exposures, cleats are more widely spaced in thicker coal beds, but observations from several localities in the northern third of the basin indicate a relation between bed thickness and cleat spacing that has marginal statistical significance (Figs. 5.7 and 5.8), even when brighter and duller varieties of medium-brightness coals are excluded. Variance of cleat spacing increases as beds become thicker.

Coal beds with many vitrain-rich layers and numerous tonsteins or shale partings tend to be densely cleated because thin beds and vitrain-rich layers tend to have closely spaced cleats. However, the cleat system may be poorly interconnected vertically because cleats tend to terminate at noncoal interbeds or margins of vitrain-rich layers.

Cleat-filling minerals

Many fractures in Fruitland coals are barren and lack macroscopically visible infill minerals, but some cleats have

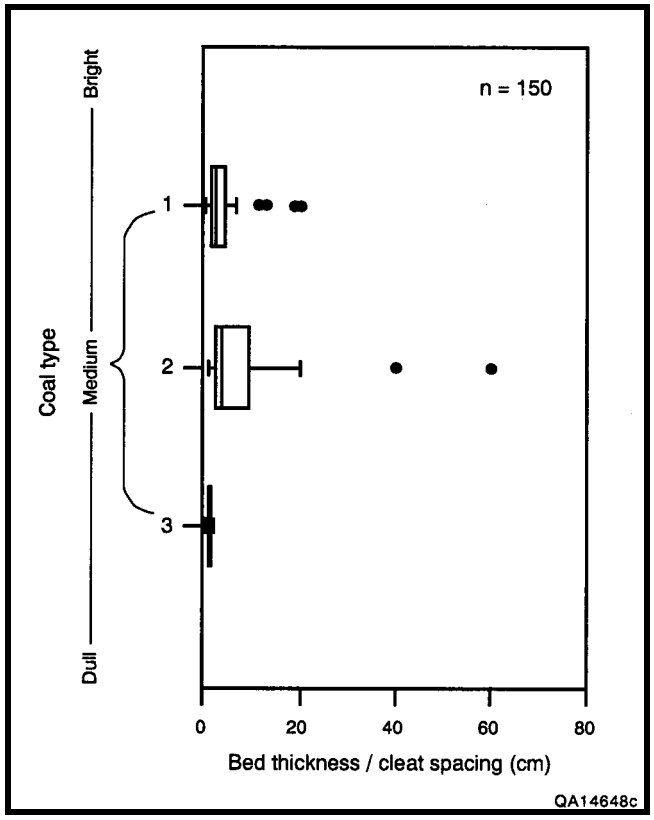

FIGURE 5.6—Coal type versus bed thickness/cleat spacing ratio (spacing index) for three classes of medium-brightness coal, Fruitland Formation, San Juan Basin. Center half of data is represented by a rectangle (box) and median is indicated by a bar.

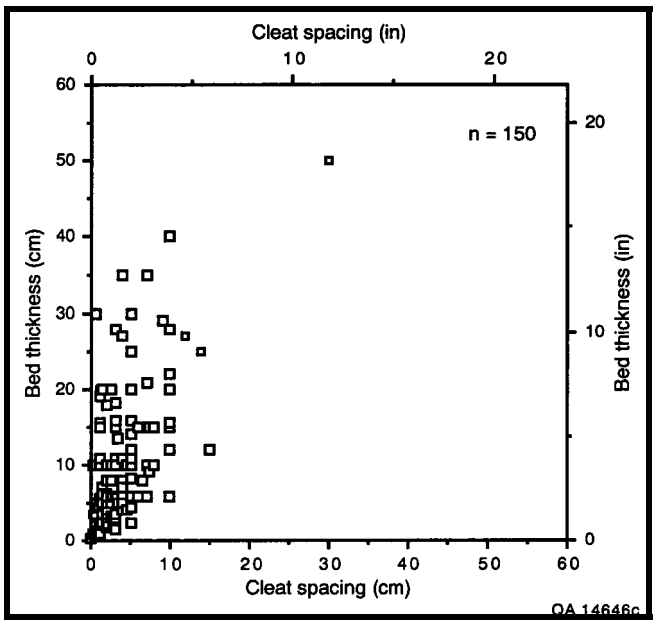

FIGURE 5.7—Cleat spacing versus bed thickness for Fruitland coal beds in northern San Juan Basin.

thin mineral veins. Principal cleat-filling minerals, pyrite, calcite, siderite, and gypsum, are present in outcrop and in core from depths ranging from 0 to 3,900 ft (0 to 1,190 m) in the northern and central basin (Table 5.2). Pyrite occurs in thin films and isolated patches on some cleat surfaces in mines and core. In outcrop, primary face cleats commonly have a reddish-brown to red stain that may represent oxidation products of finely disseminated sulfides formerly present in fractures. Near the Colorado—New Mexico border, isolated pyrite rosettes occur on both face- and butt-cleat surfaces.

Calcite fills some primary face cleats in several mines (Table 5.1, locations 2, 3, and 4) and in cores from 10 wells (Table 5.2). In sandstone of the SUTEC No. 1 Oxford core, calcite occurs in a vertical extension fracture that is parallel to, and possibly continuous with, adjacent calcite-filled cleats. Calcite-filled cleats and parallel calcite-filled fractures in sandstone also occur in the Chimney Rock mine in Colorado, and vein widths are as much as 0.05 to 0.1 inch (1.3 to 2.5 mm) in some New Mexico examples. Calcite typically has a fibrous habit.

Cleat-filling fibrous gypsum is present in several outcrops in New Mexico, in the Navajo mine, in three shallow USGS cores from New Mexico, and in core from Tenneco Pritchard No. 9 and SUTEC Oxford No. 2 wells. In exposures in the northern San Juan Basin, fine-grained clay minerals (kaolinite?) occur on some face-cleat surfaces. Fracture-filling resin is common in outcrop and in core from USGS wells in New Mexico and Colorado, and in Western Coal P-70 core (Table 5.2), but on the basis of abutting relations, most of these resin-filled veins are thought to predate regional cleat. Resin in primary face cleat is rare. Where present, pyrite and calcite mineral fill generally exists in primary face cleats in a given bed, but maps of fractures in coal pavements show that mineral fill is discontinuous along fracture traces (Fig. 5.9). Many butt cleats, and most secondary and tertiary cleats, lack mineral fill or stain.

Wide mineral-filled veins and vein networks occur near some faults and in several outcrops where presence or absence of faults could not be demonstrated. Vein widths are as much as 0.4 inch (1 cm). Veins are filled with gypsum, calcite, or quartz, and subsidiary pyrite and clay minerals. Infilling gypsum has a fibrous habit, and locally veins have medial lines and coal inclusions.

Cleat orientation

Cleat strike was measured in 7 cores (Table 5.3) and 90 outcrop stations. Core orientation was by standard down-hole orientation techniques (Nelson and others, 1987); strike uncertainty is approximately ± 10°. Outcrop stations ranged from selected areas of large, active open-pit mines and abandoned mines to natural exposures and small excavations. Most stations have areas of 100 ft^2 (9 m^2) or less. Fracture measurements in steeply dipping beds were restored to prefolding attitudes stereographically by rotation about strike of bedding. In general, change in cleat strike because of this rotation is less than 10°. In selected areas, cleat measurements were supplemented by maps of cleat patterns on bedding surfaces. Cleat maps were constructed either by mapping with reference to a grid marked on the outcrop or by mapping directly on color photographs.

Face cleats strike predominantly northwest in the northern San Juan Basin, and predominantly north or northeast in the southern part (Fig. 5.1). Cleat strike typically varies by less than 10° in individual cores and in most small (<100 ft^2 [<9 m^2]) outcrops (Table 5.1, locations 9, 14, and 19). Large, continuous or nearly continuous exposures show that in parts of the basin cleat strikes are nearly constant over large areas. For example, face-cleat strikes vary by less than 5° in a 2,300-ft (700-m) transect in the Pinto pit in the Navajo mine. In a traverse approximately 6 mi (~10 km) long in mid- to lower Fruitland coals between the Las Animas and Florida Rivers, mean face-cleat strikes at 15 stations (face n >6 per station) have a maximum variation of 37° (dispersion = 0.85), but typically vary by less than 10°

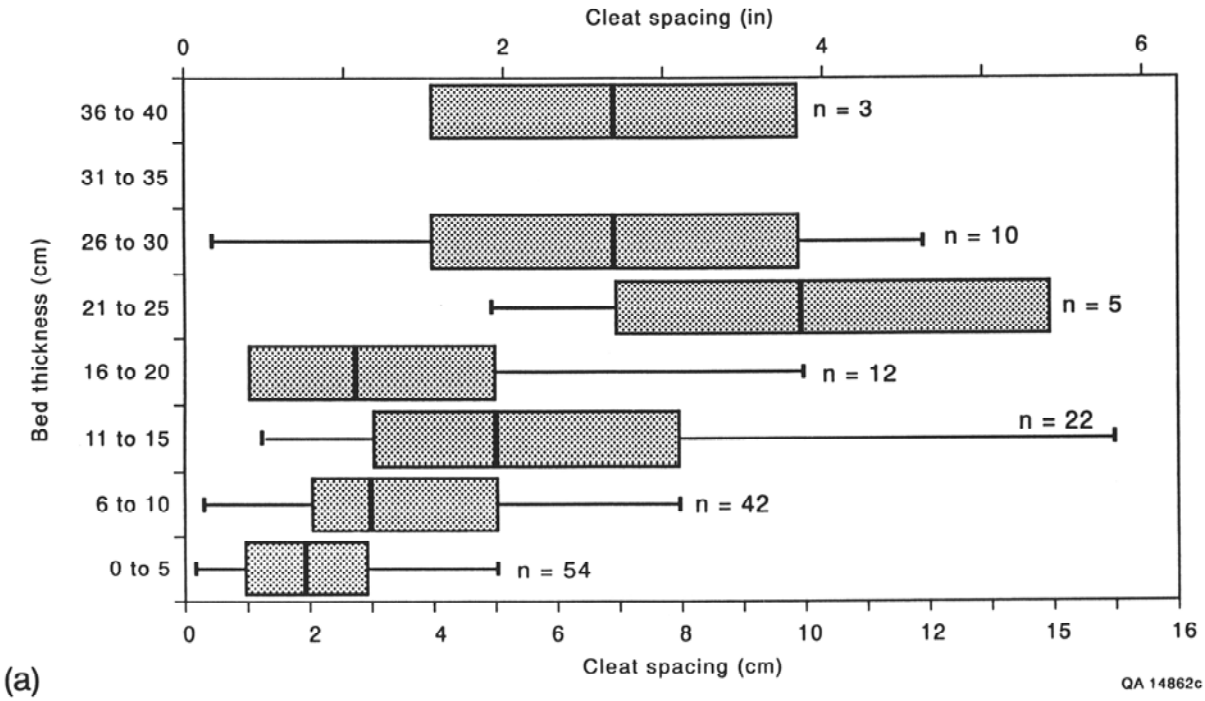

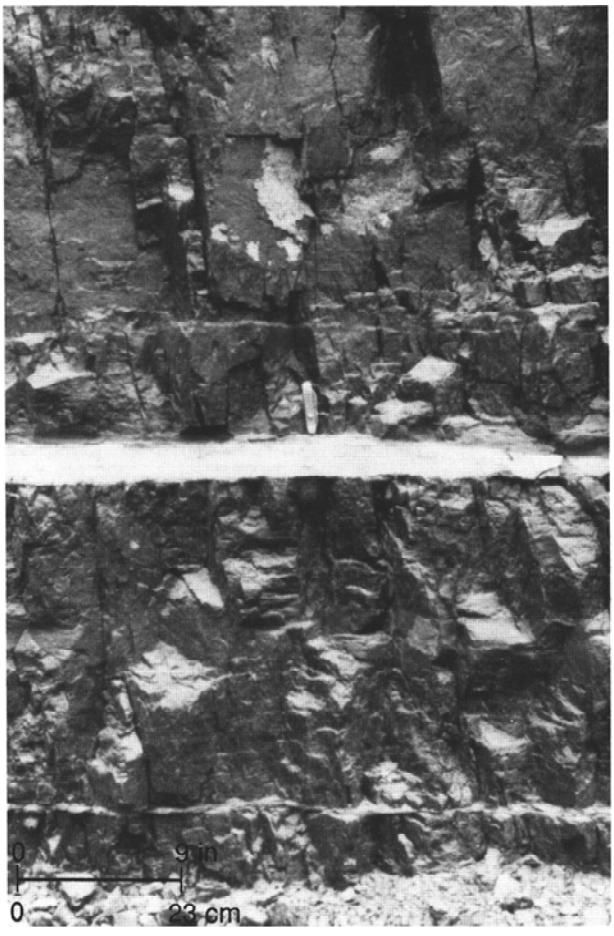

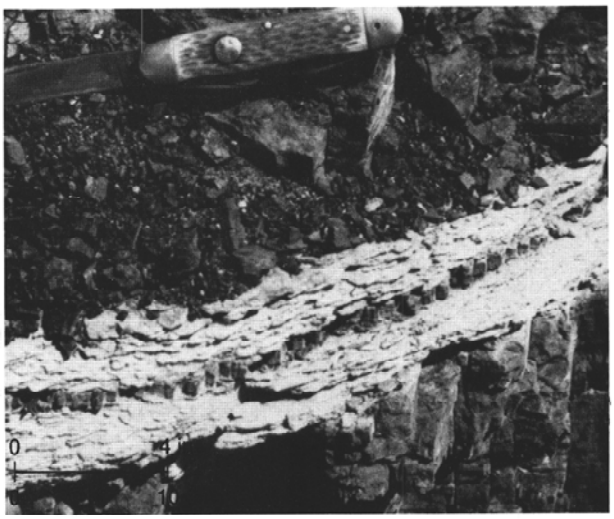

FIGURE 5.8—Illustrations of cleat spacing patterns. (a) Cleat spacing grouped by equal bed-thickness intervals. Center half of data is represented by a rectangle (box) and median is indicated by a bar. (b) Widely spaced primary cleats in thick coal bed, Navajo mine. (c) Close cleat spacing in thin coal bed, Navajo mine.

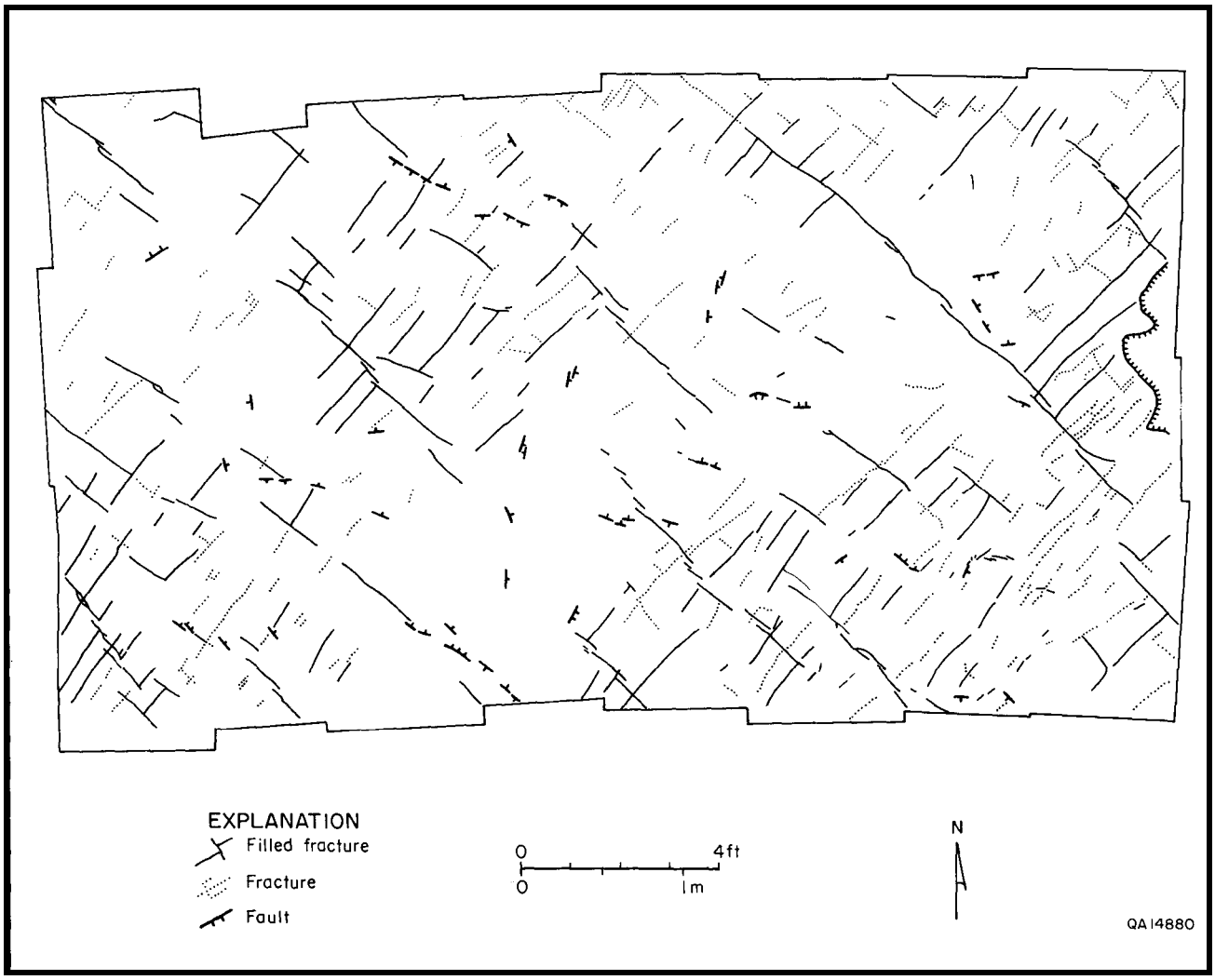

FIGURE 5.9—Cleat pavement map showing crisscrossing and mutually abutting face-cleat (fracture) pattern in a single bedding plane at Navajo mine. Natural barren and mineral-filled fractures are shown. Secondary and tertiary cleats not shown.

(Laubach and Tremain, this volume, Chapter 6). Cleat strikes are uniform between adjacent coal seams at the old La Plata mine (Table 5.1, location 11), where four coal beds in the lower Fruitland have mean face-cleat strikes between 330° and 344° (Fig. 5.10), and at the south fork of Texas Creek and East Gap (Table 5.1, locations 9 and 14), where cleat strikes in adjacent lower and lower to mid-Fruitland coal seams vary by only 11° and 5°, respectively, between basal and higher Fruitland coal beds.

Variations in face-cleat strike are due to curved cleats, gradual changes in cleat strike over wide areas, and cleats with different strikes in adjacent coal beds. Locally abrupt strike variations of 20° or more or dispersion in face-cleat strike is prominent (for example, Table 5.1, locations 3, 6, and 17). Curved cleats occur at seven stations in the Fort Lewis mine (Table 5.1, location 17) and at six widely spaced stations in the northern part of the basin (Table 5.1, locations 1, 4, 5, 6, 14, and 15). Cleat strike varies between 5° and more than 30° in distances of a few inches to several feet (centimeters to meters). Some curvature results from hooking of cleats into an adjacent fracture, probably caused by interaction between a growing and preexisting fracture (for example, Pollard and Aydin, 1988), but in several cases, the entire array of face cleats curve in unison (Table 5.1, location 6). Unlike curved cleats that define some polygonal patterns in coal, such a pattern would not be expected from brittle failure in an isotropically shrinking medium. Wavy or curved cleats have rarely been mentioned in accounts of other coal basins (one example is Ver Steeg, 1942), and because curved cleat arrays typically occur in only a small part of a given outcrop, they may have been overlooked elsewhere.

Greatest variation in cleat strike over short distances is where curved cleats occur near faults (Fig. 5.3). At the Fort Lewis mine, cleats change strike by 35° to 40° near a small graben. Cleat strikes are more nearly parallel to the fault plane within approximately 30 ft (~9 m) of the fault. In the Navajo mine, in the hanging wall of a small (6 inches [15 cm] net slip) east-striking normal fault, northeast-striking cleats change strike by 30° over a distance of only 14 inches (35 cm) as they approach the fault plane. The fault is one of several localized in the hinge of a small anticline, where difference in coalbed dip is between 2° and 5°. This fault zone differs from some that crosscut and disrupt regional cleats in that no fracture zone parallels the fault and it has an anomalously gentle dip of 20° to 30°, characteristics that are consistent with fault and cleat-curvature development during a late stage of coal compaction.

Cleat strike can vary greatly between adjacent beds. At West Gap, Beaver Creek, and Fort Lewis mine (Table 5.1, locations 15, 7, and 17), face-cleat strikes vary by 53°, 48°, and 71°, respectively, between adjacent beds. These differ-

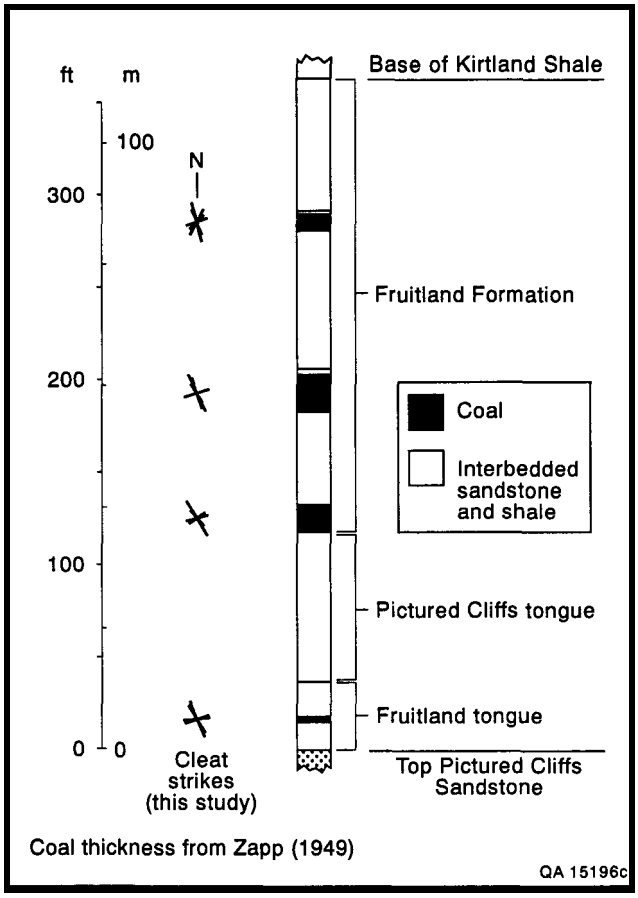

FIGURE 5.10—Cleat strikes in several coal seams at La Plata mine

ences have no consistent pattern with stratigraphic position. The area of greatest variability in cleat strike is near the Fort Lewis mine (Fig. 5.11). Some cleat-strike variation may reflect folds, faults, and fracture zones that occur in this area (Fig. 5.11) (Newman and McCord, 1980; Laubach and others, 1990; Laubach and Tremain, this volume, Chapter 6). However, this region is also part of a wider zone, described in the following section, where face-cleat strike shifts by nearly 90°.

Basin-scale cleat-strike domains

Face-cleat strikes are typically uniform throughout large areas of the San Juan Basin, but they are not the same throughout the entire basin (Figs. 5.1 and 5.12). Face-cleat strikes delineate two principal domains of regional extent. In the northern part of the basin, northwest-striking face cleats predominate (mean strike, 344°), but south of the New Mexico-Colorado State Line, north-northeast- and northeast-striking face cleats predominate (mean strike, 020°). These domains are separated by a boundary domain that extends eastward from the Colorado-New Mexico border, at the western margin of the basin, to T32N R7W, where it turns southward into New Mexico (Fig. 5.12).

In addition to the difference in polarity of the earliest formed (face) cleat from northeast in the southern part of the basin to northwest in the northern part, face cleats in the northern domain strike approximately 10° to 15° more northerly than butt cleats in the southern domain. Yet within each domain, face and butt cleats are orthogonal. The northern area (domain 1) is further characterized by gentle west-to west-northwest-trending folds, thick sandstones and coal beds with northwest depositional trends (Ayers and others, this volume, Chapter 2), and higher coal rank (high volatile A bituminous or greater) (Scott and others, this volume, Chapter 9). In contrast, the southern area (domain 2) of north to northeast face-cleat strikes is developed on a gentle northeast-dipping homocline, the Chaco slope. Fluvial channel-fill sandstone and coal deposits have predominantly northeast or north trends, and coals generally are lower rank (high volatile B bituminous or lower). Cleat spacing is apparently wider in the southern domain. Based solely on face-cleat strike, the southern part of the basin can be further subdivided into a domain of northeast-striking cleat in the west and a domain of north-striking cleat in the east (Fig. 5.12, domains 2a and 2b).

The boundary between domain 1 and domain 2 is a wide area of variable face-cleat strike that is exposed in T33N R11 and 12W near the Colorado-New Mexico border. We interpret the domain 1 boundary region to be between 15 and 20 mi (24 and 32 km) wide on the basis of the width of outcrop that has nonuniform or opposed face-cleat strikes. In the subsurface to the east, the boundary is constrained to strike east or southeast by divergent face-cleat strikes in widely spaced wells, suggesting that the boundary is approximately parallel to the east-trending Late Cretaceous basin hingeline and several gentle folds (the Bondad and Ignacio anticlines). Greatest cleat-strike variability occurs at the outcrop of the boundary zone, and northwest- and northeast-striking cleats are typically equally prominent in a given bed in this area. As a result, coal is generally friable. Near Soda Springs, Cinder Buttes, and the Fort Lewis mine, face-cleat strike (defined by abutting relations) is either northeast or northwest in adjacent beds. Beds with mutual abutting cleat relations and crossing cleat patterns are prominent. These patterns suggest two interfering face-cleat trends.

The location and nature of the boundary between domains 2a and 2b is difficult to determine accurately because well information on cleat strike in the central basin is lacking. The transition may be gradual because difference in strike is slight. There is no indication that crosscutting or interfering cleat sets exist along the boundary. Cleats in low-rank domain 2b coal may have a greater tendency to be open in the subsurface because north-striking fractures are normal to modern least horizontal stress (Zoback and Zoback, 1980, 1989).

Faults and associated fractures

East-, northeast-, and northwest-striking faults are present in the basin (Wood and others, 1948; Zapp, 1949; Barnes, 1953; Barnes and others, 1954; Newman and McCord, 1980; Condon, 1988; Tremain and Whitehead, 1990, fig. 41). Faults and associated fractures are superimposed on cleat patterns in some areas, but elsewhere cleats curve near faults, suggesting that faults and cleats formed together. Faults in coal seams are poorly exposed, except where they occur in mines in the west-central part of the basin. West-northwest- to northwest-striking normal faults occur on the western margin of the basin in the La Plata and Fort Lewis mines. Northeast- and northwest-striking faults occur near Bondad, and northeasterly striking faults occur south of Durango. Cat Creek fault in Archuleta County strikes northeast, and faults near the southern boundary of the basin have northeast or east-northeast strikes.

Some large faults are marked by zones that are as much as several tens of feet (several meters) wide composed of intensely fractured rock. Fractures within and adjacent to these zones are taller and more vertically continuous than is typical of primary face cleats, and fractures commonly extend across noncoal interbeds. Cleat strike at stations near some large faults show marked variations (Fig. 5.11), and abrupt cleat curvature occurs near some small faults (Fig 5.3). Many fault-related fractures are closed, and they may

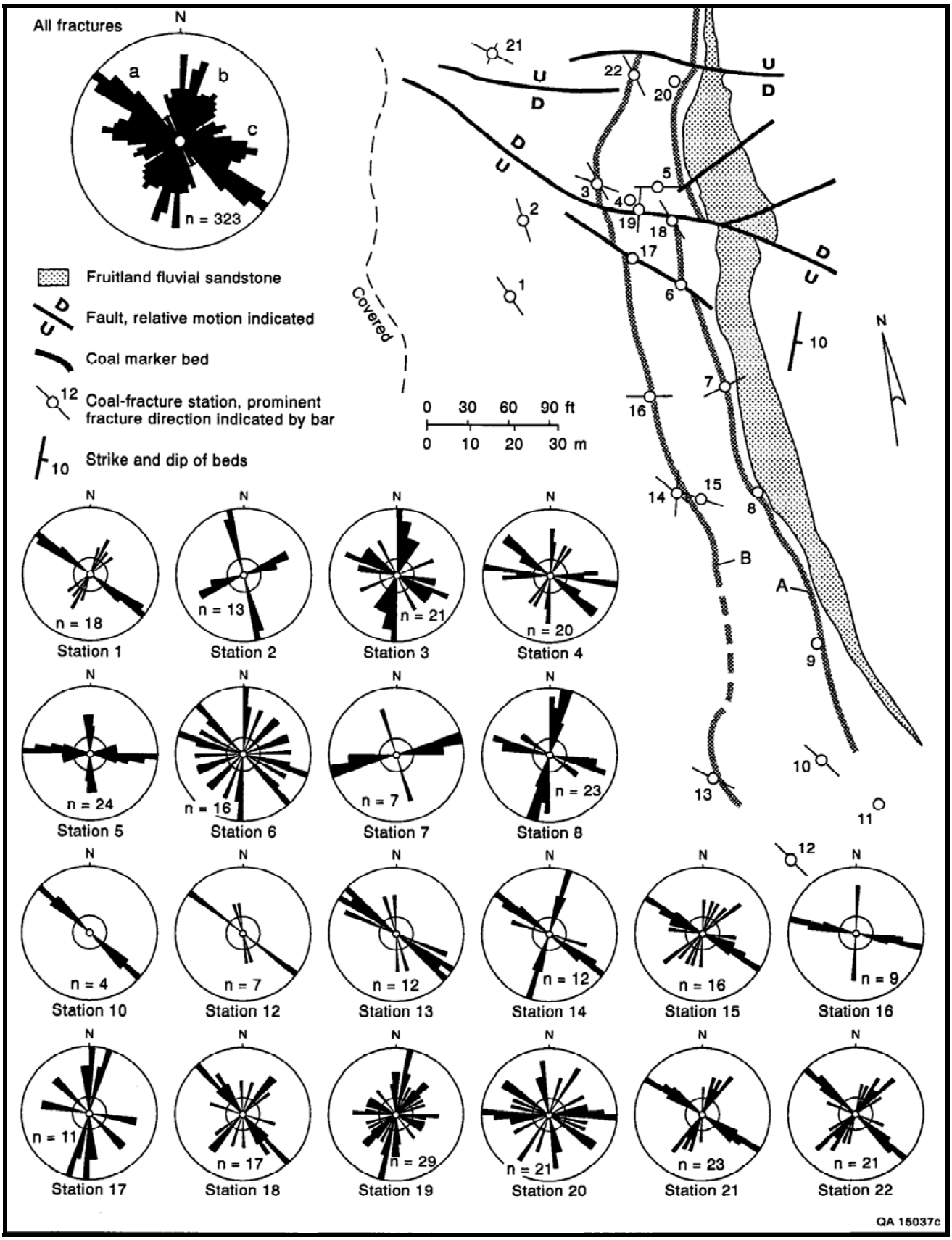

FIGURE 5.11—Faults and fracture (cleat) strikes in a part of Fort Lewis mine area.

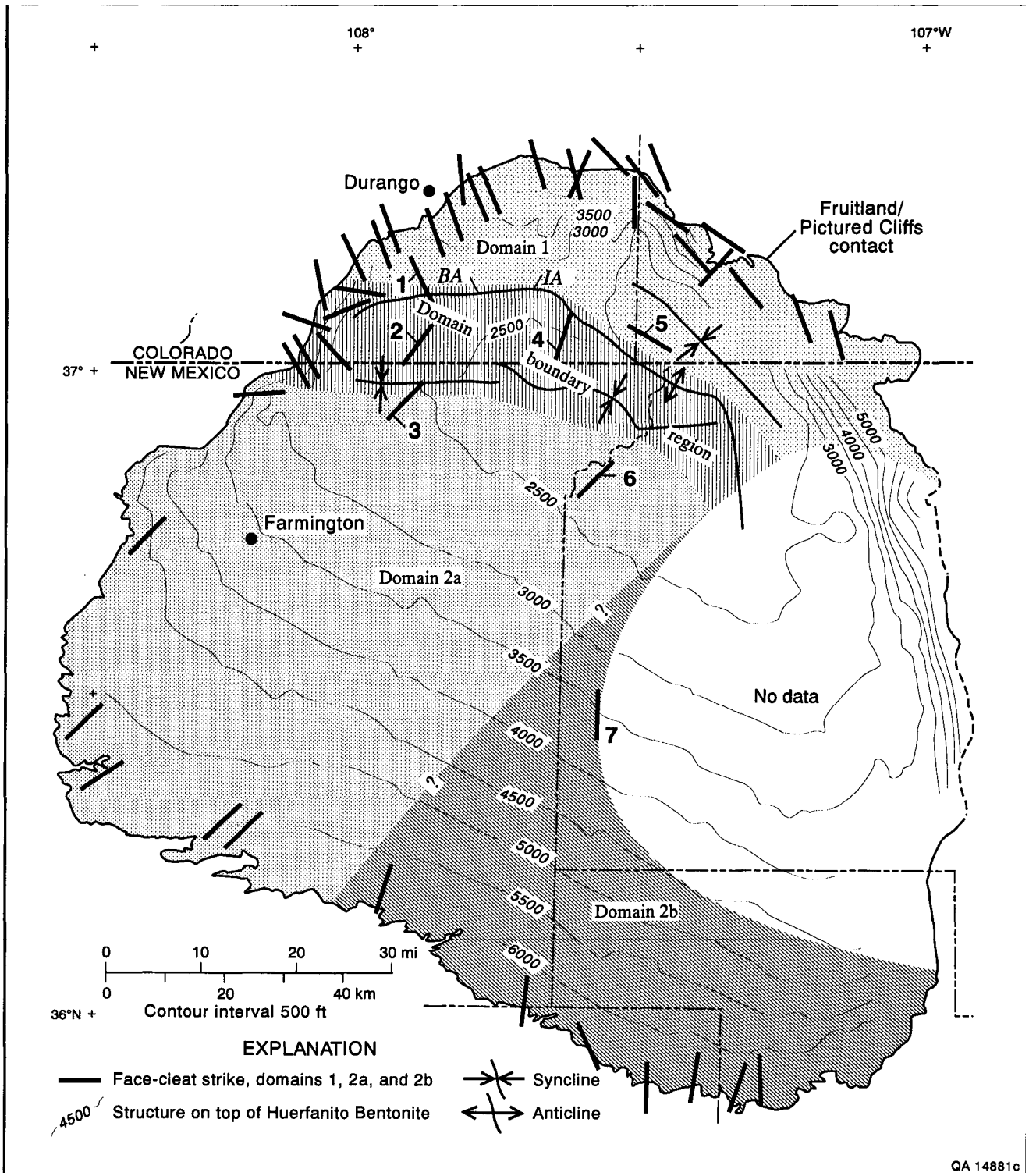

FIGURE 5.12—Structure map of San Juan Basin, contoured on the Huerfanito Bentonite, and face-cleat strikes and face-cleat-strike domains of the Fruitland Formation coal seams in the San Juan Basin. Domain boundaries are gradational and approximately located. Boldface numbers indicate wells with oriented core used in this study (see Table 5.3). Locations of stations are indicated in Table 5.1. BA–IA = Bondad–Ignacio anticline.

be barriers to, rather than conduits of, fluid flow. Faults large enough to juxtapose coal and noncoal layers could disrupt continuity of regional flow paths in coal seams. Such faults are visible in mines and can be mapped in the subsurface in areas of dense well control in the northwestern and north-central parts of the basin.

Small faults (net slip <3 ft [<1 m]) at the Fort Lewis and Navajo mines and at Squaw Creek are isolated, polished, and striated slip surfaces with little or no variation in cleat spacing adjacent to the fault. Commonly, such faults either do not have associated fracture zones or have narrow fracture zones (Fig. 5.13). As little as 0.4 to 0.8 inch (1 to 2 cm) of slip on such faults can interconnect cleat sets in adjacent coal layers that would otherwise be isolated by unfractured interbedded tonsteins.

Another type of fault zone comprises many small striated,

FIGURE 5.13—Small normal fault with associated fractures, Navajo mine. Width of fracture zone is indicated by a bar. Note offset tonstein. View is to west.

polished slip surfaces in anastomosing arrays. Although these zones are locally as much as 3 to 6 ft (1 to 2 m) wide, net slip on microfault arrays is commonly less than 4 inches (<10 cm) (Table 5.1, location 6). Because small faults and microfault zones are not open fractures but have polished surfaces consisting of dense, comminuted coal, they may be permeability barriers. Intensity of faulting and proportions of different fault types are unknown, but observations in extensive mine highwalls suggest that faults are widely spaced in the west-central part of the basin. For example, in part of the Navajo mine, only four such faults were visible in approximately 650 ft (~200 m) of highwall. Faulting is more intense in the La Plata mine.

West-northwest- and northeast-striking fracture zones, where fracture intensity dramatically increases, occur in Pictured Cliffs Sandstone and adjacent Fruitland coal on the western margin of the basin (Laubach and others, 1990; Laubach and Tremain, this volume, Chapter 6). Zones are locally associated with and parallel to small normal faults. In such areas, coal and sandstone have greater fracture frequency and density, have significantly higher fracture connectivity (Laubach and Tremain, this volume, Chapter 6), and might have greater permeability. Pictured Cliffs fractures that continue into coal seams such as those seen at the Fort Lewis mine and near Durango may be viable exploration targets. Studies are needed to further characterize these fractures to guide exploration and development efforts.

Timing and cause of cleat formation

Coalification converts initially ductile, fluid-rich organic sediment into brittle rock at shallow depths. As a consequence of tectonic strain and/or differential volume loss/ compaction, organic sediments develop fractures when coal maturation and coalification have progressed to the point where the deposits are brittle (McCulloch and others, 1974). Occurrence of cleat in shallowly buried Tertiary lignites in several basins confirms that fractures can form early in the burial history of coal (Kendall and Briggs, 1933).

Cleat sets in the San Juan Basin probably formed in the Late Cretaceous (post-Early Maastrichtian), prior to folds that define the basin margin. Timing of cleat development in the Fruitland Formation is constrained by age of cleat relative to dated folds and burial history. Where beds are reoriented by folds along the northern and western San Juan Basin margin, systematic regional face and butt cleats remain orthogonal to bedding, indicating that cleat formation predates fold development. Folds on the northern and western basin margin formed during the early Tertiary (Paleocene to Eocene) (Fassett, 1985). Crosscutting relations between cleat and bedding-parallel coal compaction fabrics indicate that brittle failure of coal occurred after a significant amount of compactional flattening. Lack of distorted or folded cleats shows that little vertical shortening of coal occurred after cleat development. Compaction of sufficient magnitude to account for current dimensions of coal beds could have been accomplished at minimum burial depths of approximately 2,000 to 3,000 ft (600 to 900 m) that were achieved prior to Late Cretaceous to early Tertiary tilting and uplift. Early formation of butt cleat is suggested by tilted mineral-filled butt cleat along basin-margin folds and in core from depths of as much as 3,000 ft (900 m).

Cleat formation was broadly contemporaneous with orogenic shortening of the Cordilleran belt that was already in progress during Campanian deposition of the Fruitland Formation and that continued, marked in the Cordilleran foreland by intermittent uplift, subsidence, or tilting, into the early Tertiary. Other structures in Fruitland coals, such as faults, local fractures discordant to cleat, and some fracture zones, may have developed during Laramide folding and faulting or during one or several of the numerous epeirogenic events that have affected the northeastern Colorado Plateau during the Cenozoic.

Face cleats are opening-mode fractures that form parallel to greatest horizontal compressive stress. Uniformity of face-cleat strikes within large domains in the San Juan Basin indicates that these fractures developed in response to a regionally coherent stress pattern, such as one resulting from orogenic processes of shortening or uplift. During coalification of the Fruitland Formation, the San Juan Basin was in the foreland of an active thrust belt and adjacent to a major bend in the belt (Fig. 5.14). This part of the foreland was probably subjected to both northeast- and southeast-directed tectonic shortening events from mid-Cretaceous time through the early Tertiary. Such events could have controlled stress patterns in the basin, and basinwide strains could have accompanied early stages of these events, accounting for cleat development prior to folding and parallelism of shortening directions indicated by face cleats and northeast- and northwest-trending folds. The Fruitland cleat pattern could be accounted for by lateral elongation of the foreland, a common response to shortening in neighboring mountain belts (Hancock and Bevan, 1987). Cleat patterns elsewhere in the Rocky Mountains and Appalachian Plateau have been interpreted to result from orogenic shortening (Ver Steeg, 1942; McCulloch and others, 1974; Henkle and others, 1977; Hucka, 1989; Kulander and Dean, 1980).

It is not yet possible to link Fruitland cleat development

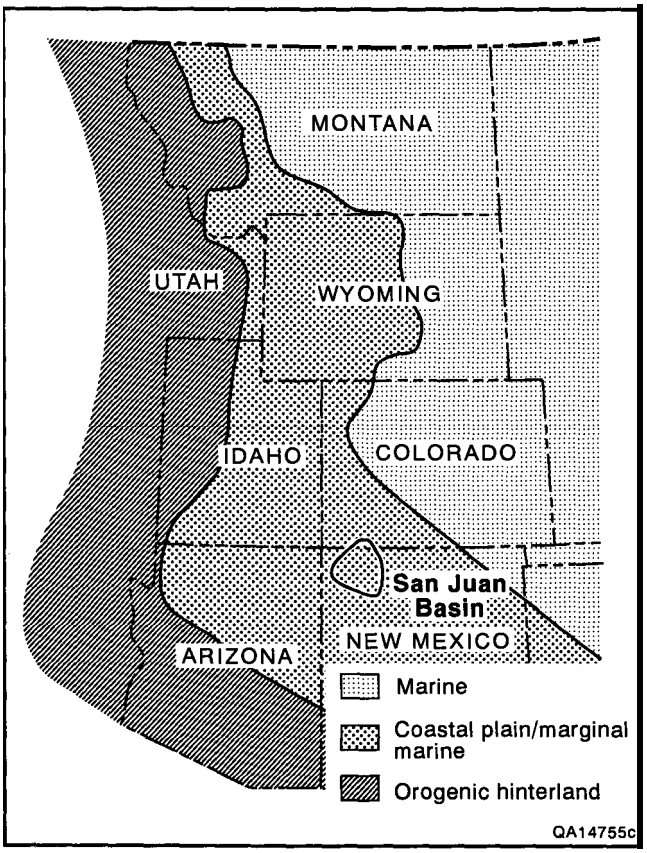

FIGURE 5.14—Tectonic/paleogeographic setting of San Juan Basin area in latest Campanian (after Cumella, 1983). Tectonic movements in orogenic hinterland may have affected cleat trends in San Juan Basin.

to specific tectonic events because the precise time of cleat development is unknown; the Late Cretaceous tectonic setting and history of the basin indicate that several Late Cretaceous tectonic events occurred while coalification was underway in the Fruitland Formation. Coal-occurrence and coal-rank maps indicate that the basin hingeline, and folds such as the Bondad and Ignacio anticlines, may have been initiated by late Campanian time (Ayers and others, this volume, Chapter 2; Scott and others, this volume, Chapter 9). During this time, extensive volcanism and possibly fault movement occurred in southeastern Arizona (Cumella, 1983; see also Laubach and others, 1989). Orogenic uplift to the southwest may have caused persistent northwest depositional strike and northeast sediment transport direction in the Fruitland Formation, and northeast-trending maximum horizontal stress. In late Maastrichtian (or possibly Paleocene) time, depositional patterns of the McDermott Member of the Animas Formation indicate a short-lived volcanic and tectonic event northwest of the San Juan Basin, and the sub-Ojo Alamo Formation unconformity indicates uplift and erosion of the basin prior to late Early Paleocene time (Fassett, 1985).

Cleat domains may represent separate deformation events or contemporaneous paleostress provinces. Abutting relations in the domain boundary region are inconclusive, but northeast-striking face cleats abut very widely spaced (3 to 6 ft [1 to 2 ml) northwest-striking fractures in the northern Navajo mine, suggesting that domain 1 face cleats in the north formed before domain 2 cleats in the south. If this is the case, it implies early southeast-trending maximum horizontal stress during domain 1 deat development replaced by northeast-trending maximum horizontal stress during domain 2 cleat development. In the north, coalification may have advanced earlier to the stage where cleat development could occur, as suggested by current pattern of coal rank and deeper burial of the northern section of the basin in the Late Cretaceous. Northwest-striking domain 1 cleats are in highest rank, high volatile A and B coals, whereas domain 2 cleats are primarily in high volatile C coal. Multiple cleat-forming events have been inferred in other basins (Spears and Caswell, 1986). Alternatively, crisscrossing or mutually abutting relations and alternations in face-cleat polarity in adjacent beds in the domain 1-2 boundary region may be due to the position of this region between two distinct, contemporaneous paleostress provinces, as Kulander and Dean (1980) suggested for some cleat domains in the Allegheny Plateau of West Virginia. The boundary region may have had complex stress patterns during coalification, because the coal-rank map suggests that folds such as the Ignacio anticline were developing then. Thus, the overall tectonic setting and structural history of the San Juan Basin may govern cleat intensity and orientation patterns.

Implications for coalbed methane exploration and development

Coalbed permeability may be 3 to 10 times greater in the face-cleat direction than in other directions (Ammosov and Eremin, 1960; McCulloch and others, 1974). This permeability anisotropy reflects the strong preferred orientation and greater length of interconnected fractures in the face-cleat direction. Potential permeability anisotropy arising from face cleat, and differences in face-deat strike in various cleat domains in the San Juan Basin, can be taken into account in the design of development-well-drilling programs and stimulation procedures such as hydraulic fracture treatment. Fruitland face-cleat strike, and thus greatest potential permeability anisotropy, shifts by 90° between domains 1 and 2, from northwest to northeast. However, only in the southern domain and in the domain boundary region are face cleats aligned normal to regional least horizontal compressive stress, the most favorable orientation for them to be open in the subsurface.

A closely cleated coal may yield more gas than a coal with wide cleat spacing. For example, cores from some friable coal beds in the Appalachian basin yield approximately 94% of total gas content, whereas the same amount of otherwise similar blocky coal from the same area yields only 60 to 65% of total gas content (McCulloch and others, 1975). Coal reservoir simulations emphasize the importance of cleat spacing (Paul, 1990), and intense fracture development may enhance the rate of gas production. Cleats are closely spaced in the boundary between domains 1 and 2 because two face-cleat sets overlap and interfere, and coals have relatively high rank. Moreover, folds and faults that locally enhance fracture development occur in this area. High gas yields are suggested by gas seeps along fractures at Soda Springs mine (Table 5.1), and gas evolved from coal core from depths of as little as 200 ft (61 m) (Roberts, 1989). The highly productive Cedar Hill field and Meridian 400 area occur in or near this boundary domain (Fig. 5.1).

Observations of cleat patterns between domains 1 and 2 suggest that two interfering face-cleat sets result in highly cleated coal that may be more isotropic and may have higher overall fracture connectivity and permeability. Furthermore, prevalence of two directions of strongly developed fractures in the domain boundary region and the resulting increased coal friability may enhance the success of well completion by open-hole cavity methods in this area. In cavity completions, the borehole in coal is allowed to col-

lapse, causing adjacent parts of the coal seam to expand toward the cavity. This process tends to open fractures near the borehole and may produce additional fractures (Logan, 1989). Conversely, potential production of coal fines and attendant production problems may be greater here.

Great lateral continuity of volcanic ash layers (tonsteins) on interwell scales, combined with a tendency for cleat to terminate at interbedded noncoal layers, should isolate cleat systems in adjacent beds. This isolation would produce a significant element of permeability layering within Fruitland coal seams and decrease the attractiveness of these seams as targets for horizontal drilling. Because tonsteins are generally thin, however, small faults with net slip of as little as 0.4 inch (1 cm) can interconnect cleat systems in adjacent beds, even without subsidiary fractures along fault zones. On the other hand, some small faults such as those at Squaw Creek (Table 5.1) are closed and unlikely to enhance permeability (Raistrick and Marshall, 1939; Ammosov and Eremin, 1960). Local fracture intensification and greater fracture continuity in coal and adjacent sandstone are associated with some faults as well as with folds and fracture zones. Through-going fractures may provide significant conduits of gas flow in areas of high gas production. This underscores the importance of determining distribution of faults that are below seismic resolution; they could play a role in connecting otherwise isolated cleat systems.

Acknowledgments

We thank the owners and operators of the Carbon Junction, Chimney Rock, La Plata, and Navajo mines for access to their property, and W. B. Ayers, Jr., and M. A. Grout for reviews.

6. Fracture swarms: potential targets for methane exploration in Upper Cretaceous sandstone and coal, northern San Juan Basin, Colorado

S. E. Laubach[1] and C. M. Tremain[2]

[1]*Bureau of Economic Geology and* [2]*Colorado Geological Survey*

Abstract—Fractures in discrete swarms, separated laterally by unfractured domains, characterize Upper Cretaceous Pictured Cliffs Sandstone along the San Juan Basin margin in Colorado. Although some fracture swarms in sandstone terminate at overlying Upper Cretaceous Fruitland Formation coal or shale beds, others extend into them, increasing fracture connectivity and intensity. In coal beds, fracture swarms are marked by vertically extensive joints, anomalous cleat strikes, closely spaced fractures, and/or small normal faults. Swarms with northwest and northeast strike are potential targets for gas exploration.

Introduction

Fractures enhance fluid flow in low-permeability coal beds and sandstones. With the increasing importance of these rock types as unconventional reservoirs of natural gas, information on their fracture patterns is becoming critical for design of exploration, development, and completion strategy, including application of horizontal drilling (Finley and others, 1990). Accurate determination of subsurface fracture patterns is difficult in mildly deformed sedimentary rocks because fracture-detection methods, such as the use of geophysical well logs and core (particularly from vertical wells), may fail to detect fractures and at best sample only a small part of the fracture network. One approach to predicting the types of fracture patterns that may exist in the subsurface is to map fractures in outcrop. Such maps provide a view of fracture spatial distribution, trace length, connectivity, and size and shape of fracture-bounded blocks that can be used to help understand hydrocarbon production patterns.

This study focuses on fractures in Pictured Cliffs Sandstone and overlying Fruitland Formation coal. We present maps and descriptions of fractures in sandstone and coal in large (up to ± 1,000,000 ft^2 [± 100,000 ml) exposures on the margin of the Late Cretaceous—early Tertiary San Juan Basin of Colorado and New Mexico (Fig. 6.1). In these sandstones the fractures are not regularly spaced or in orthogonal sets. Instead, they are in swarms that are separated laterally by domains as much as hundreds of feet wide that lack fractures. Our observations in the San Juan Basin and in the Green River Basin of Wyoming (Laubach, 1991) suggest that *irregularly spaced* swarms with unidirectional strike, such as those in the Pictured Cliffs Sandstone, are an important type of regional fracture set (Figs. 6.2-6.4).

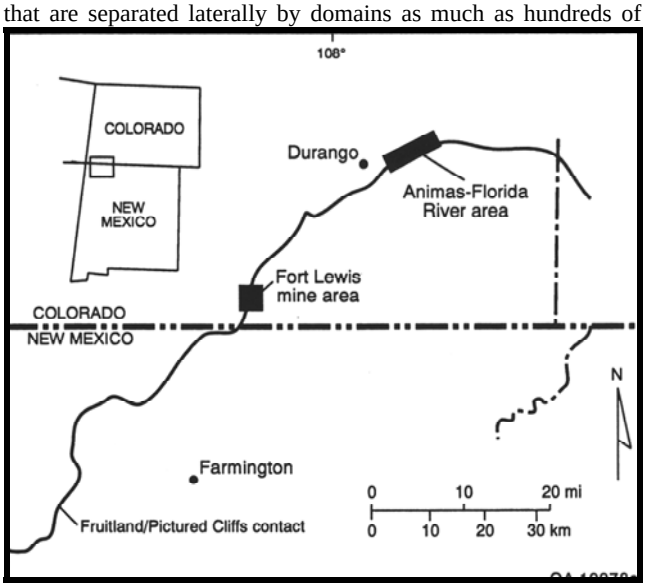

FIGURE 6.1—Location map of pavement study areas, northern San Juan Basin, Colorado and New Mexico.

The aim of this paper is to illustrate an example of fracture swarms in sandstone and adjacent coal beds. Our study builds on previous studies of the northwestern margin of

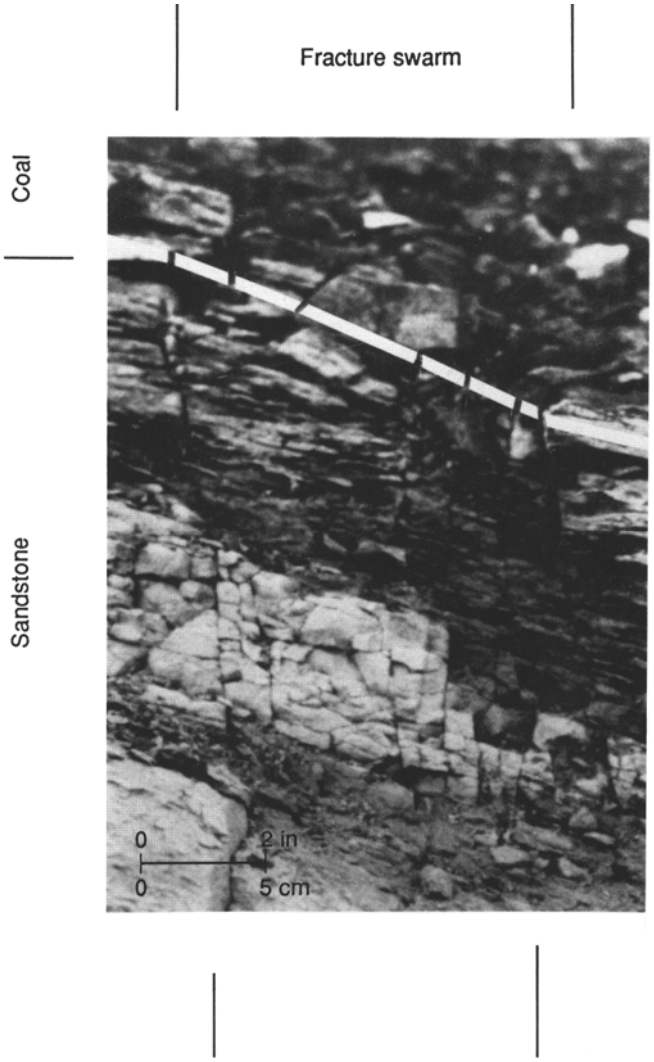

FIGURE 6.2—Fracture swarm in upper Pictured Cliffs Sandstone and overlying Fruitland Formation coal, Carbon Junction exposure.

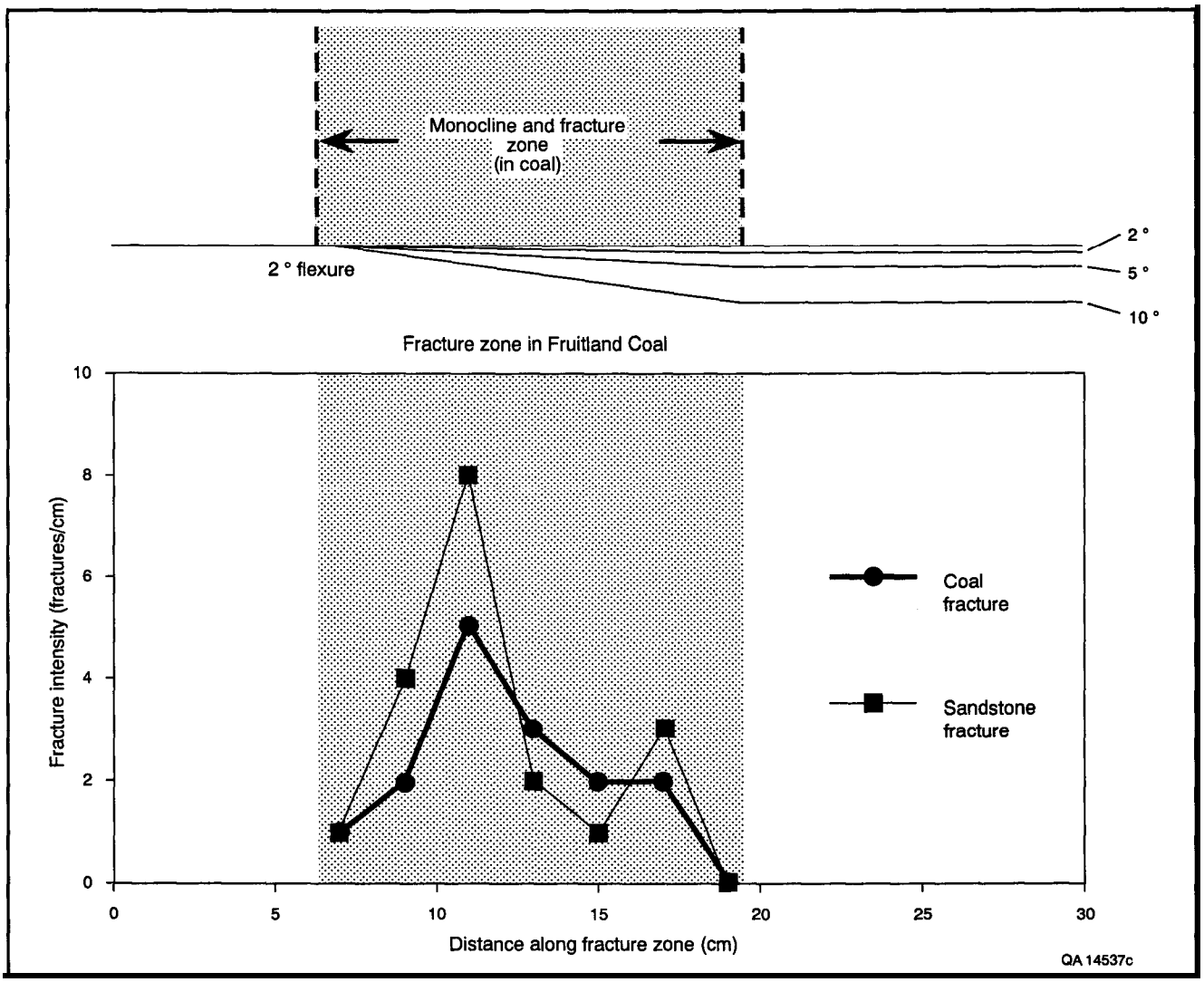

FIGURE 6.3—Fracture intensity (fractures/distance) in narrow fracture swarm that crosses both sandstone and coal. Outside the fracture swarm, fracture intensity is less than 0.02/cm. Sandstone/coal contact is deflected by 2° or less across swarm. Carbon Junction exposure. Upper part of diagram illustrates the observed 2° bed dip, and for comparison, the bed dips in monocline hinge of 5° and 10°.

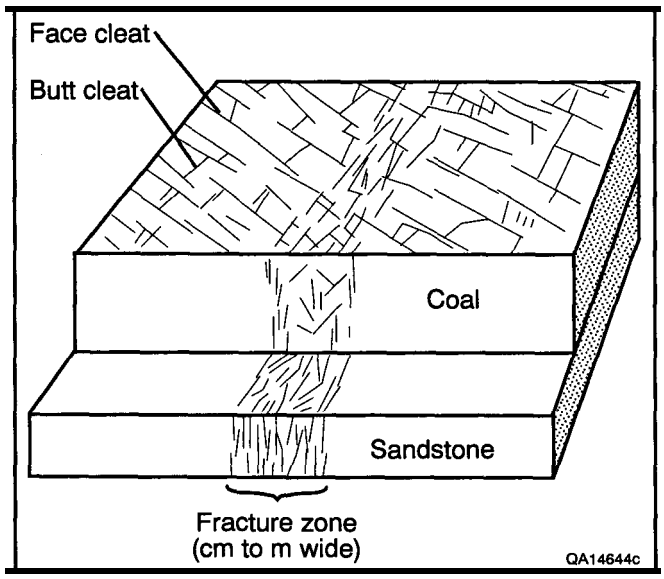

FIGURE 6.4—Block diagram illustrating fracture swarm crossing sandstone and coal. Based on relations observed at Carbon Junction exposure (Animas—Florida Rivers area) and Fort Lewis mine.

the San Juan Basin that documented fracture (cleat) and joint orientations and distinguished several fracture sets on the basis of abutting relations and orientation (Newman and McCord, 1980; Condon, 1988; Tremain and others, this volume, Chapter 5).

Regional cleats and joints

Regional cleat patterns in San Juan Basin coal are described by Tremain and others (this volume, Chapter 5). Face-cleat patterns are uniform over large areas of the Colorado part of the basin, but significant local variations in cleat strike exist. Exposures near the Animas River south of Durango and at the Fort Lewis mine indicate that variation in cleat strike in some places is associated with fracture swarms that cut both coal bed and sandstone.

Joints in sandstone on the northwestern margin of the San Juan Basin are opening-mode fractures that are commonly subvertical and at right angles to bedding planes. They generally have northwest and northeast strikes (Newman and McCord, 1980; Condon, 1988). Abutting relations among fractures suggest that several generations of joints are present, some of which may result from near-surface or surficial processes such as spalling near cliff edges (Tremain and Whitehead, 1990). Some prominent joints in the

Fruitland Formation and the Pictured Cliffs Sandstone parallel northwest-striking face cleat in overlying Fruitland Formation coal beds. Northwest-striking normal faults occur along the western margin of the San Juan Basin, and it is possible that some joints and some northwest-striking faults accommodated northeast-southwest extension during Late Cretaceous and/or early Tertiary, possibly at about the same time that regional face cleat was developing (Tremain and others, this volume, Chapter 5).

Fracture-trace maps

Maps that show the traces of fractures on bedding planes portray fracture network characteristics such as fracture spatial distribution, connectivity, trace length, and fracture-bounded block size and shape in a way that measurements at isolated stations cannot (LaPointe and Hudson, 1985; Barton and others, 1987; LaPointe, 1988). Maps have been made of quarry floors (LaPointe, 1988) or of outcrops that have been artificially cleared (Barton and others, 1987). In our study, we made maps of natural outcrops and mine floors.

Upper Cretaceous sandstones form natural dip-slope pavements along the margins of many early Tertiary basins in the western United States. On the northwestern and northern margins of the San Juan Basin, outcrops of Pictured Cliffs Sandstone bedding planes have areas ranging from hundreds to thousands of square feet. These exposures, nearly devoid of vegetation, debris, and fractures related to surficial processes, include moderately dipping (~10° to 15°) and steeply dipping (30° to 50°) beds with a range of strikes. Fracture patterns are well exposed in plan view on these bedding planes, and cross sections of fractures are visible along the upturned edges of hogbacks. Such exposures are ideal for fracture-trace map studies.

Map areas: Fort Lewis mine and Animas–Florida river transect

Two large exposures of Pictured Cliffs Sandstone were mapped in detail. They are at the abandoned Fort Lewis coal mine near the Colorado—New Mexico border (sec. 1 T32N R12W) and along a 2.8-mi-long (4.5-km) ridge southeast of Durango between the Animas and Florida Rivers (Fig. 6.1). These exposures were chosen because they are exceptionally free of debris, vegetation, and surface-related fractures and because differences in strike between the two areas permit comparison of fracture patterns along different parts of the basin margin. We made observations of fracture patterns at four other pavements in the western and northern parts of the basin to test regional consistency of fracture patterns.

The Fort Lewis mine exposure is a north—northeast-striking (020°) bedding plane of Pictured Cliffs Sandstone that dips southeast about 10°, forming the dip slope of a subdued northeast-trending hogback (Fig. 6.5). The part of the outcrop we mapped is approximately rectangular, with an area of more than 1,000,000 ft^2 (100,000 m^2) and a length of more than 1,970 ft (600 m) parallel to strike. Fractures are visible in cross section in low cliff exposures on the northwestern side of the hogback. Coal directly overlies sandstone but the sandstone-coal contact is not exposed.

The Animas—Florida river exposure near Durango is on upper Pictured Cliffs Sandstone. Strike is more easterly here than at the Fort Lewis mine, and dips are generally steeper, ranging from 20° to 55°. A sharp contact between sandstone and coal is well exposed in a number of locations along this outcrop. One part of the Animas—Florida river exposure near Durango, on US-550, has a well-exposed small-scale fracture swarm that illustrates several characteristics of these structures.

Fractures were mapped on large-scale base maps. The Fort Lewis mine outcrop was mapped at a scale of 1:1,000 using an air photograph base map, plane table, and acoustic distance-measuring devices. Within the outcrop, smaller areas were mapped at a scale of approximately 1:50 on unregistered photograph mosaics taken from an elevation of 8 ft (2.5 m). The exposure of Pictured Cliffs Sandstone along the Animas—Florida river transect was mapped at smaller scale (1:24,000 and 1:12,000) on a topographic base map, supplemented with local larger-scale maps and oblique photographs of bed surfaces. The Fort Lewis mine and Animas—Florida river maps illustrate fracture patterns at different scales over distances that are comparable to interwell spacing in some gas reservoirs.

Coal in the Fruitland Formation tends to have small exposures in natural outcrops in the San Juan Basin; bedding plane exposures of coal in active open-pit coal mines are difficult to map and interpret because of debris and fractures generated by mining operations. For mapping coal in natural outcrops and selected areas of open-pit mine floors, we used color photographs as base maps. Adjacent to sandstone pavements, coal fractures were described in closely spaced outcrops and excavations.

Fracture swarms

Small-scale fracture swarm: Carbon Junction outcrop

A narrow swarm of closely spaced fractures that crosses sandstone and overlying coal is exposed in the Pictured Cliffs Sandstone at the top of the US-550 road cut near Carbon Junction mine, south of Durango (Fig. 6.1). This exposure demonstrates that fracture swarms may extend from sandstone into overlying coal. Away from the fracture swarm, Pictured Cliffs Sandstone has few fractures, and many of these are surficial features. Coal has well-developed face cleat and a northwest (345°) strike and primary spacing of 1 to 2 inches (3 to 5 cm).

In sandstone, the fracture swarm is composed of numerous curved, anastomosing fractures that are subperpendicular to bedding (Figs. 6.2-6.4). Most fractures within the swarm strike west—northwest, parallel to the overall strike of the swarm itself. Some fractures are slightly curved and have sharp, well-defined boundaries and continuous traces through approximately 5 ft (1.5 m) of exposure. Other fractures are strongly curved, have diffuse margins, and are relatively short (0.4 to 4 inches [1 to 10 cm]). The widest fractures have widths less than 0.02 inch (0.05 cm). Most are marked by a slight orange-brown stain, but no fracture-filling minerals are visible; elsewhere in the basin similar fractures locally have calcite or siderite fill. There is no evidence for slip on fractures, and the contact between sandstone and overlying coal is not offset across the swarm. The swarm is within a monocline, with bed dips within the monocline differing from adjacent areas by 2°.

The swarm is tabular and is between 5 and 6 inches (12 and 15 cm) wide. Fracture intensity within the swarm is high but variable, ranging from 1 to 8 fractures/cm (Fig. 6.3). Decrease in fracture intensity at the swarm boundary is abrupt. Fractures that parallel the swarm are absent over an area of at least 30 ft (9 m) wide outside of the swarm itself.

In coal, the swarm consists of short (<2-inch [<5-cm] long) fractures subparallel to the swarm boundary (Fig. 6.4). In this area fracture-swarm strike is oblique to face-cleat strike. Only about 25% of fractures in sandstone extend into coal. Consequently, the fracture intensity of 2 to 3 fractures/cm in the fracture swarm (measured perpendicular to the boundary) is considerably higher than that of surrounding coal. Fracture density (fracture length per unit area) is

2 to 10 times greater within the swarm than in adjacoent coal. Connectivity, or the proportion of fractures that intersect other fractures, is markedly greater in the swarm than in adjacent coal. Cleats having greater dispersion in strike than typical outcrops (Tremain and others, this volume, Table 5.1) occur locally in the northwestern San Juan Basin. Such fractures locally have inconsistent crosscutting and abutting relations. In these outcrops, the usual face and butt cleats are accompanied by additional coal fractures ("third cleat set") having a wide range of strikes. Coal outcrops with these fractures tend to have greater fracture densities than coal of similar rank and composition with only regional cleat. Because exposures adjacent to these outcrops are limited, it is not possible to demonstrate that these anomalous areas are arranged in swarms, but the pattern of fractures within them is consistent with this interpretation.

Reservoir-scale fracture swarms: Fort Lewis mine

Swarms of closely spaced west-northwest-striking fractures are exposed at the Fort Lewis mine in an outcrop of Pictured Cliffs Sandstone (Figs. 6.5 and 6.6). The swarms have a pattern similar to those at the Durango/US-550 outcrop, but they are much larger. Fracture maps from this outcrop provide information on patterns within swarms and evidence for relationships among swarms. Cleat and fault patterns are visible in coals that overlie fracture swarms.

Surficial (set II) fractures at Fort Lewis mine—Surficial fractures must be separated from fractures that may exist at depth if outcrops are to be used as guides for subsurface exploration. Two sets of fractures, with west-northwest (set I) and north (set II) strikes, are evident in the Fort Lewis pavement. They can be distinguished as separate sets on the basis of abutting relations, orientation, and differences in style. Fracture set I is the most prominent and is composed of steeply dipping, curviplanar fractures that occur singly or in swarms. Set II fractures either cross or abut set I fractures, indicating that set I fractures are older than those of set II. Both sets dip at right angles to bedding, but they differ in their characteristic shapes, microstructure, and associated alteration.

The attributes of set II fractures are consistent with formation at shallow depths. They may be surface-related fractures that are not present in buried rocks deeper in the basin. We therefore only briefly describe their traits. They are composed of long, planar segments arranged in en echelon or relay patterns (Fig. 6.6). Overlapping segments are straight rather than curved, and small fractures connecting segments are rare. No infilling minerals are evident. Widths are 0.008 to 0.02 inches (0.02 to 0.05 cm). There is no offset parallel to fracture walls, which are smooth except for subdued arrest lines and plume structures. These charaoteristics are consistent with opening-mode propagation with movement normal to fracture walls (Pollard and Aydin, 1988). They are bordered by a reddish-brown to reddish-yellow halo of stained rock that is as much as 12 inches (30 cm) wide, and fracture surfaces oan have a similar but darker

FIGURE 6.5—Bedding-plane pavement outcrop, Upper Cretaceous Pictured Cliffs Sandstone, Fort Lewis mine. FS = fracture swarm; FI = isolated fracture. Note wide extent of unfractured rock between fractures. Scale is indicated by figure in center of outcrop.

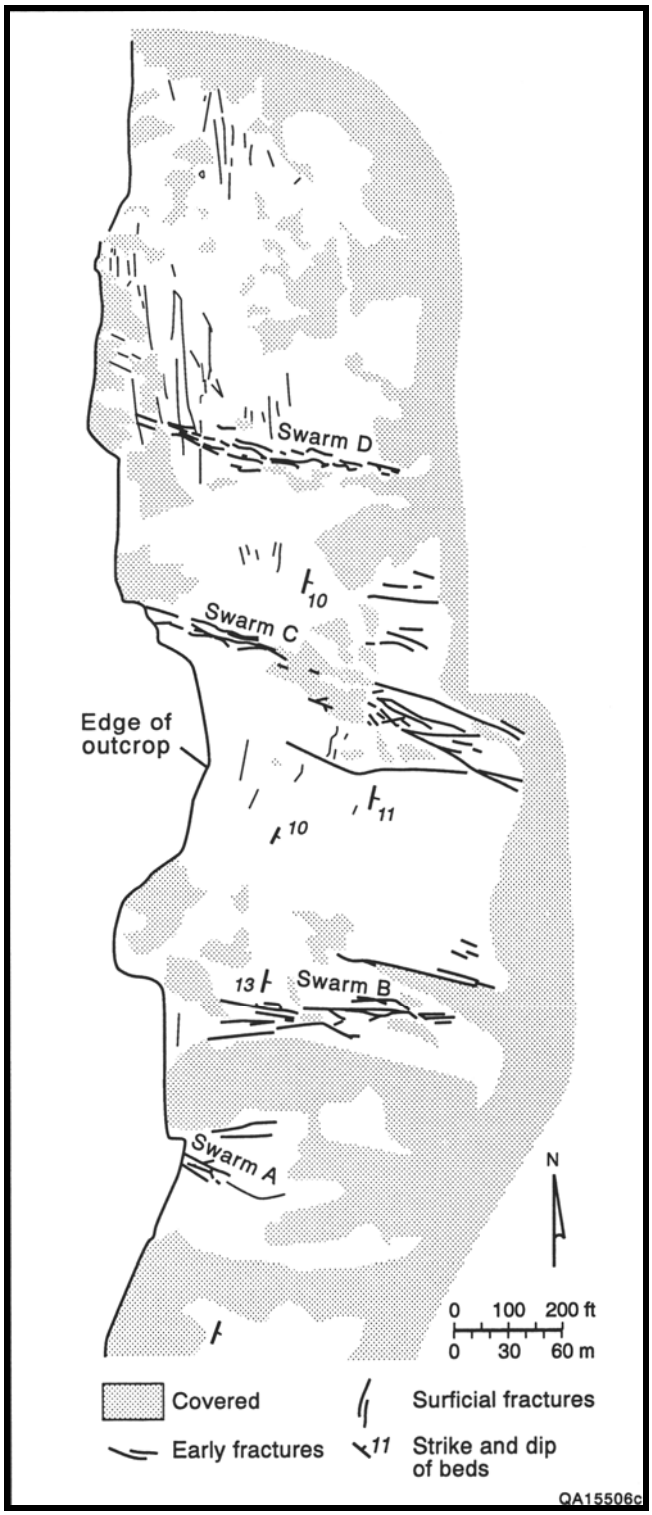

FIGURE 6.6—Simplified map of bedding-plane pavement and fracture network in Upper Cretaceous Pictured Cliffs Sandstone, Fort Lewis mine. See Fig. 6.1 for location.

stain. Set II fractures are mostly within 150 ft (45 m) and parallel to the escarpment of the Pictured Cliffs hogback at Fort Lewis mine. Fractures are longer, wider, and more abundant near the escarpment, and some fractures near the cliff edge curve gradually to approach the free surface at right angles or to parallel the cliff face.

Set II fractures are similar in appearance to other fractures along the northwestern margin of the basin that have been interpreted to be surficial fractures (Tremain and Whitehead, 1990). In the Pictured Cliffs Sandstone, these fractures tend to be subparallel to topographic escarpments and to be best developed within 75 to 100 ft (20 to 30 m), or less, of cliff edges. Along the Animas-Florida river outcrop belt, similar-appearing fractures parallel the ridge crest and are developed only within 15 ft (4.5 m) of the cliff edge. A younger set of orthogonal, abutting fractures commonly develop where this fracture set is prominent. Apparently because their orientation varies with topography, fractures with set II characteristics have a wide range of strikes regionally.

Additional surficial fracture sets are locally prominent in Pictured Cliffs outcrops. Abutting relations indicate that these are younger than set II fractures. They include polygonal fractures and exfoliation joints that are locally associated with pop-up structures. Polygonal fracture patterns are generally hexagonal and are typically composed of straight and curved fractures. Polygon diameters range from several tens of inches (centimeters) to more than 5 yds (5 m); locally, several scales of polygon are developed in the same exposure. Exfoliation joints are fractures that parallel the outcrop surface; in massive sandstone they commonly separate a slab of rock 1 to 2 inches (2 to 5 cm) or less thick. On steeply dipping outcrops, downslope movement of thin slabs can result in tentlike pop-up structures consisting of slabs that have fractured and pivoted about an axis generally parallel to the strike of the slope. Even where these features are well developed at the surface, they do not extend far into bedrock. Extensive development of polygonal fractures, exfoliation joints, and pop-ups can result in a highly disrupted bedding-plane surface, where older fracture sets are difficult to recognize. We therefore avoided such surfaces in our mapping.

Shape and microstructure of swarm (set I) fractures— Outcrop and petrographic observations are consistent with opening-mode propagation of set I fractures. For most fractures in the outcrop, there is no evidence of fracture-parallel slip, but fractographic features indicative of opening-mode propagation, such as plume structures and arrest lines, are difficult to distinguish because exposed fracture surfaces are rare. The morphology and microstructure of set I fractures distinguish them from set H fractures. Set I fractures typically have widths of 0.02 to 0.04 inch (0.5 to 1 mm), although locally they have widths of as much as 0.2 inch (0.5 cm). Narrow fractures are marked by a dark-brown seam of infilling of clay and carbonate minerals. Carbonate (calcite) or gypsum is present in some veins at the Fort Lewis mine and in exposures between the Animas and Florida Rivers (Fig. 6.7). Set I fractures commonly are surrounded symmetrically by a halo of lighter colored rock 0.4 to 1.2 inches (1 to 3 cm) wide (Fig. 6.8a).

Individual fractures within swarms are perpendicular to bedding and generally terminate vertically within homogeneous sandstone or at shale partings, so that they typically are confined to individual beds. Fracture height is therefore only 1.6 to 16 ft (0.5 to 5 m), even where map traces are tens or hundreds of yards (meters) long.

Set I fractures are composed of short (<30 ft [<10 m]) segments that either curve gradually throughout their length or curve on the ends (Fig. 6.9). Many set I fractures represented by a single trace on the pavement map are made up of several parallel fracture strands or narrow fracture zones (Figs. 6.8a-6.8c). The numerous anastomosing fracture strands give some fractures a "braided" appearance (Figs. 6.8b, 6.8c, and 6.10a). These multistrand fractures can be as much as 2 inches (5 cm) wide. Some wide fractures have inclusions of wall rock that combine with anastomosing fracture strands to create irregular or rough fracture cross sections.

High-angle abutting relations and crossing fractures are rare (Fig. 6.9); fractures intersect at a low angle. In map view, set I fractures have distinctive termination styles (Fig. 6.9). Fractures that have isolated terminations within the rock matrix commonly have small-scale splays, or numerous small segments that may be arranged en echelon or in a diffuse array of parallel microfractures and fracture strands (Fig. 6.10b). Where fracture segments overlap, fractures curve abruptly (hook) toward adjacent fractures. Within the areas of overlap, various types of interconnected, partly connected, and blind splay fractures and curving fracture strands are developed (Figs. 6.9, 6.10b, and 6.10c). One distinctive overlap pattern is *ladder structure* (Figs. 6.9h and 6.10b), a pattern in which subparallel, nearly equally spaced straight fractures link two overlapping, parallel strands. Fractures defining ladder structure are at an acute angle (15° to 60°) to the main fracture strands, rather than at right angles, as would be expected in a well-designed ladder. Fractures defining such structures may curve into parallelism with main-strand fractures or may curve abruptly to intersect them. Fracture arrangements associated with terminations and main strands are in larger scale combinations within swarms, defining an overall network pattern.

Fracture swarm dimensions and orientation—Four fracture swarms cross the Fort Lewis outcrop (Fig. 6.6). Swarms are composed of anastomosing and variably interconnected straight and curved fractures with highly variable fracture spacing that ranges from approximately 0.4 to approximately 40 inches (~0.01 to ~1 m). Many fractures within swarms are subparallel to the length of the swarm (Figs. 6.11 and 6.12). Swarm widths are defined by fracture occurrence, as illustrated in Fig. 6.13.

Swarms strike west-northwest, with a range from 290° to 310° (Fig. 6.12). They are tabular and oriented normal to sandstone beds. In plan view, swarm lengths range from 82 ft (25 m) to 755 ft (230 m), and widths range from 23 ft (7 m) to more than 165 ft (>50 m). Three of four swarms terminate outside the outcrop, so their lengths cannot be defined precisely, but swarm widths diminish substantially along fracture-swarm strike for several swarms (Fig. 6.13), suggesting that they gradually die out over distances of approximately 1,000 ft (~300 m). The most completely exposed swarm has a length/width ratio of greater than 6 (Figs. 6.6 and 6.14, swarm D). Swarms are separated by domains where fractures are either absent or sparse. These unfractured domains have widths that range from approximately 165 ft (~50 m) to more than 980 ft (>300 m), with an average width of more than 490 ft (>150 m).

The pattern of swarm distribution and the way in which swarms intersect or link are challenging to determine, despite the large size of the Fort Lewis outcrop, because swarms are long and widely spaced. Fractures in swarm A make up two domains that are separated and offset from each other and that have differing fracture orientations (Figs. 6.6 and 6.11). These domains might represent an en echelon step between two swarm segments, or the intersection of two nonparallel swarms. In swarm B, two overlapping, curved swarm segments can be distinguished (Figs. 6.6 and 6.15). The two subparallel main segments are connected by a nonparallel segment having numerous small fractures arranged in a network of en echelon fractures, splays, and ladder structures. Along both main strands, swarm width

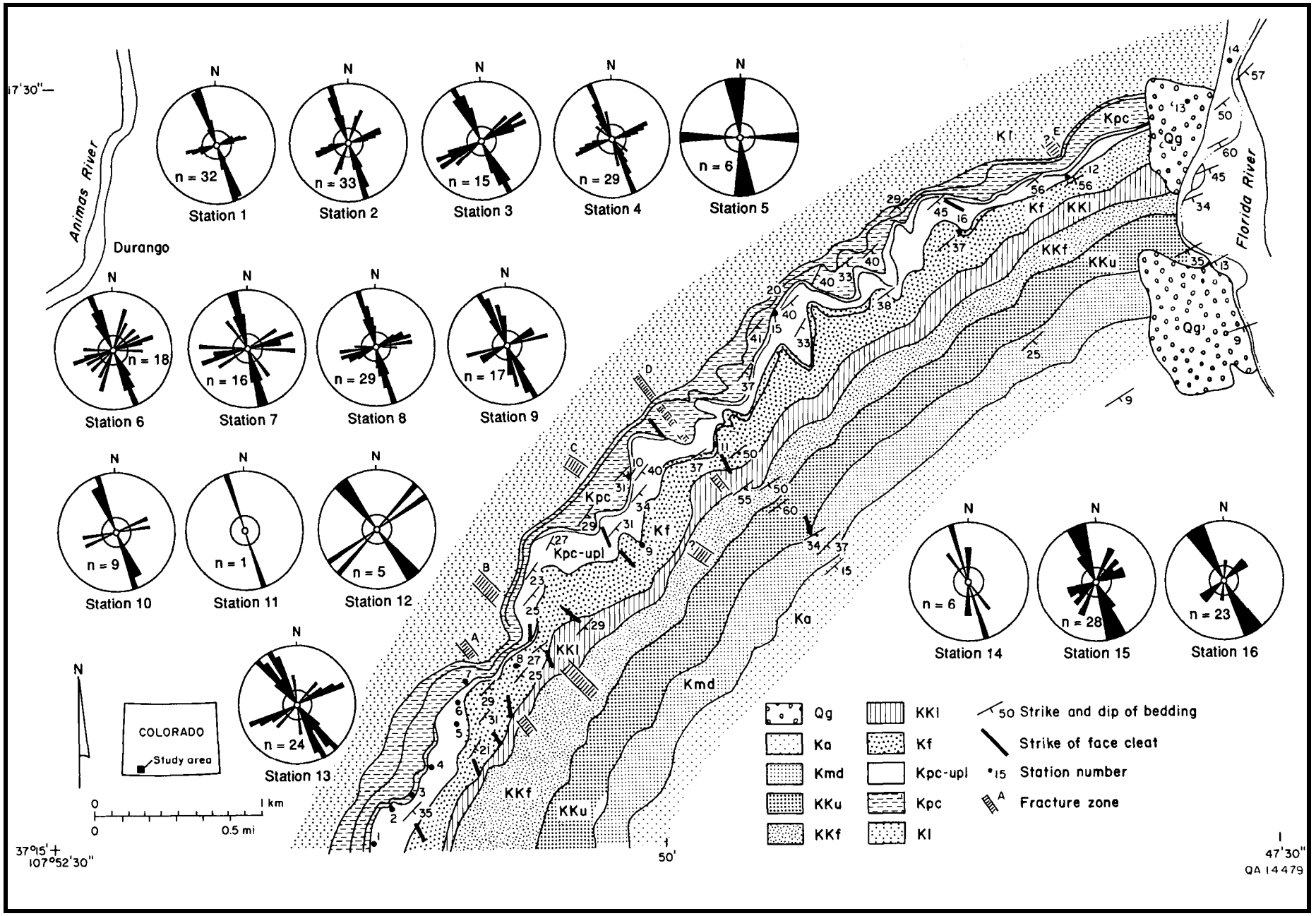

FIGURE 6.7—Fracture zones in Pictured Cliffs Sandstone and cleat strike in adjacent Fruitland Formation coal between Animas and Florida Rivers. See Fig. 6.1 for location.

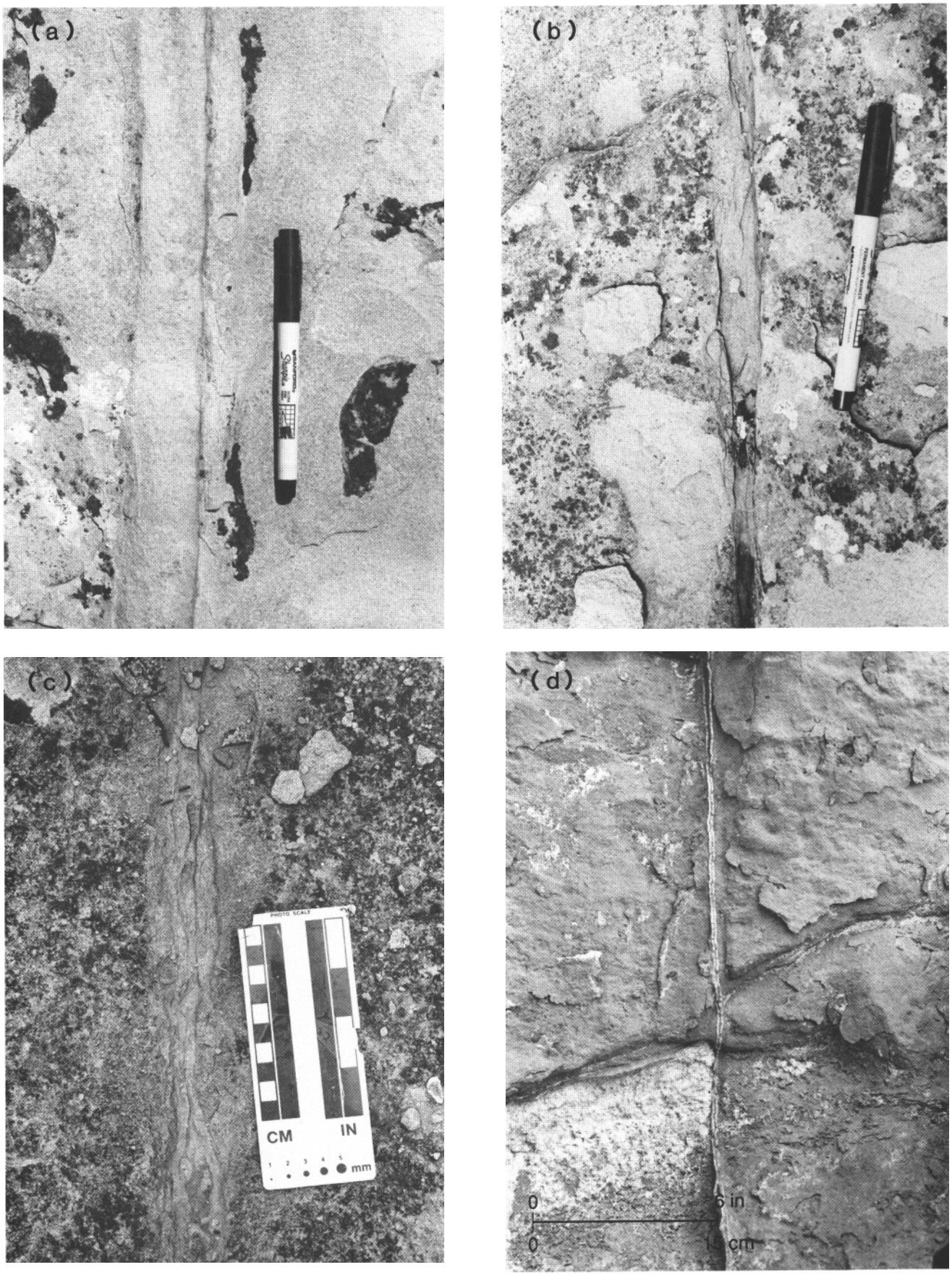

FIGURE 6.8—Morphology of individual set I fractures, Fort Lewis mine. (a) Single narrow fracture with "braided" appearance and halo of bleached rock (plan view). The morphology superficially resembles that of "deformation bands." (b) Multistrand, macroscopically segmented fracture or narrow fracture swarm with diffuse halo of bleached rock (plan view). (c) Anastomosing fractures in narrow fracture swarm (plan view). (d) Calcite-filled vein (cross-sectional view).

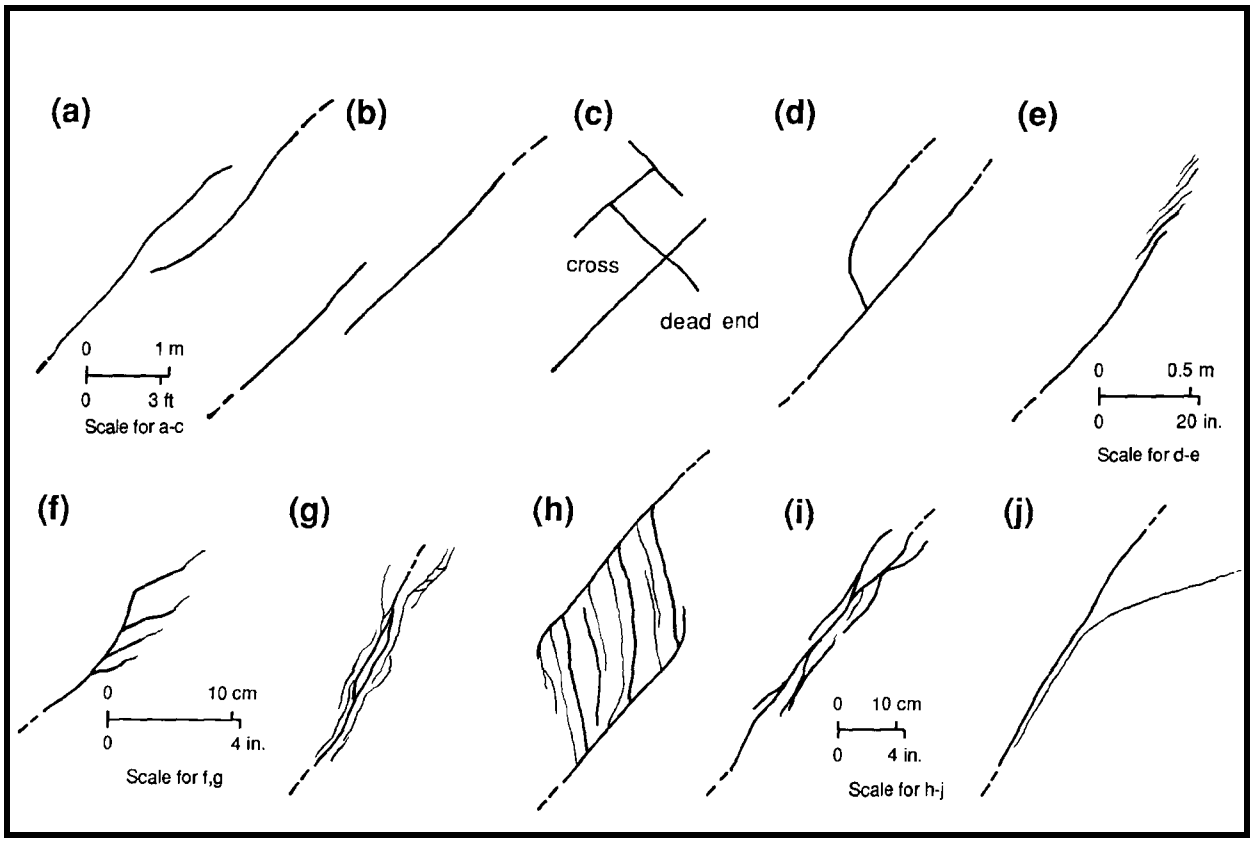

FIGURE 6.9—Fracture termination styles. (a) Approaching, nonintersecting. (b) En echelon, no curvature. (c) Abutting, crossing, and dead-end. (d) Hook intersection. (e) Segmented, en echelon step. (f) Asymmetric splay. (g) Horsetail splay. (h) Ladder structure. These patterns resemble fracture patterns developed between strike-slip fault segments. (i) Complex crossing. (j) Gradual curve into parallel strike. Examples are from field sketches.

diminishes as the area of overlap is approached (Fig. 6.15). This macrostructure resembles overlap regions of individual fractures (Fig. 6.10b).

Fractures visible on 1:1,000-scale maps are arranged in characteristic patterns that resemble the arrangements associated with terminations of individual fractures (Fig. 6.9). The most distinctive macro-scale arrangements include abruptly curving fracture segments and ladder structures. Along their strike or near their terminations, many large fractures split into smaller en echelon or arborescent arrangements of segments.

Fracture patterns within swarms—Fracture patterns within swarms are defined by fracture spacing, length, shape, orientation, and arrangement. Spacing is highly variable and ranges from 0.5 inch to approximately 3 ft (1 cm to ~1 m) or more. Average between-fracture distance is approximately 3 ft (~1 m), so fracture spacing is close only in comparison to domains adjacent to swarms that lack fractures. Areas within swarms may have regular spacing over large areas. For example, within swarm C, an area of approximately 2,420 ft^2 (~225 m^2) has parallel fractures with approximately 6 ft (~2 m) spacing. Some of these fractures are part of a large ladder structure, and their strike is oblique to that of the swarm as a whole. Fracture density can vary widely within swarms but is generally highest where fracture segments overlap. A general measure of fracture density is the number of fractures within a given swarm. A representative example is swarm C, which consists of 36 individual fractures less than 3 ft (<1 m) long in an area of 36,315 ft^2 (3,375 m^2).

Individual fractures within swarms have a wide range of trace lengths, from microfractures having millimeter-long traces to fractures with traces longer than 320 ft (>100 m). The mean length of individual, continuous fractures in the four swarms is 35 ft (10.5 m) (Fig. 6.16), but this number does not include the many short (<3 ft [<1 m]) fracture strands and segments that occur within fracture swarms.

Fractures have a wide range of strikes (250° to 340°), but mean fracture strike is west-northwest, similar to the overall strike of the swarms (Figs. 6.11 and 6.12). Fracture strikes typically differ from swarm strikes by 10° or less, but individual fractures can differ from swarm strike by 60° to 70°. Fractures with lengths less than approximately 3 ft (~1 m) have the greatest dispersion in strike, reflecting the large number of fractures in this length range that occur in splays, overlap zones, and ladder structures. Many fractures with lengths of 3 to 30 ft (1 to 10 m) have strikes at a high angle (60°) to the strike of the swarm in which they occur, in part reflecting their occurrence in large splays and ladder structures. Most fractures are straight or slightly curved, but some strongly curved fractures are present. Many fractures with lengths greater than 60 ft (>20 m) are significantly curved, and one 130-ft-long (40-m) fracture ranges in strike from approximately 275° to 345°.

Fracture connectedness—The degree to which fractures are interconnected will affect the flow properties of a fracture system; fractures that are not interconnected make little contribution to fracture flow (Long and Billaux, 1987; Barton and Hsieh, 1989). One way to assess connectedness is by noting the number of fractures that intersect or *connect* with other fractures by abutting, crossing, or splaying relative to those that end within the rock matrix with blind, or *dead-end,* terminations or that are partly (or poorly) interconnected with other fractures, such as where fractures are

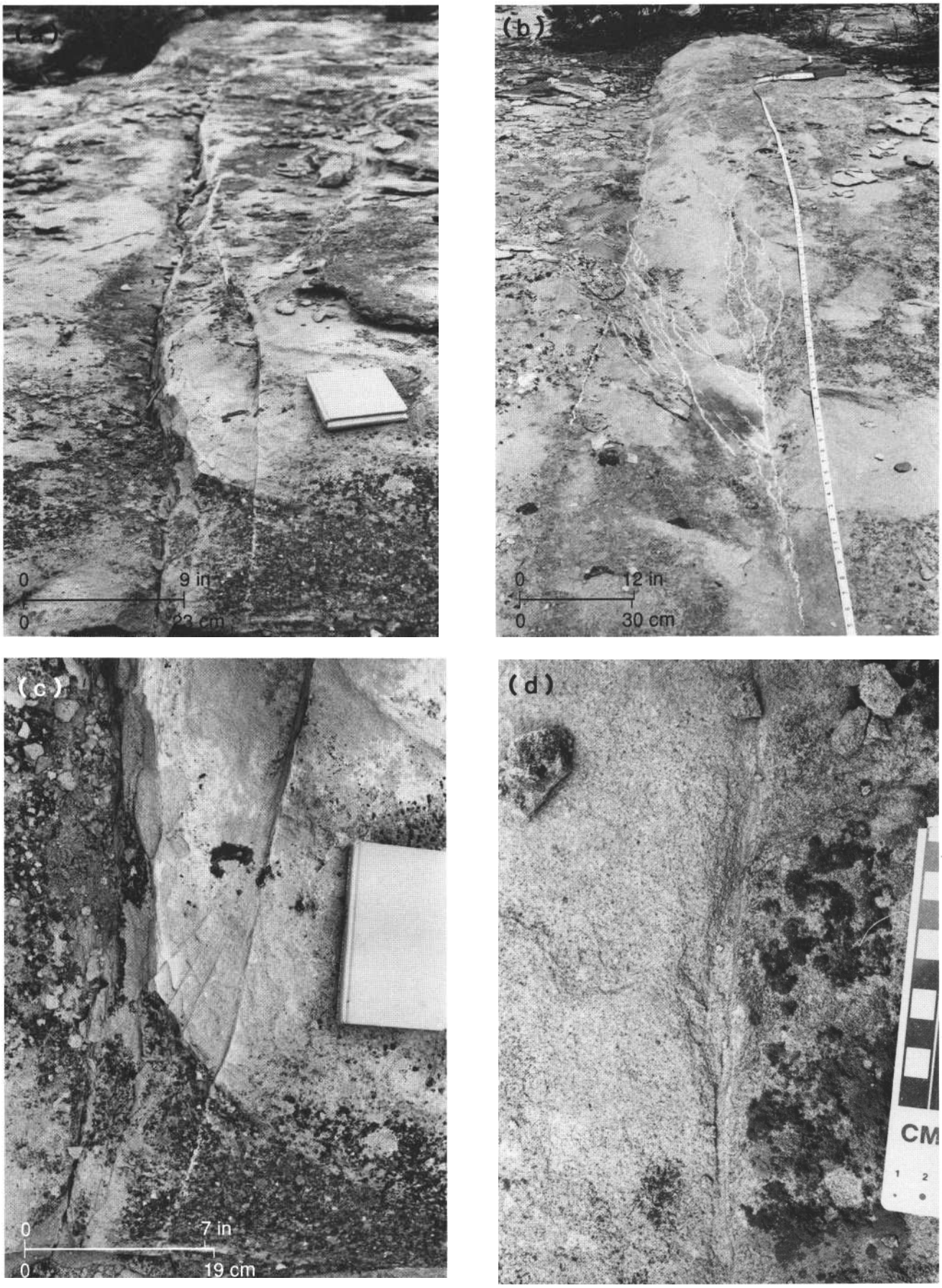

FIGURE 6.10—Fracture connectedness and termination style, Fort Lewis mine. (a) braided fracture stranus. (b) Overlapping fracture strands connected by an array of thin subsidiary fractures, "ladder" structure. (c) Curved and branching fracture termination against a larger fracture. (d) Dead-end fracture termination and associated diffuse microfracture array.

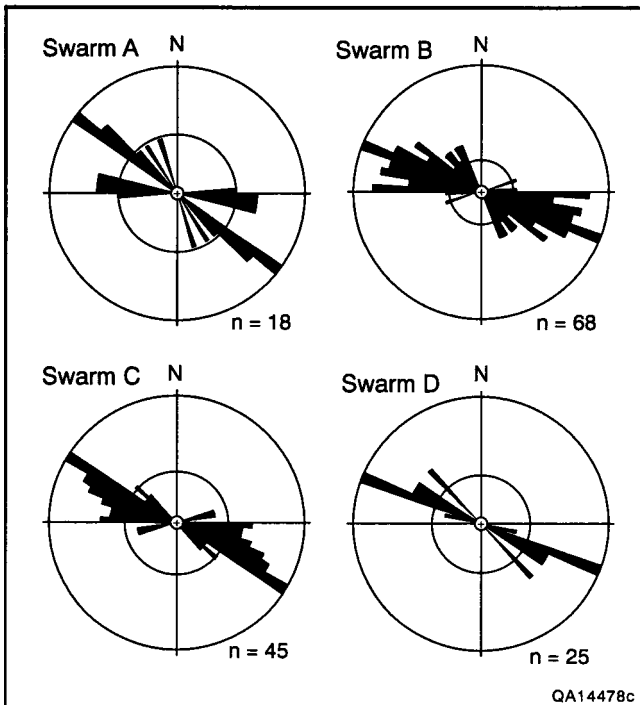

FIGURE 6.11—Fracture strikes in four main fracture zones, Fort Lewis mine. Equal-area rose diagrams; data are plotted as percentages of total number of measurements (n) in 5° intervals. See Fig. 6.6 for locations.

linked by *constricted,* thin, tapering tips or microfractures. Connectedness can be represented on a triangular graph that shows the ratios of connected, constricted, and dead-end termination types (Fig. 6.17). Detailed outcrop maps, such as the field maps that form the basis of Fig. 6.6, are needed to assess interconnectedness and to count fracture termination types, and the scale of the map may influence which fractures are deemed connected, constricted, or dead end (Fig. 6.18).

In Pictured Cliffs outcrops, fracture connectedness is surprisingly low in comparison with that which might be expected for orthogonal arrays of regional fractures (Stearns and Friedman, 1972) or simple cubic networks of fractured-reservoir models (for example, see Aguilera, 1980). Such networks would be well connected by numerous abutting intersections and would plot near or on the "connected" apex of the plot. At the Fort Lewis mine, fracture connections across the width of fracture swarms (normal to overall fracture strike) are infrequent. Few abutting or crosscutting fractures occur within swarms, except between set I and set II fractures, and these would be irrelevant for subsurface fluid flow if set II fractures are surficial phenomena. Most connections at the mapped level of exposure are through low-angle intersections and microfracture arrays where fracture strands overlap. Such intersections tend to connect fractures parallel to the length of the swarm, but not across the width, so some sections of swarms may be partly or completely isolated from others. Some fractures appear to be completely isolated both along and across strike, and many fractures or linked arrays of fractures have one blind termination.

The fracture-trace maps are two-dimensional slices through a three-dimensional fracture network, so fractures may be connected to each other above or below the surface we

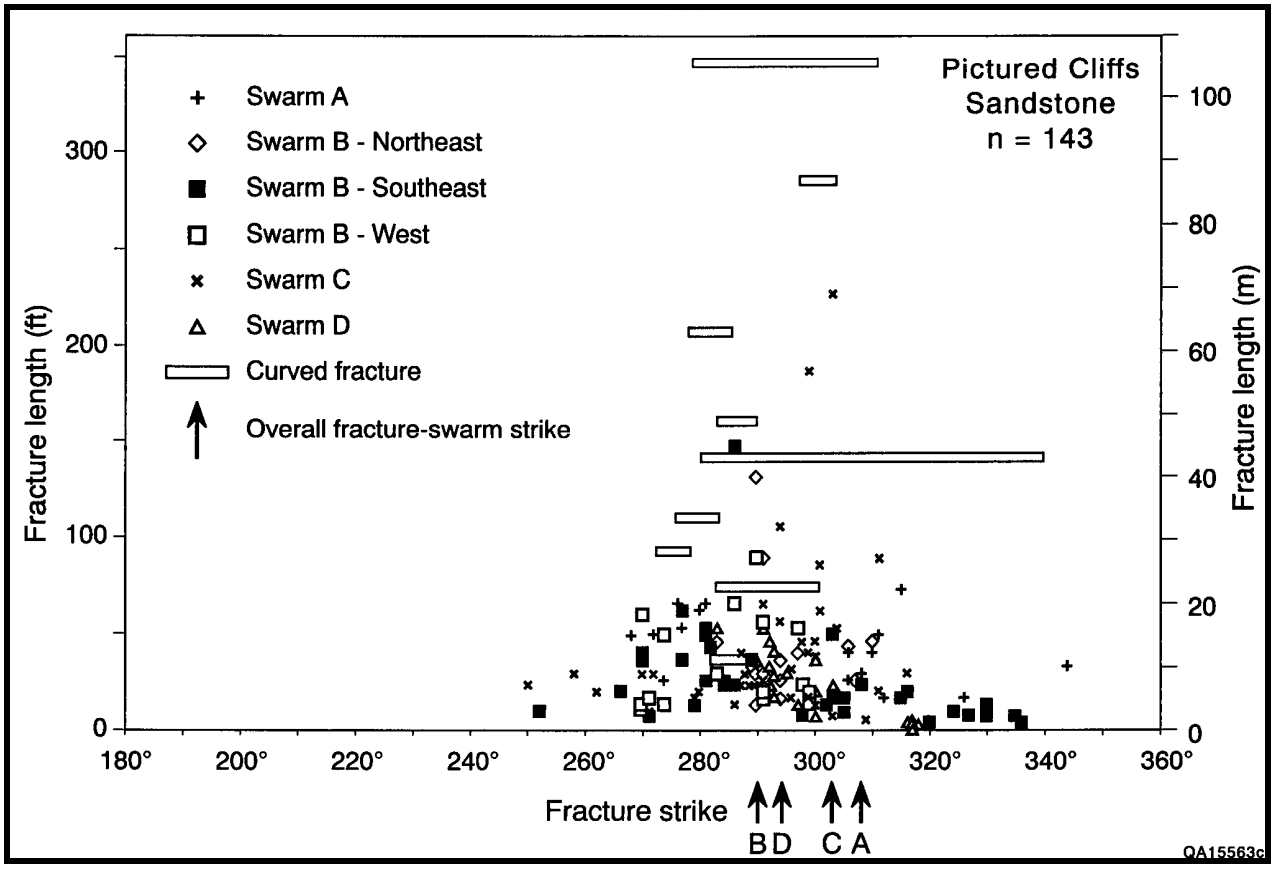

FIGURE 6.12—Fracture length versus fracture strike, Fort Lewis mine. Arrows indicate overall strike of four main fracture swarms. Bars indicate strike range of long, curved fractures. Fracture swarms are shown in Fig. 6.6.

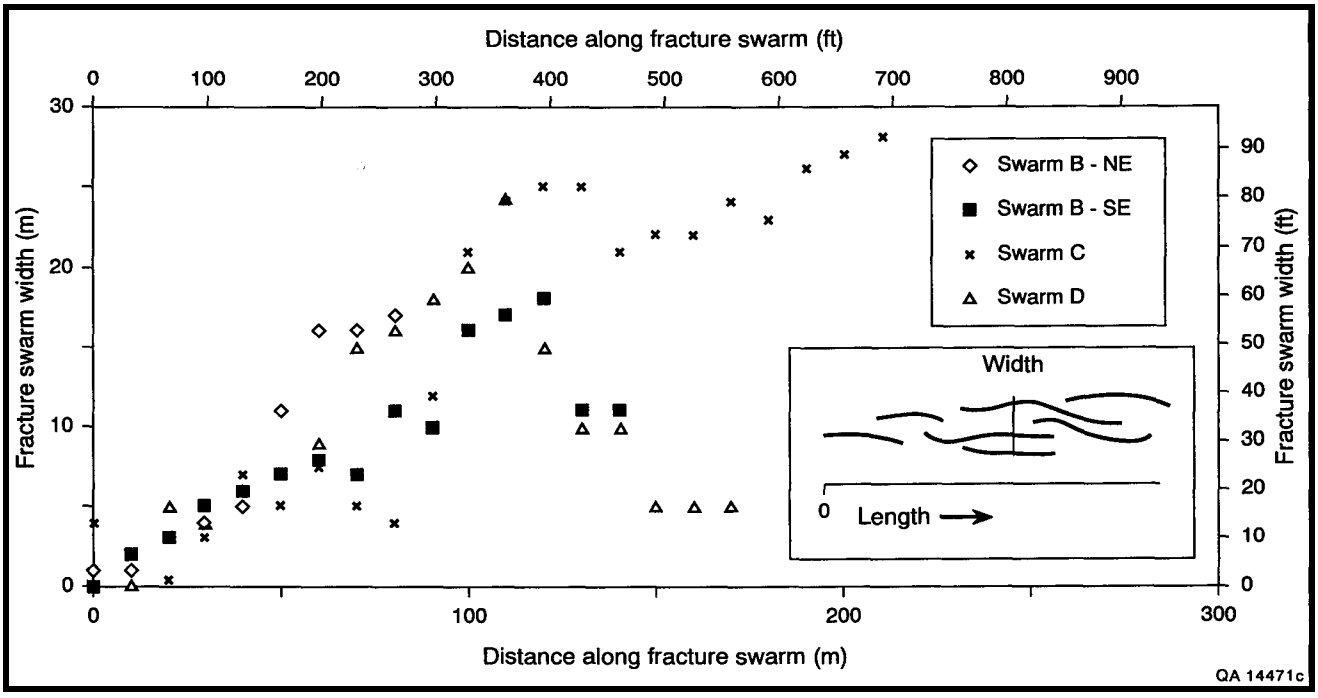

FIGURE 6.13—Fracture swarm width versus distance along fracture swarm for swarms B, C, and D. Inset defines fracture swarm width and length.

mapped. Most fractures are perpendicular to the mapper surface (a bedding plane), however, so connectivity pat terns on the map are probably representative of the system

Relation of swarms in sandstone to coal fracture patterns—At the Fort Lewis mine, coal directly overlies sandstone, but the mine has been reclaimed and the contact between coal and sandstone is not exposed in remaining outcrops. Coal is exposed within 10 ft (3 m) of the coal-sandstone contact, and cleat patterns were studied in 20 small natural outcrops and shallow excavations adjacent to the pavement. Cleat strikes and spacing are typical for the northern San Juan Basin throughout much of the outcrop. Face cleats strike northwest and have little dispersion in strike. In contrast, where fracture swarm D projects into the coal outcrop, numerous small normal faults and highly variable cleat patterns are evident. We interpret this to be the continuation of fracture swarm D in the Fruitland coal seam.

The disturbed zone in coal is approximately 90 ft (~30 m) wide. Within it. six map-scale normal faults have west-

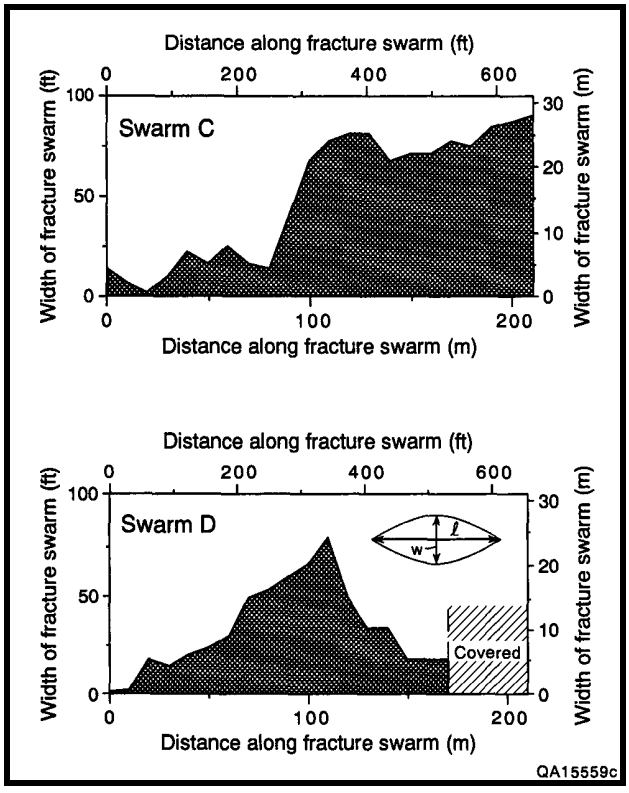

FIGURE 6.14—Profiles of fracture swarm width and length for swarms C and D. Swarm C has two sections of approximately constant width, connected by a segment near the middle of the exposure where it abruptly widens, whereas swarm D gradually tapers away from a wide central part.

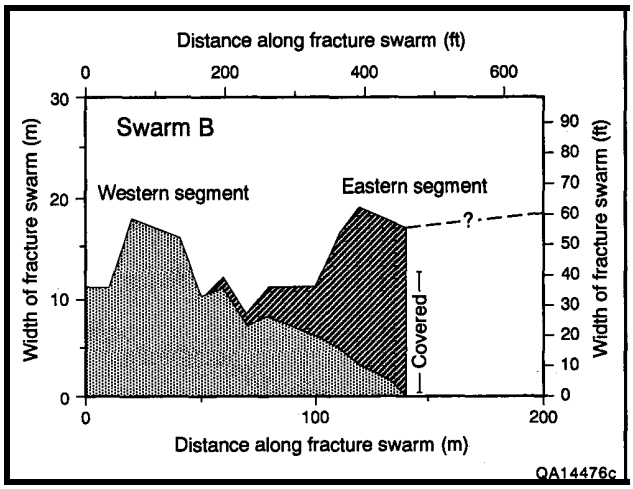

FIGURE 6.15—Width versus length measurements of overlapping western and eastern segments of swarm B. Gradual sympathetic narrowing of swarm segments in their region of overlap suggests a pattern of swarm interaction and dilation similar to that observed between segments of individual overlapping fracture segments. Dotted line shows inferred continuation of eastern swarm B segment in covered area.

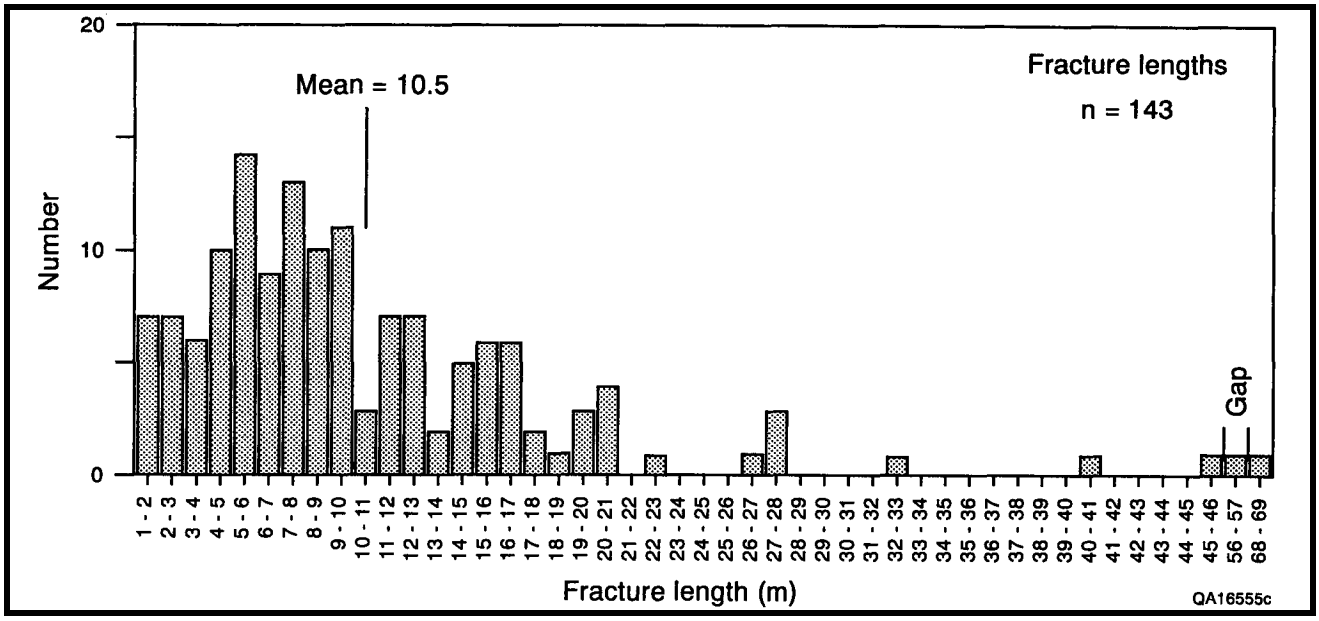

FIGURE 6.16—Histogram of fracture segment lengths greater than 3 ft (>1 m) long, Fort Lewis mine pavement.

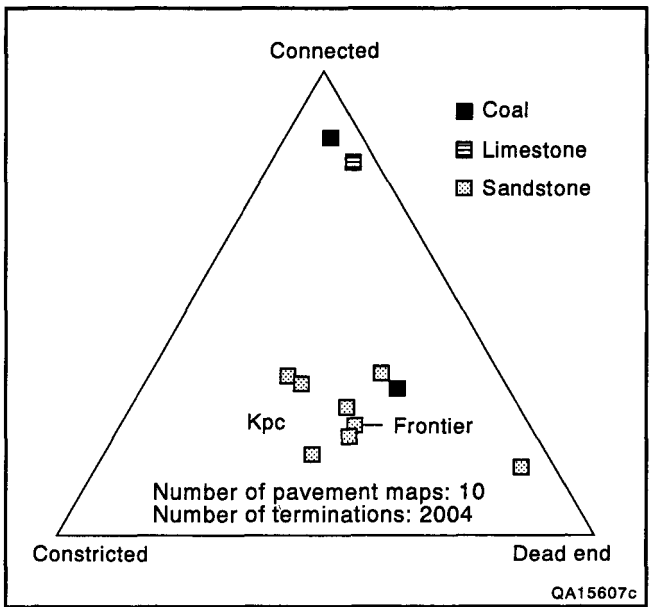

FIGURE 6.17—Termination-type diagram showing proportion of connected, constricted, and dead-end fracture terminations. Connected fractures are those that abut or cross. Constricted fractures are those connected only by narrow subsidiary fractures or micro-fractures; typically these are where segmented fracture strands overlap (see Fig. 6.10). Dead-end (or blind) fractures have isolated terminations. Sandstone measurements are from seven detailed maps of the Fort Lewis mine near the Colorado–New Mexico border and of a pavement in the Cretaceous Frontier Formation in Wyoming (Laubach, 1991). Coal measurements are from a map of lower Fruitland Formation coal at the Navajo mine in New Mexico (Tremain and others, this volume, Chapter 5); a seemingly anomalous pattern of poor interconnectedness in one coal example is evident. For comparison, Cretaceous Edwards Limestone, Balcones fault zone, central Texas, shows a well-interconnected fracture pattern (Collins and others, 1990).

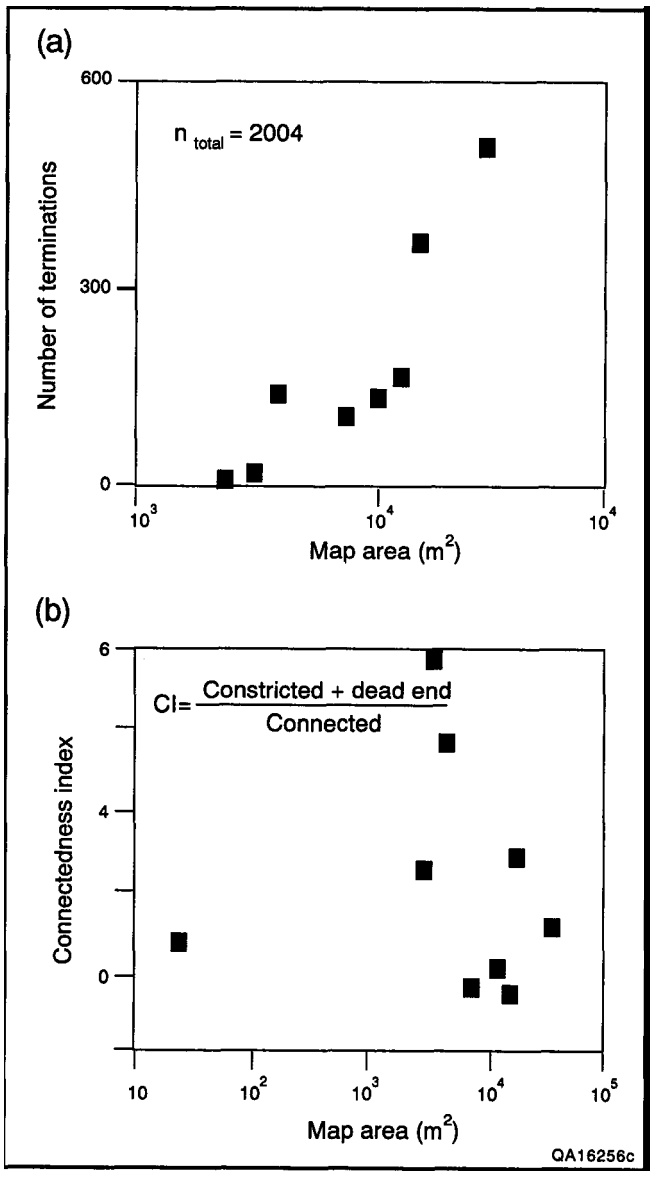

FIGURE 6.18—Fracture connectedness. (a) Number of fracture terminations versus size of mapped area and (b) connectedness index versus map area. As expected, larger maps have more terminations, but the proportion of termination types relative to the degree of connectedness does not change systematically with map size.

northwest strikes and throws of 3 ft (1 m) or less. Most faults are confined to the coal-bearing section and do not cut the main sandstone pavement. Fractures in coal include small faults, nonsystematic or widely spaced systematic "third" cleats with a range of strikes, curved cleat, and vertically extensive joints. Fracture density is greatest near faults. Changes in cleat strikes are evident at distances of as much as 50 ft (15 m) from mapped faults. These characteristics resemble the fracture pattern in coal associated with the fracture swarm at Durango/US-550 described above.

Elsewhere in Fruitland coal exposures are cleat patterns that suggest that nonuniform, swarmlike fracture arrangements are present, despite highly cleated and generally superficially uniform fracture systems. A map of master cleats in an exposure of Fruitland coal in the Navajo mine that is distant from any known swarm in sandstone shows connectivity ratios similar to those of Pictured Cliffs swarms (Fig. 6.17; Tremain and others, this volume, Fig. 5.9) because the connections between master fractures are through smaller, short, discontinuous fractures. In coal, high overall fracture connectivity is expected because numerous right-angle abutting relations are evident in most bedding-plane outcrops. The clustering of long fractures in this coal bed shows that the fracture pattern has domains of contrasting fracture density, hinting that domains with varying degrees of cleat development may exist within coal fracture patterns in Fruitland Formation coal beds.

Regional-scale fracture swarms: Animas—Florida river exposure

Discrete west-northwest-, northwest-, and north-striking fracture swarms are present in Pictured Cliffs pavements between the Animas and Florida Rivers, southeast of Durango (Fig. 6.7). Preferential erosion along north-striking fracture swarms may account for some of the linear topographic features along this outcrop. West-northwest fracture swarms tend to be less well exposed. The northwest-striking swarms are subparallel to face-cleat strikes in overlying Fruitland Formation coal. Exposed swarm lengths are as much as 1,000 ft (305 m), and widths range from 50 to greater than 100 ft (15 to >30 m). Smaller swarms, such as the one that occurs at Carbon Junction (Fig. 6.2), are present locally elsewhere along the ridge. Spacing between large swarms is irregular and ranges from more than 4,000 ft (>1,220 m) to approximately 200 ft (~60 m). Near Durango most swarms have north-northwest strike. Several of the swarms are confined to individual sandstone beds; they are isolated vertically as well as laterally by rock that lacks fractures. We were not able to link swarms in sandstone to specific coal fracture swarms or faults, but changes in mean face-cleat strike and development of "third cleat" trends (cleats with anomalous strike) in some exposures suggest that swarms may exist in coal.

Swarms in the Animas-Florida river exposure show that the Fort Lewis mine fracture style of discrete, irregularly spaced fractures is not an isolated occurrence.

Causes of fracture development

Most rocks near the Earth's surface behave as brittle-elastic materials in response to natural stresses. Consequently, under the influence of compression, extension, flexure, uplift, cooling, and fluid migration, many rocks acquire networks of fractures of various types and sizes. Determining which process(es) caused a given fracture set is challenging because many loading paths can result in fractures that appear similar (Engelder, 1985). However, knowledge of processes responsible for fractures can provide insight into the probable distribution and orientation of fractures on local and regional scales. We interpret fractures in Pictured Cliffs Sandstone to have formed in response to west-northwest tectonic shortening that caused lateral elongation subparallel to the Cordilleran overthrust belt (Fig. 6.19). This model is the same as that proposed to explain regional face-cleat patterns in the San Juan Basin (Tremain and others, this volume, Chapter 5).

Evidence that fractures grew before folding is consistent with orientation of fractures normal to bedding where beds are tilted, and with similar pre-folding fracture strikes at the Fort Lewis mine and Animas-Florida river exposure, despite regional change in fold trend, an interpretation consistent with the conclusions of previous workers that in Cretaceous rocks many joints predate development of early Tertiary folds (Condon, 1988; Tremain and Whitehead, 1990). Fractures similar to those in outcrop also occur in core from areas distant from any fold. Fracture timing is broadly consistent with fracture growth driven by movements in the adjacent orogenic belt.

Normal faults in coal are associated with swarms in sandstone at the Fort Lewis mine. These faults are compatible with foreland extension. However, northeast- and northwest-striking normal faults in Cretaceous and Tertiary rocks in the San Juan Basin have a long movement history, including Laramide movement. According to Huffman and Taylor (1991), east-west shortening may have resulted in left-lateral movement on northwest-striking faults and in

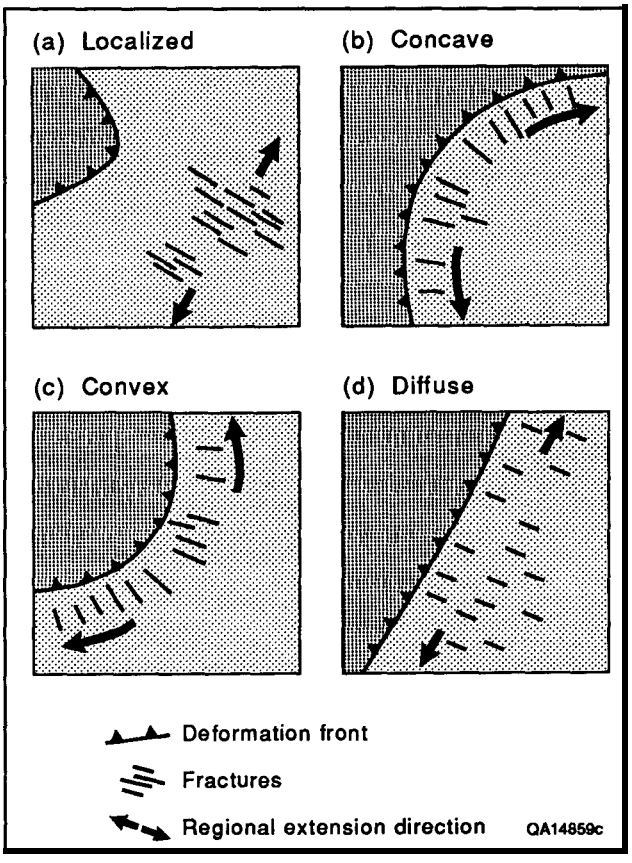

FIGURE 6.19—Map view of deformation fronts of various shapes and fracture strikes in foreland areas that may result from lateral foreland extension (modified from Hancock and Bevan, 1987). (a) Uniform extension direction and localized extension in advance of convex front. (b) Concave arc of extension directions with concave front. (c) Convex arc with convex front. (d) Slightly convex arc of extension directions with nearly rectilinear front. Fracture strikes are not precisely parallel to shortening directions, but rotate in sympathy with them. Obstacles and indentors within the foreland and the deformation front may cause fracture strikes to vary on subregional scale.

right-lateral movement on northeast-striking faults, but evidence for transcurrent slip is ambiguous and not apparent on the small exposed faults and fractures we studied. In the Fort Lewis fracture swarms, ladder structures resemble fracture patterns associated with small strike-slip faults, but strike-slip motion does not appear to have occurred on these faults.

Fracture swarms: targets for natural gas exploration

The existence of fracture swarms in the subsurface of the San Juan Basin has yet to be demonstrated. Fractures occur in several Fruitland Formation and Pictured Cliffs Sandstone cores from vertical wells in the basin (Table 6.1); some resemble set I fractures at the Fort Lewis mine. In sandstone they are subvertical and are composed of multiple strands; several have calcite vein fill. Striated and inclined fractures not evident at the Fort Lewis mine are present in these cores, but they are generally found only in shales, which are poorly exposed at the mine. Core orientation data indicate north, northeast, and east strikes for the steeply dipping sandstone fractures, but the number of oriented fractures is too limited to draw any conclusions about fracture orientations within the basin. If face-cleat strikes are a guide to sandstone fracture patterns, fracture strikes may vary considerably in the northern part of the basin. If fractures are associated with faults, then northwest and northeast strikes should be expected. Our interpretation predicts that swarms with west–northwest strike should exist within the northern third of the basin. If fault patterns are a guide to fracture swarm orientations, northeast-striking fractures may also be expected.

The abrupt contrast in fracture intensity (or density) between swarms and adjacent rocks suggests that these features may be visible with advanced seismic techniques (such as cross-polarized S-waves) and possibly as velocity anomalies on conventional seismic lines. Our observations indicate that it may be difficult to fully assess the role of fractures in Rocky Mountain low-permeability gas reservoirs with current fracture-detection methods or fractured-reservoir models because the vertical dimension of fractures at the wellbore does not show how the fracture is interconnected (or isolated) from the fracture network, and because predicting swarm occurrence is challenging. These conclusions are likely to apply elsewhere in the western United States because the Pictured Cliffs and Fruitland share a similar tectonic setting and other characteristics with many Cretaceous gas reservoir rocks of this region. Swarms are present in Cretaceous sandstones in the Piceance and Green River Basins (Cozzette and Frontier sandstones [Laubach, 1991]) and in Cretaceous chalk of central Texas (Austin Chalk [Collins and others, 1990]).

In the San Juan Basin, Pictured Cliffs sandstones and Fruitland coal beds form gas reservoirs (Ayers and others, this volume, Chapter 2), and local high gas and/or water production and abrupt differences in well performance that cannot be explained by other aspects of reservoir geology or completion practices indicate that fracture-enhanced permeability is present (Fig. 6.20) (Gorham and others, 1979; DuChene, 1989; Kaiser and Ayers, this volume, Chapter 10). Predicting the location and pattern of fractures in the subsurface is important for exploration, engineering evaluation, and development because fractures may control the size and shape of the rock volume contacted by a given borehole.

Summary

On the northwestern margin of the San Juan Basin, a prominent set of fractures in the Pictured Cliffs Sandstone

TABLE 6.1—Fractures in cores (exduding coal).

Well name, location	Fm	Core depth (ft)	Lithology	Fracture description and mineralization	References
USGS Core[2] Hole A-15 Sec. 1 T23N R13W	Kf	248-257	sandstone	Gypsum veins	Wilson and Jentgen, 1980
El Paso Natural[2] Gas Gasbuggy No. 1 Sec. 36 T29N R4W	Tn, Tka, Kkf, Kf, Kpc, Kl	3436-4316	sandstone, siltstone shale	Shale in all formations striated; vertical fractures in shale in Kkf and Kf, and KI-commonly filled with calcite in Kkf and Kf plus some clay. Sandstones in Tn and Tka have 75° to vertical fractures; sandstone and siltstones in Kkf, Kf and Kpc have many 70° to vertical fractures, commonly lined with calcite plus low-angle (<30°) fractures. Kpc sandstone has one 10-ft wet vertical fracture with gas odor.	Fassett, 1967
Blackwood & Nichols[1,2] NEBU No. 403 Sec. 9 T30N R7W	Kf	3025-3192	sandstone, siltstone, shale	Fractures are open to filled, open trend N and E, partially open N and NE, filled N and NE. Fractures arranged in strands.	Mayor and Close, 1989a, GRI-90/0041
Western Coal[2] P-70 Sec. 22 T30N R15W	Kf	370-414	carbonaceous shale	Horizontal fractures with calcite veins and pyrite on glossy surfaces	TRW Preliminary Well Test Report, 1978
Tiffany[1,2] Glover No. 1 Sec. 2 T32N R6W	Kf	3062-3111	siltstone	Horizontal to vertical microfractures (0.5 mm wide) filled with white mineral (calcite?)	COGCC files
Mobil Colorado[1,2] 32-7, No. 9 Sec. 4 T32N R7W	Kf	2759-3064 2899-2927	sandstone, shale	"Some gouge and calcite filled fractures in sandstone below coals, strike same as cleats." Low-angle striated in shale; moderate-high-angle filled fractures in sandstone, averaging 7 cm long and 0.1 mm wide plus high-angle calcium-filled fractures 0.2 mm wide and 10 cm long (one 24 cm)—not visibly porous, 28 filled fractures	Mayor and Close, 1989c, GRI-90/0043

TABLE 6.1 (continued)

Well name, location	Fm	Core depth (ft)	Lithology	Fracture description and mineralization	References
Ladd 2-3 North Cox Canyon Sec. 3 T32N R10W	Kf	3084-3114	carbonaceous shale	4 striated horizontal to 40°, 1 with calcite	CGS files
Mesa Hamilton No. 3[1] Sec. 30 T32N R10W	Kf	2652-2887	sandstone and shale enclosing coals	Prominent set of open fractures N70-80E	Mayor and Close, 1989d, GRI-90/0040
USGS No. 1 Sec. 23 T32N R12W	Kf	181-226	siltstone	45° fractures	Roberts, 1989
USGS No. 2[2] Sec. 23 T32N R12W	Kf	61-119	shale, siltstone	Two 45° fractures	Roberts, 1989
El Paso Natural Gas 14-20, 33-7 Sec. 20 T33N R7W	Sano-stee Kd	7253-7418 7646-7694	sandstone sandstone, shale	Calcite veins Vertical and horizontal fractures	COGCC; Petroleum Information completion card
Amerada No. 1 Harmon Sec. 17 T33N R8W	Kd	7796-7810	sandstone	Fractures	COGCC files
U.S. Smelting-Mining 1-x Brown Sec. 15 T33N R9W	Kf Kd	2669-3086 7725-7965	sandstone, shale sandstone	Fractures, with gas odor in sandstone; vertical fractures	COGCC; Petroleum Information completion card
USGS No. 17 Sec. 17 T33N R11W	Kf	226-271	0.8-ft siltstone, 1-ft claystone	High-angle fracture Two 45° fractures	Roberts, 1989
USGS No. 14 Sec. 30 T33N R11W	Kf	46-58 161-265	siltstone	45° fractures	Roberts, 1989
USGS No. 11 Sec. 31 T33N R11W	Kf	71-137	siltstone, sandstone	45° fracture Calcite-filled fractures	Roberts, 1989
Benson-Montin Greer Ute A-1 Sec. 35 T33N R12W	Kd	3634-3686	sandstone	Good fracture system at 3662-3686.5 ft	COGCC files
USGS No. 8[2] Sec. 36 T33N R12W	Kf	75-129	siltstone	Pyrite on fractures	Roberts, 1989
SUTEC[2] Oxford No. 1 Sec. 25 T34N R8W	Kf	2769-2787 2804-2822	shale	Striations with calcite, pyrite, and gypsum	CGS files
SUTEC[2] Oxford No. 2 Sec. 25 T34N R8W	Kf	2832-2850	carbonaceous shale, siltstone	Striations with calcite on faces, trace pyrite	CGS files
Bowen and Edwards SE Durango Federal 3-1 Sec. 3 T34N R9W	Kf	1890-1918 2010-2040 2132-2160	shale	Fractures at 2040 ft	COGCC files
Tenneco[2] Fassett 2-13 Sec. 13 T34N R9W	Kf	2468-2482	carbonaceous shale	Striations dipping 30-50°, two vertical fractures	CGS files
Tenneco Larson 1-12 Sec. 13 T34N R9W	Kf	2291-2297 2303-2361	carbonaceous shale, sandstone	2 striations at 50-60° 60° vertical fractures	CGS files
Bowen and Edwards[1] McCulloch Well No. 28-1 Sec. 28 T34N R10W	Kf	3140-3168	shale	Striations	COGCC files
Bayles Jicarilla 459 No. 5	Kf	3803-3883	carbonaceous shale, sandstone	Fractures with striations; vertical fractures	BEG files

[1] Oriented cores
[2] Also have mineralized coal cleats (see Table 5.2, Tremain and others, this volume)
Tn = Nacimiento Formation; Tka = Animas Formation; Tkkf = Kirtland Shale; Kf = Fruitland Formation; Kpc = Pictured Cliffs Sandstone; Kl= Lewis Shale; Kd = Dakota Sandstone
CGS = Colorado Geological Survey; COGCC Colorado Oil and Gas Conservation Commission (geological well report); BEG = Bureau of Economic Geology, The University of Texas at Austin

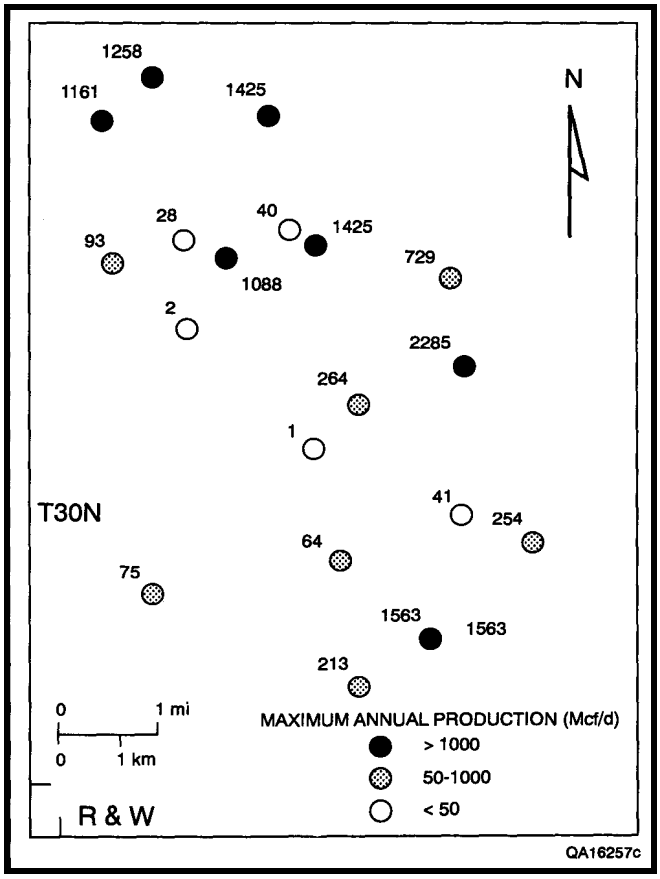

occurs in west–northwest-striking swarms. Locally, swarms extend into overlying Fruitland coal seams, where they are marked by more, and better interconnected, fractures and small normal faults. These may be areas of enhanced permeability and are potential targets of coalbed methane exploration.

Acknowledgments

We thank W. A. Ambrose, W. B. Ayers, Jr., R. W. Baumgardner, Jr., and N. H. Whitehead, III, for assistance and discussions, and W. B. Ayers, Jr., Robin H. Hill, and Roger Tyler for reviews.

FIGURE 6.20—Maximum annual production maps of coalbed methane wells from an area in the northern San Juan Basin (Joseph Yeh and W. R. Kaiser, pers. comm. 1990). Abrupt and substantial differences in maximum annual production may indicate local differences in reservoir quality that could in part be accounted for by discrete fracture zones such as those at Fort Lewis mine. Map is not contoured; this emphasizes that "sweet spots" may be controlled by fracture swarms of unknown size and position. If patterns such as those at Fort Lewis mine extend to field-scale fracture zones, outcrop examples could provide a guide for understanding distribution of exceptionally productive wells.

7. Use of lineament attributes to predict coalbed methane production in the northern San Juan Basin

R. W. Baumgardner, Jr.

Bureau of Economic Geology

Abstract—This study tested the use of lineaments in identifying highly productive coalbed methane wells in the Fruitland Formation of the San Juan Basin. Lineaments were mapped on 1:250,000-scale Landsat Thematic Mapper images and compared with lineaments from three previous studies. Little spatial correspondence exists between lineaments reported in the four studies. Statistically significant lineament trends from the studies varied from subparallel to perpendicular. Lineament attributes from all studies were compared with water and gas production. Data showed that wells on lineaments do not have consistently higher production values than those not on lineaments. Azimuths of lineaments nearest wells with high production values varied between studies and even within one study, for those lineaments derived from different imagery. Only limited significant correlation exists between well production data and attributes of the nearest lineament. Therefore, lineament attributes cannot be used to predict production volumes.

Purpose

The purpose of this study was to map lineaments and to assess their relationships with Fruitland coalbed methane production. Permeability in conventional reservoirs is enhanced by fractures in many areas of the San Juan Basin (Gorham and others, 1979). Depth to gas-producing intervals in the Fruitland Formation varies from 150 ft (45 m) near the basin margins to 3,900 ft (1,200 m) near the center of the basin (W. R. Kaiser, pers. comm. 1990). Lineaments may be spatially correlated with fractures in the subsurface. However, unlike some empirical studies, which regard spatial coincidence between lineaments and highly productive wells as proof that lineaments or their subsurface counterparts are enhancing production, in this study strict statistical criteria were applied to determine whether lineament attributes have a statistically significant correlation with production data. If a significant correlation between lineaments and subsurface fractures can be demonstrated, then the location and orientation of these surface features can be used to help select drilling sites for enhanced production of coalbed methane.

Review of lineament and fracture studies in the San Juan Basin

Previous lineament studies in the San Juan Basin (Fig. 7.1) used imagery at scales different from that used in the present study (Table 7.1). Kelley and Clinton (1960) produced a fracture map of the entire basin based on aerial photographs and photoindices. They grouped fractures in the basin into six trends and concluded that the fracture pattern was too complex to be the result of uniform stress. The pattern reflects irregular deformation of the basin from place to place. They identified a "dominant" fracture trend between 45° and 60°.

TABLE 7.1—Imagery used for lineament studies in the San Juan Basin.

Authors (date)	Scale	Imagery type
Kelley and Clinton (1960)	?	aerial photos
Kelley and Clinton (1960)	1:62,500	photoindex
Newman and McCord (1980)	1:160,000	Landsat Multispectral Scanner, false-
Knepper (1982)	1:800,000	Landsat Multispectral Scanner, black-
Decker and others (1989)	1:28,000	aerial photographs, black-and-
Decker and others (1989)	1:58,000	aerial photographs, color
Decker and others (1989)	1:80,000	aerial photographs, black-and-
Decker and others (1989)	<1:80,000	Landsat image
Wandrey (1989)	1:15,840	aerial photographs, color
Wandrey (1989)	1:20,000	aerial photographs, black-and-
Baumgardner (this study)	1:250,000	Landsat Thematic Mapper, false-color

Newman and McCord (1980) mapped 333 lineaments on Landsat images covering the northern part of the San Juan Basin (southern Colorado). They reported localized similarity between linear features and mapped fracture patterns, which are oriented predominantly north–northwest, in the northern part of their study area.

Knepper (1982) mapped more than 6,000 lineaments in the southern Colorado Plateau (Fig. 7.1) using Landsat images (Table 7.1). He then interpreted 19 "derivative" lineaments, which mark clusters of linear features interpreted from maps of trend-interval concentration and linear features. Three of these derivative lineaments are in the San Juan Basin and spatially correspond to gravity highs, magnetic anomalies, and dike swarms.

Decker and others (1989) mapped lineaments on aerial photographs and Landsat images of the Cedar Hill field area (Fig. 7.1; Table 7.1). Their study revealed linear features oriented predominantly 20° to 40°, 80° to 90°, and 300° to 310°. Locally, linear features they mapped on aerial photos are parallel to coal cleat (joint) directions and subparallel to open fractures in core from the Mesa Hamilton No. 3 well in Cedar Hill field (Fig. 7.1). However, not all photolinears were faults or fractures.

Wandrey (1989) mapped lineaments on aerial photographs of the northwestern San Juan Basin (Fig. 7.1; Table 7.1). He found recurring lineament trends at 60° to 80° and 290° to 325°. They proved to be joints on larger-scale photos.

Because fractures enhance oil and gas production in the San Juan Basin, several authors have studied fractures at the surface and in the subsurface (Fig. 7.2). Gorham and others (1979) studied fractures in the Verde and Puerto Chiquito oil fields of the San Juan Basin (Fig. 7.2). They found competent beds are fractured in areas of maximum curvature along the Hogback monocline. Open joints trend parallel to axes of local folds. In Puerto Chiquito field, oil reservoirs are composed of low-permeability blocks separated by highly permeable fractures. Apparently the fracture zones extend horizontally for miles, but their height is mostly restricted to less than 100 ft (<30 m). Gorham and his coworkers (1979) observed that joint trends in older rocks do not necessarily appear in overlying strata.

Condon (1988) studied fractures on the northwestern side of the San Juan Basin (Fig. 7.2), where he documented four discrete sets of joints. Average orientations of the joint sets were 15°, 53°, 282°, and 317°. The mean orientation of face cleats was 339°; that of butt deats was 48°.

Emmendorfer (1989) studied dipmeter fracture logs from 15 wells in the Gavilan Mancos oil field in the eastern San Juan Basin (Fig. 7.2). Most fractures were oriented north-northwest.

Orientations of cleats and joints in the basin range from northeast to northwest. Most face cleats along the southern and western margins of the basin are oriented northeast (Fig. 7.2) (Tremain and others, this volume, Chapter 5). Along the northern and northwestern sides of the basin (southern Colorado), face cleats trend mostly northwestward (Condon, 1988; Tremain and others, this vol.). Joints near the center of the basin trend mostly northwestward (Tremain and Whitehead, 1990, fig. 37). Northeast and northwest face cleats are found in cores from the northern half of the basin (Fig. 7.2).

These studies indicate that for the San Juan Basin as a whole there is a bimodal distribution of cleat and joint orientations. In the northwestern part of the basin this prob-

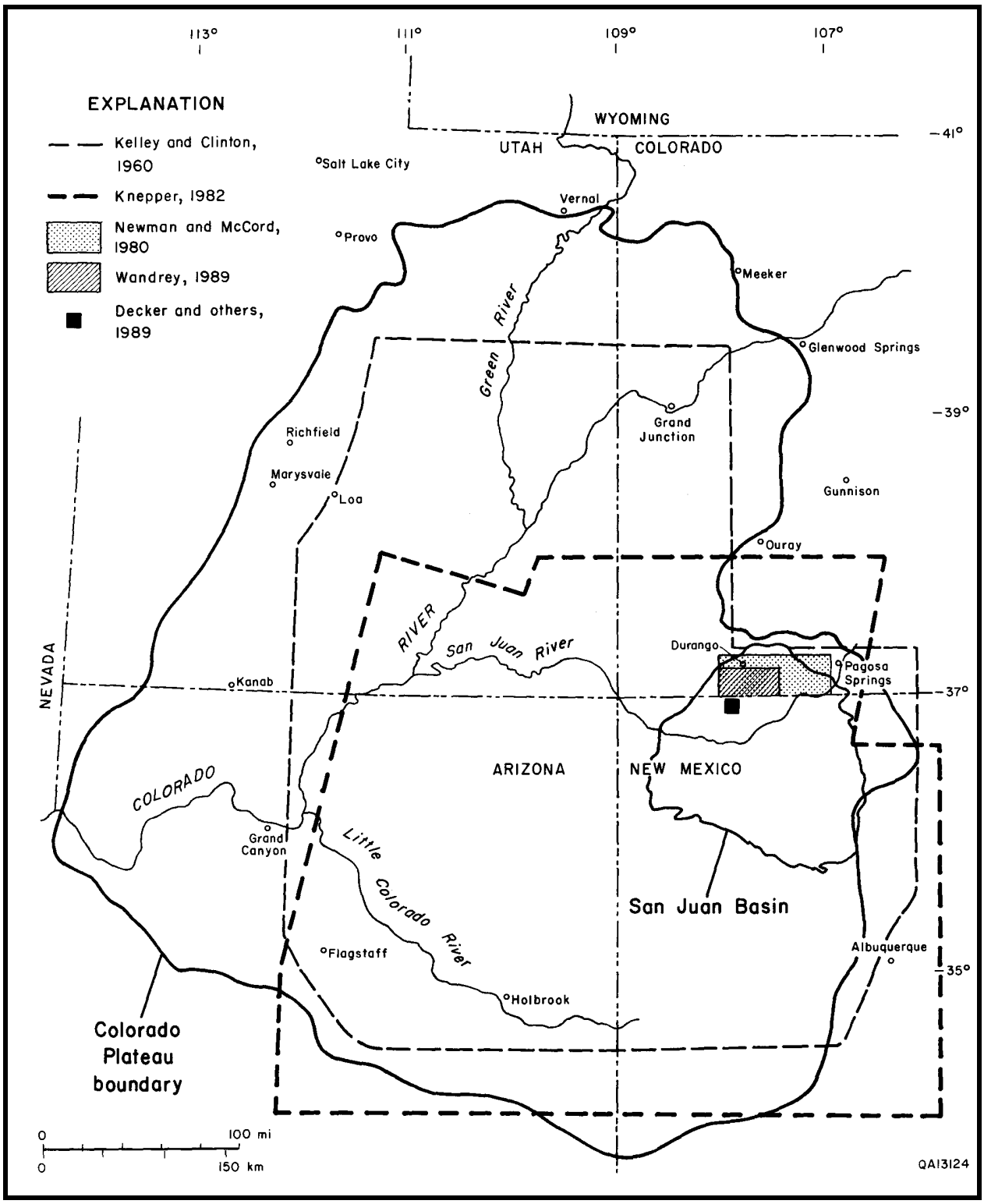

FIGURE 7.1—Previous lineament studies in the vicinity of the San Juan Basin. From Tremain and Whitehead (1990).

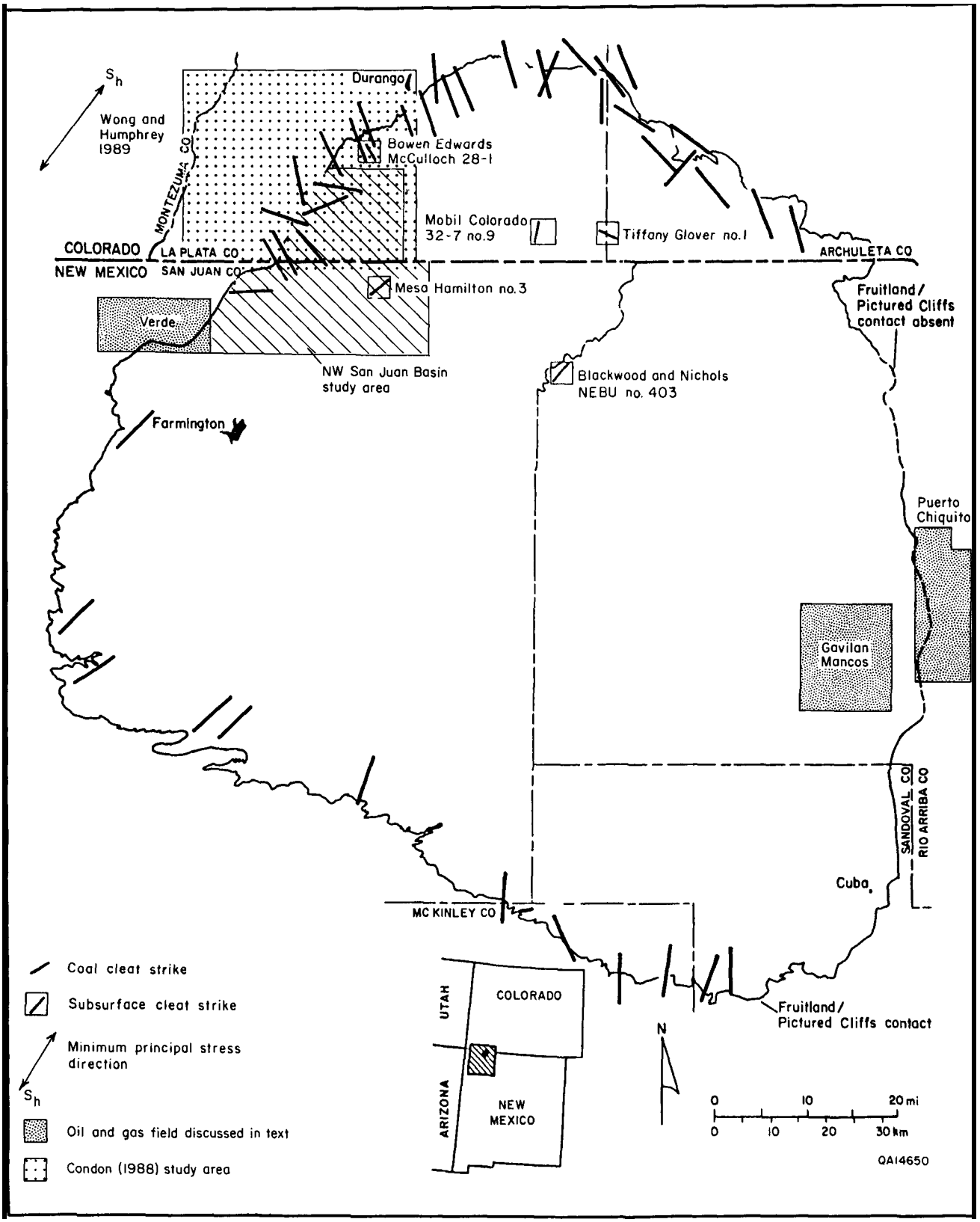

FIGURE 7.2—Map of fracture studies, selected gas fields, stress directions (Wong and Humphrey, 1989), and coal cleat orientations in the San Juan Basin. Cleats in Colorado are from Newman and McCord (1980), Condon (1988), and Tremain and Whitehead (1990). Cleats in New Mexico are from Tremain and Whitehead (1990). After Tremain and others, this volume, Chapter 5.

ably is also true, based on Condon's (1988) joint and cleat measurements and Tremain and others' (this volume, Chapter 5) cleat studies. However, a northwestern face-cleat trend may predominate locally.

These results suggest that if lineaments are controlled by surface fractures, there may be considerable local variability in lineament azimuth. Furthermore, fracture-controlled lineaments may be perpendicular to each other, as cleats are, if these fracture trends are continuous into rocks overlying coals. If the trend of lineaments is controlled by fractures, then orientations of lineaments should change as cleat and joint directions change across the basin.

Data sources and procedures

Standard Landsat Thematic Mapper (TM) images (scale 1:250,000) were used for this study. False-color composite (FCC) images were generated with data from bands 7 (red), 4 (green), and 2 (blue). In bands 4 and 7 the contrast between vegetation and soil is relatively large. Some variations in soil and rock composition, such as might occur along a fault or a formation contact, are more visible in FCC images composed of these three bands. Visibility of lineaments demarcated by vegetation changes, faults, or formation contacts is enhanced by these image characteristics.

Lineaments were mapped from edge to edge on each Landsat image without regard to boundaries of the San Juan Basin. Of the 5,855 lineaments mapped in this study, 969 are within the boundary of the San Juan Basin (Fig. 7.3). Most lineaments in the basin were checked against 1:250,000-scale U.S. Geological Survey topographic maps, and 116 lineaments were also checked against 1:24,000-scale topographic maps. Another 23 lineaments were field checked. Man-made features that were erroneously mapped as lineaments (53) amounted to 5.7% of the lineaments checked (925). It is possible that other man-made features were mapped as lineaments but were not detected. Therefore, this error rate should be considered a minimum. Lineaments were compared with maps of surface geology (scale 1:250,000) to determine whether spatial correspondence exists between lineaments and mapped geologic features, such as faults and formation contacts. More than a third (35%) are straight streams or valley axes (Table 7.2). Straight formation contacts account for 11% of the lineaments checked. Locally, these are probably represented on the ground by slight topographic relief. No mapped faults were recognized on Landsat imagery. More than half of the lineaments checked are straight ridges, tonal anomalies, and other linear features.

Lineaments from the three previous studies that covered a selected area in the northwestern San Juan Basin (Fig. 7.1) were digitized directly from published maps. They were not checked against original imagery. No judgment was made in this study regarding the "validity" of the lineaments in previous studies. Their attributes were analyzed just as those from this study were.

Values of initial water production (IPW), maximum monthly gas production (MMG), and daily averages of maximum annual water production (MAW) and maximum annual gas production (MAG) were obtained from Petroleum Information, Dwight's Oil and Gas Reports (1990a, b), and the Colorado Oil and Gas Conservation Commission. Water and gas production are assumed to correlate with fracture permeability. Production data were not "normalized" for different well-completion techniques, different completion dates, or possible interference effects from nearby wells. Nor were wells from overpressured and underpressured areas examined separately.

TABLE 7.2—Landsat lineaments mapped in the San Juan Basin that were checked against geologic maps.

Description	Number	Percent
Straight stream or valley	320	35
Straight formation contact	103	11
Straight fault	0	0
Straight igneous dike	22	2
Other (tonal anomaly, etc.)	480	52
TOTAL	925	100

Results

Definition of significant lineament azimuths

To an extent, lineament analysis is subjective, depending on vagaries of interpretation (including operator bias). Moreover, in many studies lineament trends are reported in qualitative terms such as "prominent" and "dominant." In this study lineaments were checked against other maps and were field checked. Numerically significant lineament trends were defined by standard statistical analysis of orientation data. Length-weighted frequency (F) and Bernshtein accuracy criterion (H) (Dix and Jackson, 1981) were defined for each set of lineament data. In this way, the interpretation of the data is as objective as possible, although some subjectivity of the original mapping probably remains.

Lineament-azimuth data were initially displayed as rose diagrams of length-weighted frequency (F) (Fig. 7.4). This parameter expresses the total lineament length in a 10°-wide sector of the graph, weighted in proportion to the number of lineaments in the area in question:

$$F = (L_s \times n)/L_t \qquad (1)$$

where F = length-weighted frequency, L_s = total lineament length in 10° sector, L_t = total lineament length in area, and n = number of lineaments in area.

A peak on a polar graph of $(F)^{1/2}$ is defined as any 10°-wide sector with a magnitude larger than the average for that graph. To determine which greater-than-average peaks were significant, a chi-square test was used to measure the difference between each peak and the mean F value for each data set (Siegel, 1956). The 99% confidence level ($p = 0.01$) was used to define geologically meaningful peaks because Dix and Jackson (1981) found that computer-generated random "lineaments" had statistically significant peaks at lower levels.

Although significant azimuths of lineament orientation data can be determined using 10°-wide sectors, significant trends that are split between two adjacent sectors may be obscured. To avoid this potential loss of important data, vector sums of adjacent greater-than-average peaks were calculated (Fig. 7.4b). All vector sums of greater-than-average peaks are not statistically significant, however. To determine which vector sums are significant, a chi-square test was applied to each one (Fig. 7.4c). As a further refinement, the chi-square value for each significant peak was divided by the degrees of freedom to yield the Bernshtein accuracy criterion (H) (Vistelius, 1966; Dix and Jackson, 1981). Landsat lineaments mapped in this study have two statistically significant vector sums: 5° and 68° (Fig. 7.4c).

Despite this objective approach to lineament orientation data, it is possible that there is some inherent bias in the data because of preferential shading of linear features perpendicular to the sun's azimuth. The sun's azimuth was between 133° and 148° for all four Landsat images. As a result, linear features between 43° and 58° probably are easier to see, and those between 313° and 238° probably are harder to see, than lineaments with orientations at some other angle to the sun's azimuth. Indeed, the 10°-wide sec-

tors with the lowest length-weighted frequencies (290° tc 339°, Fig. 7.4a) are subparallel to the sun azimuths, suggesting that there may have been some relative suppressior of lineaments with these orientations. However, the evidence for preferential enhancement of northeast-trending lineaments is equivocal. The largest significant azimuth (68°, Fig. 7.4c) is composed of five 10°-wide sectors (50° to 279°, Fig. 7.4a) that overlap with only half of the 43° to 58° window. Furthermore, the greater-than-average peaks are not symmetrical about the 43° to 58° window, the 50° sector is not significantly larger than the mean at the 99% confidence level, and the 40° sector is not even larger than the average (Fig. 7.4a).

Coincidence of lineaments from different studies

Lineaments from three published studies that covered the northwestern San Juan Basin (Table 7.3; Fig. 7.5, inset; Figs.

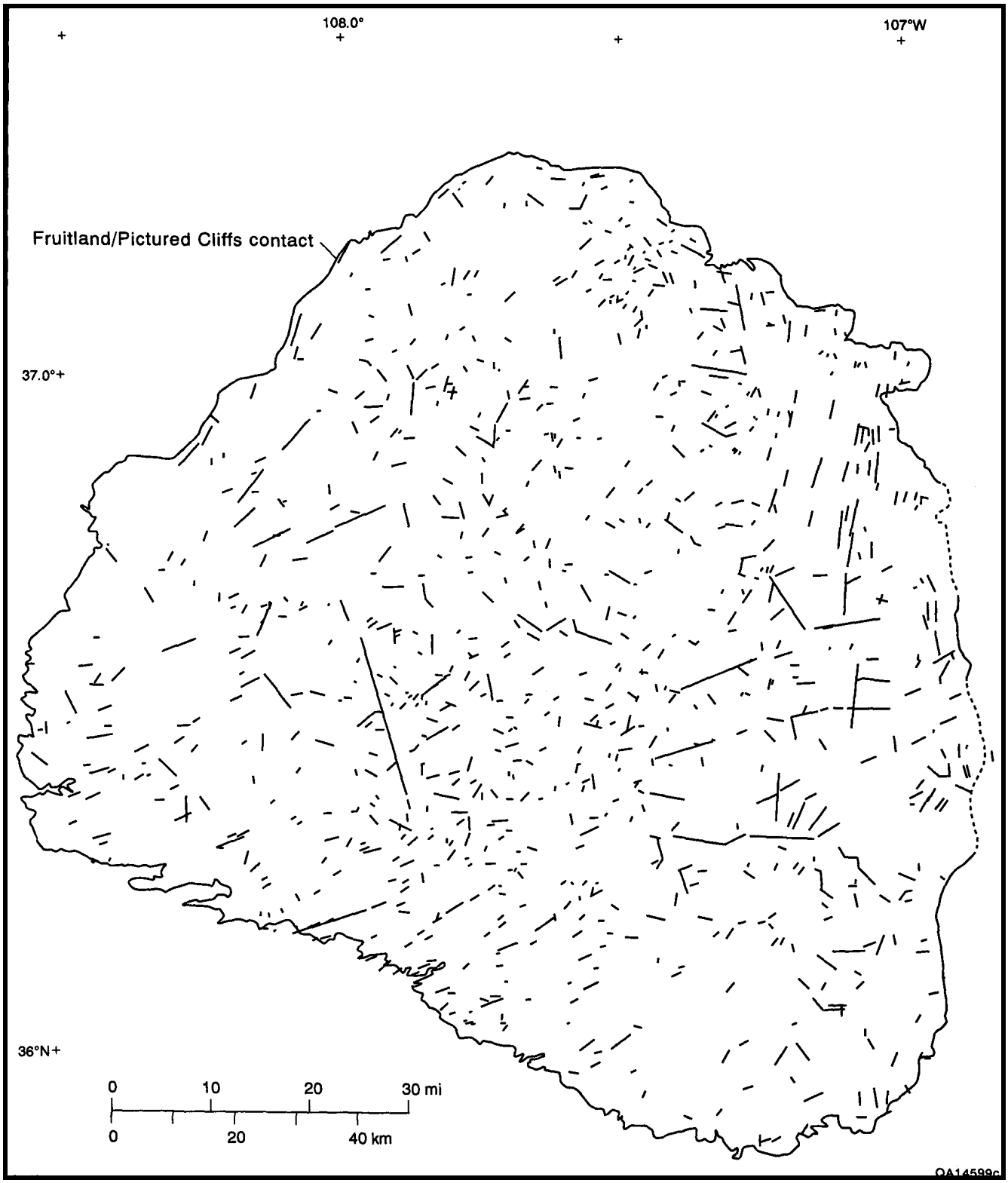

FIGURE 7.3—Landsat lineaments in the San Juan Basin mapped in this study. See Fig. 7.1 for location of San Juan Basin.

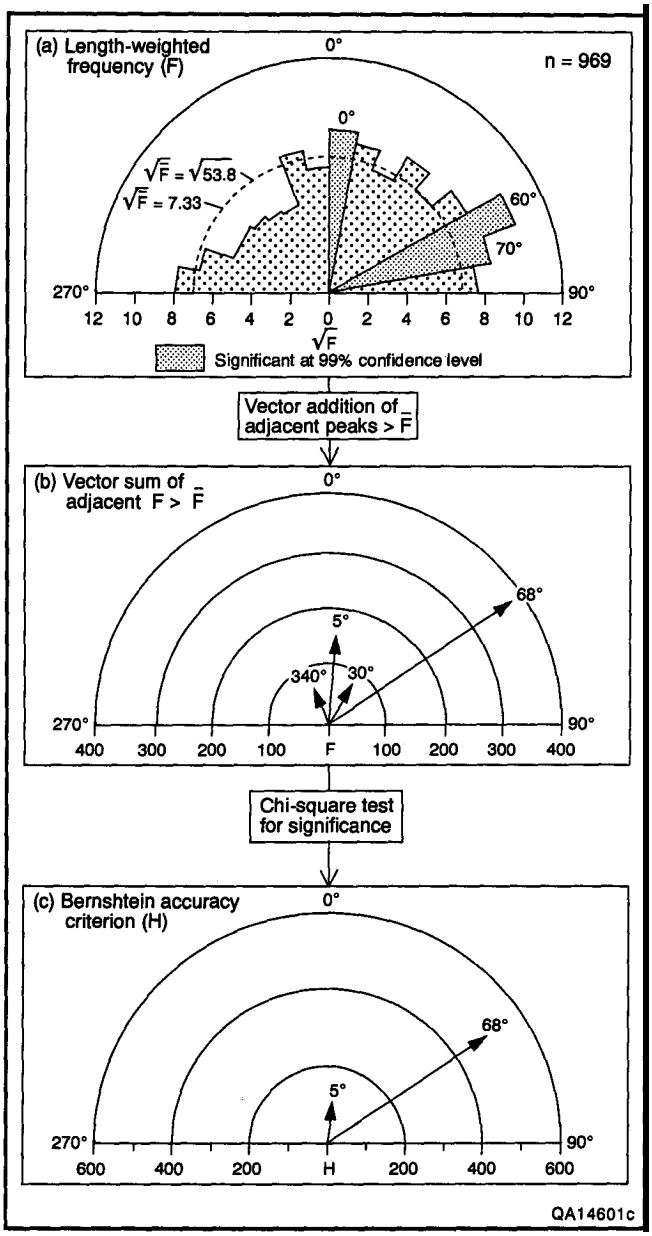

FIGURE 7.4—Procedure for statistical evaluation of lineament orientation data and polar graphs of orientation data for all 969 Land-sat lineaments mapped in this study of the San Juan Basin. (a) Length-weighted frequency (F) of lineaments has three peaks significant at the 99% confidence level, as determined by a chi-square test. The square root of F is plotted to prevent areal exaggeration of large peaks. (b) The vector sum of adjacent larger than average peaks of F has four peaks, but orientations are different from the F peaks. The data at 270° (= 90°) are adjacent to the 80° peak and are added to them in this step. (c) Two peaks of Bernshtein accuracy criterion (H) are significant at the 99% confidence level: 5° and 68°.

7.6-7.9) were compared with one another, with lineaments mapped in this study, and with gas and water production. This technique allowed comparison of lineaments mapped on different images, at different scales, by different observers. For the same area of the northwestern San Juan Basin, the number of lineaments ranged from 51 to 914, largely as a result of differences in scale of the imagery (Table 7.3). For a smaller area near Cedar Hill field (Fig. 7.5, inset), Decker and others (1989) mapped 11 lineaments on Landsat images and 249 lineaments on aerial photos (Table 7.3). Of the 1,284 lineaments from all studies, only 52 coincided between any two studies. Lineaments were considered to coincide if they (1) had the same azimuth within ± 5°, (2) overlapped for part of their length, and (3) were less than 1 mm apart, as measured on the original imagery. For a Landsat image at 1:250,000 scale, this 1 mm represented 250 m on the ground. This lack of coincidence indicates that lineament mapping is strongly dependent upon subjective analysis of the interpreter and on the scale and type of imagery used.

Lineament azimuth

Lineament azimuths were analyzed to determine (1) if a consistent lineament trend existed for all studies and (2) if that trend was associated with production values. For two of the three previous studies that cover the northwestern San Juan Basin (Fig. 7.5, inset), statistically significant lineament azimuths are similar. The maximum lineament azimuth for Landsat lineaments in this study (35°, Fig. 7.5a) is subparallel to the significant lineament azimuth (38°, Fig. 7.5b), based on aerial photographs studied by Kelley and Clinton (1960). However, the maximum lineament azimuth (302°, Fig. 7.5c) mapped on Landsat images by Knepper (1982) is nearly perpendicular to these azimuths.

The effect of this variability in lineament azimuth is shown in Fig. 7.10. The highest values of maximum monthly gas production (MMG) are closest to northeast-trending lineaments in this study (Fig. 7.10a). However, the same high values of MMG, which are from the same wells, are closest to northwest-trending lineaments from Knepper's study (Fig. 7.10b). Similar results were obtained for the daily average of maximum annual gas production (MAG) data. Clearly, lineament azimuth from one study cannot be used in other lineament studies to predict MMG or MAG values.

Even different types of imagery in the same study can produce divergent azimuths. Decker and others (1989) reported lineaments mapped on aerial photographs and Landsat images. Highest values of initial water production (IPW) (>100 barrels of water per day [bwpd]) are closest to northwest-trending Landsat lineaments, but the same wells are closest to northeast-trending aerial photolineaments.

It is clear from these comparisons that the azimuths of nearest well lineaments from different studies or even from different imagery in the same study can be quite different, even perpendicular, and that no lineament azimuth can be described as more useful than any other for predicting these

TABLE 7.3—Lineaments in the northwestern San Juan Basin.

Authors (date)	Number of lineaments	Scale of imagery	Well-lineament distance (m) min.	Well-lineament distance (m) max.	Radius (km)
Decker and others (1989)	249	≥1:80,000	6	370	1
Decker and others (1989)	11	<1:80,000	30	2,170	2
Kelley and Clinton (1960)	914	1:62,500	20	4,110	2
Baumgardner (this study)	59	1:250,000	30	2,340	4
Knepper (1982)	51	1:800,000	130	7,910	5
TOTAL	1,284				

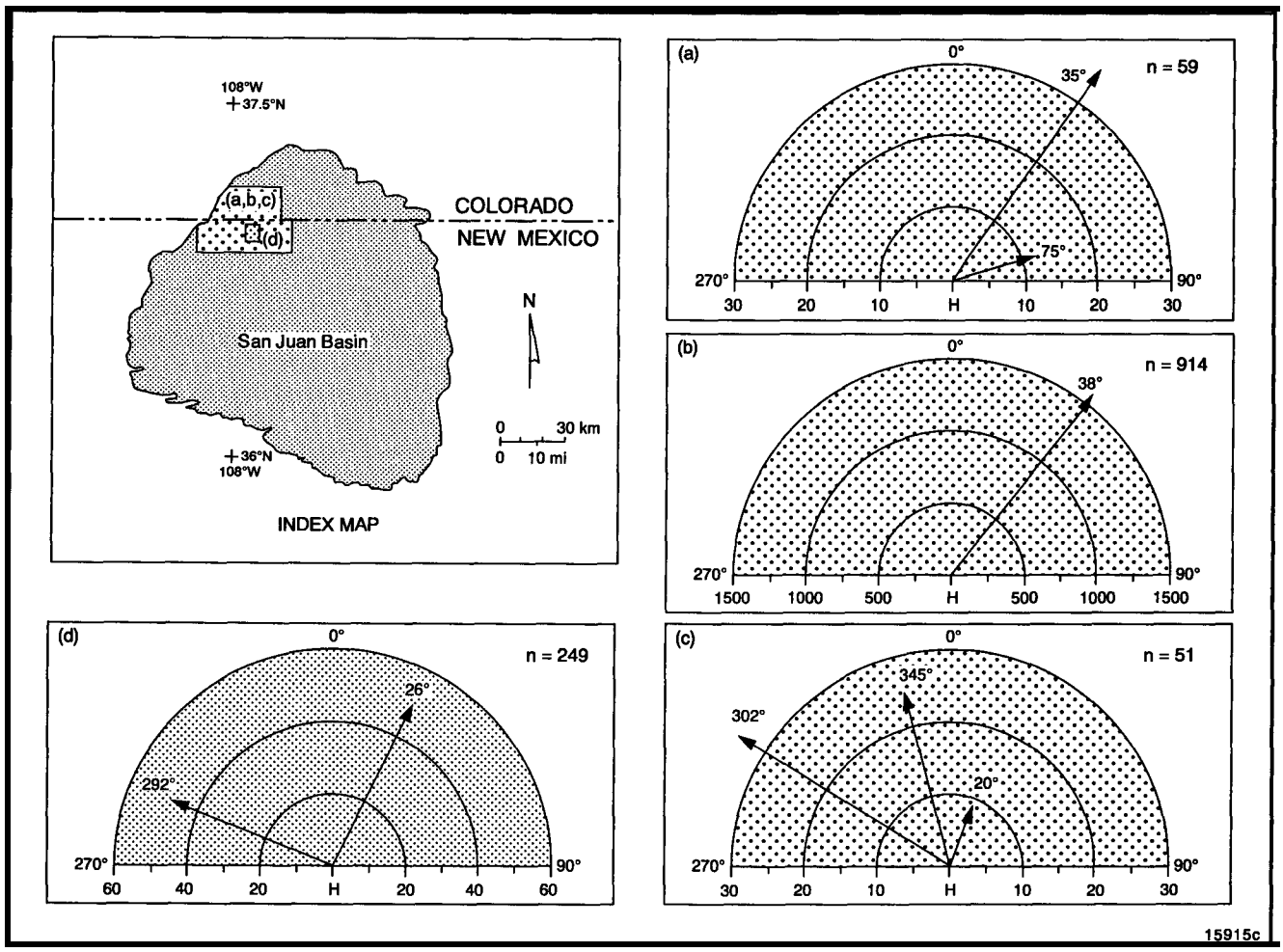

FIGURE 7.5—Polar graphs of Bernshtein accuracy criterion (*H*) for lineaments in this and three previous studies. Only vector sums of lineament azimuths that are significant at the p = 0.01 level are shown. See inset for area covered by each study. Stipple patterns represent areas that correspond to like data on graphs. Note that a, b, and c lineaments are from different studies in the northwestern San Juan Basin. (a) Landsat lineaments, this study. (b) Aerial photolineaments, Kelley and Clinton (1960). (c) Landsat lineaments, Knepper (1982). (d) Aerial photolineaments in Cedar Hill field area, Decker and others (1989). Landsat lineaments mapped by Decker and others (1989) are insufficient (*n* = 11) to produce a meaningful value for *H*.

production values. Furthermore, most other comparisons between lineament azimuth and production data showed no preferential distribution of high values at any lineament azimuth. This lack of a single lineament azimuth common to all studies and related to highly productive wells is not surprising, given the variability in fracture orientations reported in the basin. Imagery at different scales interpreted by different observers also accounts for some of this variability. However, if lineaments are functions of open subsurface fractures, regardless of orientation, then their proximity to wells should affect production.

Well-lineament distance

Two comparisons were made to determine whether wells on lineaments had higher production values than wells that were not on lineaments. Wells less than 660 ft (<200 m) from a lineament were considered to be on the lineament. A distance of 660 ft (200 m) was chosen on the basis of width of a pencil line at the original scale of the imagery and on possible positioning error when digitizing the lineaments. First, mean production values from wells on lineaments were compared with mean production values from wells not on lineaments (Table 7.4a). Second, mean distance to the nearest lineament from wells with greater-than-average production values was compared with mean distance from wells with less than average production value (Table 7.4b). This comparison tested whether wells with greater-than-average production were significantly closer to lineaments than wells with below average production. No distinction was made for the relative position of the well-lineament pairs. Wells along the trend of a lineament were treated the same as wells off the trend of, but near, a lineament.

This analysis revealed no consistent relationship between production data and a well's location on or off a lineament. These results do not replicate those reported in the Warrior Basin, Alabama (Briscoe and others, 1988), where coalbed methane wells within 200 ft (60 m) of fracture zones had higher methane and water production. In this study few mean values of MMG, IPW, or MAG are significantly different for wells on or off lineaments (Table 7.4a). In fact, for some data (Knepper, 1982; Decker and others, 1989), IPW values are significantly higher from wells that are off lineaments, the opposite of the expected result. Wells with above average MMG values are significantly closer to lineaments than those with below average MMG values in three studies (Table 7.4b). Similarly, in two data sets the mean distance from lineaments for wells with MAG greater than the mean is significantly less than the mean distance from lineaments for wells with MAG less than the mean (Table 7.4b). These results are consistent with the hypoth-

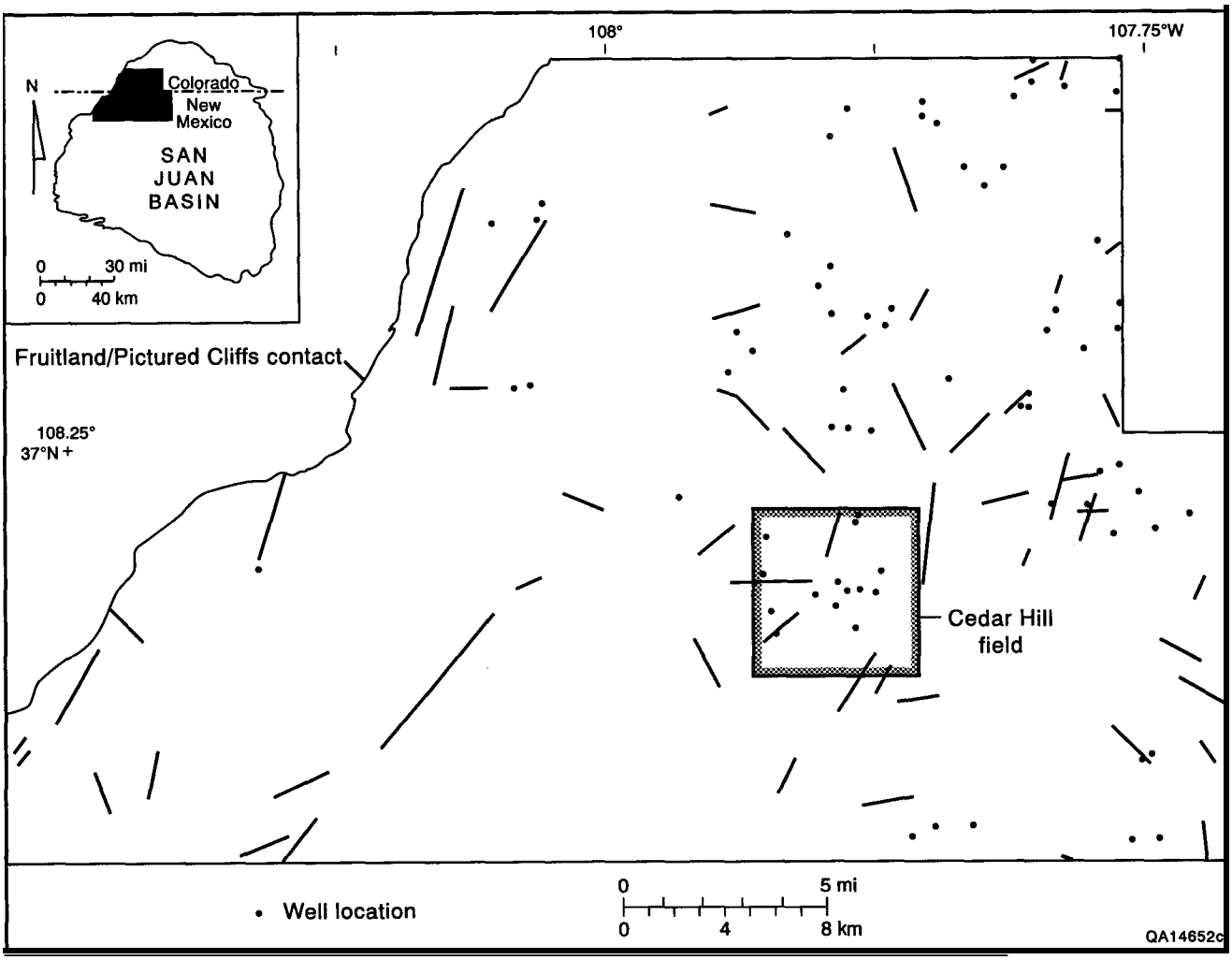

FIGURE 7.6—Landsat lineaments in northwestern San Juan Basin mapped in this study. Polar graph of these lineaments is shown in Fig. 7.5a.

TABLE 7.4—Comparison between distance to nearest lineament and production data.

a. Mean production data from wells on lineaments and wells off lineaments.

	Mean MMG (mcf) at well-lineament position		Mean IPW (bwpd) at well-lineament position		Mean MAG (Mcf/d) at well-lineament position	
Study	**On**	**Off**	**On**	**Off**	**On**	**Off**
Decker and others (1989)[1]	39,877	30,071	100	4	1,397	1,059
Decker and others (1989)[2]	46,997	34,235	0	101*	1,522	1,243
Kelley and Clinton (1960)[1]	15,220	17,278	210	278	292	558
Knepper (1982)[2]	14,270	16,873	50	267*	509	484
Baumgardner (this study)[2]	13,712	16,980	137	265	257	502

b. Mean distance from well to lineament for wells with production values greater than and less than the mean.

	Mean distance from well to nearest lineament (m) for MMG		for IPW		for MAG	
Study	**>mean**	**<mean**	**>mean**	**<mean**	**>mean**	**<mean**
Decker and others (1989)'	156	117	90	137	155	119
Decker and others (1989)[2]	565	764	1,011	486	373	1,033
Keltey and Clinton (1960)'	919*	1,830	2,236	1,425	837*	1,808
Knepper (1982)[2]	1,465*	3,997	3,946	2,680	1,048*	3,923
Baumgardner (this study)[2]	1,148*	1,735	1,784	1,443	1,235	1,667

[1] Based on aerial photographs.
[2] Based on Landsat images.
*Mean vatues are significantly different at p = 0.05 level.

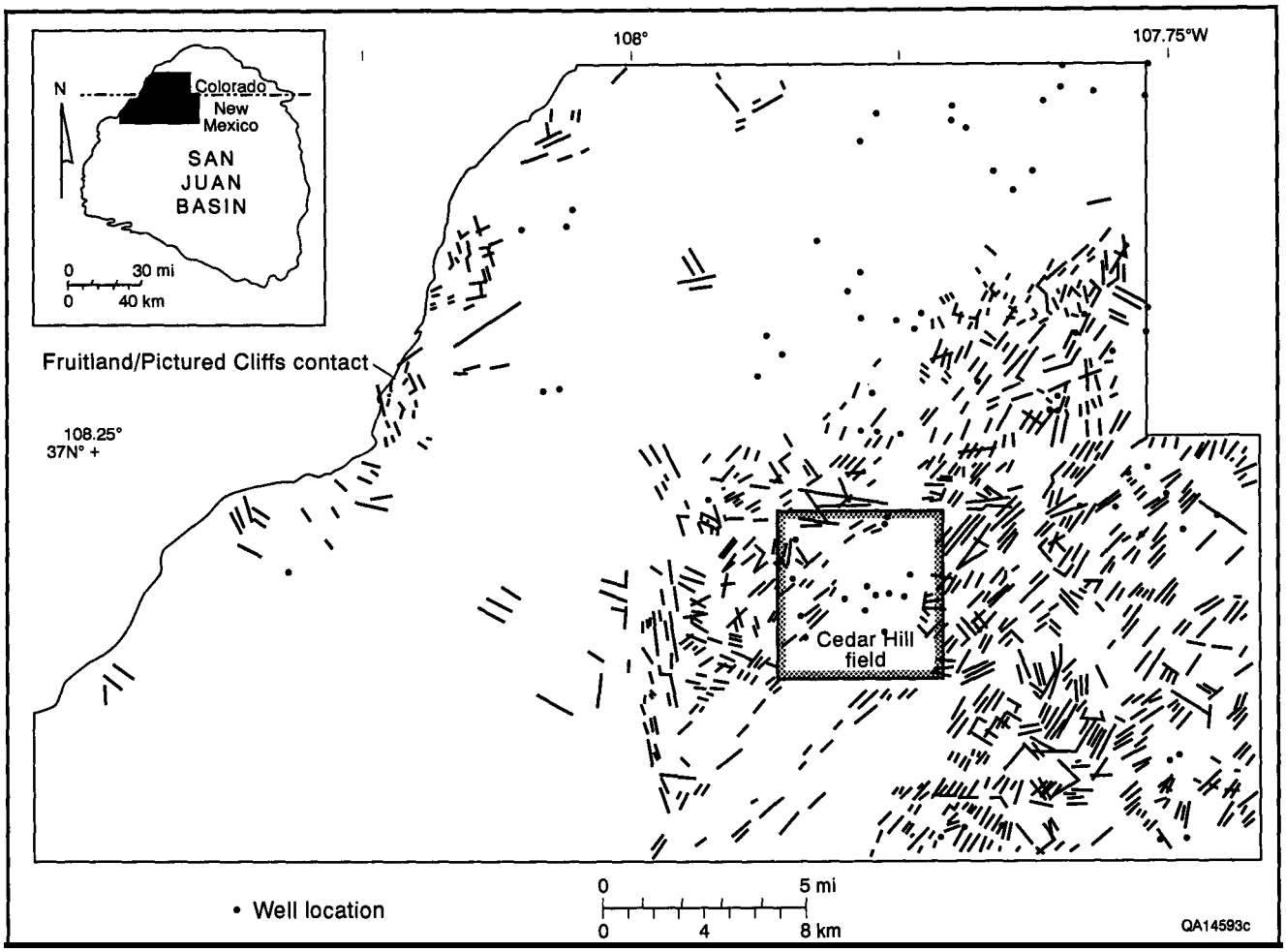

FIGURE 7.7—Aerial photolineaments in northwestern San Juan Basin mapped by Kelley and Clinton (1960). Potar graph of these lineaments is shown in Fig. 7.5b.

esis that lineaments enhance gas production, but similar results were not obtained for the Cedar Hill field area (Decker and others, 1989), where some of the highest gas production values in the San Juan Basin have been observed (MMG as high as 67,837 Mcf, equivalent to 2,261 Mcf/d).

Correlation between lineament attributes and production

To assess the relationship between lineaments and coalbed methane production, data from wells were compared with various attributes of the nearest lineament from each study, assuming that lineaments are surficial manifestations of vertical fracture zones. Linear regressions were carried out between lineament attributes (independent variables) and production data (dependent variables). As in most statistical analyses, only correlation coefficients significant at a confidence level of p = 0.05 or better were accepted as significant. Ninety-six linear regressions were done (Fig. 7.11), but only 11 were statistically significant. Most significant regressions are between production data and number of lineaments within a given radius.

Distance from well to nearest lineament—The first linear regression correlated production data and distance to the nearest lineament (Fig. 7.11, inset). Distance varied according to scale of the imagery (Table 7.3). Only 4 out of 2C linear regressions (4 kinds of production data versus 5 sets of lineaments) produced significant correlation coefficients (Fig. 7.11). One of those is made significant by a single data point. The correlation coefficient for Kelley and Clinton (1960) data is positive (Fig. 7.12a), indicating that the farther the well from a lineament, the higher the IPW, the opposite of the expected effect of lineaments on production. The Knepper (1982) data show a negative correlation between MMG and MAG and distance to lineament (Fig. 7.12b and c), but these correlations ($|r| < .0.40$) explain only about 16% ($r^2 = 0.16$) of the variability in MMG values.

Length of nearest lineament—The length of the nearest lineament was significantly correlated with MAG only in data from this study (Figs. 7.11 and 7.13). MAG increases as lineament length increases, as expected, but the trend is not well defined. The well with the highest MAG (2,710 Mcf/d) is near the second longest lineament, but the well near the longest lineament has one of the lowest MAG values (60.4 Mcf/d), and the correlation (r = 0.33) accounts for only 10% ($r^2 = 0.10$) of the variability in MAG values.

Lineament intersections within a given radius—The number of nearby lineament intersections was compared with production data because if lineaments represent fractures in the subsurface, then intersections of these zones should represent areas of increased permeability, which should enhance production. Radii of 1 km and a "scale-determined" radius were used. The size of this radius varied with the scale of the original imagery (Table 7.3). However, there was no significant correlation between the number of lineament intersections and production for any radius (Fig. 7.11).

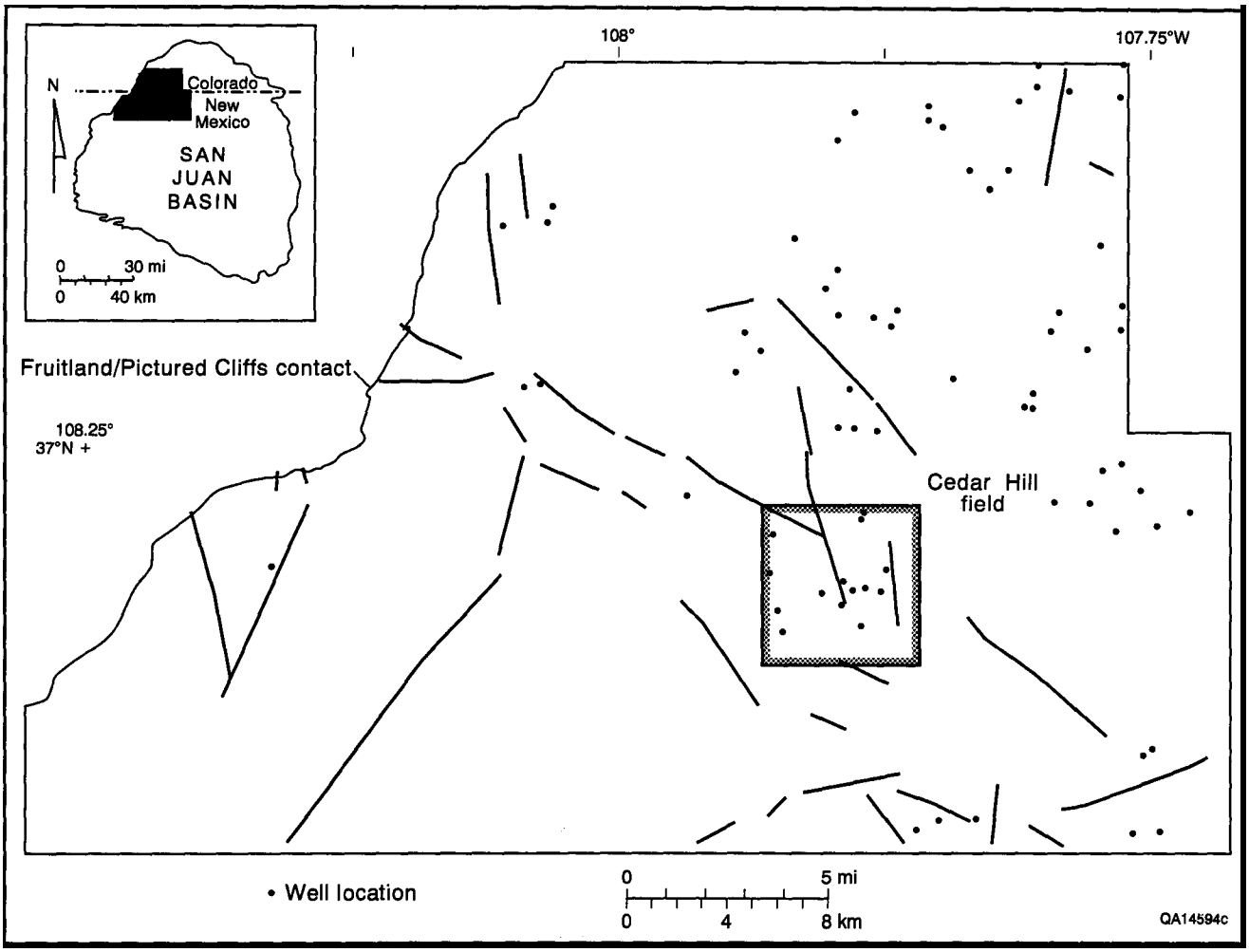

FIGURE 7.8—Landsat lineaments in northwestern San Juan Basin mapped by Knepper (1982). Polar graph of these lineaments is shown in Fig. 7.5c.

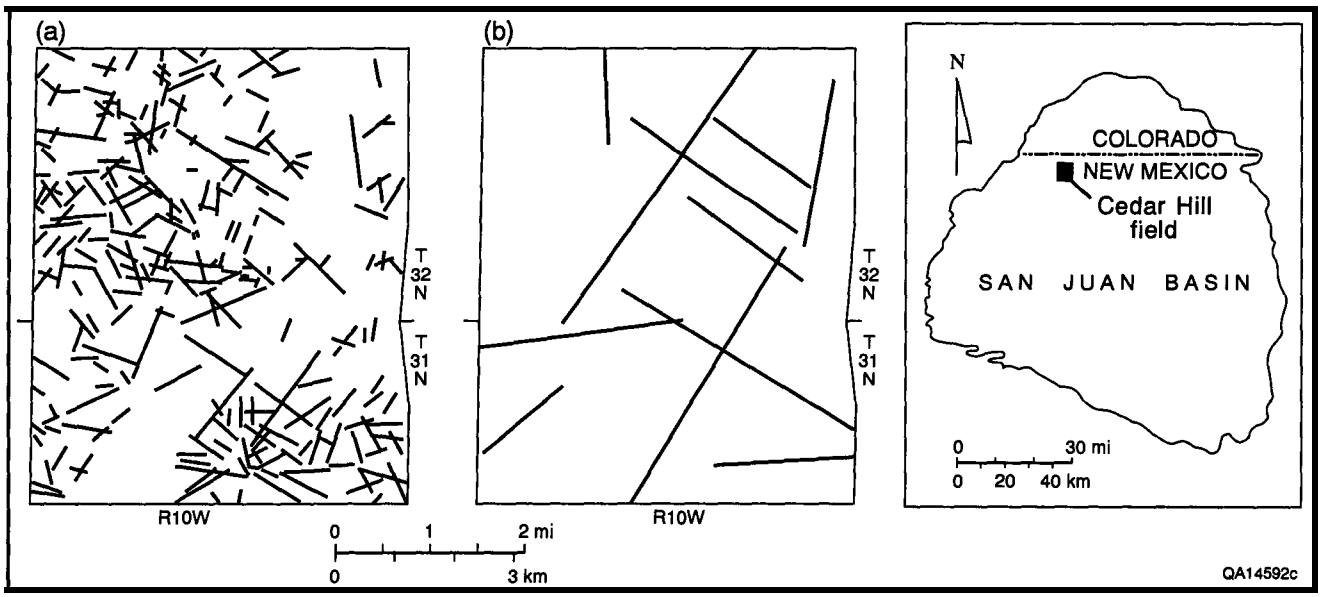

FIGURE 7.9—Lineaments in Cedar Hill field area mapped by Decker and others (1989). (a) Aerial photolineaments. (b) Landsat lineaments. Polar graph of aerial photolineaments is shown in Fig. 7.5d.

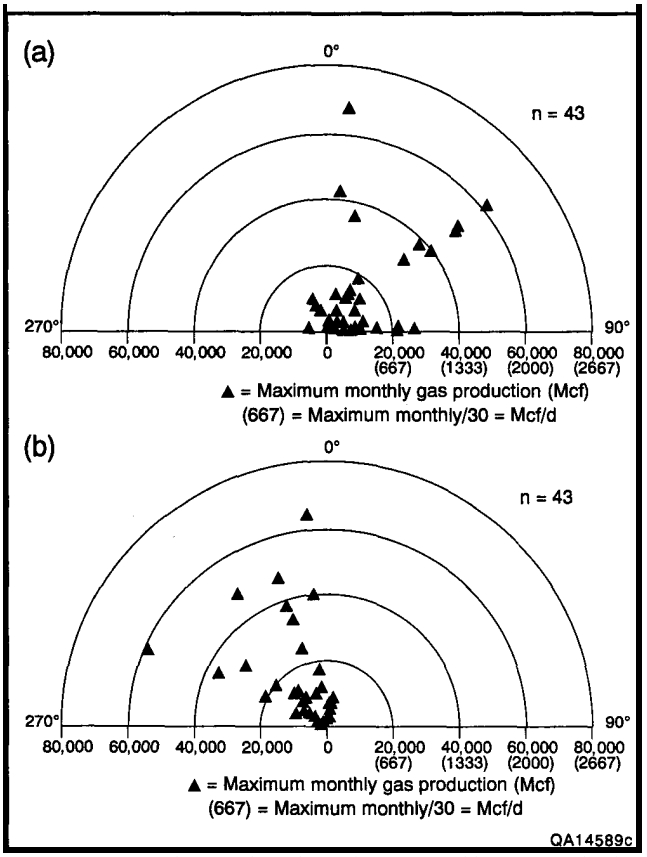

FIGURE 7.10—Polar graphs of maximum monthly gas production (MMG) versus azimuth of nearest lineament. MMG data are from welts in northwestern San Juan Basin for 1988 and 1989. (a) This study: all values of MMG greater than 11,000 Mcf are in the northeastern quadrant. (b) Knepper (1982): att values of MMG greater than 11,000 Mcf are in the northwestern quadrant. MMG values in both graphs are from the same wells. This relationship shows that tineament azimuths for the same area may be quite different, depending on the study.

Number of lineaments within a given radius—The number of lineaments within a given radius of each well was compared with production (Fig. 7.11, inset). Six regressions produced significant correlation coefficients (Figs. 7.11, 7.14, and 7.15), but these regressions ($|r| \leq 0.59$) explain, at most, only about one-third of the variability in the production data ($r^2 \leq 0.35$). These correlations are surprising for two reasons. First, all significant correlations are for Landsat lineaments, not aerial photolineaments. A previous study of lineaments in the Cedar Hill field area concluded that aerial photolineaments are more useful than Landsat lineaments for exploration programs (Decker and others, 1989). Second, these results show that the only lineament attribute that is significantly correlated with production values from Cedar Hill field is the number of Landsat lineaments within a given radius of the well (Fig. 7.11). However, the number of lineaments is negatively correlated with IPW (Fig. 7.14a), indicating that the fewer lineaments there are within a 0.6 mi (1-km) radius of a well, the higher its IPW. This is the reverse of the relationship usually expected in lineament studies. Even where a positive correlation with production values was seen (Figs. 7.14b, 7.14c, and 7.15), the utility of this relationship for exploration purposes is questionable because the radii used are as large as 3.1 mi (5 km).

A comparison of lineament density (length/area measured on 100-km^2 blocks) and initial water production (IPW) showed no consistent spatial coincidence between wells with high values of IPW (>400 bwpd) and either high (>15 km/100 km^2) or low (<5 km/100 km^2) values of lineament density. Some high values of IPW coincided with low density values, but others occurred in areas with intermediate values (10 to 15 km/100 km^2).

Discussion

Stress in the study area

The present stress regime in the San Juan Basin is extensional, with minimum horizontal stress oriented northeast (Fig. 7.2; Wong and Humphrey, 1989). Regional opening-mode fractures in this stress field would be oriented west-

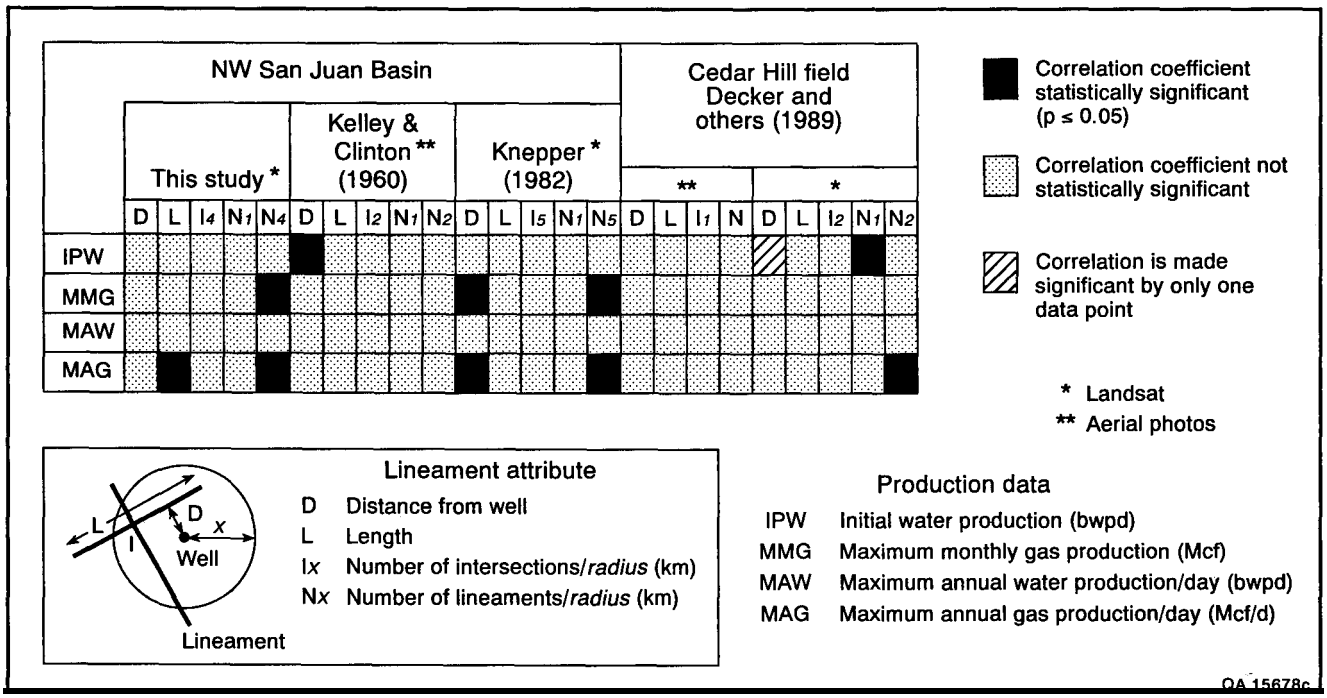

FIGURE 7.11—Results of linear regressions of production data versus lineament attributes. Onty 11 of 96 regressions produced statistically significant (p= 0.05) correlation coefficients.

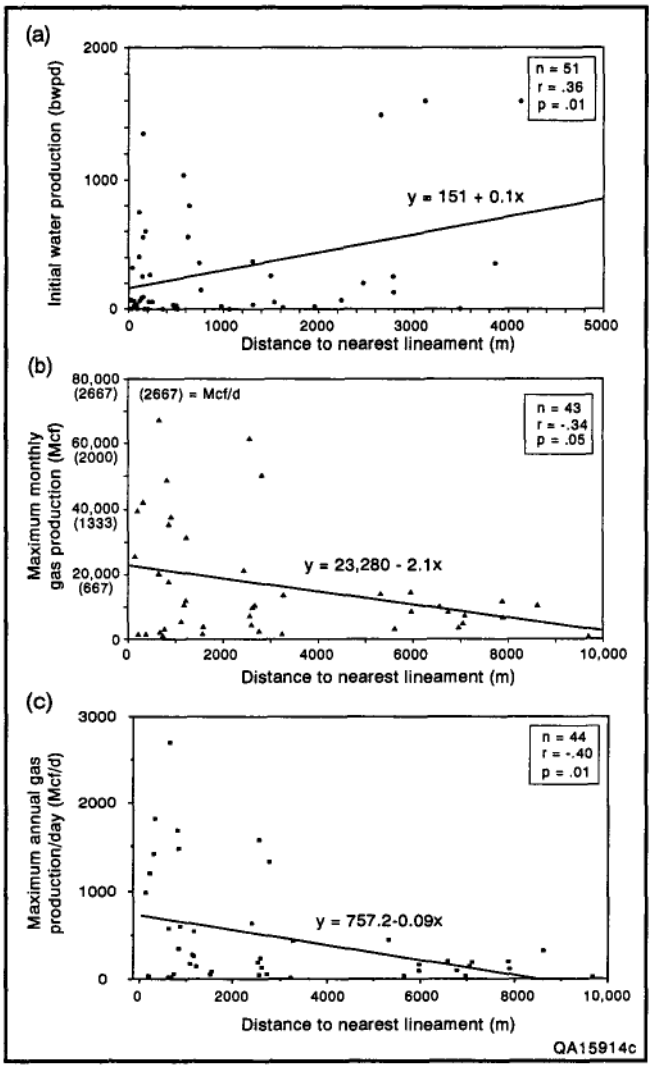

FIGURE 7.12—Graphs of production data versus distance from well to nearest lineament. (a) IPW versus distance to nearest lineament (Ketley and Clinton, 1960). Positive correlation coefficient indicates that IPW increases as distance to lineament increases, contrary to the expected result. (b) MMG versus distance to nearest tineament (Knepper, 1982). Negative corretation coefficient shows that MMG decreases as distance to lineament increases, as expected. (c) MAG versus distance to nearest lineament (Knepper, 1982). MAG decreases as distance to lineament increases, as expected.

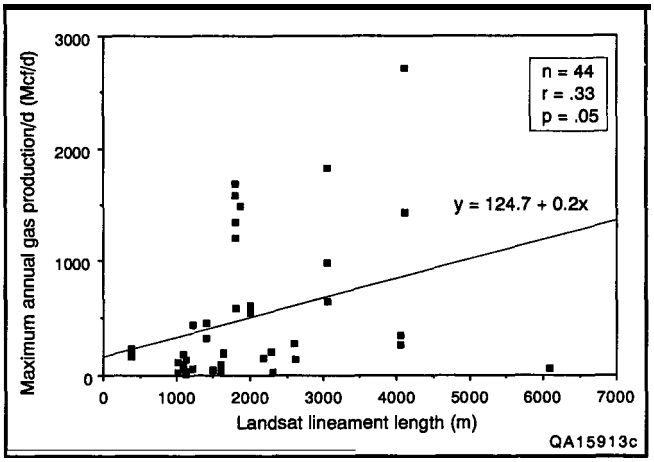

FIGURE 7.13—Graph of MAG versus length of Landsat lineaments (this study). MAG increases as lineament length increases, as expected.

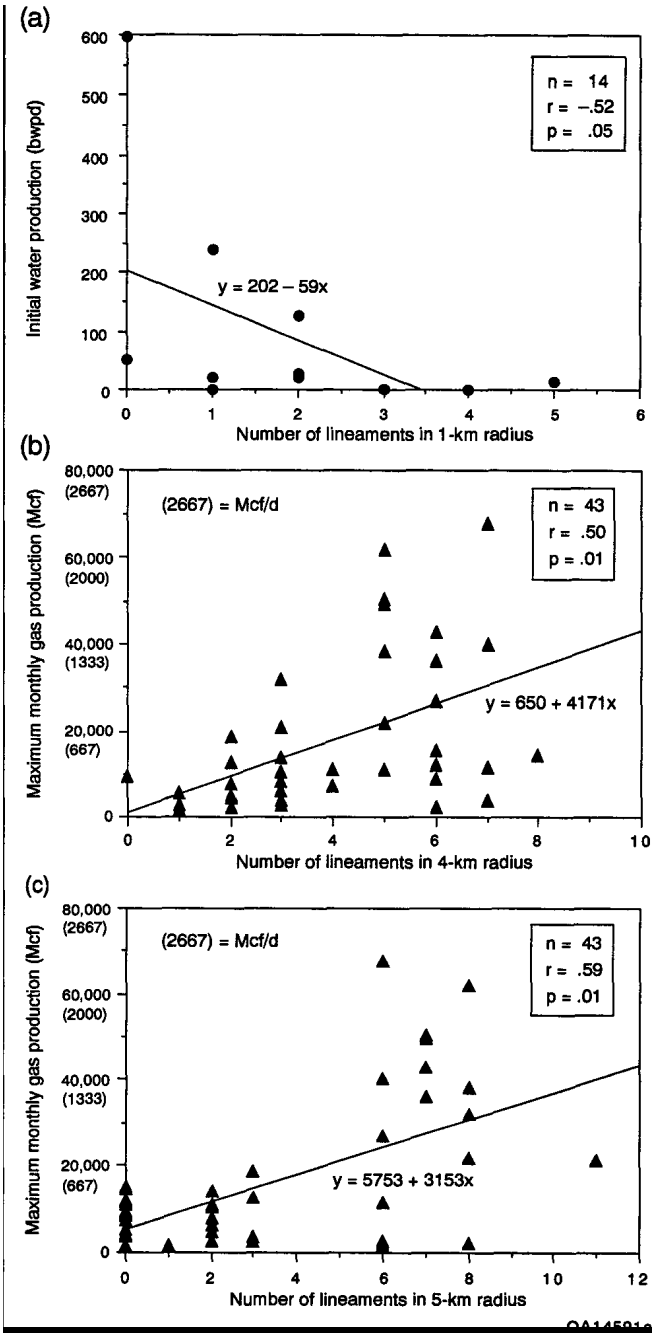

FIGURE 7.14—Graphs of production data versus number of Land-sat lineaments within a given radius of a well. (a) IPW versus lineaments in a 0.6-mi (1-km) radius (Decker and others, 1989). Negative correlation coefficient indicates that as number of lineaments near a well increases, IPW decreases, the reverse of the expected result. (b) MMG versus Landsat lineaments in a 2.5-mi (4-km) radius (this study). (c) MMG versus Landsat lineaments in a 3.1-mi (5-km) radius (Knepper, 1982). Positive correlations for (b) and (c) indicate that production increases as the number of lineaments increases, as expected. Applicability of these correlations to exploration is questionable, given the size of the radii around the wells.

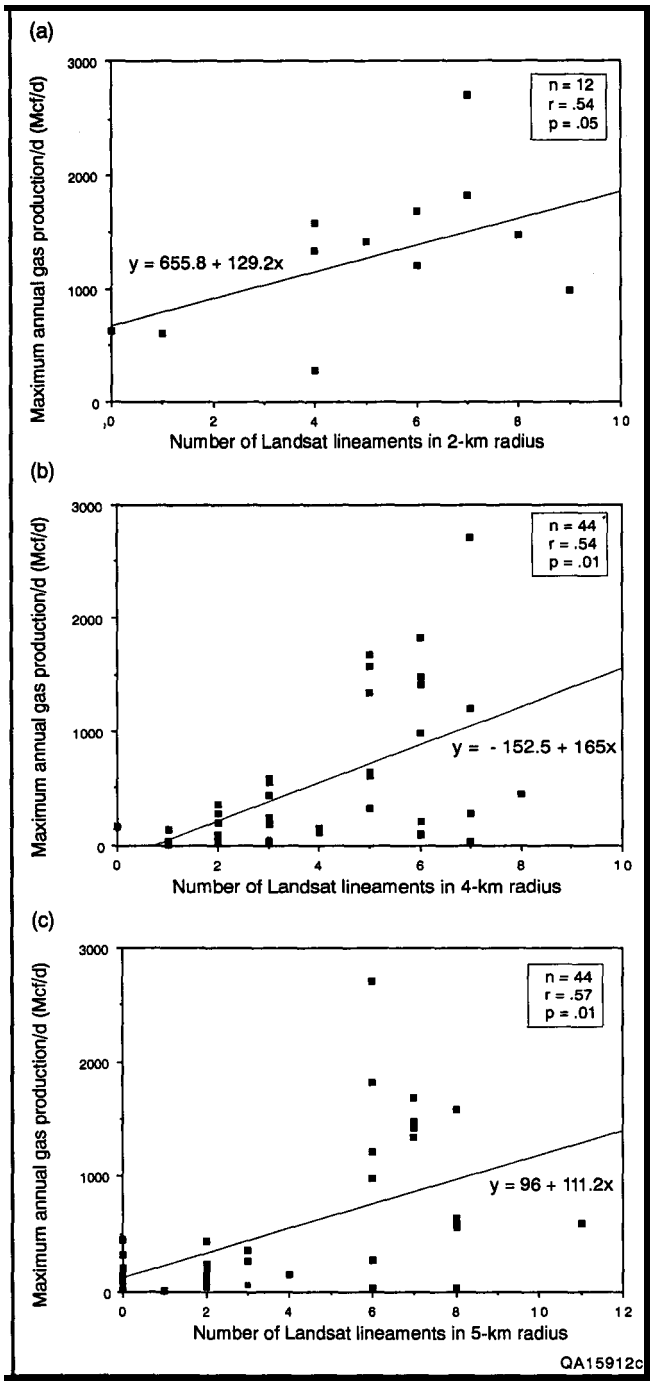

FIGURE 7.15—Graph of MAG versus number of Landsat lineaments within a given radius of a wetl. (a) 1.2-mi (2-km) radius (Decker and others, 1989). (b) 2.5-mi (4-km) radius (this study). (c) 3.1-mi (5-km) radius (Knepper, 1982). Positive correlations indicate that MAG increases as number of tineaments increases, as expected. However, the applicability of these correlations to exptoration is questionable, given the size of the radii around the wells.

northwest. Near the boundary between the Colorado Plateau and Rio Grande Rift provinces, which is adjacent to the eastern side of the San Juan Basin, maximum compressive horizontal stress is predominantly north—northeast (Zoback and Zoback, 1989, fig. 1). Opening-mode fractures formed in this stress regime would be oriented north—northeast if aligned with maximum horizontal stress, approximately perpendicular to fractures farther to the northwest.

Several studies have shown that northeast- and northwest-trending faults, fractures, and foliations are present in the San Juan Basin (Laubach and Tremain, this volume, Chapter 6; Tremain and others, this volume, Chapter 5; and references therein). Precambrian foliations and age-province boundaries trend predominantly northeastward beneath the San Juan Basin (Kelley, 1955a). Northeast-trending fault zones with major displacements of Precambrian age have influenced later Phanerozoic fracture trends (Shoemaker and others, 1974). Northeast—northwest conjugate joint sets and northeast-trending extensional fractures were recognized by Woodward and Callender (1977). Statistically significant (p = 0.01 level) cleat directions from the Mesa Hamilton No. 3 well in Cedar Hill field are 32° and 303°. These orientations are very similar to significant azimuths (26° and 292°) for lineament data from the Cedar Hill field area (Fig. 7.5d). This result suggests that cleat and aerial photolineament directions may coincide locally. However, this study did not detect a consistent relationship between lineaments and production data.

Lineaments and stress

Most linear topographic features probably form as a result of weathering and erosion along linear fractures. Surface fractures form in response to stresses in near-surface rocks, which may be different from those in the deep subsurface. Differences in age, thickness, and tectonic history of rocks at the surface from those at depth are likely to produce differences in orientation, length, and location of fractures at the surface from those at depth. Local topography, weathering, and erosion may cause shallow, horizontal stresses (<330 ft [<100 m] deep) to differ from deeper stresses at the same site (Haimson, 1978, 1979; Zoback and others, 1980; Zoback and Zoback, 1980). As a result, lineaments that form along surface fractures may not be representative of fractures or stress directions at depth in reservoir rocks.

However, measurement of lineaments over a large area may cancel the random effects of local topography and reveal patterns that are related to more deeply seated stresses. Longer lineaments may result from deeper fractures (Nur, 1982). If these linear patterns are the result of present-day stresses or deep fractures in the rock, they could provide information about the orientation of permeable fractures in the subsurface, because the minimum horizontal compressive stress direction determines the orientation of open vertical fractures in the subsurface.

Even so, the relationship between lineaments and fractures commonly is not straightforward in sedimentary basins. Natural fractures in the subsurface may parallel joints mapped at the surface (Hickman and others, 1985). One study in an area of flat and gently dipping rocks reported vertical fractures in the subsurface subparallel to lineaments (Komar and others, 1971). However, subsurface fractures were nearly perpendicular to surface fractures. Judging from these different studies, the relationship between orientations of linear features at the Earth's surface and in the subsurface is not the same everywhere. Indeed, in an area of complex fracture patterns, surface and subsurface fractures can be either parallel or perpendicular because of differences in lithology and burial and thermal histories of the rocks (Grout and Verbeek, 1985). The greater the differences in age, thickness, and tectonic history between reservoir rocks and those at the surface, the less likely it is that lineaments will reflect fracture patterns at depth or be useful for identifying productive gas zones.

Conclusions

This study has shown that lineaments are not reliable predictors of production from coalbed methane wells in the San Juan Basin. There is little agreement between lineaments mapped in independent studies of the San Juan Ba-

sin. More than 95% of lineaments mapped in four separate studies do not coincide. Statistically significant ($p = 0.01$) vector sums of lineament azimuths vary from subparallel to perpendicular among studies. Azimuths of lineaments nearest wells with high production values vary between studies and even within one study, for lineaments derived from different imagery. Wells on lineaments do not have consistently higher production values than those not on lineaments. There is no consistently significant correlation between production data and any lineament attribute tested. The most common correlation is between the number of lineaments within a given radius (≤3.1 mi [≤5 km]) and production values. However, it explains only about one-third [$r^2 = (0.59^2) = 0.35$] of the variability in production values.

Acknowledgments

The Gas Research Institute provided funding for this work under contract no. 5087-214-1544. The author wishes to acknowledge the following persons who assisted in completion and improvement of this report. Consultation with Walter B. Ayers, Jr., and W. R. Kaiser improved the analysis and presentation of results. Neil H. Whitehead, III, assisted with field checking of lineaments. Rick Edson, Joseph S. Yeh, and Arten J. Avakian provided invaluable assistance in the use of computer-based mapping and contouring programs. Ting—Ya Hsieh assisted with integration of lineament and well data files. Insightful reviews by Walter B. Ayers, Jr., Tucker F. Hentz, W. R. Kaiser, Dan H. Knepper, Jr. (USGS), and Stephen E. Laubach improved the report and the conclusions presented herein.

8. Hydrologic framework of the Fruitland Formation, San Juan Basin

W. R. Kaiser, T. E. Swartz, and G. J. Hawkins

Bureau of Economic Geology

Abstract—The hydrology of the Upper Cretaceous Fruitland Formation was evaluated from its potentiometric surface, pressure regime, and hydrochemistry and through numerical ground-water modeling. The Fruittand Formation receives recharge mainly from the elevated, wet, northern and northwestern margins of the basin, where aquifer coal seams crop out. Regionally, the Fruitland Formation is a single hydrologic unit, but compartmentalization is indicated locally by large vertical and lateral pressure gradients. Abnormal pressuring requires permeability contrasts in the Fruitland and is explained hydrodynamically; overpressuring in the north-central part of the basin is artesian in origin. Underpressure in the remainder of the basin endures because it is insulated from recharge by low-permeability rocks. Fruitland formation waters reflect their hydrologic setting. Na–HCO3 waters coincide with overpressure and Na–Cl waters with underpressure. These waters are meteoric or modified marine in origin, and HCO^{-3} is mainly of bacterial origin. Fruitland hydrodynamics were simulated in a regional, cross-sectional ground-water flow model by imposing regionat permeability contrasts. Enhanced permeability is inferred from gentle hydraulic gradients, overpressure, and low-chloride formation waters.

Introduction

Little is known about the hydrology of coal basins and its relation to the producibility of coalbed methane. Locally, its significance is evident in the need to dewater (depressure) some coal seams to stimulate gas desorption for commercial production. However, beyond this correlation, few associations have been established between the regional hydrologic setting and methane producibility. Lacking knowledge of ground-water circulation and hydrochemistry, we can say little about favorability of production in recharge or discharge areas or its association with potentiometric anomalies. Moreover, the relative importance of unconventional and conventional structural/stratigraphic trapping remains clouded without an understanding of the hydrologic framework and the pressure regime. Thus, the objective of this study was to establish the Fruitland Formation's hydrologic setting for subsequent evaluation of hydrology's role in the producibility of coalbed methane.

Fluid dynamics and trapping mechanisms in coal seams are not well understood. Decker and Horner (1987) suggested that overpressured coal beds have better deliverabilities and are preferred exploration targets, overlooking sustained production from underpressured coal beds. They contended that overpressure is relict, a product of earlier compaction, dewatering, and reservoir isolation. However, we propose that overpressuring and trapping mechanisms in the Fruitland Formation can be explained in the context of the regional hydrology and hydrodynamics. Furthermore, Decker and others (1987) concluded that bicarbonate-rich water in coal seams indicates reservoir isolation and the presence of fresh connate water. In contrast, our study indicates that low-chloride water reflects active groundwater circulation and the presence of meteoric water and suggests enhanced permeability.

Whether hydrologic parameters such as fluid flow, pressure regime, and chemical composition of formation waters are important controls of methane producibility or simply indicators of permeability has not been previously established. To evaluate these parameters in the San Juan Basin, we made (1) regional Fruitland potentiometric-surface, pressure-gradient, and bottom-hole pressure (BHP) maps using shut-in pressures (SIP) recorded in drill-stem tests (DST) and BHPs calculated from wellhead SIPs (WHSIP), (2) pressure-elevation and pressure-depth plots, (3) Piper (trilinear) and Stiff ionic-ratio diagrams and histograms of Fruitland formation waters, and (4) a Fruitland chlorinity map. The conceptualization of the ground-water flow system was further tested in numerical modeling.

A discussion of the elements of Fruitland hydrodynamics (hydraulic head, pressure regime, and hydrochemistry) is followed by an examination of hydrostratigraphy and regional ground-water flow. Hydrodynamic elements are used to define components of the Fruitland—Pictured Cliffs aquifer system and the degree of hydraulic communication between coal beds and sandstones. Abnormal formation pressure and the origin of overpressuring in the Fruitland are explained hydrodynamically. Finally, the testing of our assumptions about ground-water flow in the San Juan Basin, using a regional cross-sectional model, is summarized.

Hydrodynamics

Approximately 250 WHSIPs, 50 SIPs recorded in DSTs, and 10 BHPs measured or extrapolated in well tests were used to prepare the potentiometric-surface map. Static water levels (approximately 30) along the northern and southern margins of the basin and outcrop elevations of perennial streams at the northern margin were used to map the Fruitland water table.

Static BHP equals the sum of the surface pressure, gas-column pressure, and liquid-column pressure; its estimation from WHSIPs involves calculating the additive pressure exerted by the weight of the static fluid column. In this study, BHPs were calculated using the Cullender and Smith (1956) method, the most accurate method of calculating BHPs in dry-gas wells. To accommodate water production, we modified the Cullender and Smith method by treating the gas-liquid system as a pseudohomogeneous mixture (Peffer, 1985; Peffer and others, 1986). Gas-compressibility factors (Z-factors) were calculated using the Hall and Yarborough equation of state, which accurately represents the Standing—Katz Z-factor chart for calculation of Z-factors as a function of pressure and temperature (Hall and Yarborough, 1973; Yarborough and Hall, 1974).

We tested our modified Cullender and Smith method on three wells in Cedar Hill field (Cahn No. 1, Schneider B No. 1S, and State BW No. 1) for which measured BHPs, WHSIPs, and associated production data were available. When average daily water and gas production were matched with the month of the well test, good agreement between measured and calculated BHPs was achieved (Table 8.1). Absolute difference (AP) from the measured BHP ranged

TABLE 8.1-Comparison of calculated and measured BHP, Cedar Hill field.

Well	Water[b] bwpd	Gas[b] Mcf/d	WHSIP[c]	BHP calculated	BHP[d] measured	|ΔP|[e]
Amoco	0	694	1,293	1,396	1,362	34
Schneider B 1S[f]	0	356	1,313	1,418	1,362	56
	83	661	1,208	1,371	1,362	11
Amoco	0	547	1,293	1,391	1,421	30
State BW 1	0	272	1,313	1,412	1,421	09
	44	784	1,208	1,329	1,421	92
Amoco	239	350	1,098	1,405	1,465	60
Cahn 1	207	738	1,258	1,494	1,465	29
	126	901	1.323	1.507	1.465	42
	120	976	1,323	1,498	1,465	33

[a] All pressures in psi.
[b] Average daily water and gas production for month of well test. Zero indicates no water reported, not necessarily that none was produced.
[c] Surface pressure on date of well test as reported by Amoco.
[d] BHP reported to NMOCD by Amoco June 8, 1983.
[e] Absolute pressure difference.
[f] BHP in wetl B 1S approximately 1,525 psi in 1979 prior to production (Amoco to NMOCD July 6, 1988).

from 9 to 92 psi; most calculated BHPs were within 9 to 60 psi of the measured value. The most difficult problem was matching appropriate WHSIPs with the corresponding production data. For most tests, only surface pressures were available, and the calculated BHPs in effect represent those of dry-gas wells. Extremely high water productivities may cause calculated BHPs to be too high.

In a comparison of calculated BHPs and DST SIPs in the same well, absolute differences in pressure were as large as 151 psi (Table 8.2). Typically, the DST SIP is higher than the calculated value. There is no single explanation for this, but it probably reflects such factors as pressure depletion caused by production, shut-in time, and unreported water production. Certainly the former is evident in the Schneider B No. 1S (Table 8.1), where original reservoir pressure of approximately 1,525 psi declined to less than 1,400 psi upon production. In low-permeability strata such as that of the Fruitland Formation, pressure equilibrium is attained slowly, if at all, and shut-in times probably were never long enough to achieve equilibrium. Thus, we classified DST's on the basis of shut-in time, using the highest pressure recorded, whether initial or final SIP. Approximately two-thirds of the DST shut-in times were between 30 and 60 min. WHSIPs were not classified because shut-in times were seldom recorded; rarely did they exceed 7 days. In general, most of the BHPs used here represent something less than original reservoir pressure.

Hydraulic head

Equivalent fresh-water head-BHPs were converted to pressure heads using a fresh-water hydrostatic gradient of 0.433 psi/ft and were combined with elevation heads to calculate equivalent fresh-water heads. Although equivalent fresh-water heads may be inexact for inferring vertical flow direction, because of variable density, they are commonly used to represent heads in aquifers containing fluid of varying density where the prime concern is lateral flow (Bair and others, 1985). Variable density is treated with great difficulty and was not accounted for in this study. In the north-central part of the basin, formation waters are fresh to brackish and rarely exceed total dissolved solids (TDS) contents of 30,000 mg/L. In the south, waters are more saline, exceeding 35,000 mg/L in some cases, and the flow pattern may be different than that inferred from equivalent fresh-water heads. Because saline water is denser and will not freely rise as high as fresh water, the effect of increased salinity is to steepen the potentiometric surface basinward. For example, if BHP were 433 psi, equivalent fresh-water and seawater pressure heads would be 1,000 ft (305 m) and 975 ft (297 m), respectively.

The calculation of heads is also affected by the presence of a gas phase. The effect is negligible in coal seams prior to gas production, where water and gas reservoir pressure are approximately equal (McKee and others, 1987). Thus, BHPs measured early in the well history are representative of formation water pressure. Furthermore, available gas- water capillary pressure measurements in coal seams (Dabbous and others, 1976; Way and others, 1985) show low capillary pressures (<10 psi) at high water saturations, which exist initially in many coal seams. Free gas may also be present to contribute a buoyant force (the difference between hydrostatic and gas gradient). However, BHPs were not computed back to the gas/water contact because either

TABLE 8.2-Comparison of calculated BHP and DST SIP[a].

Well	Location	BHP calculated	DST SIP	|ΔP|[b]
Bondad 3-8	8 33N 9W	1,367	1,365	02
Gallegos 1	12 33N 8W	1,439	1,525	86
Ute 1	36 33N 7W	1,249	1,370	121
Mesa 3-18	18 32N 7W	1,534	1,610	76
San Juan 32-5, 2	35 32N 5W	1,597	1,550	47
Northeast Blanco Unit 212	1 31N 7W	1,640	1,675	35
San Juan 29-4, 2	35 29N 4W	1,214	1,375	151

[a] All pressures in psi.
[b] Absolute pressure difference.

there were no contacts or data on such contacts were unavailable. Moreover, Fruitland sandstone gas reservoirs, where a buoyant force is most likely, are at most a few tens of feet thick and the corresponding gas caps would be thin. Hence, if the buoyant force is unaccounted for, only a small error would be introduced relative to the 200-ft (61-m) con tour interval of Fig. 8.1. For example, the presence of a 50 ft (15-m) gas column would cause the head to be approximately 43 ft (13 m) too high. A 232-ft (71-m) gas column would be required to introduce an error equal to the contour

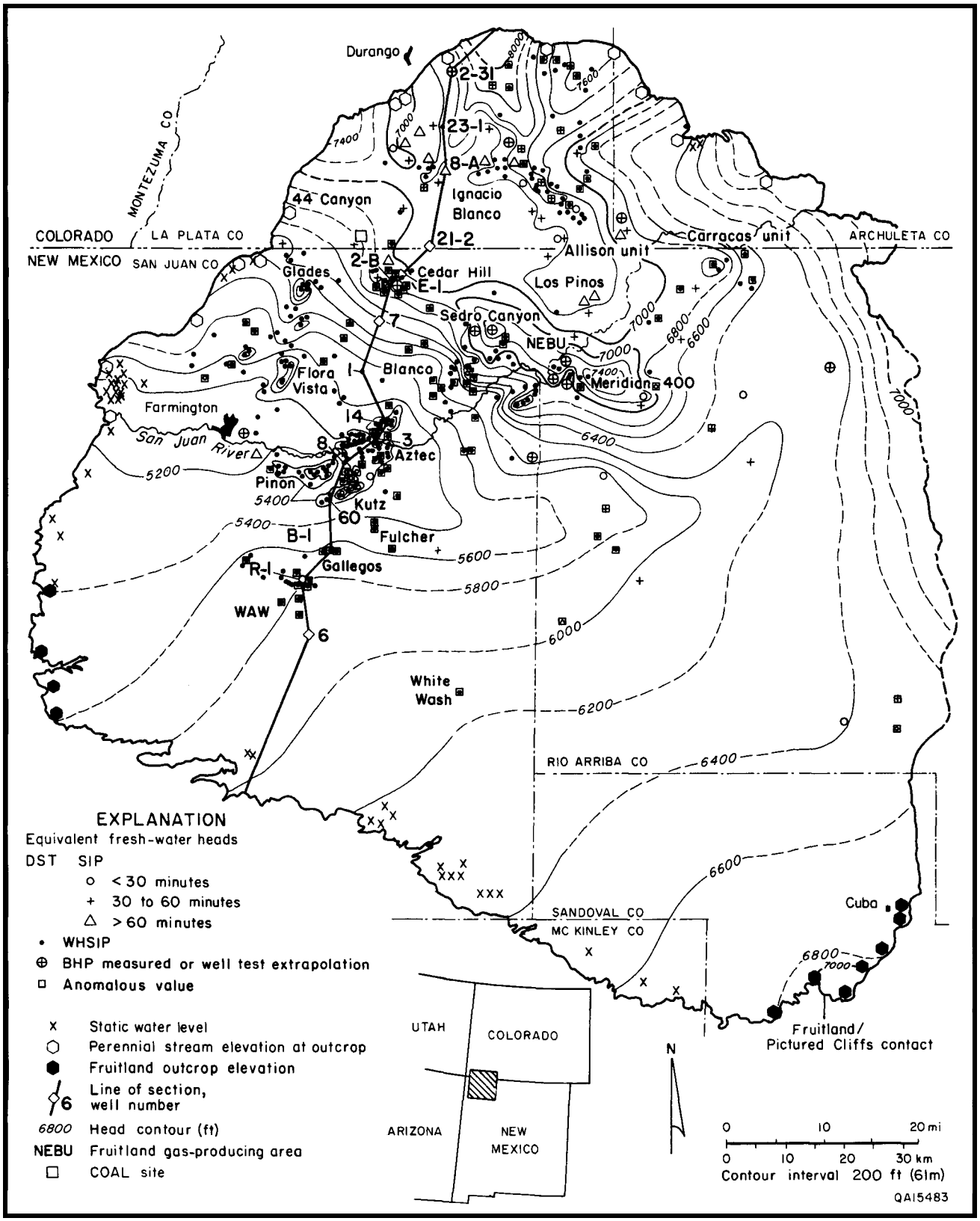

FIGURE 8.1—Fruitland Formation potentiometric-surface map. Surface is high in the northern part of the basin, flattens markedly basinward, and shows that recharge is from the northern margin of the basin. Marked steepening of surface coincides with southwestward pinch-out of aquifer coal seams and/or their offset along a structural hingeline (see Figs. 8.8 and 8.19).

interval. Finally, if water is in transit through the sandstones, as implied by the potentiometric-surface map, then capillary pressures will be low (Berry, 1959) and BHPs will reflect formation water pressure.

Potentiometric surface—A Fruitland potentiometric-surface map was made from equivalent fresh-water heads (Fig. 8.1). The potentiometric surface is highest along the northern margin of the basin, slopes basinward, where it flattens markedly, and then steepens conspicuously to separate areas of high and low potential. Recharge is mainly at the elevated northern margin of the basin (Fig. 8.2) in the foothills of the San Juan Mountains, where numerous thick coal seams crop out in the wettest part of the basin (precipitation 20 to 30 inches/yr [51 to 76 cm/yr]). Ground water flows laterally from there toward the San Juan River valley. Recharge from the eastern margin is limited because (1) the Fruitland is absent along much of the margin (Ayers and others, this volume, Figs. 2.3 and 2.11) and where present it is dominated by low-permeability, fine-grained rocks, (2) annual precipitation (12 to 20 inches/yr [30 to 51 cm/yr]) is less than that on the northern margin, and (3) the continental divide lies within the basin, diverting potential recharge eastward out of the basin that would otherwise be available through leakage. Moreover, much of the recharge is captured by the overlying, high-permeability Ojo Alamo Sandstone (Ayers and others, this volume, Figs. 2.2-2.4). Recharge from the southern and western margins of the basin also is limited, having annual precipitation lower than that in the east (4 to 12 inches/yr [10 to 30 cm/yr]). Furthermore, the Fruitland-Pictured Cliffs outcrop along the southwestern margin of the basin is topographically lower than the basin interior (Fig. 8.2) and lies just east and northeast of the Chaco River. Consequently, recharge to the unconfined Fruitland-Pictured Cliffs aquifer is diverted westward out of the basin as discharge to the Chaco River and its tributaries and is thus unavailable as recharge basin-ward to the confined aquifer system. This is demonstrated on the southern margin, where saline springs issue from Fruitland coal seams in topographically low areas associated with tributaries of the Chaco River. Widely spaced head contours in the southeastern part of the basin reflect limited recharge from the southern margin of the basin and reduced fluxes in low-permeability strata, whereas widely spaced contours in the San Juan River valley reflect discharge (upward flow) to the river as well as low permeability.

Potentiometric mounds—Potentiometric mounds at Sedro Canyon, Meridian 400, Aztec, Kutz, Pinon, Flora Vista, and Glades areas (Figs. 8.1 and 8.2) are of uncertain origin. The largest of these are in the Sedro Canyon-Meridian 400 area (SC-M) and the Aztec-Kutz-Pinon area (A-K-P) (Figs. 8.1 and 8.2). The mound in the SC-M area trends northwest-southeast as a continuous potentiometric ridge 25 mi (40 km) long, as defined by the 7,000-ft (2,135-m) head contour. Mounds in the A-K-P area trend northeast-southwest and east-west for 4 to 8 mi (6.4 to 13 km). Topography, elevation of completion intervals, presence of free gas, and cross-formational flow were examined to explain the potentiometric mounds.

The mounds probably do not represent recharge mounds (downward flow) because there is no apparent source for the recharge. The SC-M area is unassociated with any topographic highs and is situated well within the basin (Fig. 8.2). In fact, topography is higher northwest of SC-M and elevation heads at SC-M are lower than those of wells to the southwest, which have much lower total heads, proving that elevation head cannot explain the high total heads at SC-M. On the other hand, A-K-P is located in the San Juan River valley, the regional discharge area where upward flow is expected. Some A-K-P wells are slightly overpressured and located mainly along the San Juan River. Overpressuring in these wells is explained hydrodynamically as evidence of upward flow.

The presence of free gas causes heads to be higher, which may contribute to the potentiometric anomalies, particularly at A-K-P, where gas is conventionally trapped in sandstone reservoirs. However, free gas is not the main contributory factor. Gas columns that are many times the thickness of sandstone reservoirs at A-K-P would be required to account for these anomalies. At SC-M, the presence of gas has a negligible effect on heads because water and gas reservoir pressures are approximately equal.

The alternative explanation for potentiometric mounds at SC-M and A-K-P, having eliminated recharge, topography, and buoyant force as primary causes, is that they indicate areas of upward flow. Potential for upward flow was determined from the vertical pressure gradient, or slope of the line established by plotting BHP versus elevation above mean sea level (msl). Pressure-elevation (msl) plots for SC-M and A-K-P show vertical pressure gradients of approximately 0.80 psi/ft, which is much greater than hydrostatic gradient (0.433 psi/ft), indicating a very strong potential for upward flow (Figs. 8.3 and 8.4). The large vertical pressure gradients imply that the Fruitland strata are not well interconnected vertically and that a large driving force is needed to move fluid vertically. Shale interbeds and abundant tonsteins limit vertical connectivity between and within coal seams, contributing to reservoir compartmentalization.

The SC-M area is thought to represent a pressure ridge coinciding with upward ground-water flow caused by pinch-out of thick, laterally continuous coal seams (aquifers) in the area and their possible offset by faults along the basin's structural hingeline (Ayers and others, this volume, Chapter 2). Wells in the SC-M area are highly overpressured and have the highest reported Fruitland bottom-hole temperatures (up to 140°F [60°C]). Aquifer coal seams transmit ground water from the northern and northwestern margins of the basin under high pressure; upon aquifer pinch-out and/or offset this water must turn upward. Note that the potentiometric mound is associated with thick coal seams (Ayers and others, this volume, Figs. 2.17 and 2.19) and marked steepening of the potentiometric surface (Fig. 8.1), indicating lower permeability across a facies change. Focused flow in the high-permeability coal aquifers and resistance to horizontal flow cause a buildup of fluid pressure and, in turn, a reversal of the vertical pressure gradient from downward, which is shown regionally for the north-central part of the basin (Fig. 8.5), to strongly upward at SC-M (Fig. 8.3). Consequently, there is a substantial downward increase in pressure heads such that total heads exceed those up and down hydraulic gradient, resulting in a potentiometric mound. Because the potentiometric surface of successively deeper coal aquifers is predicted to exceed that of those above, the mound is thought to be generated within the stratified Fruitland Formation without regard to underlying units.

Pressure regime

Two Fruitland pressure gradients were calculated: simple pressure gradient and vertical pressure gradient. The simple pressure gradient is usually calculated over a much larger interval than is the vertical pressure gradient, which is usually determined for a specific formation or aquifer. Each has a different meaning and use. Simple pressure gradient is the quotient of BHP divided by the depth from land surface of the test interval's midpoint and is used to define the pressure regime in the Fruitland. The basinal pressure-depth plot shows two distinct populations and reflects both overpressured and underpressured conditions in the basin (Fig. 8.6). In the north-central part of the basin, BHPs are greater

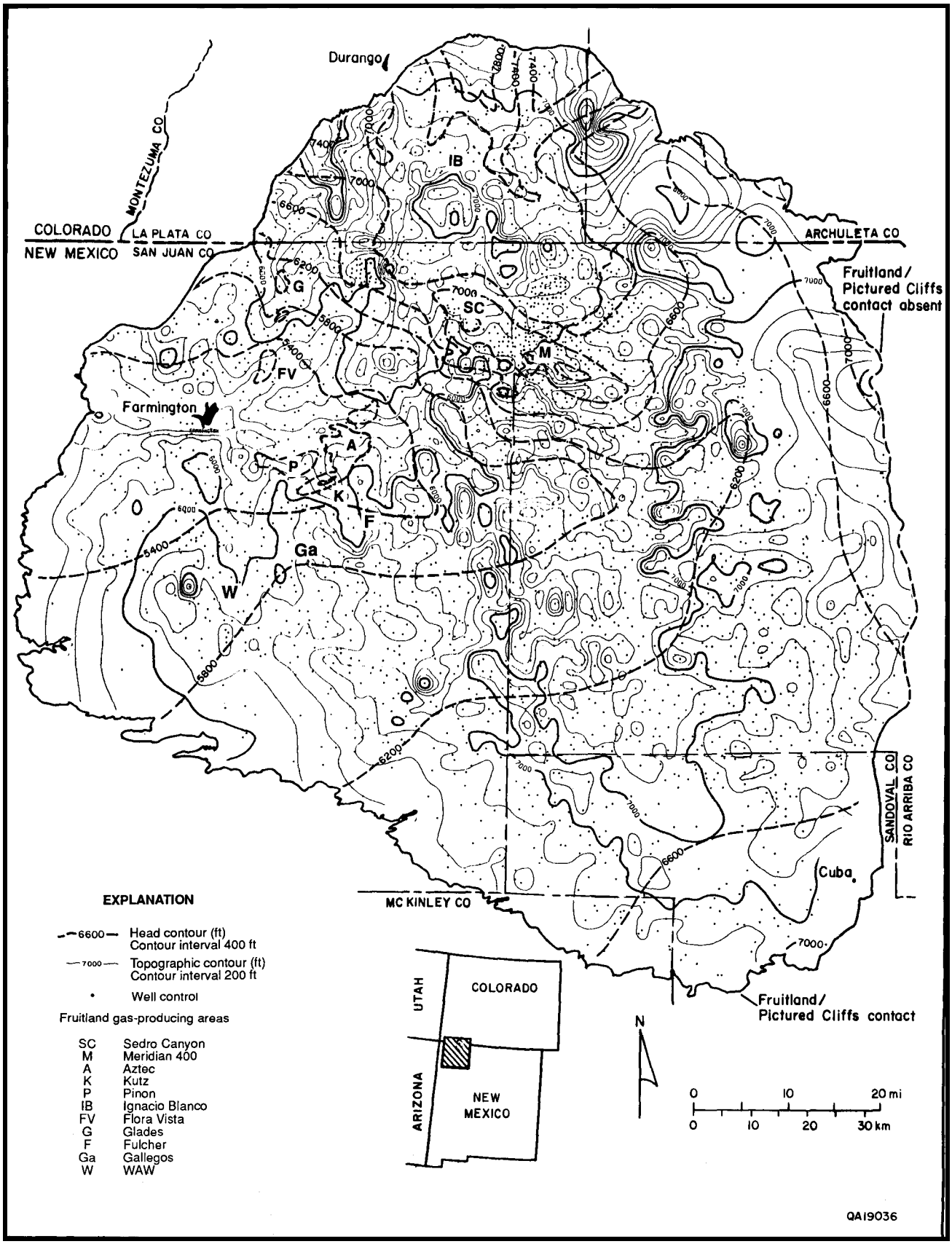

FIGURE 8.2—Fruitland Formation potentiometric-surface map and topographic map of land surface, San Juan Basin (from Kaiser and Swartz, 1990).

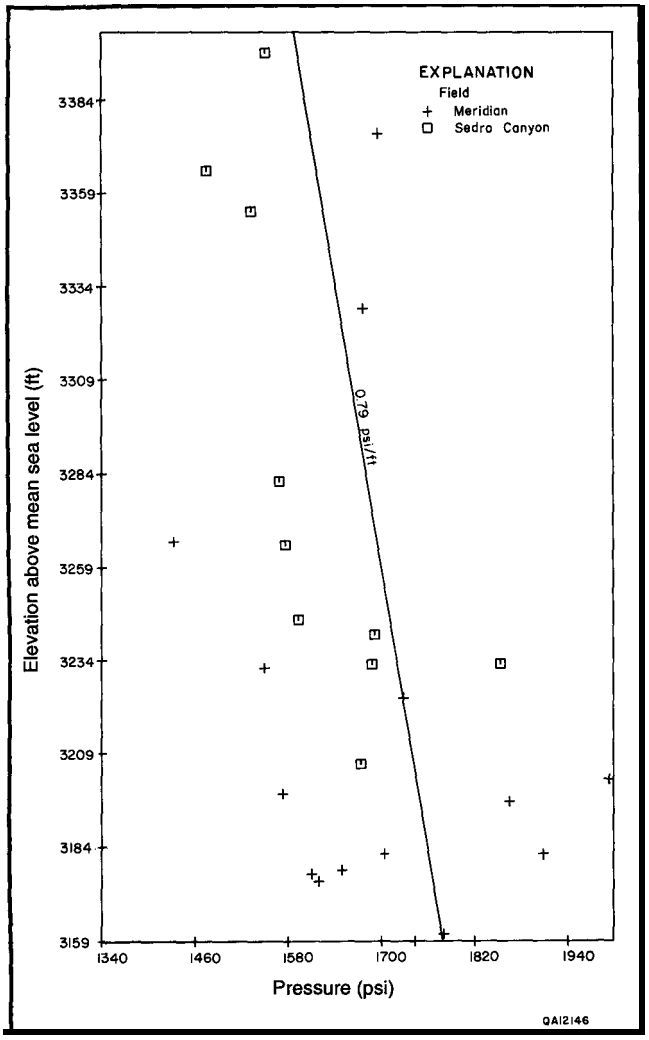

FIGURE 8.3—Fruitland Formation pressure-elevation plot, Sedro Canyon—Meridian 400 area (from Kaiser and Swartz, 1990). See Fig. 8.1 for area location. Vertical pressure gradient (~0.79 psi/ft) is the slope of the trend line and is much greater than hydrostatic gradient (0.433 psi/ft), which indicates strong potential for upward flow. Large vertical pressure gradient indicates reservoir heterogeneity and low vertical permeability. Large lateral pressure gradient (note wide pressure range at 3,184 ft [970 m]) also indicates reservoir heterogeneity.

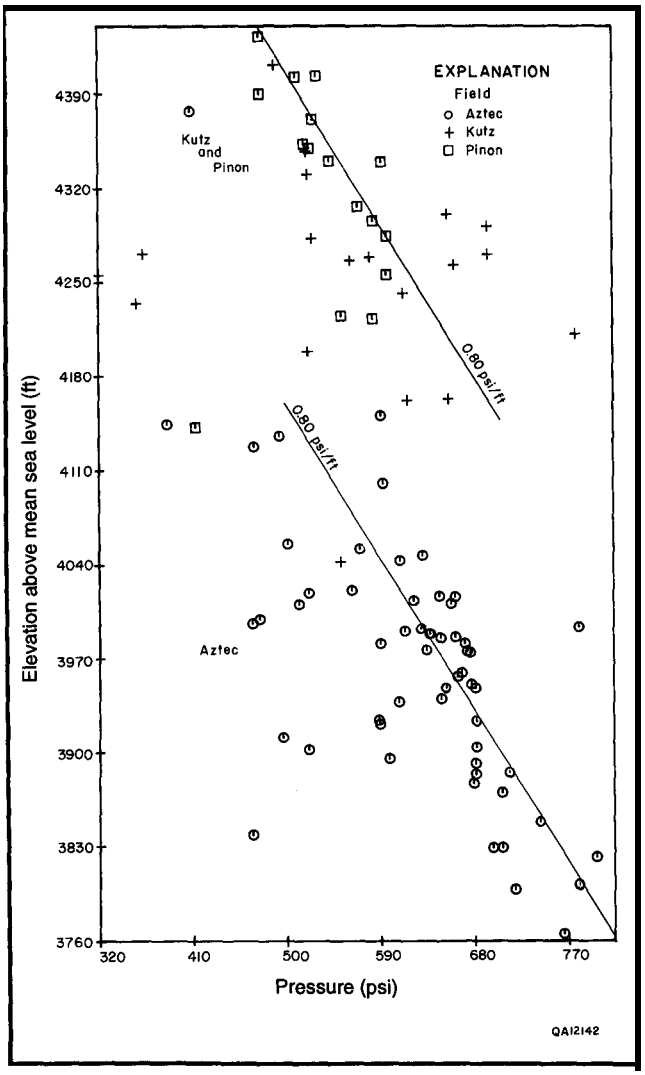

FIGURE 8.4—Fruitland Formation pressure-elevation plot, Aztec-Kutz-Pinon area (from Kaiser and Swartz, 1990). See Fig. 8.1 for area location. Vertical pressure gradient (~0.80 psi/ft) is the slope of the trend line and shows strong potential for upward flow.

than fresh-water hydrostatic pressure (overpressured), whereas those in the west-central basin are less than hydrostatic pressure (underpressured).

As discussed above, vertical pressure gradient, or slope of the pressure-elevation plot, is used to indicate vertical flow direction. Regionally, BHPs lie along two trend lines to define vertical pressure gradients of approximately 0.30 and 0.60 psi/ft, indicating potential for downward and upward vertical flow, respectively, in the northern and southern parts of the basin (Fig. 8.5). In both areas, coal beds and sandstones cluster together and fall along the same trend lines, showing no significant difference in pressure to indicate regional pressure communication between interbedded coal seams and sandstones.

The Fruitland Formation is divided into overpressured and underpressured areas. The overpressured, north-central part of the basin is surrounded by a much larger under-pressured area (Fig. 8.7). The overpressured area (simple pressure gradient >0.44 psi/ft) is a large, roughly rectangular area (~1,000 mi^2 [~2,590 km^2), trending northwest-southeast from the outcrop in T34N R10W, basinward to T31N R5W, and extending north and northeast to the outcrop. Note that the overpressured area is regional in extent and is not confined to isolated areas delineated by drilling mud weight (Kelso and others, 1988). Except to the northwest, the overpressured area is surrounded in all directions by an area of underpressure (pressure gradient <0.44 psi/ ft). The transition between the pressure regimes is marked by pronounced steepening of the potentiometric surface (Figs. 8.1 and 8.6) and coincides with pinch-out of thick aquifer coal seams and possible faulting along the basin's structural hingeline (Ayers and others, this volume, Chapter 2).

Anomalous islands of overpressure in the regionally underpressured west-central part of the basin occur at Kutz, Aztec, Flora Vista, and Glades and are explained hydrodynamically by local upward flow of ground water. The vertical pressure gradient at Kutz and Aztec is well in excess of the hydrostatic gradient (Fig. 8.4), indicating strong potential for upward flow. Flora Vista and Glades lie in a dip-elongate belt of thick coal seams (Ayers and others, this volume, Fig. 2.19) and thus may receive recharge directly from the nearby outcrop to the north, contributing to over-pressure. Anomalous underpressuring in the overpres-

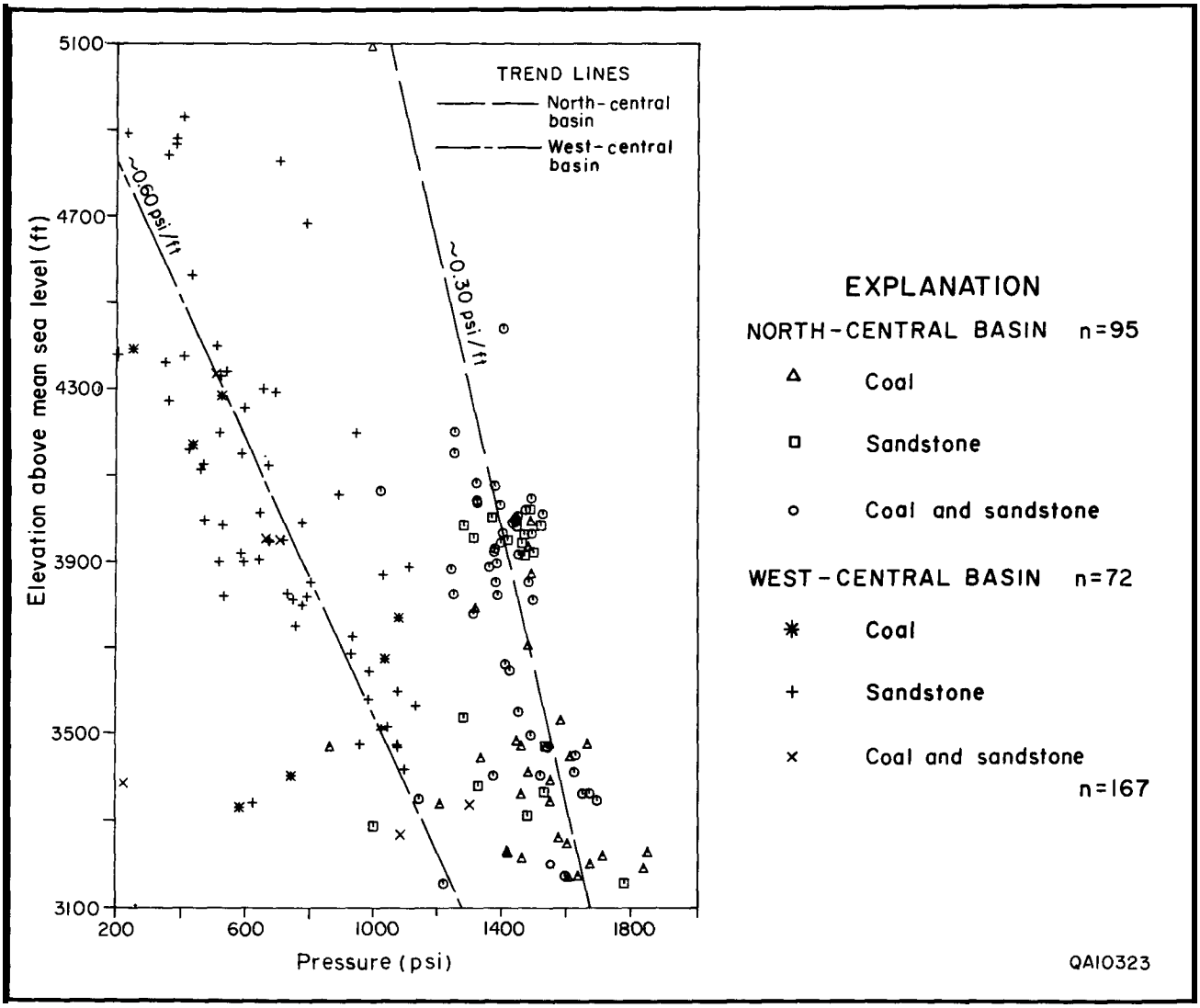

FIGURE 8.5—Fruitland Formation pressure-elevation plot, San Juan Basin (modified from Kaiser and Swartz, 1990). Vertical pressure gradient (~0.30 and ~0.60 psi/ft) is the slope of the respective trend line. Ground-water flow is potentially downward in the north-central part of the basin (vertical gradient < hydrostatic gradient, 0.433 psi/ft) and upward in the west-central part of the basin (vertical gradient > hydrostatic gradient). Coal and sandstone values lie along the same trend lines, indicating regional pressure communication between interbedded coal seams and sandstones.

sured north-central part of the basin is attributed to pressure decline because of production in the Ignacio Blanco field. Seventeen wells, clustered near Tiffany (Fig. 8.7) and completed in the early 1980s, are thought to have undergone pressure decline caused by long-term production (dating from the 1950s) from nearby wells. Alternatively, under-pressure may reflect low permeability and poor communication with regionally overpressured coal seams.

BHPs in the north-central part of the basin typically range from 1,400 to 1,900 psi, translating into simple pressure gradients of 0.50 to 0.63 psi/ft, whereas BHPs in the southern part of the basin commonly range from 400 to 1,000 psi (0.30 to 0.40 psi/ft). The 1,200-psi contour (Fig. 8.8) encloses the approximate area of overpressure. The area of highest pressure (BHPs >1,600 psi) is northwest-trending, parallel to depositional strike (Fig. 8.8), and is south of the basin's structural axis (Ayers and others, this volume, Fig. 2.5). Meridian 400, Northeast Blanco (NEBU), Sedro Canyon, and Los Piños are in this region. To the southwest, between Sedro Canyon and Blanco, the pressure drops abruptly from approximately 1,500 to 800 psi over a distance of approximately 10 mi (16 km). Low permeability and reservoir compartmentalization are inferred from this steep, lateral pressure gradient, which coincides with the pinch-out of thick coal seams (Ayers and others, this volume, Fig. 2) and conspicuous steepening of the potentiometric surface (Fig. 8.1). From Blanco, pressure uniformly decreases southwest to approximately 700 psi at Aztec and to less than 400 psi at Gallegos South. The lowest reported BHPs (<200 psi) occur in the San Juan River valley near the western margin of the basin.

Hydrochemistry

Hydrochemistry reflects rock-water interaction and prevailing ground-water flow rates and directions and indicates ground-water circulation through distribution of mass or dissolved solids in ground water, whereas hydraulic head indicates circulation through distribution of potential energy. In other words, chemical composition records actual ground-water movement (mass transfer), whereas head shows the direction of force that drives ground-water flow. Because ground water evolves chemically along its flow path, hydrochemistry can be used to help define recharge

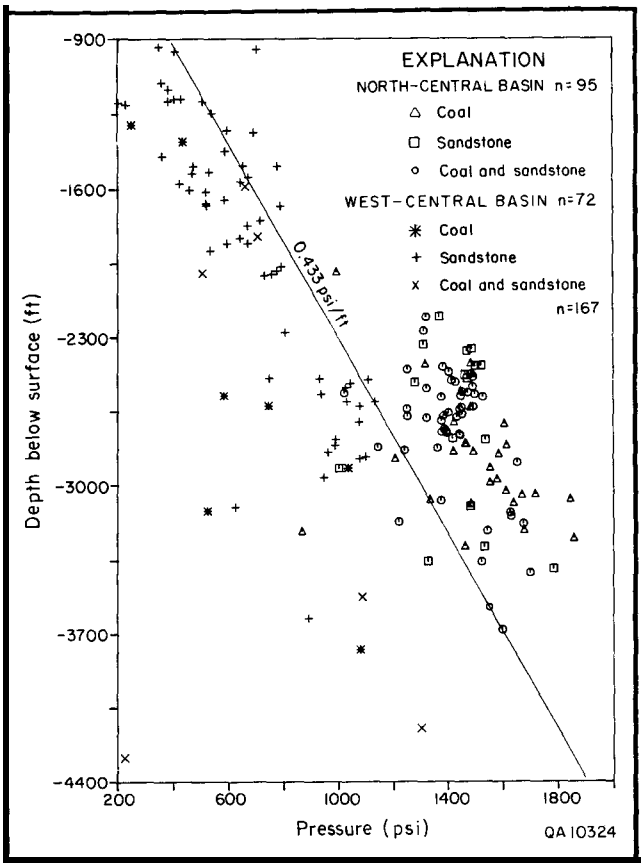

FIGURE 8.6—Fruitland Formation pressure-depth plot, San Juan Basin (from Kaiser and Swartz, 1988). Depth relative to land surface. Fresh-water hydrostatic gradient is 0.433 psi/ft. Fruitland is overpressured in north-central basin, underpressured in west-central.

and discharge areas. Generally, ground water is freshest at the outcrop in recharge areas and penetration of this fresh water into a basin marks the most permeable flow paths and implies an active, dynamic flow system.

To evaluate Fruitland hydrochemistry, Piper (trilinear) and Stiff ionic-ratio diagrams, histograms, and a chlorinity map were prepared from approximately 250 chemical analyses of produced waters that were separated by geographic region and producing lithology. Most of the analyses are from the north-central part of the basin. Few analyses were available from other parts of the basin. Ten GRI/BEG samples were collected, preserved, and analyzed for major ions, organic acids, stable isotopes, and selected trace metals to investigate sources of alkalinity and CO_2 in Fruitland waters and the extent of meteoric circulation in the basin. Chemical analyses were performed by the Bureau of Economic Geology's Mineral Studies Laboratory. Stable isotope analyses were done by Coastal Science Laboratories, Inc., Austin, Texas.

Piper diagrams were used to identify chemical facies or water type. However, Piper diagrams cannot be used to differentiate between waters of the same type, whereas ionic ratios can be used to fingerprint waters of the same facies (Novak and Eckstein, 1988). Thus, we modified the Stiff diagram and plotted eight ionic ratios: (Ca + Mg)/(Na + K), Mg/Ca, Ca/(Na + K), SO_4/(Na + K), (Na + K)/(HCO_3 + CO_3), (Ca + Mg)/(HCO_3 + CO_3), CI/(Na + K), and SO_4/Cl.

North-central basin—Chemical analyses of Fruitland waters produced from coal seams were selected from across the north-central part of the basin for wide geographic coverage. They are Na-HCO_3-type waters, complemented bya smaller number of Na-Cl waters (Fig. 8.9a). At least five Na-Cl waters came from wells that were stimulated with HCl or KCl, or both, and may not represent formation water. One Na-Cl water sample came from coal in the shallow subsurface on the western margin of the basin. These waters are mainly brackish and saline but are not brines (Fig. 8.10a and 10b). Fruitland waters produced from sandstone in the north-central part of the basin are also mainly Na-HCO_3 type, with only a few Na-Cl-type waters (Fig. 8.9b), contrary to previous reports on chemical facies of sandstone waters (Decker and others, 1987). Only waters produced from intervals thought to be mainly sandstone (based on log analysis) were plotted in Fig. 8.9b. Several of the $NaHCO_3$ waters came from open-hole completions in upper Fruitland sandstone in the Ignacio Blanco field made in the 1950s by Stanolind Oil & Gas; one sample came from a perforated interval in a well in Cedar Hill field. Apparently, sandstone waters are somewhat less saline (fresher) than coal waters, being lower in TDS and Cl- (Fig. 8.10c and 10d).

To further evaluate chemical characteristics of Fruitland waters produced from coal beds and sandstones in the north-central basin, we plotted Stiff ionic-ratio diagrams of samples from wells in T33N R7W. Waters from coal and sandstone are Na-HCO_3 type and have ionic-ratio diagrams of similar shape and ionic ratios (Fig. 8.11); that is, the variations are common to waters from each lithology, showing that chemical composition cannot be used to identify completion lithology. Moreover, similar chemical facies and diagram shapes for waters from each lithology, as shown at Cedar Hill field, indicate hydraulic communication between coal seams and sandstones.

Commonly, coal waters have large Mg^{2+}/Ca^{2+} ratios, giving the diagram a distinctive triangular segment, or magnesium triangle. Coal waters from the Meridian 400 area have Mg^{2+}/Ca^{2+} ratios as large as 12, whereas those from Cedar Hill are not unusually large but are similar to those in T33N R7W (Fig. 8.11) and the NEBU area (Fig. 8.12). Apparently, the Mg^{2+}/Ca^{2+} ratio increases basinward down hydraulic gradient along the flow path (Figs. 8.12 and 8.13). Mg^{2+} enrichment and/or Ca^{2+} depletion basinward is evident in a number of analyses in the Meridian 400 and NEBU areas. Ca^{2+} concentration may be reduced by precipitation of calcite and gypsum and by ion exchange. Fibrous calcite and gypsum occur as discontinuous mineral fill along the primary coal cleat (Tremain and others, this volume, Table 5.2). Moreover, solubility of calcite is less than that of Mg-carbonates, and Ca^{2+} is more strongly adsorbed than Mg^{2+}in ion exchange.

Waters in the north-central part of the basin are unique in their very high HCO_3^- contents (several thousand mg/ L up to 20,000 mg/L), high Na contents (thousands of mg/ L), low Ca^{2+} and Mg^{2+} contents, low Cl^- contents (tens to hundreds of mg/L), negligible SO_4^{2-} contents, and Ba2+ enrichment (Table 8.3). Earlier, on the basis of the existing suite of water analyses, organic-acid anions were thought to be important contributors to total alkalinity (Kaiser and Swartz, 1990). Very high reported HCO_3- contents and the neutral to slightly alkaline pHs (7 to 8) of produced waters suggested that organic acids were abundant and that inorganic alkalinities (HCO_3^- contents) were lower than those reported in available analyses. Although organic acids are present (200 to 300 mg/L as acetic acid), they are secondary contributors to the very high total alkalinities that are due mainly to HCO_3^- (Table 8.3). The dominance of HCO_3^- is shown by vigorous effervescence of the samples upon acidification in the laboratory, equivalence of inorganic C analyses and field alkalinities expressed as HCO_3^-, and titration-curve shapes typical of waters dominated by inorganic alkalinity (Fig. 8.14).

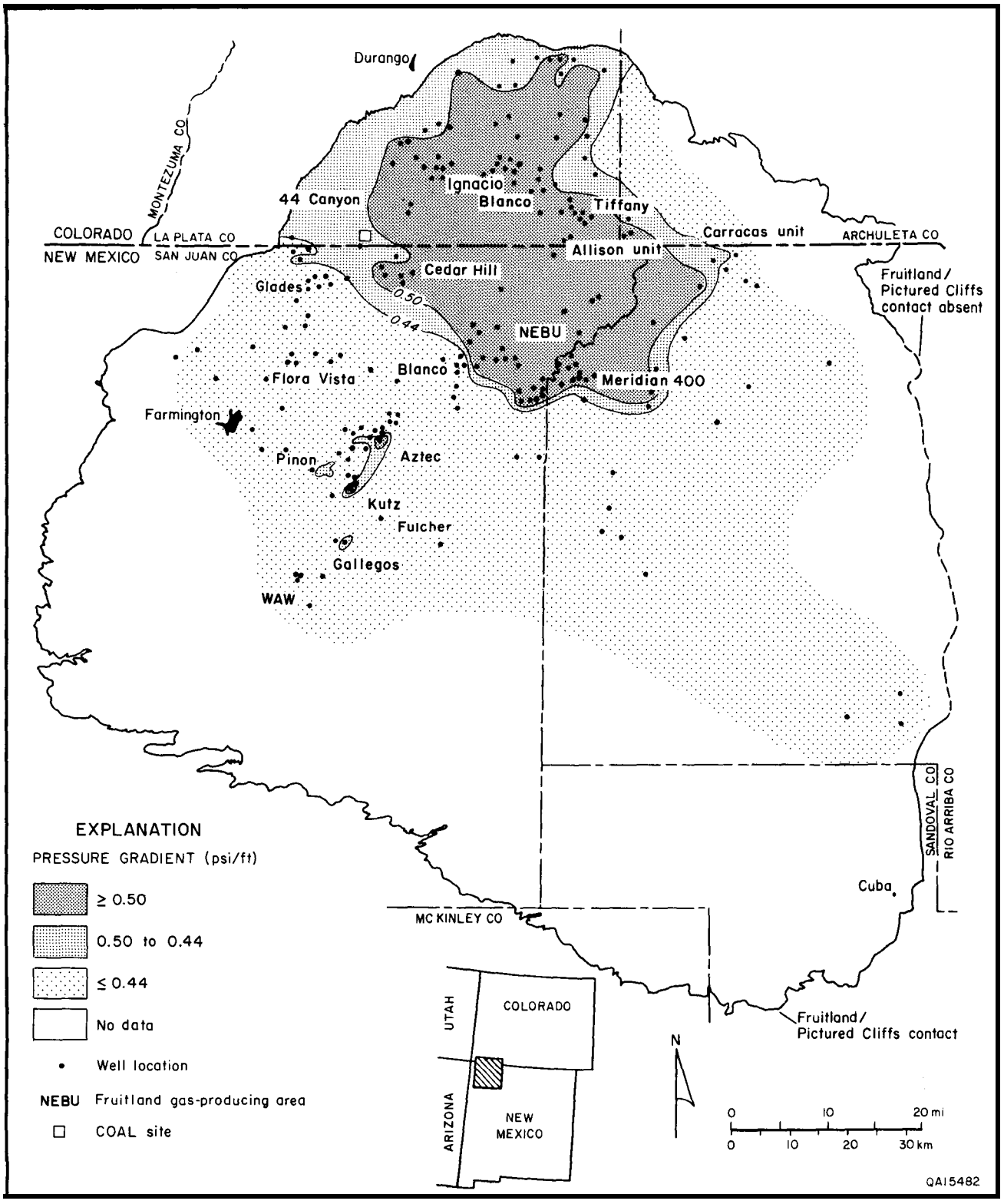

FIGURE 8.7—Fruitland Formation pressure-gradient map, San Juan Basin. Gradients are pressure-depth quotients. Overpressure is adapted to the basin's present-day geomorphology, extending to the northern outcrop (recharge area), and is nearly coincident with thick aquifer coal beds and freshest formation waters.

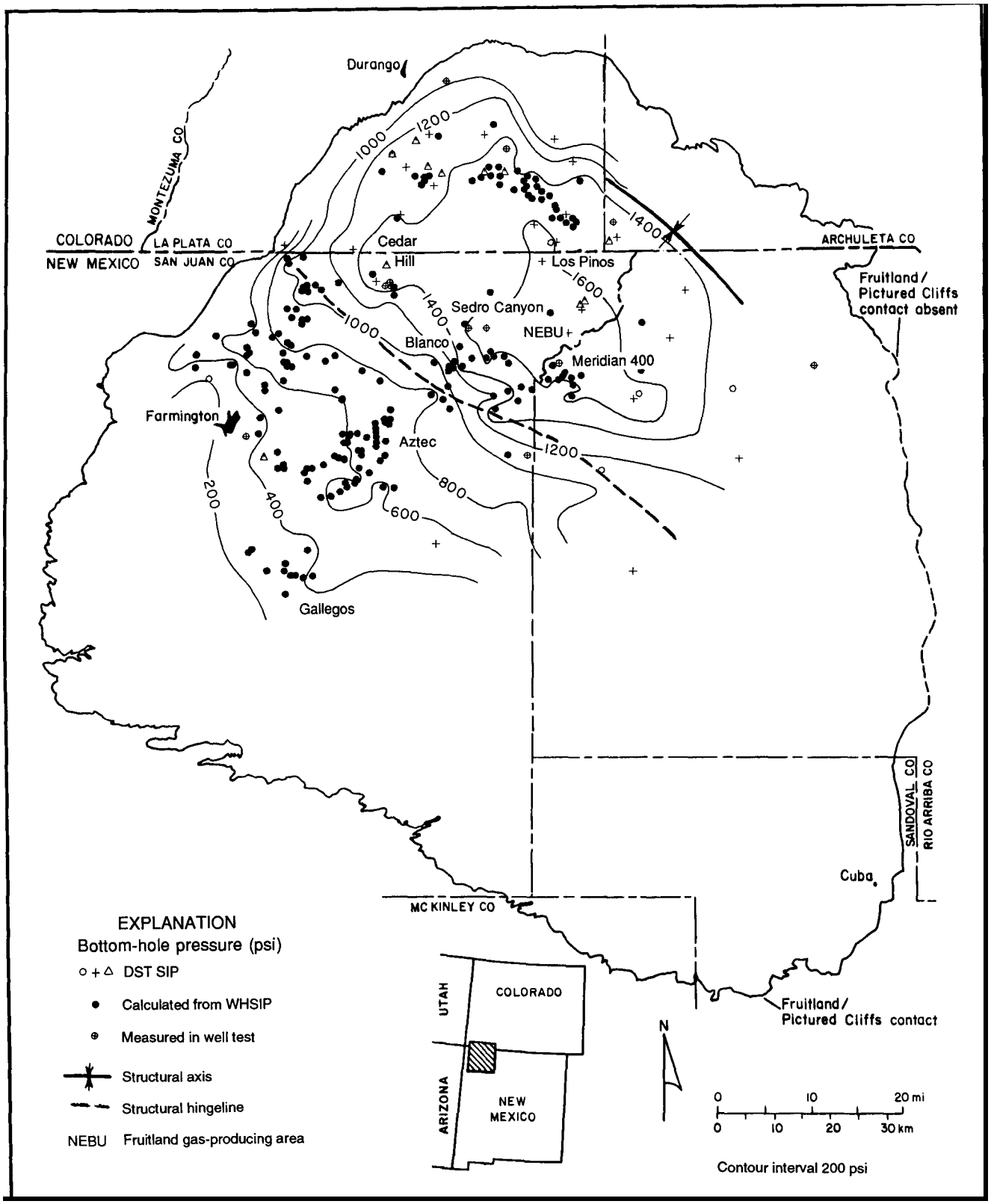

FIGURE 8.8—Fruitland Formation bottom-hole pressure map, San Juan Basin (from Kaiser and Swartz, 1990). Typical BHPs are 1,500 psi in the north-central part of the basin and 600 psi in the west-central part of basin. Highest pressures (>1,600 psi) occur south of the structural axis of the basin. Note steep pressure gradient northeast of structural hingeline at transition between overpressure and underpressure (Fig. 8.7).

High HCO_3^- content and lack of correlation with pH suggests an open chemical system and addition of organically sourced CO_2. Results of analyses for ^{13}C of total dissolved carbonate species (HCO_3^-, H_2CO_3, CO_2, and CO_3^{2-}) show extreme enrichment in ^{13}C. Values of $\delta^{13}C$ range from + 16.7 to +26.0%0 (Table 8.3) and are much heavier than those derived from thermogenic CO_2 or marine carbonates. Formation of CH_4 by degradation of organic acids and reduction of CO_2 by methanogenic bacteria yield isotopically heavy HCO_3^- (Carothers and Kharaka, 1980; Grossman and others, 1989). Lower $\delta^{13}C$ values (+16.7 and +17.5‰) near the northern outcrop (recharge area) may reflect dilution by isotopically light CO_2 formed diagenetically in the soil zone (Phillips and others, 1989) or greater abundance of isotopically light thermogenic CO_2. Heavier values basin-ward (+24.0 to +26.0%0) may indicate less dilution or that little CO_2 is being generated, while CH_4 continues to form by reduction, enriching the remaining CO_2 in ^{13}C (Carothers and Kharaka, 1980).

Abundant organic acids are thought to have been generated by the late Oligocene thermal event (Bond, 1984). Organic acids probably are not forming today because subsurface temperatures are too cool (~125°F [~50°C]). At 158°F (70°C), organic acids are generated faster than they are destroyed by bacteria (Y. K. Kharaka, pers. comm. 1989). In waters low in Ca^{2+} and Mg^{2+} such as these, HCO_3^- contents of more than 1,000 mg/L can be generated when CO_2-releasing processes (methanogenesis and sulfate reduction) occur. Methanogenesis is dominant here because sulfate reduction produces isotopically light HCO_3^- and is pervasive at low-SO_4^{2-} concentrations (Claypool and Kaplan, 1974; Whiticar and others, 1986). Sulfate reduction and methanogenesis in peat swamps were postulated by Decker and others (1987) to account for high HCO_3- contents in

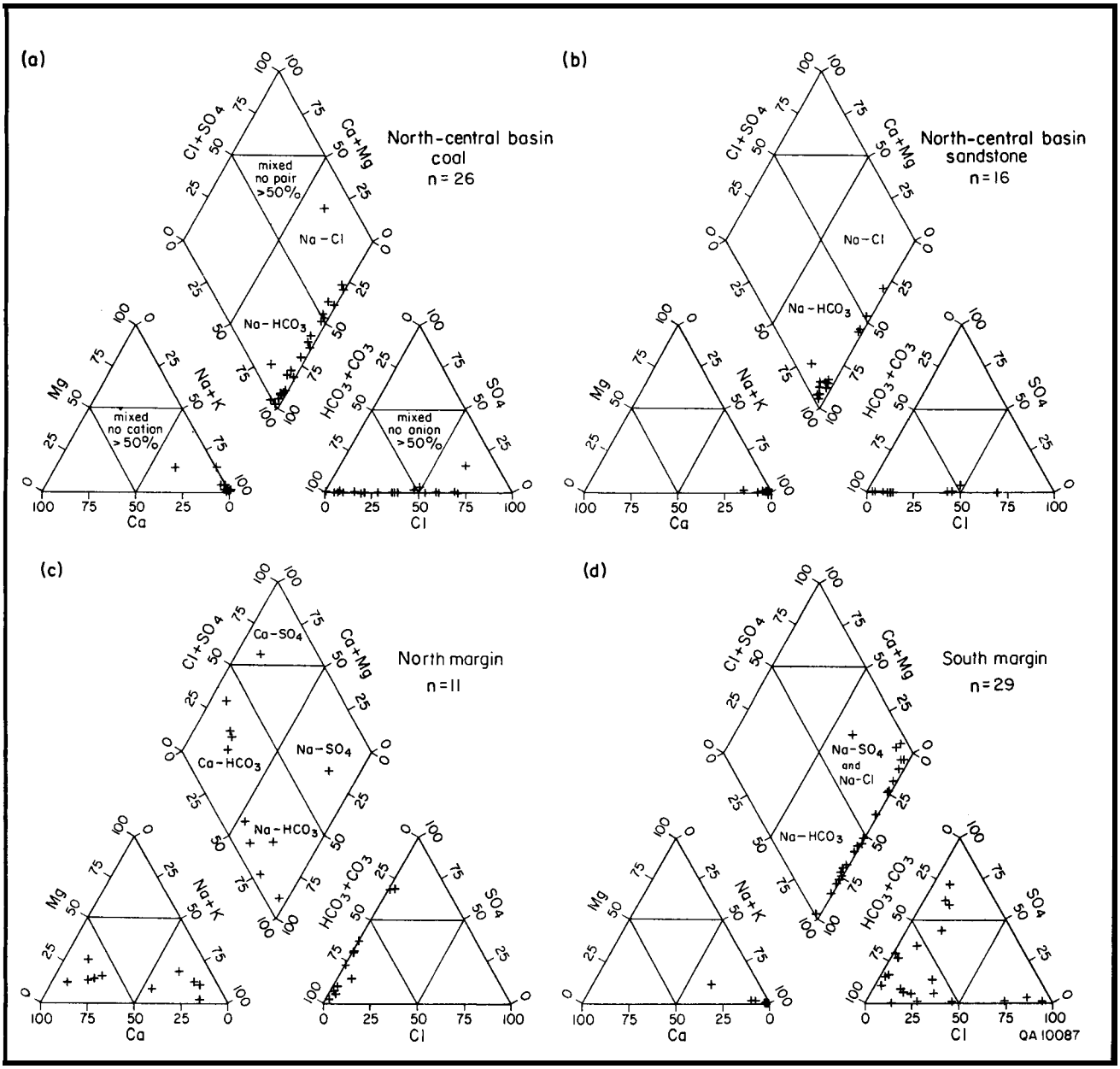

FIGURE 8.9—Piper diagrams of Fruitland waters, San Juan Basin (from Kaiser and Swartz, 1988). North-central part of basin by lithology (a and b), and northern (c) and southern (d) margins of basin undifferentiated by lithology. Similar chemical facies in coalbed and sandstone waters indicate hydraulic communication between strata. Note diversity of facies types in Fruitland waters. Diagrams plotted in meq/L.

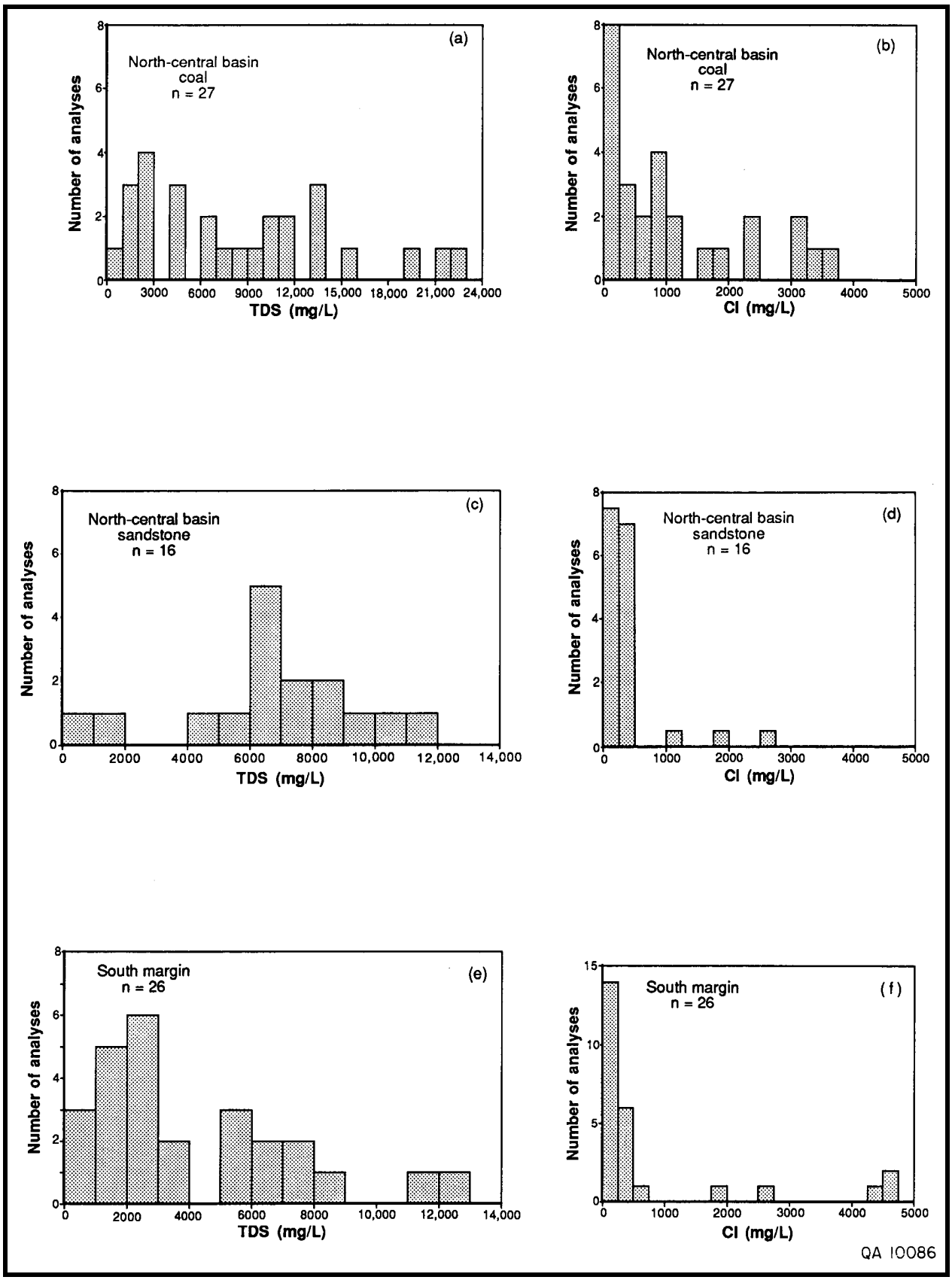

FIGURE 8.10—Histograms of Fruitland water composition, San Juan Basin (from Kaiser and Swartz, 1988). North-central part of basin by lithology, southern margin undifferentiated.

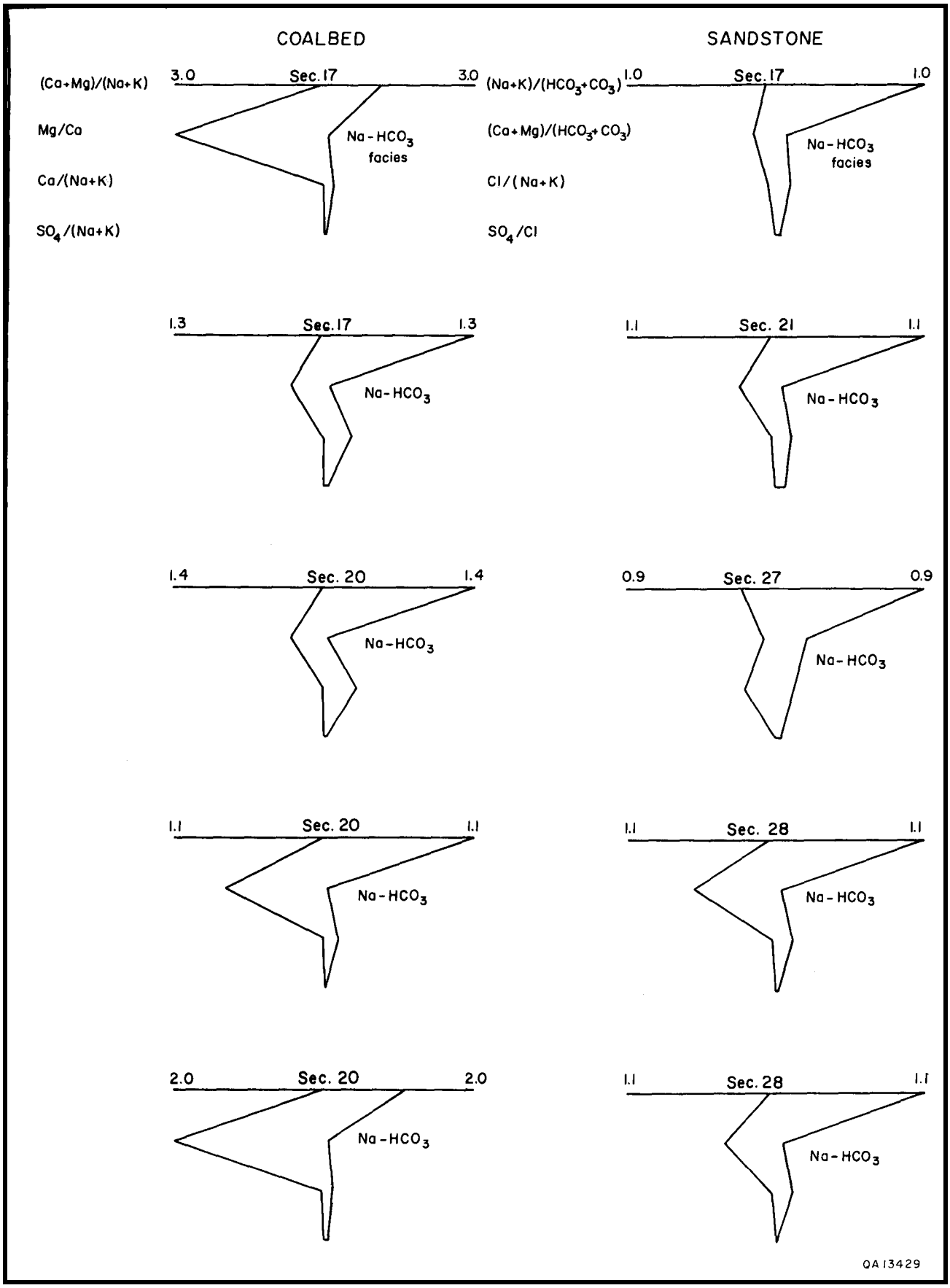

FIGURE 8.11—Stiff ionic-ratio diagrams, Fruitland coalbed and sandstone waters, T33N R7W, San Juan Basin (from Kaiser and Ayers, 1990). Similar shapes are common to waters from both rocks, suggesting hydraulic communication between them. Diagrams plotted in meq/L. See Fig. 8.13 for area location.

coalbed waters. However, these waters are meteoric and not fresh connate waters. They plot above and close to the meteoric water line, showing enrichment of D but not of ^{18}O (Fig. 8.15). A possible explanation of D enrichment is isotopic exchange with hydrogen gases (CH_4, C_2H_6, H_2, and H_2S) (Welhan, 1987) or between H_2O and HCO_3^- in methanogenesis. During methanogenesis, coexisting formation waters are enriched in D (values of 6D range from 0.0 to –80‰) (Whiticar and others, 1986). This enrichment in Fruitland waters is shown by a close correlation between δD of water and $\delta^{13}C$ of total dissolved carbonate species (Fig. 8.16). Exchange with H_2S is not likely because it is not present in these waters. Basinward enrichment of ^{18}O (samples 5-8) may, in view of isotopically light oxygen upflow, represent mixing of lighter water with older, isotopically much heavier water downflow or it may represent older recharge events, when past recharge was enriched in 180.

Chemical evolution—Waters from the northern and southern margins of the basin are chemically diverse and evolve, respectively, to Na—HCO_3^- and Na—Cl-type waters basinward. Margin waters are discussed collectively because host lithology is usually not reported. Waters from

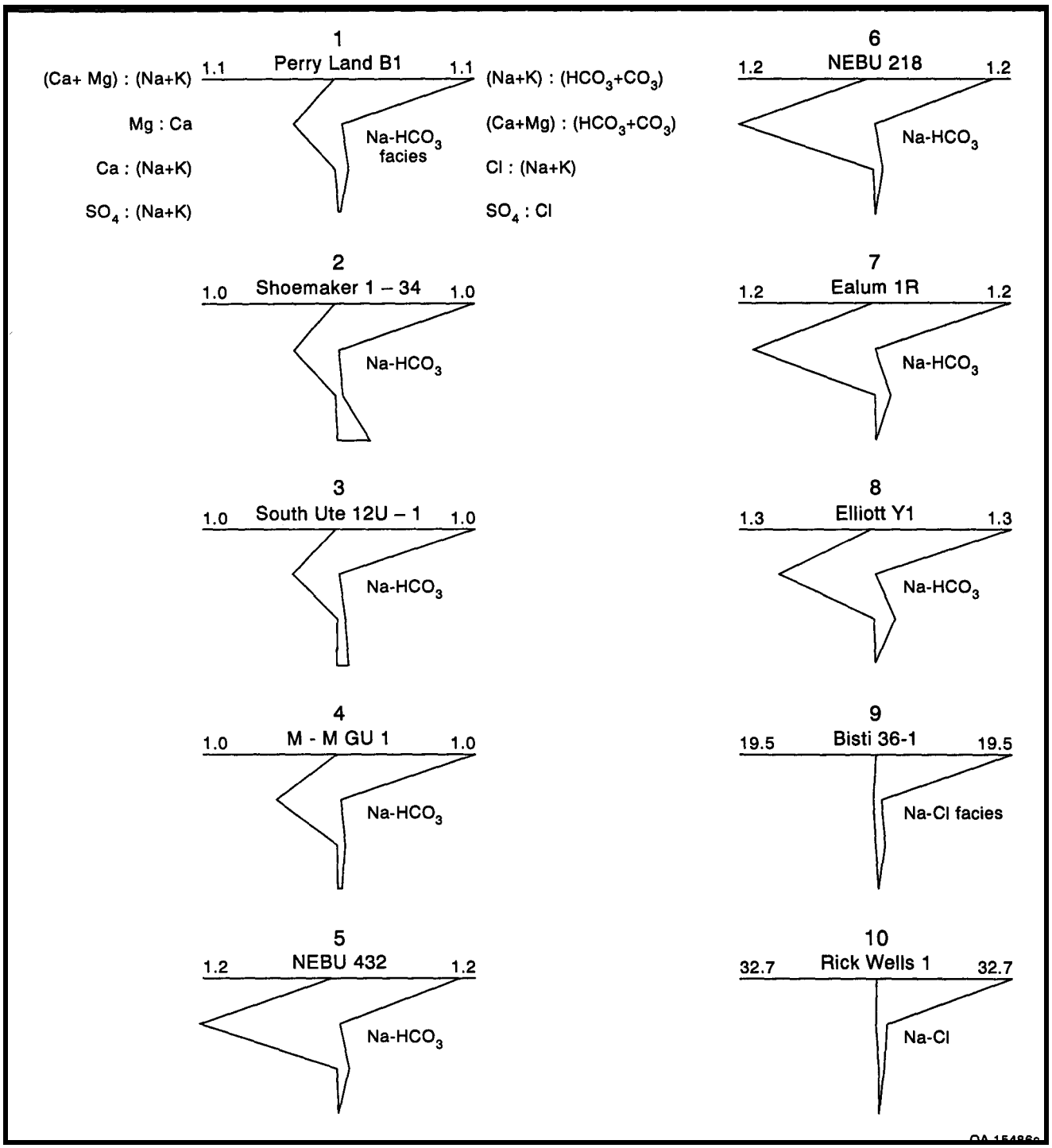

FIGURE 8.12—Stiff ionic-ratio diagrams, GRI/BEG Fruitland coalbed water samples (see Fig. 8.13 for location and Table 8.3 for analyses). Northern waters are Na–HCO_3 type and southern waters Na–Cl type. Note increase in Mg^{2+}/Ca^{2+} ratio down flow path (samples 2, 3, 4, and 7). Samples 9 and 10 resemble seawater (see Fig. 8.17); meteoric dilution is indicated by $\delta^{18}O$ and δD values (see Fig. 8.15) and small (Na + K)/(HCO_3+ CO_3) ratios relative to seawater.

the northern margin are dominantly Ca-Mg-HCO_3 and $NaHCO_3$ types (Fig. 8.9c) and are fresh to brackish (TDS content of 180 to 3,015 mg/L and chlorinities of 2 to 45 mg/L). Northern waters graphically differ from those basinward. They have large SO_4^{2-} /Cl^- ratios (up to 116), giving the Stiff ionic-ratio diagram a distinctive triangular foot, or sulfate triangle (Kaiser and others, 1991, fig. 20). Apparently, meteoric waters in the northern part of the basin evolved basin-ward by addition of $SO4_2^-$ and Mg^{2+}, followed downflow by loss of SO_4^{2-}, addition of Cl^-, Na^+ (ion exchange), and HCO_3^- (methanogenesis), and possible addition of Mg^{2+}, as well as loss of or no addition of Ca^{2+} (mineral precipi-

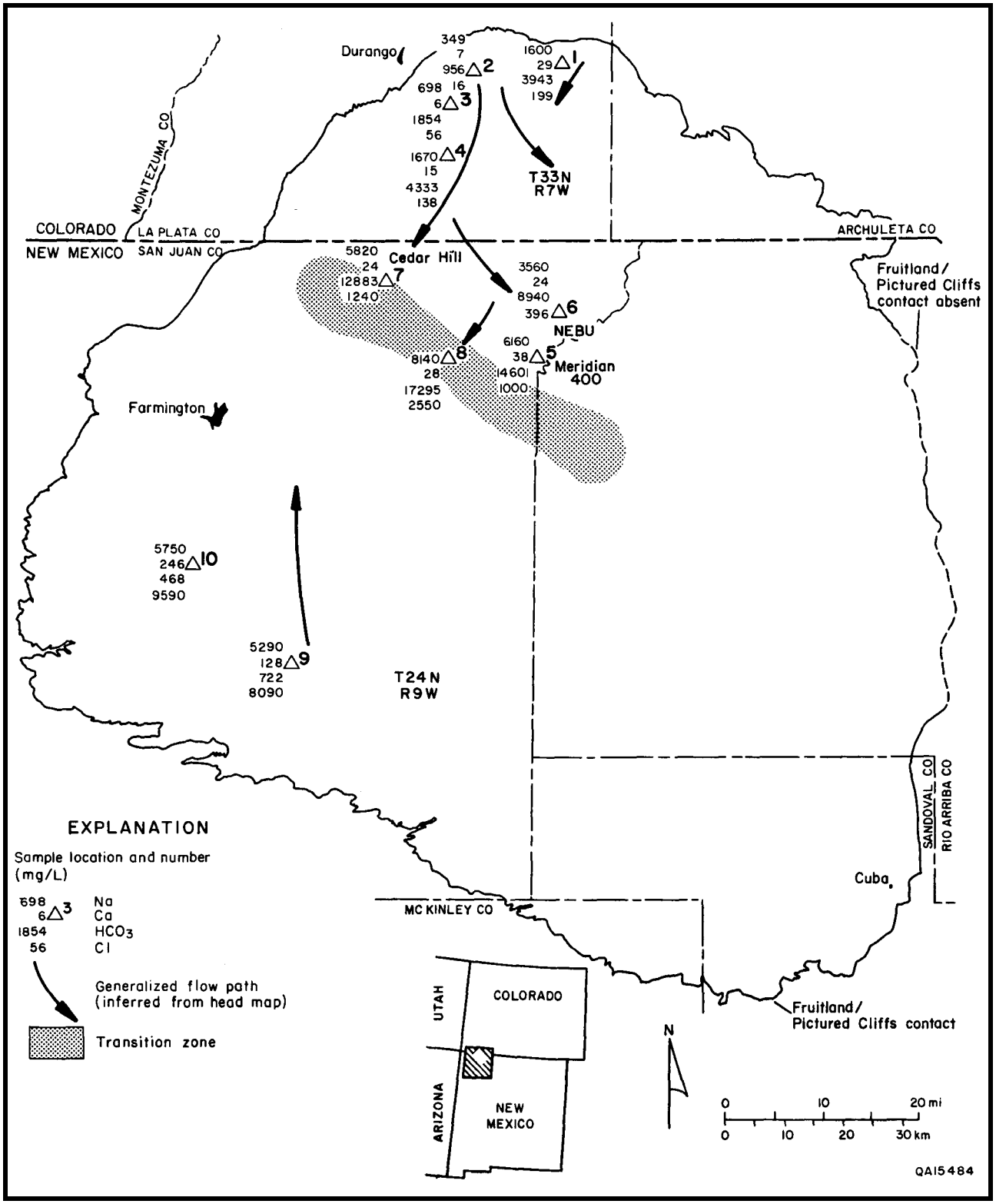

FIGURE 8.13—Location of GRI/BEG Fruitland coalbed water samples. In the north-central part of the basin, Na^+ and HCO_3^- increase down flow path, reaching their highest concentration in the transition zone. Southern waters are enriched in Cl^- and Ca^{2+}. The transition zone is a regional facies, potentiometric, pressure, and hydrochemical boundary. Complete chemical analyses in Table 8.3.

tation and ion exchange), to become Na-HCO_3 waters. Sulfate reduction occurs rapidly along the flow path because waters within 2 mi of the outcrop have negligible 5042 contents (Fig. 8.13 and Table 8.3).

Waters from the southern margin of the basin are sodium dominated, showing Na-HCO_3, Na-SO_4, and Na-Cl types (Fig. 8.9d) that have salinities similar to those in the north-central part of the basin (Fig. 8.10). When plotted as Stiff ionic-ratio diagrams, these waters display a variety of shapes, reflecting their chemical diversity. Among 29 analyses plotted, 19 have a sulfate triangle, 7 a magnesium triangle, and 3 a north-central basin signature (Kaiser and others, 1991, figs. 21 and 22).

Na-SO_4 waters are thought to be the chemically evolved shallow ground water because thenardite (Na_2SO_4) is deposited by area spring waters (Stone and others, 1983). Apparently, these waters evolve basinward to Na-Cl domination through loss of SO_4^{2-} and addition of Cl^-. Coal waters sampled in the southern basin have TDS contents of 14,000 to 42,000 mg/L, chlorinities of 8,000 to 26,000 mg/ L, and are the only brines identified in the Fruitland Formation. These waters have ratio diagrams very similar to that of seawater, especially the diagrams of waters sampled in T24N R9W (Figs. 8.12 and 8.17). However, their (Na+K)/(HCO_3+CO_3) ratios are considerably less than that of seawater but greater than those of Na-Cl waters from the southern margin, suggesting meteoric dilution, which was confirmed by the stable isotope analysis of samples 9 and 10 (Fig. 8.15 and Table 8.3). Their $\delta^{18}O$ and SD values are similar to those of Holocene, Ojo Alamo, and Nacimiento ground waters (Phillips and others, 1986). They plot near the meteoric water line for northwest New Mexico but are shifted slightly to the right, which strongly suggests evaporation during recharge, a common process in semiarid environments (Phillips and others, 1986). Thus, these Fruitland waters probably represent modified marine waters. Apparently, coal beds have been flushed of their fresh connate water by saline waters moving upward and laterally toward the San Juan River valley. Their presence further indicates limited recharge from the southern margin of the basin and implies low permeability. These waters can be preserved only where strata are tight and poorly flushed by meteoric recharge.

Chlorinity-Ground-water flow patterns were also defined by a chloride map. Chloride was mapped because it is a conservative chemical species unaffected by rock-water interaction. In the north-central part of the basin, the chlorinity map (Fig. 8.18) and isotopic data (Fig. 8.15) show a

TABLE 8.3-Chemical analyses of produced Fruitland coalbed waters.

Sample number	1	2	3	4	5	6	7	8	9	10
Well	Perry Land GU B1	Shoemaker 1-34	Southern Ute 12U-1	Mayfield-Melton GU 1	NEBU 432	NEBU 218	Ealum Gas Com C IR	Elliott Gas Com Y 1	Bisti Coal 36-1	Rick Wells 1
Location	30 35N 6W	34 35N 8W	12 34N 9W	1 33N 9W	7 30 N 7W	16 31N 7W	33 32N 10W	9 30N 9W	36 25N 12W	8 26N 13W
Production interval	1,304-1,480	1,896-2,026	2,400-2,478	2,530-2,747	3,004-3,216 (OH)	3,200-3,346 (OH)	2,777-2,813	2,790-2,944	1,074-1,092	1,383-1,427
Source	wellhead	wellhead	wellhead	separator[a]	separator[a]	wellhead	wellhead	wellhead	wellhead	wellhead
TDS	5,820	1,360	2,650	6,220	21,970	13,030	20,110	28,210	14,330	16,190
Na	1,600	349	698	1,670	6,160	3,560	5,820	8,140	5,290	5,750
K	9.9	4.3	5.8	5.4	19.5	13.2	33.3	53.1	22.5	27.5
Ca	28.8	6.5	5.8	15.1	37.7	24.4	23.6	28.1	128	246
Mg	6.2	1.2	1.2	4.2	27.4	17.3	15.5	15.1	36.4	57.7
Sr	4.3	0.6	0.7	5.0	17.7	13.2	12.3	19.4	6.9	12.3
Ba	6.5	0.7	1.1	6.1	62.9	21.1	36.2	51.5	8.4	7.6
Fe	0.12	0.80	0.04	0.05	0.64	0.72	1.24	0.59	0.57	2.37
Mn	0.06	0.03	0.03	0.01[b]	0.01	0.01	0.03	0.01	0.49	0.15
Li	0.88	0.34	0.94	1.54	1.39	1.11	0.58	1.13	0.50	0.53
B	1.08	0.21	0.63	1.55	2.15	0.98	8.54	9.17	1.18	1.09
SiO_2	21.0	22.8	26.1	31.5	26.6	27.1	24.7	26.1	12.5	15.0
Field alkalinity (as HCO_3)	3,943	956	1,854	4,333	14,601	8,940	12,883	17,295	722	468
Organic acids (as CH_3COOH)	270	220	210	330	330	210	210	220	120	160
NH_3	2.53	1.50	1.11	4.47	11.3	8.57	9.13	16.2	4.99	6.20
organic-N	0.39	0.78	0.85	1.04	1.45	1.59	0.85	1.50	0.60	0.48
CI	199	16	56	138	1,000	396	1,240	2,550	8,090	9,590
SO,	<5[c]	<5	<5	<5	<5	<5	<5	<5	<5	10.4
Br	0.85	0.14	0.50	0.76	4.65	3.49	3.99	6.19	7.64	8.68
I	0.38	0.10	0.33	1.13	0.41	0.11	0.52	0.87	0.60	0.56
Field pH	7.65	8.21	8.23	7.73	7.62	7.89	8.06	8.02	7.39	7.33
$\delta^{18}O$[d]	-14.0	-14.6	-14.6	-14.1	-7.4	-7.9	-7.7	-7.6	-10.8	-10.5
δD	-85	-98	-102	-85	-32	-43	-28	-36	-81	-80
$\delta^{13}C$[e]	+23.5	+17.5	+16.7	+24.0	+25.6	+24.7	+26.0	+24.9	+19.7	+19.5
Σ cations	71.94	15.73	30.92	74.03	273.71	158.30	257.14	359.07	240.27	268.10
Σ anions	70.28	16.13	31.98	74.95	267.66	157.78	246.25	355.55	239.98	278.33

[a]Flowing well.

[b]Near detection limit of 0.01 mg/L.

[c]Detection limit 5 mg/L.

[d]$\delta^{18}O$ and δD in per mil relative to SMOW.

[e]$\delta^{13}C$ of total dissolved carbonate species in per mil relative to PDB.

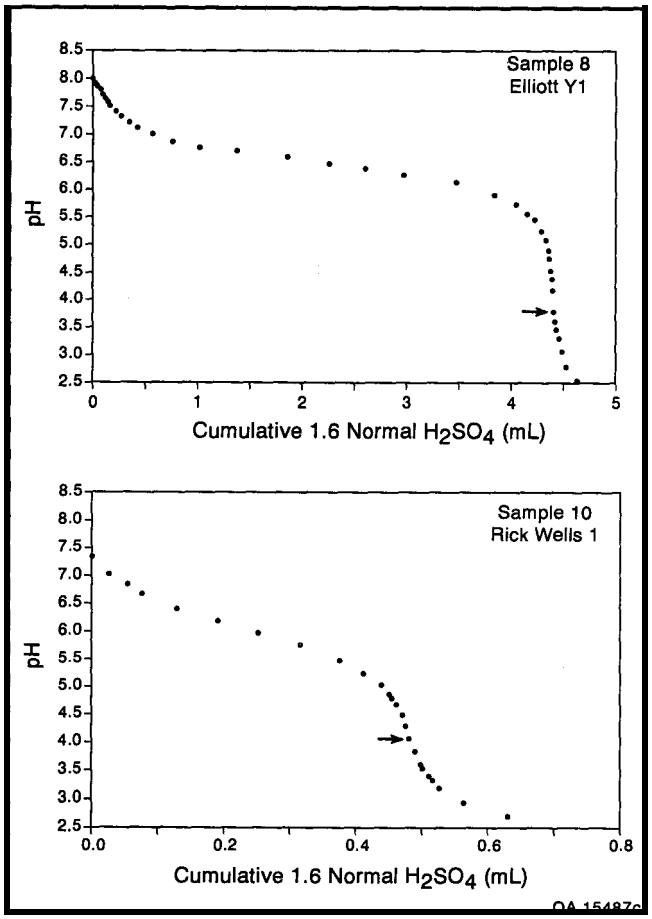

FIGURE 8.14—Representative titration curves for field alkalinity, GRI/BEG water samples. Curve shape is characteristic of waters dominated by inorganic atkatinity. Inflection points (arrows) are shifted to lower pH by organic acids. Curve flattens and inflection point becomes less well defined as relative percentage of organic acids increases (Table 8.3).

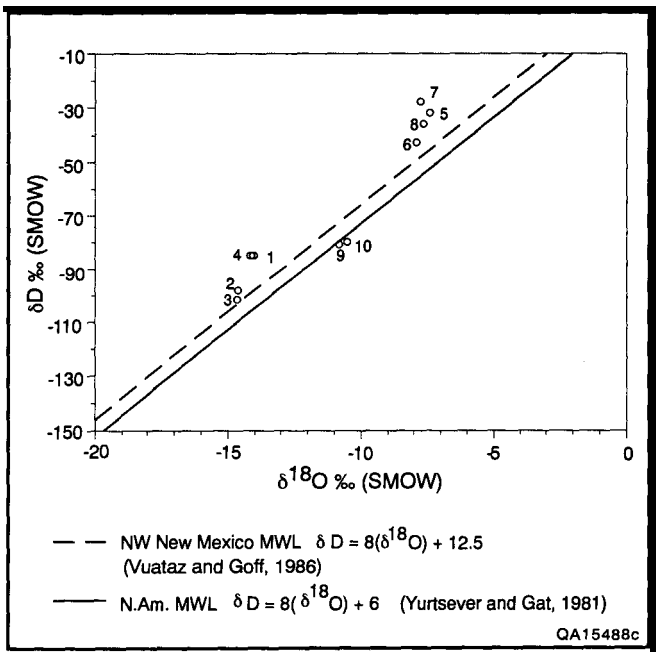

FIGURE 8.15—Plot of δD versus $\delta^{18}O$, GRI/BEG water samples. Northern waters plot above the meteoric water line (MWL) and are enriched in D but not ^{18}O, which indicates isotopic exchange with hydrogen gases or water and bicarbonate in methanogenesis. Southern waters (samples 9 and 10) plot to right of New Mexico MWL, indicating evaporation during recharge in the semiarid climate.

fresh-water plume of meteoric origin extending basinward from the northern and northwestern margins, as predicted from the potentiometric-surface (or head) map (Fig. 8.1). The distribution of dissolved solids, or mass, shows that low-chloride water coincides with flow patterns inferred from the head map and that flow is in the directions inferred from the map. For example, the Southern Ute—Mobil No. 36-1 well receives recharge directly from the northwestern margin of the basin; its produced waters have a TDS content of approximately 1,500 mg/L and contain 2 mg/L chloride. In contrast, the Southern Ute No. 1-24 well, although closer to the outcrop, should receive little direct recharge from the outcrop, as predicted from the chloride (Fig. 8.18) and head (Fig. 8.1) maps. Indeed, its produced waters have a TDS content of approximately 10,000 mg/L and contain about 600 mg/L chloride. The correlation between chlorinity and the present-day flow system and the presence of meteoric water show conclusively that these low-chloride waters are not fresh connate waters but evolved meteoric waters. Further evidence of geologically young waters is a ^{14}C age date of 33,176 yrs (Mayor and others, 1991) for dissolved bicarbonate in Fruitland formation water at the COAL site (Fig. 8.1). This date may be a maximum age because some of the carbon in the system could be older or "dead" carbon derived from the coal. From Darcy's law, travel (residence) times of Fruitland waters to the site were calculated to be approximately 15,000 and 28,000 yrs, using 16- and 27-mi (26- and 43-km) flow paths from the northwestern and northern margins of the basin, respectively, and a coal permeability of 10 and and porosity of 2%.

Tongues of low-chloride water project basinward along generalized flow paths inferred from the head map, defining the configuration of fresh-water recharge (Fig. 8.18). Major tongues are oriented northwest—southeast, parallel to depositional strike and to the orientation of aquifer coal seams. The largest tongue of low-chloride water extends from the northwestern margin of the basin southeast to beyond the San Juan River and coincides with thick coal seams. Similarly, the northerly tongue in eastern La Plata County coincides with thick coal seams that extend to the outcrop as probable conduits for recharge (Ayers and others,

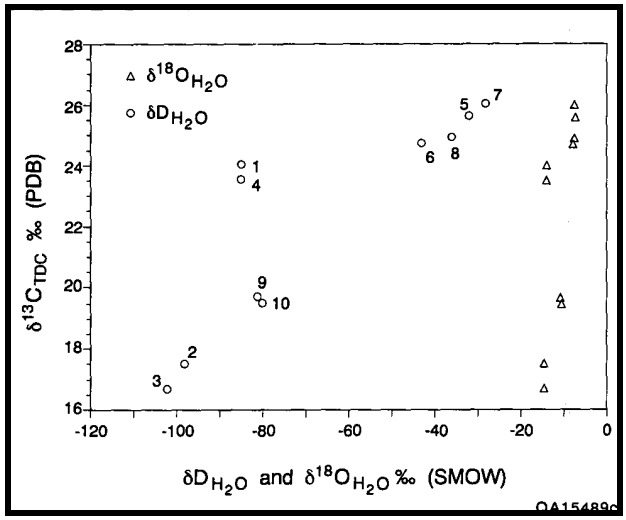

FIGURE 8.16—Plot of δD and $\delta^{18}O$ in water versus $6^{13}C$ of total dissolved carbonate species (TDC). D enrichment during methanogenesis is indicated by correlation of SD with S13C.

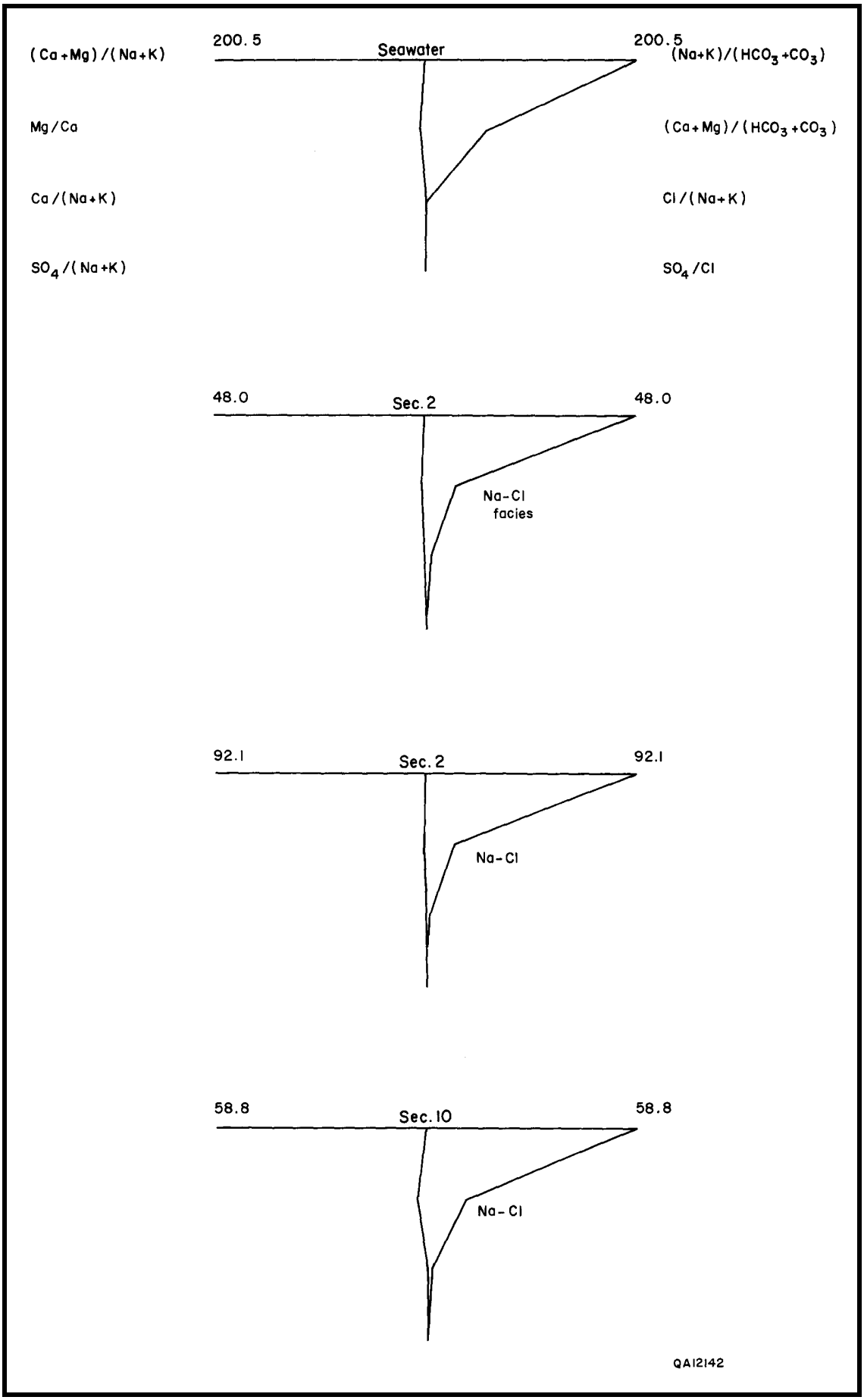
(Ca+Mg)/(Na+K)
Mg/Ca
Ca/(Na+K)
SO4/(Na+K)
200.5
Seawater
200.5
(Na+K)/(HCO3+CO3)
(Ca+Mg)/(HCO3+CO3)
Cl/(Na+K)
SO4/Cl
48.0
Sec.2
48.0
Na-Cl facies
92.1
Sec.2
92.1
Na-Cl
58.8
Sec.10
58.8
Na-Cl
QA12142

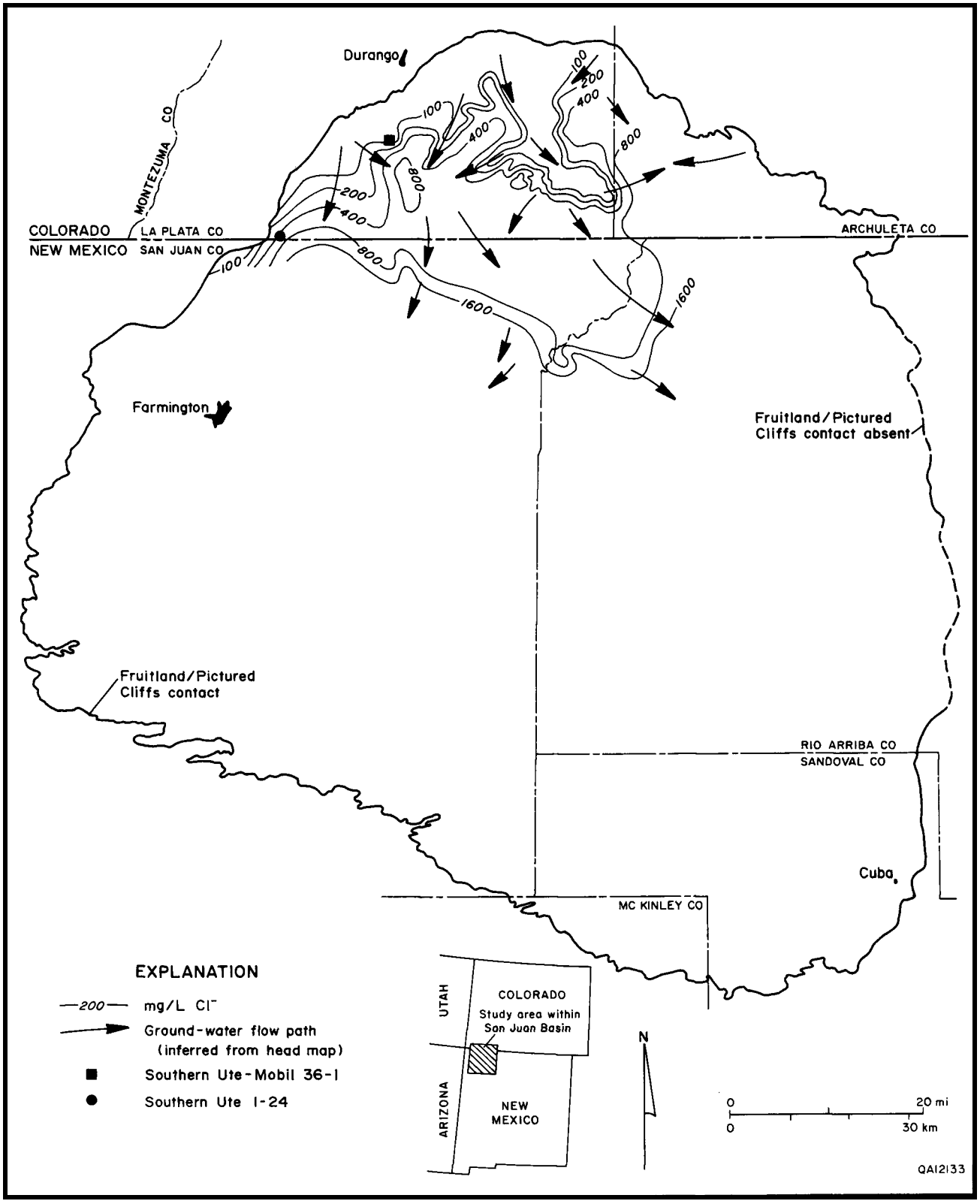

FIGURE 8.18—Chlorinity map of Fruitland waters, north-central part of the San Juan Basin (from Kaiser and Swartz, 1990). Distribution of chloride shows that flow is in directions inferred from the head map (Fig. 8.1). Low chlorinities coincide with overpressure (Fig. 8.7).

FIGURE 8.17—Stiff ionic-ratio diagrams, Fruitland coalbed waters, T24N R9W, San Juan Basin (from Kaiser and Swartz, 1990). Their similarity to seawater suggests the presence of marine waters. See Fig. 8.13 for area location.

this volume, Fig. 2.19). Secondary tongues are oriented northeast—southwest and may reflect the dominant fracture trend (Tremain and others, this volume, Fig. 5.12), dip-elongate coal seams (Ayers and others, this volume, Fig. 2.19), Fruitland channel sandstone belts (Ambrose and Ayers, this volume, Fig. 3.5), or a combination of all three. Some extremely low-chloride waters, located in T33N R6W at the end of a 20-mi (32-km) flow path, have chloride contents of less than 5 mg/L. The reason for their low chlorinities is ambiguous. Analytical error has been eliminated because the technique used (argentometric titration) tends to produce results that err on the high side. Possibly, the low chlorinities reflect recharge of fresh Pleistocene waters, which commonly are very low in chloride and depleted in ^{18}O and D (Phillips and others, 1986), and therefore indicate relatively fast ground-water flow rates and short residence times. Calculations based on Darcy's law, using highest coal permeability values from well tests (20 to 40 md) and a porosity of 2%, yield travel (residence) times of between 16,500 and 8,300 yrs (late Pleistocene to early Holocene) over a 20-mi (32-km) flow path. Use of Fruitland coal permeabilities (10 md or less) that are typically reported from well tests yield longer travel times of greater than 33,000 yrs. Calculated Fruitland travel times are consistent with ages of major recharge events (~5,000, 17,000, and 22,000 yrs B.P.) reported for the San Juan Basin (Phillips and others, 1986) and absolute age.

Hydrostratigraphy and regional flow

The Fruitland—Pictured Cliffs aquifer system was defined by Kaiser and Swartz (1988) on the basis of hydraulic head, pressure gradients, hydrochemistry, relative permeability, topography, and geography to include the Fruitland Formation, upper Pictured Cliffs sandstone tongues that inter-tongue with the Fruitland, and the Pictured Cliffs Sandstone, which underlies the coal-bearing Fruitland (Ayers and others, this volume, Figs. 2.1 and 2.13; Ayers and Zellers, this volume, Fig. 4.1). The aquifer system is overlain by the Kirtland Shale and underlain by the Lewis Shale. Previously, the Fruitland Formation had been combined with the Kirtland Shale to form the Kirtland/Fruitland confining unit (Stone and others, 1983). More recently, McCord (1988) proposed a major Fruitland aquifer in the north-central part of the basin composed of thick, laterally extensive coal seams. These seams have permeabilities that are orders of magnitude greater than those of associated sandstones (Ayers and Zellers, this volume, Fig. 4.5).

In the northern part of the basin, the Fruitland Formation is composed of interbedded coal beds and sandstones in apparent hydraulic communication, as shown by their similar reservoir pressures and water chemistry (Figs. 8.5 and 8.11). Little is known about the scale of interconnectedness. However, because permeability in fractured reservoirs is scale dependent, or increases with sample size (Garven, 1986), higher regional than local permeability is inferred from scale dependency. Fruitland permeabilities calculated from regional heat-flow data (McCord, 1988) are higher than those typically obtained from well tests and are thought to reflect scale dependency. Consequently, on that basis the Fruitland is postulated to behave regionally as a homogeneous, hydraulically interconnected aquifer, or single hydrologic unit, and locally as a heterogeneous, disconnected aquifer. Local heterogeneity is indicated by large vertical and lateral pressure gradients (Fig. 8.3). Hydraulic communication between the Fruitland Formation and upper Pictured Cliffs sandstone tongues is inferred from similar heads and their intertonguing relation (Ayers and Zellers, this volume, Fig. 4.1; Ayers and others, this volume, Fig. 2.2). Therefore, the two units are considered a single hydrostratigraphic unit that transmits ground water mainly south and southwest.

The hydraulic relation of the Fruitland—upper Pictured Cliffs hydrostratigraphic unit to the underlying main Pictured Cliffs Sandstone, or to that part of the Pictured Cliffs exclusive of the sandstone tongues, is uncertain. Available pressure data indicate that Fruitland heads are considerably higher than those of the low-permeability main Pictured Cliffs Sandstone and that the two are not in hydraulic communication in the northern part of the basin. Pictured Cliffs heads are highest (6,200 to 7,000 ft [1,890 to 2,134 m]) in the northwestern part of the basin, adjacent to the outcrop, and decrease southeast to approximately 6,000 ft (1,829 m), parallel to the Pictured Cliffs depositional strike and dominant fracture trend (Laubach and Tremain, this volume, Figs. 6.6 and 6.7). Except for the northwestern part of the basin, Pictured Cliffs heads in the northern basin are 800 to 1,000 ft (244 to 305 m) lower than those in the Fruitland Formation.

The large head difference between the Fruitland. Formation and the main Pictured Cliffs Sandstone partly reflects failure to attain pressure equilibrium during short-term well testing, which implies low permeability in the Pictured Cliffs Sandstone. Even though strong potential for downward flow (leakage) is indicated from the Fruitland Formation to the main Pictured Cliffs Sandstone, this potential, particularly in low-permeability strata, does not mean that significant flow actually occurs. The very large head difference between the Fruitland Formation and the main Pictured Cliffs Sandstone indicates hydraulic separation and low permeability in the main Pictured Cliffs Sandstone, which is too tight to receive and transmit appreciable recharge basin-ward (Cumella, 1981; Kaiser and Swartz, 1988, 1989). If they were connected vertically and the Pictured Cliffs was permeable, head differentials and vertical pressure gradients would be much less. Separation is further indicated in the hydrochemistry; Pictured Cliffs waters are Na-Cl type, whereas Fruitland waters are a unique, low-chloride, Na-HCO_3 type (Table 8.3). Thus, ground-water flow is mainly in the Fruitland Formation, especially in the more permeable coal seams, and in the upper Pictured Cliffs sandstone tongues, which are confined by the low-permeability main Pictured Cliffs Sandstone below and the Kirtland Shale above. Consequently, in the northern part of the basin, the Fruitland—Pictured Cliffs aquifer system consists of the Fruitland Formation and upper Pictured Cliffs sandstone tongues (Fig. 8.19; Ayers and others, this volume, Fig. 2.2).

The Fruitland—upper Pictured Cliffs aquifer transmits ground water under high head from the northern and northwestern margins of the basin. Vertical flow is down the steep northern limb (Fig. 8.19), as indicated by a regional vertical-pressure gradient (~0.30 psi/ft) that is less than hydrostatic gradient (Fig. 8.5). Basinward, flow must eventually turn upward as cross-formational flow along the pinch-out of thick aquifer coal seams and/or their offset by faults along the basin's structural hingeline (Ayers and others, this volume, Chapter 2). At this point, the vertical pressure gradient exceeds the hydrostatic gradient, and upward flow is indicated (Fig. 8.3). In the vicinity of Cedar Hill field, pronounced steepening of the potentiometric surface between the Southern Ute No. 21-2 and Crandell No. 7 wells coincides with aquifer pinch-out and a zone of minor normal faults (Ambrose and Ayers, this volume, Fig. 3.3). The Fruitland potentiometric surface is above land surface (overpressured conditions) to a point just beyond the Crandell No. 7 well (Fig. 8.19). Hydraulic head is independent of land surface, indicating a confined aquifer and little gravity-driven cross-formational flow, that is, artesian conditions (Fig. 8.20).

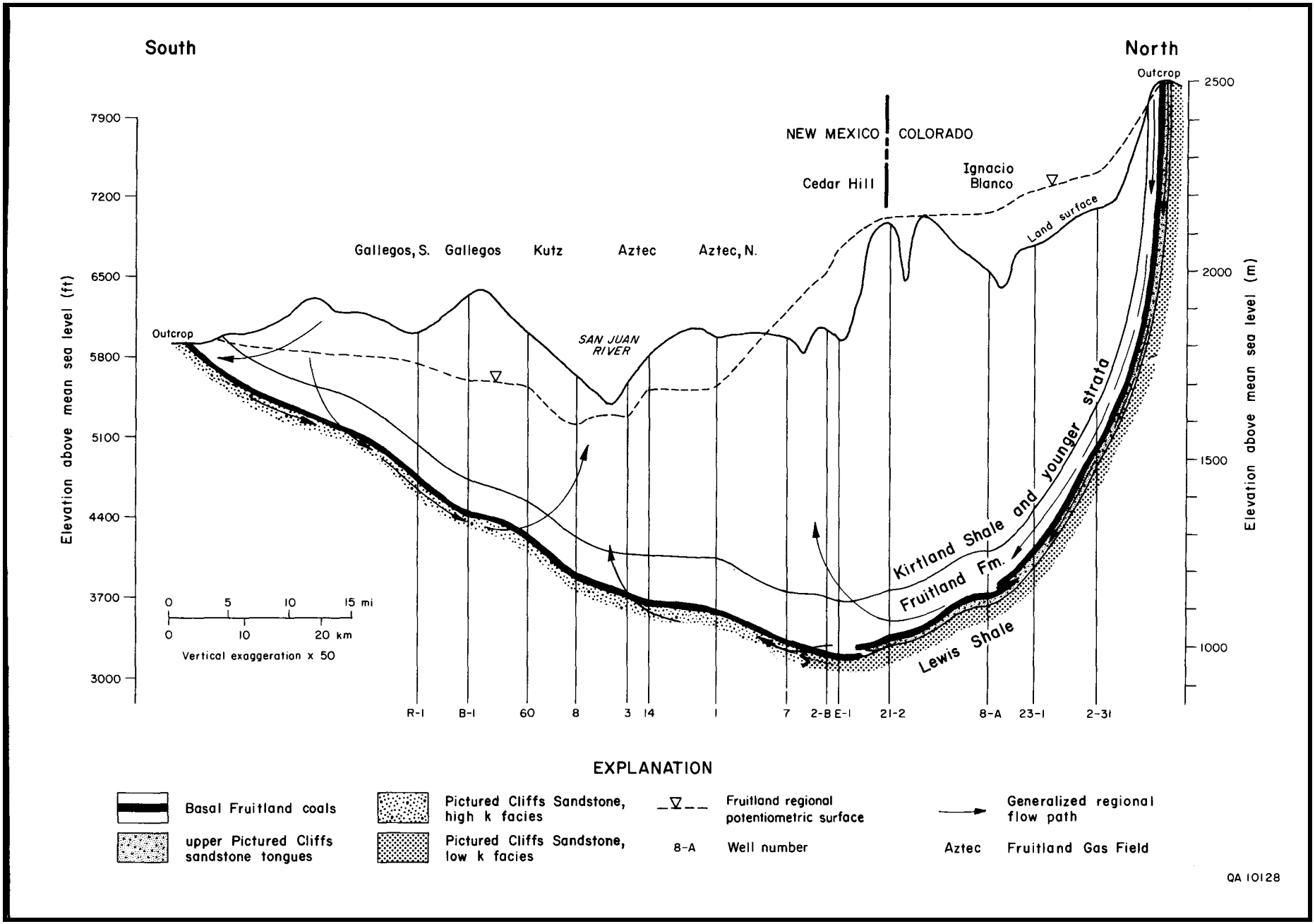

FIGURE 8.19—Schematic of cross-sectional ground-water flow, Fruitland-Pictured Cliffs aquifer system (modified from Kaiser and Swartz, 1988). See Fig. 8.1 for line of section. Basal Fruitland coal seams pinch out in vicinity of Cedar Hill field between wells 21-2 and E-1 and upward flow is initiated at this point. In the north, the potentiometric surface is above and independent of land surface, indicating artesian overpressured conditions. The southern outcrop is a discharge area.

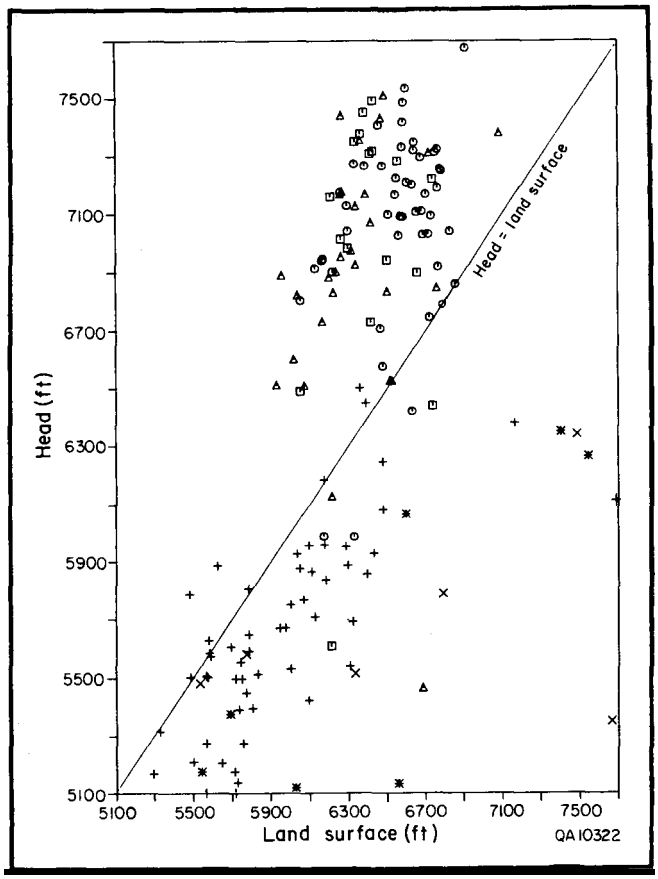

FIGURE 8.20—Fruitland fresh-water equivalent head versus land surface (from Kaiser and Swartz, 1988). Geometric symbols for north-central part of basin, stick symbols for west-central part of basin. In the north, independence of head and land surface indicates artesian conditions, whereas in the southwest, dependence indicates cross-formational flow.

In the southern part of the basin, major upper Pictured Cliffs sandstone tongues are absent, and the Fruitland Formation rests conformably on the Pictured Cliffs Sandstone. Heads and hydrochemistry in the basal coal beds and Pictured Cliffs Sandstone are similar; the waters of both are dominantly Na-Cl type with similar salinities. In the San Juan River valley, Pictured Cliffs heads are similar to or slightly greater than those of the Fruitland. Elsewhere, in the west-central part of the basin, Pictured Cliffs heads are slightly less or about equal to Fruitland heads, indicating a single aquifer system. Thus, hydraulic communication between the basal Fruitland coal beds and Pictured Cliffs Sandstone is inferred from their similar heads and water chemistry. This communication accounts for occasional water production in wells completed in the basal coal. However, in the southeastern part of the basin, where Pictured Cliffs heads are as much as 700 ft (213 m) lower than Fruitland heads, the two units are hydraulically separate. Consequently, in the west-central part of the basin, the Fruitland—Pictured Cliffs aquifer system consists of the basal Fruitland Formation (mainly coal beds) and the Pictured Cliffs Sandstone (Fig. 8.19); it is underpressured and transmits ground water from the northeast and southeast for eventual discharge to the San Juan River. Upward cross-formational flow is centered on the San Juan River valley, where the potential for upward flow is indicated by a regional vertical-pressure gradient (~0.60 psi/ft) that is greater than the hydrostatic gradient (Fig. 8.5). At the basin's southern margin, downward flow occurs across the Kirtland Shale as discharge to the outcrop and as recharge basinward to the confined aquifer system (Fig. 8.19). The plot of head versus land surface (Fig. 8.20) shows correlation of head and land surface, indicating a partially confined aquifer experiencing gravity-driven cross-formational flow (Tóth, 1978).

Abnormal formation pressure

The Fruitland Formation is characterized by an overpressured area surrounded by a much larger underpressured area (Fig. 8.7). Factors that contribute to under-pressuring are reduced temperature, uplift, and erosion (Bradley, 1975), heterogeneous permeability, and better hydraulic connection to the discharge area than to the recharge area (Belitz and Bredehoeft, 1988). Overpressuring indicates increased temperature, basinal subsidence, compaction, and hydrocarbon generation or artesian conditions.

Temperature reduction is an important cause of abnormal pressure, especially underpressuring (Bradley, 1975), which in the San Juan Basin can be explained in the context of basin evolution. During the Oligocene Epoch the Fruitland Formation was buried under approximately 9,000 ft (2,743 m) of sediment and subjected to igneous intrusion. Overpressuring developed in response to burial and intense hydrocarbon generation. Following the Oligocene thermal event, basinwide deterioration to an underpressured state occurred after uplift and erosion (Bond, 1984).

An example illustrates evolution of the basinal pressure regime. First, assume that the Oligocene overpressured gradient was a realistic 0.80 psi/ft; formation pressure at 9,000 ft (2,743 m) would have been 7,200 psi. Next, assume the formation was sealed and that 6,000 ft (1,829 m) of sediment was eroded in post-Oligocene time, yielding a burial depth similar to that of today (3,000 ft [914 m]). Finally, using today's temperature gradient (1.9°F/100 ft [1.1°C/30 m]), an assumed pressure change of 75 psi/°F, and a hydrostatic gradient of 0.433 psi/ft, one can calculate the pressure gradient per foot of depth change according to Bradley (1975):

$$\Delta PG_f - \Delta PG_h = PG_{\Delta d} \qquad (8.1)$$

$$(0.019°F/ft \times 75\ psi/°F) - 0.433\ psi/ft = 0.992\ psi/ft$$

This corresponds to a pressure reduction of 5,952 psi (6,000 ft x 0.992 psi/ft) due to temperature reduction, uplift, and erosion. Predicted formation pressure is 1,248 psi (7,200 psi – 5,952 psi), 51 psi less than hydrostatic pressure at 3,000 ft (1,299 psi), and underpressured as observed throughout most of the basin.

Fruitland overpressuring is not an artifact of Oligocene hydrocarbon generation and overpressuring, or a fossil geopressure; it is thought to represent a repressuring event of probable Pliocene age that occurred after basinwide deterioration to an underpressured state. It is postulated here that repressuring occurred during the mid-Pliocene in response to establishment of the basin's present topography and hydrodynamics (Kelley, 1955b; Berry, 1959). Thus, overpressuring is attributed to artesian conditions; that is, to an elevated recharge area on the basin's northern margin and to aquifer confinement and basinward pinchout (Fig. 8.19). Hydraulic head is elevated, raising pressures down hydraulic gradient well above the hydrostatic gradient so that head rises above land surface (overpressured). This interpretation is supported by the fact that overpressuring is adapted to the present-day geomorphology and not to the basin's tectonic axis (Ayers and others, this volume, Fig. 2.5) or most thermally mature area (Scott and others, this volume, Fig. 9.3). The overpressured area lies north and west of the basin axis, extends northward to the recharge area at the basin rim, and coincides with the presence of flowing wells. Most of the overpressured area lies south of

the area of highest vitrinite reflectance and only partially overlaps the highest rank coals. The pressure transition parallels the 0.78 isoreflectance line (boundary between high volatile A and B bituminous) on the southwest but is discordant to isoreflectance in the remainder of the basin (Scott and others, this volume, Fig. 9.3). Disparity between overpressuring and the inferred region of maximum Oligocene gas generation is not surprising because today's formation temperatures are too low to generate gas (Spencer, 1987). Moreover, overpressure coincides with modern hydrologic elements such as the freshest (low-chloride) formation waters (meteoric water) (Figs. 8.7, 8.15, and 8.18) and distribution of aquifer coal seams and upper Pictured Cliffs sandstone tongues (Ayers and others, this volume, Fig. 2.15).

Cross-sectional modeling

Regional ground-water flow was modeled in a cross section across the San Juan Basin to further conceptualize ground-water flow and to elucidate cross-formational flow. Numerical modeling, a logical extension of head, pressure, and hydrochemical mapping, was used to test assumptions about ground-water circulation patterns, causes of abnormal pressuring, and regional permeability contrasts made from potentiometric-surface and pressure-gradient maps (Figs. 8.1 and 8.6) and from stratigraphic cross sections (Ayers and others, this volume, Figs. 2.2 and 2.3). Modeled strata include the Pictured Cliffs Sandstone and all younger strata. FREESURF (Neuman and Witherspoon, 1970), a two-dimensional, steady-state flow model, was used to solve the equation describing ground-water flow in porous media. Specifically, our objective was to better understand Fruitland hydrodynamics by simulating potentiometric anomalies and abnormal pressuring.

Hydrostratigraphy

The ground-water flow model was constructed from geophysical logs along a 90-mi (145-km), north-south cross section in the western San Juan Basin oriented nearly perpendicular to the head contours, or parallel to the inferred flow path (Fig. 8.1). Hydrostratigraphic boundaries follow the stratigraphy of Ayers and others (this volume, Chapter 2) and were chosen on the basis of hydrologic characteristics and log response. Three major Cretaceous hydrostratigraphic units (Pictured Cliffs Sandstone, Fruitland Formation, and Kirtland Shale) and two Tertiary units (Ojo Alamo Sandstone and undivided Tertiary) were defined.

The base of the Pictured Cliffs Sandstone is defined on geophysical logs as the base of upward-coarsening log patterns above the Lewis Shale. Its top is directly below the lowest Fruitland coal seams. Northern and southern Pictured Cliffs units are defined on the basis of permeability. On the northern limb of the basin, upper Pictured Cliffs sandstone tongues are included in the Pictured Cliffs Sandstone, but basinward, where the basal Fruitland coal is thick, a separate basal coal/upper Pictured Cliffs Sandstone unit is defined. The Fruitland Formation was divided for modeling into three units. In the lower Fruitland Formation, northern and southern coal units containing coal, sandstone, and shale are defined. The northern coal unit contains numerous, thick, continuous coal seams, whereas the southern coal unit contains fewer, thinner, and less continuous coal seams. Consequently, the northern coal unit is assigned a higher permeability than the southern unit. The upper Fruitland Formation is defined as a sandstone unit, composed mainly of sandstone and shale. The Kirtland Shale was divided into three units: lower Kirtland Shale, Farmington shale and sandstone unit, and upper Kirtland Shale. The Farmington unit is a sequence of interbedded shale and thin sandstones (Ayers and others, this volume, Fig. 2.1). The Ojo Alamo Sandstone unconformably overlies the Kirtland Shale and is defined by its blocky log pattern. The Ojo Alamo formation is continuous throughout the southern part of the basin but is indistinguishable from other Tertiary units in the northern part. The undivided Tertiary includes the Nacimiento-Animas Formations and San Jose Formation, which consist of alluvial sandstones and mud-stones. The Nacimiento and Animas Formations are strati-graphic equivalents and are considered a single hydrostratigraphic unit (Stone and others, 1983; Phillips and others, 1989); this unit is overlain by the San Jose Formation.

Computer program

The ground-water flow model was implemented with FREESURF, a computer program developed by Neuman and Witherspoon (1970). FREESURF solves the partial differential equation describing two-dimensional steady-state flow through porous media:

$$\frac{\partial}{\partial x}\left(K_x \frac{\partial h}{\partial x}\right) + \frac{\partial}{\partial z}\left(K_z \frac{\partial h}{\partial z}\right) = 0 \qquad (8.2)$$

using a finite-element method and noniterative Gaussian elimination scheme (variational method of Rayleigh-Ritz). FREESURF computes hydraulic head at each node and calculates fluxes (recharge and discharge) along a prescribed head boundary; it was modified to compute stream functions (streamlines) and Darcy velocities (Fogg and Senger, 1985; Senger and others, 1987; Senger, 1989) to show groundwater flow patterns and fluxes. These are difficult, if not impossible, to establish from contour maps of computed hydraulic heads, because of permeability anisotropy and extreme vertical exaggeration on cross-sectional models.

FREESURF output was evaluated using three plotting routines developed by R. K. Senger of the Bureau of Economic Geology (pers. comm. 1990). One routine contours hydraulic head and delineates the pressure regime. Another plots velocity vectors to show direction and rate of flow. The third routine uses velocity and a unit thickness of 1 ft (0.3 m) to plot stream tubes that show magnitude of flow for consequent delineation of the most transmissive units.

Modeling

The finite-element mesh was designed to represent the cross-sectional model's hydrostratigraphy and basin geometry (Fig. 8.21). The steep northern limb was constructed by manually projecting modeled units updip from the northernmost geophysical log to the outcrop along a section parallel to the lateral flow direction inferred from the head map (Fig. 8.1). The southern limb was similarly constructed, but along a section oblique to flow direction, into an area having values of Fruitland static-water levels.

The model's lower boundary is the contact between Pictured Cliffs Sandstone and Lewis Shale, a thick 600-ft (183 m) marine shale and regional confining unit. This contact is modeled as a no-flow boundary (Fig. 8.21). The model's upper boundary is the water table in the undivided Tertiary. To establish the water table, a topographic profile was made along the model's line of section, and static-water levels in the vicinity of the section were documented from the literature to constrain depth below land surface. In the absence of water-level data, the water table was approximated by assuming that it is a subdued replica of the topography. Where the section crosses perennial rivers, the water table was set to their surface elevation. The water table is a con-

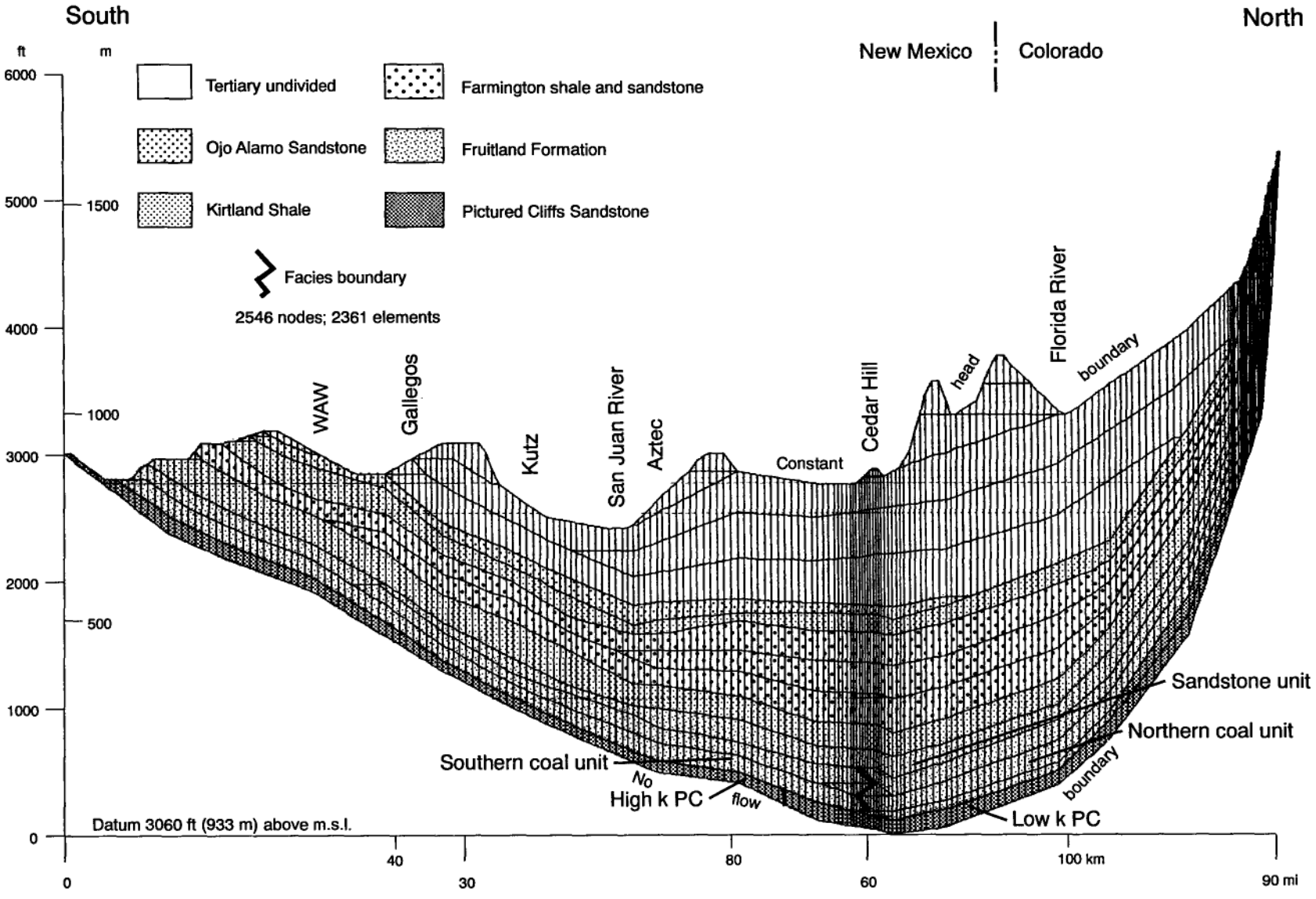

FIGURE 8.21—Finite-element mesh of major hydrogeologic units above the Lewis Shale, San Juan Basin. Units are assigned permeabilities that vary among simulations. The upper surface is a constant head boundary corresponding to the water table. The lower surface is a no-flow boundary corresponding to the contact between the Pictured Cliffs Sandstone and Lewis Shale. Vertical exaggeration 50×. See Fig. 8.1 for line of section.

stant head boundary for the model simulations and a prescribed flux boundary for investigation of recharge and discharge.

The finite-element mesh was constructed (discretized) by passing vertical lines through the cross section and lateral lines parallel to hydrostratigraphic boundaries. Vertical lines are approximately 0.5 mi (0.8 km) apart, except at the regional facies change and on the basin's steep northern limb. Additional verticals were added in those areas to ensure more accurate modeling of flow. Additional lateral lines were placed parallel to hydrostratigraphic boundaries to subdivide the units more uniformly and to decrease their thickness for more accurate modeling. The intersection of vertical and lateral lines defines 2,546 nodes, which in turn enclose the model's 2,361 elements (Fig. 8.21).

Model limitations

The largest potential source of error is in the permeability distribution and assumed anisotropies of hydrostratigraphic units. Only meager permeability data are available, which indicate low permeabilities (0.1 to 10 md) in the Fruitland Formation and Pictured Cliffs Sandstone. Permeability of Fruitland coal seams is orders of magnitude greater than that of associated sandstones (Ayers and Zellers, this volume, Fig. 4.5). Moreover, discretization required simplification of the hydrostratigraphy. Complexity at the local scale (Ambrose and Ayers, this volume, Fig. 3.3; Ayers and Zellers, this volume, Fig. 4.17) is far greater than can be depicted in a regional model. The model simulates north-south ground-water flow across the San Juan Basin, which is oblique to the direction of regional flow south of Gallegos (Fig. 8.1). Thus, results of the model may not be directly comparable to observed conditions.

The model assumes steady-state conditions; that is, groundwater flow pattern and velocity do not change with time and are governed by basin geometry, topography, and permeability distribution. The present flow system was established in the mid-Pliocene upon establishment of the basin's present topography. Uplift, erosion, and retreat of the basin margins since then have been limited and have had minor effect on the flow system. One possible cause of transient conditions is extensive hydrocarbon production from the Pictured Cliffs Sandstone and subsequent decline of reservoir pressure below virgin conditions.

Although Darcy's law assumes flow through porous media, the strata in this model have low matrix permeability and are fractured. Fracture flow dominates in coal beds. Nevertheless, because the Fruitland coal beds are pervasively fractured (cleated), they should behave regionally as a porous medium. Sandstone, however, is discretely fractured (Tremain and others, this volume, Chapter 5), and local fracture flow is possible if fracture permeability exceeds matrix permeability.

Another limitation of the model is the assumption of a homogeneous fluid (fresh water) throughout the basin, which neglects effects of variable density and temperature. A denser, more viscous fluid basinward would result in a decrease of hydraulic conductivity, which influences flow rates linearly. TDS content of formation waters increases basinward along the cross section, but does not exceed 35,000 mg/L. Because hydraulic gradients are steep, topographically driven flow undoubtedly dominates buoyancy-driven flow associated with these slightly denser formation waters (Senger, 1990). Thus, density and viscosity effects are probably minimal and may even be balanced by a basinward increase in temperature. Other factors that may affect the model are the assumption of no flow into or out of the Lewis Shale and no consideration of flow perpendicular to the cross section.

Model simulations

The simulations investigated the relative importance of such factors as permeability anisotropy and confinement on ground-water flow in the San Juan Basin. Three simulations are presented here to illustrate the interactions of geology and hydrology that explain the hydrodynamics of the Fruitland-Pictured Cliffs aquifer system. Because of uncertainty about permeability and inherent limitations of the model, simulation design was kept simple to reduce the chance for error and to facilitate interpretation of results. The simplest simulation is model simulation 1, in which all hydrostratigraphic units were assigned the same permeability. In model simulation 2, the Kirtland Shale is a confining unit. The most complex simulation is model simulation 3, where regional permeability contrasts were imposed to approximate observed data. Recharge and discharge were also investigated to further test simulation 3. Permeabilities assigned for each simulation are given in Table 8.4. Flow paths reflect direction and magnitude as determined from plots of flow velocity and stream tubes for each simulation.

Model simulations 1 and 2—In simulation 1, no permeability constraints were imposed. Consequently, gravity-driven, cross-formational flow dominates the entire section (Fig. 8.22). Flow is downward under topographic highs and upward under topographic lows. Note slight underpressuring (deep heads lower than surface heads) at the base of the cross section on either side of the state line. This reflects a lower vertical than lateral permeability, topographic highs in the area, and the absence of confinement. In simulation 2, a low-permeability confining layer (Kirtland Shale) was added to the section, whereas permeability

TABLE 8.4—Model permeabilities and k_h/kv ratios.

Modeled hydrostratigraphic units	Simulation 1 md, k_h/k_v	Simulation 2 md, k_h/k_v	Simulation 3 md, k_h/k_v
Undivided Tertiary	1.0, 100	1.0, 100	10.0, 100
Ojo Alamo Sandstone	1.0, 100	1.0, 100	10.0, 100
Kirtland Shale			
Upper shale unit	1.0, 100	0.01, 1,000	0.01, 100
Farmington shale and sandstone unit	1.0, 100	0.01, 1,000	0.1, 100
Lower shale unit	1.0, 100	0.01, 1,000	0.01, 100
Fruitland Formation			
Sandstone unit	1.0, 100	1.0, 100	0.1, 100
Southern coal unit	1.0, 100	1.0, 100	0.1, 100
Northern coal unit	1.0, 100	1.0, 100	10.0, 100
Basal coal/upper Pictured Cliffs sandstone unit	1.0, 100	1.0, 100	10.0, 100
Pictured Cliffs Sandstone			
Southern Unit	1.0, 100	1.0, 100	1.0, 100
Northern Unit	1.0, 100	1.0, 100	0.1, 10,000

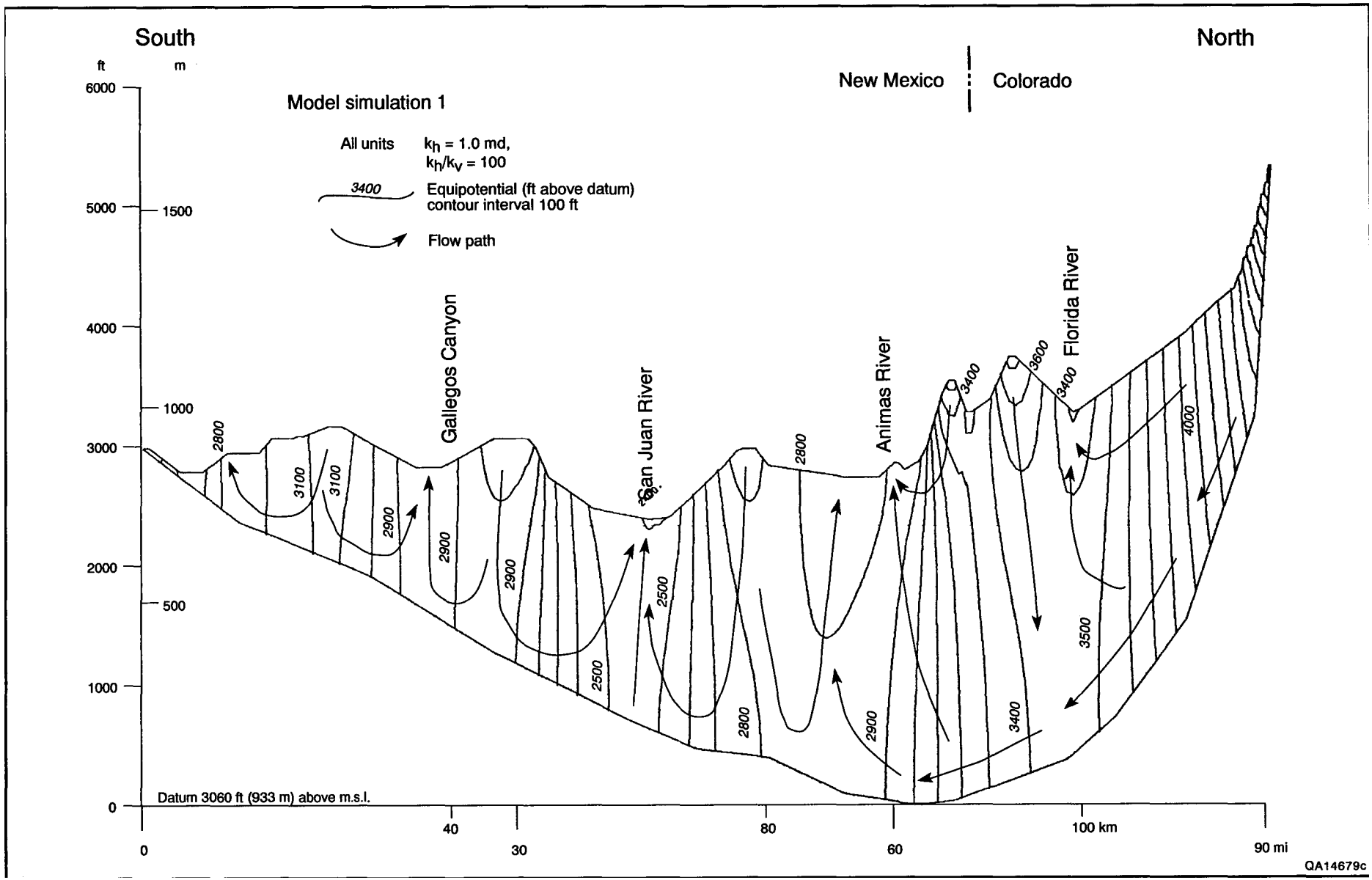

FIGURE 8.22—Equipotentials and generalized flow paths from model simulation 1, San Juan Basin. All units have the same permeability. Gravity-driven cross-formational flow dominates the entire section. Flow is downward under topographic highs and upward under topographic lows.

values in the upper and lower sections were unchanged (Fig. 8.23). The Kirtland Shale in the center of the section separates two flow systems (1) one above, which consists of a series of intermediate flow systems, and (2) one below, which is regional. In this simulation, flow is cross-formational in the upper section, similar to that of simulation 1. Recharge over topographic highs and discharge to topographic lows divide flow into a series of intermediate cells. Minor upward flow occurs across the Kirtland confining layer. In the lower section, ground water enters the basin at the northern margin, flows basinward down the steep northern limb, passes laterally beneath the San Juan River, and exits at the southern margin. Overpressured conditions are simulated and extend nearly across the entire basin. Agreement between simulated and observed heads in the Fruitlan,d Formation is good in the northern part of the basin and poor in the southern part. Note that the hydraulic gradient shows no change as flow turns updip (Fig. 8.23), indicating that this is not the cause of the steep Fruitland gradient mapped south of Cedar Hill field (Fig. 8.1).

If vertical permeability is increased from 0.00001 md (k_h/k_v = 1,000 [Table 8.4]) to 0.0001 md (k_h/k_v = 100) in the Kirtland Shale, flow would still be confined but would turn upward at the San Juan River, converging from the north and south. If k_v was 0.001 (k_h/k_v = 10), the Kirtland Shale would no longer be a confining unit, and gravity-induced cross-formational flow would extend across the entire cross section to hydraulically connect all units. A k_v of 0.001 md was too high and permitted vertical connectivity, allowing heads to equalize in the vertical direction. Flow increases because the cross-sectional area through which vertical flow can take place is large compared with that available for horizontal flow.

Model simulation 3—In simulation 3, we calibrated the model in order to yield good agreement between computed and observed data. To approximate observed Fruitland heads, we imposed permeability contrasts that were inferred from the head map (Fig. 8.1) and stratigraphic studies (Ambrose and Ayers, this volume, Chapter 3; Ayers and others, this volume, Chapter 2). Permeabilities assigned to the hydrostratigraphic units are consistent with available permeability data.

Flow patterns in Tertiary strata, despite an increase in lateral permeability from 1.0 to 10 md (Table 8.4), differ little from those in simulation 2 (Figs. 8.23 and 8.24). Flow in these strata is separated from that in the lower section by the Kirtland Shale. Plots of velocity vectors and streamlines show that ground-water flow is concentrated in the permeable Tertiary section. The Fruitland-Pictured Cliffs aquifer system is insulated in the north and is in poor communication with Tertiary strata on the south, experiencing minor cross-formational flow. Only on the southern end of the section, where strata approach the outcrop, does appreciable flow move downward across the Kirtland Shale into the Fruitland-Pictured Cliffs aquifer. Correlation of Fruitland heads and land surface in the southern part of the basin indicates a poorly confined aquifer with substantial cross-formational flow (Fig. 8.20). The southern outcrop is a discharge area. Consequently, on the southern margin of the basin, recharge occurs by vertical leakage through Tertiary strata rather than by infiltration at the outcrop.

In the absence of a permeability barrier, hydraulic gradient in the Fruitland-Pictured Cliffs is uniform across the basin (Fig. 8.23). When the barrier is imposed in the vicinity of Cedar Hill field, where thick, lower Fruitland aquifer coals pinch out, the model simulates flat and steep potentiometric surfaces, consistent with those mapped at Cedar Hill (Fig. 8.1), and Fruitland hydraulic heads are close to the observed values (Fig. 8.24). The steep hydraulic gradient is located downgradient of the permeability barrier in low-permeability strata and reflects a modeled permeability contrast of two orders of magnitude between the northern and southern coal units across the barrier (Table 8.4). Groundwater flow turns steeply upward at this point and is mainly upward across the Kirtland Shale to the Animas River in the Cedar Hill area rather than to the San Juan River. Upward flow across the Kirtland to the San Juan River, a consequence of regional discharge to the river, is negligible (Oldaker, 1991). Thus, the flattened potentiometric surface north of the barrier probably reflects higher permeability and diversion of lateral flow upward. Most flow in the lower section is concentrated in the northern coal unit, which has permeabilities that are orders of magnitude greater than those of the sandstone units (Table 8.4).

Abnormal pressuring in the Fruitland Formation is simulated by modeling the permeability barrier as a regional facies boundary or fault zone. Assuming a facies change, the Fruitland is significantly overpressured in the north (Fruitland heads well above land surface). Overpressuring requires high permeability in the Fruitland Formation (10 md), confinement by the Kirtland Shale, and recharge at an elevated outcrop. In the southern part of the basin, regional underpressuring requires limited recharge at the basin's southern margin (it is actually a discharge area), low permeability in the Fruitland (0.1 to 1.0 md), poor hydraulic connection with the northern recharge area, and insulation from Tertiary water-table aquifers by the Kirtland Shale. The model simulates slightly underpressured, slightly overpressured, and normally pressured conditions in the south that require a permeability barrier in the Fruitland Formation at the basin's center to achieve hydraulic insulation from northern recharge. Slight overpressure reflects convergent, upward flow under topographic lows such as to the San Juan River valley, whereas underpressure occurs under topographic highs. Normal pressure is expected where there is communication with Tertiary aquifers, such as on the basin's southern margin.

The regional transition from overpressured to under-pressured conditions may be wider than mapped; the modeled pressure transition is regionally in the correct position, but shifted slightly southwest of the mapped transition (Figs. 8.7 and 8.24). A few overpressured wells are present in the underpressured area. This may reflect interbedding of overpressured and underpressured coal seams, or seams connected and disconnected from the regional aquifer system, as expected in a transition zone. Discontinuity is also evident in the hydrochemistry of neighboring wells that have chemically disparate formation waters.

Offset of aquifer coals by faults may also be a barrier to lateral flow (Ambrose and Ayers, this volume, Fig. 3.3). Faulting was simulated in the Cedar Hill area by imposing a low-permeability barrier (0.1 to 0.01 md) of variable width (2.5 to 7.0 mi [4 to 11 km]) between the northern and southern coal units and increasing the permeability of the southern coal unit. Permeability of the northern coal unit was not changed, and its heads were unchanged in these simulations. At 1.0 md permeability, underpressuring in the south expanded under topographic highs—a better fit to observed conditions, whereas heads under the San Juan River valley were much higher than observed. Hydraulic gradients also became gentler. When the permeability of the southern coal unit was increased to 10 md, overpressure was simulated from the barrier south to Gallegos (Fig. 8.24), and there was essentially no hydraulic gradient across the southern half of the basin. Only locally under topographic highs was underpressuring simulated. Explicit in the modeling is the need for low-permeability strata in underpressuring. In all cases, the simulated hydraulic gradient was very steep within the barrier and gentler than that observed to the south.

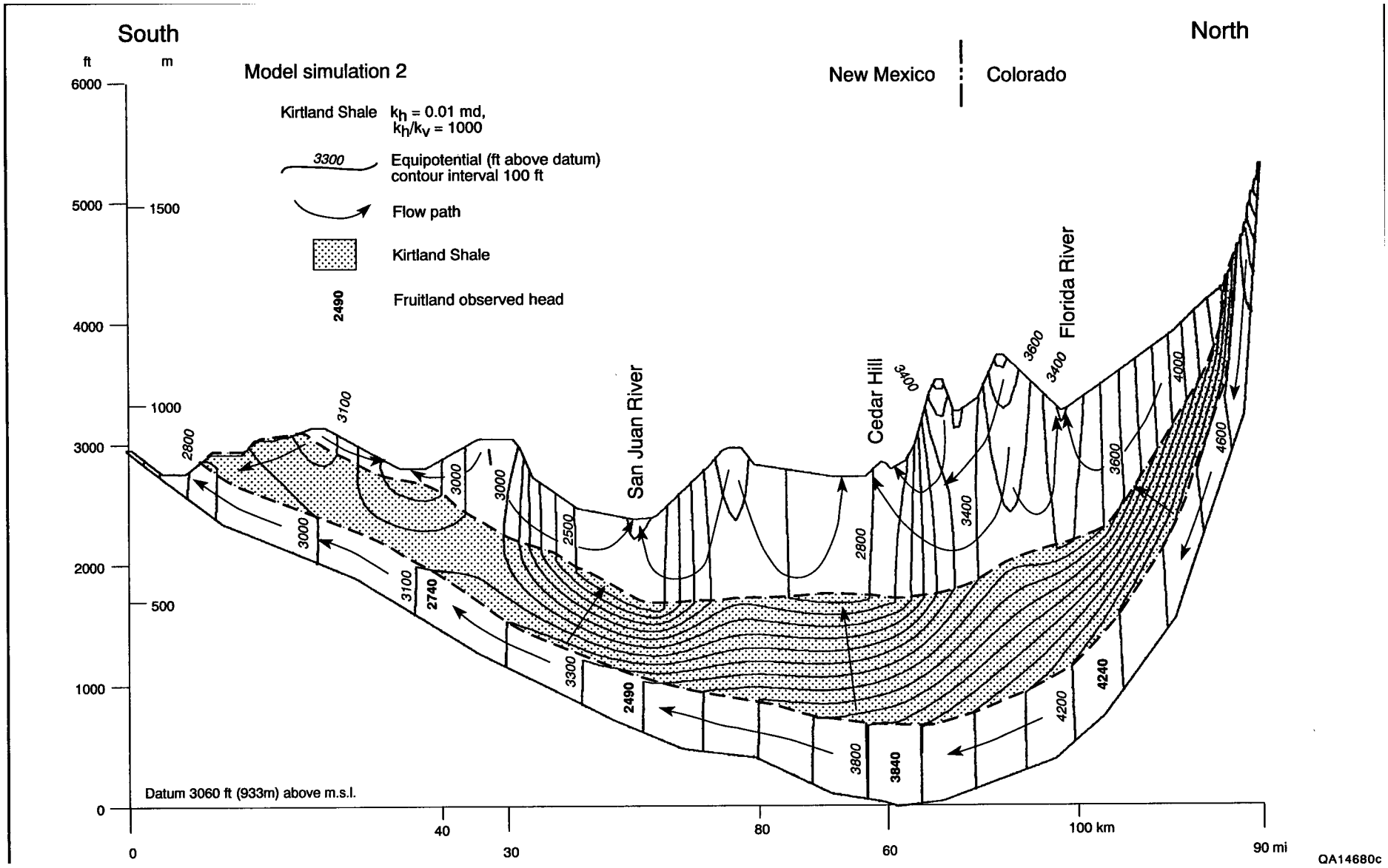

FIGURE 8.23—Equipotentials and generalized flow paths from model simulation 2, San Juan Basin. Kirtland Shale is an aquitard. Flow in Tertiary strata is cross formational, whereas that in the Fruitland Formation is lateral (confined). Ground water enters the basin at the northern margin, flows across the basin, and exits at the southern margin. Overpressure extends almost across the entire basin. Note the close agreement between simulated and observed heads in the northern part of the basin.

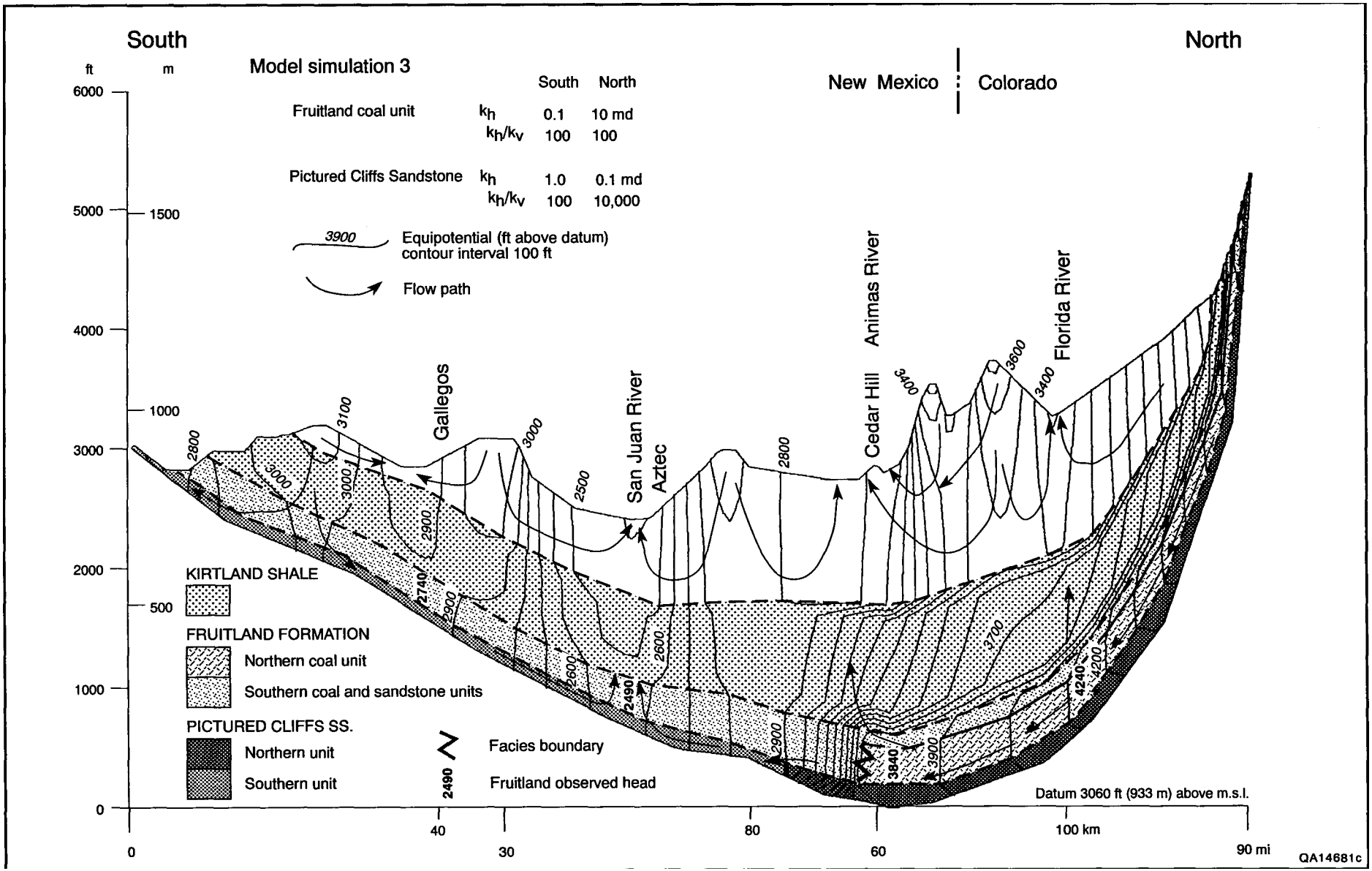

FIGURE 8.24—Equipotentials and generalized flow paths from model simulation 3, San Juan Basin. ln the Cedar Hill area, a permeability barrier is imposed in the Fruitland Formation. Consequently, the hydraulic gradient is steep. Flow in the northern coal unit turns steeply upward at this point. South of the transition, flow is mainly in the basal Fruitland coal and Pictured Cliffs Sandstone. The southern margin of the basin is a discharge area. Slight overpressuring is simulated in the San Juan River valley, consistent with observation. Pictured Cliffs overpressuring is simulated in the north, contrary to observation.

Abnormal pressuring is also simulated in the Farmington shale and sandstone unit on the basin's northern limb (Fig. 8.24). Overpressure in the Farmington has not been, reported, and data are unavailable to assess that prediction. However, assuming sandstone interconnectedness, it is not an unreasonable prediction, given an elevated northern outcrop and confinement between shales.

The model shows overpressured Pictured Cliffs Sandstone in the northern part of the basin and only slightly lower heads than those in the overlying Fruitland Formation, contrary to observed conditions. A combination of conditions may explain this phenomenon. Nonattainment of static reservoir conditions during short-term well testing of low-permeability strata would result in apparent under-pressuring. Thus, the main Pictured Cliffs Sandstone, although underpressured, may not be as underpressured as available pressure data indicate. Similarity of observed heads in the Fruitland Formation and upper Pictured Cliffs sandstone tongues indicates hydraulic communication between these units. Thus, the model simply reflects the fact that the Fruitland Formation and Pictured Cliffs Sandstone were modeled in communication. The presence of a thin aquiclude between them is possible but was not modeled.

In the Pictured Cliffs Sandstone, hydraulic gradient dramatically steepens, as in the Fruitland Formation, at a permeability facies boundary imposed between low- and high-permeability units in the central part of the basin (Fig. 8.24; Table 8.4). Its presence is inferred from the literature (Meissner, 1984), head data, and log analysis. The hydraulic gradient here steepens upgradient in low-permeability sandstone, and simulated Pictured Cliffs heads are slightly above Fruitland heads, contrary to observations. Perhaps transient conditions are reflected in the observed data because extensive hydrocarbon production from the Pictured Cliffs Sandstone has caused pressure depletion and thus present pressures are less than those modeled under steady-state conditions. If the facies boundary is moved northward, closer to the Fruitland facies boundary, the hydraulic gradient in the Fruitland Formation becomes gentler. If the Pictured Cliffs facies boundary is moved southward, there is little effect on flow because the two facies boundaries are too far apart to interact. Southwest of the Pictured Cliffs facies boundary, heads drop and flow is focused in the higher permeability Pictured Cliffs Sandstone (Fig. 8.24). Plots of velocity vectors and streamlines show that groundwater flux is slight and concentrated in the Pictured Cliffs Sandstone and basal Fruitland coal seams. For the most part, the Fruitland Formation is an aquitard in the southern part of the basin (Stone and others, 1983).

Clearly, simulation 3 shows that permeability contrasts are critical to describing ground-water flow in the San Juan Basin. Furthermore, modeling showed that flow is particularly sensitive to vertical permeability. Thus, well productivity may depend as much on vertical as on horizontal permeability. For example, vertical-permeability values less than 0.1 md caused a dramatic decrease in simulated heads relative to observed heads in the northern coal unit, whereas at higher values there was only a minor increase in simulated heads. A vertical permeability in the Kirtland Shale of 0.0001 md was required to achieve confinement without a large increase or decrease of Fruitland heads relative to observed heads. In the southern part of the basin, a decrease in Kirtland permeability expanded the area of under-pressure and caused higher heads under the San Juan River valley. An unrealistically low vertical permeability in the northern Pictured Cliffs Sandstone was required to simulate heads less than those in the Fruitland Formation. Finally, higher lateral permeabilities (>1.0 md) in the Pictured Cliffs Sandstone caused heads to decrease in the northern coal unit.

Recharge and discharge

To further evaluate the cross-sectional model's approximation of observed data, recharge and discharge were calculated along its upper boundary at the constant potential nodes of the water table. FREESURF makes the calculations such that the amount of recharge to and discharge from the cross section is equal. Calculations were also made under prescribed flux boundaries to investigate the effect of recharge on the pressure regime. Recharge and discharge were calculated for the permeability distribution of model simulation 3.

Recharge rates in the San Juan Basin range from 1 to 4% of annual precipitation (Roybal and others, 1983; Mattick and others, 1987). A rate of approximately 1% was calculated from chloride mass balance in arid areas near Socorro and Las Cruces, New Mexico (Mattick and others, 1987), where annual precipitation is less than 9 inches/yr (23 cm/ yr) and less than the amount received in the northern part of the basin. Rates higher than 1% are predictable for the topographically higher and wetter northern part of the basin, which receives 20 to 30 inches/yr (51 to 76 cm/yr) precipitation. Phillips and Tansey (1984) postulated that most of the recharge in the San Juan Basin occurs at high elevations during the cool, wet, winter months of December through March.

In simulation 3, most of the constant potential nodes were discharge points of less than 0.1 inch/yr (<0.25 cm/yr) in topographic lows and on lower slopes of topographic highs. Highest discharge rates were from the outcrop of the Fruitland northern coal unit (>0.9 inch/yr [>2.3 cm/yr]) and where perennial rivers (Florida, Animas, and San Juan) intersect the cross section (>0.1 inch/yr [>0.25 cm/yr]). Recharge nodes were located on topographic highs and on their upper slopes. Recharge rates over the highs ranged from 0.1 to 0.6 inch/yr (0.25 to 1.5 cm/yr), or 0.5 to 3% of an annual precipitation rate of 20 inches/yr (51 cm/yr) and 0.33 to 2.0% of a rate of 30 inches/yr (76 cm/yr). Recharge rates as high as 2.5 inches/yr (6.4 cm/yr) occur in the outcrop of the northern coal unit. When recharge and discharge rates in the northern coal unit were summed, the net recharge rate was 0.4 inch/yr (1.0 cm/yr), or 2% of a 20—inch (51—cm) annual precipitation.

Finally, simulations were made that varied recharge rates to evaluate their effect on overpressuring. To evaluate the amount of recharge required to overpressure the Fruitland Formation, the rate of recharge to the Fruitland outcrop was varied, while no recharge was permitted to the Kirtland Shale and Pictured Cliffs Sandstone. Recharge rates as low as 0.05 inch/yr (0.13 cm/yr) (0.25% of 20 inches/yr [51 cm/ yr]) simulated overpressuring, suggesting that overpressuring does not require extraordinary recharge rates. Even though no recharge was permitted to the outcrop of the Pictured Cliffs Sandstone, it was overpressured. The Fruitland Formation and Pictured Cliffs Sandstone were modeled in hydraulic communication. Consequently, the Fruitland Formation must be leaky to the Pictured Cliffs. It is possible that the Pictured Cliffs Sandstone is slightly overpressured or at least only slightly underpressured and that true reservoir pressures are obscured in short-term well testing by its low permeability. Underpressure may represent transient conditions associated with low permeability.

Conclusions

1. In the Fruitland Formation, recharge is mainly along the northern margin of the basin, where aquifer coal seams crop out in the foothills of the San Juan Mountains; recharge is limited at the eastern, southern, and western margins because of low rainfall, a topographically low outcrop, and poor aquifer quality. The potentiometric surface is highest

near the recharge area; in the north-central part of the basin, the surface flattens nearly coincident with the distribution of thick Fruitland coal seams, the primary aquifers. Regionally, lateral ground-water flow converges from the northeast and southeast toward the San Juan River valley.

2. The Fruitland Formation is regionally overpressured (0.44 to 0.63 psi/ft) in the north-central part of the basin (BHPs 1,200 to 1,900 psi) and underpressured (0.30 to 0.40 psi/ft) in the remainder of the basin (BHPs 400 to 1,200 psi). Overpressuring is attributed to artesian conditions, which explains the need to dewater coalbed methane wells in the northern part of the basin. Underpressuring is due to basinal uplift, erosion, and cooling following the Oligocene thermal event. Underpressure endures in the southern part of the basin because it is insulated from Tertiary water-table aquifers and the northern recharge area by low-permeability rocks.

3. Fruitland waters are chemically diverse, reflecting their hydrologic setting rather than the producing lithology. Low-chloride, high-bicarbonate ($Na\text{-}HCO_3$) waters coincide with overpressure, and high-chloride, saline (Na-Cl) waters coincide with underpressure. Consequently, hydrochemistry cannot be used to identify completion lithology. The northern waters are evolved meteoric waters rich in bacterially derived HCO_3-, whereas southern waters are modified marine waters. Because of high-bicarbonate contents in Fruitland waters, scaling by carbonate minerals during production and plugging of perforations and artificial permeability upon injection are expected.

4. In the northern San Juan Basin, the Fruitland Formation and upper Pictured Cliffs sandstone tongues form a hydrostratigraphic unit in which coal seams are the primary aquifers. Fruitland coal beds and sandstones are in regional hydraulic communication. Large vertical and lateral pressure gradients indicate local compartmentalization. The Fruitland Formation and main Pictured Cliffs Sandstone are hydraulically separate. In the southern part of the basin, the basal Fruitland coal and Pictured Cliffs Sandstone form a hydrostratigraphic unit. Primarily, the Fruitland is an aquitard in the south, accounting for water-free gas production in that part of the basin.

5. The regional cross-sectional model simulates hydraulic heads and gradients, potentiometric anomalies, abnormal pressure, and recharge rates observed in the Fruitland Formation. The model requires large ratios of horizontal to vertical permeability (k_h/kv) to simulate observed heads and is very sensitive to this ratio. Vertical permeability is an important but overlooked flow parameter in the production of coalbed methane. Modeled potentiometric anomalies reflect regional permeability contrasts. Enhanced and reduced permeability can be inferred from gentle and steep hydraulic gradients, respectively. Barriers to lateral flow (facies changes and/or faults), rather than topography, are the most important causes of upward flow. Areas of upward flow correspond to potentiometric mounds. Abnormal pressure is a consequence of steady-state regional ground-water flow. In the northern part of the basin, overpressure is simulated, affirming its hydrodynamic origin. The degree of under-pressure in the southern part of the basin may be more apparent than real because of low permeability.

6. Hydrologic elements define an aquifer's ability to accept and transmit fluid; hence, they are indicators of permeability. Enhanced permeability in the Fruitland Formation is inferred from gentle hydraulic gradients, overpressure, and low-chloride formation waters. Permeability is inferred to be enhanced where the potentiometric surface is flat and reduced where it is steep. Overpressuring requires enhanced permeability and, because overpressure reduces effective stress, the permeability of coal is increased. Underpressure in the Fruitland is an indicator of low permeability and insulation from recharge; strata too tight to accept and transmit measurable recharge remain under-pressured. In the north, the presence of low-chloride, meteoric waters indicates an active, dynamic flow system and permeable pathways. In the south, the presence of modified marine water implies low permeability or limited recharge or both. The distributions of potential energy (head) and mass (dissolved solids) identify regional ground-water flow paths and indicate permeability anisotropy.

Acknowledgments

John McCord collected DST data and static water levels, and A. H. Scanlon collected pressure data. R. K. Senger's assistance in the implementation of FREESURF was invaluable. We thank Amoco Production Company, Blackwood & Nichols Co., Ltd., and Giant Exploration & Production Company for allowing water sampling of their wells and the logistical support in collecting those samples. Discussions with R. S. Fisher, Y. K. Kharaka, and L. S. Land strengthened interpretation of the geochemical data. The manuscript was reviewed by R. W. Baumgardner, W. A. Ambrose, W. B. Ayers, Jr., and Ken Belitz. Their reviews tightened the presentation and improved the content.

9. Thermal maturity of Fruitland coal and composition of Fruitland Formation and Pictured Cliffs Sandstone gases

A. R. Scott, W. R. Kaiser, and W. B. Ayers, Jr.
Bureau of Economic Geology

Abstract—Fruitland coal rank largely reflects the structural configuration of the San Juan Basin except the northern part. Coals north of the basin axis are structurally higher than lower rank coals south of the axis. Coal rank and hydrodynamics control the composition and distribution of coalbed gases. Carbon dioxide content of coalbed gases ranges from less than 1 to more than 13%; C_1/C_{1-5} values range from less than 0.80 to 1.00. In most parts of the basin, Fruitland coalbed, Fruitland sandstone, and Pictured Cliffs sandstone gases cannot be distinguished by composition alone. Hydrogen-rich Fruitland coal produces chemically wet gases in the southern part of the basin. Gas compositional distributions and isotopic data suggest that some methane and carbon dioxide produced from coal beds in the northern basin have a mixed secondary biogenic and thermogenic origin.

Introduction

The process of coalification encompasses the physical and chemical changes affecting peat and coal during burial and diagenesis. The degree of coalification, or coal rank, is often determined on the basis of vitrinite reflectance or volatile matter content of coals. With increasing thermal maturity and coal rank, vitrinite reflectance values increase and volatile matter content of the coal decreases. During coalification natural gases are generated from organic matter through biogenic, early thermogenic, and late thermogenic processes. Biogenic methane is produced at relatively low temperatures through the metabolic activity of methanogenic bacteria. Gases in the Fruitland Formation are thought to be mainly thermogenic in origin (Rice, 1983). Early thermogenic gases are formed before and during the main stage of liquid hydrocarbon generation, often referred to as the oil window. Dry thermogenic gases are formed by late thermogenic processes and/or are generated by cracking heavier hydrocarbons formed from sapropelic or hydrogen-rich organic matter during the oil-generating stage. Carbon dioxide and nitrogen are also released from organic matter during thermal maturation. Carbon dioxide is derived from the oxygen-bearing functional groups of the organic matter and is released during decarboxylation stages at relatively low levels of thermal maturity (Stach and others, 1975) before significant quantities of liquid hydrocarbons and thermogenic gases have been generated. At higher temperatures, decarboxylation of organic acids can generate both carbon dioxide and methane (Carothers and Kharaka, 1980). Molecular nitrogen in coalbed gas is probably derived from the oxidation of ammonia (Rohrback and others, 1983) evolved from organic matter during coalification.

The thermal maturity of Fruitland coal beds in the San Juan Basin and the origin and migration pathways of natural gases produced from both the Pictured Cliffs Sandstone and the Fruitland Formation are important in evaluating gas reserves and in developing future exploration efforts. The distribution and compositional variations among Pictured Cliffs Sandstone and Fruitland sandstone and coalbed gases may prove useful in establishing gas migration pathways and in evaluating the environmental aspects of coalbed methane development in the San Juan Basin. Furthermore, carbon dioxide is corrosive and noncombustible (which lowers the gas BTU content) and must be removed before the gases can enter the pipeline system. Recent papers that discussed the origin and composition of gases in both the Pictured Cliffs Sandstone and Fruitland sandstones and coal beds (Rice, 1983; Rice and others, 1988, 1989, and 1990) were based on the analysis of a limited number of samples obtained primarily from the thermally more mature northern San Juan Basin. This report, based on analyses of a significantly larger data base, evaluates differences in coalbed gas compositions between the overpressured and underpressured parts of the basin and integrates this data with coal rank and Fruitland hydrodynamics.

Objectives

The objectives of this study were to (1) map and evaluate coal rank in the Fruitland Formation, (2) determine if there are significant differences in composition among Fruitland coalbed, Fruitland sandstone, and Pictured Cliffs sandstone gases, (3) determine if minor variations in gas composition can be used to determine the origin and migration history of these gases, and (4) compare regional variations in Fruitland coalbed gas compositions with coal rank and basin hydrodynamics and evaluate factors controlling gas composition.

Methods

Proximate analyses and vitrinite reflectance data from 26 Fruitland coals, which ranged in rank from subbituminous to medium volatile bituminous, were used to determine the relationship between volatile matter (dry, ash-free basis [VM_{daf}]) and measured vitrinite reflectance values (R_m). Linear regression analyses, based on reflectance data points on either side of the coalification jump, were used to determine the equations for converting volatile matter content into calculated vitrinite reflectance values (R_c). Measured vitrinite reflectance values are from Kelso and Rushworth (1982), Rice (1983), Roybal and others (1985), Rice and others (1989), Fassett and Nuccio (1990), Law (1990b), and this study. Volatile matter contents are from Fassett and Hinds (1971), Goolsby and others, 1979, Roybal and others (1985), Kelso and others (1988), Nickelson (1988), and Roberts (1989). Approximately 226 measured and 72 calculated vitrinite reflectance values were used to map the rank of Fruitland coal.

Gas compositional data from more than 5,500 Pictured Cliff sandstone wells and approximately 470 Fruitland wells were used in this study. These data were obtained from pipeline companies, published literature, and several Gas Research Institute cooperative wells. Gas samples were generally collected from the meter run downstream from production equipment or from the wellhead in nonproducing wells; collection of gas samples directly from a meter

reduces the possibility of air contamination. Samples were analyzed with a gas chromatograph using a silica column. The completion lithology (sandstone and/or coal) for Fruitland wells was confirmed by the operator or identified from completion reports and geophysical logs. If logs were not available for a well, then equivalent perforation intervals on well logs from several adjacent wells were used to determine lithology. Wells whose producing zone and producing lithology could not be determined were designated as Basin Fruitland Coal completions on the basis of information provided by Dwight's Oil and Gas Reports (1990a, b). Wells were omitted from the study if the gases were commingled, the producing lithology was uncertain, or if production could have been from both coal beds and sandstones. For Pictured Cliffs completions, only a limited number of wells were examined to verify that the perforation interval was actually in the Pictured Cliffs Formation.

Gas contents discussed in this report are given in mole percent. The ratio of methane (C_1) to total hydrocarbons (C_1 through C_5) can be used to determine a gas dryness index. Chemically very dry gases have C_1/C_{1-5} values greater than 0.99, dry gases have values ranging from 0.94 to 0.99, wet gases have values from 0.86 to 0.94, and very wet gases have C_1/C_{1-5} values of less than 0.86.

Methane, carbon dioxide, and water isotopic data were collected from the literature. The $\delta^{13}C$ values for total dissolved carbonate species is from Kaiser and others (this volume, Chapter 8). Bicarbonate is the dominant chemical species in Fruitland Formation water, and $\delta^{13}C$ values for the total dissolved carbonate species will be referred to as bicarbonate $\delta^{13}C$ values in this paper. All isotopic values are relative to the PDB standard unless otherwise designated.

Thermal maturity of Fruitland coal

Factors affecting the ability of a coal bed to generate and store natural gases include coal rank, ash content, and maceral composition. Coal rank and maceral composition, particularly the relative abundance of hydrogen-rich organic material, also control the types of gases produced from coal beds. Coal rank is often used to estimate gas reserves. In previous studies of the Fruitland Formation (Fassett and Hinds, 1971; Kelso and Rushworth, 1982; Rice, 1983; Meissner, 1984; Campbell, 1985; Roybal and others, 1985; Kelso and others, 1988; Fassett and Nuccio, 1990), vitrinite reflectance values or volatile matter were used to determine coal rank. Teichmüller (1971) and van Gijzel (1982) demonstrated that there is good relation between vitrinite reflectance and volatile matter with increasing coal rank. Therefore, volatile matter content data in this study were converted to equivalent vitrinite reflectance values using equations determined from cross plots of vitrinite reflectance and volatile matter data from Fruitland coals; this approach provided a large regional data base of more than 200 measured and calculated values for mapping coal rank variations in the Fruitland Formation.

In cross plots of measured vitrinite values versus volatile matter content, two distinct linear trends are separated by an interval where R_m values increase rapidly with minor increases in VM_{daf} values (Fig. 9.1). This sharp increase in vitrinite reflectance corresponds to the first coalification jump that represents the beginning of catagenesis (Tissot and Welte, 1978), when volatile hydrocarbons are generated from the liptinitic components of the coal as the "oil window," or oil-generating stage, is reached during thermal maturation (Teichmüller, 1987). The percent volatile matter cutoff for using Equation 1 or Equation 2 to calculate vitrinite reflectance values was set at 47% volatile matter; this value represents the approximate intersection point of these two equations (Fig. 9.1). Vitrinite reflectance values were determined using Equation 1 for samples containing more

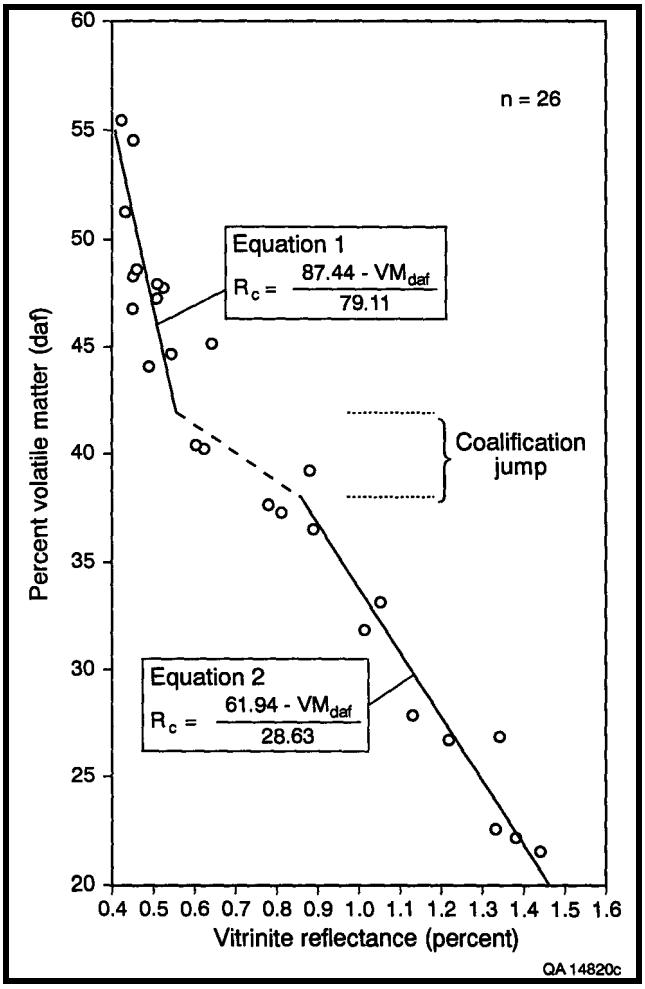

FIGURE 9.1—Relationship between vitrinite reflectance and volatile matter content of Fruitland coal. Two distinct linear trends are separated by an interval where vitrinite reflectance values increase abruptly with only a minor decrease in volatile matter (dry, ash-free basis). This coalification jump reflects the generation of bitumen from hydrogen-rich components of the coal.

than 47% volatile matter (correlation coefficient of 0.787). Equation 2 (correlation coefficient of 0.972) was used to calculate vitrinite reflectance values of samples with less than or equal to 47% volatile matter. The extension of Equation 2 to higher VM_{daf} values over the coalification jump range was necessary because (1) poor sample control over the coalification jump did not allow an equation to be calculated in this range, and (2) there was better correlation between measured and calculated vitrinite values over this volatile matter range. The excellent relationship (Fig. 9.2; correlation coefficient of 0.986) between measured (R_m) vitrinite values and calculated (R_c) vitrinite values, determined from volatile matter content, provides the basis for using these equations to convert proximate data into equivalent vitrinite reflectance values. Over 75% of the calculated vitrinite values fall within 0.06% of the measured vitrinite values. Vitrinite values from lower rank Fruitland coals (R_m <1.0%) vary by as much as 0.08% over tens of feet (Campbell, 1985; this study), suggesting that R_c values generally fall within the normal range of variability for vitrinite reflectance values over short depth intervals within the Fruitland. This relatively large change in R_m values at low levels of thermal maturity, between or within individual coal beds, may be due to differences in maceral composition, hydrogen content, and/or differences in the degree of humifica-

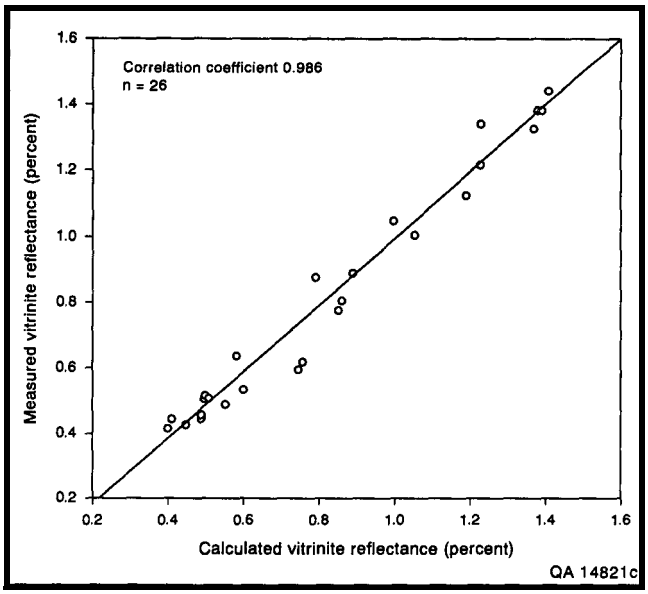

FIGURE 9.2—Calculated and measured vitrinite values. Vitrinite reflectance values calculated from volatile matter content using the equations in Fig. 9.1 show a very good correlation with measured vitrinite reflectance values.

tion attained during the peat stage of diagenesis (Teichmüller, 1987).

More than 140 measured and 72 calculated vitrinite reflectance values were used to make the coal-rank map of the Fruitland Formation (Fig. 9.3). Measured vitrinite values were selected over calculated values when both sets of data were available. Measured vitrinite reflectance values range from 0.42 to 1.51% and correspond to subbituminous to low volatile bituminous coal ranks. Low volatile bituminous Fruitland coal occurs within a northwest-trending band of medium volatile bituminous coal in the northern third of the San Juan Basin. Coal rank decreases abruptly toward the northern margin of the basin along the Hogback mono-dine (Ayers and others, this volume, Fig. 2.5) where high volatile C to high volatile A bituminous isorank lines parallel basin structure. This change in vitrinite reflectance values is most pronounced along the northwestern margin of the basin, where measured vitrinite values decrease from 1.45% to 0.8% in less than 6 mi (<10 km) (Fig. 9.3). Southward, vitrinite reflectance isorank lines generally parallel basin structural contours as coal rank gradually decreases to subbituminous in the southern third of the basin.

Overall, there is a general correlation between the structural configuration of the San Juan Basin (Ayers and others, this volume, Fig. 2.5) and Fruitland coal rank (Fig. 9.3). The anomalously low vitrinite reflectance values along the Ignacio anticline and the Hogback monocline indicate that development of these structures began before or during the main stage of coalification. In the northern third of the basin, low volatile bituminous coals are structurally higher than lower rank coals located to the south along the structural axis of the basin. North of the Bondad anticline, coal rank does not follow present-day structure. In this area, the elevation of the Huerfanito Bentonite rises from 2,800 ft (853 m; datum mean sea level) to nearly 3,800 ft (1,158 m) over a distance of 7 mi (11 km) (Ayers and others, this volume, Fig. 2.5), with no significant change in vitrinite reflectance values within Fruitland coals. The presence of structurally higher coal adjacent to structurally lower coal of equivalent rank (R_m values of 1.45%) suggests that significant postcoalification uplift and/or higher heat flux occurred locally in the northern part of the basin.

Anomalously high vitrinite reflectance values (R_m >1.4%) in the northern San Juan Basin have been attributed to higher heat flux derived from the emplacement of the San Juan Batholith to the north (Rice, 1983; Bond, 1984), heat advection from ground-water movement (Clarkson and Reiter, 1987), or the presence of a localized, deeply buried heat source (Rice and others, 1989). Regional heat-flow studies of the San Juan Basin and surrounding areas (Reiter and Mansure, 1983; Clarkson and Reiter, 1987) indicate that heat flow increases from south to north in the San Juan Basin (Fig. 9.4). According to Reiter and Mansure (1983), these trends are consistent with seismic, geomagnetic, and gravity data from the Colorado Plateau. The relatively large (10 by 40 mi [15 by 60 km]), eastward-trending gravimetric low (< – 250 mGal) in the northern San Juan Basin (Fig. 9.4) may represent areas of higher heat flow. However, magnetic anomalies (Zietz and others, 1982) that would support a deep igneous heat source are absent, which suggests that the low gravity values may indicate increased thickness of lower-density sedimentary rocks, regions of higher heat flow within the Colorado Plateau, vertical migration of fluids at depth as suggested by Law (1990a), and/or a combination of these factors.

The correlation between vitrinite reflectance and structure in the San Juan Basin suggests that burial depth and structural evolution of the basin were probably the major factors controlling the thermal maturity of Fruitland coals. The rather abrupt increase in vitrinite reflectance values greater than 0.70% in the northern basin coincides with a structural hingeline (Ayers and others, this volume, Figs. 2.5 and 2.9). Coal-rank trends and basin structure coincide with gravity trends in this area (Figs. 9.3 and 9.4). Along the structural hingeline, closely spaced northwest-trending isogals may suggest the presence of a deep-seated structural feature. Ayers and others (this volume, Chapter 2) hypothesized that the structural hingeline is a northwest zone of normal faults with the downthrown side of the basement floor to the northeast. Significantly, offset of coal beds across the northwest-trending fault zone and the southwestward pinch-out of coal beds may have inhibited the southwestward migration of fluids derived from thermally more mature parts of the basin. This would explain the closely spaced isorank contours (R_m >0.65%) in the northern basin as well as the southwest boundary of overpressuring.

Composition and distribution of Fruitland and Pictured Cliffs gases

Both Fruitland and Pictured Cliffs reservoirs produce nonassociated gas and minor condensate. Fruitland coal alone is estimated to contain 43 to 49 Tcf of gas (Ayers and others, this volume, Chapter 2). Understanding the origin, migration, and compositional variability of these gases in the San Juan Basin is important for future exploration and production efforts. Most previous studies indicated that Fruitland coalbed gases are genetically distinct from Fruitland sandstone and Pictured Cliffs sandstone gases (Rice and others, 1988, 1989). However, these studies were based on relatively few samples, and the extrapolation of these conclusions to all parts of the basin may be invalid. Hanson (1990) used gases desorbed from subsurface samples of Fruitland coal cores to demonstrate that these coals contain a broad range in gas chemistry that is not necessarily distinct from Pictured Cliffs sandstone gases.

Composition of gas produced from Fruitland coal beds does not appear to change significantly with time (Hale and Firth, 1988; Hanson, 1990), indicating that the length of production should not be a major factor affecting gas compositional data and that gas compositional trends revealed in this study are probably valid. Carbon dioxide, ethane,

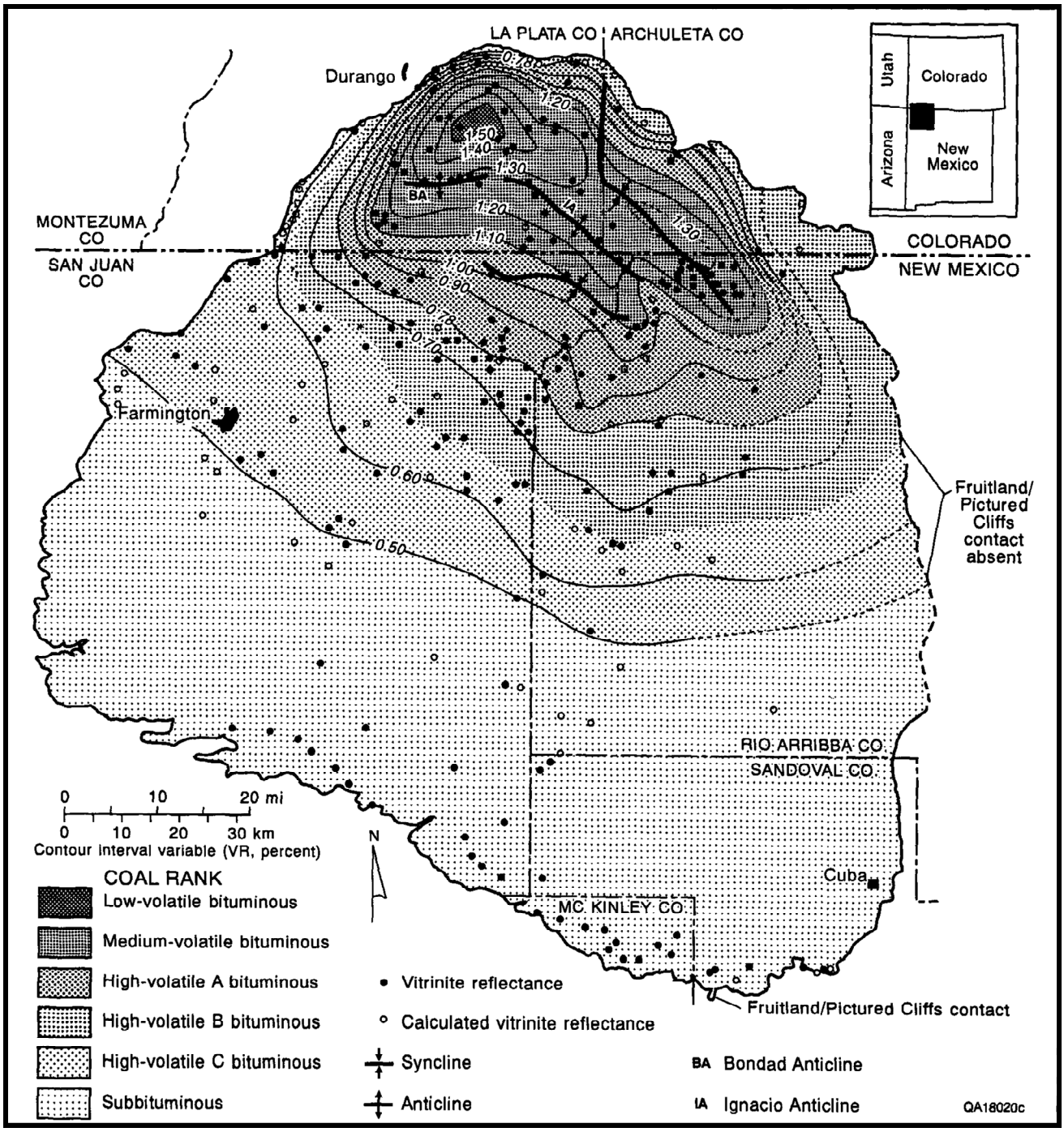

FIGURE 9.3—Fruitland Formation coal-rank map. The rank of coal generally reflects the structural configuration of the basin. Low, vitrinite reflectance values over the Ignacio anticline and along the Hogback monocline suggest that these structural features were present during coalification. Structural axes are from the Huerfanito Bentonite datum (Ayers and others, this volume, Fig. 2.5).

and nitrogen were evaluated to characterize variations in composition among Fruitland coal beds, Fruitland sandstones, and Pictured Cliffs sandstone gases. These three gas components, instead of methane, were used so that minor variations in gas compositions could be recognized. If methane had been used as an end member, gas compositional data points would have clustered at that corner of the ternary diagram. Furthermore, there appears to be a very good correlation between methane content and these three components (Fig. 9.5) and between ethane and heavier gas components (C_3 through C_5 hydrocarbons). Coalbed gases from the overpressured parts of the basin follow gas compositional trend A, which has a correlation coefficient of 0.990 (Fig. 9.5a). These gases are composed predominantly of methane and carbon dioxide and of very minor amounts of other hydrocarbon gases. Gases from underpressured Fruitland coal beds and sandstones generally follow trend B (Fig. 9.5b, correlation coefficient of 0.907). Both underpressured coalbed and sandstone gases follow trend B, suggesting that there may be communication between sandstones and coals in the southern part of the basin. Overpressured sandstone and coalbed gases follow different trends (Fig. 9.5). However, hydrochemical data indicate that sandstones and coal beds in overpressured parts of the basin are in regional hydraulic communication (Kaiser and others, this volume, Chapter 8). Communication between sandstones and coal

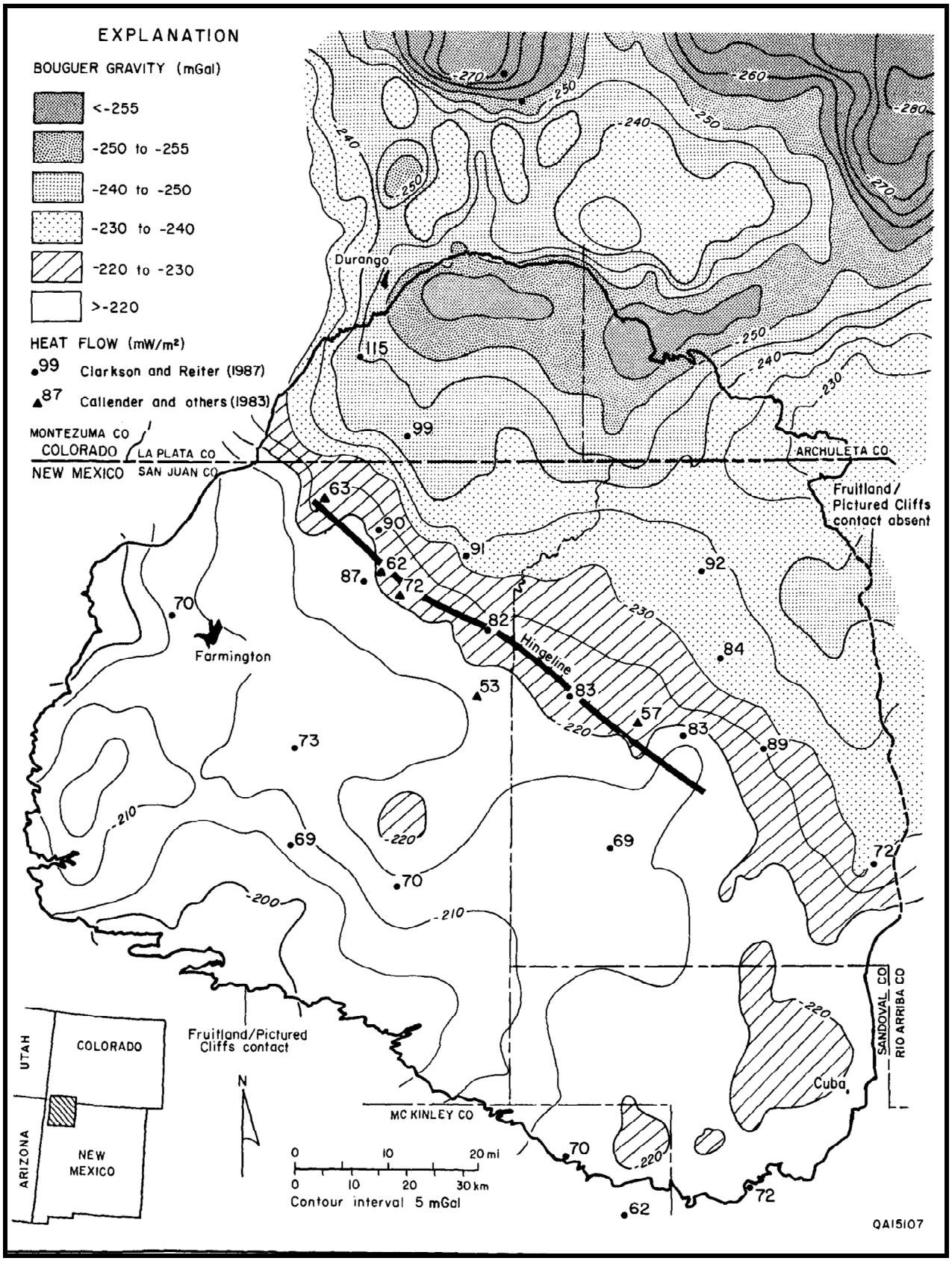

FIGURE 9.4—Bouguer gravity map and heat-flow data from the San Juan Basin. Bouguer gravity contour trends are northwest and highly spaced north of a structural hingeline, suggesting that there may be a change in the relative position of crustal blocks in this area. The negative gravity anomalies (< –250 mGal) in the northern basin may be due to increased heat flux, vertical migration of fluids at depth, a thicker sequence of sedimentary rocks, or any combination of these factors. Data are modified from Suits and Cordell (1981), Callender and others (1983), and Clarkson and Reiter (1987).

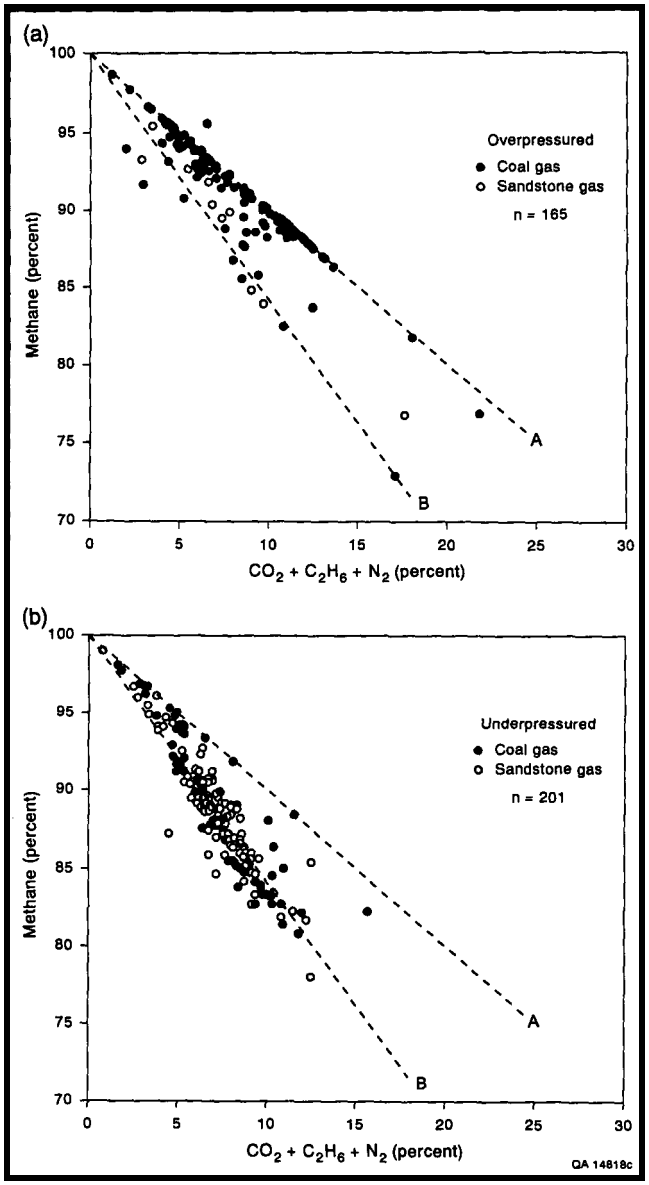

FIGURE 9.5—Relationship between major gas components in the (a) overpressured and (b) underpressured parts of the San Juan Basin. The correlation coefficients of trends A and B are 0.990 and 0.907, respectively, indicating a good relationship between methane and other gas components.

beds probably occurred over geologic time rather than as a result of drilling and production activities. Therefore, differences between sandstone and coalbed gas compositional trends in the northern basin probably reflect the way gases are stored in and released from these reservoirs rather than noncommunication between reservoirs.

Fruitland Formation gases

Previous studies indicated that Fruitland coalbed gas composition is distinctly different from the composition of Fruitland sandstone gases (Rice and others, 1988, 1989). Differences in gas composition were attributed to different organic source materials; chemically dry gases were derived from coal beds, and chemically wet gases were thought to have been generated from dispersed type III kerogen found in adjacent carbonaceous shales. The presence of wet gases produced from Fruitland coal beds was attributed to unspecified completion practices instead of to production directly from the coal. However, this study indicates that Fruitland coals are the source of wet coalbed gases. Furthermore, coalbed and sandstone gas compositions are very similar in the southern part of the basin, indicating that gas composition alone cannot always determine gas origin.

Fruitland sandstone gases

Gases produced from Fruitland sandstones have C_1/C_{1-5} values ranging from 0.80 to 1.00, and a mean of 0.90 (Table 9.1). Underpressured sandstone gases are wetter than overpressured sandstone gases (mean C_1/C_{1-5} values of 0.90, and 0.94, respectively). Low C_1/C_{1-5} values (<0.91) in Fruitland sandstone gases occur in a southeast-trending band in the central part of the basin (Fig. 9.6). This area generally falls between vitrinite reflectance values of 0.49 and 0.70%, which corresponds to the oil-generating stage of the organic matter. The ethane content of sandstone gases ranges from less than 1% to nearly 11%; gases from the underpressured region contain significantly more ethane than gases from the overpressured region. Overpressured and underpressured sandstone gases have similar ranges of carbon dioxide content (Table 9.1). However, Fruitland sandstone gases in the northern part of the basin generally contain more than 1% carbon dioxide (Fig. 9.7) and have a mean carbon dioxide content of 2.2%. Gases in the southern basin generally have less than 1% carbon dioxide (mean of 0.50%), but some wells may contain more carbon dioxide. Nitrogen content ranges from less than 1% to more than 9%. Overpressured sandstone gases have a higher mean nitrogen content (1.8%) than gases from underpressured sandstones (mean of 0.6%). However, high nitrogen content in gases produced from overpressured sandstones may reflect sample contamination by air rather than the actual nitrogen content of these gases.

Ternary diagrams also reflect the relatively high ethane content of Fruitland sandstone gases (Fig. 9.8). Gases from overpressured sandstones and UP1 tongues have similar gas compositions and generally contain more carbon dioxide and less ethane than gases from underpressured Fruitland sandstones. Some Fruitland wells completed in sandstones have coal-decline production behavior, indicating that these sandstones are producing gases from adjacent coal beds (Kaiser and Ayers, this volume, Chapter 10). Gases from some of these wells have proportionally higher carbon dioxide and/or nitrogen contents (Fig. 9.8), indicating that a portion of the gas contained in these sandstones may have been derived from adjacent coalbeds. However, other wells with coal-decline production behavior do not follow this trend and have gas compositions that are similar to other Fruitland sandstones; either the coalbed gas composition is similar to the sandstone gas composition, the contribution of coalbed gases to the total production is relatively minor, or the gas composition changed during migration from coal beds to sandstones.

Fruitland coalbed gases

Methane and other gases are generated from coal during coalification as temperatures increase with increasing burial depth. Coal rank, ash content, reservoir pressure, and maceral type, particularly the amount of hydrogen-rich components, all affect final gas composition. Analysis of Fruitland coalbed gases showed that although many coalbed gases are chemically dry, a significant number of gases are chemically wet. Hanson (1990) found that C_1/C_{1-5} values of gases desorbed from Fruitland coals ranged from 0.81 to 1.00. The range of C_1/C_{1-5} values of Fruitland coalbed gases (0.77 to 1.00) is similar to that of Fruitland sandstone gases (Table 9.1) and to the C_1/C_{1-5} values of desorbed coalbed gases reported by Hanson (1990) (0.81 to 1.00). Chemically dry

to very dry coalbed gases, located in both the overpressured, northern part and the underpressured, southern part of the basin, are separated by a west–northwest-trending band of relatively wet coalbed gases (Fig. 9.9). Overpressured coalbed gases are chemically drier (mean C_1/C_{1-5} value of 0.98) than underpressured gases, which have a mean C_1/C_{1-5} value of 0.92. However, underpressured coalbed and sandstone gases have similar mean C_1/C_{1-5} values (0.92 and 0.90, respectively). Ethane content of Fruitland coalbed gases ranges from 0 to more than 11% (Table 9.1). The wet gases from underpressured coal beds have a significantly higher mean ethane content (4.8%) than do gases from overpres-

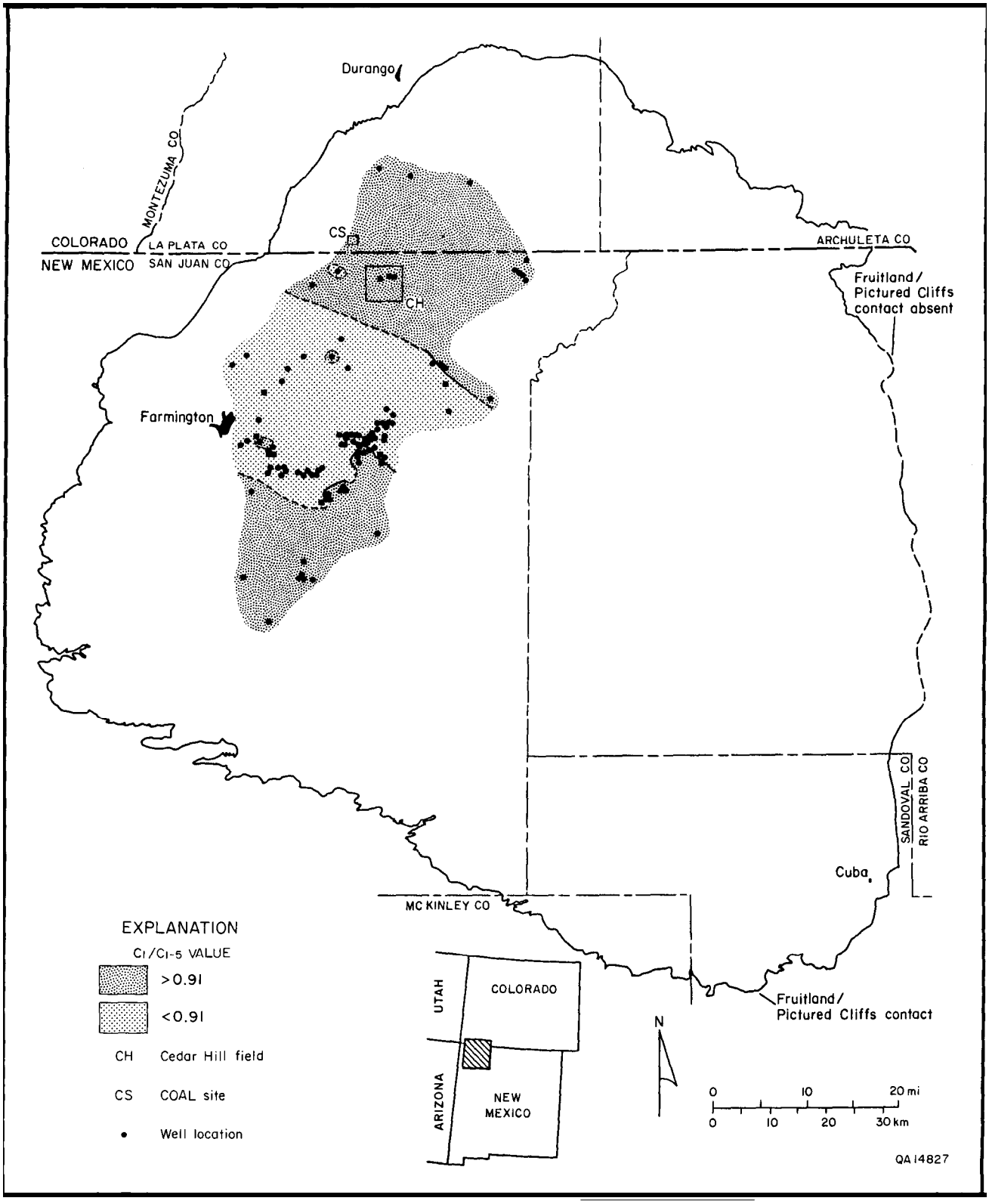

FIGURE 9.6— C_1/C_{1-5} values of Fruitland sandstone gases. Fruitland sandstone gases in the northern and southern parts of the basin are generally chemically drier than gases from the central basin. The wet gases coincide with vitrinite reflectance values between 0.50 and 0.70% and were probably derived from adjacent shales and/or coal beds.

sured coal beds (mean of 1.1%). Underpressured coalbed and sandstone gases have similar mean ethane values (Table 9.1).

Carbon dioxide content in Fruitland coalbed gases ranges from less than 1% to more than 13% (Table 9.1). Coalbed gases with the highest carbon dioxide content (>10%) are from the north-central part of the basin. This area is characterized by very dry gases (C_1/C_{1-5} values of 1.00) and highly productive coalbed methane wells. From this area, carbon dioxide content of coalbed gases decreases gradually northwestward and very abruptly southward. Carbon dioxide content of Fruitland coalbed gases is generally less than 1% in the southern part of the basin (Fig. 9.10). The ranges of carbon dioxide values for underpressured and overpressured coalbed gases are similar (Table 9.1); however, the mean carbon dioxide of overpressured coalbed gases (6.4%) is significantly higher than underpressured coalbed gases (1.4%). Coalbed gases generally contain more carbon dioxide than underpressured and overpressured sandstone gases (Table 9.1).

Underpressured and overpressured coalbed gases have similar ranges of nitrogen content. Nitrogen content in Fruitland coalbed gases is generally low (mean of 0.7), and more than 95% of the samples contain less than 3% nitrogen, indicating that contamination of the gas samples by air was not a major problem. Most of the data on gas samples having elevated nitrogen contents were obtained from published sources, and the nitrogen reported in these samples may represent air contamination. Nitrogen contents of sandstone and coalbed gases are similar, although sandstone gases contain slightly more nitrogen than coalbed gases (Table 9.1).

Major differences exist between overpressured and underpressured Fruitland coalbed gases (Fig. 9.11). Gases from overpressured coal beds are generally drier and have significantly more carbon dioxide than gases from underpressured coal beds, which are characterized by a higher proportion of ethane (C_2H_6). Coalbed gases from the transition zone, located between overpressured and under-pressured areas, have composition ranges that are similar to both pressure regimes (Fig. 9.11). Underpressured coalbed gases generally have C_1/C_{1-5} values of less than 0.94 and a carbon dioxide content of less than 2% (Fig. 9.12). Gases from overpressured coal beds are significantly drier (C_1/C_{1-5} values generally >0.97) and have more carbon dioxide (>3%) than gases produced from underpressured coal beds. The anomalously high carbon dioxide content of Meridian 400 coalbed gases (>10%) is reflected in the bimodal distribution of carbon dioxide values (Fig. 9.12). The compositions of gases produced from underpressured coalbed and sandstone reservoirs are similar. Gases produced from these reservoirs have relatively high ethane and generally minor carbon dioxide and nitrogen contents (Figs. 9. 8b and 9.11c). Histograms of C_1/C_{1-5} values and carbon dioxide content of gases from underpressured coalbeds and sandstones show that both sandstones and coalbed gases are chemically wet to very wet and contain only minor carbon dioxide (Fig. 9.13).

Pictured Cliffs Sandstone gases

Gases produced from Pictured Cliffs sandstones are similar to gases produced from Fruitland sandstones and underpressured Fruitland coal beds. (Figs. 9.11, 9.14, and 9.15). Pictured Cliffs gases show a normal distribution of C_1/C_{1-5} values that range from 0.72 to 1.00 (mean of 0.88); they may contain nearly 15% ethane (Table 9.1). The ranges of carbon dioxide and nitrogen contents of these gases are also similar to those ranges found in Fruitland sandstone gases. However, Fruitland coalbed gases are generally chemically drier and contain more carbon dioxide than Pictured Cliffs sandstone gases (Table 9.1). The mean nitrogen content of Pic-

TABLE 9.1-Composition ranges of Fruitland sandstone, Fruitland coalbed, and Pictured Cliffs sandstone gases.

		Fruitland sandstone gases			Fruitland coalbed gases			Pictured Cliffs sandstone gases
		All n=101	UP n=91	OP n=10	All* n=288	UP n=111	OP n=157	All n=1,533
C_1/C_{1-5} value	$\bar{X}$	0.90	0.90	0.94	0.96	0.92	0.98	0.88
	S	0.04	0.03	0.04	0.05	0.04	0.03	0.04
	C	0.04	0.04	0.05	0.05	0.05	0.03	0.04
	Min.	0.80	0.80	0.86	0.77	0.83	0.85	0.75
	Max.	1.00	1.00	1.00	1.00	1.00	1.00	1.00
Ethane (percent)	$\bar{X}$	5.7	6.2	3.8	2.5	4.8	1.1	6.7
	S	2.0	1.86	2.00	2.69	2.35	1.70	1.83
	C	0.35	0.30	0.53	1.08	0.49	1.55	0.27
	Min.	0.3	0.3	0.6	0	<0.1	0	<0.5
	Max.	10.7	10.7	6.4	11.9	9.7	8.5	14.8
Carbon dioxide (percent)	$\bar{X}$	0.8	0.5	2.2	4.5	1.4	6.4	0.7
	S	0.73	1.86	0.87	3.90	1.54	3.71	0.64
	C	0.93	0.31	0.41	0.87	1.10	0.58	0.91
	Min.	0	0	<0.1	<0.1	<0.1	0.2	<0.1
	Max.	3.4	3.4	3.2	13.5	11.4	13.5	10.1
Nitrogen (percent)	$\bar{X}$	0.8	0.6	1.8	0.7	0.8	0.7	0.7
	S	1.28	0.90	2.95	1.56	1.32	1.79	0.52
	C	1.60	1.50	1.64	2.23	1.65	2.56	0.72
	Min.	0.1	0.1	0.3	0	0	0	0
	Max.	9.7	8.5	9.7	13.3	11.2	13.3	5.3

$\bar{X}$ = arithmetic mean

S = standard deviation

C = coefficient of variation

UP = underpressured parts of basin

OP = overpressured parts of basin

*Includes 20 samples from transition zone

tured Cliffs gases (0.7%) is similar to the mean nitrogen content of Fruitland gases. The higher nitrogen content in some Pictured Cliffs gases may be related to the presence of sapropelic organic material (which contains nitrogen-rich proteins) in the underlying Lewis Shale relative to terrestrial organic matter. The highest nitrogen contents occur in the southeastern part of the basin.

The wettest Pictured Cliffs gases also occur in the southeastern part of the basin (Fig. 9.16). The wetter gases in this area may reflect lower levels of thermal maturity and/or differences in kerogen type. Elongate trends of relatively dry gas (C_1/C_{1-5} values >0.85) parallel depositional strike in the southeastern corner of the basin, suggesting that localized variations of gas composition may be due to (1)

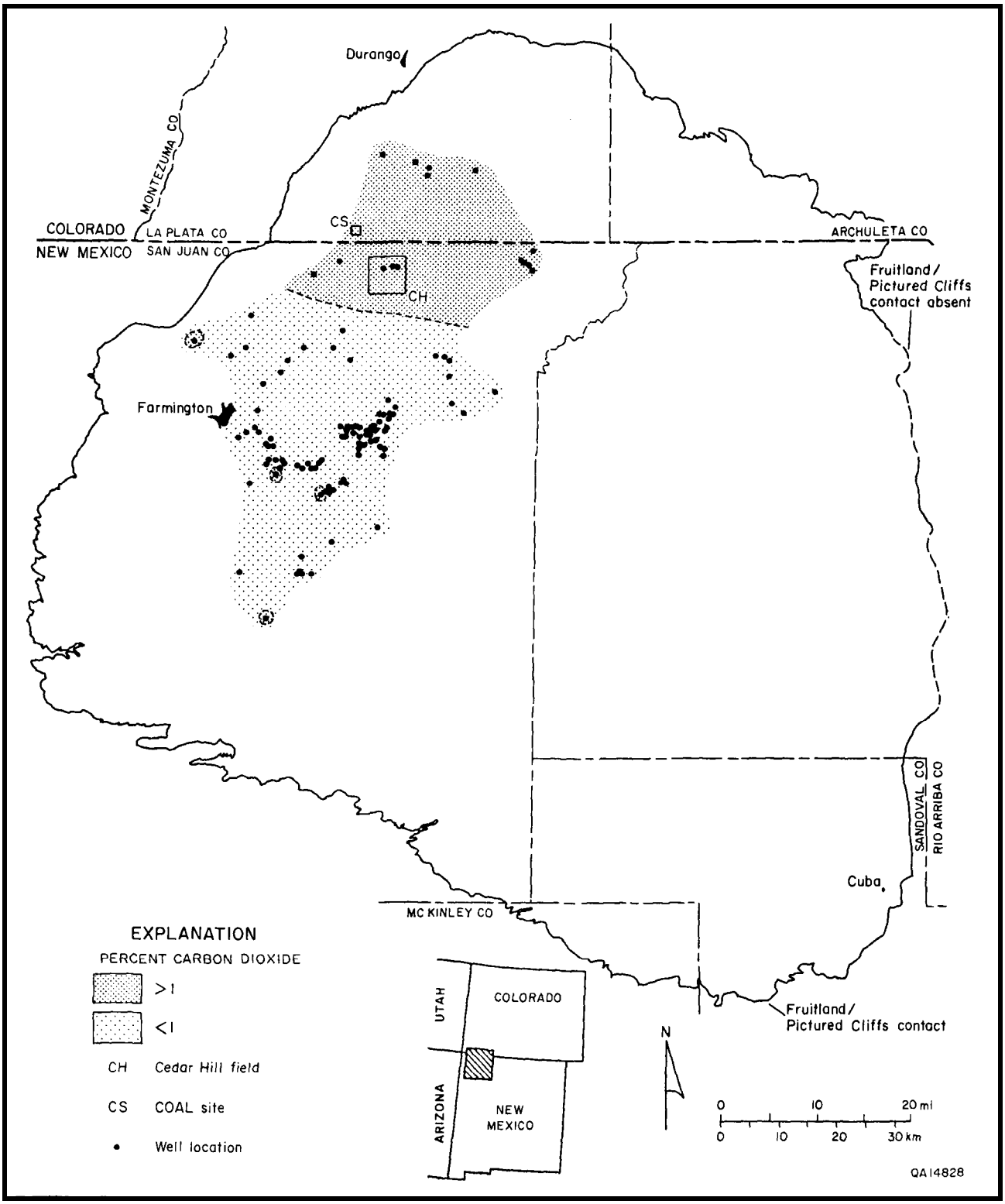

FIGURE 9.7—Carbon dioxide content of Fruitland sandstone gases. Fruitland sandstone gases in the northern basin contain slightly more carbon dioxide than do gases in the southern basin.

migration effects across shale/sandstone contacts that would enrich the gases in methane relative to the other components (Leythaeuser and others, 1979), or (2) migration of dry gas through more permeable sandstones. Although significant volumes of Pictured Cliffs gases were probably derived from the underlying Lewis Shale, some of these gases could have migrated from overlying Fruitland coal beds, and mixing of gases from these two sources is possible. Choate and others (1984) suggested that Pictured Cliffs reservoirs are sourced by Fruitland coal beds where pressure differences between the two formations result in the downward migration of chemically drier coalbed gases. Relatively dry (C_1/C_{1-5} values >0.88) sandstone gases occur in the northwestern part of the basin, where thick basal coal beds lie directly on top of Pictured Cliffs sandstones. The dip-elongate bands of coal are not found in the southeastern corner of the basin (Ayers and others, this volume, Fig. 2.17). The driest Pictured Cliffs gases (C_1/C_{1-5} values >0.91), which occur in a dip-elongate band in eastern San Juan County, may result from completion practices (dual completion in Fruitland coal beds and Pictured Cliffs sandstones) or downward migration from adjacent Fruitland coal beds. This trend of dry gases coincides with dip-elongate bands of basal Fruitland coal beds that may be in excess of 20 ft (>6 m) thick (Ayers and others, this volume, Fig. 2.17). The C_1/C_{1-5} values of coalbed gases in western Rio Arriba County are similar to C_1/C_{1-5} values of gases from underlying Pictured Cliffs sandstone gases. Fruitland coal cores taken throughout central Rio Arriba County emit relatively wet gases (C_1/C_{1-5} values of 0.81 to 0.98) (Hanson, 1990). The similarity of underpressured Fruitland coalbed and Pictured Cliffs sandstone C_1/C_{1-5} values and gas composition distributions (Figs. 9.9 and 9.16) indicates that gas composition alone will not necessarily distinguish coalbed from sandstone gases in parts of the southern basin. More detailed analytical methods, including hydrogen and carbon isotopic analyses of both Fruitland and Pictured Cliffs gases on a basinwide scale, are probably required to establish the origin and migration pathways of these gases.

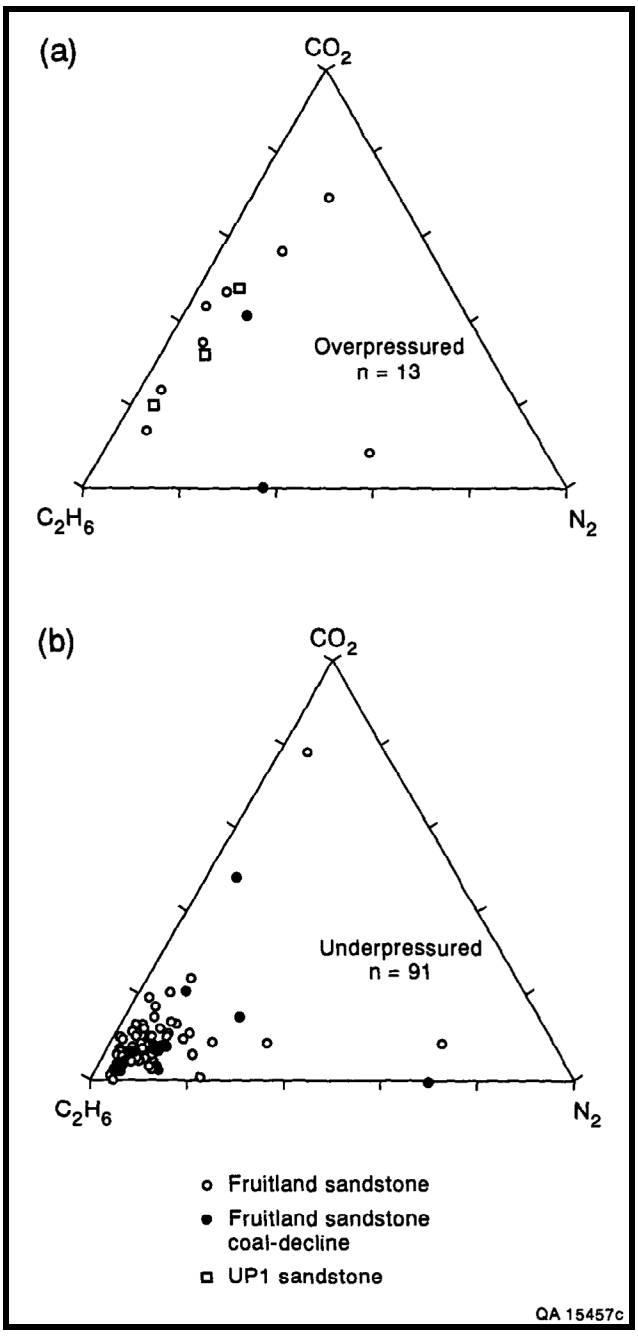

FIGURE 9.8—Ternary diagrams of gases produced from Fruitland sandstones in the (a) overpressured and (b) underpressured parts of the San Juan Basin. Overpressured sandstone gases generally contain proportionally lower ethane and more carbon dioxide than underpressured sandstone gases. Sandstones with known coal-decline behavior are believed to be in communication with coal beds; some, but not all, of these gases contain proportionally higher carbon dioxide and/or nitrogen, which suggests that the gases were derived from the coal. Gases produced from upper Pictured Cliffs tongues have compositions similar to overpressured Fruitland sandstone gases.

Carbon dioxide content of Pictured Cliffs sandstone gases is generally less than 1% (Fig. 9.17). The highest carbon dioxide values of Pictured Cliffs sandstone gas occur in the northwestern part of the basin in the Cedar Hill area (Figs. 9.10 and 9.17); gases from the southwestern part of the basin are chemically drier and also contain unusually high amounts of carbon dioxide (Figs. 9.16 and 9.17). These areas of higher carbon dioxide content may represent communication between Fruitland coal beds and/or result from dual completions in Fruitland coal beds and Pictured Cliffs sandstones.

Relation of gas composition to thermal maturity and pressure regime

Previous interpretations of gas origin and composition in the Fruitland Formation and Pictured Cliffs sandstones were based upon the assumption that coal rank and burial history controlled gas composition. Furthermore, fossil geopressure in the Fruitland was thought to result from earlier compaction, dewatering, and reservoir isolation during coalification (Decker and others, 1987; Rice and others, 1989, 1990). However, this study suggests that compositional variations in Fruitland coalbed gases and the regional distribution of these gases result from thermal maturity and basin hydrology. The Fruitland Formation is a regional aquifer, with recharge occurring in the northern basin where thick northwest-trending coal beds crop out along the Hogback monocline (Kaiser and others, this volume, Chapter 8). Upon confinement and basinward pinch-out of coal beds and/or localized faulting (Ayers and others, this volume, Chapter 2), regional overpressuring is developed in the Fruitland (Kaiser and others, this volume, Chapter 8). Rice and others (1988 and 1989) suggested that Fruitland coalbed gases are chemically very dry (C_1/C_{1-5} values >0.99) and that Fruitland coalbed gases with lower C_1/C_{1-5} values result from unspecified completion practices. However, Rice and others (1989) also cited geochemical evidence that Fruitland coal is hydrogen rich and may be the source of condensate produced from the coals; they did not explain why hydrogen-rich coals would produce only very dry gases. According

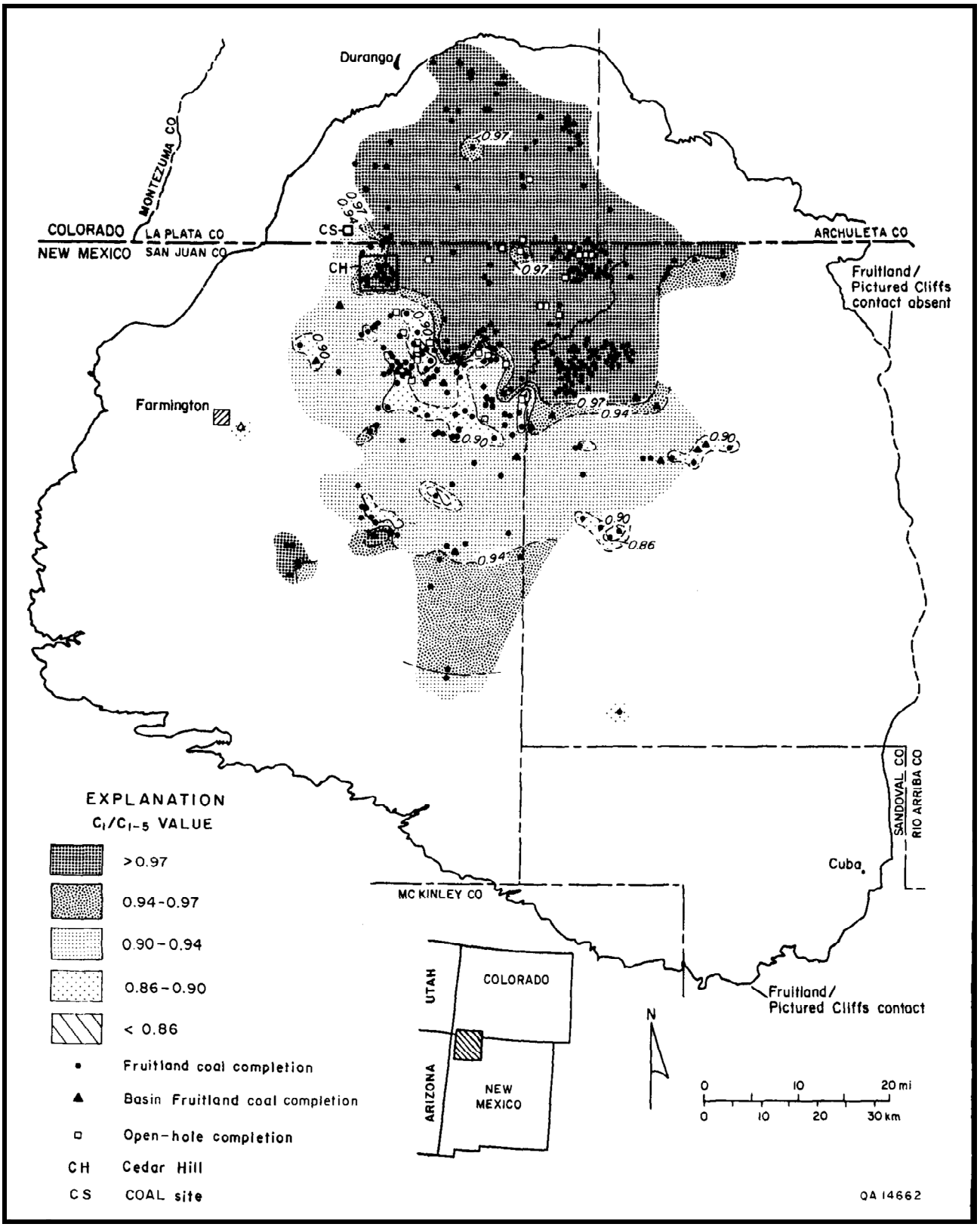

FIGURE 9.9— C_1/C_{1-5} values of Fruitland coalbed gases. Gases derived from higher rank coals (vitrinite reflectance values >0.8%) in the overpressured area generally have C_1/C_{1-5} values greater than 0.97. Isotopic data and the abrupt transition from very dry to wet gases suggest that dry gases in the northern basin are derived from both thermogenic and biogenic sources.

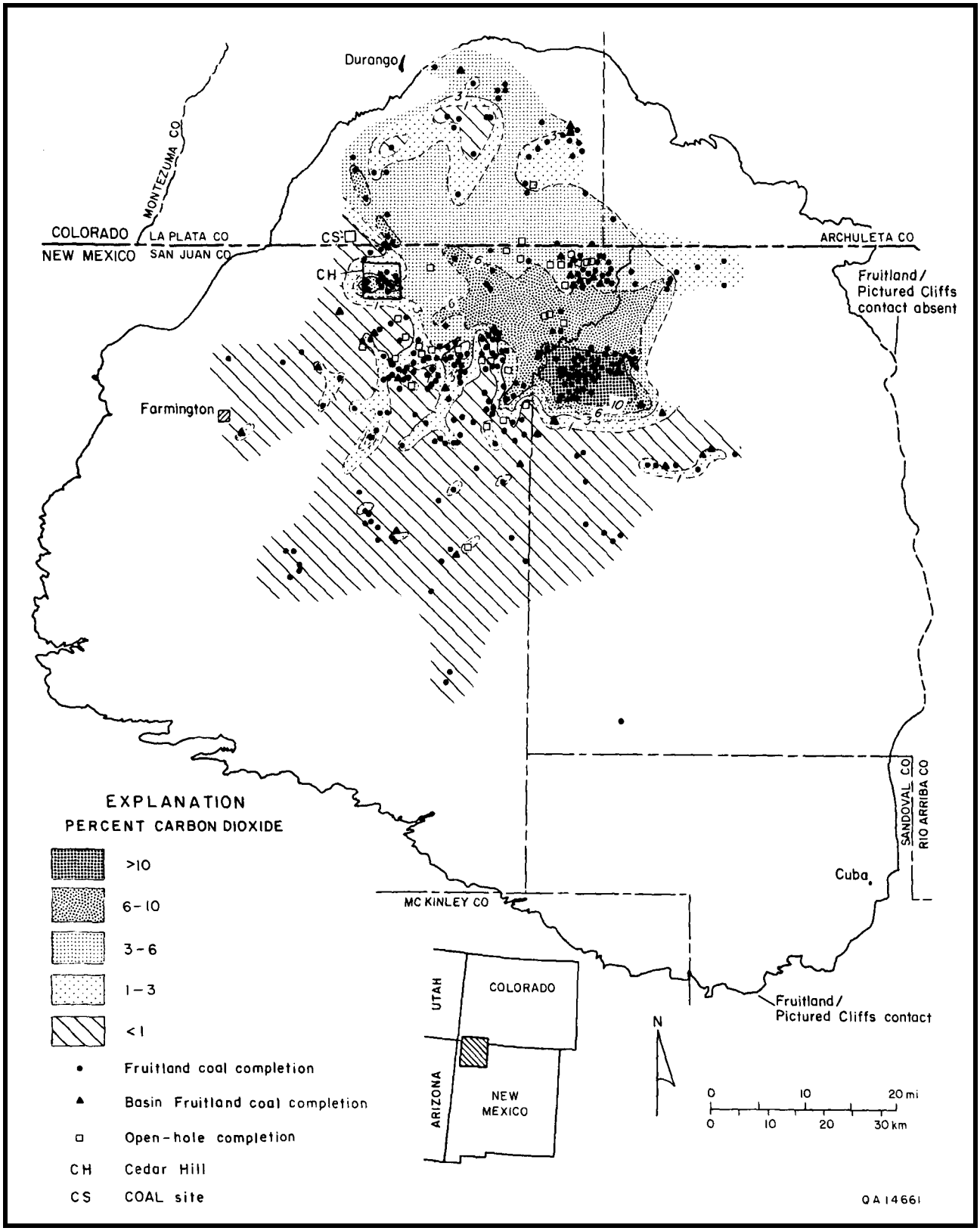

FIGURE 9.10—Carbon dioxide content of Fruitland coalbed gases. Gases containing relatively large amounts of carbon dioxide occur in the north-central basin. Highest carbon dioxide content (>6%) corresponds with coal rank (high volatile A bituminous) and high bottom-hole pressures. Coalbed gases with more than 10% carbon dioxide correspond with highest bottom-hole pressures (>1,600 psi) (Kaiser and others, this volume, Fig. 8.8).

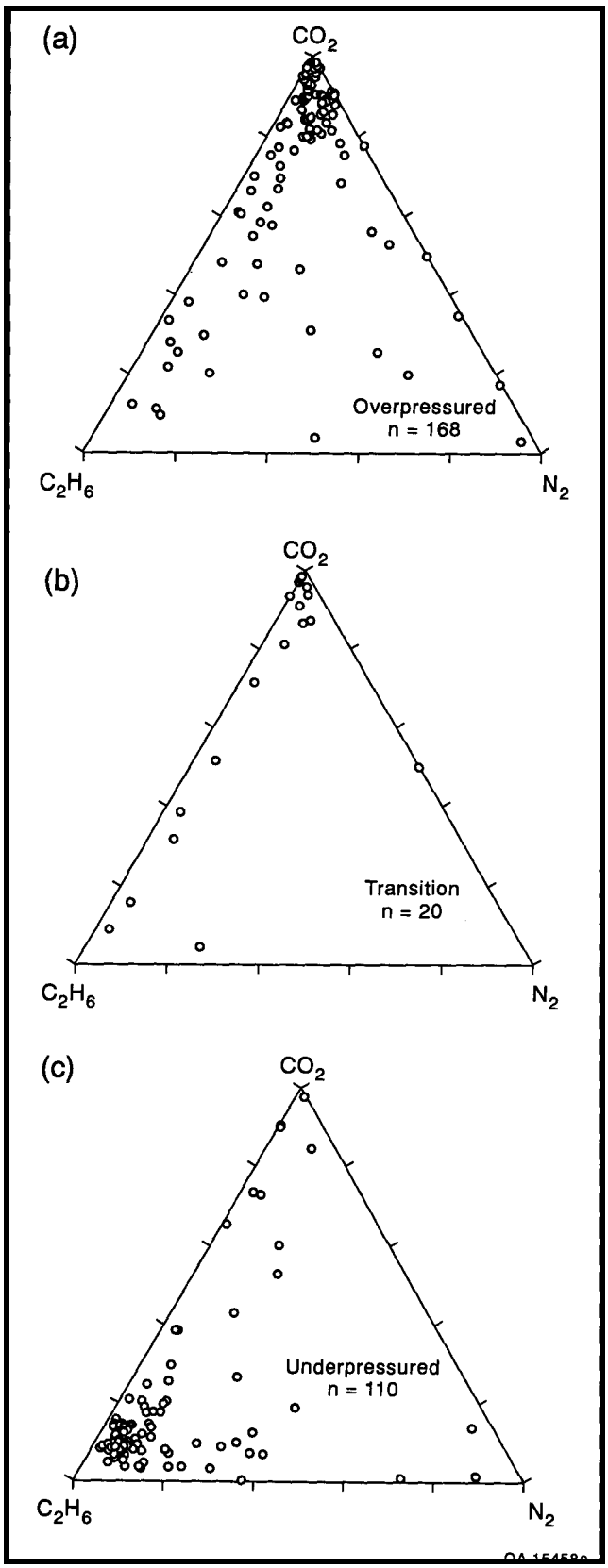

FIGURE 9.11—Ternary diagrams of Fruitland coalbed gases. (a) Coalbed gases from the overpressured part of the basin generally contain significant amounts of carbon dioxide and minor ethane. (b) Coalbed gases from the transition zone between overpressuring and underpressuring contain variable amounts of carbon dioxide and ethane and relatively little nitrogen. (c) Coalbed gases from the underpressured area contain higher amounts of ethane and variable amounts of carbon dioxide and nitrogen.

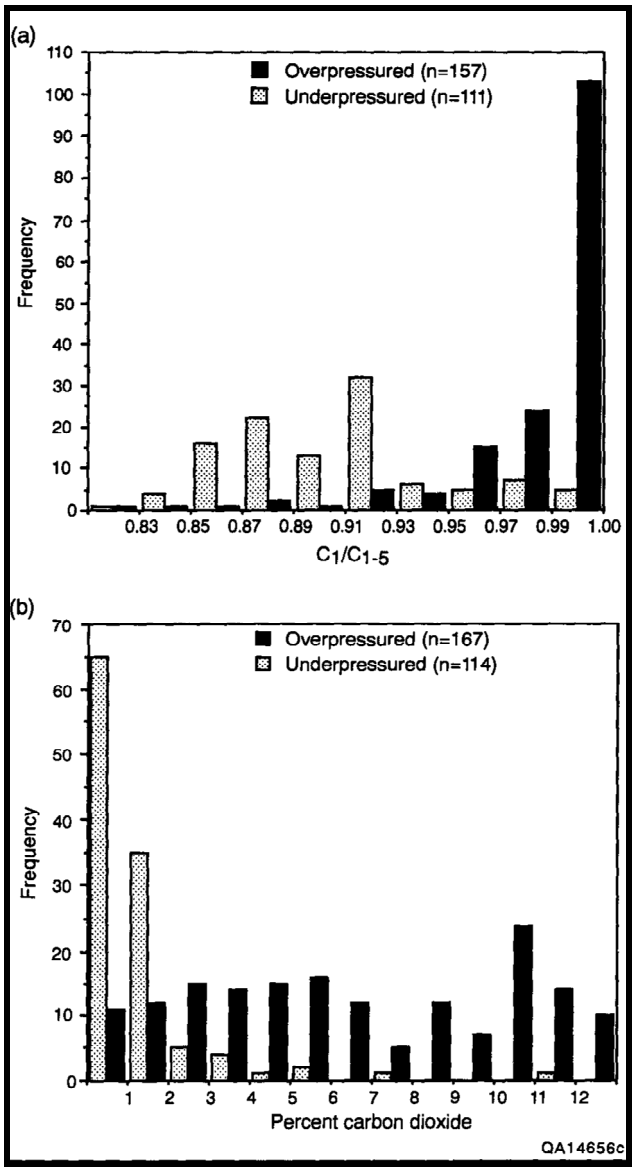

FIGURE 9.12—Histograms of (a) C_1/C_{1-5} values and (b) carbon dioxide content of gases from overpressured and underpressured Fruitland coal beds. Gases from the overpressured, thermally more mature coal in the northern basin are significantly drier than coalbed gases from the underpressured area. Gases from underpressured coal beds generally contain less than 2% carbon dioxide, whereas gases from overpressured coal beds commonly contain more than 2% carbon dioxide. The bimodal distribution of carbon dioxide in the overpressured gases primarily reflects the high carbon dioxide content in samples from the Meridian 400 area.

to Hanson (1990), although desorbed coalbed gases are commonly dry to very dry, some gases may be wet to very wet, with gas wetness depending on coal rank and maceral composition. Furthermore, coalbed gas composition may vary between individual coal beds and laterally within a given coal bed if maceral content is highly variable.

Thermogenic gases become chemically drier with increasing thermal maturity. Predictably, coalbed gases from the thermally more mature northern part of the basin are chemically dry to very dry. However, the regional distribution of these gases (Fig. 9.9) suggests that coal rank is not the only factor controlling the chemical composition of the gas. The eastern boundary of chemically dry coalbed gases does not coincide with coal-rank trends (Fig. 9.3). Furthermore, a gradational contact between very dry and wet coal gases

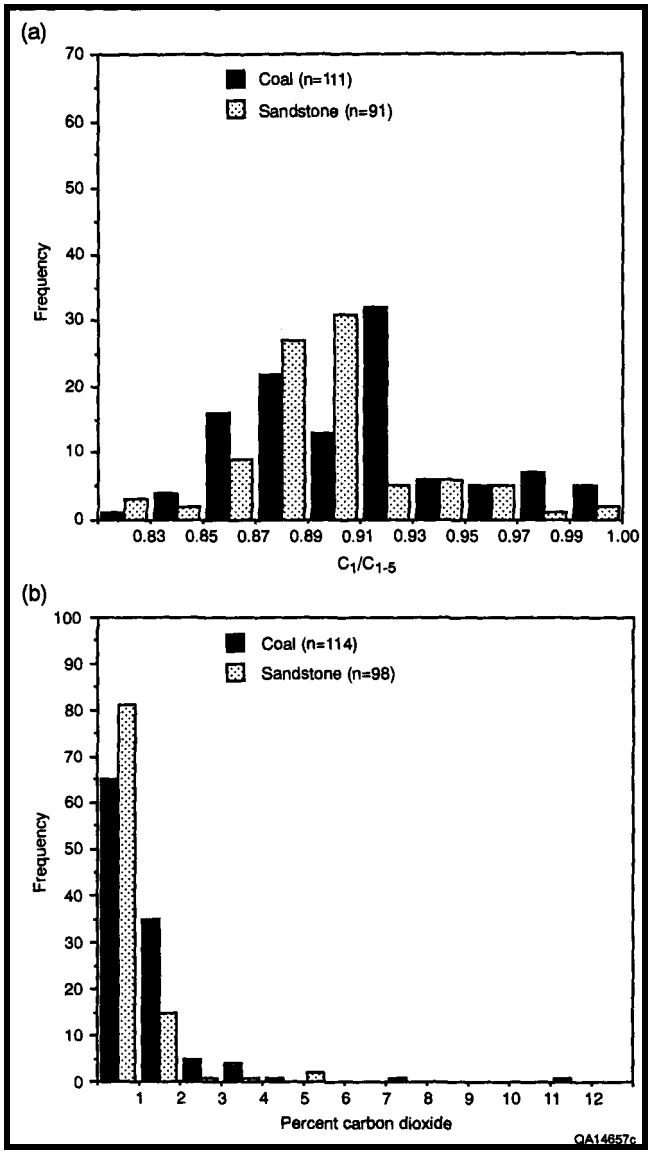

FIGURE 9.13—Histograms of (a) C_1/C_{1-5} values and (b) carbon dioxide content of gases from underpressured Fruitland coal beds and sandstones. Both coal and sandstone gases usually contain less than 2% carbon dioxide and have C_1/C_{1-5} values between 0.85 and 0.93.

paralleling vitrinite reflectance trends would be expected if coal rank alone controlled gas composition. Instead, there is an abrupt transition from very dry (C_1/C_{1-5} value of 1.00) to wet (C_1/C_{1_5} value of 0.87) coalbed gases over distances of less than 1.5 mi (<2 km) along some parts of the overpressured/underpressured boundary. In fact, gas composition coincides more with pressured conditions in the Fruitland Formation (Kaiser and others, this volume, Chapter 8) than with coal rank. Therefore, basin hydrology is thought to be a major factor controlling coalbed gas composition. The origin of these gases will be discussed in the following section.

Previous studies suggested that coalbed carbon dioxide content decreases with increasing coal rank (Rice and others, 1988, 1989, 1990). Gases from low and medium volatile bituminous coals from the northern basin and high volatile bituminous B to subbituminous coals in the southern part of the basin generally have lower carbon dioxide content (<3%), indicating a carbon dioxide content maximum for coalbed gases in the high volatile A bituminous range (Fig.

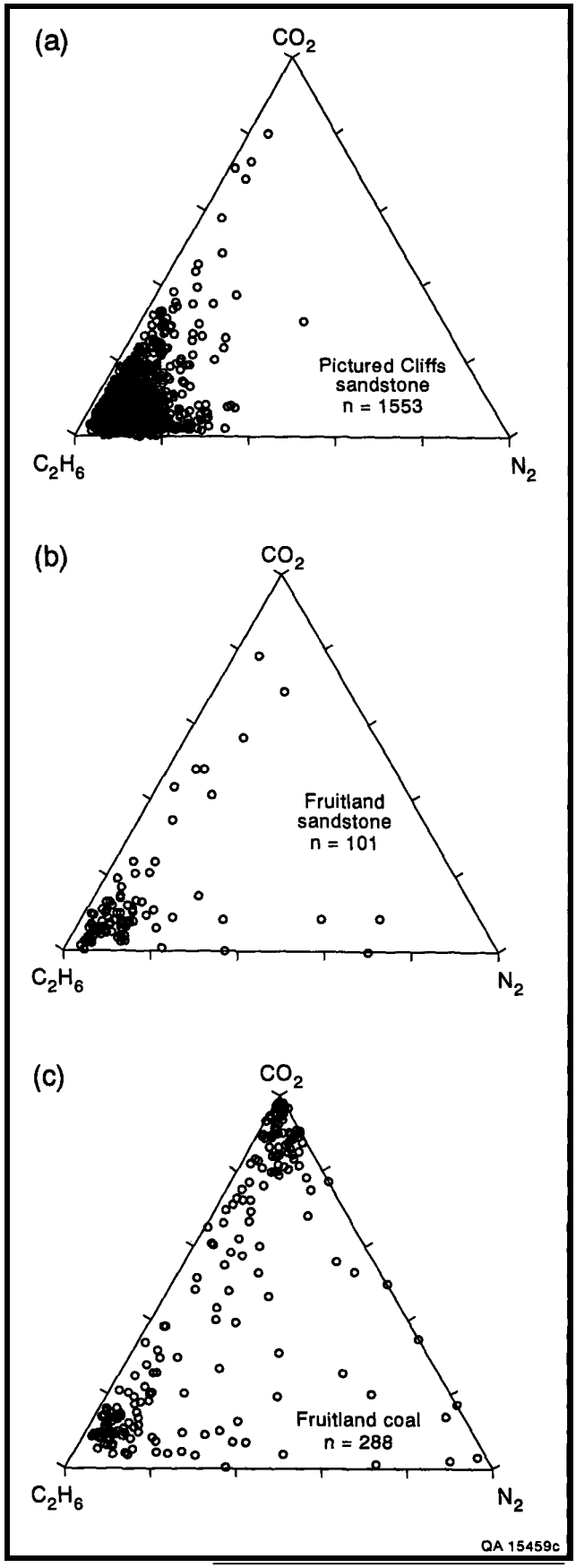

FIGURE 9.14—Ternary diagrams of Pictured Cliffs and Fruitland gases. The proportion of carbon dioxide, ethane, and nitrogen cannot be used to confidently differentiate between gases derived from (a) Pictured Cliffs sandstones, (b) Fruitland sandstones, and (c) Fruitland coal beds.

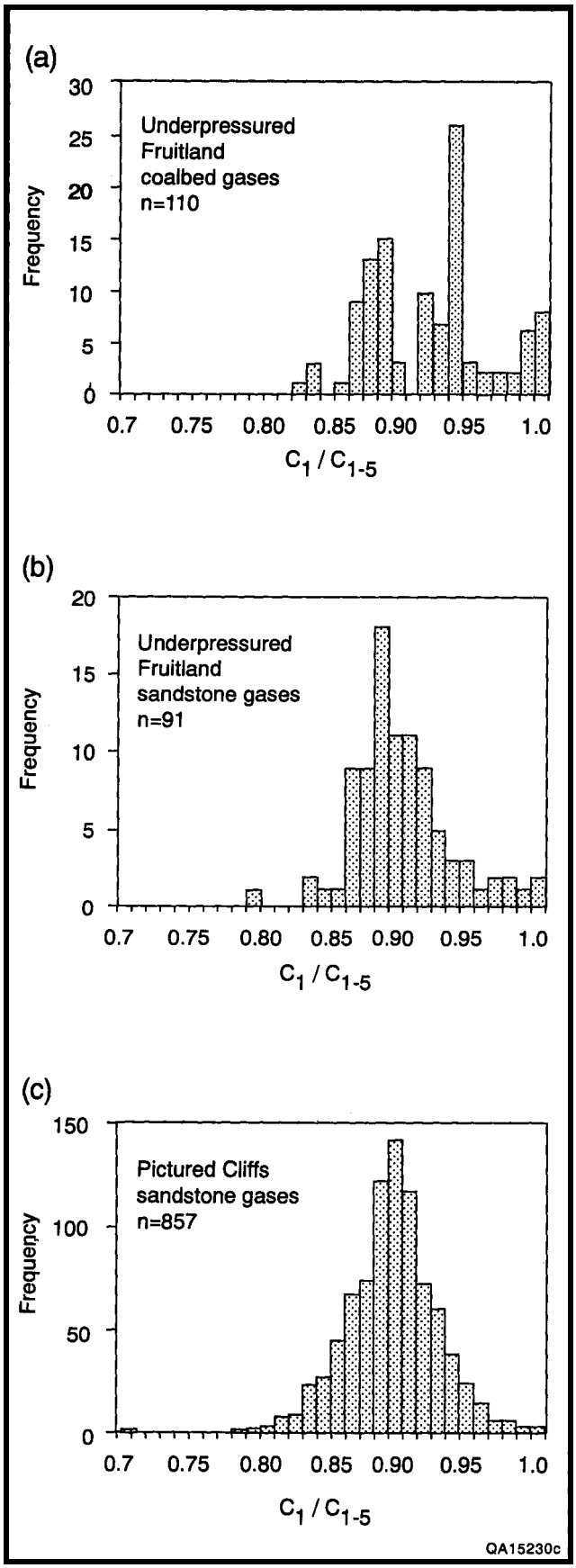

FIGURE 9.15—Histograms of gases from underpressured (a) Fruitland coal beds, (b) Fruitland sandstones, and (c) Pictured Cliffs sandstones. Pictured Cliffs gas data used in this histogram are from the same part of the basin from which Fruitland gas data were available.

9.10). However, carbon dioxide content of gases from high volatile A bituminous coal varies from less than 1% to more than 10%, indicating that coal rank is not the only factor controlling carbon dioxide content. High carbon dioxide content in coalbed gases coincides with the overpressured part of the basin and with the highest bottom-hole pressures (Fig. 9.10; Kaiser and others, this volume, Figs. 8.7 and 8.8), indicating that the carbon dioxide content is partly controlled by basin hydrology and regional overpressure. Dip-elongate bands of slightly higher carbon dioxide content in the southern basin represent diffusion of carbon dioxide and/or flow of dissolved bicarbonate from the overpressured part of the basin southwestward through coal beds that were offset by the northwest-trending fracture zone along the structural hingeline (Ayers and others, this volume, Chapter 2). These higher carbon dioxide content trends parallel dip-elongate coal beds, hydraulic gradients, and northeast–southwest productivity trends (Ayers and others, this volume, Chapter 2; Kaiser and Ayers, this volume, Chapter 10; Kaiser and others, this volume, Chapter 8). The bands of relatively high carbon dioxide content terminate near the San Juan River valley in northern San Juan County, which acts as a regional flow boundary (Kaiser and others, this volume, Chapter 8).

Chemically dry gases with low carbon dioxide contents are associated with higher rank coal in the northern part of the basin, whereas chemically wet, low carbon dioxide content coalbed gases occur in the underpressured, southern region. Coalbed gases in high volatile A bituminous coal are characterized by variable C_1/C_{1-5} values and carbon dioxide contents. The coincidence between regional overpressuring and the distribution of chemically dry to very dry, carbon dioxide-rich gases, and the abrupt transition between these gases and wetter gases with low carbon dioxide contents in the underpressured, southern part of the basin indicate that coalbed gas composition is related to basin hydrology in addition to coal rank.

Origins of Fruitland coalbed gases

Previous studies using gas wetness and carbon isotopic values of methane suggested that most of the gases produced from the Fruitland Formation are thermogenic; only a few gas samples in the southern basin were believed to have a possible biogenic origin (Rice and others, 1988, 1989). The wet gases produced from Fruitland coal beds have been attributed to unspecified completion practices that allowed gases to migrate or drain from adjacent reservoirs (Rice and others, 1988, 1990). However, the distribution of carbon dioxide content and C_1/C_{1-5} values for Fruitland coalbed gases do not necessarily support these conclusions. The distribution of wet gases in the Fruitland Formation and previous geochemical studies (Rice and others, 1989; Law and others, 1990) suggest that these gases are indigenous to the coal. Although most of the gases produced from Fruitland coal beds probably have a thermogenic origin, mixing of thermogenic and biogenic gases can better explain gas compositional distributions and the VC isotopic signatures of methane, total dissolved carbonate, and carbon dioxide found in the Fruitland Formation.

Wet coalbed gases (C_1/C_{1-5} values <0.94) occur between vitrinite reflectance values of 0.49 and 0.75% in the high volatile C and B bituminous coal range (Figs. 9.3 and 9.9). This range of vitrinite reflectance values corresponds to the early stages of oil and gas generation; vitrinite reflectance values for the principal zone of oil and gas generation, or the oil window, range from approximately 0.5 to 1.3% (Tissot and Welte, 1978). This relationship between the distribution of chemically wet coalbed gases and vitrinite reflectance values suggests that wet coalbed gases in the

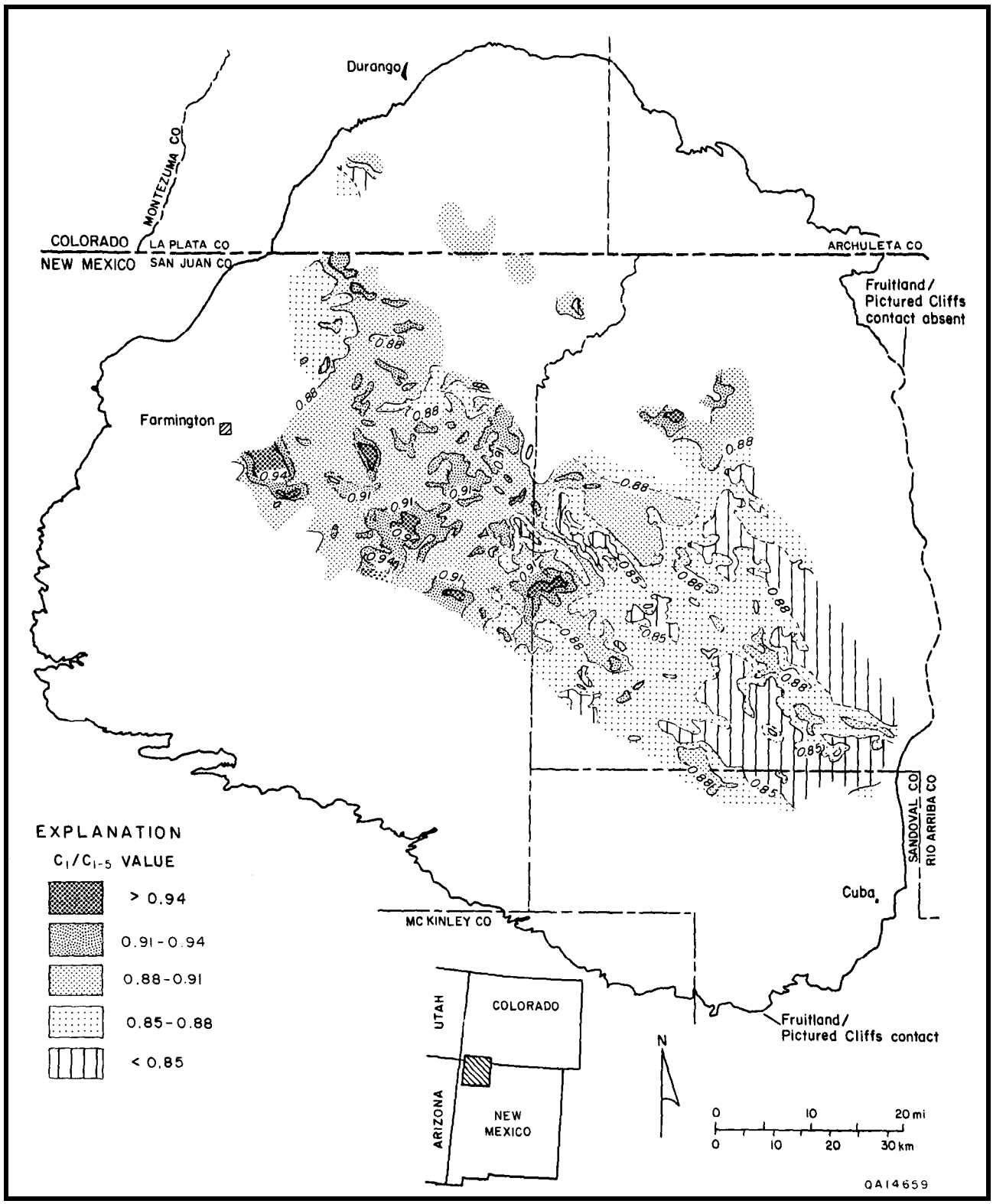

FIGURE 9.16— C_1/C_{1-5} values of Pictured Cliffs sandstone gases. Pictured Cliffs gases in the southeastern part of the trend are chemically wetter than gases produced from the northwestern part of the trend. The northeast-trending area of drier gases (C_1/C_{1-5} values >0.91) in east-central San Juan County coincides with areas where thicker Fruitland coal beds overlie the sandstones, suggesting that coalbed gases may have migrated downward. Gas analyses from more than 5,500 wells were used to construct this map.

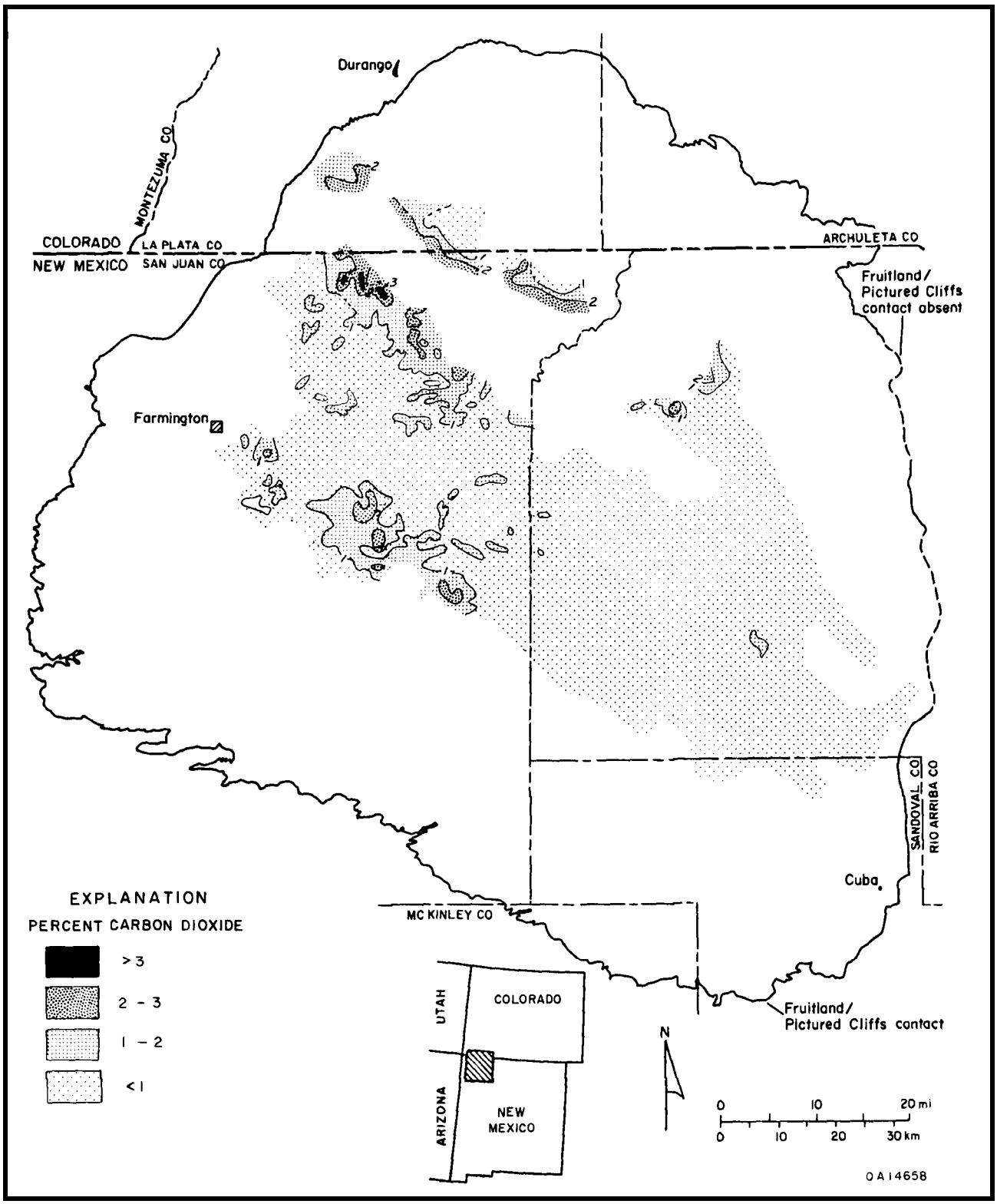

FIGURE 9.17—Carbon dioxide distribution in Pictured Cliffs sandstone gases. Gases from the Pictured Cliffs Sandstone generally have less than 1% carbon dioxide. Wells with higher carbon dioxide values may be completed in or immediately below the basal Fruitland coal beds. Gas analyses from more than 5,500 wells *were* used to construct this map.

Fruitland may be directly related to the thermal maturation of organic matter and not to completion practices.

Coal has traditionally been thought of as a major source of dry gas that has little potential for generating liquid hydrocarbons. However, hydrogen-rich (liptinite-rich) coal is capable of generating liquid hydrocarbons (Khorasani, 1987). Furthermore, coals composed predominantly of vitrinite may contain submicroscopic particles of hydrogen-rich organic matter in the vitrinite; however, these particles would not be identified during microscopic studies of the kerogen, resulting in an interpretation of coal as being composed predominantly of vitrinite (Bertrand and others, 1986, and references therein). Furthermore, petrographic analyses of Fruitland coal made under visible light can significantly underestimate the actual percentage of liptinitic macerals (Kuellmer, 1987).

Rock-Eval pyrolysis analyses of Fruitland coals (Rice and others, 1989; Law and others, 1990) indicate that these coals are hydrogen rich and have a moderate potential for generating liquid hydrocarbons (Fig. 9.18a). Fruitland coals have hydrogen indices similar to oil-prone coals from Australia (Khorasani, 1987). However, these analyses suggest that Fruitland coals are composed of type I and II kerogen rather than type III kerogen, which is characteristic of terrestrial organic matter (Law and others, 1990). The relatively high hydrogen indices of Fruitland coal are probably related to the early generation of bitumen (probably the exsudatinite reported by Rice and others, 1989) during coalification. Bitumen released during the early stages of oil generation can result in unusually high hydrogen indices (Clementz, 1979), making it difficult to correctly identify kerogen type on the basis of Rock-Eval data alone. Most of the hydrogen-rich material found in Fruitland coals is presumably indigenous and has not migrated from adjacent shales (Rice and others, 1989). Elemental analyses, in which the bitumen has been extracted before analysis, indicate that Fruitland coals are composed of type III kerogen (Fig. 9.18b), which is consistent with conclusions from petrographic studies (Rice and others, 1989; Law and others, 1990). Law and others (1990) reported correlation between the amount of generated bitumen and increasing vitrinite reflectance values, which suggests that Fruitland coals are progressively generating more hydrocarbons with increasing coal rank. These observations suggest that Fruitland coal beds are capable of producing wet gases and that areas of wet coalbed gases in the southern basin are directly related to coal rank.

Saturated hydrocarbon distributions on gas chromatograms of Fruitland coal and carbonaceous shale extracts are similar to condensates produced from Fruitland coal beds, indicating that the condensates originated from the coals (Rice and others, 1989; Clayton and others, 1991). The similar compositional range of Fruitland sandstone and coalbed gases and the similarity between coalbed gas condensates and coal and carbonaceous shale extracts (Rice and others, 1989; Clayton and others, 1991) are consistent with the migration of wet gases derived from carbonaceous shales and coal beds to adjacent Fruitland sandstones.

The generation of significant volumes of dry thermogenic gases from coal usually begins at vitrinite reflectance values of approximately 0.7% (Meissner, 1987). This lower limit of thermogenic methane generation from coal beds coincides with the southwestern limit of dry coalbed gases (Fig. 9.9), suggesting that the dry gases in the northern San Juan Basin are predominantly thermogenic in origin, as indicated previously (Rice and others, 1988, 1989). However, if Fruitland coalbed methane is entirely thermogenic, the $\delta^{13}C$ values of methane should become less negative (isotopically heavier) with increasing thermal maturation (thermogenic $\delta^{13}C$ values from - 55‰ to -15‰) (Jenden, 1985). Instead, the isotopic signature of methane from Fruitland coal beds is relatively consistent throughout the basin and does not vary

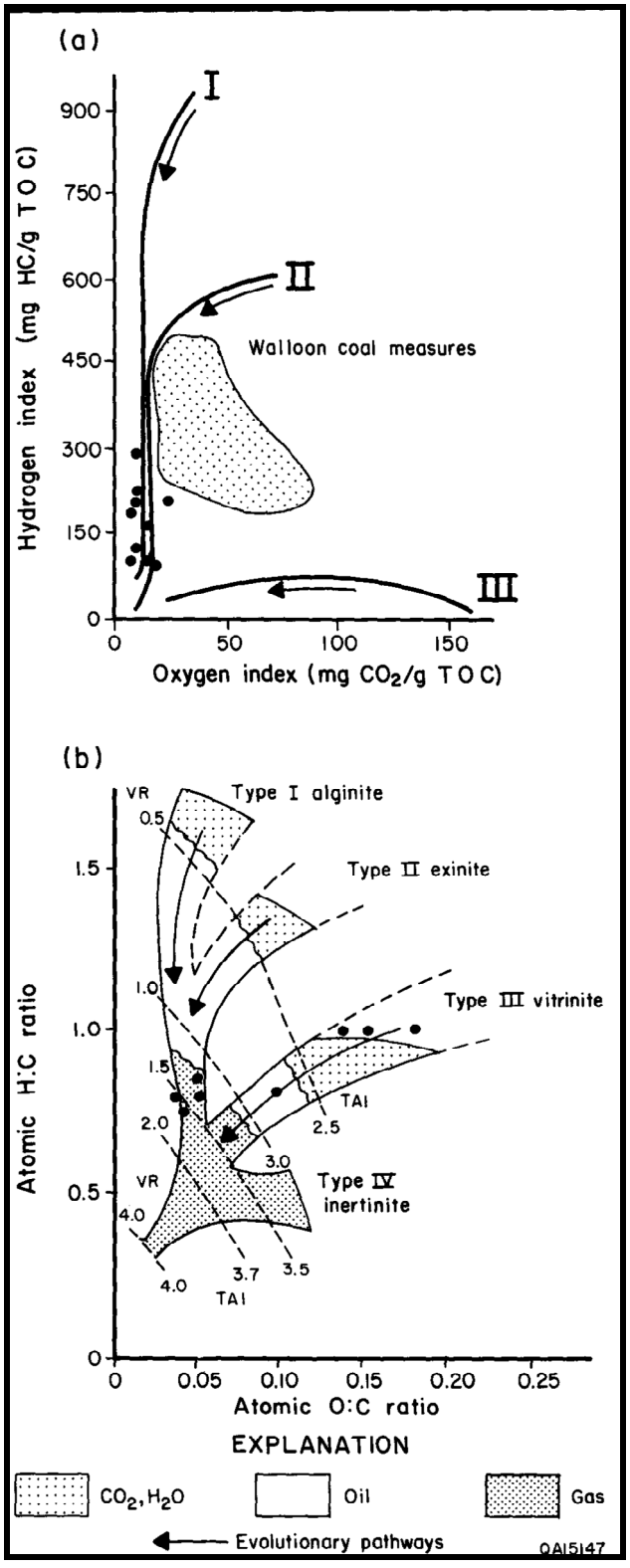

FIGURE 9.18—Geochemical characterization of Fruitland coal. Fruitland coals (solid circles) contain significant amounts of hydrogen-rich components and are capable of generating wet gases. (a) Rock-Eval pyrolysis of Fruitland coal indicates that the coal is hydrogen rich, but it incorrectly identifies the coal as types I and II kerogen. Hydrogen indices of Fruitland coals approach those of the oil-prone Walloon coal measures in Australia. (b) Elemental analyses correctly identify the Fruitland organic matter as type III terrestrial kerogen (vitrinite). Figures modified from Espitalie and others (1977), North (1985), Khorasani (1987), and Rice and others (1989). VR = vitrinite reflectance (percent); TAI = thermal alteration index; TOC = total organic carbon.

significantly with coal rank (Fig. 9.19). Either the process of thermogenic gas generation from coal is significantly different from gas generation from other types of organic matter, resulting in a relatively narrow range of $\delta^{13}C$ methane values, or the Fruitland coalbed gases represent a mixture of thermogenic and biogenic gases.

Biogenic methane $\delta^{13}C$ values range from less than -90‰ to -40‰ (Jenden, 1985), indicating that biogenic and thermogenic gases can have similar methane $\delta^{13}C$ isotopic values over the range of -55‰ to -40‰. Biogenic gases produced from carbonate reduction and/or acetate dissimilation can produce both chemically very dry gases (C_1/C_{1-5} values of 1.00) and isotopically heavy bicarbonate (Carothers and Kharaka, 1980). Furthermore, bacterial alteration of chemically wet gases can remove nearly all of the heavier gas components, producing chemically dry gases that re-

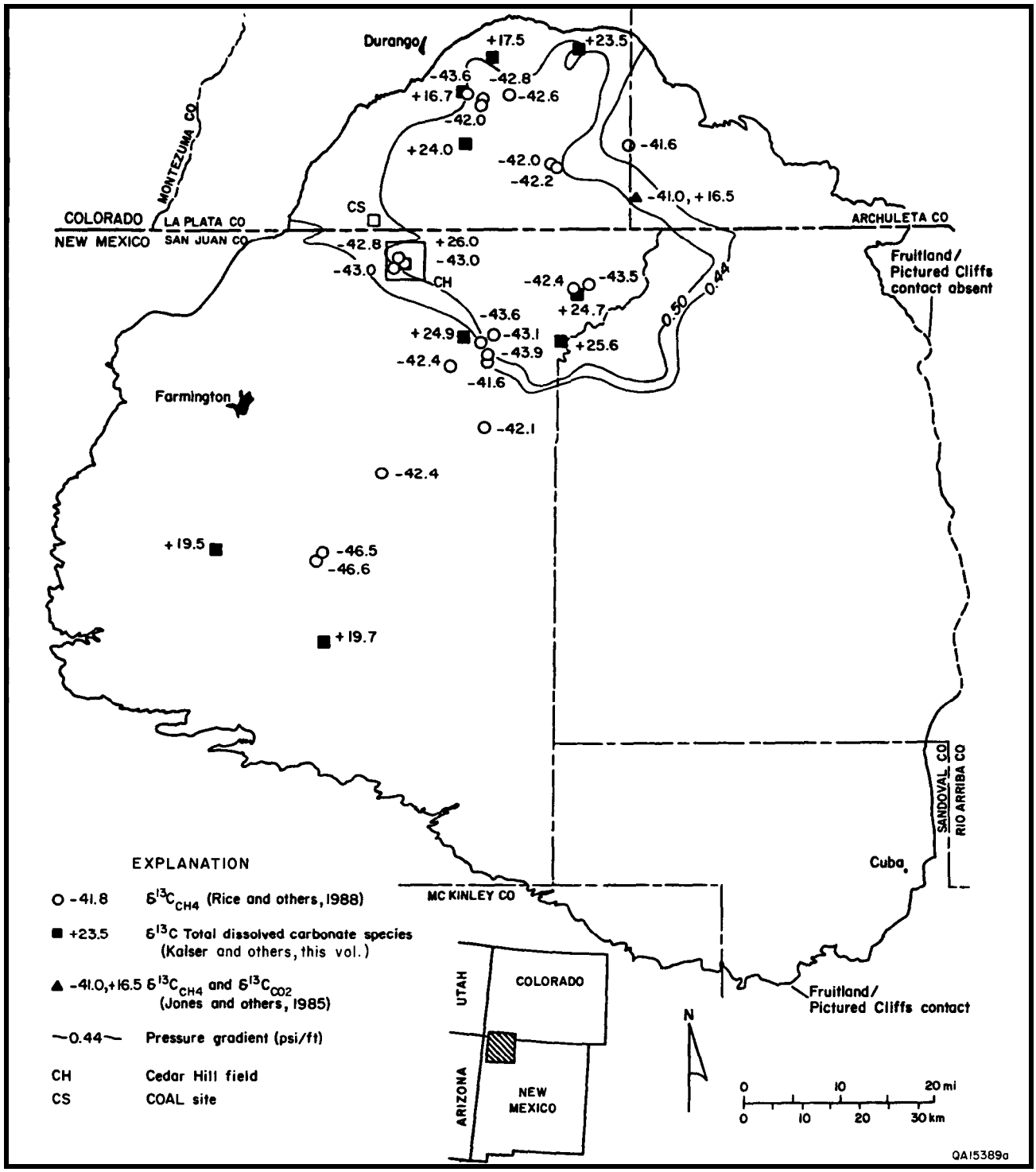

FIGURE 9.19—Distribution of $\delta^{13}C$ isotopic values of methane and carbon dioxide produced from Fruitland coal beds and PC values of total dissolved carbonate species (predominantly bicarbonate) in Fruitland formation waters. The consistency of PC methane values across the basin, light isotopic signature of methane associated with higher rank coals, isotopically heavy carbon dioxide from Fruitland coal beds, and isotopically heavy bicarbonate in Fruitland formation waters suggest that at least some coalbed gases in the overpressured, northern basin are biogenic. Data from Jones and others (1985), Jenden (1985), Rice and others (1988), and Kaiser and others (this volume, Chapter 8).

semble thermogenic gases (James and Burns, 1984). Therefore, the composition and distribution of coalbed gases and isotopic composition of bicarbonate from formation water must be considered in addition to methane $\delta^{13}C$ values to determine the origin of Fruitland coalbed methane.

Regional variations of carbon dioxide content and chemical composition (C_1/C_{1-5} values) of Fruitland coalbed gases coincide with regional overpressuring, indicating that there is a relationship between basin hydrology and gas composition. Waters from the overpressured, northern basin are dominantly Na–HCO_3 type and are characterized by high alkalinity and low chloride content (Kaiser and others, this volume, Chapter 8). Relatively minor amounts of organic acids are present in these waters, and alkalinity is predominantly inorganic (Kaiser and others, this volume, Table 8.3). The $\delta^{13}C$ values of the total dissolved carbonate species (predominantly composed of the bicarbonate ion) are isotopically heavy, ranging from + 16.7‰ to + 26.0‰ (Kaiser and others, this volume, Table 8.3). These values are consistent with isotopically heavy carbon dioxide values of + 16.8‰ for coalbed gases reported in the Glover No. 1 well (sec. 2 T32N R6W; Jones and others, 1985) and + 16.9‰ at the COAL site (sec. 17 T32N R10W; J. Close, pers. comm. 1991). Isotopically heavy values such as these can be derived from isotopically heavy carbonate cement and/or bacterial activity.

Isotopically heavy bicarbonate can be derived from the dissolution of isotopically heavy carbonate cements. Carbonates from the NEBU No. 403 well (sec. 9 T32N R7W) in the overpressured part of the basin have a wide range of $\delta^{13}C$ values (Table 9.2). Although the fracture-filling calcite is isotopically heavy ($\delta^{13}C$ of +17.2‰), the $\delta^{13}C$ isotopic values of authigenic carbonates from Fruitland sandstones and siltstones are negative, ranging from – 2‰ to –15.3‰ (Table 9.2). Carbonate cement is also present in Fruitland coal cleats (Tremain and others, this volume, Table 5.3), but the coal and/or adjacent sandstones may not contain sufficient carbonate cement to account for the large quantities of carbon dioxide present in some coal beds. Furthermore, carbonate dissolution would have to be demonstrated; precipitation of isotopically heavy carbonate in the cleat system may have occurred rather than dissolution of isotopically heavy carbonate cement. Geochemical modeling indicates that Fruitland waters, under in situ conditions, are super-saturated with respect to all carbonate phases. Furthermore, the $\delta^{18}O$ isotopic value of the fracture-filling calcite suggests that the calcite precipitated at a temperature of approximately 33°C (91°F) (Friedman and others, 1977) assuming a $\delta^{18}O$ value of – 7.4‰ for the formation water (Kaiser and others, this volume, Table 8.3, sample 5). This estimated precipitation temperature is similar to present-day formation temperatures. Therefore, bacterial degradation of organic acids and/or reduction of carbon dioxide by methanogenic bacteria may have produced both isotopically heavy carbon dioxide and bicarbonate, and biogenic methane in some parts of the basin.

A combination of thermogenic and biogenic gases can explain both methane $\delta^{13}C$ values and the heavy isotopic signature of total dissolved carbonate species in Fruitland waters. Methanogenic degradation of short-chained organic acids through acetate fermentation would produce both positive $\delta^{13}C$ total dissolved carbonate values and methane that would be depleted in ^{13}C by 66‰ to 73‰ relative to the bicarbonate at present-day in situ formation temperatures of 50° to 30°C, respectively (Friedman and others, 1977). Furthermore, acetate dissimilation is probably the major source of biogenic gas in fresh-water environments (Whiticar and others, 1986, and references therein). Biogenic carbonate reduction of carbon dioxide will also produce isotopically heavy bicarbonate and isotopically light methane.

Assuming a formation temperature of 40°C (104°F) and a bicarbonate $\delta^{13}C$ value of +23‰, the fractionation factor between methane and bicarbonate would be +71‰ (Friedman and others, 1977), and the corresponding biogenic methane would have an estimated $S^{13}C$ of –48‰. Thermogenic coalbed methane isotopic values adjacent to the overpressured north-central part of the basin range from – 42.4‰ to – 41.6‰ (Fig. 9.19). Therefore, a mixture of 85% thermogenic methane ($\delta^{13}C$ of –42‰) and 15% biogenic methane ($\delta^{13}C$ of –48‰) would produce methane with an average isotopic value of –42.9‰. These isotopic values are similar to isotopic ranges seen in Fruitland coalbed gases and formation waters (Fig. 9.19; Kaiser and others, this volume, Table 8.3). The less positive $\delta^{13}C$ values of total dissolved carbonate (+16.7‰ and +17.5‰) in the northwestern part of the basin (Fig. 9.19) may indicate the dilution of isotopically heavy bicarbonate with fresh ground water containing isotopically light bicarbonate derived from atmospheric and/or soil sources.

Thermogenic methane becomes less negative with increasing coal rank (Schoell, 1983; Jenden, 1985), suggesting that the methane $\delta^{13}C$ values of Fruitland gases should also become more positive. However, methane PC values from Fruitland coal beds remain constant (~ –42‰) over a wide range of vitrinite reflectance values (0.6 to 1.5%), suggesting that a portion of the gases desorbed from coal surfaces during early production is isotopically lighter biogenic methane. These isotopically light gases found in the over-pressured part of the basin may represent biogenic methane present in the cleat system as free gas and on coal surfaces as adsorbed gas. Adsorption of methane onto coal surfaces is controlled by the amount of methane in the gas phase (Puri and Yee, 1990). Therefore, as the concentration of biogenic methane increases in the cleat system, the methane will be adsorbed onto coal surfaces. If the concentration of biogenic methane is insufficient for adsorption to occur, the methane would remain as a free gas phase in the cleat system or be removed from the system.

During initial production, gases desorbed from coal surfaces would have a relatively large biogenic component (isotopically light methane), whereas subsequently desorbed

TABLE 9.2—Isotopic composition of Fruitland Formation and Pictured Cliffs carbonates.*

Formation	Depth (ft)	Carbonate	Comments	$\delta^{13}C_{PDB}$	$\delta^{18}O_{PDB}$
Fruitland	3086.5	calcite	fracture-filling	+17.2	–11.1
Fruitland	3093.2	dolomite	very fine sandstone	–15.3	–14.6
Fruitland	3097.3	siderite	concretion	–2.0	–12.5
Fruitland	3112.4	dolomite	siltstone	–9.6	– 16.7
Pictured Cliffs	3131.8	dolomite	fine sandstone	–8.0	–15.2
Fruitland	outcrop	calcite	cone-in-cone	–2.2	–13.7

*All samples are from the NEBU No. 403 well in Rio Arriba County, New Mexico (sec. 9 T32N R7W), except the Fruitland outcrop sample, which was collected from Ft. Lewis mine, Colorado.

gases would be progressively enriched in thermogenic methane (isotopically heavier). If this hypothesis is correct, $\delta^{13}C$ values of the produced methane should become less negative with time as the proportion of biogenic methane decreases and the amount of thermogenic gases desorbed from coal surfaces increases. The amount of change in methane $\delta^{13}C$ values over time would depend on the proportion of biogenic gases in the system and the difference between thermogenic and biogenic methane $\delta^{13}C$ values. The change in methane $\delta^{13}C$ values would be most pronounced in the northern basin, where coal is higher rank.

The presence of biogenic methane in coalbed gases is supported in part by studies involving the desorption of gases from Fruitland coal, which reported that desorbed methane from coal samples was isotopically heavier than the methane produced from nearby wells (Rice and others, 1988; Hanson, pers. comm. 1991). This suggests that $\delta^{13}C$ values of produced gases could represent a mixture of biogenic methane occurring as a free or dissolved gas in the cleat system and thermogenic methane desorbed from the coal surfaces. The presence of free gas in some wells may be indicated by a geometric mean for initial production (195 Mcf/d) that is significantly larger than that for maximum annual production (93 Mcf/d) (Kaiser and Ayers, this volume, Figs. 10.3 and 10.4).

Previous studies suggested that dry coalbed gases in the southern basin may be biogenic in origin; the light isotopic signature of the methane ($\delta^{13}C$ values of –46.6‰ to –46.5‰) results from acetate dissimilation instead of carbonate reduction during methanogenesis (Rice and others, 1988, 1989). The $\delta^{13}C$ values of bicarbonate from Fruitland Formation water produced from two wells in this area are + 19.5‰, supporting the conclusion that these gases are probably biogenic. The difference in $\delta^{13}C$ values between methane and bicarbonate from Fruitland Formation waters in this area is approximately 65‰, which is consistent with the fractionation between biogenic methane and bicarbonate reported by Carothers and Kharaka (1980) at low temperatures. Some relatively dry gases in the southwestern part of the basin also may have an early thermogenic origin, as suggested by Rice and others (1989). Recent work (Galimov, 1988) on the origin of gases in the supergiant gas fields of western Siberia indicates that early thermogenic gases can be generated from terrestrial organic matter at low levels of thermal maturity (R_m from 0.4 to 0.5%). The isotopic signatures of these early thermogenic gases ($\delta^{13}C$ values of –50‰ to –46‰) are similar to those of Fruitland coalbed gases. The boundary between chemically dry and chemically wet gases in the southern basin is near the vitrinite reflectance isorank contour of 0.5% (Figs. 9.3 and 9.9), which corresponds to the initial stage of liquid hydrocarbon generation. This boundary may represent the transition from predominantly biogenic and early thermogenic gases in the southwestern part of the basin to predominantly wet gases associated with liquid hydrocarbon generation in the west-central part of the basin.

Some coalbed gases in the overpressured part of the basin contain significant amounts of carbon dioxide (Fig. 9.10). These areas of higher carbon dioxide content (>3%) coincide with regional overpressuring, lower rank coal (low volatile A bituminous) and highest bottom-hole pressures, but do not follow regional productivity trends (Kaiser and Ayers, this volume, Chapter 10). The high production rates and large quantities of carbon dioxide (>10%) in gases produced from coal beds of the Northeast Blanco Unit (NEBU) and Meridian 400 areas may be a function of several factors, including (1) the presence of thick coal beds, which increases the resource, and folding, which increases fracture porosity and permeability in the coal (Ayers and Zellers, this volume, Chapter 4); (2) coal rank, which may control the amount of carbon dioxide and organic acids in the system; (3) fluid movement, where a general southeastward movement of water transported organic compounds, bicarbonate, and methane southeastward to this area; (4) permeability controls, which restrict lateral flow in this area; (5) bacterial degradation of organic compounds, which produces significant amounts of isotopically heavy carbon dioxide and isotopically light biogenic methane; and (6) a decrease in reservoir pressures during production, which results in the release of carbon dioxide from the formation waters.

Lower rank coals contain more oxygen-bearing functional groups and are capable of generating larger amounts of carbon dioxide and organic acids than higher rank coals, in addition to n-alkanes and other hydrocarbons. Therefore, lower rank coal would contain significantly more organic compounds that could be utilized by bacteria as food sources. Gas chromatograms of the C_{10+} alkane fraction extracted from Fruitland coals in the northern, overpressured part of the basin show an almost total absence of n-alkanes (Clayton and others, 1991; Nelson, 1991). The preferential removal of n-alkanes relative to isoprenoid hydrocarbons is a characteristic feature of biodegradation, suggesting that bacteria may have metabolized organic compounds in the coal in addition to the wet gas components. Microbial degradation of these compounds would produce chemically very dry methane with $\delta^{13}C$ isotopic values similar to methane isotopic values reported by Rice and others (1988) and would account for the isotopically heavy bicarbonate, low organic acid concentrations, high alkalinities of formation waters in this area (Kaiser and others, this volume, Table 8.3), and isotopically heavy carbon dioxide. There is a positive correlation between the carbon dioxide content of coalbed gases and the $\delta^{13}C$ of the carbon dioxide sampled at the COAL site (J. Close, pers. comm. 1991). Coalbed gases with less than 1% carbon dioxide have negative isotopic values (– 19.3‰), whereas gases with more than 10% carbon dioxide have positive isotopic values (up to +16.9‰).

Carbon dioxide is very soluble in water, and a significant portion of the isotopically heavy carbon dioxide produced from acetate dissimilation was probably dissolved in the formation water. Bicarbonate may have been transported southeastward (basinward) in Fruitland Formation waters. Because pressure increases basinward, progressively more carbon dioxide would be dissolved in the water, and total alkalinity would increase. As reservoir pressure is reduced during production, less carbon dioxide can remain dissolved in water, and carbon dioxide is released from the formation water to be produced along with coalbed gases. Desorption of biogenic and thermogenic carbon dioxide and methane from coal surfaces would also occur. The interpretation of exsolution of carbon dioxide from water is partly justified by the presence of isotopically heavy carbon dioxide produced from coal beds at the Glover No. 1 well in southern Colorado and at the COAL site (Jones and others, 1985; J. Close, pers. comm. 1991). These isotopically heavy $\delta^{13}C$ values indicate a predominantly biogenic origin for this carbon dioxide because thermogenic carbon dioxide has negative $\delta^{13}C$ values (Jenden, 1985). Furthermore, bicarbonate from Fruitland waters is enriched in ^{13}C relative to coalbed carbon dioxide by 6‰ to 9‰, which is similar to the fractionation factor of the bicarbonate and carbon dioxide system (5‰ to 6‰ at 50°C) reported by Friedman and others (1977). However, the relatively large difference (>6‰) between coalbed carbon dioxide $\delta^{13}C$ values and some Fruitland water bicarbonate isotopic values suggests that at least some carbon dioxide from coalbed gases in the northern basin may be derived from the desorption of isotopically light (isotopically negative) thermogenic carbon dioxide from coal surfaces. A mixture of 95% biogenic carbon dioxide

($\delta^{13}C$ of + 18.0‰) and 5% thermogenic carbon dioxide ($\delta^{13}C$ of – 20‰) would produce a carbon dioxide with an average $\delta^{13}C$ value of + 16.1‰, which is similar to Fruitland coalbed $\delta^{13}C$ carbon dioxide values reported by Jones and others (1985). As reservoir pressures decrease during production, progressively more isotopically light, thermogenic carbon dioxide should be desorbed from the coal surface. Therefore, the isotopic composition of carbon dioxide produced from coal beds in the northern part of the basin should become isotopically more negative with time.

Conclusions

1. Subbituminous and high volatile C bituminous coals are found in the southern basin and along the Hogback monocline. The low vitrinite reflectance values over the Ignacio anticline and along the Hogback monocline indicate that these structures formed before or during coalification. Northward of a structural hingeline, Fruitland coal rank increases abruptly, reaching the low volatile bituminous coal rank in the northern basin. The presence of structurally higher coals adjacent to structurally lower coal of the same rank in the northwestern corner of the basin suggests local postcoalification uplift and/or higher heat flux.

2. Wet coalbed gases (C_1/C_{1-5} values <0.94) in the southern part of the basin are probably indigenous to the hydrogen-rich Fruitland coal and therefore would not result from completion practices and/or migration of gases from adjacent shales. Chemically dry to very dry coalbed gases in some parts of the southern basin are most likely biogenic in origin, although some early thermogenic methane may be present.

3. The similar composition of Pictured Cliffs sandstone, Fruitland sandstone, and underpressured Fruitland coalbed gases in the southern part of the basin makes determinations of gas origin, on the basis of gas composition alone, difficult or impossible. However, minor differences in carbon dioxide content and gas wetness between Fruitland coalbed and Pictured Cliffs and/or Fruitland sandstone gases in some parts of the southern basin may allow coalbed gases to be distinguished from sandstone gases locally.

4. The similarity between Fruitland coalbed and sandstone gases in some areas suggests that these two types of reservoirs are in communication and/or that the gases were derived from similar types of organic matter. Gas compositional data also suggest that gases from Pictured Cliffs sandstones may have originated from basal Fruitland coal beds in the western part of the basin, where thick coal beds directly overlie Pictured Cliffs sandstones. However, additional data are required to determine the timing and extent of gas migration.

5. Basin hydrology and coal rank control Fruitland coalbed gas composition. The effect of basin hydrology on coalbed gas compositions is shown by the abrupt transition from carbon dioxide rich, chemically dry to very dry gases in the overpressured, northern part of the basin to carbon dioxide poor, chemically wet gases in the underpressured, southern part of the basin.

6. Bacterial degradation of organic acids by acetate dissimilation and/or the microbial reduction of carbon dioxide are required to produce the isotopically heavy bicarbonate ($\delta^{13}C$ ranges from +16.7‰ to +26‰) found in Fruitland coalbed waters. A mixture of 85% thermogenic methane ($\delta^{13}C$ of – 42‰) and 15% biogenic methane ($\delta^{13}C$ of – 48‰) would produce methane with an average isotopic value of – 42.9‰. The $\delta^{13}C$ value of the corresponding bicarbonate would be +23‰, assuming a fractionation factor of 71‰ between the biogenic methane and bicarbonate. These isotopic values are similar to isotopic ranges reported for Fruitland coalbed gases and formation waters. Furthermore, the presence of free and dissolved biogenic methane in the cleat system of Fruitland coal and/or biogenic methane adsorbed onto coal surfaces would explain the relatively constant PC methane values in the northern basin reported in earlier studies.

7. The large amounts of carbon dioxide in gases produced from coal beds in the Northeast Blanco Unit (NEBU) and Meridian 400 areas may result from a combination of factors. Isotopic data suggest that some of the carbon dioxide produced from Fruitland coal beds is biogenic in origin and that it may originate from the formation water. We suggest that bacterially generated carbon dioxide was dissolved in formation waters and transported basinward. As pressure decreases during production, carbon dioxide exsolves from the formation water and mixes with carbon dioxide, methane, and other gases desorbed from coal surfaces.

Acknowledgments

We thank Jeff Peace and George Lippman of El Paso Natural Gas Company, Brent W. Hale of Northwest Pipeline Corporation, Tom Hemler of Jerome P. McHugh and Associates, and Ernie Busch of the New Mexico Oil and Gas Conservation Commission for providing the gas data used in this study. We also thank William B. Hanson of Amoco Production Company and Peter D. Jenden of Chevron Production Research for their valuable comments concerning coalbed gas chemistry. We thank Joseph Yeh for handling and digitizing the large gas data base. Finally, we thank Tucker F. Hentz and William B. Hanson for their constructive reviews of the manuscript.

10. Coalbed methane production, Fruitland Formation, San Juan Basin: geologic and hydrologic controls

W. R. Kaiser and W. B. Ayers, Jr.
Bureau of Economic Geology

Abstract—Production from Fruitland coalbed methane wells in the San Juan Basin ranges from 30 to 15,000 Mcf/d. Production varies markedly from one well to another, even where wells are closely spaced; both regional and local controls on coalbed production exist. To determine geologic and hydrologic controls on the production of coalbed methane, we analyzed production of gas and water from Fruitland coal beds, mapped gas and water production, and compared production maps with geologic and hydrologic maps. Coalbed methane production is greatest where wells are completed in northwest-trending, thick coal deposits in the overpressured, northern part of the basin. Within these northwest-trending belts, the basin's highest production occurs in smaller, northeast-trending pods, consistent with the depositional fabric. Although production is greatest from wells in the overpressured part of the basin, production rates from the underpressured, southern part of the basin overlap those of the north. Because wells in the underpressured part of the basin are shallow and produce little or no water, they are inexpensive to drill and operate. On the basis of geology, hydrology, and production, the San Juan Basin was divided into three areas in which Fruitland coal beds have similar reservoir characteristics.

Introduction

The San Juan Basin is the largest producer of coalbed methane in the United States. Production increased from 2 Bcf in 1985 to 67 Bcf in 1989 and was 447 Bcf in 1992. The number of producing coalbed methane wells in the Fruitland Formation also increased from fewer than 50 in 1985 to more than 500 in 1989 and more than 2,100 in 1992. Production rates from coalbed methane wells vary locally and regionally. The increasingly large production data base affords an opportunity to evaluate production trends to determine controls on coalbed methane production and thereby develop exploration strategies for frontier areas.

The objectives of this paper are to (1) evaluate gas and water production from Fruitland coalbed methane wells, (2) map gas and water production from coalbed methane wells, (3) identify geologic and hydrologic controls on occurrence and producibility of coalbed methane by comparing production maps with geologic and hydrologic maps, and (4) characterize the regional variations in Fruitland coalbed reservoirs.

We first analyze Fruitland production and present summary statistics by lithology and pressure regime. This discussion is followed by a review of physical and economic controls on the production of coalbed methane. Among these are size, thickness, and orientation of coal seams, reservoir pressure, permeability, and water production. Finally, potential for future coalbed methane production is evaluated in a basinwide characterization of reservoir parameters of Fruitland coal beds.

Production

Analysis of Fruitland production is based on (1) annual gas and water production data through 1987, collected by the Colorado Geological Survey, and (2) all reported Fruitland completions from Dwight's Oil and Gas Reports (Dwight's, 1990a and b). Updated production and new well data through 1989 were obtained from Dwight's. We evaluated each well to confirm Fruitland completions and to determine the lithology of the producing interval. We identified approximately 780 coalbed completions and 225 sandstone completions in the Fruitland Formation as well as more than 100 coal and sandstone and 52 indeterminate (no log or poor log) but probable Fruitland completions through 1989. A review of wells listed as Fruitland/Pictured Cliffs completions showed that most of these are Pictured Cliffs completions. A few were completed in Fruitland coal seams and Pictured Cliffs sandstones; none were completed in only coal seams.

Because of recent orders by the New Mexico Oil Conservation Division (orders no. R-8768 and R-8769) designating all Fruitland coalbed methane wells as "Basin-Fruitland Coal Gas Pool," this report refers to productive areas in New Mexico by geographical area or by the name of the operator most active in an area. Order no. R-8768 established the Coal Gas Pool, and order no. R-8769 restricted the vertical limits of 26 existing Fruitland and Fruitland/Pictured Cliffs Gas Pools to include only the sandstone completions. In Colorado, Ignacio Blanco field is the only Fruitland field, and it includes production from both coal beds and sandstones.

Decline behavior

Decline behavior was evaluated to establish a profile of coalbed methane performance and to compare performance of coalbed methane wells with that of Fruitland sandstone wells. We evaluated decline behavior by comparing production histories of coalbed and sandstone completions, using decline curves and Q plots. In the Q plot (REC, 1989a and b), first-year production (Q_1) divided by cumulative production to date (Q_{total}) is plotted against years of production. This technique can be used to analyze decline behavior of wells individually, by reservoir, and by stratigraphic interval. To facilitate analysis, type decline curves were generated for selected decline-rate factors of 5, 10, 20, 30, 50, and 75%/yr, assuming exponential decline. With time, the curves asymptotically approach the selected rate factor.

Because long production histories are required to establish decline rates and there are many old sandstone wells, a basinwide plot of Fruitland sandstone production is used to introduce Q plots. Sandstone wells commonly show steep decline (20 to 50%) early in their production and typically less than 20% decline later, beyond 15 yrs of production (Fig. 10.1). Low decline rates are expected in the oldest wells because they should be little affected by depletion in offset wells. Newer wells (<15 yrs production) showing steep decline probably are experiencing depletion because of production from older offset wells, whereas those with little decline (<10%) probably represent completions in new reservoirs. Scatter over the entire range of the Q plot reflects completions in a great number of different reservoirs. Such a plot for a single reservoir would indicate a highly compartmentalized reservoir.

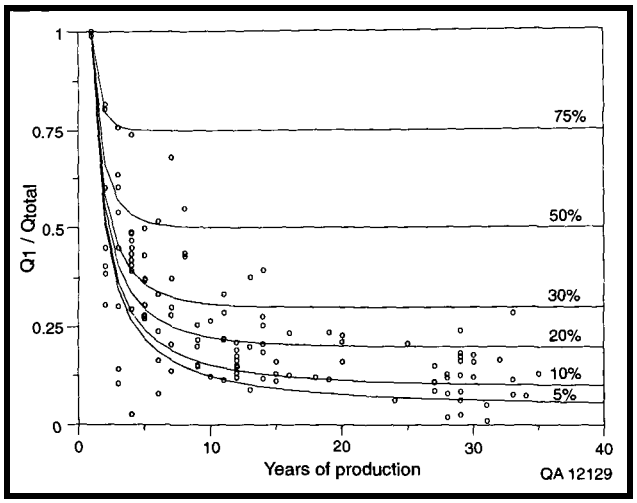

FIGURE 10.1—Q plot, Fruitland Formation sandstone wells.

Sandstone wells commonly have decline curves that cross the exponential-decline type curves in the early years (gently curved) and then flatten in the late years to parallel the type curves at decline rates of 10 to 20%/yr (Fig. 10.2). From the Q plots, we condude that sandstones exhibit exponential decline late, as reported by operators in personal communications, and hyperbolic decline early in their production. Sandstone Q plots by pressure regime show that overpressured wells have decline rates greater than 10% and little scatter, whereas underpressured wells show great scatter and have lower decline rates (<10%).

Although the Q plot was designed to evaluate sandstone reservoirs, it can be used to analyze coalbed reservoirs. Because many coalbed reservoirs show negative decline, or increased production with time in the early years, there will be an obvious effect on the Q plot, giving the well a decline rate in its late history much lower than that for sandstone. To compare coal and sandstone decline behavior, we made Q plots for 40 selected wells-7 completed in coal beds and 33 in sandstones.

Q plots for coalbed wells show that production from coal beds declines exponentially at rates of less than 5%/yr (Fig. 10.3). The San Juan 32-7 unit No. 6 well (Phillips No. 617) has a decline rate of 2.5% beyond 15 yrs of production. Coal reservoirs in the Black Warrior Basin also display exponential decline (David Bolin, pers. comm. 1989). Fruitland wells exhibiting classic negative decline (Cahn and Knauff wells) fall well below the exponential curve early (sharply curved), whereas others (Clay and Western Federal wells) exhibit no negative decline and closely follow the type curve. The latter two wells are in the underpressured, west-central part of the basin, and they produce little or no water.

Several wells in the underpressured, west-central part of the basin, reported to be sandstone completions, have anomalously low decline rates of less than 10%/yr (Fig. 10.1). These wells display coal decline behavior (negative decline and very low decline rates) and probably are producing methane from coal seams adjoining sandstones (Fig. 10.4). The Scott No. 21 is such a well at Cedar Hill field. Sandstone wells that show greater decline (hyperbolic) early (gently curved Q plot) and exponential decline later (for example, Schultz Corn F No. 11) may reflect initial production directly from a conventional sandstone reservoir and later production indirectly from coal seams (Fig. 4). Early production from sandstones and mainly late production from coal beds may have occurred at the San Juan 32-7 unit No. 6 well (Fig. 10.3), which is completed open hole in interbeddedsandstones and coal seams. Sandstone wells that show exponential decline throughout their productive histories may have been in early communication with coal seams.

In summary, three distinct Fruitland production Q plots, exhibiting decline behavior characteristic of production from coal seams, sandstone beds, and sandstone beds in communication with coal seams, are recognized (Fig. 10.5). The representative coalbed Q plot drops quickly (sharply curved early) to exponential decline rates of less than 5%/yr, whereas the sandstone Q plot is gently curved early and exhibits decline rates of 10 to 20%. The Q plot of a sandstone completion inferred to be in contact with a coal bed (coalbed behavior) has features of both curves, gentle curvature early and low exponential decline (less than 5%) later in its production history. These decline-curve characteristics may allow Q plots to be used to distinguish wells producing from coal beds, sandstones, or both.

Production statistics

We analyzed gas and water production from Fruitland coal beds in the overpressured and underpressured areas of the San Juan Basin to provide an overview of production statistics and to determine the contour interval to be used on production maps. Production statistics are subject to several pitfalls or limitations. Among these are (1) variations in completion techniques, (2) complications of negative decline, (3) limited production history, (4) incomplete reporting by operators, and (5) demand-related shut-ins. Despite these limitations, enough coalbed methane has been produced in the San Juan Basin to provide a data base adequate to begin identification of geologic and hydrologic controls on coalbed methane production.

To compare the productivity among wells having either long or short productive lives and to minimize the time variable inherent in cumulative production data, we evaluated initial potential (IP) and maximum annual production (MAP), where MAP is the average daily production of a well's most productive year. There was no adjustment to account for negative decline in the early production. Commonly, IPs were run for 3 hrs on a ¾-inch choke and were from both stimulated and unstimulated wells. There were more IP than MAP data available because many completions are recent, and in dually completed wells, IPs usually are conducted separately for each formation, whereas production is commingled so that MAP cannot be determined.

Maximum annual gas production—Histograms of MAP for Fruitland coalbed and sandstone completions show overlapping lognormal distributions (Figs. 10.6 and 10.7), suggesting that coalbed reservoirs have production rates similar to sandstone reservoirs, after initial depressurization and the onset of desorption in coal beds. In other words, the two reservoir types have similar production rates at the end of negative decline. On the basis of similar production rates and statistical distributions, permeability of similar magnitude is inferred for coalbed and sandstone reservoirs.

Basinwide, the geometric mean (GM) for MAP from coal beds is slightly larger than that from sandstones, whereas by pressure regime the GM for coal is less than that for sandstones. Overpressured coal seams are more productive than underpressured seams, although there is considerable overlap between pressure regimes (Fig. 10.6). High productivities from overpressured sandstones reflect high deliverabilities from high-pressure, conventional reservoirs (Fig. 10.7). Production from underpressured coal seams and sandstones is lower than that from overpressured reservoirs (Figs. 10.6 and 10.7). In all cases, the mode for coal is less than that for sandstone (Figs. 10.7 and 10.8). Lower GMs and modes for coal are not readily explained. Negative decline is the likely explanation in that many coalbed wells,

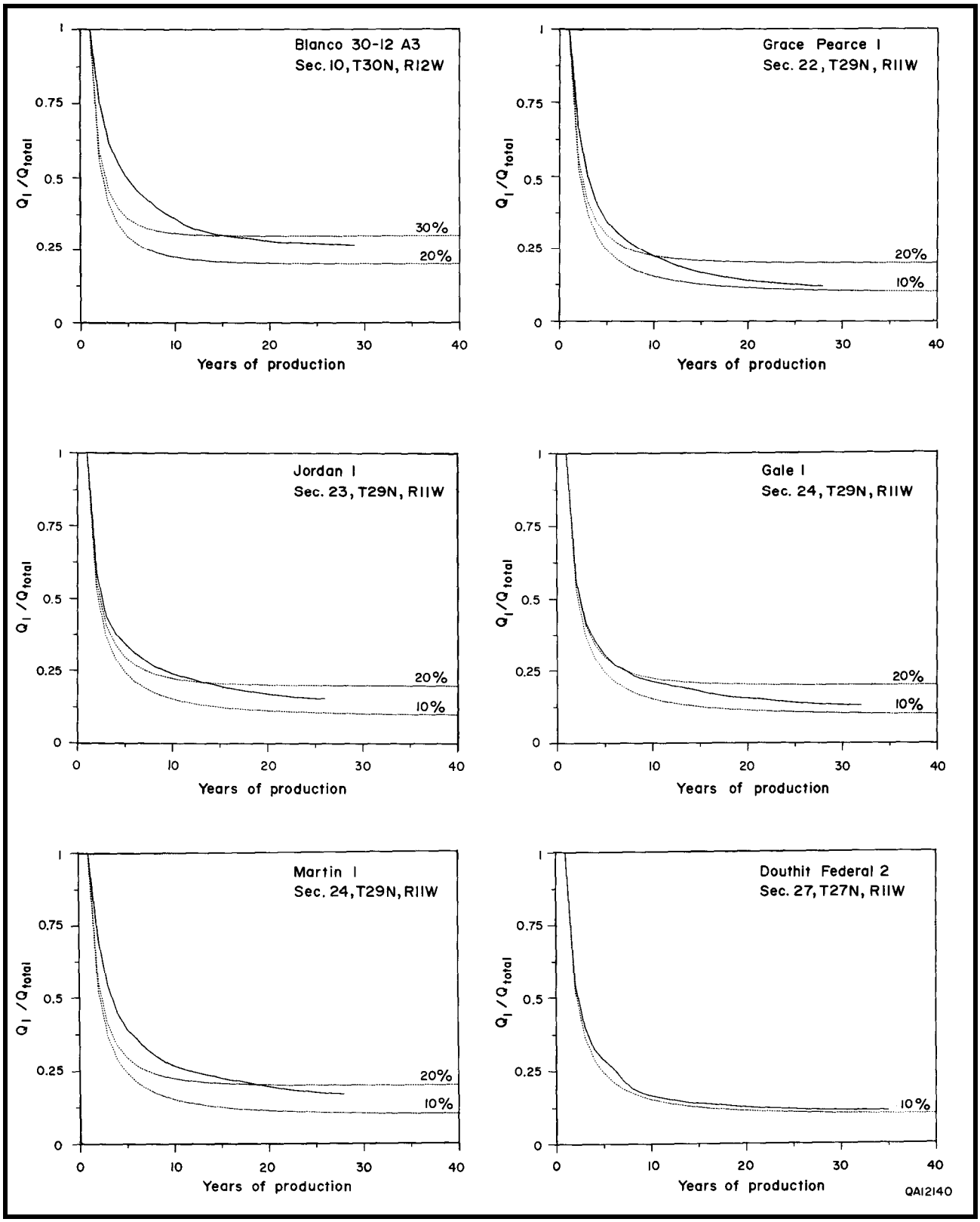

FIGURE 10.2—Q plots, individual Fruitland Formation sandstone wells.

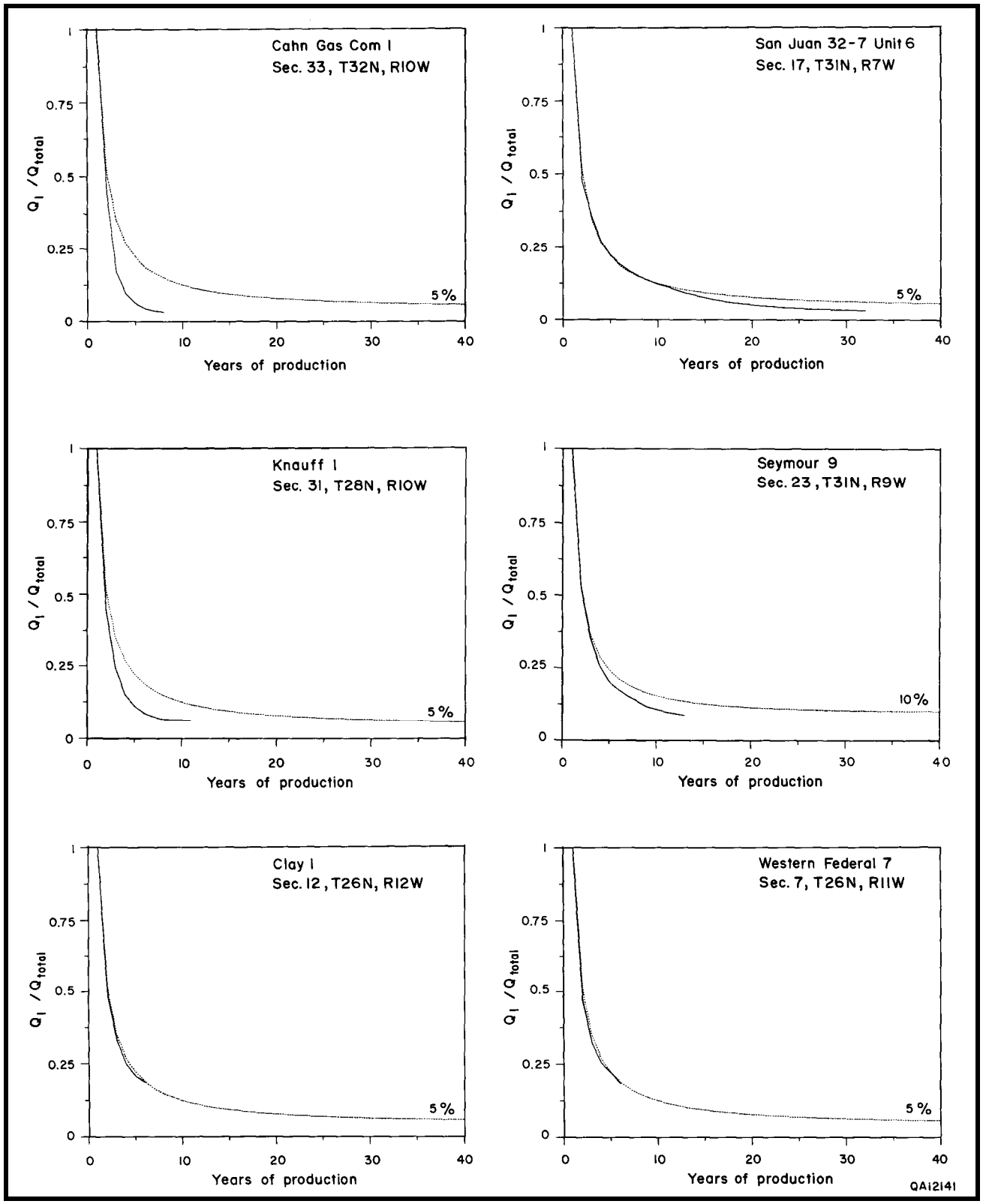

FIGURE 10.3—Q plots, individual Fruitland Formation coalbed wells.

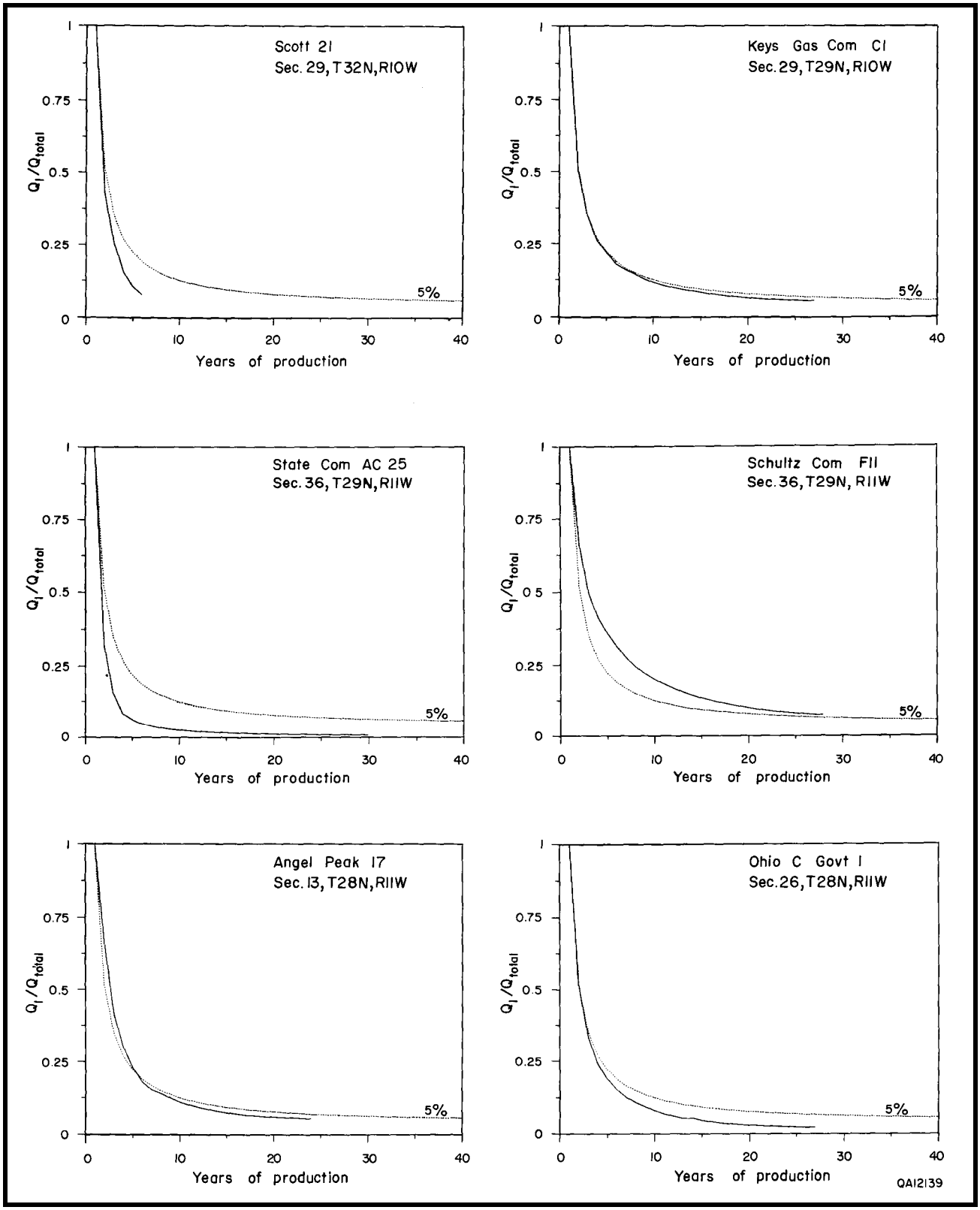

FIGURE 10.4—Q plots, individual Fruitland Formation sandstone wells that exhibit coal-decline behavior.

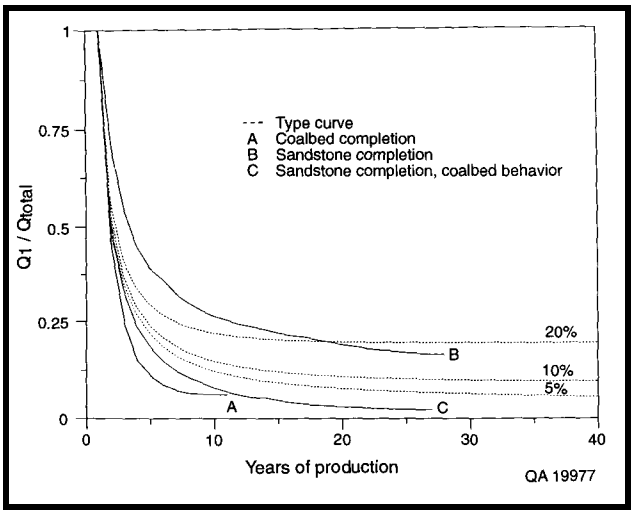

FIGURE 10.5—Q plots representative of gas production from coal beds, sandstones, and sandstones in communication with coal beds.

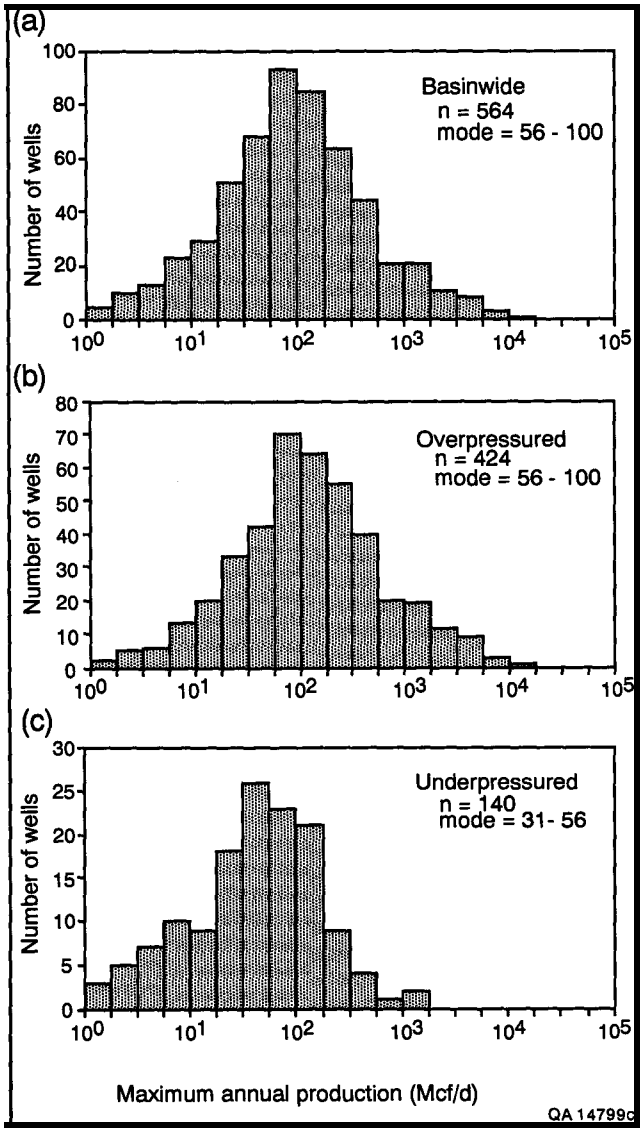

FIGURE 10.6—Histograms of maximum annual gas production from Fruitland coalbed wells, San Juan Basin for (a) basinwide, (b) overpressured, and (c) underpressured areas. Maximum annual production is most productive year, normalized to daily production; it is plotted in 0.25-log units. Production is lognormally distributed.

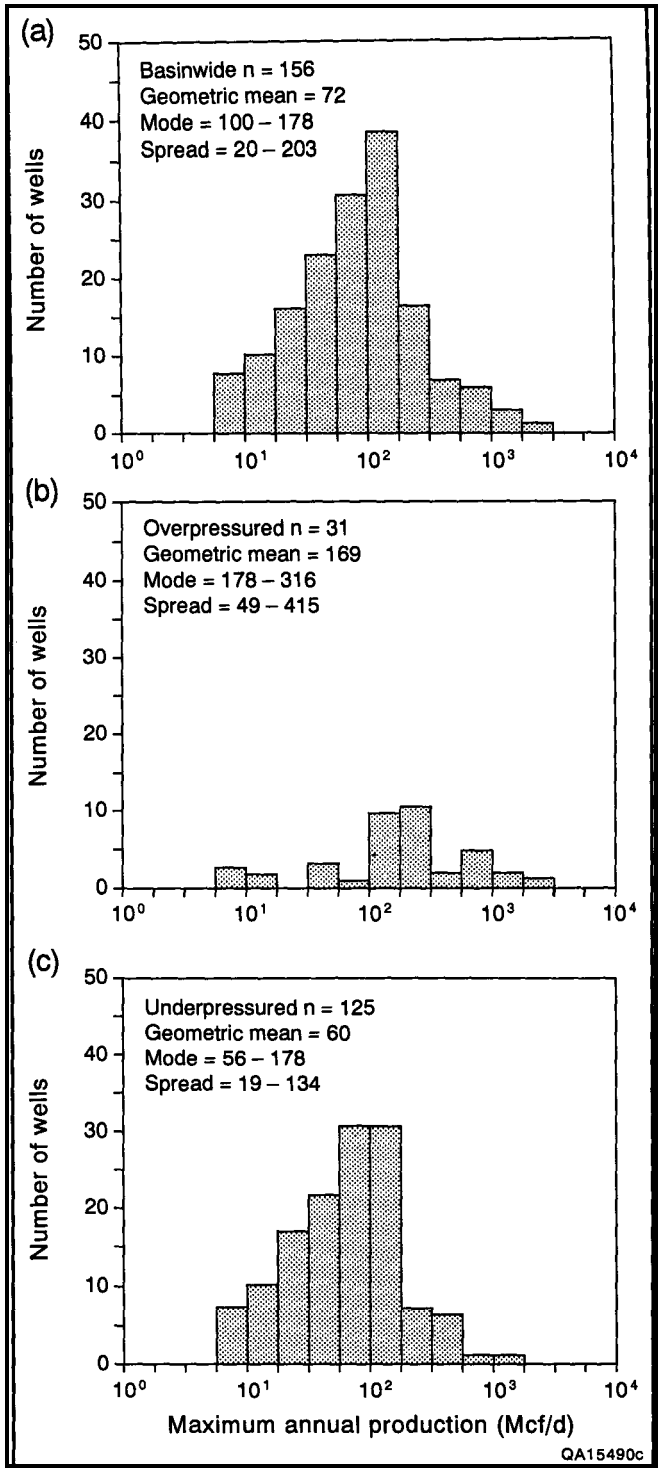

FIGURE 10.7—Histograms of maximum annual gas production from Fruitland sandstone wells, San Juan Basin, for (a) basinwide, (b) overpressured, and (c) underpressured areas.

because of short production histories, have not yet reached peak production. Few coalbed methane wells have produced for 5 yrs or more.

Initial gas potential—On initial potential (IP), the GM of coalbed wells (195 Mcf/d) is much less than that of sandstones (726 Mcf/d), which undoubtedly reflects the early production behavior of coalbed reservoirs, when fluid pressure and water saturation are high (negative decline characteristics). The central 68% of the distribution, or spread between 16 and 84% probability, for coalbed completions

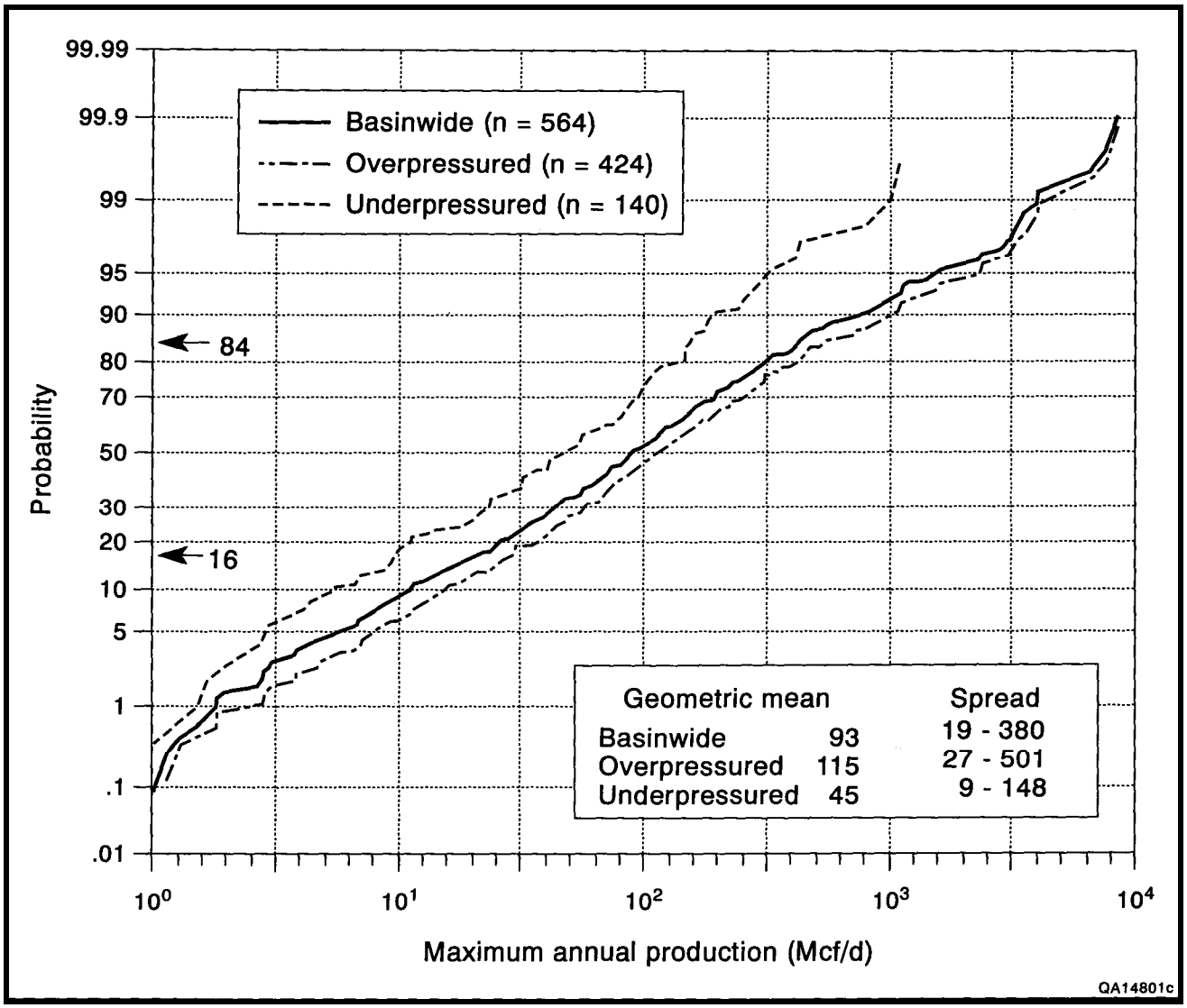

FIGURE 10.8—Probability plots of maximum annual gas production from Fruitland coalbed wells, San Juan Basin. Production is plotted in 0.1 -log units.

exceeds that for sandstones, reflecting a large number of highly productive, overpressured coal wells. The probability of an overpressured coal well producing more than 1,000 Mcf/d is 10% (Fig. 10.8). Overpressured coalbed wells are most productive, but production values from overpressured and underpressured wells overlap.

Free gas in some coal seams is indicated by the similarity of MAP for underpressured coal seams and sandstones (Figs. 10.6 and 10.7) and by higher productivities upon initial testing than upon sustained production in some wells (Figs. 10.8 and 10.9). Note that the GMs for IP are about twice those for MAP. On initial potential, coalbed production is bimodal (Fig. 10.10). The high second mode (3,162 to 5,623 Mcf/d) reflects high IPs in the Meridian 400 area and is comparable to IPs from Fruitland sandstone reservoirs (562 to 5,623 Mcf/d). Here, the presence of free gas (significant fracture porosity) and/or fluid pressures close to desorption pressure, allowing gas to desorb upon only slight depressurization, are suspected.

Water production—Initial water potential was also evaluated, because it has been shown to increase with permeability (Oldaker, 1991). The distribution of water IPs, like those of gas, is lognormal (Fig. 10.11). Production is greatest from overpressured wells; GM of initial tests in overpressured coal beds is 211 barrels of water per day (bwpd). By water-well standards, most coalbed methane wells are low-yield wells (1 to 100 gallons per minute [gpm]). For example, 100 bwpd is equivalent to 3 gpm, which is well below a moderate-yield water well producing hundreds of gallons per minute (100 gpm = 3,430 bwpd). Wells testing water free are most common in underpressured coal seams. Their anomalous occurrence in the overpressured region reflects low permeability, gas-saturated coal seams, or unreported water production; although operators are required to report water production, they do not always comply.

To identify predictors of productivity, we made scatter plots of IP and MAP for gas and water. The only correlation was between IP and MAP for gas (Fig. 10.12). In overpressured wells with IPs greater than 30 Mcf/d, IP is a predictor of long-term productivity, as indicated by MAP. Lack of correlation below 30 Mcf/d probably reflects high water yield during early production. Underpressured wells show a correlation between IP and MAP for gas over the entire range of IPs. A plot of MAP gas versus MAP water (Fig. 10.13) shows a correlation at gas production rates of 10 to 500 Mcf/ d. The scatter of this plot shows that highly productive gas wells are not always prolific producers of water, suggesting the presence of free gas. IP water is a poor predictor of well

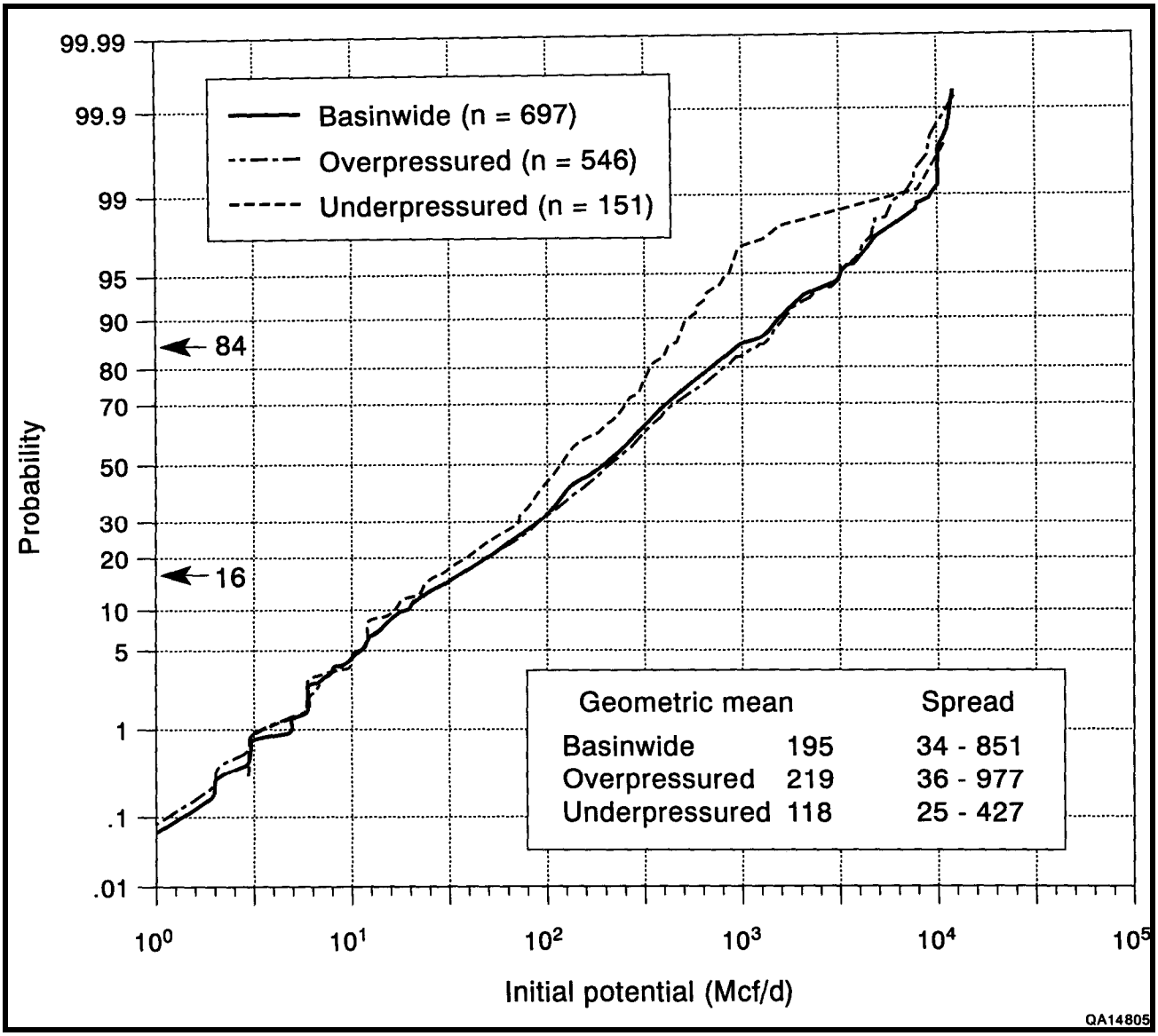

FIGURE 10.9—Probability plots of initial gas potential from Fruitland coalbed wells, San Juan Basin. Production is plotted in log units.

performance. A plot of IP water versus MAP gas showed no correlation (Fig. 10.14), which was unexpected, because high water productivities (several 100 bwpd) are indicative of enhanced permeability. Many wells are still being de-watered and have yet to reach peak gas production. Wells that produce large volumes of water but little gas may have tapped coal seams that are hydraulically well interconnected and thus more difficult to dewater (depressurize).

Coalbed methane production history and trends

In 1989, coalbed methane production from the Fruitland Formation in the San Juan Basin was 67 Bcf from more than 500 wells, a dramatic increase from the 19 Bcf produced from fewer than 200 wells in 1988. Most production is from the north-central part of the basin. The Meridian 400 area and Cedar Hill and Ignacio Blanco fields (Fig. 10.15) accounted for approximately 90% of the basinwide production in 1989. Although most coalbed methane production and pre-1987 activity were in the north-central part of the basin, in 1988 and 1989 considerable coalbed methane activity occurred in the southern part, including new wells and old Pictured Cliffs wells recompleted in Fruitland coal seams. This activity is primarily in eastern San Juan County and secondarily in western Rio Arriba County, New Mexico, but it extends as far south as T24N and as far east as R2W. From maps of maximum annual gas production (MAP) and of initial gas and initial water production (Figs. 10.15, 10.16, and 10.17), productivity trends were delineated. On all production maps, the boundary of regionally overpressured Fruitland strata, defined by the 0.44 psi/ft pressure-gradient contour (Kaiser and others, this volume, Fig. 8.7), is included for reference.

Two major trends—northwest and northeast—are evident in gas-production maps. The most productive coalbed methane wells occur in the overpressured, northern part of the basin (Figs. 10.15 and 10.16), as was shown in production histograms (Figs. 10.6 and 10.10). On the basis of the production histogram (Fig. 10.6), highly productive wells were defined as those with MAP greater than the modal class of 100 Mcf/d. These highly productive wells occur in a northwest-trending belt (primary trend) in New Mexico, where MAP and IP for gas generally exceed 100 Mcf/d and locally are greater than 316 Mcf/d (Figs. 10.15 and 10.16). This primary belt includes the Meridian 400 wells and Cedar Hill field. Two other less continuous, northwest-trending

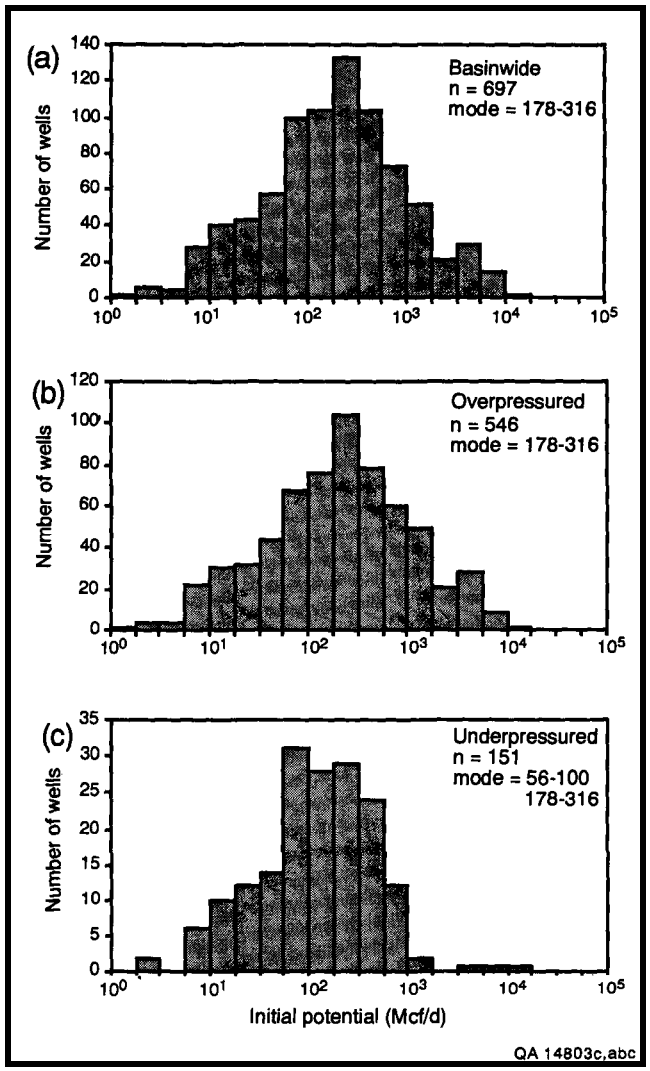

FIGURE 10.10—Histograms of initial gas potential from Fruitland coalbed wells, San Juan Basin, for (a) basinwide, (b) overpressured, and (c) underpressured areas.

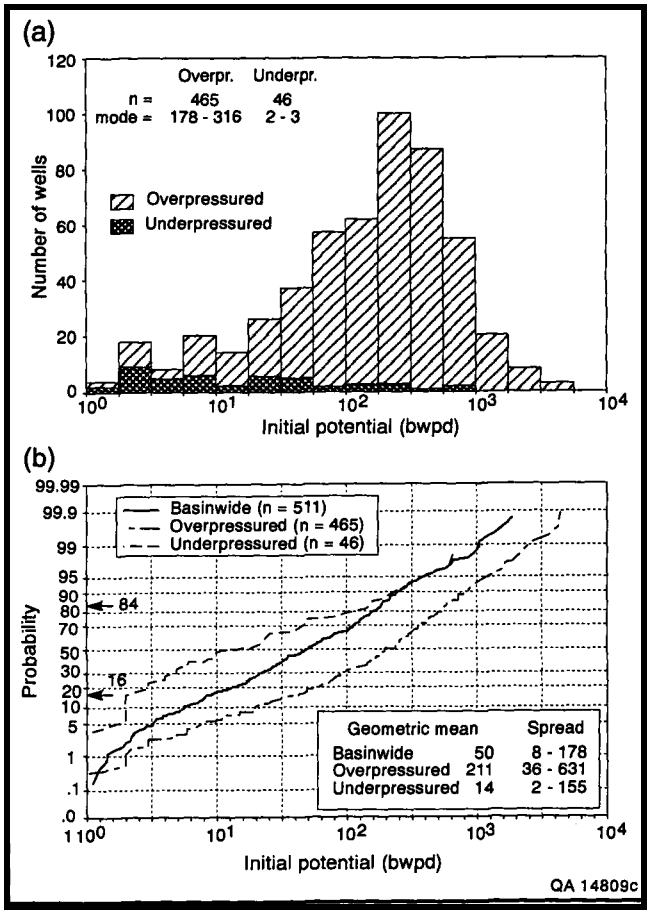

FIGURE 10.11—(a) Stacked histograms and (b) probability plots of initial water potential from Fruitland coalbed wells, San Juan Basin. Production, plotted in log units, correlates with pressure regime.

belts of highly productive wells occur in Colorado, northeast of the primary belt. The first is delineated on the map of maximum annual production, where it is located southeast of Durango (Fig. 10.15), and the second is apparent on the IP map, near the northern margin of the basin (Fig. 10.16).

A prominent northeast trend is present on both gas-production maps (Figs. 10.15 and 10.16) but is particularly evident in the map of maximum annual production (Fig. 10.15). In New Mexico, in the northwest-trending primary belt of production greater than 100 Mcf/d (Meridian 400 to Cedar Hill areas), the most productive wells (300 to 3,000 Mcf/d) occur in smaller northeast-trending pods. Northeast-trending pods of highly productive wells are present throughout the overpressured part of the basin. However, in the underpressured, southwestern part of the basin, highly productive wells occur in broad northeast-trending belts (Figs. 10.15 and 10.16).

Most water-productive coalbed methane wells are in the overpressured, northern part of the basin (Fig. 10.17), where initial water production from coalbed wells is greatest. Generally, areas of high water production coincide with areas of high gas production (compare Figs. 10.15, 10.16, and 10.17). The dominant trend of high water production (defined as >316 [or $10^{2.5}$] bbls/d [Fig. 10.11]) is northeast, with secondary northwest and north trends present (Fig. 10.17). Because of poor reporting practices, these trends may be as much an artifact of incomplete data as a reflection of the physical system. Note that the dominant water-production trend is a secondary, but highest, trend for gas production. Water production in the underpressured, southwestern part of the basin is minimal.

Controls on coalbed methane production

Production characteristics of Fruitland coalbed reservoirs vary across the San Juan Basin, reflecting regional differences in geologic and hydrologic settings, which were described in the preceding papers of this volume. These differences include coal and coal-gas resources, pressure regime, permeability, gas composition, and water production. By comparing geologic and hydrologic maps with production trends, controls on Fruitland coalbed methane production were identified. In this section, we first discuss physical controls on production, or reservoir characteristics: coalbed occurrence, thickness, and rank; formation pressure; and fracturing. We then describe two economic controls on production: gas composition and water production.

Coal occurrence, trends, and thickness

Coalbed thickness determines gas resources and affects production by influencing the size of the dewatered area, or cone of depression. Assuming economic dewatering, equal permeability, and artesian overpressure, gas productivity will be greater in a thicker seam because a larger cone of

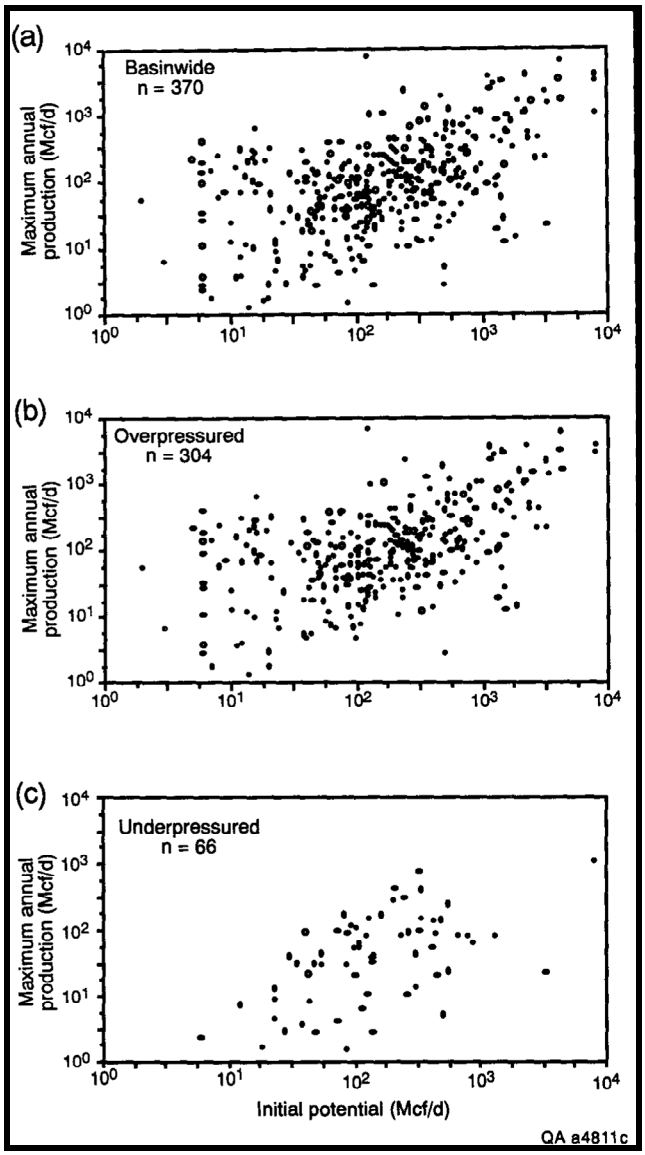

FIGURE 10.12—Scatter plots of maximum annual gas production versus initial gas potential from Fruitland coalbed wells, San Juan Basin, for (a) basinwide, (b) overpressured, and (c) underpressured areas. Annual and initial production shows positive correlation above 30 Mcf/d ($10^{1.5}$). Production is plotted in log units.

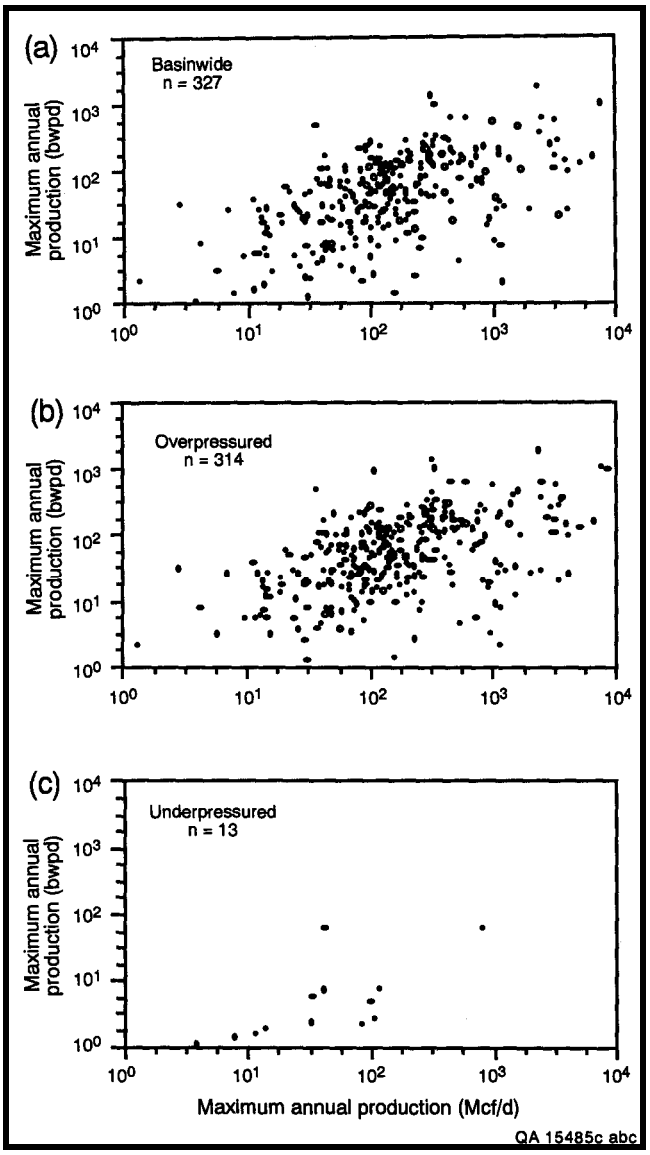

FIGURE 10.13—Scatter plots of maximum annual gas production versus maximum annual water production from Fruitland coalbed wells, San Juan Basin, for (a) basinwide, (b) overpressured, and (c) underpressured areas. A correlation is present between 10 and 500 Mcf/d ($-10^{2.7}$) and is absent above 500 Mcf/d.

depression is induced upon dewatering, freeing a larger volume of gas. Coal occurrence and thickness are controlled by depositional systems. The thickest coal seams occur in three northwest-trending belts landward (southwest) of the pinch-outs of upper Pictured Cliffs tongues and northeast of a structural hingeline at the basin floor (Ayers and others, this volume, Fig. 2.15, belts E, F, and G, and Figs. 2.2 and 2.5). Southwest of the hingeline, coal deposits are thinner and are northeast-trending, lying between Fruitland channel-sandstone belts.

Depositional trends are reflected in the production maps. Production trends (Figs. 10.15 and 10.16) parallel coal-thickness trends (Ayers and others, this volume, Figs. 2.16 and 2.19). Production is greatest from the northwest-trending coal deposits in the northern part of the basin; within these northwest-trending belts, secondary northeast trends of very high production are present. In the northern basin, coalbed gas in place generally exceeds 15 Bcf/mi^2 and locally exceeds 35 Bcf/mi^2 (Ayers and others, this volume, Fig. 2.21). In the southwestern part of the basin, production patterns trend predominantly northeastward and gas in place is commonly 5 to 15 Bcf/mi^2.

Coal rank

The volume of gas generated in a coal bed is rank related. Fruitland coal rank is greatest in the northern San Juan Basin, where it is medium to low volatile bituminous. Coincidence of coal of high rank with the occurrence of thick coal beds and high reservoir pressure results in large coalbed methane resources in this part of the basin. The area encompassed by high volatile A bituminous or higher rank coal (Scott and others, this volume, Fig. 9.3) makes up one-fourth of the basin, yet it contains more than one-half of the Fruitland coalbed methane resources. Coal of lower rank does not preclude presence of economic coalbed methane resources; coalbed methane production is well established in the southern San Juan Basin, where coal (subbituminous

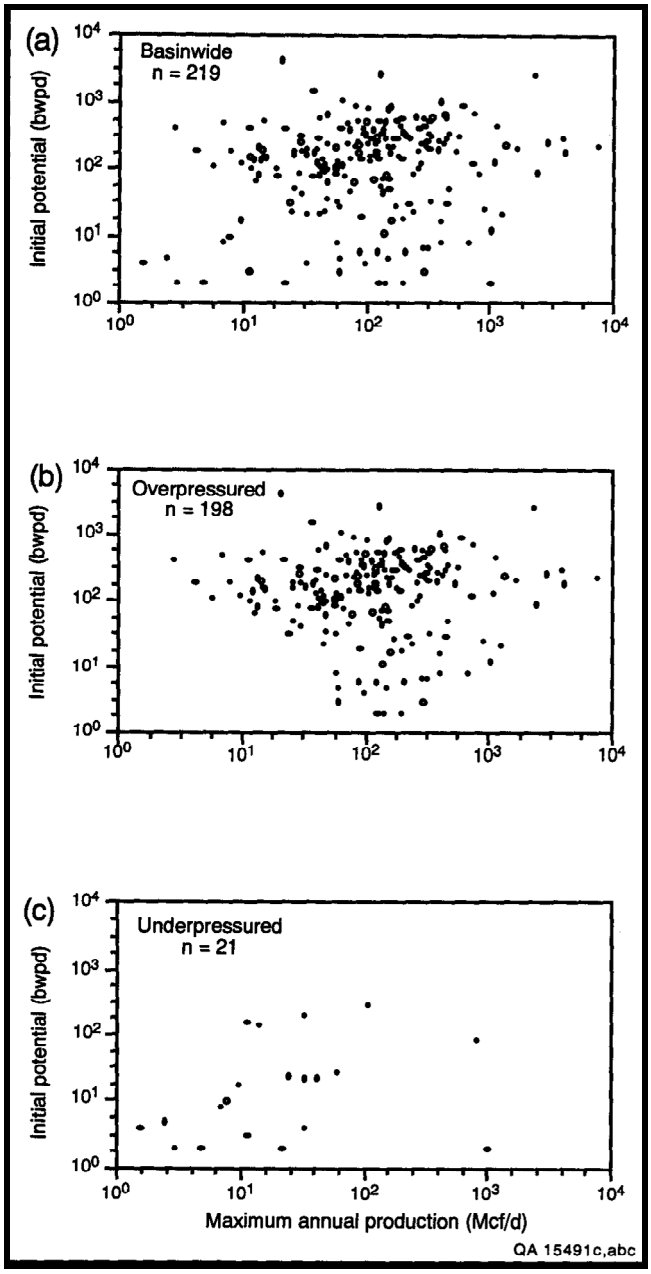

FIGURE 10.14—Scatter plots of maximum annual gas production versus initial water potential from Fruitland coalbed wells, San Juan Basin, for (a) basinwide, (b) overpressured, and (c) underpressured areas, showing no correlation.

and high volatile C bituminous rank) has not entered the thermogenic gas-generation window. Methane in the southern part of the basin may be late-forming biogenic methane or early or main stage thermogenic methane that migrated either (1) upward along faults connected to older source rocks or (2) laterally (up the basin flank) from deeper, mature Fruitland coal beds.

Reservoir pressure

The volume of gas stored in coal varies with reservoir pressure. In the Fruitland Formation, pressure is greatest in the overpressured, northern part of the basin, where it exceeds 1,600 psi (Kaiser and others, this volume, Figs. 8.7 and 8.8). The southwest boundary of overpressure is caused by pinch-out of aquifer coal seams (Kaiser and others, this volume, Chapter 8) and/or the offset of seams by faults along the basin's structural hingeline (Ayers and others, this volume, Chapter 2). The southeast boundary is thought to reflect (1) a major Fruitland channel sandstone belt that interrupts coal seam (aquifer) continuity and (2) minor normal faults that offset coal beds.

Because more methane is adsorbed on coal at higher pressure, overpressure enhances gas content in coal beds. Moreover, because permeability in coal seams is stress dependent, it may be enhanced in the overpressured part of the basin (McKee and others, 1987). Wells in the overpressured area are the basin's most productive (Figs. 10.6 and 10.8); highest MAPs correlate with high BHPs (Fig. 10.18). In Fig. 10.18, two distinct production populations are evident, reflecting the overpressured, north-central part of the basin and the underpressured, west-central part of the basin. BHPs of coalbed methane wells in the west-central part are as low as 300 psi; yet some of these wells have MAPs comparable to coalbed wells in the north-central part that have BHPs of approximately 1,400 psi. Clearly, overpressure is not required for economic production of coalbed methane in the San Juan Basin, as shown by sustained production from underpressured Fruitland coal beds (Figs. 10.6 and 10.18).

Because the desorption curve for many Fruitland coals flattens above 900 to 1,300 psi, pressure must be lowered considerably to release a small amount of gas; at reservoir pressures greater than 1,000 psi significant dewatering may be needed (Koenig and others, 1989). However, if original reservoir pressure is too low, adsorbed gas volume may be small. Therefore, original reservoir pressure that is either too high or too low is probably detrimental to the producibility of coalbed methane. The optimum initial reservoir pressure range is unknown but is thought to be large. Commercial production in the San Juan Basin has been established in coal seams having original reservoir pressures as high as 1,900 psi and as low as 120 psi. Because coalbed methane is ultimately produced at low pressures, compression is required, adding to the operating costs.

Tectonic fractures and cleats

Fractures are the primary control on coalbed permeability and include the regional cleat systems, formed during coalification, and local fractures of tectonic origin. In the San Juan Basin, coalbed methane is produced from a variety of structural settings, induding the low-relief central-basin floor, northern hogbacks and flexures, flanks of the structural axes, and southern monocline. Production from these varied structural settings suggests mainly unconventional trapping of methane and little direct control on methane occurrence by major structural elements. For example, some of the basin's most productive coalbed wells are located in a syncline at Cedar Hill field. The importance of major structural elements is mainly in the associated fracture-enhanced permeability. For example, wells at the Carracas unit are located on the plunging Ignacio anticline, where permeability may be fracture enhanced in the anticlinal nose.

Minor folds and faults not recognized on regional maps may be more important to the production of coalbed methane than major structural elements, because these small structures may be sites of fracture-enhanced permeability and conventional traps. Northwest- and northeast-trending normal faults with as much as 75 ft (23 m) of throw have been identified in the transition zone from overpressured to underpressured Fruitland strata and may account for abrupt pressure boundaries and offsets in productivity trends (Fig. 10.15). A northwest-trending boundary, separating high and low production, extends from the Cedar Hill field southeastward to the Blanco area, parallel to the pressure transition, and may reflect faulting along the transition zone associated with the basin's structural hingeline (Ayers and

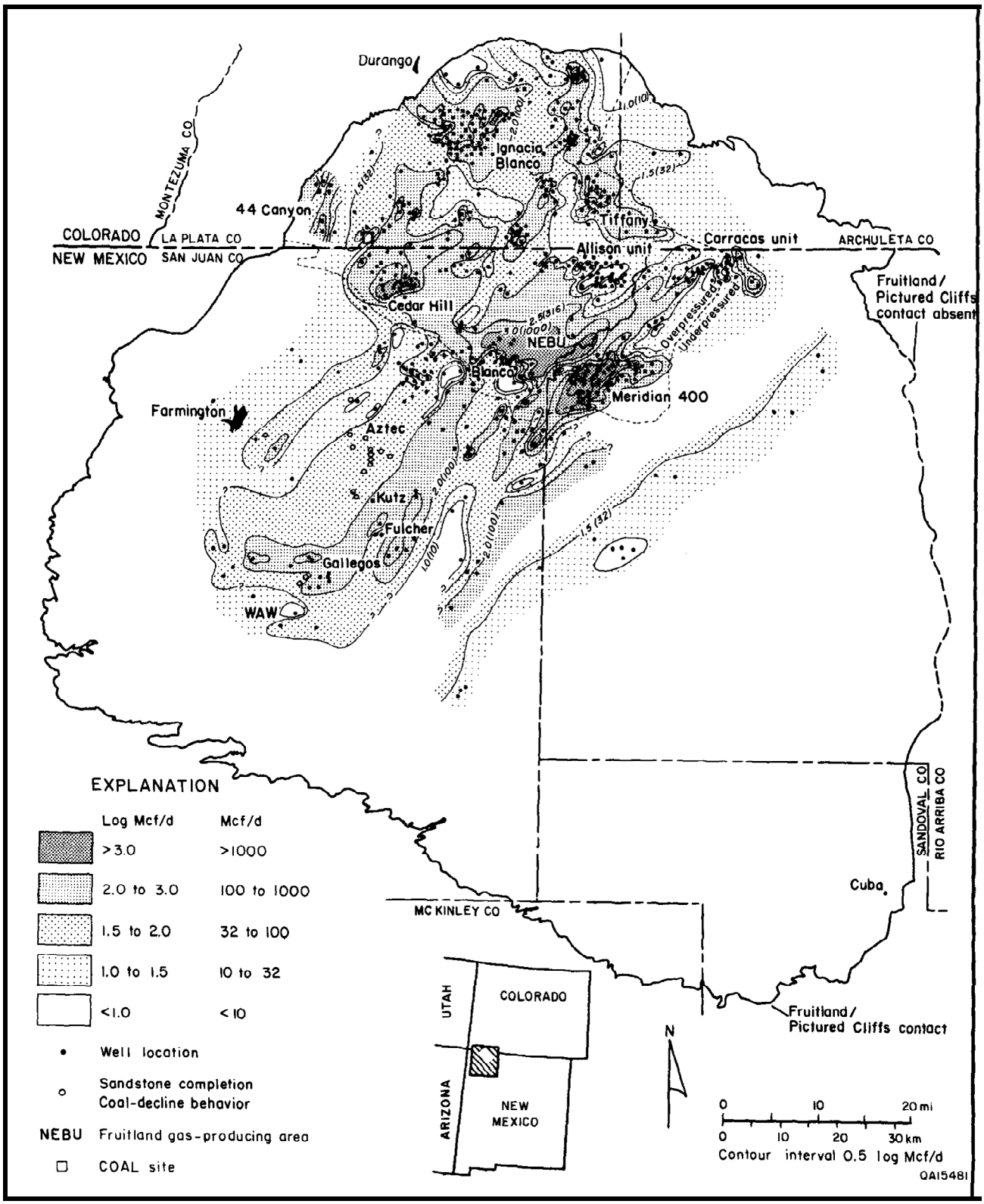

FIGURE 10.15—Map of maximum annual gas production from Fruitland coalbed wells, San Juan Basin. The dominant productivity trends are oriented northwest and northeast. Production is lognormally distributed; therefore, log of production was mapped.

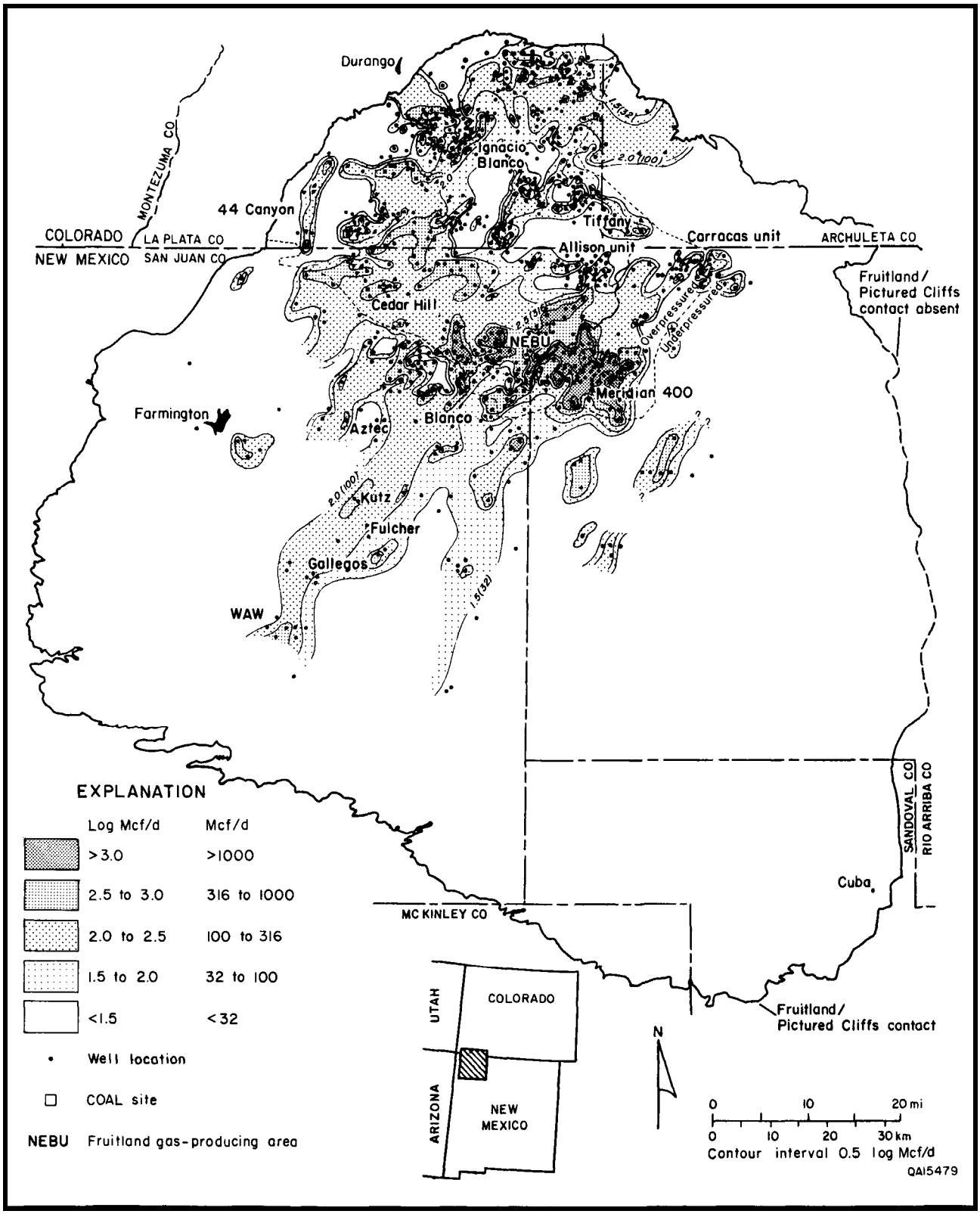

FIGURE 10.16—Map of initial gas potential from Fruitland coalbed wells, San Juan Basin. In northern New Mexico, areas of highest production trend eastward and northward.

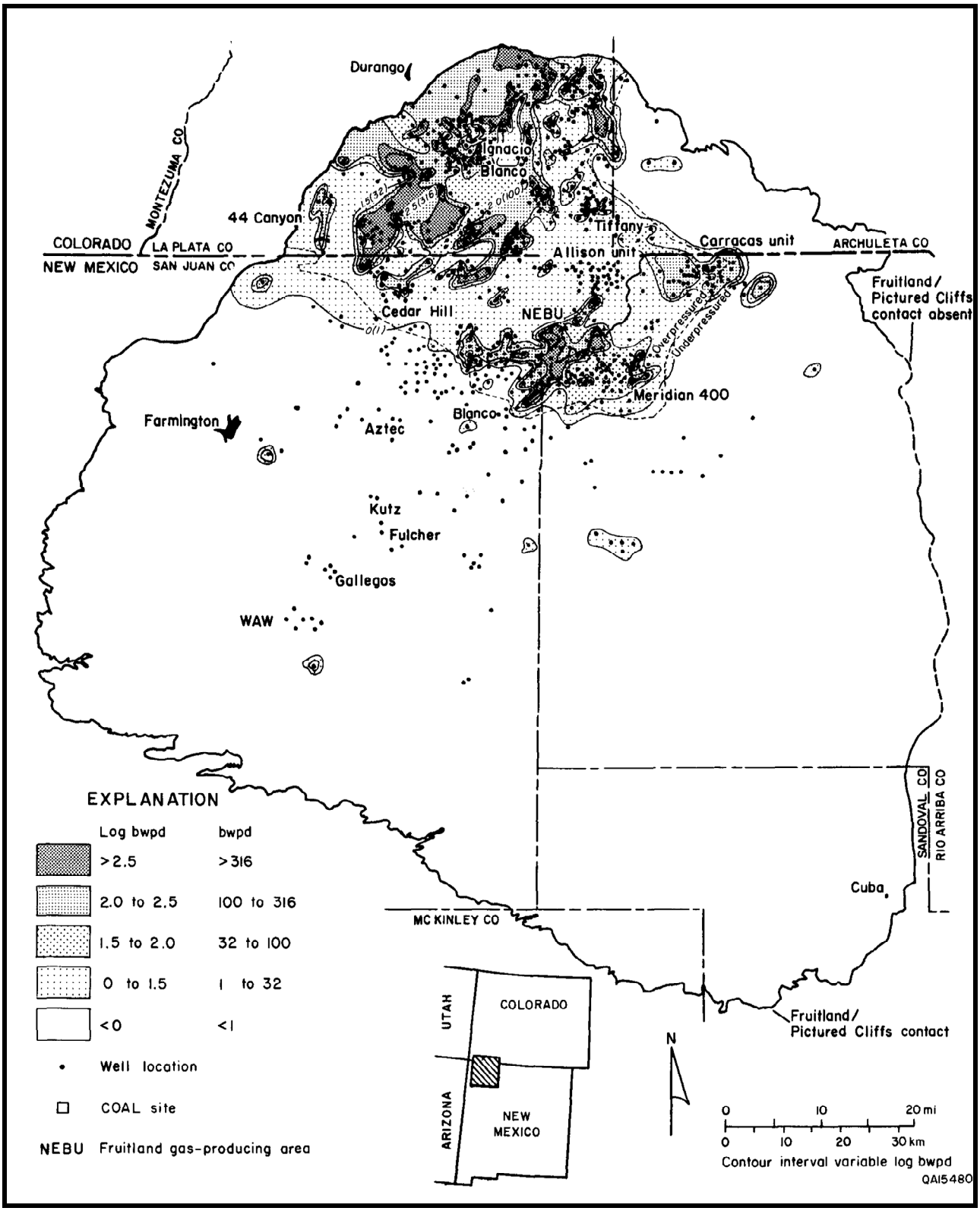

FIGURE 10.17—Map of initial water potential from Fruitland coalbed wells, San Juan Basin. Water-productive wells occur mainly in the overpressured, northern part of the basin. Areas of low water production shown within the overpressured area may reflect unreported water production.

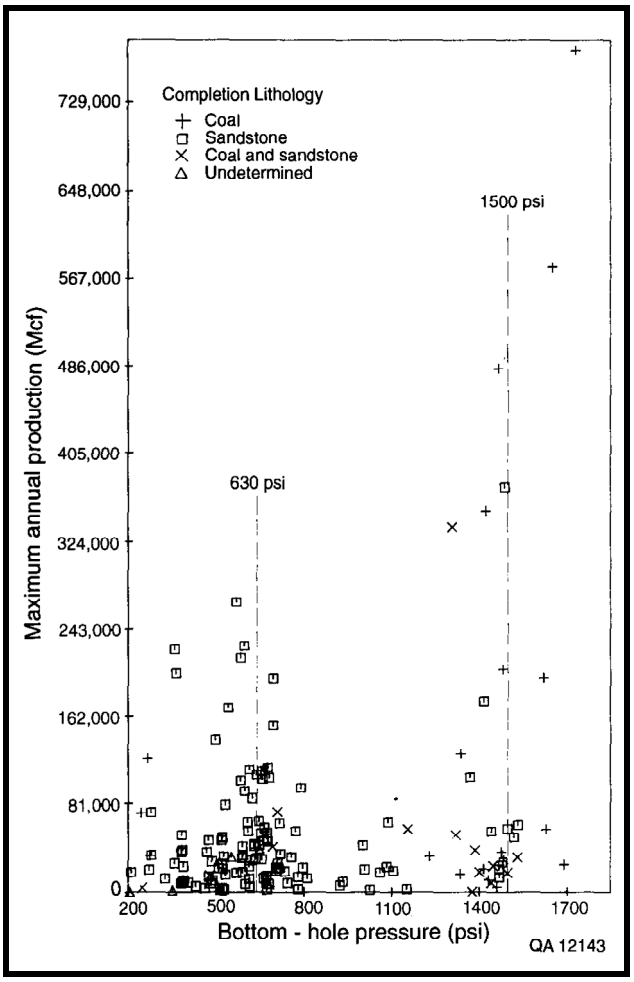

FIGURE 10.18—Cross plot of bottom-hole pressure versus maximum annual gas production by producing lithology (from Kaiser and others, 1990).

others, this volume, Chapter 2). In the Blanco area, this boundary is offset to the northeast, coinciding with the northwestward projection of a prominent northwest-trending segment (lineament) of the San Juan River.

Regional studies have shown two principal face-cleat domains in Fruitland coal beds in the basin; a north-to-northeast domain is present in the southern part of the basin, whereas a northwest face cleat is dominant in the northern part (Tremain and others, this volume, Fig. 5.12). Primary cleat directions parallel the coalbed methane productivity trends (Fig. 10.15). Coalbed permeability may be higher and success of open-hole cavitation may be favored where the two fracture domains overlap. Faults also trend northwestward and may favor flow in that direction because present maximum horizontal stress direction is northwest (Laubach and Tremain, this volume, Chapter 6; Tremain and others, this volume, Chapter 5). Southeast of Durango, productivity trends are oriented northwest and northeast (Fig. 10.15), consistent with northwest-trending faults and the regional cleat system.

Gas composition

The composition of coalbed gas is important because it affects production costs. The composition of Fruitland coalbed gases varies across the basin. Chemically dry to very dry gases occur in the overpressured, northern part and under-pressured, southern part of the basin and are separated by a northwest-trending band of relatively wet gases (Scott and others, this volume, Fig. 9.9). Significantly, carbon dioxide content is highest (commonly 3 to 10%) in coalbed gases from the overpressured, north-central part of the basin (Scott and others, this volume, Fig. 9.10). In the under-pressured, southern part of the basin, coalbed gases commonly contain less than 1% carbon dioxide. Carbon dioxide is a noncombustible, corrosive diluent that lowers the heating value of coalbed gas; it must be stripped from the produced gas at a cost of approximately $0.15/Mcf (Lon Mayhan, pers. comm. 1990). Therefore, coalbed methane produced from the overpressured part of the basin (high carbon dioxide) has a cost penalty relative to coalbed methane produced from the underpressured part of the basin (low carbon dioxide).

Produced water

Water content of coal beds also significantly impacts production costs. Both gas- and water-saturated coal beds occur in the San Juan Basin. Fruitland coal beds in the under-pressured part of the basin produce little or no water, whereas wells in the overpressured part of the basin commonly are water productive in response to artesian overpressuring. Wells in the overpressured area that produce little or no water probably are located on structural highs or have been dewatered by nearby production.

The San Juan 32-7 unit No. 6 well (Phillips No. 6-17) has produced essentially water free since 1953; it is in pressure communication with and structurally high to a well 0.25 mi away (NEBU No. 218) that produces water at the rate of 50 bbls/d. A gas-saturated seam and structural trapping are implied for the San Juan No. 32-7 well. The Seymour No. 9 well, located at Sedro Canyon, has produced water free since 1978; this well was drilled on an anticline mapped on the top of the Pictured Cliffs Sandstone. Likewise, the Ross No. 1 well (sec. 18 T32N R5W), structurally high to the Glover No. 1 well, blew out and flowed gas during completion, whereas the Glover was water productive. Depletion by earlier production on the Ignacio anticline is suspected as the cause of low water production in the Tiffany area as well as at Cedar Hill field, where 10 yrs of production has reduced cumulative water production from Amoco's wells to less than 200 bbls/d.

Disposal cost of Fruitland-produced waters ranges from $0.25 to $6.00/bbl, depending on transportation and disposal method. Water transport is far more expensive by truck than pipeline. Water is disposed of in evaporation ponds or, more commonly, by injection into the Entrada Sandstone, Morrison Formation, or Mesaverde Group. Entrada disposal wells cost $1 to $2 million to drill and complete; the very low permeability sandstone (~0.01 md) must be fraced (200,000 to 1,000,000 lbs of sand and 100,000 to 200,000 gals of fluid) to accept Fruitland water. Moreover, there is high risk of limited capacity and short well life. Water analyses (Kaiser and others, this volume, Table 8.3) and reports from operators suggest that scaling of production wells is a concern in parts of the San Juan Basin, adding to operational costs in these areas. The fact that coalbed methane wells in the underpressured, southern part of the basin are shallow and produce little or no water improves their economics relative to those of wells in the overpressured part of the basin, which are deeper and produce more gas but require considerable dewatering (depressuring) and subsequent disposal of produced water.

Regional characterization of Fruitland coalbed reservoirs

On the basis of hydrodynamics and geology, the San Juan Basin was divided into three regions in which Fruitland coal beds have similar reservoir characteristics: Area 1, the

regionally overpressured, north-central part of the basin; area 2, the underpressured, regional discharge area in the west-central part of the basin; and area 3, the underpressured, eastern part of the basin (Fig. 10.19). In the following discussion, we summarize the salient characteristics of coalbed reservoirs in these areas and illustrate the effects of these characteristics, using production histories of selected coalbed methane wells. To further describe reservoir conditions in the basin, characteristics of Fruitland coal beds in area 1 are detailed in a discussion of the Meridian 400 area, Cedar Hill field, and Allison unit, whereas those of area 2 are elucidated in a review of the WAW-Gallegos area.

Area 1: regionally overpressured area

Large coalbed methane resources in the north-central San Juan Basin result where thick coal deposits, high-rank coal, and high reservoir pressures coincide. The maximum coal bed is at least 10 ft (3 m) thick, and in several northwest-trending and smaller, northeast-trending belts, maximum coal thickness exceeds 20 ft (>6 m). Highly productive wells coincide with thick maximum coal (>20 ft [>6 m]) in several areas (Fig. 10.15; Ayers and others, this volume, Fig. 2.17). The correlation of productivity trends with maximum coal thickness is superior to correlations with average and net coal thickness. Within the regionally overpressured area, defined by simple pressure gradients of approximately 0.50 psi/ft or greater and BHPs greater than 1,200 psi, three subregions are identified: areas A, B, and C (Fig. 10.19).

Area 1A has thick coastal plain and alluvial coal beds (Ayers and others, this volume, Fig. 2.15) and exhibits high BHPs (locally >1,800 psi), low-chloride waters (Kaiser and others, this volume, Chapter 8). About 90% of the basin's coalbed methane production is from areas producing low-chloride water. The basin's most productive coalbed methane wells are in the Cedar Hill, NEBU, and Meridian 400 areas (Fig. 10.15), which are areas of upward fluid flow occurring north of the structural hingeline in association with a regional permeability barrier. This setting is favorable to hydrocarbon entrapment owing to a combination of conventional stratigraphic and structural trapping and hydrodynamics. This highly productive setting is up hydraulic gradient (northeast) from the area of marked steepening of the potentiometric surface and the regional pressure and hydrochemical transitions (Kaiser and others, this volume, Figs. 8.1, 8.7, and 8.18). Wells here commonly produce more than 1,000 Mcf/d, a production rate achieved by only about 1 in 10 coalbed methane wells in the San Juan Basin (Fig. 10.8). The structural hingeline is a no-flow boundary. Northeast of the boundary appreciable free and dissolved gas are inferred to be present, in addition to that sorbed on the coal surface. At the structural hingeline, low permeability is inferred from the steep potentiometric surface (Kaiser and others, this volume, Fig. 8.1). Consequently, wells in the Blanco area, which occur along this steep surface and within the pressure transition, have low gas and water productivities (Fig. 10.15; Kaiser and others, this volume, Figs. 8.1 and 8.7). In the Blanco area, the hydraulic gradient is very steep (~0.045), indicating poor lateral permeability.

Area 1B is along the northern and northwestern margins of the basin (Hogback monocline). Productive wells occur in an area of downward flow, close to the recharge area, and associated with a potentiometric high (Fig. 10.15; Kaiser and others, this volume, Fig. 8.1). In this area, fracture permeability may be high because of the presence of tight folds. Production near the northwestern (44 Canyon area) and northeastern (Carracas unit) hogbacks (Figs. 10.15 and 10.19) may be high owing to fractures associated with such tight folds. Likewise, wells clustered just southeast of Durango occur at a flexure, or abrupt change in dip, in an area of implied enhanced permeability.

Area 1C (Fig. 10.19) is defined by a conspicuously flat potentiometric surface, which is thought to indicate enhanced permeability in a dynamic aquifer (Kaiser and others, this volume, Chapter 8). Vertical flow is potentially downward in this area. To the east, wells in the Carracas unit, similar to those at Blanco, are in an area of steep potentiometric surface and are in the transition from overpressure to underpressure. To date, Carracas wells, like those at Blanco, have not been highly productive (Fig. 10.15).

In area 1, maximum annual gas production (MAP) ranges from less than 30 to 15,000 Mcf/d (Fig. 10.15). Productivities in areas 1B and 1C are lower than those in area 1A. Many water-productive coalbed methane wells had IPs of several hundred barrels of water per day (Fig. 10.17). Their occurrence is predictable from artesian overpressuring, which extends to the northern and northwestern rims of the basin. Wells near that rim, or recharge area, may be difficult to dewater (depressurize), especially if they are completed in coal seams that are hydraulically well interconnected. Nevertheless, some wells within 2 mi of the outcrop produce at high rates (>300 Mcf/d) and apparently were successfully dewatered.

High water productivities indicate enhanced permeability (Oldaker, 1991). Good examples are the McKenzie Methane Southern Ute-Mobil No. 36-1 well and ARCO wells in south-central La Plata County, which lie in the area of flat potentiometric surface and inferred high permeability (area 1C, Fig. 10.19). Coal seams of the No. 36-1 well have natural permeabilities of approximately 40 md, and when stimulated produced low-chloride water at rates greater than 2,000 bbls/d. Some ARCO wells produce gas at rates of 2,000 Mcf/ d and water at rates of 1,000 bbls/d. Wells in the Meridian 400 area are also prolific producers of water (cumulative productions of several hundred thousand barrels).

Although most wells in area 1 produce water, some produced little or no water on initial testing (Fig. 10.17). Examples are clustered wells (for example, eastern La Plata County), isolated individual wells, and individual wells within clusters of water producers. These wells are thought to be associated with structural anomalies, areas of little direct recharge from the outcrop, and/or areas of low coalbed permeability. Such a well is the Forty-four Canyon No. 222 (sec. 22 T33N R11W), which initially produced too little gas to gauge and no water. When stimulated, it produced 281 Mcf/d and 17.5 bwpd. The phenomenon of either isolated wells of low water (<30 bbls/d) or high water potential (hundreds of barrels of water per day) probably reflects a high degree of reservoir heterogeneity or compartmentalization in the coal seams. For example, faults may serve to compartmentalize the coal reservoirs along the northwestern margin of the basin.

Meridian 400 area—The Meridian 400 area, in area 1A, is the basin's "sweet spot," where individual wells typically produce from 300 to 15,000 Mcf/d (Fig. 10.15) with considerable water. Produced gases are carbon dioxide rich (commonly >10%), very dry (C_1/C_{1-5} values of 1.00) (Scott and others, this volume, Chapter 9), and reflect their hydrodynamic setting. The area is overpressured, coincides with a conspicuous potentiometric mound, flanks the pressure-transition zone, lies at the basin floor, and has thick coal seams.

The highly productive Meridian 400 area extends southwestward and southeastward to the limits of overpressure. This boundary results from pinch-out and/or faulting of aquifer coal seams. On the southeast, a major Fruitland channel-sandstone belt interrupts coal seam (aquifer) continuity, causing overpressuring and underpressuring on the northwest and southeast sides, respectively, of the channel

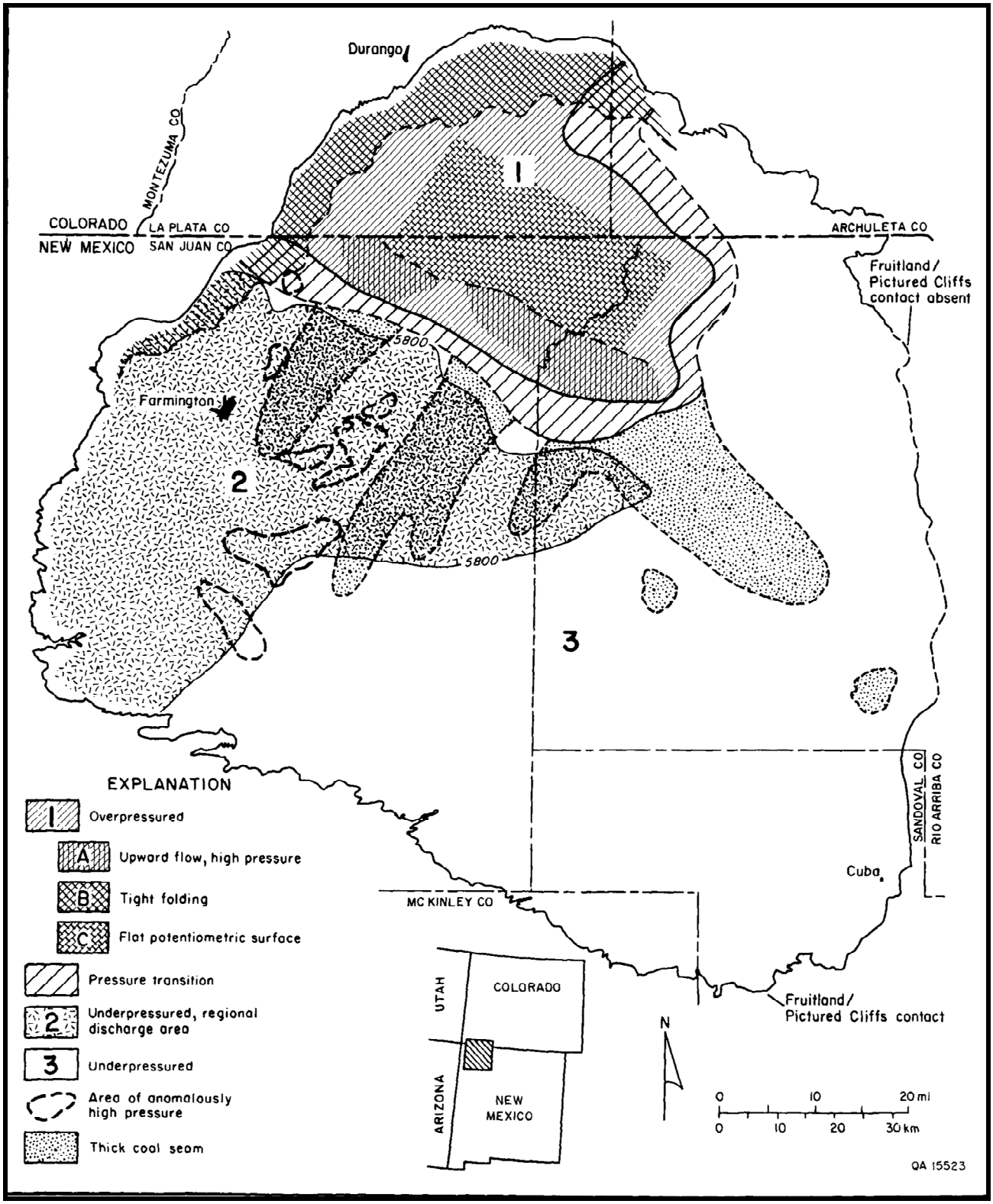

FIGURE 10.19—Hydrogeologic regions in the Fruitland Formation, San Juan Basin. Numbers refer to major regions and letters to subregions discussed in text. Major regions are the (1) overpressured (north-central) area, (2) underpressured regional discharge area, and (3) underpressured area outside of the regional discharge area (from Kaiser and others, 1990).

belt. Minor faulting may also contribute to aquifer separation. The loss of aquifer continuity causes a no-flow boundary and results in conventional trapping of gas and upward fluid flow. Upward flow is indicated by a vertical pressure gradient of approximately 0.80 psi/ft (Kaiser and others, this volume, Fig. 8.3) and is manifest in a pressure ridge, or potentiometric mound.

On the basis of the postulated no-flow boundary, we infer that considerable free gas is concentrated in conventional stratigraphic and/or structural traps in combination with hydrodynamic trapping along the transition between overpressure and underpressure. Moreover, convergent, upward flow and basinward lateral flow would serve to concentrate dissolved gas at this point and prevent its escape updip. Additional gas trapped in combination conventional/hydrodynamic traps is inferred to be available for production beyond that predicted only from the sorption isotherm. This inference cannot be tested in the absence of gas volumetric data. However, above approximately 1,500 psi pressure, little additional gas is sorbed by the coal. Meridian BHPs exceed that value, ranging from 1,600 to 1,900 psi. In open-hole completions, some additional gas may also be contributed by carbonaceous shales and sandstones.

The Meridian 400 area lies at the edge of the basin floor and in an area of many minor structural features (Ayers and Zellers, this volume, Figs. 4.16 and 4.19). The face cleat is oriented northeast (Tremain and others, this volume, Fig. 5.12), parallel to the productivity trend, and permeability anisotropy is inferred across the area to favor flow in the northeast direction. This trend parallels a prominent northeast-trending segment of the San Juan River, a lineament that may reflect regional faulting or northeast-trending coal seams (Ayers and others, this volume, Fig. 2.17). Individual coal seams of high volatile A bituminous rank commonly exceed 20 ft (6 m) in thickness (Scott and others, this volume, Fig. 9.3).

Minor folds may contribute fracture permeability to the coal seams and form conventional structural traps (Ayers and Zellers, this volume, Figs. 4.2 and 4.19). In the Meridian 400 area, there is instantaneous production of gas before pressure drawdown. Several wells initially tested for little or no water but upon production yielded large volumes of water. For example, the Meridian San Juan 30-6 unit No. 402 produced no water upon initial testing but subsequently produced water at an average annual rate of 108,780 bbls. This behavior, coupled with a high gas IP (2,460 Mcf/d), suggests initial production of free gas from a structurally high coal seam with high fracture permeability (secondary porosity) followed by invasion of structurally low water. In summary, exceptional permeability and contribution from conventionally trapped free gas and dissolved gas, or non-sorbed gas, are thought to explain high production in the Meridian 400 area.

Cedar Hill field—At Cedar Hill field, production trends (Fig. 10.15), face cleats (Tremain and others, this volume, Fig. 5.12), coal seams, and channel-sandstone belts are all oriented northeastward (Ambrose and Ayers, this volume, Figs. 3.5 and 3.8a). Individual wells typically produce 300 to more than 1,000 Mcf/d (Fig. 10.15). The field is overpressured, lies at the transition from a flat to steep potentiometric surface (Kaiser and others, this volume, Fig. 8.1), and has thick (some individual seams >20 ft [>6 m]) coal seams of high volatile A and B bituminous rank (Scott and others, this volume, Fig. 9.3). Numerical modeling shows strong potential for upward flow of ground water at Cedar Hill field (Kaiser and others, this volume, Fig. 8.24). High productivity in this area is associated with a no-flow boundary (lateral flow restricted by southwestward pinch-out of aquifer coal seams and/or offset along faults) and probable upward flow, which favor concentration of free gas in conventional traps. Productivity at Cedar Hill field is also influenced by the structural setting and distribution of Fruitland coal seams. Cedar Hill field lies along the structural axis of the basin (Ayers and others, this volume, Fig. 2.5). The most productive wells (>1,800 Mcf/d) are on the southern flank of the synclinal axis that crosses Cedar Hill field, where flexure along the syncline may have caused fracture-enhanced permeability. However, the map of maximum annual production (Ambrose and Ayers, this volume, Fig. 3.13) shows that northeast-trending belts of high production (>1,000 Mcf/d) in the southwestern part of the field, also coincide with similar trending belts of thick net coal (Ambrose and Ayers, this volume, Figs. 3.8b and 3.9). Production on the southern and southwestern flanks of the field may be limited by a zone of northwest-trending, normal faults (Ambrose and Ayers, this volume, Fig. 3.3) associated with the structural hingeline of the basin. A northwest-trending boundary separates high and low production and continues southeastward to the Blanco area (Fig. 10.15). As at Meridian, exceptionally high permeability and presence of non-sorbed gas are thought to explain high production in Cedar Hill field.

Allison unit—The Allison unit (T32N, R6W and R7W) is an area of low production that is surrounded by areas of higher production, is overpressured, and has a flat potentiometric surface in association with thick coal seams (Fig. 10.15; Kaiser and others, this volume, Figs. 8.1 and 8.7; Ayers and others, this volume, Fig. 2.17). Over a short production history (1 to 2 yrs), individual wells commonly have MAP rates of 30 to 100 Mcf/d (Fig. 10.15) that have been disappointing and erratic, contrary to that expected from the hydrologic setting. Water production ranges from 50 to 200 bbls/d. Negative decline only partially explains low production, because several wells scattered throughout the unit produced at rates of 100 to 300 Mcf/d in early 1990. Variable production probably reflects reservoir heterogeneity and variable permeability. The unit lies in an area of gentle hydraulic gradient between an area of downward flow to the northwest and one of strong upward flow to the southeast. Consequently, in the absence of a no-flow boundary, there may be little or no potential for concentration of free gas and vertical flow in the Fruitland Formation. Coal thickness does not appear to be a limiting factor because the unit coincides in part or in whole with the thickest maximum, average, and net coal thicknesses.

The Allison unit is at the basin's structural floor and is bounded to the northeast by the plunging Ignacio anticline (Ayers and others, this volume, Fig. 2.5). Free gas may have migrated up structure, possibly reducing gas content of coal beds. Structural and stratigraphic complexity locally may serve to compartmentalize the coal seams, contributing to reservoir heterogeneity. A minor, northwest-trending normal fault (~40 ft [~12 m] throw), which has been identified just to the southwest of the unit, occurs at the transition between high and low production (Fig. 10.15). Coalbed continuity is uncertain and is complicated by coalbed termination, splitting, and overriding of UP2 sandstones (Ayers and others, this volume, Figs. 2.2 and 2.17). Currently, reservoir heterogeneity (because of highly variable permeability and minor faulting) and little contribution from non-sorbed gas are thought to explain erratic production in the Allison unit.

Area 2: underpressured, regional discharge area

The west-central part of the basin (Fig. 10.19, area 2) is regionally underpressured (simple pressure gradients of 0.30 to 0.40 psi/ft and BHPs <1,000 psi), except for local pressure anomalies. It is an area of regional convergence and discharge, as generally defined by the 5,800-ft head contour

(Kaiser and others, this volume, Fig. 8.1) and, consequently, such areas are favorable for hydrocarbon accumulation (Roth, 1980). Available chemical analyses show Na-Cl-type waters. Coal seams may be thicker than 10 ft (>3 m) and they occur primarily in northeast-trending belts (Ayers and others, this volume, Figs. 2.15 and 2.17). A northeast-trending, dip-elongate belt of thick coal extends almost to the southwestern margin of the basin (Ayers and others, this volume, Figs. 2.17 and 2.19) and coincides with a similar trending belt of high gas production (>100 Mcf/d) (Fig. 10.15). This belt includes productive wells (200 to 500 Mcf/d) in the Fulcher and WAW-Gallegos areas (Fig. 10.15) completed in coal seams of subbituminous and high volatile C bituminous rank (Scott and others, this volume, Fig. 9.3), and it flanks a major northeast-trending Fruitland channel-sandstone belt. Sandstone wells of the Aztec, Kutz, and Gallegos fields (Fig. 10.20) are completed in channel-sandstone belts (thin-coal areas) that flank northeast-trending belts of thick coal (Ayers and others, this volume, Fig. 2.15).

Northeast-trending coal seams may have served as pathways that allowed gas to migrate out of the north-central part of the basin, either entrained or dissolved in ground water, or by diffusion in response to the concentration gradient. Carbon dioxide appears to have migrated. Plumes of high carbon dioxide content gases extend updip (southwestward) from the overpressured area, coincident with northeast-trending coal belts (Scott and others, this volume, Fig. 9.10), and terminate at the San Juan River valley, a regional no-flow boundary (Kaiser and others, this volume, Figs. 8.1 and 8.24).

In the west-central part of the basin (area 2), the Fruitland Formation is mainly an aquitard, and gas is produced water free (Kaiser and others, this volume, Chapter 8). Water-free production in this regional discharge area is explained in terms of the low flow, hydrostratigraphy, trapping mechanism, and coal wettability. Limited flow in the basal Fruitland coal and Pictured Cliffs Sandstone accounts for water production from some wells completed in the basal coal. Conventional trapping and low gas permeability relative to water are also important factors. Stratigraphic trapping is postulated to be more important than structural trapping on the basis of gentle, northeast monoclinal dip and associated updip (southwestward) pinch-out of reservoir coal seams (Ayers and others, this volume, Fig. 2.2). Coal seams in the southern part of the basin are lower rank (subbituminous to high volatile C bituminous) and may be water wet; hence, in these low-permeability strata, water is less mobile than gas.

In the west-central, underpressured part of the basin, Fruitland coalbed wells have MAPs ranging from 30 to 300 Mcf/d, similar to productivities of many wells in the north-central, overpressured part of the basin (Ignacio Blanco field) in areas 1B and 1C (Fig. 10.19). Although coalbed methane production is highest from overpressured coal seams, economic production occurs over a wide pressure range. Cumulative production of some wells exceeds 1 Bcf in area 2 (for example, Clay 1, Gallegos area, >1 Bcf in 14 yrs). However, most wells in this area have cumulative productions of a few hundred million cubic feet, and some have produced oil at the rate of 2 or 3 bbls/d. Numerous Fruitland sandstone gas fields occur in the southwestern part of the basin (Fig. 10.20). Several of them, such as Aztec field, are associated with potentiometric mounds (Kaiser and others, this volume, Fig. 8.1). Analysis of production decline has shown that many wells identified as sandstone completions actually have coal-decline behavior and probably are producing coalbed methane indirectly from coal seams (Fig. 10.4). In some cases, sandstone volumetrics require gas production from the associated coal seams. Some wells are dually completed in Fruitland coal seams and Pictured Cliffs Sandstone or Mesaverde sandstones, and the production is commingled. Consequently, the contribution of Fruitland coalbed methane to total gas production in the west-central part of the basin is substantial but unquantifiable.

WAW-Gallegos area—Coalbed methane wells in the WAW-Gallegos area, which is located in area 2 in the southwestern corner of the basin (Figs. 10.15 and 10.20), produce at rates of 30 to more than 300 Mcf/d. Wells completed in 1990 average about 180 Mcf/d. Long-term productivity is demonstrated by the Clay 1 well (sec. 12 T26N R12W), which was completed as a coalbed well in 1976 and had an average production rate of 185 Mcf/d in 1989. The area is under-pressured and lies mostly within the regional discharge area. Structural dip is homoclinal to the northeast at less than 1° (~80 ft/mi [~15 m/km]). Strike- and dip-elongate coal seams of subbituminous rank have maximum thicknesses of 10 to 20 ft (3 to 6 m) (Ayers and others, this volume, Fig. 2.17). Stratigraphic and hydrodynamic trapping may account for considerable gas volume beyond that adsorbed at reservoir pressures below or near hydrostatic pressure. Coal seams pinch out updip (southwestward), and ground water flows downdip (northward). Enhanced permeability is inferred for wells producing water from the basal Fruitland coal. Gas may in part come from the underlying Pictured Cliffs Sandstone. Thus, the presence of significant free gas and enhanced permeability are thought to combine to explain relatively high gas productivities in the WAW-Gallegos area.

Area 3: underpressured, eastern area

Little is known about the hydrogeology of the eastern part of the basin. Area 3 (Fig. 10.19) is regionally under-pressured, and because of limited data, it appears to be hydrologically featureless. Widely spaced head contours suggest sluggish ground-water flow (Kaiser and others, this volume, Fig. 8.1). Fruitland-produced waters are Na-Cl type that resemble seawater. An area of thick coal, corresponding to coals of belt E (Ayers and others, this volume, Fig. 2.15), trends northwestward across Rio Arriba County, parallel to depositional strike. There are only a few producing Fruitland wells (coal and/or sandstone completions) in the area. After 1 or 2 yrs of production, these wells have average annual productions of less than 1 to 3 MMcf, accompanied by little or no water.

Conclusions

1. Coalbed methane production in the Fruitland Formation is lognormally distributed. Production histograms and probability and scatter plots suggest that coal beds having free gas may be common. Production from overpressured coal seams is greater than that from underpressured seams, although production rates from the two pressure regimes overlap. Initial gas potential is a predictor of longterm productivity. Highly productive wells produce both gas and water, reflecting superior permeability and artesian overpressure. Decline curves of coalbed and sandstone reservoirs differ. Coalbed wells have negative decline early in their production history, followed by exponential decline at less than 5%/yr late in their lives. Sandstone wells that exhibit coal-decline behavior probably are producing coalbed methane indirectly from adjoining coal seams.

2. Approximately 90% of the Fruitland coalbed methane production is from the Meridian 400 area and Cedar Hill and Ignacio Blanco fields in the overpressured part of the basin. Wells in the Meridian 400 area are the most productive (>1,000 Mcf/d), whereas those in Ignacio Blanco field are the least productive (~30 to 300 Mcf/d) and may still be dewatering. Coalbed wells in the west-central (underpres-

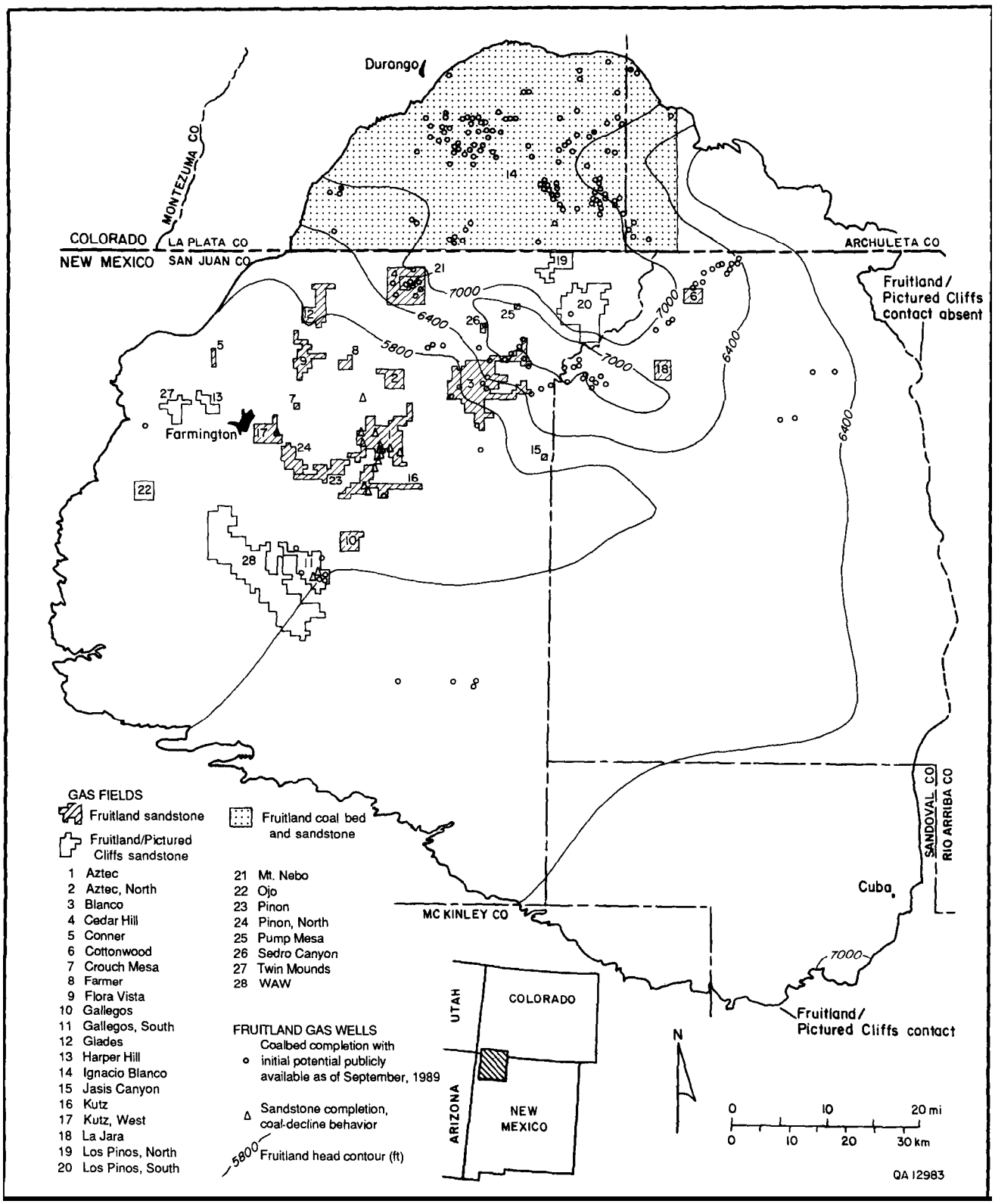

FIGURE 10.20—Fruitland Formation potentiometric-surface map (fresh-water head, in feet) and the distribution of Fruitland and Fruitland/Pictured Cliffs gas fields and tested Fruitland coalbed wells (from Kaiser and others, 1990).

sured) part of the basin (area 2), which produce little or no water, are as productive as those in the Ignacio Blanco field (area 1).

3. Dominant productivity trends are oriented northwestward and northeastward and reflect shoreline and fluvial depositional systems, which controlled coal occurrence and seam thickness. Maximum coal thickness is a critical parameter for the production of coalbed methane and is inferred to be an indicator of productivity, whereas net coal thickness indicates gas resources. Coalbed methane production has been established from coal beds of wide rank (subbituminous to low volatile bituminous); economic production in the San Juan Basin is not limited by rank. The producibility of coalbed methane is ultimately controlled by the thickness and permeability of the coal reservoirs.

4. Major structural elements exert little direct control on production. Minor folds and faults may be more important to production as sites of fracture-enhanced permeability and conventional trapping. Primary cleat direction parallels productivity trends, which are thought to reflect the domihant fracture trends and resultant permeability anisotropy. A northwest-trending fault zone along the basin hingeline is inferred from abrupt changes in production and the coincidence of regional depositional facies, potentiometric, pressure, chemical-facies, and gas-composition boundaries in the hinge area.

5. Coalbed methane is produced in a variety of hydrologic settings. Production is greatest near no-flow boundaries in areas of upward flow that are manifest in potentiometric mounds. Overpressure is not required for the production of coalbed methane. Commercial production of coalbed methane is possible over a very wide pressure range but is highest from overpressured coal seams.
The most productive wells produce low-chloride water and carbon-dioxide-rich gases.

6. Permeability is the most critical parameter for coalbed methane production. Regional permeability contrasts can be inferred from the potentiometric surface, pressure regime, and hydrochemistry. Exceptional permeability and the presence of free and dissolved gas are thought to account for high production in the Meridian 400 area.

7. Regionally, coalbed methane production is greatest in the north-central part of the San Juan Basin (area 1). However, water production is highly variable in this area, reflecting compartmentalization, or heterogeneity, in reservoir coals. In the west-central part of the basin (area 2), production of coalbed methane is substantial either directly or indirectly from underpressured coal seams. Coal seams in this part of the basin are viable exploration targets. The eastern part of the basin (area 3) is largely unexplored but appears to have less potential for coalbed methane production than other areas. Low permeability and thin coal seams, except in west-central Rio Arriba County, limit the potential in this area.

Acknowledgments

Production data through 1987 were collected by A. H. Scanlon and Nancy Oltmanns. Dwight's Energydata, Inc., provided initial potential data. Numerous operators patiently answered questions about their wells' production histories and completion lithology and intervals. Dugan Production Corporation was particularly helpful with wells in the southern part of the basin. J. L. Thurber reviewed the manuscript to improve its content.

References

Aguilera, R., 1980, Naturally fractured reservoirs: PennWell Books, Tulsa, Okla., 619 pp.

Aldrich, M. J., Jr., Chapin, C. E., and Laughlin, A. W., 1986, Stress history and tectonic development of the Rio Grande Rift, New Mexico: Journal of Geophysical Research, v. 91, no. B6, pp. 6199-6211.

Ammosov, I. I., and Eremin, I. V., 1960, Fracturing in coal: IZDAT Publishers, Moscow, 109 pp. (translated from Russian, available from the Office of Technical Services, Washington, D.C.).

Armstrong, R. L., 1968, Sevier orogenic belt in Nevada and Utah: Geological Society of America, Bulletin, v. 79, no: 4, pp. 429-458.

Ayers, W. B., Jr., and Ambrose, W. A., 1990, Geologic controls on the occurrence of coalbed methane, Fruitland Formation, San Juan Basin; *in* Ayers, W. B., Jr., and others, Geologic evaluation of critical production parameters for coalbed methane resources; Part 1, San Juan Basin: The University of Texas at Austin, Bureau of Economic Geology, annual report prepared for the Gas Research Institute, GRI-90/0014.1, pp. 9-72.

Ayers, W. B., Jr., Kaiser, W. R., Ambrose, W. A., Swartz, T. E., Laubach, S. E., Tremain, C. M., and Whitehead, N. H., III, 1990, Geologic evaluation of critical production parameters for coalbed methane resources; Part 1, San Juan Basin: The University of Texas at Austin, Bureau of Economic Geology, annual report prepared for the Gas Research Institute, GRI-90/0014.1, 175 pp.

Ayers, W. B., Jr., and Kaiser, W. R., 1984, Lacustrine interdeltaic coal in the Fort Union Formation (Palaeocene), Powder River Basin, Wyoming and Montana, U.S.A.; *in* Rahmani, R. A., and Flores, R. M. (eds.), Sedimentology of coal and coal-bearing sequences: International Association of Sedimentologists, Special Publication No. 7, pp. 61-84.

Ayers, W. B., Jr., and Zellers, S. D., 1988, Sedimentologic and structural controls on the occurrence and producibility of coalbed methane, Fruitland Formation, northern San Juan and Rio Arriba Counties, New Mexico; *in* Ayers, W. B., Jr., and others, Geologic evaluation of critical production parameters for coalbed methane resources; Part 1, San Juan Basin: The University of Texas at Austin, Bureau of Economic Geology, annual report prepared for the Gas Research Institute, GRI-88/0332.1, pp. 3-59.

Bair, E. S., O'Donnell, T. P., and Picking, L. W., 1985, Potentiometric mapping from incomplete drill-stem test data: Palo Duro Basin area, Texas and New Mexico: Ground Water, v. 23, no. 2 (April 1985), pp. 198-211.

Baltz, E. H., 1967, Stratigraphy and regional tectonic implications of part of Upper Cretaceous and Tertiary rocks in east-central San Juan Basin, New Mexico: U.S. Geological Survey, Professional Paper 552, 101 pp.

Barnes, Harley, 1953, Geology of the Ignacio area, Ignacio and Pagosa Springs Quadrangles, La Plata and Archuleta Counties, Colorado: U.S. Geological Survey, Oil and Gas Investigations Map OM-138, scale 1:63,360.

Barnes, Harley, Baltz, E. H., Jr., and Hayes, P. T., 1954, Geology and fuel resources of the Red Mesa area, La Plata and Montezuma Counties, Colorado: U.S. Geological Survey, Oil and Gas Investigations Map OM-149, scale 1:62,500.

Barton, C. C., and Hsieh, P. A., 1989, Physical and hydrogeologic flow properties of fractures: 28th International Geological Congress, Field Trip Guidebook T385, 36 pp.

Barton, C. C., Larsen, Eric, Page, W. R., and Howard, T. M., 1987, Characterizing fractured rock for fluid-flow, geomechanical, and paleostress modeling: methods and preliminary results from Yucca Mountain, Nevada: U.S. Geological Survey, Open-file Report 87 (preliminary report).

Beach, L. J., and Jentgen, R. W., 1978, Coal test drilling for the San Juan Mine extension, San Juan County, New Mexico: U.S. Geological Survey, Open-file Report 78-960, 87 pp.

Belitz, K., and Bredehoeft, J. D., 1988, Hydrodynamics of Denver Basin: explanation of subnormal fluid pressures: American Association of Petroleum Geologists, Bulletin, v. 72, no. 11, pp. 1334-1359.

Berry, F. A. F., 1959, Hydrodynamics and geochemistry of the Jurassic and Cretaceous systems in the San Juan Basin, northwestern New Mexico and southwestern Colorado: unpublished PhD dissertation, Stanford University, 192 pp.

Bertrand, Philippe, Behar, Francoise, and Durand, Bernard, 1986, Composition of potential oil from humic coals in relation to their petrographic nature: Organic Geochemistry, v. 10, pp. 601-608.

Bond, W. A., 1984, Application of Lopatin's method to determine burial history, evolution of the geothermal gradient, and timing of hydrocarbon generation in Cretaceous source rocks in the San Juan Basin, northwestern New Mexico and southwestern Colorado; *in* Woodward, J., and others (eds.), Hydrocarbon source rocks of the greater Rocky Mountain region: Rocky Mountain Association of Geologists (Denver), pp. 433-447.

Bradley, J. S., 1975, Abnormal formation pressure: American Association of Petroleum Geologists, Bulletin, v. 59, no. 6, pp. 957-973.

Briscoe, F. H., Camp, B. S., Lottman, L. K., and Malone, P. G., 1988, A study of coal-bed methane production trends as related to geologic features, Warrior Basin, Alabama; *in* Coal-bed methane, San Juan Basin: Rocky Mountain Association of Geologists, pp. 237-246.

Britten, R. A., Smyth, M., Bennett, A. J. R., and Shibaoka, M., 1975, Environmental interpretations of Gondwana coal measure sequence in the Sydney Basin of New South Wales; *in* Campbell, K. S. W. (ed.), Gondwana geology: Australian National University Press, Canberra, pp. 233-247.

Burchfiel, B. C., and Davis, G. A., 1975, Nature and controls of Cordilleran orogenesis, western United States: extensions of an earlier synthesis: American Journal of Science, v. 275 A, pp. 363-396.

Callender, J. F., Seager, W. R., and Swanberg, C. A., 1983, Late Tertiary and Quaternary tectonics and volcanism: geothermal resources of New Mexico: Scientific Map Series, New Mexico State University Energy Institute; work performed under U.S. Department of Energy contract number AS07-781D01717, scale 1:500,000.

Campbell, F. W., 1985, Chemical characteristics of the coals; *in* Roybal, G. H., Campbell, F. W., Beaumont, E. C., Cohen, A. D., Kuellmer, F. J., and Kottlowski, F. E., Quality assessment of strippable coals in New Mexico, Phase I, Fruitland and Cleary coals in the San Juan Basin of northwestern New Mexico: New Mexico Energy Research and Development Institute, Report No. 2-73-4304, 89 pp.

Carothers, W. W., and Kharaka, Y. K., 1980, Stable carbon isotopes of HCO_3- in oil field waters-implications for the origin of CO_2: Geochimica et Cosmochimica Acta, v. 44, pp. 323-332.

Chapin, C. E., and Cather, S. M., 1981, Eocene tectonics and sedimentation in the Colorado Plateau-Rocky Mountain area; *in* Dickinson, W. R., and Payne, M. D. (eds.), Relations of tectonics to ore deposits in the southern Cordillera: Arizona Geological Society Digest, v. 14, pp. 173-198; *also in* Lowell, J. D. (ed.), Rocky Mountain foreland basins and uplifts: Rocky Mountain Association of Geologists, Guidebook, 1983 Field Conference, pp. 33-56.

Choate, Raoul, Lent, J., and Rightmire, C. T., 1984, Upper Cretaceous geology, coal, and the potential for methane recovery from coalbeds in San Juan Basin-Colorado and New Mexico; *in* Rightmire, C. T., Eddy, G. E., and Kirr, J. N. (eds.), Coalbed methane resources of the United States: American Association of Petroleum Geologists, Studies in Geology Series No. 17, pp. 185-222.

Choate, Raoul, and Rightmire, C. T., 1982, Influence of the San Juan Mountain geothermal anomaly and other Tertiary igneous events on the coalbed methane potential in the Piceance, San Juan and Raton Basins, Colorado and New Mexico; *in* Proceedings of the Unconventional Gas Recovery Symposium, May 1618, 1982, Pittsburgh, Pennsylvania: Society of Petroleum Engineers/U.S. Department of Energy (SPE Paper 10805), pp. 151-164.

Clarkson, Gerry, and Reiter, Marshall, 1987, The thermal' regime of the San Juan Basin since Late Cretaceous times and its relationship to San Juan Mountains thermal sources: Journal of Volcanology and Geothermal Research, v. 31, no. 3-4, pp. 217-237.

Clarkson, Gerry, and Reiter, Marshall, 1988, An overview of geothermal studies in the San Juan Basin, New Mexico and Colorado; *in* Fassett, J. E. (ed.), Geology and coal-bed methane resources of the northern San Juan Basin, Colorado and New Mexico: Rocky Mountain Association of Geologists, pp. 285-291.

Claypool, G. E., and Kaplan, I. R., 1974, The origin and distribution of methane in marine sediments; *in* Kaplan, I. R. (ed.), Natural gases in marine sediments: Plenum Press, New York, pp. 99139.

Clayton, J. L., Rice, D. D., and Michael, G. E., 1991, Oil-generating coals of the San Juan Basin, New Mexico and Colorado, USA: Organic Geochemistry, v. 17, pp. 735-742.

Clementz, D. M., 1979, Effect of oil and bitumen saturation on source-rock pyrolysis: American Association of Petroleum Geologists, Bulletin, v. 63, no. 12, pp. 2227-2232.

Collins, E. W., Laubach, S. E., and Vendeville, B. C., 1990, Faults and fractures in the Balcones Fault Zone, Central Texas: Austin Geological Society, Guidebook 13, 34 pp.

Colorado Geological Survey (CGS) files, various years, informal reports available from the Colorado Geological Survey, unpaginated.

Colorado Oil and Gas Conservation Commission (COGCC) well file, geological well data files, various years: reports available from Colorado Oil and Gas Conservation Commission, Denver, Colorado.

Condon, S. M., 1988, Joint patterns on the northwest side of the San Juan Basin (Southern Ute Indian Reservation), southwest Colorado; in Fassett, J. E. (ed.), Geology and coal-bed methane resources of the San Juan Basin, Colorado and New Mexico: Rocky Mountain Association of Geologists, pp. 61-68.

Cordell, Lindrith, and Grauch, V. J. S., 1985, Mapping basement magnetization zones from aeromagnetic data in the San Juan Basin, New Mexico; *in* Hinze, W. J. (ed.), The utility of regional gravity and magnetic anomaly maps: Society of Exploration Geophysicists, pp. 181-197.

Cullender, M. H., and Smith, R. V., 1956, Practical solutions of gas-flow equation for wells and pipelines with large temperature gradients: American Institute of Mining, Metallurgical, and Petroleum Engineers, Transactions, v. 207, pp. 281-287.

Cumella, S. P., 1981, Sedimentary history and diagenesis of the Pictured Cliffs Sandstone, San Juan Basin, New Mexico and Colorado: The University of Texas at Austin, Texas Petroleum Research Committee, Report No. UT 81-1, 219 pp.

Cumella, S. P., 1983, Relation of Upper Cretaceous regressive sandstone units of the San Juan Basin to source area tectonics; in Reynolds, M. W., and Dolly, E. D. (eds.), Mesozoic paleogeography of west-central United States: Society of Economic Paleontologists and Mineralogists, Rocky Mountain Section, pp. 189-199.

Dabbous, M. K., Reznik, A. A., Mody, B. G., Fulton, P. F., and Taber, J. J., 1976, Gas-water capillary pressure in coal at various overburden pressures: Society of Petroleum Engineers, Journal, v. 16, no. 5, pp. 261-268.

Dane, C. H., 1936, The La Ventana-Chacra Mesa coal field; part 3A, Geology and fuel resources of the southern part of the San Juan Basin, New Mexico: U.S. Geological Survey Bulletin 860C, pp. 81-161.

Decker, A. D., Close, J. C., and McBane, R. A., 1989, The use of remote sensing, curvature analysis, and coal petrology as indicators of higher coal reservoir permeability; *in* Proceedings, 1989 Coalbed Methane Symposium: University of Alabama, School of Mines and Energy Development (Tuscaloosa), pp. 325-340.

Decker, A. D., and Homer, D. M., 1987, Origin and production implications of abnormal coal reservoir pressure; *in* Proceedings, 1987 Coalbed Methane Symposium: University of Alabama, School of Mines and Energy Development (Tuscaloosa), pp. 51-62.

Decker, A. D., Jeu, S. J., Cooper, J. D., and Wicks, D. E., 1988, Geology, geochemistry, reservoir engineering, and completion methods at the Cedar Hill field, San Juan County, New Mexico: a field study of classic coal degasification behavior; *in* Fassett, J. E. (ed.), Geology and coal-bed methane resources of the northern San Juan Basin, Colorado and New Mexico: Rocky Mountain Association of Geologists, Guidebook, pp. 221-235.

Decker, A. D., Klusman, R., and Horner, D. M., 1987, Geochemical techniques applied to the identification and disposal of connate coal water; *in* Proceedings, 1987 Coalbed Methane Symposium: University of Alabama, School of Mines and Energy Development (Tuscaloosa), pp. 229-242.

Devine, P. E., 1980, Depositional patterns in the Point Lookout Sandstone, northwest San Juan Basin, New Mexico: Unpublished MS thesis, The University of Texas at Austin, 238 pp.

Dickinson, W. R., Klute, M. A., Hayes, M. J., Janecke, S. U., Lundin, E. R., McKittrick, M. A., and Olivares, M. D., 1988, Paleogeographic and paleotectonic setting of Laramide sedimentary basins in the central Rocky Mountain region: Geological Society of America, Bulletin, v. 100, pp. 1023-1039.

Dilworth, O. L., 1960, Upper Cretaceous Farmington Sandstone of northeastern San Juan County, New Mexico: New Mexico, Unpublished MS thesis, University of New Mexico (Albuquerque).

Dix, O. R., and Jackson, M. P. A., 1981, Statistical analysis of lineaments and their relation to fracturing, faulting, and halokinesis in the East Texas Basin: The University of Texas at Austin, Bureau of Economic Geology, Report of Investigations No. 110, 30 pp.

Donaldson, A. C., 1979, Origin of coal seam discontinuities; in Donaldson, A. C., Presley, M. W., and Renton, J. J. (eds.), Carboniferous coal guidebook: West Virginia Geological and Economic Survey, Bulletin B-37-1, pp. 102-132.

Donaldson, A. C., Presley, M. W., and Renton, J. J. (eds.), 1979, Carboniferous coal guidebook: West Virginia Geological and Economic Survey, Bulletin B-37-1, 301 pp.

DuChene, H. R., 1989, Fracture reservoirs in the San Juan Basin, Colorado and New Mexico; *in* Lorenz, J. C., and Lucas, S. G. (eds.), Energy frontiers in the Rockies, Albuquerque Geological Society, pp. 101-109.

Dwight's Oil and Gas Reports, 1990a, Natural gas well production histories: Colorado Statewide Coal Bed Methane Report, v. 1, 373 pp.

Dwight's Oil and Gas Reports, 1990b, Natural gas well production histories: New Mexico Statewide Coal Bed Methane Report, v. 1, 853 pp.

Emmendorfer, Alan, 1989, Fracture orientation: use of the dipmeter type fracture log: The Mountain Geologist, v. 26, no. 2, pp. 63-67.

Engelder, Terry, 1985, Loading paths to joint propagation during a tectonic cycle: an example from the Appalachian Plateau, U.S.A.: Journal of Structural Geology, v. 7, no. 3/4, pp. 459-476.

Epis, R. C., and Chapin, C. E., 1975, Geomorphic and tectonic implications of the post-Laramide, late Eocene erosion surface in the southern Rocky Mountains; *in* Curtis, B. F. (ed.), Cenozoic history of the southern Rocky Mountains: Geological Society of America, Memoir 144, pp. 45-74.

Erpenbeck, M. F., 1979, Stratigraphic relationships and depositional environments of the Upper Cretaceous Pictured Cliffs Sandstone and Fruitland Formation, southwestern San Juan Basin, New Mexico: Unpublished MS thesis, Texas Tech University, 78 pp.

Espitalie, J., Laporte, J. L., Madec, M., Leplat, P., Paulet, J., Boutfeu, A., 1977, Méthode rapide de caractérisation des roches mères, de leur potentiel petrolier et de leur degré devolution: Revue de l'Institut Francais du Pétrole, v. 32, pp. 23-42.

Fassett, J. E., 1967, Core description from GB-1 (Gasbuggy 1) in the northeastern part of the San Juan Basin, Rio Arriba County, New Mexico: U.S. Geological Survey, Open-file Report, 37 pp.

Fassett, J. E., 1985, Early Tertiary paleogeography and paleotectonics of the San Juan Basin area, New Mexico and Colorado; *in* Flores, R. M., and Kaplan, S. S. (eds.), Cenozoic paleogeography of the west-central United States: Society of Economic Paleontologists and Mineralogists, Rocky Mountain Section, Rocky Mountain Paleogeography Symposium 3, pp. 317-334.

Fassett, J. E., 1986, The non-transferability of a Cretaceous coal model in the San Juan Basin of New Mexico and Colorado; *in* Lyons, P. C., and Rice, C. L. (eds.), Paleoenvironmental and tectonic controls in coal-forming basins in the United States: Geological Society of America, Special Paper 210, pp. 155-171.

Fassett, J. E., 1987, Geometry and depositional environments of Fruitland Formation coalbeds, San Juan Basin, New Mexico and Colorado: anatomy of a giant coal-bed methane deposit; *in* Proceedings, 1987 Coalbed Methane Symposium: University of Alabama, School of Mines and Energy Development (Tuscaloosa), pp. 19-35.

Fassett, J. E., 1988, Second day-road log from Durango, Colorado around northeast rim of San Juan Basin via Bayfield, Chimney Rock, Arboles, Allison, and Ignacio, Colorado and back to Durango; *in* Geology and coalbed methane resources of the San Juan Basin, Colorado and New Mexico: Rocky Mountain Association of Geologists, pp. 337-351.

Fassett, J. E., and Hinds, J. S., 1971, Geology and fuel resources of the Fruitland Formation and Kirtland Shale of the San Juan

Basin, New Mexico and Colorado: U.S. Geological Survey, Professional Paper 676, 76 pp.

Fassett, J. E., and Nuccio, V. F., 1990, Vitrinite reflectance values of coals from drill-hole cuttings from the Fruitland and Menefee Formations, San Juan Basin, New Mexico: U.S. Geological Survey, Open-file Report 90-290, 22 pp.

Finley, R. J., Laubach, S. E., Holtz, M. H., and Tyler, Noel, 1990, Opportunities for horizontal drilling in Texas: The University of Texas at Austin, Bureau of Economic Geology, Geological Circular 90-2, 32 pp.

Fisher, W. L., Brown, L. F., Scott, A. J., and McGowen, J. H., 1969, Delta systems in the exploration for oil and gas: The University of Texas at Austin, Bureau of Economic Geology Research Colloquium, 212 pp.

Flores, R. M., and Erpenbeck, M. F., 1981, Differentiation of delta front and barrier lithofacies of the Upper Cretaceous Pictured Cliffs Sandstone, southwestern San Juan Basin, New Mexico: The Mountain Geologist, v. 18, no. 2, pp. 23-34.

Fogg, G. E., and Senger, R. K., 1985, Automatic generation of flow nets with conventional ground-water modeling algorithms: Ground Water, v. 23, no. 3, pp. 336-344.

Friedman, Irving, O'Neil, J. R., and Fleischer, Michael (technical ed.), 1977, Compilation of stable carbon isotope fractionation factors of geochemical interest: U.S. Geological Survey, Professional Paper 440-KK, 12 pp.

Galimov, E. M., 1988, Sources and mechanisms of formation of gaseous hydrocarbons in sedimentary rocks: Chemical Geology, v. 71, pp. 77-95.

Garven, G., 1986, The role of regional fluid flow in the genesis of the Pine Point deposit, western Canada sedimentary basin-a reply: Economic Geology, v. 81, pp. 1015-1020.

Goolsby, S. M., Reade, N. S., and Murray, D. K., 1979, Evaluation of coking coals in Colorado: Colorado Geological Survey, Department of Natural Resources, Resource Series No. 7, 72 pp.

Gorham, F. D., Jr., Woodward, L. A., Callender, J. F., and Greer, A. R., 1979, Fractures in Cretaceous rocks from selected areas of San Juan Basin, New Mexico-exploration implications: American Association of Petroleum Geologists, Bulletin, v. 63, no. 4, pp. 598-607.

Grossman, E. L., Coffman, B. K., Fritz, S. J., and Wada, W., 1989, Bacterial production of methane and its influence on groundwater chemistry in east-central Texas aquifers: Geology, v. 17, no. 6, pp. 495-499.

Grout, M. A., and Verbeek, E. R., 1985, Fracture history of the Plateau Creek and adjacent Colorado River valleys, southern Piceance Basin: implications for predicting joint patterns at depth: U.S. Geological Survey, Open-file Report 85-744, 17 pp.

Haimson, B. C., 1978, Near surface and deeper hydrofracturing stress measurements in the Waterloo Quartzite (abs.): American Geophysical Union, Transactions, v. 59, pp. 327-328.

Haimson, B. C., 1979, New hydrofracturing measurements in the Sierra Nevada Mountains and the relationship between shallow stresses and surface topography: 20th U.S. Symposium on Rock Mechanics, Austin, Texas, pp. 675-682.

Hale, B. W., and Firth, C. H., 1988, Production history of the San Juan Unit No. 6 well, northern San Juan basin, New Mexico; *in* Fassett, J. E. (ed.), Geology and coal-bed methane resources of the northern San Juan Basin, Colorado and New Mexico: Rocky Mountain Association of Geologists, pp. 199-204.

Hall, K. R., and Yarborough, L., 1973, A new equation of state for Z-factor calculations: Oil & Gas Journal, v. 71, no. 25, pp. 8292.

Hancock, P. L., and Bevan, T. G., 1987, Brittle modes of foreland extension; *in* Coward, M. P., Dewey, J. F., and Hancock, P. L. (eds.), Continental extensional tectonics: Geological Society of London, Special Publications No. 28, pp. 127-138.

Hanson, W. B., 1990, Chemistry of western interior USA coal-bed gases based upon desorption of subsurface coal samples (abs.): American Association of Petroleum Geologists, Bulletin, v. 74, no. 8, pp. 1326.

Hattin, D. E., 1965, Stratigraphy of the Graneros Shale (Upper Cretaceous) in central Kansas: Kansas Geological Survey, Bulletin 178, 83 pp.

Heller, P. L., Bowdler, S. S., Chambers, H. P., Coogan, J. C., Hagen, E. S., Shuster, M. W., and Winslow, N. S., 1986, Time of initial thrusting in the Sevier orogenic belt, Idaho-Wyoming and Utah: Geology, v. 14, no. 5, pp. 388-391.

Henkle, W. R., Jr., Muhm, J. R., and DeBuyl, M. H. F., 1977, Cleat orientation in some subbituminous coals of the Powder River and Hanna Basins, Wyoming; *in* Hodgson, H. E. (ed.), Proceedings of the Second Symposium on the Geology of Rocky Mountain Coal-1977: Colorado Geological Survey, Resource Series No. 4, pp. 129-144.

Hickman, S. H., Healy, J. H., and Zoback, M. D., 1985, In situ stress, natural fracture distribution, and borehole elongation in the Auburn geothermal well, Auburn, New York: Journal of Geophysical Research, v. 90, no. B7, pp. 5497-5512.

Horne, J. C., Ferm, J. C., Caruccio, F. T., and Baganz, B. P., 1978, Depositional models in coal exploration and mine planning in Appalachian region: American Association of Petroleum Geologists, Bulletin, v. 62, no. 12, pp. 2379-2411.

Houseknecht, D. W., and Iannacchione, A. T., 1982, Anticipating facies-related coal mining problems in Hartshorne Formation, Arkoma Basin: American Association of Petroleum Geologists Bulletin, v. 66, no. 7, pp. 923-946.

Hucka, B. P., 1989, Analysis of cleats in Utah coal seams: Utah Geological and Mineral Survey Open-file Report 154, 156 pp. Huffman, A. C., and Taylor, D. J., 1991, Basement fault control on the occurrence and development of San Juan Basin energy resources (abs.): Geological Society of America, Abstracts with Programs, v. 23, no. 4, pp. 34.

Irving, E., 1979, Paleopoles and paleolatitudes of North America and speculations about displacement terrains: Canadian Journal of Earth Sciences, v. 16, pp. 669-694.

James, T. A., and Burns, B. J., 1984, Microbial alteration of subsurface natural gas accumulations: American Association of Petroleum Geologists, Bulletin, v. 68, no. 8, pp. 957-960.

Jenden, P. D., 1985, Analysis of gases in the Earth's crust: Gas Research Institute, GRI-85/0106, 110 pp.

Jones, A. H., 1985, Methane production characteristics of deeply buried coalbed reservoirs: Gas Research Institute, GRI-85/0033, NTIS PB85-223386, 144 pp.

Jones, A. H., Kelkar, S., Bush, D., Hanson, J., Rakop, K., Ahmed, U., Holland, M., Tibbitts, G., Owen, L. B., and Bowman, K. C., 1985, Methane production characteristics of deeply buried coalbed reservoirs: Gas Research Institute, GRI-85/0033, 176 pp.

Jordan, T. E., 1981, Thrust loads and foreland basin evolution, Cretaceous, western United States: American Association of Petroleum Geologists, Bulletin, v. 65, no. 12, pp. 2506-2520.

Kaiser, W. R., and Ayers, W. B., Jr., 1990, Hydrologic evaluation of coalbed methane producibility: Gas Research Institute, Coalbed Methane Workshop, Technical Session II, Part B, 23 pp.

Kaiser, W. R., Johnston, J. E., and Bach, W. N., 1978, Sand-body geometry and the occurrence of lignite in the Eocene of Texas: The University of Texas at Austin, Bureau of Economic Geology, Geological Circular 78-4, 19 pp.

Kaiser, W. R., and Swartz, T. E., 1988, Hydrology of the Fruitland Formation and coalbed methane producibility; *in* Ayers, W. B., Jr., and others, Geologic evaluation of critical production parameters for coalbed methane resources; Part 1, San Juan Basin: The University of Texas at Austin, Bureau of Economic Geology, annual report prepared for the Gas Research Institute, GRI-88/ 0332.1, pp. 61-81.

Kaiser, W. R., and Swartz, T. E., 1989, Fruitland Formation hydrology and producibility of coalbed methane in the San Juan Basin, New Mexico and Colorado; *in* Proceedings, 1989 Coalbed Methane Symposium: University of Alabama, School of Mines and Energy Development (Tuscaloosa), pp. 87-97.

Kaiser, W. R., and Swartz, T. E., 1990, Hydrodynamics of the Fruitland Formation; *in* Ayers, W. B., Jr., and others, Geologic evaluation of critical production parameters for coalbed methane resources; Part 1, San Juan Basin: The University of Texas at Austin, Bureau of Economic Geology, annual report prepared for the Gas Research Institute, GRI-90/0014.1, pp. 99-126.

Kaiser, W. R., Swartz, T. E., Ambrose, W. A., and Ayers, W. B., Jr., 1990, Hydrogeologic parameters for the producibility of coalbed methane; *in* Ayers, W. B., Jr., and others, Geologic evaluation of critical production parameters for coalbed methane resources; Part 1, San Juan Basin: The University of Texas at Austin, Bureau of Economic Geology, annual report prepared for the Gas Research Institute, GRI-90/0014.1, pp. 127-155.

Kaiser, W. R., Swartz, T. E., and Hawkins, G. J., 1991, Hydrology of the Fruitland Formation, San Juan Basin; *in* Ayers, W. B., Jr., and others, Geologic and hydrologic controls on the occurrence and producibility of coalbed methane, Fruitland Formation, San Juan Basin: The University of Texas at Austin, Bureau of Eco-

nomic Geology, topical report prepared for the Gas Research Institute, GRI-91/0072, pp. 195-241.

Kauffman, E. G., 1977, Geological and biological overview-Western Interior Cretaceous basin; *in* Kauffman, E. G. (ed.), Cretaceous facies, faunas, and paleoenvirorunents across the Western Interior basin: The Mountain Geologist, v. 6, pp. 227-245.

Kelley, V. C., 1951, Tectonics of the San Juan Basin: New Mexico Geological Society, Guidebook to 2nd Field Conference, pp. 124-131.

Kelley, V. C., 1955a, Regional tectonics of the Colorado Plateau and relationship to the origin and distribution of uranium: University of New Mexico Publications in Geology, no. 5, 120 pp.

Kelley, V. C., 1955b, Tectonics of the Four Corners region; *in* Geology of parts of Paradox, Black Mesa, and San Juan Basin: Four Corners Geological Society, First Field Conference Guidebook, pp. 108-117.

Kelley, V. C., and Clinton, N. J., 1960, Fracture systems and tectonic elements of the Colorado Plateau: University of New Mexico, Publications in Geology, no. 6, 104 pp.

Kelso, B. S., Decker, A. D., Wicks, D. E., and Homer, D. M., 1987, GRI geologic and economic appraisal of coalbed methane in the San Juan Basin; *in* Proceedings, 1987 Coalbed Methane Symposium: University of Alabama, School of Mines and Energy Development (Tuscaloosa), pp. 119-125.

Kelso, B. S., Goolsby, S. M., and Tremain, C. M., 1980, Deep coalbed methane potential of the San Juan River coal region, southwestern Colorado: Colorado Geological Survey, Open-file Report 80-2, 56 pp.

Kelso, B. S., and Rushworth, Peter, 1982, Southern Ute/Department of Energy coalbed methane test wells: Colorado Geological Survey, Open-file Report 82-4, 21 pp.

Kelso, B. S., Wicks, D. E., and Kuuskraa, V. A., 1988, A geologic assessment of natural gas from coal seams in the Fruitland Formation, San Juan Basin: Gas Research Institute, GRI-88/034, 56 pp.

Kendall, P. F., and Briggs, H., 1933, The formation of rock joints and the cleat of coal; *in* Proceedings: Royal Society of Edinburgh, v. 53, pp. 164-187.

Keystone, 1986, 1986 Keystone coal industry manual: McGraw-Hill, New York [Colorado-description of seams, pp. 431-452; New Mexico-description of seams, pp. 514-523].

Khorasani, G. K., 1987, Oil-prone coals of the Walloon coal measures, Surat Basin, Australia; *in* Scott, A. C. (ed.), Coal and coal-bearing strata: recent advances: Blackwell Scientific Publications, Geological Society Publication No. 32, pp. 303-310.

Kluth, C. F., and Coney, P. J., 1981, Plate tectonics of the Ancestral Rocky Mountains: Geology, v. 9, no. 1, pp. 10-15.

Knepper, D. H., Jr., 1982, Lineaments derived from analysis of linear features mapped from Landsat images of the Four Corners region of the southwestern United States: U.S. Geological Survey, Open-file Report 82-849, 79 pp.

Koenig, R. A., Bumb, A. C., McKee, C. R., Murphy, C. L., Ramesh, M. S., Reverand, J. M., and Way, S. C., 1989, Application of hydrology to evaluation of coalbed methane reservoirs: Gas Research Institute, GRI-89/0031, 114 pp.

Komar, C. A., Overbey, W. K., Jr., Rough, R. L., and Lambert, W. G., 1971, Factors that predict fracture orientation in a gas storage reservoir: Journal of Petroleum Technology, v. 23, May, pp. 546-550.

Kuellmer, E J., 1987, Preliminary petrographic analyses; *in* Roybal and others, Quality assessment of strippable coals in New Mexico, Year II, Phase II, Fruitland, Menefee, and Crevasse Canyon Formation coals in the San Juan Basin of northwestern New Mexico: New Mexico Research and Development Institute, NMRDI 2-74-4331, pp. 86-90.

Kulander, B. R., and Dean, S. L., 1980, Fracture trends in the Allegheny Plateau of West Virginia: West Virginia Geologic and Economic Survey, Map WV-11.

Ladeira, F. L., and Price, N. J., 1981, Relationship between fracture spacing and bed thickness: Journal of Structural Geology, v. 3, no. 2, pp. 179-183.

LaPointe, P. R., 1988, A method to characterize fracture density and connectivity through fractal geometry: International Journal of Rock Mechanics and Geomechanics Abstracts, v. 25, no. 6, pp. 421-429.

LaPointe, P. R., and Hudson, J. A., 1985, Characterization and interpretation of rock mass joint patterns: Geological Society of America, Special Paper 199, 37 pp.

Laubach, S. E., 1991, Fracture patterns in low-permeability-sandstone gas reservoir rocks in the Rocky Mountain region; *in* Proceedings: Society of Petroleum Engineers Joint Rocky Mountain Regional Meeting and Low-Permeability Reservoirs Symposium, SPE Paper 21853, pp. 501-510.

Laubach, S. E., Reynolds, S. J., Spencer, J. E., and Marshak, Stephen, 1989, Progressive deformation and superposed fabrics related to Cretaceous crustal underthrusting in western Arizona, U.S.A.: Journal of Structural Geology, v. 11, no. 6, pp. 735-749.

Laubach, S. E., Tremain, C. M., Whitehead, N. H., and Baumgardner, R. W., 1990, Fracture-trace maps of Upper Cretaceous Pictured Cliffs Sandstone pavements, San Juan Basin, Colorado: implications for coalbed methane exploration (abs.): Geological Society of America, Abstracts with Programs, v. 22, no. 7, p. A202.

Law, B. E., 1990a, Thermal evolution of the Upper Cretaceous Fruitland Formation, San Juan Basin, Colorado and New Mexico; *in* Carter, L. M. H. (ed.), U.S. Geological Survey Research on Energy Resources, 1990, Programs and Abstracts, pp. 49-50.

Law, B. E., 1990b, Vitrinite reflectance data from Cretaceous and Tertiary rocks, San Juan Basin, New Mexico and Colorado: U.S. Geological Survey, Open-file Report 90-659, 19 pp.

Law, B. E., Anders, D. E., and Michael, G. E., 1990, Use of RockEval pyrolysis and vitrinite reflectance data in characterizing type and maturity of organic matter in coal, Upper Cretaceous Fruitland Formation, San Juan Basin, New Mexico and Colorado (abs.): American Association of Petroleum Geologists, Bulletin, v. 74, no. 8, pp. 1333.

Leckie, D. A., Singh, Chaitanya, Goodarzi, Fariborz, and Wall, J. H., 1990, Organic-rich, radioactive marine shale: a case study of a shallow-water condensed section, Cretaceous Shaftesbury Formation, Alberta, Canada: Journal of Sedimentary Petrography, v. 60, no. 1, pp. 101-117.

Levey, R. A., 1985, Depositional model for understanding geometry of Cretaceous coals: major coal seams, Rock Springs Formation, Green River Basin, Wyoming: American Association of Petroleum Geologists, Bulletin, v. 69, no. 9, pp. 1359-1380.

Leythaeuser, D., Schaefer, R. G., Cornford, C., and Weiner, B., 1979, Generation and migration of light hydrocarbons (C_2-C_7) in sedimentary basins: Organic Geochemistry, v. 1, pp. 191-204.

Lipman, P. W., Doe, B. R., Hedge, C. E., and Steven, T. A., 1978, Petrologic evolution of the San Juan volcanic field, southwestern Colorado; Pb and Sr isotope evidence: Geological Society of America, Bulletin, v. 89, no. 1, pp. 59-82.

Logan, T. L., 1989, Coalbed methane-6, western basins dictate varied operations: Oil & Gas Journal, v. 87, no. 49, pp. 35-39.

Long, J. C. S., and Billaux, D. A., 1987, From field data to fracture network modeling: an example incorporating spatial structure: Water Resources Research, v. 23, no. 7, pp. 1201-1216.

Manfrino, Carrie, 1984, Stratigraphy and palynology of the upper Lewis Shale, Pictured Cliffs Sandstone, and lower Fruitland Formation (Upper Cretaceous) near Durango, Colorado: The Mountain Geologist, v. 21, no. 4, pp. 115-132.

Mattick, J. L., Duval, T. A., and Phillips, F. M., 1987, Quantification of groundwater recharge rates in New Mexico using bomb-36Cl, bomb-^{3}H, and chloride as soil-water tracers: New Mexico State University (Las Cruces), New Mexico Water Resources Research Institute, WRRI Report No. 220, 184 pp.

Mavor, M. J., and Close, J. C., 1989a, Western Cretaceous coal seam project, evaluation of the cooperative research area Northeast Blanco Unit operated by Blackwood & Nichols Co., Ltd.: Gas Research Institute, GRI-90/0041, variously paginated.

Mavor, M. J., and Close, J. C., 1989b, Western Cretaceous coal seam project, evaluation of the cooperative research well Southern Ute-Mobil 36-1 operated by McKenzie Methane Cooperation: Gas Research Institute, GRI-90/0042, variously paginated.

Mavor, M. J., and Close, J. C., 1989c, Western Cretaceous coal seam project, evaluation of the cooperative research well Colorado 32-7 #9 operated by Mobil Oil Corporation: Gas Research Institute, GRI-90/0043, variously paginated.

Mavor, M. J., and Close, J. C., 1989d, Western Cretaceous coal seam project, evaluation of the cooperative research well Hamilton #3 operated by Mesa Operating Limited Partnership: Gas Research Institute, GRI-90/0040, variously paginated.

Mavor, M. J., Close, J. C., and Pratt, T. J., 1991, Western Cretaceous Coal Seam Project; summary of the Completion Optimization and Assessment Laboratory (COAL) site: Gas Research Institute, GRI-91/0377, variously paginated.

McCord, J. P., 1988, Hydrogeology of a Fruitland Formation aquifer, San Juan Basin-New Mexico and Colorado, with emphasis on using temperature distribution data to estimate lateral groundwater velocity: Unpublished MS thesis, New Mexico Institute of Mining and Technology, 121 pp.

McCulloch, C. M., Deul, Maurice, and Jeran, P. W., 1974, Cleat in bituminous coalbeds: U.S. Bureau of Mines, Report of Investigations No. 7910, 23 pp.

McCulloch, C. M., Diamond, W. P., Bench, B. M., and Deul, Maurice, 1975, Selected geological factors affecting mining of the Pittsburgh Coalbed: U.S. Bureau of Mines, Report of Investigations No. 8093, 72 pp.

McGowen, J. H., 1968, Utilization of depositional models in exploration from nonmetallic minerals; *in* Brown, L. F., Jr. (ed.), Proceedings, Fourth Forum on Geology of Industrial Minerals: The University of Texas at Austin, Bureau of Economic Geology, pp. 157-174.

McKee, C. R., Bumb, A. C., and Koenig, R. A., 1987, Stress-dependent permeability and porosity in coal; *in* Proceedings, 1987 Coalbed Methane Symposium: University of Alabama, School of Mines and Energy Development (Tuscaloosa), pp. 183-193.

Meissner, F. F., 1984, Cretaceous and lower Tertiary coals as sources for gas accumulations in the Rocky Mountain area; *in* Woodward, J., Meissner, F. F., and Clayton, J. L. (eds.), Hydrocarbon source rocks of the greater Rocky Mountain region: Rocky Mountain Association of Geologists (Denver), pp. 401-431.

Meissner, E F., 1987, Mechanisms and patterns of gas generation and expulsion-migration and accumulation associated with coal measures, Green River and San Juan Basins, Rocky Mountain region, USA; *in* Doligez, Brigitte (ed.), Migration of hydrocarbons in sedimentary basins: Editions Technip, Paris, pp. 79-112.

Merewether, E. A., and Cobban, W. A., 1986, Biostratigraphic units and tectonism in the mid-Cretaceous foreland of Wyoming, Colorado, and adjoining areas; *in* Peterson, J. A. (ed.), Paleotectonics and sedimentation in the Rocky Mountain region, United States: American Association of Petroleum Geologists, Memoir 41, pp. 443-468.

Molenaar, C. M., and Baird, J. K., 1989, North-south stratigraphic cross-sections of Upper Cretaceous rocks, northern San Juan Basin, Colorado: U.S. Geological Survey, Miscellaneous Field Studies Map, MF-2068, 3 sheets.

Nelson, C. R., 1991, Basic science methane from coal seams program: Gas Research Institute, Natural Gas Supply Project Advisor Group Meeting-Coalbed Methane Project Area, Birmingham, Alabama, November 13-15, 1991, unpaginated.

Nelson, R. A., Lenox, L. C., and Ward, B. J., 1987, Oriented core: its use, error, and uncertainty: American Association of Petroleum Geologists, Bulletin, v. 71, no. 4, pp. 357-368.

Neuman, S. P., and Witherspoon, P. A., 1970, Finite element method of analyzing steady seepage with a free surface: Water Resources Research, v. 6, no. 3, pp. 889-897.

Newman, K. R., and McCord, J. P., 1980, Detailed site investigation, northern San Juan Basin: Unpublished report to TRW for U.S. Department of Energy, available for inspection at the Colorado Geological Survey, Denver, Colorado, variously paginated.

Nickelson, H. B., 1988, One hundred years of coal mining in the San Juan Basin, New Mexico: New Mexico Bureau of Mines and Mineral Resources, Bulletin, Report No. 111, 226 pp.

North, F. K., 1985, Petroleum geology: Allen & Unwin, Boston, 607 pp.

Novak, S. A., and Eckstein, Y., 1988, Hydrochemical characterization of brines and identification of brine contamination in aquifers: Ground Water, v. 26, no. 3, pp. 317-324.

Nur, Amos, 1982, The origin of tensile fracture lineaments: Journal of Structural Geology, v. 4, no. 1, pp. 31-40.

Oldaker, P. R., 1991, Hydrogeology of the Fruitland Formation, San Juan Basin, Colorado and New Mexico; *in* Schwochow, S. D. (ed.), Coalbed methane of western North America: Rocky Mountain Association of Geologists, pp. 61-66.

Palmer, J. J., and Scott, A. J., 1984, Stacked shoreline and shelf sandstone of La Ventana Tongue (Campanian), northwestern New Mexico: American Association of Petroleum Geologists, Bulletin, v. 68, no. 1, pp. 74-91.

Paul, G. W., 1990, Coalbed methane simulation: Quarterly Review of Methane from Coal Seams Technology, v. 7, no. 4, pp. 14-16.

Peffer, J. W., 1985, An improved method for calculating bottom-hole pressures in gas wells: Unpublished MS thesis, The University of Texas at Austin, 138 pp.

Peffer, J. W., Miller, M. A., and Hill, A. D., 1986, An improved method for calculating bottom-hole pressures in flowing gas wells with liquid present: Society of Petroleum Engineers, SPE Paper 15655, 6 pp.

Petzet, G. A., 1990, Devon pressing Fruitland coal seam program: Oil & Gas Journal, v. 88, no. 45, pp. 28-30.

Phillips, F. M., Peeters, L. A., Tansey, M. K., and Davis, S. N., 1986, Paleoclimatic inferences from an isotopic investigation of groundwater in the central San Juan Basin, New Mexico: Quaternary Research, v. 26, pp. 179-193.

Phillips, F. M., and Tansey, M. K., 1984, An integrated isotopic/ physical approach to a numerical model of groundwater flow in the San Juan Basin: New Mexico State University, New Mexico Water Resources Research Institute, WRRI Report No. 197, 146 pp.

Phillips, F. M., Tansey, M. K., Peeters, L. A., Cheng, S., and Long, A., 1989, An isotopic investigation of groundwater in the central San Juan Basin, New Mexico carbon 14 dating as a basis for numerical flow modeling: Water Resources Research, v. 25, no. 10, pp. 2259-2273.

Pollard, D. D., and Aydin, A., 1988, Progress in understanding jointing over the past century: Geological Society of America Bulletin, v. 100, no. 8, pp. 1181-1204.

Puri, R., and Yee, D., 1990, Enhanced coalbed methane recovery; *in* 1990 SPE Annual Technical Conference and Exhibition, Society of Petroleum Engineers, September 23-26, 1990, New Orleans, Louisiana, SPE Paper 20732, pp. 193-202.

Raistrick, A., and Marshall, C. E., 1939, The nature and origin of coal and coal seams: The English Universities Press, London, pp. 42-45.

REC, 1989a, Stratton field, preliminary engineering assessment: Research & Engineering Consultants, Inc., Englewood, Colorado, report no. REC-SGR 89.1, prepared for the Bureau of Economic Geology, The University of Texas at Austin, 31 pp.

REC, 1989b, McAllen Ranch field, preliminary engineering assessment: Research & Engineering Consultants, Inc., Englewood, Colorado, report no. REC-SGR 89.2, prepared for the Bureau of Economic Geology, The University of Texas at Austin, 65 pp.

Reiter, Marshall, and Mansure, A. J., 1983, Geothermal studies in the San Juan Basin and the Four Corners area of the Colorado Plateau; I, Terrestrial heat-flow measurements: Tectonophysics, v. 91, no. 3-4, pp. 233-251.

Rice, D. D., 1983, Relation of natural gas composition to thermal maturity and source-rock type in San Juan Basin, northwestern New Mexico and southeastern Colorado: American Association of Petroleum Geologists, Bulletin, v. 67, no. 8, pp. 1199-1218.

Rice, D. D., Clayton, J. L., and Pawlewicz, M. J., 1989, Characterization of coal-derived hydrocarbons and source-rock potential of coal beds, San Juan Basin, New Mexico and Colorado, U.S.A.: International Journal of Coal Geology, v. 13, pp. 597-626.

Rice, D. D., Threlkeld, C. N., Vuletich, A. K., and Pawlewicz, M. J., 1988, Identification and significance of coal-bed gas, San Juan Basin, northwestern New Mexico and southwestern Colorado; *in* Fassett, J. E. (ed.), Geology and coal-bed methane resources of the northern San Juan Basin, Colorado and New Mexico: Rocky Mountain Association of Geologists, pp. 51-59.

Rice, D. D., Threlkeld, C. N., Vuletich, A. K., and Pawlewicz, M. J., 1990, Nonassociated gas potential of San Juan Basin considerable: Oil & Gas Journal, v. 88, no. 5, pp. 60-61.

Roberts, L. N. R., 1989, Results of 1988 coal exploratory drilling in the Fruitland Formation, western part of the Southern Ute Indian Reservation, La Plata County, Colorado: U.S. Geological Survey, Open-file Report 89-487, 221 pp.

Roberts, L. N. R., and Uptegrove, Jane, 1991, Coal geology and preliminary coal zone correlations in the Fruitland Formation, western part of the Southern Ute Indian Reservation, La Plata County, Colorado: U.S. Geological Survey, Coal Investigations Map, C-138, scale 1:24,000.

Rohrback, B. G., Peters, K. E., Sweeney, R. E., and Kaplan, I. R., 1983, Ammonia formation in laboratory simulated thermal maturation: implications related to the origin of nitrogen in natural gas; *in* Bjoroy, M. (ed.), Advances in Organic Geochemistry, 1981: John Wiley, New York, pp. 819-823.

Ross, C. A., and Ross, J. R. P., 1986, Paleozoic paleotectonics and sedimentation in Arizona and New Mexico; *in* Peterson, J. A. (ed.), Paleotectonics and sedimentation in the Rocky Mountain

region: American Association of Petroleum Geologists, Memoir 41, pp. 653-668.

Roybal, F. E., and others, 1983, Hydrology of area 60, Northern Great Plains and Rocky Mountain coal provinces, New Mexico, Colorado, Utah, and Arizona: U.S. Geological Survey, Water Resources Investigations Open-file Report 83-203, 140 pp.

Roybal, G. H., Campbell, F. W., Beaumont, E. C., Cohen, A. D., Kuellmer, F. J., and Kottlowski, F. E., 1985, Quality assessment of strippable coals in New Mexico, Phase I, Fruitland and Cleary coals in the San Juan Basin of northwestern New Mexico: New Mexico Energy Research and Development Institute, Report No. 2-73-4304, 89 pp.

Royse, F., Jr., Warner, M. A., and Reese, D. L., 1975, Thrust belt structural geometry and related stratigraphic problems, Wyoming-Idaho-northern Utah; *in* Bolyard, D. W. (ed.), Deep drilling frontiers of the central Rocky Mountains: Rocky Mountain Association of Geologists, pp. 41-54.

Ryer, T. A., 1981, Deltaic coals of Ferron Sandstone Member of Mancos Shale: a predictive model for Cretaceous coal-bearing strata of Western Interior: American Association of Petroleum Geologists, Bulletin, v. 65, no. 11, pp. 2323-2340.

Schoell, Martin, 1983, Genetic characterization of natural gases: American Association of Petroleum Geologists, Bulletin, v. 67, no. 12, pp. 2225-2238.

Scruton, P. C., 1961, Rocky Mountain Cretaceous stratigraphy and regressive sandstones: Wyoming Geological Association Guidebook, 16th Annual Field Conference, pp. 242-249.

Sears, J. D., Hunt, C. B., and Hendricks, T. A., 1941, Transgressive and regressive Cretaceous deposits in southern San Juan Basin, New Mexico: U.S. Geological Survey, Professional Paper 193-F, pp. 101-121.

Senger, R. K., 1989, Hydrodynamics of gravity-driven flow systems in sedimentary basins: example of the Palo Duro Basin, Texas: Unpublished PhD dissertation, The University of Texas at Austin, 191 pp.

Senger, R. K., 1990, Regional characterization of variable-density fluid flow in sedimentary basins: implications on model interpretation: Paper presented at the Fifth Annual Canadian/American Conference on Hydrogeology: Parameter Identification and Estimation for Aquifer and Reservoir Characterization, Calgary, Alberta, Canada, September 18-20, 1990, 20 pp.

Senger, R. K., Fogg, G. E., and Kreitler, C. W., 1987, Effects of hydrostratigraphy and basin development on hydrodynamics of the Palo Duro Basin, Texas: The University of Texas at Austin, Bureau of Economic Geology, Report of Investigations No. 165, 48 pp.

Shoemaker, E. M., Squires, R. L., and Abrams, M. J., 1974, The Bright Angel and Mesa Butte fault systems of northern Arizona; *in* Geology of northern Arizona with notes on archaeology and paleoclimate, part 1: Geological Society of America, Rocky Mountain Section, pp. 355-391.

Siegel, Sidney, 1956, Nonparametric statistics of the behavioral sciences: McGraw-Hill, New York, 312 pp.

Sikkink, P. G. L., 1987, Lithofacies relationships and depositional environment of the Tertiary Ojo Alamo Sandstone and related strata, San Juan Basin, New Mexico and Colorado; *in* Fassett, J. E., and Rigby, J. K., Jr. (eds.), The Cretaceous-Tertiary boundary in the San Juan and Raton Basins, New Mexico and Colorado: Geological Society of America, Special Publication 209, pp. 81-104.

Silver, Caswell, 1951, Cretaceous stratigraphy of the San Juan Basin: New Mexico Geological Society, Guidebook to 2nd Field Conference, pp. 104-118.

Silver, Caswell, 1957, Relation of coastal and submarine topography to Cretaceous stratigraphy (New Mexico): Four Corners Geological Society Guidebook, Geology of southwestern San Juan Basin, Second Field Conference, pp. 128-137.

Spears, D. A., and Caswell, S. A., 1986, Mineral matter in coals: cleat minerals and their origin in some coals from the English Midlands: International Journal of Coal Geology, v. 6, pp. 107-125.

Spencer, C. W., 1987, Hydrocarbon generation as a mechanism for overpressuring in Rocky Mountain region: American Association of Petroleum Geologists, Bulletin, v. 71, no. 4, pp. 368-388.

Stach, E., Mackowsky, M.-Th., Teichmüller, M., Taylor, G. H., Chandra, D., and Teichmüller, R., 1975, Stach's textbook of coal petrology (2d ed.): Gebrüder Borntraeger, Berlin, Stuttgart, 428 pp.

Stearns, D. W., and Friedman, M., 1972, Reservoirs in fractured rock; *in* Stratigraphic oil and gas fields: American Association of Petroleum Geologists, Memoir 16, pp. 82-106.

Steven, T. A., 1975, Middle Tertiary volcanic field in the southern Rocky Mountains; *in* Curtis, B. F. (ed.), Cenozoic history of the southern Rocky Mountains: Geological Society of America, Memoir 144, pp. 75-94.

Stone, W. J., Lyford, F. P., Frenzel, P. F., Mizell, N. H., and Padgett, E. T., 1983, Hydrogeology and water resources of San Juan Basin, New Mexico: New Mexico Bureau of Mines and Mineral Resources, Hydrologic Report 6, 70 pp.

Suits, V. J., and Cordell, Lindrith, 1981, Bouger gravity map of the San Juan Basin area, Colorado, Arizona, and New Mexico: U.S. Geological Survey, Open-file Report No. 81-0657, scale 1:500,000.

Taylor, D. J., and Huffman, A. C., 1988, Overthrusting in the northwestern San Juan Basin, New Mexico-a new interpretation of the Hogback monocline (abs.): U.S. Geological Survey, Circular 1025, V. E. McKelvey Forum on Mineral and Energy Resources, p. 60.

Teichmüller, Marlies, 1971, Anwendung kohlenpetrographischer methoden bei der Erdöl u. Kohle, v. 24, pp. 69-76.

Teichmüller, Marlies, 1987, Recent advances in coalification studies and their application to geology; *in* Scott, A. C. (ed.), 1987, Coal and coal-bearing strata: recent advances: Blackwell Scientific Publications, London, Geological Society Publication No. 32, pp. 127-169.

TerraTek, 1990, Preliminary cleat and fracture data, Resource Enterprises, Inc. well: Southern Ute Tribal H#1, 5 pp.

Thompson, G. A., and Zoback, M. L., 1979, Regional geophysics of the Colorado Plateau: Tectonophysics, v. 61, no. 1-3, pp. 149-181.

Ting, F. T. C., 1977, Origin and spacing of cleats in coal beds: Journal of Pressure Vessel Technology, v. 99, pp. 624-626.

Tissot, B., and Welte, D., 1978, Petroleum formation and occurrence: Springer-Verlag, Berlin, 521 pp.

Tóth, J., 1978, Gravity-induced cross-formational flow of formation fluids, Red Earth region, Alberta, Canada: analysis, patterns, and evolution: Water Resources Research, v. 14, no. 5, pp. 805-843.

Tóth, J., 1980, Cross-formational gravity-flow of groundwater; a mechanism of the transport and accumulation of petroleum; the generalized hydraulic theory of petroleum migration; *in* Roberts, W. H., III, and Cordell, R. J. (eds.), Problems of petroleum migration: American Association of Petroleum Geologists, Studies in Geology No. 10, pp. 121-167.

Tremain, C. M., and Whitehead, N. H., III, 1990, Natural fracture (cleat and joint) characteristics and patterns in Upper Cretaceous and Tertiary rocks of the San Juan Basin, New Mexico and Colorado; *in* Ayers, W. B., Jr., and others, Geologic evaluation of critical production parameters for coalbed methane resources; Part I, San Juan Basin: The University of Texas at Austin, Bureau of Economic Geology, annual report prepared for the Gas Research Institute, GRI-90/0014.1, pp. 73-98.

TRW, 1978, Preliminary well test report on Western Coal Co., P07, San Juan County, New Mexico: Report on file at Colorado Geological Survey, Denver, Colorado.

Tyler, Roger, Laubach, S. E., and Ambrose, W. A., 1991, Effects of compaction on cleat characteristics: preliminary observations; *in* Ayers, W. B., Jr., and others, 1991, Geologic and hydrologic controls on the occurrence and producibility of coalbed methane, Fruitland Formation, San Juan Basin: The University of Texas at Austin, Bureau of Economic Geology, report prepared for the Gas Research Institute, GRI-91/0072, pp. 141-151.

van Gijzel, Peter, 1982, Characterization and identification of kerogen and bitumen and determination of thermal maturation by means of qualitative and quantitative microscopial techniques; *in* Staplin, F. L., and others, How to assess maturation and paleotemperatures: Society of Economic Paleontologists and Mineralogists, Short Course Number 7, pp. 159-216.

Ver Steeg, K., 1942, Jointing in the coal beds of Ohio: Economic Geology, v. 37, pp. 503-509.

Vistelius, A. B., 1966, Structural diagrams: Pergamon, New York, 178 pp.

Vuataz, F. D., and Goff, Fraser, 1986, Isotope geochemistry of thermal and nonthermal waters in the Valles Caldera, Jemez Mountains, northern New Mexico: Journal of Geophysical Research, v. 91, no. 2, pp. 1835-1853.

Wandrey, C. J., 1989, Lineament map of part of the Southern Ute

Reservation, San Juan Basin, southwestern Colorado: U.S. Geological Survey, Open-file Report No. 89-112, scale 1:100,000.

Way, S. C., Bumb, A. C., Koenig, R. A., McKee, C. R., and Reverand, J. M., 1985, Hydrologic characterization of coal seams for methane recovery, activities 5 and 7 progress report: review of single-phase hydrologic testing in coalbeds and development of unsaturated-flow well test procedures: Gas Research Institute, GRI 85/0046, 79 pp.

Weimer, R. J., 1986, Relationship of unconformities, tectonics, and sea level changes in the Cretaceous of the Western Interior, United States; *in* Peterson, J. A. (ed.), Paleotectonics and sedimentation in the Rocky Mountain region, United States: American Association of Petroleum Geologists, Memoir 41, pp. 397-422.

Welhan, J. A., 1987, Stable isotope hydrology; *in* Kyser, T. K. (ed.), Stable isotope geochemistry of low temperature processes: Mineralogical Society of Canada Short Course Handbook, v. 13, pp. 129-161.

Whiticar, M. J., Faber, E., and Schoell, Martin, 1986, Biogenic methane formation in marine and freshwater environments: CO_2 reduction vs. acetate fermentation-isotope evidence: Geochimica et Cosmochimica Acta, v. 50, pp. 693-709.

Williams, G. D., and Stelck, C. R., 1975, Speculations on the Cretaceous paleogeography of North America; *in* Caldwell, W. G. E. (ed.), The Cretaceous system in the Western Interior of North America: Geological Association of Canada, Special Paper 13, pp. 1-20.

Wilson, R. W., and Jentgen, R. W., 1980, Coal test drilling for the De-Na-Zin Bisti Area, San Juan County, New Mexico: U.S. Geological Survey, Open-file Report 80-1289, 111 pp.

Wong, I. G., and Humphrey, J. R., 1989, Contemporary seismicity, faulting, and the state of stress in the Colorado Plateau: Geological Society of America, Bulletin, v. 101, no. 9, pp. 1127-1146.

Wood, G. H., Jr., Johnson, R. B., and Dixon, G. H., 1948, Geology of the southern part of Archuleta County, Colorado: U.S. Geological Survey, Oil and Gas Investigation Preliminary Map 81, scale 1:63,360.

Woodward, L. A., and Callender, J. F., 1977, Tectonic framework of the San Juan Basin: New Mexico Geological Society, Guidebook to 28th Field Conference, pp. 209-212.

Wright, Robyn, 1986, Cyde stratigraphy as a paleogeographic tool: Point Lookout Sandstone, southeastern San Juan Basin, New Mexico: Geological Society of America, Bulletin, v. 97, no. 6, pp. 661-673.

Yarborough, L., and Hall, K. R., 1974, How to solve equation of state for Z-factors: Oil & Gas Journal, v. 72, no. 7, pp. 86-88.

Yeh, Joseph, Schultz-Ela, D. D., and Laubach, S. E., 1991, Predicting fracture permeability from bed curvature; *in* Ayers, W. B., Jr., and others, Geologic and hydrologic controls on the occurrence and producibility of coalbed methane, Fruitland Formation, San Juan Basin: The University of Texas at Austin, Bureau of Economic Geology, topical report prepared for the Gas Research Institute, GRI-91/0072, pp. 181-192.

Yurtsever, Y., and Gat, J. R., 1981, Atmospheric waters; *in Gat,* J. R., and Gonfiantini, R. (eds.), Stable isotope hydrology: deuterium and oxygen-18 in the water cycle: International Atomic Energy Agency Technical Report Series No. 210, pp. 103-142.

Zapp, A. D., 1949, Geology and coal resources of the Durango area, La Plata and Montezuma Counties, Colorado: U.S. Geological Survey, Oil and Gas Investigation Preliminary Map 109, scale 1:31,680.

Zietz, Isidore (compiler) and others, 1982, Composite magnetic anomaly map of the United States, Part A: conterminous United States: U.S. Geological Survey, Geophysical Investigation Map, GP-0954-A, scale 1:250,000.

Zoback, M. D., Tsukahara, Hiroaki, and Hickman, Stephen, 1980, Stress measurements at depth in the vicinity of the San Andreas Fault: implications for the magnitude of shear stress at depth: Journal of Geophysical Research, v. 85, no. B11, pp. 6157-6173.

Zoback, M. L., and Zoback, M. D., 1980, State of stress in the conterminous United States: Journal of Geophysical Research, v. 85, no. B11, pp. 6113-6156.

Zoback, M. L., and Zoback, M. D., 1989, Tectonic stress field of the continental United States; *in* Pakiser, L. C., and Mooney, W. D. (eds.), Geophysical framework of the continental United States: Geological Society of America, Memoir 172, pp. 523-539.

Selected conversion factors*

TO CONVERT	MULTIPLY BY	TO OBTAIN
Length		
inches, in	2.540	centimeters, cm
feet, ft	3.048 X 10^{-1}	meters, m
yards, yds	9.144 X 10^{-1}	m
statute miles, mi	1.609	kilometers, km
fathoms	1.829	m
angstroms, Å	1.0 x 10^{-8}	cm
Å	1.0 x 10^{-4}	micrometers, µm
Area		
m2	6.452	cm^2
ft^2	9.29 x 10^{-2}	m^2
yds^2	8.361 x 10^{-1}	m^2
mi^2	2.590	Km^2
acres	4.047 x 10^3	m^2
acres	4.047 x 10^{-1}	hectares, ha
Volume (wet and dry)		
in^3	1.639 x 10^1	cm^3
ft^3	2.832 x 10^{-2}	m^3
yds^3	7.646 x 10^{-1}	m^3
fluid ounces	2.957 x 10-^{2}	liters, l *or* L
quarts	9.463 x 10^{-1}	I
U.S. gallons, gal	3.785	1
U.S. gal	3.785 x 10^{-3}	m^3
acre-ft	1.234 x 10^3	m^3
barrels (oil), bbl	1.589 x 10^{-1}	m^3
Weight, mass		
ounces avoirdupois, avdp	2.8349 x 10^1	grams, gr
troy ounces, oz	3.1103 x 10^1	gr
pounds, lb	4.536 x 10^{-1}	kilograms, kg
long tons	1.016	metric tons, mt
short tons	9.078 x 10^{-1}	mt
oz mt^{-1}	3.43 x 10^1	parts per million, ppm
Velocity		
ft sec^{-1} (= ft/sec)	3.048 x 10^{-1}	m sec^{-1} (= m/sec)
mi hr^{-1}	1.6093	km hr^{-1}
mi hr^{-1}	4.470 x 10^{-1}	m sec^{-1}

TO CONVERT	MULTIPLY BY	TO OBTAIN
Pressure, stress		
lb in^{-2} (= lb/in^2), psi	7.03 x 10-^{2}	kg cm^{-2} (= kg/cm^2)
lb in^{-2}	6.804 x 10-^{2}	atmospheres, atm
lb in^{-2}	6.895 x 10^3	newtons (N)/m^2, N m^{-2}
atm	1.0333	kg cm^{-2}
atm	7.6 x 10^2	mm of Hg (at 0° C)
inches of Hg (at 0° C)	3.453 x 10^{-2}	kg cm'
bars, b	1.020	kg cm^{-2}
b	1.0 x 10^6	dynes cm^{-2}
b	9.869 x 10^{-1}	atm
b	1.0 x 10-^{1}	megapascals, MPa
Density		
lb in^{-3} (= lb/in^3)	2.768 x 10^1	gr cm^{-3} (= gr/cm^3)
Viscosity		
poises	1.0	gr cm^{-1} sec^{-1} *or* dynes cm^{-2}
Discharge		
U.S. gal min^{-1}, gpm	6.308 x 10-^{2}	1 sec^{-1}
Gpm	6.308 x 10-^{5}	m^3 sec^{-1}
Ft^3 sec^{-1}	2.832 x 10-^{2}	m^3 sec^{-1}
Hydraulic conductivity		
U.S. gal day-1ft^{-2}	4.720 x 10-^{7}	m sec^{-1}
Permeability		
darcies	9.870 x 10-^{13}	m^2
Transmissivity		
U.S. gal day^{-1} ft^{-1}	1.438 x 10-^{7}	m^2 sec^{-1}
U.S. gal min^{-1} ft^{-1}	2.072 x 10'	1 sec^{-1} m^{-1}
Magnetic field intensity		
gausses	1.0 x 10^5	gammas
Energy, heat		
British thermal units, BTU	2.52 x 10-^{1}	calories, cal
BTU	1.0758 x 10^2	kilogram-meters, kgm
BTU lb^{-1}	5.56 X 10-^{1}	cal kg^{-1}
Temperature		
°C + 273	1.0	°K (Kelvin)
°C + 17.78	1.8	°F (Fahrenheit)
°F - 32	5/9	°C (Celsius)

*Divide by the factor number to reverse conversions.
Exponents: for example 4.047 x 10^3 (see acres) = 4,047; 9.29 x 10-^{2} (see ft^2) = 0.0929.

Editors: Bobby Duncan Carol
A. Hjellming

Typeface: Palatino

Presswork: Miehle Single Color Offset
Harris Single Color Offset

Binding: Smyth sewn with softbound cover

Paper: Cover on 17-pt Kivar Text on
70-lb white matte

Ink: Cover- PMS 320/4-color process Text-
black

Quantity: 1,000